SAMHÄLLSBYGGNAD

BYGGTEKNIK

Conference proceedings, ICTB 2017, 3rd International Conference on Timber Bridges

Anders Gustafsson, RISE, Anna Pousette, RISE

Olle Hagman, LTU, Mats Ekevad, LTU

SP Rapport 2017:26

Abstract

Conference proceedings, ICTB 2017, 3rd International Conference on Timber Bridges

Conference proceedings from the conference ICTB 2017, the 3rd International Conference on Timber Bridges, 26-29 June 2017 in Skellefteå, Sweden.

A pre-tour included visits to several timber bridges between Skellefteå and Umeå. The conference had 5 Keynote presentations and 45 technical papers presented in 10 sessions, and also a technical visit to wooden buildings and bridges in Skellefteå.

Content of the conference is presented in the program.

Key words: Timber bridge, Design, Moisture, Monitoring, Testing, Joints, Durability, LCA, Timber-concrete bridge, Historical timber bridges, FEM Analyses, Case studies

RISE Research Institutes of Sweden

SP Rapport 2017:26
ISSN 0284-5172
Skellefteå 2017

ICTB 2017

3RD INTERNATIONAL CONFERENCE ON TIMBER BRIDGES

26-29 June, 2017 | Skellefteå, Sweden

Conference Programme

RI. SE
Research Institutes of Sweden

ICTB 2017

3RD INTERNATIONAL CONFERENCE ON TIMBER BRIDGES

26-29 June, 2017 | Skellefteå, Sweden

Welcome to ICTB 2017

RISE Research Institutes of Sweden in cooperation with Luleå University of Technology have the pleasure to welcome you to the Conference on Timber Bridges which will take place in Skellefteå. The conference is supported by the municipality of Skellefteå (Skellefteå kommun) and the Swedish Research Council Formas.

The successful conferences ICTB 2010 in Lillehammer, Norway, and ICTB 2013 in Las Vegas, USA, is now being followed up by a third conference in Skellefteå, Sweden. The conference will be a unique opportunity to network with an international community of experts on timber bridges, including highway, railway and pedestrian structures.

We received a lot of technical abstracts and have created a program that offers many topics concerning timber bridges. We welcome you to Skellefteå and the conference and hope you will find interesting technical sessions and meetings with speakers and attendees to learn more and maybe find new collaborations for the future.

Anders Gustafsson

Conference chair

ICTB 2017 Committes

International Scientific Committee

James Wacker, USDA Forest Service, Forest Products Lab. (USA)
Kjell Arne Malo, Norwegian University Of Science and Technology, NTNU, (Norway)
Roberto Crocetti, Lund University, (Sweden)
Robert Widmann, Empa – Structural Engineering Research Laboratory, (Switzerland)
A.J.M Jorissen, Technische Universiteit Eindhoven, (Netherlands),
Hideyuki Nasu, Nippon Institute of Technology, (Japan)
Mats Ekevad, Luleå University of Technology, (Sweden)
Anna Pousette, RISE Research Institutes of Sweden, (Sweden)

Conference Planning Committee

Anders Gustafsson, RISE Research Institutes of Sweden
Anna Pousette, RISE Research Institutes of Sweden
Per-Anders Fjällström, RISE Research Institutes of Sweden
Mats Ekevad, Luleå University of Technology
Olle Hagman, Luleå University of Technology

Keynote Speakers

 **A. J. M. Jorissen**	Professor André J. M. Jorissen at Technische Universiteit Eindhoven, the Department of the Built Environment, is expert in the research program Structural Design. Main topics are Manufacturing technology, mechanical technology, robotics; Urban and rural planning; Building technology; Architecture and building construction.
 **Kjell Arne Malo**	Professor Kjell Arne Malo got his PhD from Norwegian Institute of Technology. His professional background is from steel- aluminium and timber structures. His current research topics and fields of interests are material models for wood, strength and stiffness of connections for timber structures, vibrations and comfort issues in multi-storey timber buildings, and design of timber bridges. He has since 2002 lectured university courses on timber engineering and basic mechanics and is supervisor for MSc and PhD students in timber engineering at NTNU, Norway. He is national delegate to the European standardization committee on timber structures, convenor for committee on the new Eurocode EN 1995-2 Timber Bridges.
 **Robert Widmann**	Robert Widmann is Civil Engineer. After servicing in German Airforce for 10 years as an EOD specialist Robert studied civil engineering at the University of Biberach, Germany. Practical works in a construction company and in an engineering office followed and in 1997 Robert joined Wood Laboratory of Empa in Duebendorf Switzerland as a research engineer. His main focus was timber engineering and within this field he worked on a wide variety of topics, including timber bridges. Since 2015 Robert is working as a Test Engineer in the Structural Engineering Research Laboratory of Empa. As a group leader he is responsible for the structural test facility of this laboratory, which includes - amongs others - testing of big timber structural members.
 **James P. Wacker**	James' current position is research engineer at the Forest Products Laboratory, a national laboratory within the USDA-Forest Service. He has been involved with various aspects of timber bridge research in the field and in the laboratory. Over the past 25 years, James has led a handful of national field studies aimed at characterizing the performance or durability characteristics of highway bridges. More recently, he has been involved with the evaluation of several NDE techniques for inspection of timber bridge structures. As a member of the American Society of Civil Engineers (ASCE), Jim served as chairperson for the timber bridges technical committee, and currently serves on its technical activities executive committee. He is also a registered professional engineer in the state of Wisconsin.
 **Hideyuki Nasu**	Hideyuki Nasu is a professor at Nippon Institute of Technology, and is the head of its Architecture department. His academic degree is Doctor of Engineering and he has license of First-grade qualified Architect. His fields of expertise include wooden structural engineering. He is working with: research and development for wooden skeleton framing with high spec joints; vibration damping technology for wooden houses; middle to high-rise wooden structures with cross laminated timber (CLT), etc.

Programme overview

Pre-Tour

Monday - 26 June 2017	See separate programme

Conference programme

Place of the Conference: Forumsalen, Campus Skellefteå (Laboratorgränd 13, Skellefteå)

The duration of each presentation is scheduled 20 minutes including questions. Presentations should be about 15 minutes to allow a 5 minutes question time and discussion.

Tuesday - 27 June 2017	
7:30 – 11:00	*Attendee Registration, Presenter Check-in, Posters*
8:45 – 9:00	Opening Session
9:00 – 10:00	Keynote Presentations
10:00 – 10:30	Coffee Break
10:30 – 12:10	Technical Session 1 Design of timber bridges I
12:10 – 13:10	Lunch
13:10 – 14:50	Technical Session 2 Monitoring
14:50 – 15:50	Coffee Break / Poster session
15:50 – 17:30	Technical Session 3 Joints
17:30 – 19:00	Technical visit - Skellefteå Wooden buildings and bridges
19:00 – 21:00	Information from Timber Bridge Manufacturer including Buffet Dinner (Stiftsgården)

Wednesday - 28 June 2017		
7:30 – 11:00	*Attendee Registration, Presenter Check-in*	
7:50-8:00	Introduction to the day	
8:00 – 9:00	Keynote Presentations	
9:00 – 10:40	Technical Session 4 Durability and LCA	
10:40 – 11:10	Coffee Break	
11:10 – 12:40	Technical Session 5 Design of timber bridges II	
12:40 – 13:40	Lunch	
13:40 – 15:20	Technical Session 6 Timber concrete bridges	
15:20 – 15:50	Coffee Break	
15:50 – 17:10	Technical Session 7 Historical bridges	Technical Session 8 FEM Analyses
17:10 –	Committee Meeting, next conference	

19:00 – 21:30	Dinner Banquet Skellefteå

Thursday – 29 June 2017	
7:30 – 8:00	*Attendee Registration, Presenter Check-in*
7:50-8:00	Introduction to the day
8:00 – 8:30	Keynote Presentation
8:30 – 9:50	Technical Session 9 Testing
9:50 – 10:10	Coffee Break
10:10 – 11:300	Technical Session 10 Case studies
11:30 – 11:40	Close-out Session
11:40 – 13:00	Lunch

Poster Session

Tuesday 27 June 2017, 14:50-15:50

Folding System for Timber Truss Bridge *Hideyuki Hirasawa, Honomi Ansai, Jun Tonuma*	**Vaida footbridge – from design to demolition** *Lauri Perv, Mihkel Sinisalu, Alar Just*
Performance evaluation of the cross laminated timber for the bridge decks *Yusuke Ariyama, Takanobu Sasaki, Tomoyuki Hayashi, Atsushi Toyoda, Humihiko Gotou, Katsuhiko Takami, Shogo Araki*	**Adhesive system for acetylated wood for load bearing constructions - The GIAceWood project** *Andreas Treu, Ronny Bredesen, Ferry Bongers*
Creep behavior of oak pegs under tension in dry and wet conditions *Jiři Kunecký, Michal Kloiber, Hana Hasníková, Jaroslav Hrivnák, Václav Sebera, Jan Tippner, Jaromír Milch*	**A Covered Cross Laminated Timber Bridge - From Concept to Product** *Lars Laitila, Niclas Björngrim, Peter Bomark & Tobias Pahlberg*
Mechanical analysis of scarf joint fastened using cylindrical wooden dowel *Jan Tippner, Jaromír Milch, Jiři Kunecký, Michal Kloiber, Martin Brabec, Václav Sebera*	**Future CLT** **Mats, Elisa?**

Detailed Technical Programme

Tuesday 27 June 2017

8:45-9:00	**Opening Session,** *Olle Hagman, Luleå University of Technology*
9:00-10:00	**Keynote Presentations** *André Jorissen, Design and manufacturing of timber bridges in the Netherlands* *Kjell Arne Malo, Developments of durable timber bridges*
10:30-12:10	**Technical Session 1, Design of timber bridges I** *Moderator: James P. Wacker, USDA Forest Service, Forest Products Laboratory*
	A timber bridge across Lake Mjøsa in Norway *Ole Kristian Løke, Trond Arne Stensby, Johannes Veie, Yngve Årtun, Svein Erik Jakobssen, Per Meaas*
	Comparison of network patterns suitable for timber bridges with crossbeams *Anna Weronika Ostrycharzyk, Kjell Arne Malo*
	Effect of Nordic climate on cupping of stress laminated timber decks *Stefania Fortino, Giovanni Metelli, Petr Hradil, Federico Ossodi, Anna Pousette, Tomi Toratti*
	Anchor plates for pre-stressing rods and compression orthogonal to grain of timber *Fransesco Mirko Massaro, Kjell Arne Malo*
	Mechanical properties of acetylated radiate pine *Ferry Bongers*
13:10-14:50	**Technical Session 2, Monitoring and testing** *Moderator: Olle Hagman, Luleå University of Technology*
	Advantages of moisture content monitoring in timber bridges *Andreas Müller, Bettina Franke, Marcus Schiere, Steffen Franke*
	Moisture monitoring of nine protected timber bridges in Germany *Johannes Koch, Ralf W. Arndt, Antje Simon, Markus G. Jahreis*
	Moisture Content Monitoring in Glulam by Electrical Methods *Hang Li, Marianne Perrin, Florent Eyma, Xavier Jacob, Vincent Gibiat*
	Smart Timber Bridge on Geosynthetic Reinforced Soil (GRS) Abutments *Adam Senalik, James P. Wacker, Travis K. Hosteng, John Hermanson*
	A Robust, Passive Resistance Sensor for Moisture Content Monitoring of Timber Bridges *Niclas Björngrim, Per-Anders Fjellström, Olle Hagman*
14:50-15:50	**Poster Session**
15:50-17:30	**Technical Session 3, Joints** *Moderator: Alar Just, RISE Research Institutes of Sweden*
	Effect of on-site splice joints for timber network arch bridges *Martin Cepelka, Kjell Arne Malo*
	Parallel splitting mode of failure in dowel type connections with chamfered cuts *Katarzyna Ostapska-Luczkowska, Kjell Arne Malo*
	Effects of Notching on Timber Girder Performance *Justin Dewey, Rabin Tuladhar, Lara Mullamphy, Lucy McCormack*
	Fatigue strength of axially loaded threaded rods embedded in glulam at 45° to the grain *Haris Stamatopoulos, Kjell Arne Malo*
	Reinforcement of Sundbyveien Bridge *Magne A. Bjertnæs, Trond Arne Stensby*

Detailed Technical Programme

Wednesday 28 June 2017

7:50-8:00	**Introduction to the day,** *Anders Gustafsson RISE Research Institutes of Sweden*
8:00-9:00	**Keynote Presentations** *Robert Widmann*, From then to now: A short history of Swiss timber bridge designs *James P. Wacker*, U.S. Timber Bridges: Current Activities and Future Directions
9:00-10:40	**Technical Session 4, Durability and LCA** *Moderator: Anna Pousette, RISE Research Institutes of Sweden*
	Learning Experiences from Norwegian Timber Bridge Inspections *Hauke Burkart, Otto Kleppe*
	Rational maintenance of timber bridges *Daniel Honfi, Thomas Lechner, Jochen Köhler*
	Investigation of timber bridges in Estonia *Per-Anders Fjellström, Alar Just*
	Comparative life cycle assessment of concrete and timber road bridge deck designs *Reyn O´Born, Katalin Vertes*
	Life cycle Assessment on two design alternatives of the Driva Bridge *Yishu Niu, Lauri salokangas, Gerhard Fink*
11:10-12:40	**Technical Session 5, Design of timber bridges II** *Moderator: Mats Ekevad, Luleå University of Technology*
	A parametrized process: Design and realization of timber truss bridges *John Haddal Mork, Marcin Luczkowski, Bendik Manum, Anders Rønnquist*
	Correct geometry against water damages in Design of Timber Bridges *Tönis Teppand, Renno Reitsnik*
	New design Guidelines for structural protected timber bridges *Antje Simon, Markus G. Jahreis, Johannes Koch, Ralf Arndt*
	Improved efge design for stress-laminated decks made of spruce *Anna Pousette, Peter Jacobsson, Erik Johansson, Lars-Olof Nilsson, Christine Warg*
13:40-15:20	**Technical Session 6, Timber-concrete composite bridges** *Moderator: Kjell Arne Malo, NTNU Norwegian University of Science and Technology*
	Investigation of Early Timber-Concrete Composite Bridges in the United States *James P. Wacker, Alfredo Dias, Travis K. Hosteng*
	Design of wood-concrete composite beams under deck bridge – Theoretical development and construction examples *Fabien Renaudin, Philippe Jandin*
	Short-term analysis of timber-concrete composite bridges *Joonas Jaaranen, Lauri Salokangas, Gerhard Fink*
	Long-term analysis of timber-concrete composite bridges *Joonas Jaaranen, Lauri Salokangas, Gerhard Fink*
	Laminated Steel-Timber-Concrete Beams for Bridges *Jeno Balogh, István Szücs, Rose Holtzman*

Parallell Sessions

15:50-17:10	**Technical Session 7, Historical bridges** *Moderator: Anders Gustafsson, RISE Research Institutes of Sweden*
	A Century of a Bridge of Perfection *Liu Yan*
	Historic Timber Howe Trusses of British Columbia *Murray Johnson, Gary Farnden*
	The Cloak Bridge in Česky Krumlov – construction history research *Jiri Blaha*
	Structural Evolution of Woven Arched Covered Timber Bridges in China *Yaxin Li, Sudarshan Krishnan*
15:50-17:10	**Technical Session 8, FEM Analyses** *Moderator: André J. M. Jorissen, Technische Universitet Eindhoven*
	Mechanics of Stress-Laminated Timber Bridges with Butt End Joints *Mats Ekevad, Johannes A. J. Huber, Peter Jacobsson*
	Simulation of moisture diffusion in timber bridges exposed to rain *Petr Hradil, Stefania Fortino, Giovanni Metelli, Alessandro Musci, Jakob Dohnal, Maria Fredriksson*
	Updating of numerical timber bridges models by experimental modal analysis *Julio Vivas, Soledad Rodriguez, Juan Carlos Santos*
	Comparison of Cross- and Stress-Laminated Timber Bridge Decks *Jonas Turesson, Mats Ekevad, Sven Berg*

Detailed Technical Programme

Thursday 29 June 2017

7:50-8:00	**Introduction to the day,** *Anders Gustafsson RISE Research Institutes of Sweden*
8:00-8:30	**Keynote Presentation** *Hideyuki Nasu, Examples of Japanese wooden bridges and Japanese wooden structures*
8:30-9:50	**Technical Session 9, Testing** *Moderator: Robert Widmann, Empa – Structural Engineering Research Laboratory*
	Inspection of a cable-stayed bridge by 3D-scanner *Balázs Major, Olle Hagman*
	The potential of acoustic Emission for Timber damage Assessment *Imen Yahyaoui, Marianne Perrin, Xiaojing Gong*
	Analysis of Mini-jack technique for in situ measurement of strength *Michal Kloiber, Jan Tippner, Jiři Kunecký,Václav Sebera, Jaromír Milch, Jaroslav Hrivnák*
	The Cloak Bridge in Česky Krumlov – measuring of mechanical properties *Michal Kloiber, Václav Sebera, Jaroslav Hrivnák Jan Tippner, Jiři Kunecký*
10:10-11:30	**Technical Session 10, Case studies** *Moderator: Per-Anders Fjellström, RISE Research Institutes of Sweden*
	Design flaws on Norwegian Timber Bridges *Hauke Burkart, Tormod Dyken*
	Björgum bridge, a roofed timber footbridge in Norway *Asmund Sveen, Trond Even Eggen, Yngve O. Aartun*
	Field condition assessment of the first vehicular timber bridge in Korea, Hanareum Bridge *Sang-Joon Lee, Kwang-Mo Kim, Kug-Bo Shim*
	Network arch bridge with glulam arches. Lessons learned and further development *Johannes Veie*
11:30-11:40	**Close-out Session,** *Anders Gustafsson, RISE Research Institutes of Sweden*

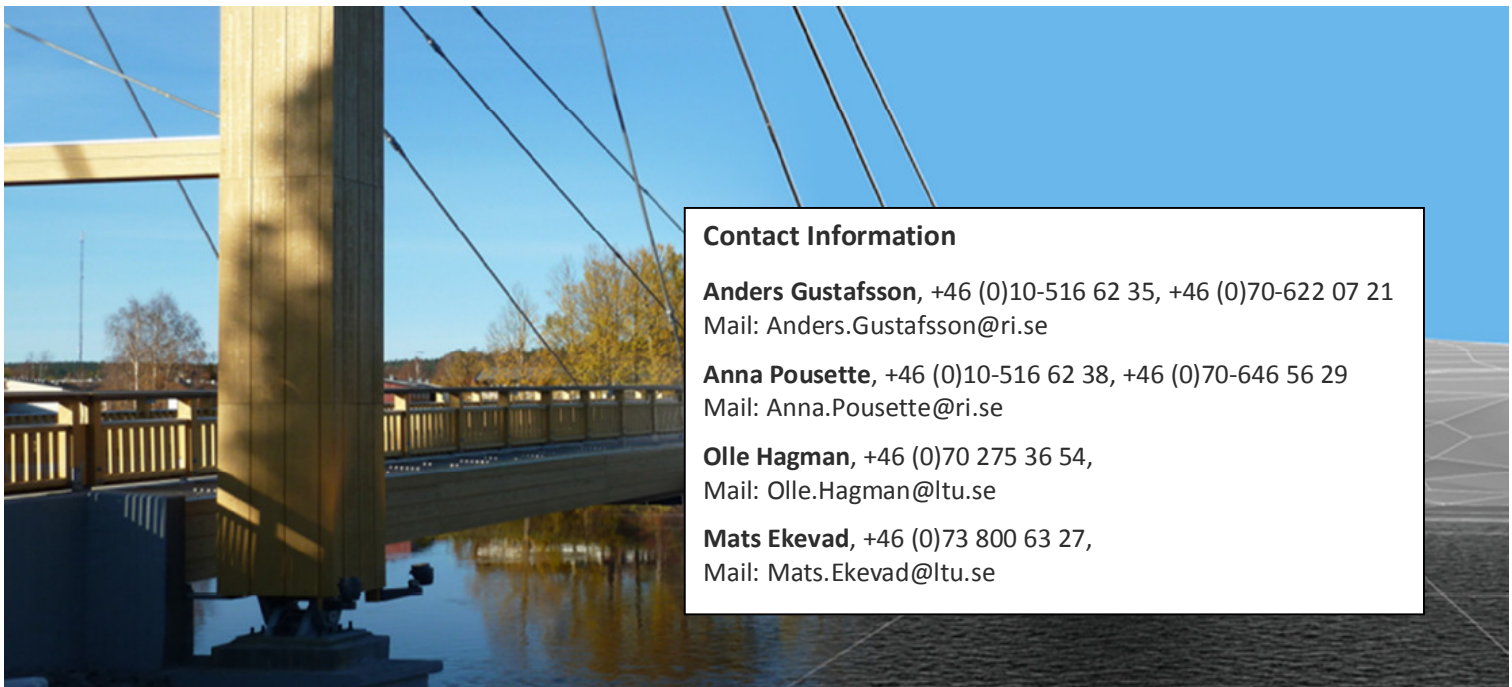

Contact Information

Anders Gustafsson, +46 (0)10-516 62 35, +46 (0)70-622 07 21
Mail: Anders.Gustafsson@ri.se

Anna Pousette, +46 (0)10-516 62 38, +46 (0)70-646 56 29
Mail: Anna.Pousette@ri.se

Olle Hagman, +46 (0)70 275 36 54,
Mail: Olle.Hagman@ltu.se

Mats Ekevad, +46 (0)73 800 63 27,
Mail: Mats.Ekevad@ltu.se

Through our international collaboration programmes with academia, industry, and the public sector, we ensure the competitiveness of the Swedish business community on an international level and contribute to a sustainable society. Our 2,200 employees support and promote all manner of innovative processes, and our roughly 100 testbeds and demonstration facilities are instrumental in developing the future-proofing of products, technologies, and services. RISE Research Institutes of Sweden is fully owned by the Swedish state.

I internationell samverkan med akademi, näringsliv och offentlig sektor bidrar vi till ett konkurrenskraftigt näringsliv och ett hållbart samhälle. RISE 2 200 medarbetare driver och stöder alla typer av innovationsprocesser. Vi erbjuder ett 100-tal test- och demonstrationsmiljöer för framtidssäkra produkter, tekniker och tjänster. RISE Research Institutes of Sweden ägs av svenska staten.

RISE Research Institutes of Sweden
Box 857, 501 15 BORÅS
Telefon: 010-516 50 00
E-post: info@ri.se, Internet: www.sp.se / www.ri.se

Byggteknik
SP Rapport 2017:26
ISSN 0284-5172

A timber bridge across Lake Mjøsa in Norway

Ole Kristian Løke
Project engineer
Aas-Jakobsen
Oslo, Norway

M.Sc. from University of New South Wales, Australia from 2003. Joined the company Aas-Jakobsen in 2003.

Trond Arne Stensby
Project Manager
Norwegian Public Roads Administration
Hamar, Norway

Project leader and central person in Norwegian development of timber bridges since 1990

Johannes Veie
Bridge department,
Norwegian Public Roads Administration
Hamar, Norway

Yngve Årtun
Chief Architect
Plan Arkitekter AS
Trondheim, Norway

M.Arch. from Norwegian Institute of Technology from 1983. Joined the company Plan Arkitekter as a partner in 1996. Specialist in bridge aesthetics and timber bridges.

Svein Erik Jakobsen
Director
Aas-Jakobsen
Oslo, Norway

M.Sc. from Norwegian Institute of Technology from 1984. Joined the company Aas-Jakobsen in 1985 and is currently Director of the Bridge Department.
.

Per Meaas
Project Manager
Aas-Jakobsen
Oslo, Norway

M.Sc. from Norwegian Institute of Technology from 1974. Joined the company Aas-Jakobsen in 1976 and is Project Manager for several Major Infrastructure Projects.

Summary

This paper summarises the results of a research program on how to cross Lake Mjøsa in Norway for a new 4-lane link on Highway E6 between the cities Hamar and Lillehammer with a timber bridge.

Based on preliminary studies the Norwegian Ministry of Transportation launched a research program to investigate critical aspects involved in construction of such a large timber bridge. The research focused on the large-scale aspects, durability and the technical solution further investigating the timber alternative. The research program finished in the autumn of 2016 with the conclusion that a timber bridge is both technically, aesthetically and economically feasible.

The timber alternative is a truss bridge with two underlay timber trusses composite with a concrete bridge deck. Typical span width is 70 m. Main spans are suggested to be cable stay spans with the same timber truss solution and span widths 120 m. Total length of the bridge is 1750 m.

Keywords: Timber truss, world record, research program, Lake Mjøsa.

1. Introduction

1.1 1st Mjøsa Bridge

Figure 1 Overview of 1st Mjøsa Bridge

The 1st Mjøsa Bridge was opened to traffic in 1985 and is a part of the main north-south highway in Norway, the E6. The bridge crosses the largest lake in Norway, Lake Mjøsa, and is in total 1311m long. It is a concrete box girder bridge with typical span widths of 69m. The bridge is founded on piles, some to rock, some as friction piles. At the bridge site, the lake is approximately 30-40m deep, giving a considerable free span in water for each pile. The bridge has two lanes of traffic and a pavement for walking/bicycling. An overview picture og the bridge is shown in Figure 1.

1.2 Feasibility study 2006

Since traffic is increasing on the E6, plans have been introduced to increase capacity across Lake Mjøsa. In 2006, Norwegian Public Roads Administration carried out a feasibility study to investigate if it was possible to cross Lake Mjøsa with a bridge in vicinity to the existing one. The feasibility study report was worked out by Aas-Jakobsen AS. The existing Mjøsa Bridge is situated on a narrow sill formed by ancient glaciers. The feasibility study concluded that it was possible to place yet another bridge at the same sill. The study also identified another possible alignment for the crossing further south, this however requiring deep sea foundations.

1.3 The timber bridge background

The Norwegian Public Roads Administration Region East plays a major role in establishing a 2nd crossing. This region has been the leading developer of timber bridges in Norway. Through a large number of timber bridge projects, the knowhow and expertise has grown over the years, making this region one of the leading timber bridge environments in the world. Since Mjøsa Bridge is situated in the very heart of this timber bridge society, it is only natural that there are strong interests to consider a timber bridge alternative for the new crossing. The fact that this will be the world's longest bridge of its kind, if carried out as a timber bridge, only strengthen this attitude. In 2010, a timber bridge seminar was held close to the bridge site to determine whether a timber bridge alternative was feasible for Mjøsa Bridge. Experts from the whole industry were invited, and the conclusion was positive. The seminar even introduced three different technical solutions as basis for further work.

1.4 Conceptual design 2012

In 2012, Norwegian Public Roads Administration launched a conceptual design phase [1] involving evaluation of all consequences of realization of the project for the 2nd crossing of Lake Mjøsa. The project was awarded Aas-Jakobsen AS. One of the basic boundary conditions of the project was that at least one timber bridge alternative should be investigated.

The first part of the project was dedicated to evaluations of road alignments as defined in the feasibility study. Along this work a broad spectre of bridge alternatives was evaluated for the different alignments. The recommendation from this part of the project was that even if the southern alignment has technical challenges from deep sea foundations, it is preferable to traffic and to public considerations.

Given the recommended alignment, it was concluded that both from technical aspects and from aesthetical aspects, the bridge should have increased mid span lengths compared to side span lengths. This led to the conclusion that the bridge type should either be a concrete box girder type with extradosed main spans, or a timber underlay truss type with main spans supported by cable

stays.

This paper further describes the latter.

A paper [2] presenting the results from the conceptual design was presented on the 2nd International conference on Timber bridges in 2013, Las Vegas.

1.5 Preliminary design 2013-2015

The preliminary design focused on the road alignments and concluded in May 2015. The bridge presented in this paper uses the road alignment from May 2015.

2. Technical challenges

The proposed new bridge has a total length of 1750m and span widths typically 70 m. The middle four spans have span widths 120 m. The bridge is founded on rock in two axes, on piles to rock on 10 axes and on friction piles on the remaining 12 axes. Deep sea foundations in the five main span axes are friction piles up to almost 110m length, with a 40m portion in soil and a water depth of 70m. The free spanning through water is restricted through a concrete caisson solution acting both as guides and as buckling constraints to the piles. The piles are steel piles with diameter 1220 mm or 1420 mm. A side overview of the bridge solution is given in Figure 2.

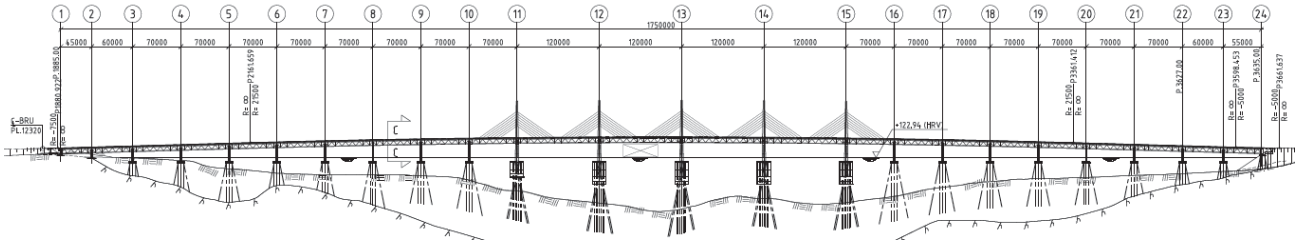

Figure 2 Side overview, timber bridge

The bridge carries four lanes of traffic, with free space between railings of 2 x 9.5m, one pedestrian lane of 3m and one service lane on the opposite side of 3m, giving a symmetric layout of the bridge as can been seen on Figure 3.

The superstructure is a two-plane timber truss with a height of 7.3 m proposed in composite action with a concrete bridge deck. The timber truss members have typical dimensions of 1600mm x 1100mm for the upper chord, 1600mm x 900mm for the lower chord and 1600mm x 600mm for the diagonals.

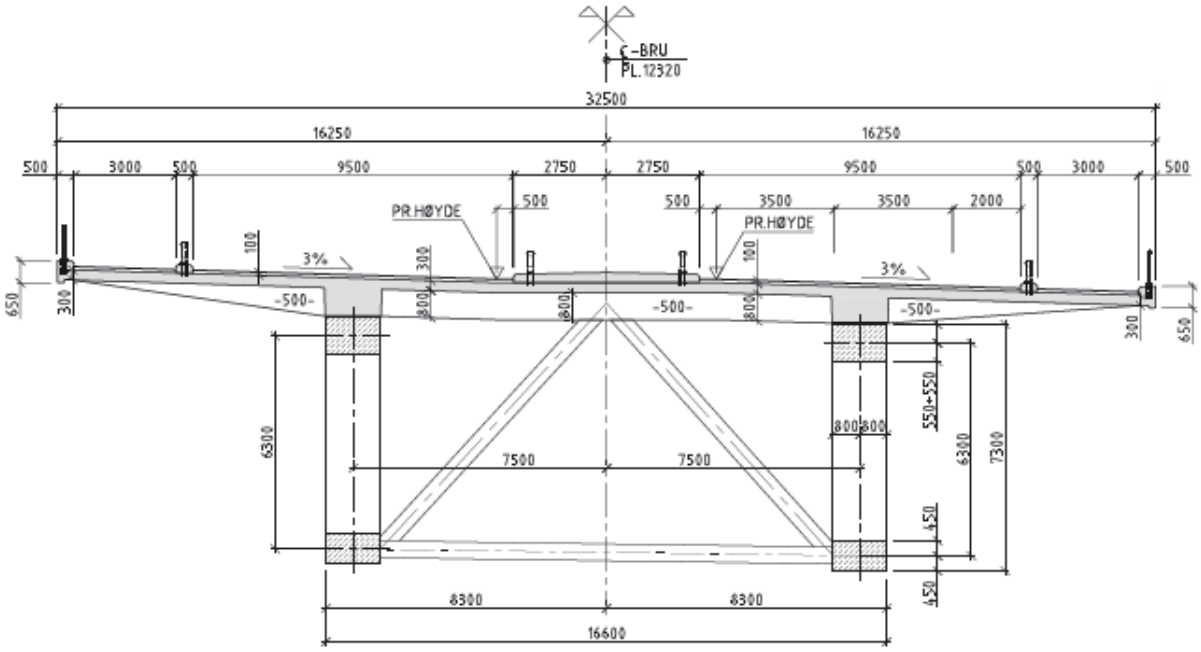

Figure 3 Typical cross section

2.1 Technical description

The single stay plane is placed in the centre, implying the introduction of single towers in between the traffic lanes. The towers are steel with steel anchor attachments.

The bridge deck is a concrete deck with typical thickness of 300 mm supported by longitudinal beams above each truss plane and transverse cross beams every approximate 5 m, every second of who is situated above the truss nodes were a composite connection is established.

Figure 4 View beneath the bridge

2.2 Structural behaviour

The overall length of the bridge requires careful considerations on global behaviour and force transfer for instance creep, shrinkage and temperature effects. The research program concludes that the bridge should be a composite bridge with regards to the timber truss and the concrete deck, and with full force transfer between these elements. The superstructure therefore will be a continuous beam from abutment to abutment. The bridge is fixed at the central pylons and has sliding bearings in side spans. This requires large expansion joints at the abutments.

The vertical forces in the main span are partly transferred through the stays to the central pylons, while the transverse forces are transferred through the bridge beam to the same pylons.

2.2.1 Large scale challenges

The bridge will be the longest timber bridge in the world if build. Hence it has been vital to the project to identify what challenges this introduces. A list of topics has been outlined as follows:

- Detailing of large scale timber connections
- Composite behaviour with concrete (internal force transfer, different material characteristics)
- Production of large scale truss elements
- Deliverance capacity (manufacturing, transportation)
- Durability (large scale effects)

2.2.2 Timber truss connection

The timber connections will be detailed as a for a typical timber truss. The width of the elements means one must take extra care regarding the tolerances for the holes to allow for insertion of the bolts. Because of the height of the elements one must also take into considerations the forces transversal to the fibres in the timber at the joints. Figure 7 shows an elevation, section and perspective of a joint detail between upper chords and diagonals.

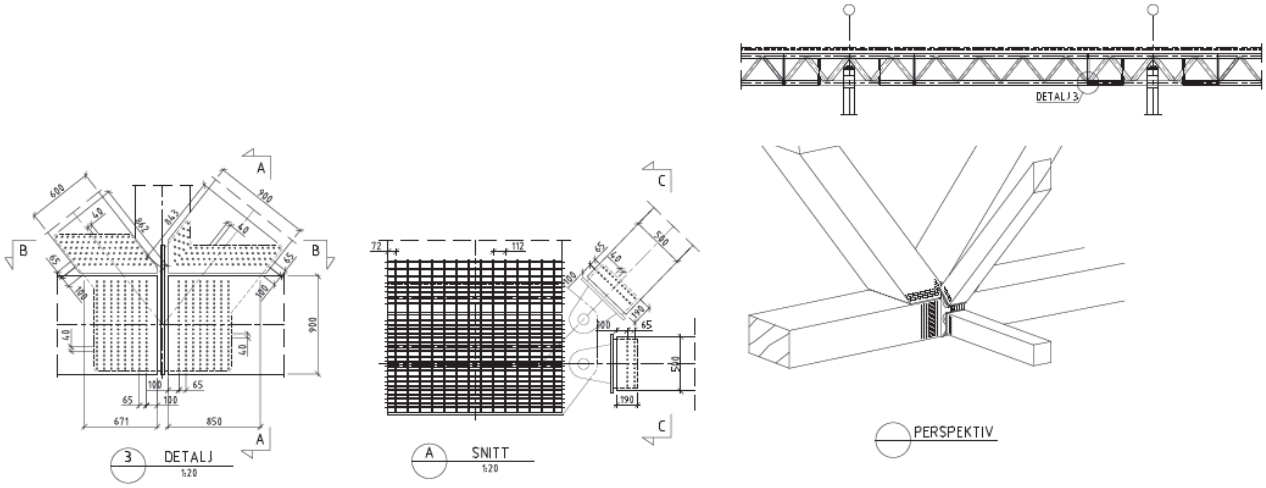

Figure 5 Example of joint detailing of lower chord to diagonals. Elevation, section and perspective.

2.2.3 Composite solution and behaviour with concrete

For the composite connection, different solutions have been tested for small scale projects but for the world's longest timber bridge there was a consensus in the research group that a well-tested system was needed. Therefore, the stud connections typically used for steel concrete composite bridges was chosen. The choice of stud connectors led to a model were the connection between the timber truss and concrete slab is limited to the area around the joints between the upper chords and diagonals. For Mjøsa Bridge a composite connection to the concrete slab is established every 10 m.

In Figure 6 one can see the vertical steel plates used in the joints for the diagonals and the upper chord. On top of the vertical steel plates is welded a horizontal plate with stud connectors. The concrete is cast towards this plate and composite connection is established.

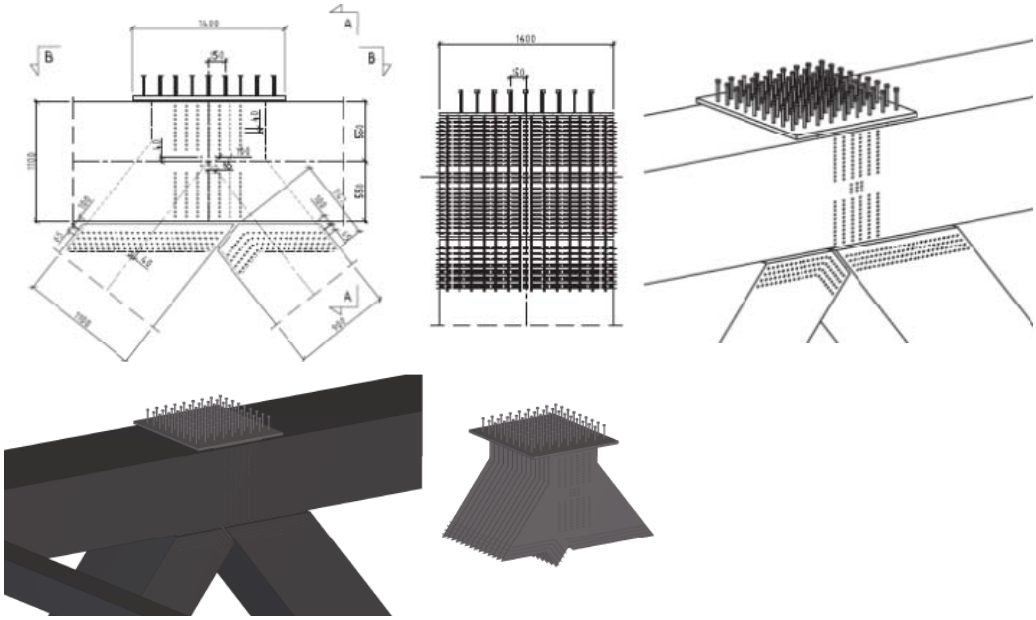

Figure 6 Detail of composite solution. Elevation, section and perspective.

The composite connection increases the capacity of the composite section but also generates the need to transfer horizontal forces from creep, shrinkage and temperature between the two materials that have different properties for these effects. Typically, timber bridges are designed with a coefficient of thermal expansion equal to $5x10^{-6}$. This is however a conservative value for considering the expansion at the joints. For the case of a timber truss composite to a concrete slab a lower bound value for the thermal expansion of timber needs to be considered as this gives the highest forces in the composite connection. A value of the thermal expansion equal to $0.2x10^{-6}$ was

chosen based on measurement performed on an existing timber bridge.

2.2.4 Large scale truss elements

The truss has a total height of 7.3 m with the lower chord having dimensions 1.6m x 0.9 m and the upper chord having dimensions 1.6 m x 1.1 m. The diagonals typically have dimensions 1.6 m x 0.6 m. The width of 1.6 m is chosen because of the height limitations in the impregnation factory of 1.1 m. To get adequate area for the upper chord the width then needs to be 1.6 m. For an effective transfer of forces between the timber elements they all have the same width.

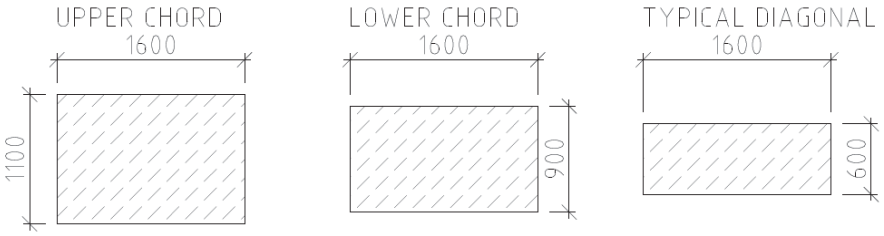

Figure 7 Section of typical truss elements

The production method used for timber elements gives limitations to the height of the elements. The maximum practical width of the elements is limited by the assembly of the elements. A width of 1.6 m is by the research group considered to be acceptable regarding the assembly.

2.3 Deliverance capacity

Building a timber bridge across lake Mjøsa is estimated to take approximately 3 years and 10 months. The amount of timer required is approximately 18 500 m3 of timber which equals to about a year productions of timber on one shift at the local Moelven factory. The current timetable means that the production of the timber truss sections must be completed in approximately two years, if not the production of timber will be on the critical path.

Figure 8 Example of large scale timber truss (Norsenga Bridge)

2.4 Durability

The bridge will be designed for a 100-year life. The project must however make sure this is feasible for such a large-scale project. For normal size bridges, it is more relevant to do repair and rehabilitation on exposed parts of the structure, but with the size of the Mjøsa Bridge it is of vital importance to ensure durability through technical solutions, treatment and planning.

To place the timber trusses beneath the wide concrete deck as proposed will make timber less exposed to sun, temperature differences, rain, salt treatment, etc. The environment should therefore be the best to increase durability. In addition, the experience from the many neighbouring timber bridges will constantly improve the durability, giving the best state of the art design available as a reference.

2.5 Foundation solutions

The suggested Mjøsa Bridge involves 5 deep water foundations with 28 piles ø1220/ø1420, with water depths of approximately 70 m, including a caisson solution for each foundation to reduce the buckling length of the piles. The caisson could be partly build in dry dock and the rest in its final position. The piles are then installed through the caisson that has pre-installed tubes working as guides for the piles.

There are otherwise 16 pile foundations with 15 piles ø1220 mm with depths 10 – 30 m.

2.6 Construction methods

2.6.1 Truss assembly

The assembly of the large-scale truss will involve challenges regarding tolerances of the trusses to be connected. One possible solution is that the truss is assembled in span lengths on shore and afterwards lifted out to its final position as shown in Figure 9. For the assembly of the trusses one will need equipment to rotate and move the truss to be installed about all axis, for the correct positioning of the truss, to allow for insertion of bolts. The total weight of each lift would be approximately 1800 kN.

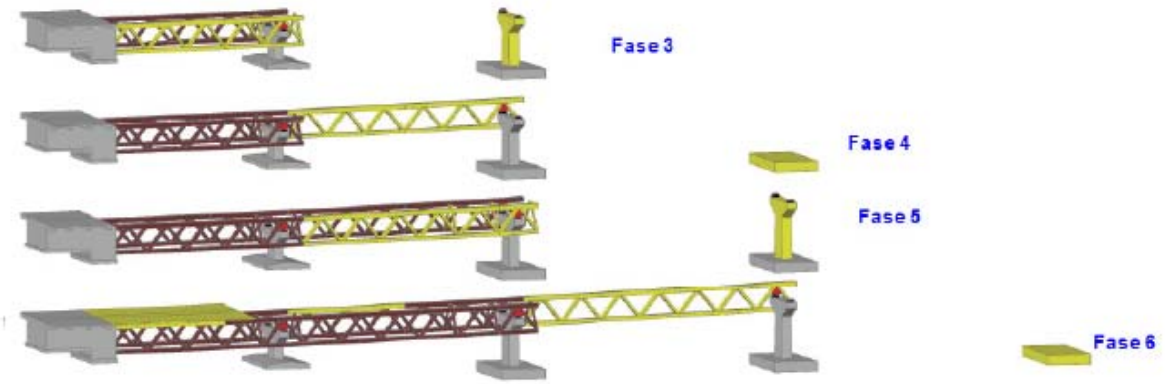

Figure 9 Truss assembly

2.6.2 Concrete deck casting

For the casting of the concrete deck it is likely that a steel composite carriage will be used. Normally this would move on supports c/c 5 m established on the steel flange. For the timber bridge, it is natural to use supports c/c 10 m on the composite joints. Per the producers of steel composite carriage these can be adjusted so that they can work with c/c 10 m.

For the viaduct, the casting will be done in sections. First the mid-spans will be cast and then afterwards the remaining parts above the supports will be cast. For the cable stayed bridge the concrete deck will be cast 5 m at a time.

Figure 10 shows the principle for the casting of the concrete deck, in blue is shown a stiffening of the timber truss for the building period that may be necessary.

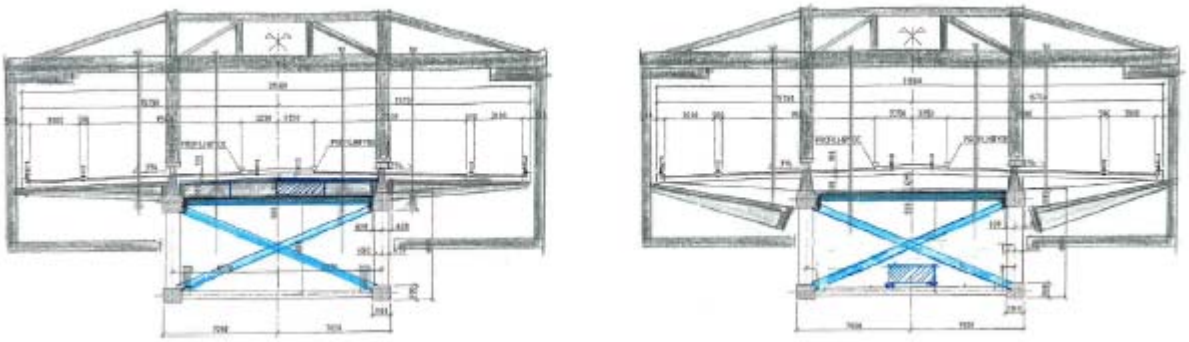

Figure 10 Steel composite carriage on Mjøsa Bridge

2.7 Aesthetics

The idea of the truss timber bridge was developed from the requirement of relatively large spans. This requirement was agreed to be vital both from aesthetical and economic reasons, to avoid costly foundations and to avoid the common barrier look that the long strait crossings with small spans often tend to have.

It was also agreed that the introduction of longer mid spans was beneficial to the overall looks of the bridge. These spans underline the bridge as an icon, and emphasize the proposed ship channel areas.

The final decision was to introduce 5 towers as this also minimizes the number of deep sea foundations.

3. Life cost analysis (LCA)

Two different LCA's both conclude that the timber bridge will give a substantial reduction in the CO2 emissions. Both studies focus on the different choices that can be made for the different materials regarding recycling, low-carbon, CO2-storage in the timber etc. and what impact this has on the total CO2-emissions. For all choices, the studies conclude that a timber bridge gives less CO2-emissions. The timber bridge will save approximately 25 000 tons of CO2 compared to the concrete bridge alternative.

4. Economics

The research program led to the design of a concrete bridge and a timber bridge. Both bridges were detailed to the same level and then the bill of materials were summarized, prized and compared. In general, the superstructure for the timber bridge is more expensive than the superstructure for the concrete bridge alternative and the foundation is cheaper for the timber bridge because of a lighter superstructure. In total the timber bridge alternative is calculated to cost 3,6 % more than the concrete bridge.

5. Further development

5.1 Goals

At an arrangement at Biri, right by current Mjøsa Bridge, the 18. April the project group presented the results of the research program to both local and national politicians. The project was handed over from the Norwegian public road department to Nye Veier AS. Nye Veier is a fully state-owned company operating parallel to the Norwegian public road department. The company's tasks include planning, building, operating and maintaining key main roads. Included in their allocated jobs is E6 along Mjøsa and hence also Mjøsa bridge.

There is great political interest in the project and the political demand to build the bridge in timber is increasing. It is a goal to design and construct this prestige bridge in near future, making it an iconic symbol for both the region and the country. To make it into the largest timber bridge ever built would in addition be a valuable achievement for the whole industry.

6. Conclusions

The conclusion of the research program of the 2nd Mjøsa Bridge is that a timber truss alternative is economically, technically and aesthetically competitive. With regards to CO2-emissions the timber bridge alternative give a substantial saving compared to a concrete alternative.

The timber bridge is the recommended solution based on the bridge aesthetics and its impact as a landmark.

7. Acknowledgements

Acknowledgements must be given to the rest of the members of the research program for Mjøsa Bridge:

Widar Mikkelsen	-	Norwegian Public Roads Administration
Harald R. Thoresen	–	Innovation Norway
Åge Holmestad	–	Director of Moelven Glulam AS
Tormod Dyken	–	Dyken AS

8. References

[1] Statens vegvesen: “Kommunedelplan. E6 Gardermoen-Biri. Parsell Moelv-Biri. Ringsaker og Gjøvik kommune. Konstruksjonsrapport”. B003 (Aas-Jakobsen), ver. 14.06.2013.

[2] Paper “A timber bridge across Lake Mjøsa in Norway”. Presented on the 2nd International conference on Timber bridges in 2013, Las Vegas.

Comparison of network patterns suitable for timber bridges with crossbeams

Anna Weronika OSTRYCHARCZYK
MSc, PhD Candidate
Norwegian University of Science and Technology (NTNU)
Trondheim, Norway
anna.w.ostrycharczyk@ntnu.no

Anna Weronika Ostrycharczyk is working in the field of timber structures. Current research topic is related to structural performance of network arch timber bridges.

Kjell Arne MALO
Professor, Dr. ing
Norwegian University of Science and Technology (NTNU)
Trondheim, Norway
kjell.malo@ntnu.no

Kjell Arne Malo is professor of timber structures at NTNU. His research topics are methods for increased strength and stiffness of connections for timber structures and vibrations in timber structures.

Summary

This article presents a comparison of different types of network patterns with evenly spaced hanger pairs on the deck level, which is suitable for timber bridges with transversal crossbeams. Bending moments in the arch and the number of relaxed hangers, obtained for skew loading, have been the comparative criteria. The numerical parametric studies focus of three pattern types, two arch shapes and six different arch rises. In conclusion, values of geometric parameters are suggested in order to achieve optimal structural performance of bridges with network hanger patterns.

Keywords: timber, network arch, network pattern, circular arch, parabolic arch

1. Introduction

Network arch bridge concepts are well known among bridge engineers. The concept was defined by the Norwegian engineer Per Tveit. The basic assumption for the network arch is that the hangers are crossing each other multiple times [1]. When this assumption is combined with fine-tuned hanger arrangement, it is possible to achieve approximately uniform distribution of forces in the structure, especially for bending moments in the arch and axial forces in the hangers. It can result in better material utilization and thus material savings. This is considered to be the main advantage of network arches.

In the literature, many hanger arrangements are defined [2-4]. Not all of those patterns belong entirely to the network group. The most common patterns are: vertical hangers [5], fan arrangement [5], radial network pattern [6], network pattern with constant inclination of hangers [3] or with constant change of hangers inclination [3].

In [7] Teich compared four network patterns to a pattern with vertical hangers, in terms of i.a. arch utilization related to axial forces, bending moments or both. Moreover, necessary amount of steel weight of the arch was also presented. It was shown that arch with vertical hangers required almost double amount of steel in comparison to arches with network patterns.

In the other article [3], Teich presented parametric studies of five different network patterns, with varying parameters like number of hangers, bridge span, arch rise or hangers inclination. The main comparative criteria were related to stress values in hangers.

Schanack [6] compared bending moment distributions in upper and lower chords of network bowstring arches with different hanger arrangements with radial patterns as well as patterns with vertical hangers.

De Zotti et al. [8] compared structural performance of arches with vertical hangers, network and fan patterns for different arch to span ratios. The same set of patterns as in [8] was considered by Pellegrino et al. [5]. The main comparative criteria were related to stress values in hangers. In the paper, individually arranged outline of hangers located close to supports were tested and compared.

The vast majority of the patterns from the described studies share a common feature, namely hanger attachment points are evenly distributed along the arch; the distribution along the deck is hence likely to be uneven. Such distributions are suitable for network bridges made of steel or concrete, i.e. hanger attachment on the deck level can be located anywhere on edge beams of the deck.

In this paper however, the network concept is adapted to the timber bridges with light timber deck supported by transversal crossbeams. It is assumed that hangers are attached to the crossbeams. Consequently, the hangers should be evenly distributed along the deck. Although all the previously published papers studied different patterns in detail, the results are most useful for outlines with even distribution of hangers on the arch. This publication attempts to extend the results for outlines suitable for timber bridges with crossbeams.

The present study focuses on comparison of three network patterns adapted for even distribution of hangers along the deck. The comparison is performed for two types of arch shapes and six different arch rises.

2. Methodology

2.1 Analysed patterns

In the paper three types of network patterns are discussed: radial, pattern with constant inclination of hangers (CIH) and pattern with constant change of hanger inclination (CCI).

The radial pattern [6] is characterised by a constant angle between arch radius and hanger. The pattern was developed by Brunn and Schanack [9] as a result of parametric studies performed on the 100 m long steel bridge with concrete deck. Fig.1a shows the outline of the radial pattern. In this specific instance hangers are equally distributed along the arch. Fig. 1b presents corresponding pattern with uniform distribution of hangers on the deck level.

The tested range of angles α for the radial pattern spreads from $0°$ to $70°$ with steps of $1°$. It should be highlighted that patterns with angle α above a certain value depending on the arch rise, bridge span and number of hangers, can be classifies as a network pattern. Moreover, the pattern where $\alpha = 0°$ is denoted a fan arrangement [5].

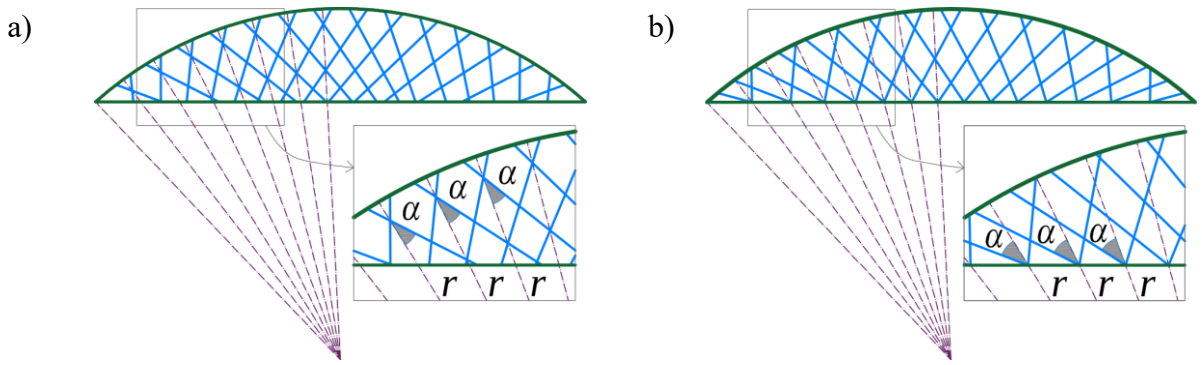

Fig. 1 Radial pattern with hangers equally distributed along the arch (a); along the deck (b)

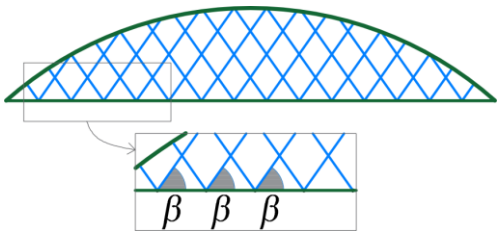

Fig. 2 Pattern with constant inclination of hangers (CIH)

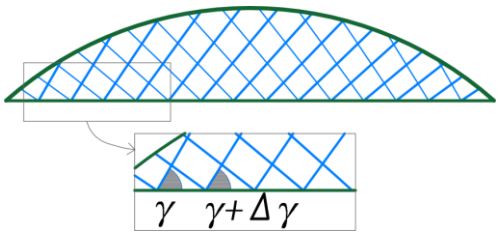

Fig. 3 Pattern with constant change of hangers inclination (CCI)

In the pattern with constant inclination of hangers (CIH), as the name suggests, the angle between the deck and each hanger is constant for the whole pattern, see Fig. 2. This pattern, with the hangers evenly distributed along the deck, is known also as a rhombic pattern [10].

In the numerical study presented herein, the angle β is in range from $30°$ to $90°$ with steps of $2.5°$. When $\beta = 90°$, it becomes a special case with vertical hangers.

The third analysed pattern is a variation of the previous pattern. This pattern is often denoted pattern with constant change of hanger inclination (CCI). Here, the angle between the deck and the hanger changes its value incrementally for each consecutive hanger. The increment is constant. Two parameters are needed to unambiguously describe the pattern: a starting angle γ and an angle change $\Delta\gamma$. Depending on the desired geometrical effect, the angle change can be both positive and negative. An example of CIH pattern is depicted in Fig. 3.

The tested range of starting angle γ spreads from $45°$ to $90°$ with steps of $5°$ while the angle change $\Delta\gamma$ is from $0°$ to $4.5°$ with steps $0.5°$. For some combinations of γ and $\Delta\gamma$ certain patterns cannot be constructed, so they were excluded from the analysis.

2.2 Numerical model

A parametric numerical model was created to study the patterns and to compare them. The model is two-dimensional and consists of beam elements in arch and deck, and truss elements in hangers. In the model, the hangers are of steel and can only carry tensile forces, as in the material properties the elastic modulus is zero, for negative strains. Both the arch and the deck are made of glulam GL30c and GL24c, respectively [11]. The arch cross-section is 1000 x 600 mm, while the deck is 3000 x 500 mm. The deck width corresponds to the width of one notional car-lane, according to EN1-2 [12]. The density of timber associated to the deck takes into account the presence of 18 steel crossbeams and an asphalt layer of 120 mm. Moreover, pinned boundary conditions are applied both to the arch and the deck.

In this paper all comparisons are made with bridge length $l = 100$ m and number of crossbeams $n = 18$. Other parameters, like an arch rise f and angles are varied. In the study, six arch rises are considered, i.e. $f = (11,14,17,20,23,26)$ expressed in meters. For a 100 m bridge span, $f = 11$ m (14 m) constitutes 11% (14%) of the deck length and represents a shallow arch. Accordingly, $f = (17,20)$ refers to medium arch rises and $f = (23,26)$ refers to high-rise arches. The values of the considered angles α, β and γ are given in Section 2.1. For an instance given by f and l, it is possible to construct only one particular circle or one particular parabola that will constitute the arch. Both shapes are considered and compared.

All analyses have been performed with Abaqus software [13] with implicit procedure allowing nonlinear analysis. Abaqus software was extended with Python [14] scripting, in order to create pattern outlines automatically.

2.3 Comparison criteria

One of the advantages of network arches is a possibility to achieve uniformly distributed bending moments along the arch. Bending moment is sensitive to skew loading, and therefore different skew load cases are considered in the numerical studies. The loading was applied on the deck structure in 11 steps, leading to 11 load cases. Starting from left, the loaded part of the deck was increased by 10% of the deck length in each step. The first step includes only the self-weight, while the last step represents uniformly loaded deck.

For different network patterns with the same arch rise, the values of axial forces are similar (they only differ by approximately 5%). Therefore, the main comparative criterion takes into account solely bending moments. For a given pattern, the absolute maximum bending moment along the arch M is obtained for the most unfavourable load case. The value M for each hanger outline is then used to compare the structural performance of the network arch layouts.

The arch utilization is usually the governing design criterion. However, in the considered patterns, analysis of the bending moments and the utilization function leads to similar conclusions. In Fig. 4 an example of maximum bending moment M and utilization U for a range of patterns is presented. The utilization U is calculated as combination of the bending moment and an axial force, according to EN5-1-1 [15]. Both functions reach minimum for similar geometric feature of the pattern, i.e. angle. Moreover, the same behaviour can be observed for all types of tested patterns.

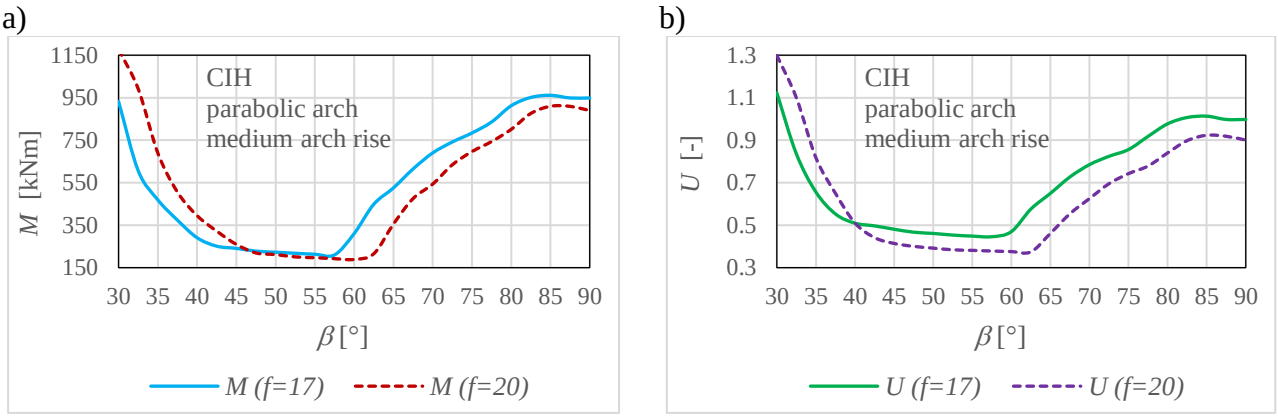

Fig. 4 Maximum bending moment M (a) and arch utilization U (b) as a function of angle β, for patterns with constant inclination of hangers(CIH), n=18 and arch rise f=17m and f=20m

A secondary comparative criterion is the maximum percentage of relaxed hangers, H, chosen from all load cases. It might be an important design characteristic since, as opposed to a heavy concrete deck, the self-weight of a light timber deck is insufficient for adequate hanger prestressing.

3. Results

For each studied pattern type two comparative criteria are presented in a single figure. In each figure, the left-hand-side vertical axis corresponds to the bending moment value, while the right-hand side vertical axis refers to the percentage of relaxed hangers. The horizontal axis, depending on tested pattern type, refers to angle α, β or γ and $\Delta\gamma$.

In most figures, the results for two arch rises are presented simultaneously. The bending moment is marked as solid or dotted line, while open dots and plus symbols mark the percentage of relaxed hangers.

3.1 Radial pattern

The results for the radial pattern are presented in Fig. 5 and Fig. 6. Only the medium arch rises are chosen for visualisation, since the results for all tested arch rises have common characteristic. The critical values for all arch rises and pattern types are gathered in Tab.1 in Section 3.4.

The function of bending moment to angle α, presented in Fig. 5, is decreasing for increasing α, until function starts to rise with fluctuations. The function of percentage of relaxed hangers is constantly decreasing with increasing angle. The highest M and lowest H is achieved for $\alpha = 0°$, i.e. the fan arrangement of hangers.

For the radial pattern, the most promising angle is corresponding to the lowest value of M. In Fig. 5a this angle is $\alpha \approx 45°$. For such angle, the number of relaxed hangers is around 10% what is an acceptable value. It can be noticed that for angles $\alpha \geq 55°$, values of H reach zero, which is of course desired. However for such inclination some hangers are located almost horizontally, which should be avoided.

Comparing the results for circular and parabolic shape of the arch, the latter reaches slightly higher values of M and H. The results have the same characteristic, but are shifted up and right.

The results presented in Fig. 5 refer to the model of 100 m long bridge with 18 transversal crossbeams, while the results presented in Fig. 6 refer to a similar bridge with 24 transversal crossbeams. By comparing both figures, it can be concluded that number of crossbeams does not change the characteristics of the results. Only the negligible changes of M and H values, are direct consequences of a change of the number of hangers.

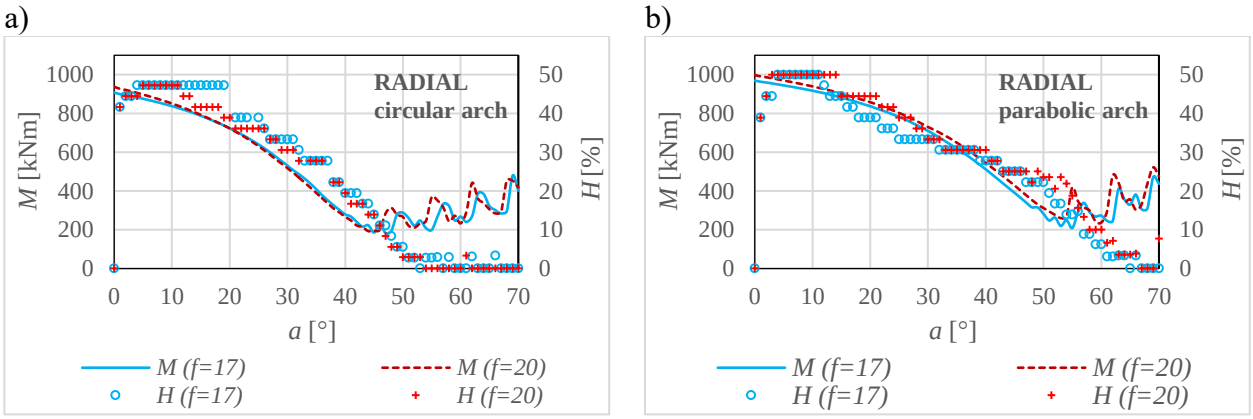

Fig. 5 Bending moment and percentage of relaxed hangers for medium arch raises and arch shape as circle (a); parabola (b). Number of crossbeams n=18. Radial pattern.

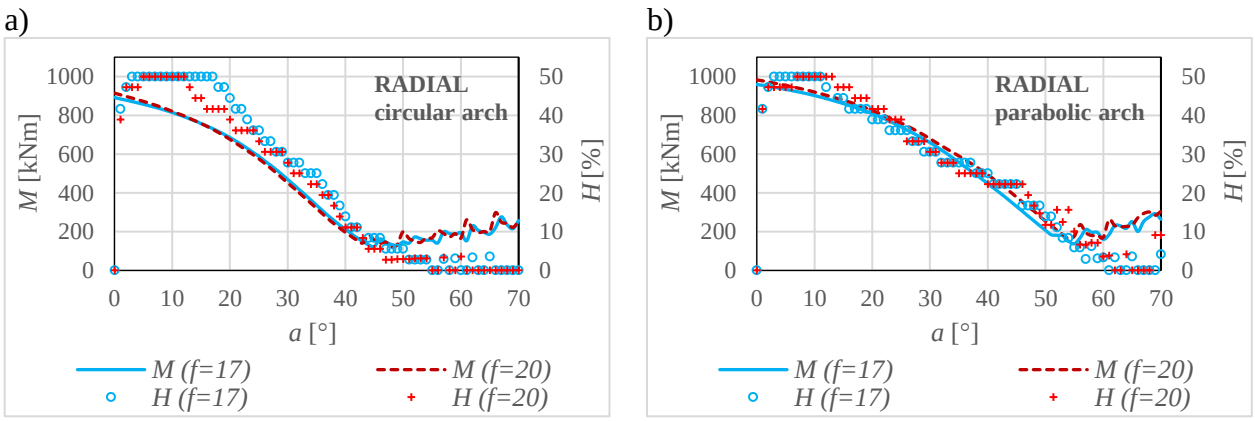

Fig. 6 Bending moment and percentage of relaxed hangers for medium arch raises and arch shape as circle (a); parabola (b). Number of crossbeams n=24. Radial pattern.

3.2 Pattern with constant inclination of hangers

The results related to the pattern with constant inclination of hangers for medium arch rises are depicted in Fig. 7. The function of the bending moments has similar characteristics for both arch shapes. Clearly it has an optimal range of β around $40° - 50°$.

The functions of hanger relaxation H for both arch shapes also have similarities. The graph shows, approximately, independence of β for small values, but for $\beta > 45°$ a steady increase of H takes place for increasing β.

The outline with angle $\beta \approx 50°$ seems to be most promising, regardless the arch shape. It is worth to notice that for parabolic shape the pseudo optimal range of angles is wider than for circular shape and spreads from $\beta \approx 40°$ to $\beta \approx 60°$.

Note that the highest values of M and the lowest value of H are for $\beta = 90°$, thus for a pattern with vertical hangers. Such pattern often constitutes the basic pattern for comparison of network patterns to show a scale of improvement from inclined hangers.

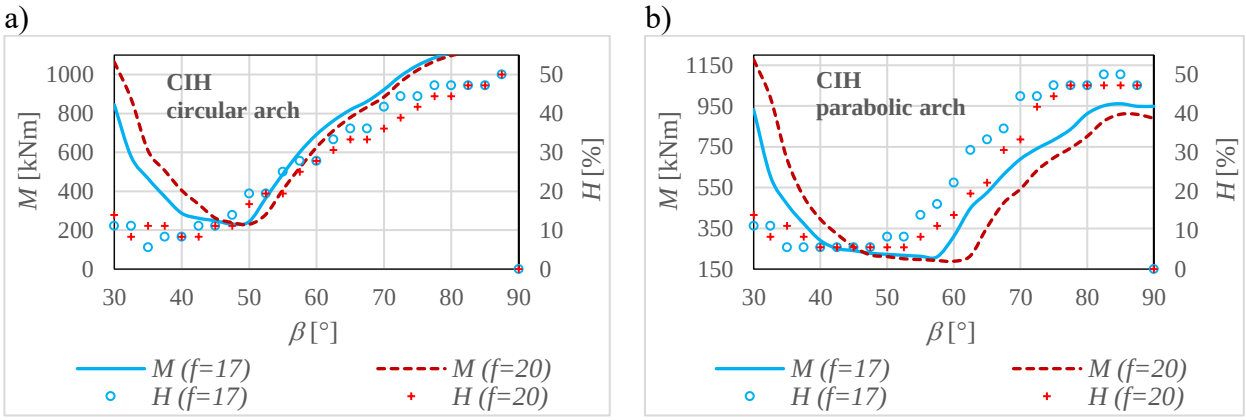

Fig. 7 Bending moment and percentage of relaxed hangers for medium arch raises and arch shape as circle (a); parabola (b). Number of crossbeams n=18. Pattern with constant inclination of hangers (CIH).

3.3 Pattern with constant change of hangers inclination

In this section the pattern with constant change of hangers inclination is taken under consideration. In Fig. 8 the bending moment and the percentage of relaxed hangers are shown as a function of the starting angle γ and angle change $\Delta\gamma$. The arch rise is 17 m and arch shape is circular. In Fig. 9 similar results are presented for parabolic arch shape. Further results have been obtained for other arch rises, thus Fig. 8 and Fig. 9 are only shown as examples.

The lowest values of M can be obtained for various combinations of γ and $\Delta\gamma$. In general, the higher the starting angle, the bigger angle change shall be used. It applies to both arch shapes.

The percentage of relaxed hangers is low for starting angle $\gamma = 45°$ for any angle change $\Delta\gamma$. For the circular arch shape, H increases with increasing γ, and is larger for small changes $\Delta\gamma$. For the parabolic shape, H remains low for $\gamma \leq 60°$ and increases drastically with an increase of γ, regardless of $\Delta\gamma$.

On the plots in Fig. 8 and Fig. 9, zero values of M or H correspond to pattern outlines which cannot be geometrically constructed.

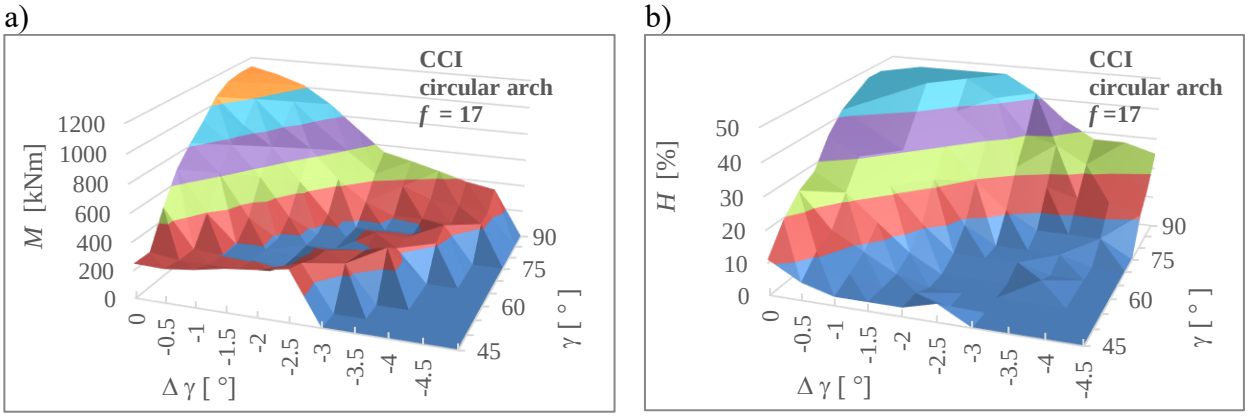

Fig. 8 Bending moment (a) and percentage of relaxed hangers (b) in circular arch with $f = 17$ and $n = 18$. *Pattern with constant change of hanger inclination.*

a)

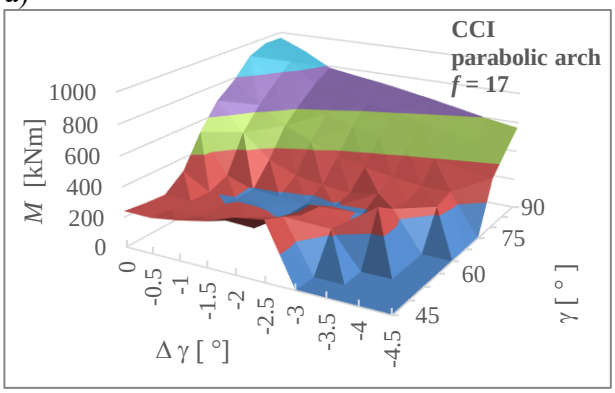

b)

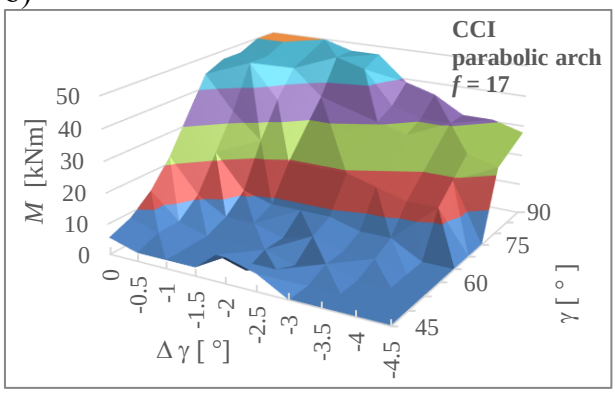

Fig. 9 Bending moment (a) and percentage of relaxed hangers (b) in parabolic arch with $f = 17$ and $n = 18$. *Pattern with constant change of hanger inclination.*

3.4 Collected results

The most promising outlines are those with the lowest value of M and possibly the lowest value of H. The lowest values of the bending moment for all tested arch rises f, two arch shapes, and three pattern types are collected in Tab. 1. Percentages of relaxed hangers, corresponding to M values from Tab.1, are given in Tab. 2.

Table 1 Lowest given bending moment in the arch for different arch rises, shape of the arch, and type of the pattern

Arch rise	Lowest bending moment on the arch M [kNm]					
	radial		constant inclination of hangers (CIH)		constant change of inclination (CCI)	
f	circular	parabolic	circular	parabolic	circular	parabolic
11	185	209	328	327	195	224
14	176	209	261	250	183	199
17	183	208	231	210	163	172
20	193	237	230	189	153	173
23	209	256	239	175	146	158
26	223	316	281	165	156	152

* the lowest values for particular arch rise is highlighted in grey

Table 2 Percentage of relaxed hangers corresponding to lowest M in the arch, for different arch rises, shape of the arch, and type of the pattern

Arch rise	H [%] corresponding to M from Tab. 1					
	radial		constant inclination of hangers (CIH)		constant change of inclination (CCI)	
f	circular	parabolic	circular	parabolic	circular	parabolic
11	6	11	19	17	8	3
14	8	11	14	17	3	3
17	11	14	14	17	3	8
20	14	10	17	14	3	3
23	3	18	14	14	6	3
26	0	23	17	11	8	3

In Tab. 1, for each arch rise the lowest value of M is highlighted in grey. It can be noticed that for shallow arches radial pattern strikes as best, while for medium and high arch rises it is the pattern with constant change of hangers inclination. In addition, for radial and CCI patterns, the circular arch shape is more beneficial. The parabolic arch shape is better for CIH.

The percentage of relaxed hangers corresponding to *M*-results from Tab. 1, is smallest for CCI patterns, while it is the highest for CIH pattern and varies for circular and parabolic arch shape.

4. Conclusions

In the literature related to network patterns, most studies are focused on patterns with equal distribution of hangers along the arch. It results from technological solutions used in steel and concrete bridges. For timber bridges, equal distribution of hangers along the deck is desired. Therefore in this paper, three types of network patterns with hangers spread uniformly along the deck are compared. Circular and parabolic arch shape as well as six different arch rises are taken into account.

The present study, based on numerical analyses of more than 2000 pattern outlines, shows that, depending on arch rise, different pattern types are most efficient. For shallow arches the radial pattern appears to be slightly better than the others, while for medium and high-rise arches, pattern with constant change of hangers inclination is preferable. Moreover, for these patterns circular arch shape is recommended. On the other hand, for pattern with constant inclination of hangers, parabolic arch shape yields better results.

The recommended angle range for radial pattern and circular arch shape spreads from $\alpha = 45°$ to $\alpha = 55°$ for shallow arches, and from $\alpha = 40°$ to $\alpha = 50°$ for medium and high-rise arches. Recommended angle range for parabolic arch shape is from $\alpha = 45°$ to $\alpha = 60°$ for all arch rises.

For hangers with constant inclination (CIH), and for both arch shapes, best performance is obtained for the range between $\beta = 35°$ and $\beta = 45°$ for shallow arches, between $\beta = 40°$ and $\beta = 50°$ for medium arches and between $\beta = 45°$ and $\beta = 55°$ for high-rise arches.

For the last pattern, CCI, and circular arch shape, the suggested starting angle spreads from $\gamma = 50°$ to $\gamma = 65°$ for shallow arches, from $\gamma = 60°$ to $\gamma = 80°$ for medium arches and from $\gamma = 65°$ to $\gamma = 85°$ for high-rise arches. Suggested angle change spreads from $\Delta\gamma = -1.5°$ to $\Delta\gamma = -3.0°$ for all arch rises. For parabolic arch shape, the suggested starting angle spreads from $\gamma = 50°$ to $\gamma = 60°$ for shallow arches, and from $\gamma = 60°$ to $\gamma = 70°$ for medium and high-rise arches. The recommended angle change is from $\Delta\gamma = -1.5°$ to $\Delta\gamma = -3.0°$, and from $\Delta\gamma = -1.0°$ to $\Delta\gamma = -3.0°$, and from $\Delta\gamma = -0.5°$ to $\Delta\gamma = -2.5°$ for shallow, medium and high arch rises respectively.

The percentage of relaxed hangers corresponding to the best outlines is acceptably low, however some relaxation of hangers always takes place. Patterns without hanger relaxation, according to criterion *H*, have higher values of bending moments, and often hangers become located almost horizontally. Such location of hangers results in high value of stress range in the pattern and therefore should be avoided.

5. Acknowledgements

This work has been made possible by a project grant received from The Research Council of Norway (208052) and financial and technical support from The Association of Norwegian Glulam Producers, Skogtiltaksfondet and Norwegian Public Road Authorities. These contributions are gratefully acknowledged. This work was also supported by the WoodWisdom-Net+ project DuraTB ("Durable Timber Bridges") and the support from the partners is appreciated.

6. References

1. Tveit P., *The design of network arches.* The Structural Engineer, 1966. **44**(7): p. 249-259.
2. Pipinato A., *Innovative Bridge Design Handbook: Construction, Rehabilitation and Maintenance*. 2016: Elsevier Science.
3. Teich S., *Entwicklung allgemeiner Entwurfsgrundsätze für Hängernetze von Netzwerkbogenbrücken, (Development of general design principles for the hanger arrangements of network arch bridges).* Stahlbau, 2011. **80**(2): p. 100-111.

4. Schanack F., *Puentes en Arco Tipo Network, (Network Arch Bridges). Doctoral Thesis*. 2008, Department of Structural Engineering and Mechanics, Technical College of Road, Channel and Port Engineering, University of Cantabria, Spain.
5. Pellegrino C., G. Cupani, and C. Modena, *The effect of fatigue on the arrangement of hangers in tied arch bridges.* Engineering Structures, 2010. **32**(4): p. 1140-1147.
6. Schanack F. and B. Brunn, *Analysis of the structural performance of network arch bridges.* Indian Concrete Journal, 2009. **83**(1): p. 7-13.
7. Teich S., *Die Netzwerkbogenbrücke, ein überaus effizientes Brückentragwerk - Tragwirkung und Konstruktion, (The network arch bridge, an extremely efficient structure - Structural behaviour and construction).* Stahlbau, 2005. **74**(8): p. 596-605.
8. De Zotti A., C. Pellegrino, and C. Modena. *A parametric study of the hanger arrangement in arch bridges*. in *5th international conference on arch bridges ARCH '07*. 2007.
9. Brunn B. and F. Schanack, *Calculation of a double track railway network arch bridge applying the european standards. Graduation thesis*. 2003, Dresden University of Technology.
10. Schanack F. and B. Brunn, *Netzgenerierung von Netzwerkbogenbrücken, (Generation of network arch hanger arrangements).* Stahlbau, 2009. **78**(7): p. 477-483.
11. CEN, *EN 14080: Timber structures - Glued laminated timber and glued solid timber - Requirements*. 2013: Brussels, Belgium.
12. CEN, *EN 1991-2: Eurocode 1: Actions on structures -Part 2: Traffic loads on bridges*, in 2003: Brussels, Belgium.
13. Hibbit K., Sorensen, *ABAQUS/Standard Analysis User's Manual* 2007.
14. *Python Software Foundation*. https://www.python.org/.
15. CEN, *EN 1995-1-1: Eurocode 5: Design of timber structures -Part 1-1: General - Common rules and rules for buildings*, in 2004: Brussels, Belgium.

Effect of Nordic climate on cupping of stress laminated timber decks

Stefania Fortino
Senior Scientist
VTT
Espoo, Finland

Senior Scientist at VTT technical Research Centre of Finland Ltd, PhD in computational mechanics. Main expertise in hygro-thermo-mechanical analysis of wood-based products and biomaterials. Management of WW-Net projects and participation in Cost actions related to timber structures.

Giovanni Metelli
Professor
University of Brescia
Brescia, Italy

Assistant professor at University of Brescia in Structural Design teaches Design of Steel and Timber Structures. Main research topics: behaviour of steel braced frames, bond of reinforcements in concrete and the design criteria of timber structures in seismic areas.

Petr Hradil, Senior Scientist,
VTT, Espoo, Finland

Federico Ossoli, MSc student,
University of Brescia, Italy

Anna Pousette, Scientist
SP Wood Building Technology, Skellefteå, Sweden

Tomi Toratti, Senior Advisor,
Federation of the Finnish Woodworking Industries, Helsinki, Finland

Summary

In this paper a numerical method based on a single-Fickian moisture diffusion model coupled with an orthotropic-viscoelastic-mechanosorptive model for wood, previously developed by some of the authors, is used to study the effect of moisture content on stress laminated timber decks (SLTDs) of bridges under different Northern climates. In particular, SLTD specimens tested during the earlier Nordic Timber Bridge project and the deck of Umeå bridge in Sweden are analysed. The results obtained by moisture-stress analyses carried out by Abaqus FEM code show the capabilities of the numerical approach to predict cupping and losses of bar forces in these structures. The proposed method can be useful to improve the performance control and the maintenance of the SLTDs during their service life.

Keywords: timber bridges, SLTD, moisture content, mechanosorptive creep, cupping, FEM

1. Introduction

Stress–laminated timber decks (SLTDs) of bridges are widely used in Northern European countries [1]. The monitoring of timber bridges exposed to natural climate fluctuations is important to predict their long-term performance in terms of durability, serviceability and safety. As shown in earlier research, numerical hygro–thermal methods are useful, alongside with sensor techniques, for monitoring the moisture content (*MC*) in timber bridge elements [2]. Previous numerical studies based on the finite element method (FEM) have shown that the yearly variations of relative humidity (*RH*) in Northern Europe (average values over 80%), cause higher moisture gradients compared to the Southern Europe variations of *RH* in structures sheltered from rain and sun (see references in [3]). In addition, the differences in shrinkage and swelling due to moisture gradients generate the moisture induced stresses (*MIS*) that can cause the onset of cracks and their propagation in wooden elements. Numerical analyses carried out within the WoodWisdom–Net+ project Durable Timber Bridges (2014-2017) revealed high moisture gradients and *MIS* also in sheltered glulam beams of poorly coated timber bridges [4]. Nowadays the protection of timber bridges is a challenging topic since the high protective but toxic creosote is expected to be banned in the future. Measurements taken on stress-laminated timber specimens within the Nordic Timber Bridge project [1] and, more recently, *in-situ* measurements carried out by Pousette and Fjellström within Durable Timber Bridges project [5], revealed cupping phenomena in SLTDs of bridges. Losses of bar forces varying during wetting and drying seasonal periods were also measured during the Nordic Timber Bridges project.

From the material point of view, in the literature it is widely proved that rheological behaviour of wood as well as its mechanosorptive creep in timber elements can cause large deflections in service conditions, even in indoor environment (see [6] and references in [3]). The phenomenon of cupping in stress laminated timber decks refers to the curvature of the cross section of a timber deck, originated from the difference in moisture content between the upper surface and lower surface of the structure. Due to the environmental conditions and mainly to the moisture effects, the bottom surface tends to swell increasing the risk of fractures and water infiltration, and consequently decreasing the useful life of the bridge. Moreover, cupping generates a vertical deformation of the deck edges causing a visible uplift in the deck structure of the bridge with respect to the end supports. This may cause damage to the asphalt paving and expansion joint at the bridge end entailing a risk of water infiltration. Several examples of cupping phenomena in Swedish bridges can be found in [5].

The structural integrity and serviceability of stress-laminated decks depends on the compressive stress maintained among the wooden laminations [7]. In order to distribute the dead and live loads among the parallel laminations, this compression must be sufficient to prevent vertical slip because of transverse shear and bending actions acting between the laminations. This initial compressive stress is applied by assuming that 40 to 60% of the initial stress will be lost over the life of the structure because of wood stress relaxation and changes in wood moisture content. Some studies have shown the phenomenon of the slip between the laminations due to the reduction of the interlaminar compression [8-9].

The numerical method proposed in this work has been used to calculate the moisture induced cupping in stress laminated timber decks. The models allow also the bar force losses to be evaluated during time. However, in this work the computational models do not take into account the slip between laminations.

2. Moisture-stress analysis for timber members

2.1 Single-Fickian method for moisture transport in wood

According to [3], the so-called single-Fickian theory of moisture transport in wood is based on the three dimensional Fick equation:

$$\frac{\partial MC}{\partial t} = \nabla \cdot (\mathbf{D} \nabla MC) \tag{1}$$

where *MC* is the moisture content of wood and D the diffusion tensor of moisture transfer. This form of the Fick equation can be used when the density of wood (ρ) is constant. For varying density, the variable concentration $c = \rho MC$ instead of *MC* should be considered (where *c* represents the concentration in kg/m^3). In the literature the assumption of isotropic diffusion is usually made and only the diagonal coefficients of the corresponding matrix are considered to be nonzero. The moisture flow through the surface is given by the following equation:

$$q_n = rS(MC_{air} - MC_{surf}) \tag{2}$$

where q_n is the value of the flow across the boundary, ρ represents the wood density in absolute dry conditions, *S* is the surface emissivity (that can take into account also eventual protective coatings), MC_{surf} is the moisture content on the wood surface and MC_{air}, also known as sorption isotherm, represents the equilibrium moisture content of wood corresponding to the air humidity. The expression for the sorption isotherm used in [3] is:

$$MC_{air} = 0.01\left(\frac{-T\ln(1-RH)}{0.13(1-T/647.1)^{-6.46}}\right)^{\frac{1}{110T^{-0.75}}} \tag{3}$$

where *T* is the temperature of the air and *RH* the relative humidity of the air. Expressions for surface emission parameters are provided in [3] while the diffusion values proposed by Nilsson [10] are used. Very recently the described model has been further developed in [11] to analyse also cases of *MC* above the fibre saturation point by using a coupled diffusion-permeability approach.

2.2 Orthotropic-viscoelastic-mechanosorptive model for wood and moisture-stress analysis

The calculation of moisture induced stresses (*MIS*) is based on three-dimensional orthotropic-viscoelastic-mechanosorptive material model used in [3] and developed in earlier works by Fortino and Toratti (see references in [3]). The model is composed of five deformation mechanisms in series which provide a decomposition of strain into elastic response, hygroexpansion, viscoelastic creep, recoverable mechanosorption and mechanosorptive irrecoverable creep. Both the viscoelastic and the mechanosorptive recoverable creep are described through Kelvin type elements. In particular, the elastic strain of the model is defined as

$$\boldsymbol{\varepsilon}^{e} = \boldsymbol{\varepsilon} - \boldsymbol{\varepsilon}^{u} - \sum_{i=1}^{p} \boldsymbol{\varepsilon}_i^{ve} - \sum_{j=1}^{q} \boldsymbol{\varepsilon}_j^{ms} - \boldsymbol{\varepsilon}^{ms,irr} \tag{4}$$

being $\boldsymbol{\varepsilon}$ the total strain, $\boldsymbol{\varepsilon}^{u}$ the hygroexpansion strain, $\boldsymbol{\varepsilon}_i^{ve}$ and $\boldsymbol{\varepsilon}_j^{ms}$ the viscoelastic and mechanosorptive elemental creep strain and $\boldsymbol{\varepsilon}^{ms,irr}$ the irrecoverable mechanosorptive strain tensor. The elastic moduli of the model are expressed as functions of density, temperature and *MC*.

The surface moisture flux described in the previous section is implemented in subroutine Dflux of Abaqus code while the constitutive model is implemented in subroutine UMAT of Abaqus code [3]. Because of the analogy between the moisture diffusion and the heat transfer analysis, the moisture-stress analysis for wood is performed by using the available temperature-displacement analysis of Abaqus Standard. An algorithm allows the calculation of moisture-induced stresses. The elastic properties used for the moisture-stress analysis, adopted for Norway spruce material in earlier research, are listed in Table 1.

Table 1: Elastic properties used for the moisture-stress analysis.

E_R (MPa)	E_T (MPa)	E_L (MPa)	G_{RT} (MPa)	G_{RL} (MPa)	G_{TL} (MPa)	ν_{RT} (-)	ν_{RL} (-)	ν_{TL} (-)
600	600	12000	40	700	700	0.558	0.038	0.015

3. Numerical evaluation of cupping and bar force losses

The single-Fickian approach for moisture transport described in the previous sections, coupled with the three-dimensional orthotropic-viscoelastic-mechanosorptive model for wood, has been used in the present work to calculate the moisture induced cupping in SLTDs as well as the bar force losses during time.

3.1 FEM analysis of deck specimens tested within the Nordic Timber Bridge project

The purpose of the Nordic Timber Bridge project [1] was to study the influence of different climates on stress-laminated timber deck plates in the Nordic countries. Test specimens were placed outdoor (in contact with the external environmental conditions) in Skellefteå, Oslo, Copenhagen and Helsinki. For each test specimen measurements of moisture content, forces in the pre-stressed bars and cupping/uplift of wood deck were measured monthly, from 1.5.1995 to 1.8.1996.

Four timber deck specimens were manufactured at Trätek in Skellefteå. They had a length of 2.94 m, width of 0.8 m, a height of 0.36 m and were made of laminations of glulam beams, of dimensions 140 × 360 × 800 mm and strength class L40. Each lamella had dimensions 140 × 45 × 800 mm (eight lamellas per each glulam beam). The glulam beams were stressed together with two steel bars Dywidag 15.1 mm anchored with steel plates (200 × 200 × 43.25 mm) with a force of 144 kN, which generates a transverse compressive stress of 1.0 MPa between laminations. An insulating bitumen mat was put on top of the deck plate and down on the edges. On the top there was also a 25 mm thick layer of asphalt paving. The underside of the specimen was coated with two applications of penetrating stain.

The measuring equipment was installed and one deck specimen was then placed in the test yard at Trätek in Skellefteå. The other test specimens were sent to the Norwegian Institute of Wood Technology in Oslo, to the Danish Technological Institute in Copenhagen, and to the University of Technology in Helsinki for measurements.

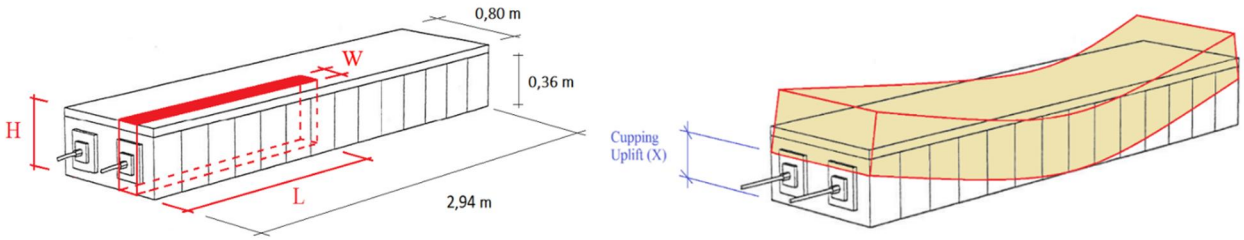

Figure 1: Left: sketch of the specimen tested within the Nordic Timber Bridge project and geometry of the slice deck analysed in Abaqus (in red). Right: sketch of the cupping phenomenon and measured uplift

Figure 1 shows the scheme of tested specimen with the slice deck analysed in Abaqus as well as the phenomenon of cupping and the measured uplift (X).

The test specimens were placed outdoor on a frame on stands at a height above ground of about 0.8 m. The frame had two supports for the deck plate with a centre distance of 1800 mm. Load cells were used to measure the steel bar forces. The load cells were manufactured and calibrated at IUC in Skellefteå. One load cell was installed on each bar, and readings of voltage were then converted to force levels using calibration graphs. Measurements of moisture content were made in three locations with electrical resistance measuring equipment.

The cupping of deck was determined measuring with the yardstick the uplift at the corner in the bottom surface of the specimen in correspondence of the steel bar; the value is the difference

between the deformed configuration (originated by environmental humidity changes) and the undeformed shape taken at the beginning of the tests.

In order to decrease the duration of calculation without compromising the quality of the analysis, the geometry model used in Abaqus, for all the cases explained in the following, is a smaller portion but nonetheless representative of the specimens that were actually tested [12]. The slice geometry has a width of 0.082 m and the half length of the specimen (Figure 1, left). A global coordinate system with vertical axis along the tangential direction of wood and horizontal axis along the radial direction was considered in the analyses. The elastic properties are the ones listed in Table 1 and the other material properties proposed in [3] are used. The steel bar is connected to the wooden deck by using the contact TIE of Abaqus code (Figure 2, left).

The weather data for the cities of Skellefteå , Oslo, Copenhagen and Helsinki were taken from the European ECMWF website [13] referring to the airport locations. The vertical displacements are shown in Figure 2 (right) for the specimen in the city of Skellefteå. The cupping and moisture content *MC* at the deck underside during time is presented in Figure 3 that shows the increase of cupping during a period of 15 months. It should be observed a sharp increase of cupping during wetting and only a partial decrease during drying. The bar force losses are presented in Figure 4 in comparison with the measurements taken in the two load cells in the specimen. The numerical losses are evaluated as average along the steel bar and show a decrease of bar losses during the whole period of analysis and this trend was observed for all studied cases. However, the measurements show an increase of the bar stress starting from winter 1996. It has to be noticed that a force loss during a time step corresponds to a drying step while a gain of force corresponds to a wetting step.

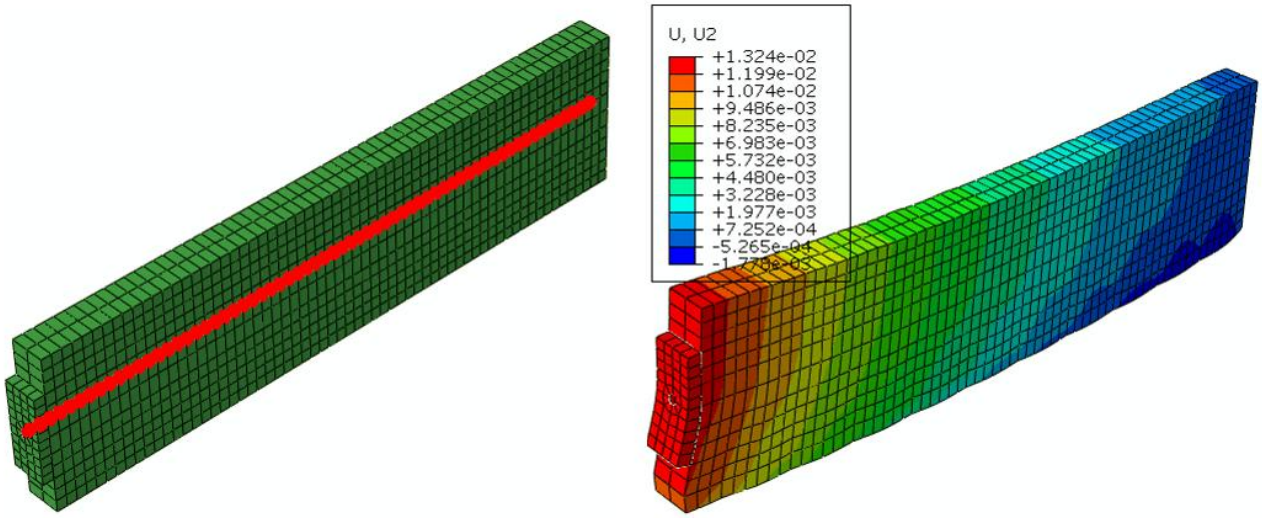

Figure 2. Left: Abaqus model (steel bar in red). Right: vertical displacements (right) at the end of the 15 month analysis (1st August 1996) for the specimen tested in Skellefteå, Sweden

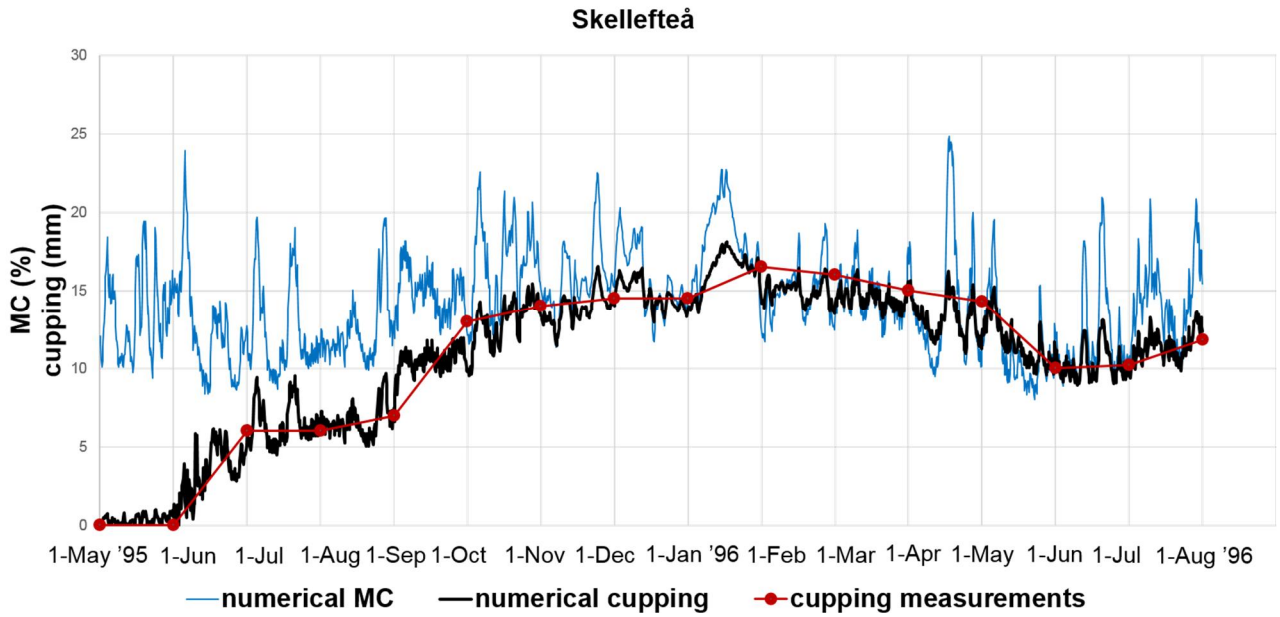

Figure 3. Numerical moisture content (MC), measured and numerical cupping at the underside of deck specimen in Skellefteå, Sweden

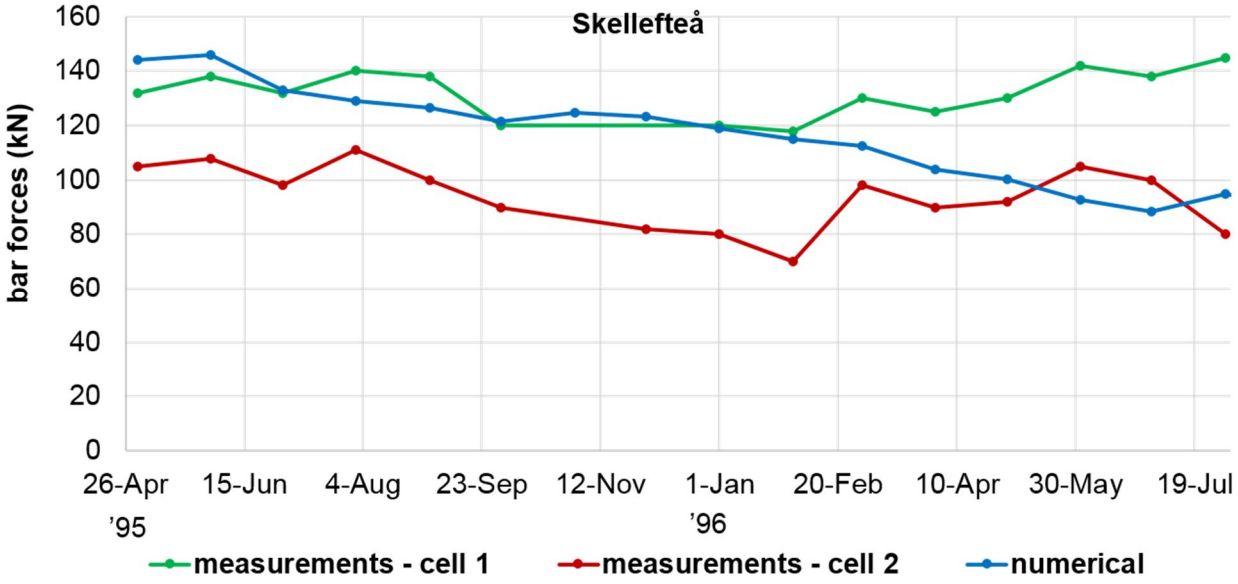

Figure 4. Measured and numerical bar forces of the deck specimen in Skellefteå, Sweden

3.2 Numerical analysis of cupping in deck of Umeå bridge

From 2011 to 2015 the SP Technical Research Institute of Sweden inspected 142 timber bridges built between 1990-2015. The inspections were made on behalf of the Swedish Transport Administration, local authorities or engineering consultants, for bridges geographically spread all over in Sweden, from Lund in the south to Kiruna in the north.

Among all the inspected bridges, the one in Umeå (Figure 5) shows similar technological characteristics as the specimens tested within the Nordic Timber Bridge project and, due to this, it has been selected for the numerical analysis in the present work. This is a pedestrian bridge over

water with stress laminated glulam deck, built in 2010. The deck has a width of 3.875 m, a depth of 0.36 m and the span is 10.720 m long. It is composed of 21 glulam beams in spruce of strength class L40 (similar to GL30), with section 94.5 × 360 mm each, compressed by a Dywidag steel bar, diameter ø 20, see [5] for the details.

Figure 5. Left: pedestrian bridge with SLTD in Umeå, Sweden; Right: Cupping in every corner of the deck (Pousette and Fjellström 2016).

The climate data have been taken from the European ECMWF website referring to the real bridge position for the year 2013 during which the *in situ* measurements were carried out [13].

The information in [5] about the inspections carried out on the bridge in Umeå reports that the initial moisture content in the glulam was about 12.5% when the bridge was constructed (year 2010). Since the presence of the river under the bridge induces a higher concentration of moisture in the air around the bottom surface of the bridge compared to other areas, the moisture content under the waterproof membrane on the top surface is still around 12.5% but the underside of the deck has a *MC* around 18% (end of year 2013). The cupping is found to be 15-30 mm in all corners of the bridge deck (Figure 5, right).

The material properties used for the Abaqus analysis are the same as the ones adopted for the deck specimens in the previous sections. The analysis provides results in terms of cupping, moisture content and stress in pre-tensioned bar. The measurements of tension in the bar are not reported in [5]. However, it is possible to compare the numerical results in terms of cupping and moisture content at the point on the lower surface of deck in line with the steel bar. The cupping versus time is shown in Figure 6. Numerical result of *MC* starts from 12.5% as initial condition imposed in Abaqus and grows up to 18% in the last months. For the top surface of deck, where the lamellas are insulated from the external atmosphere due to the road paving and the waterproof mat, *MC* remains stabilized at 12.5%. These values are in agreement with *in-situ* measurements which showed a moisture content of 12% for the viable surface on top and about 20% for the lower surface of the bridge. The numerical cupping values appear to be in agreement with the measured cupping since, after a transition time at the beginning of the analysis, these values are in the range of 15-30 mm for the entire duration of measurement, as stated in [5].

Table 2 shows all results in terms of numerical *MC*, cupping and bar force losses obtained for the deck specimens of the Nordic Timber Bridge project and for the deck of Umeå bridge. It can be observed that the loss of bar forces after 15 months of analysis is about 33-34% for all studied cases.

The maximum cupping is found during the month of January for all the studied cases. This corresponds to the high peaks of relative humidity coupled with low peaks of temperature in winter. It is recommended to check the conditions of SLTDs during the autumn before the eventual peak of cupping in January or other winter months.

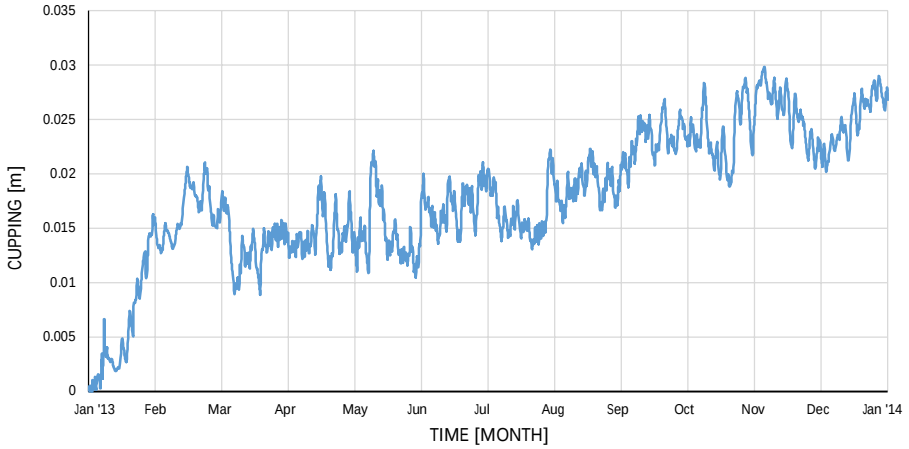

Figure 6. Numerical cupping trend at the underside of timber deck in Umeå, Sweden

Table 2: Summary Table for numerical MC, cupping and bar force losses

City and period of analysis	MC_{ini} (%)	MC_{avrg} (bottom deck) (%)	MC_{avrg} (middle deck) (%)	MC_{avrg} (top deck) (%)	Max cupping (mm)	Bar force loss (%)
Helsinki (15 months)	12	16.86	13.24	12.00	17.00	34
Copenhagen (15 months)	12	17.16	14.67	12.00	21.60	33
Oslo (15 months)	12	15.65	12.96	12.00	19.40	33
Skellefteå (15 months)	12	14.36	12.59	12.00	18.10	33
Umeå (12 months)	12.5	17.58	13.57	12.5	27.0	34

4. Conclusions

In this paper the effect of cyclic variations of the moisture content on the deformation of stress laminated timber decks of bridges is studied by means of finite element analysis with Abaqus code. The numerical method, based on a single-Fickian moisture diffusion model coupled with an orthotropic-viscoelastic-mechanosorptive model for wood, was validated by means of the experimental results on SLTD small specimens tested during the earlier Nordic Timber Bridge project. Finally, the model was used to study the behaviour of the deck of Umeå bridge in Sweden.

The numerical model is able to predict both the deformation (cupping) and the pre-stressed bar losses in a laminated timber deck, thus showing that the moisture-stress analysis is an effective tool for addressing the maintenance of SLTDs during their service life. However, further experimental research is needed to better investigate the role of the moisture content variation on the stress in the bars, which governs the interactions between the laminations of timber decks.

Acknowledgements

This work was funded by the WoodWisdom-Net+ project DuraTB (Durable Timber Bridges) which is gratefully acknowledged. The funding program for MSc theses (University of Brescia, Italy) that allowed MSc student Federico Ossoli to undertake a research stage at VTT is gratefully acknowledged.

References

[1] Pousette A., Nordic Timber Bridge Project, Influence of different climates on moisture content, bar forces and cupping (2000).

[2] Fortino S., Genoese A., Genoese A., Nunes L. and Palma P. "Numerical modelling of the hygro-thermal response of timber bridges during their service life: A monitoring case-study", *Construction and Building Materials*, Vol. 47, 2013, pp. 1225-1234.

[3] Fragiacomo M., Fortino S., Tononi D., Usardi I., Toratti T. Moisture-induced stresses perpendicular to grain in timber sections exposed to European climates. *Engineering Structures*, Vol. 33, 2011, pp. 3071-3078,.

[4] Hradil P., Fortino S., Salokangas L., Musci A., Metelli G. Effects of moisture induced stresses on the mechanical performance of glulam beams of Vihantasalmi bridge. Proceedings of World conference in Timber Engineering (WCTE 2016) conference, August 22-25.2016, Vienna, Austria.

[5] Pousette, A., Fjellström, P. A. *(2016)*, "Experiences from timber bridge inspections in Sweden - examples of influence of moisture", SP Technical Research Institute of Sweden, SP Rapport 2016:45.

[6] Metelli G., Preti M., Giuriani E. On the delamination phenomenon in the repair of timber beams with steel plates. *Construction and Building Materials*, Vol. 102, 2016, pp. 1018–1028.

[7] Ritter M.A., Geske E.A., , McCutcheon W.J., Moody R.C., Wacker, J.P., Mason L.E. Methods for assessing the field performance of stress-laminated timber bridges. In: Proceedings of the 1991 International timber enigneering conference; 1991 September 2-5; London. London:TRADA; 1991:3.319-3.326. Vol. 3.

[8] Ritter M.A., Wacker J.P., Field Performance of Stress-Laminated Timber Bridges on Low-Volume Roads, In Proceedings of the 6th International conference on low-volume roads; 1995 June 25-29; Minneapolis, MN. Washington DC: National Academy Press; 1995. Vol 2. 1995.

[9] Carlberg J., Toyib B. (2012), Finite Element Modelling of Interlaminar Slip in Stress-Laminated Timber Decks, Sweden. Master Thesis.

[10] Nilsson L.-O. "Moisture transport properties of wood and wood-based boards – an inventory and analysis of knowledge and required knowledge (in Swedish)", Report P-88:4, dept. Of building materials, Chalmers University of Technology, Göteborg, Sweden, 1988.

[11] Musci A. Effects of Moisture Content on Timber Structural Elements; Case Study: Vihantasalmi Bridge, Master Thesis, DICATAM, University of Brescia, Italy, 2015.

[12] Ossoli F. Effects of moisture content variation on the structural behaviour of pre-stressed laminated timber bridges, Master Thesis, DICATAM, University of Brescia, Italy, 2017.

[13] ECMWF http://apps.ecmwf.int/datasets/data/interim-full-daily/levtype=sfc

Anchor plates for pre-stressing rods and compression orthogonal to grain of timber

Francesco Mirko MASSARO
MSc, PhD Candidate
NTNU, Dep. of Str. Eng.
Trondheim, Norway
francesco.m.massaro@ntnu.no

Francesco Mirko Massaro received his structural engineering master degree from the Polytechnic University of Turin in Italy in 2011. He is currently a PhD candidate at NTNU.

Kjell Arne MALO
Professor
NTNU, Dep. of Str. Eng.
Trondheim, Norway
kjell.malo@ntnu.no

Kjell Arne Malo is professor of timber structures at NTNU. His research topics are method for increased strength and stiffness of connections for timber structures and vibrations in timber structures

Summary

A better knowledge of the mechanical behaviour of timber loaded in compression perpendicular to grain is essential for design of stress-laminated timber bridge decks to guarantee their proper behaviour during their whole lifetime. Several compression orthogonal to grain tests have been performed on timber. The paper presents numerical simulations of these aforementioned compression tests. The Tsai-Wu criterion is used in the numerical model to determine the change between the elastic and plastic behaviour of timber The comparison of the numerical simulations to the experimental results allows the use of the same numerical approach to analyse different geometrical and mechanical configurations than the one used in the experimental tests. Hence, it allows widening of the range of applications and a brief study of different geometrical layouts is presented herein.

Keywords: compression orthogonal to grain, stress-laminated timber decks, anchor plates, pre-stressing force.

1. Introduction

1.1 Stress laminated timber decks

Stress-laminated timber decks have become popular due to their light weight and high lateral stiffness. The system consists of parallel timber laminations that are held together by pre-stressed rods, usually made of high-strength steel, inserted into pre-drilled holes (see Figure 1a).

The pre-stressing generates lateral stress between laminations, which then work as a plate due to the friction between the lamellas, giving a better distribution of loads. However, there is a reduction of longitudinal stiffness due to the presence of butt joints of the lamellas. They cannot transfer bending moment so the full flexural capacity is reached only at a certain distance from the butt joints. In order to avoid weak sections the timber lamellas are displaced lengthwise relative to each other, spreading the butt joints (see Figure 1a) [1].

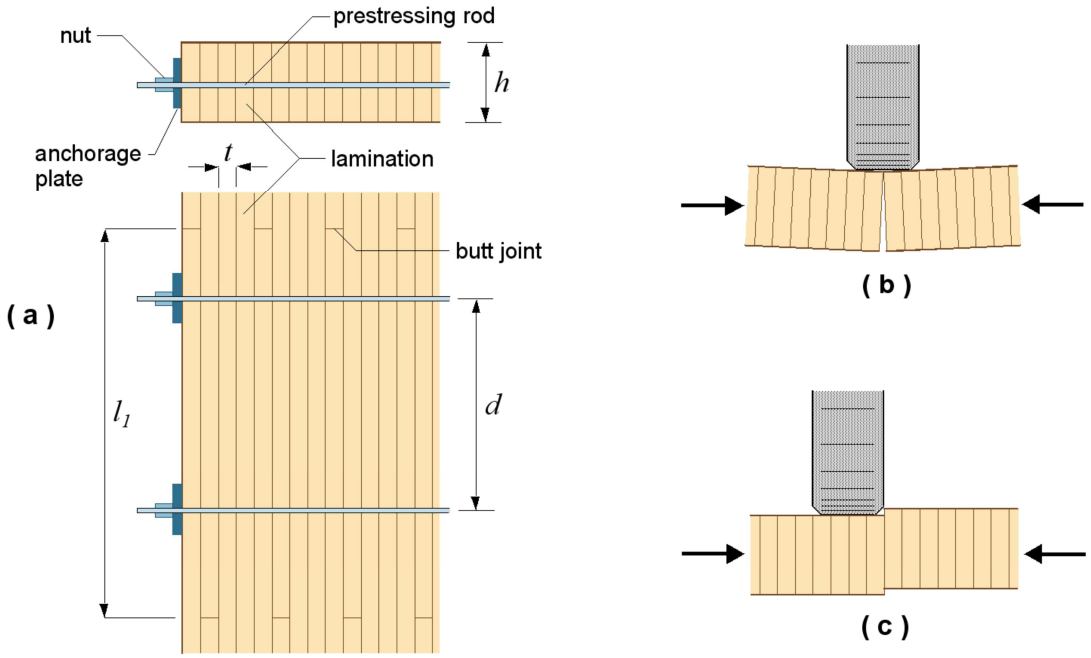

Figure 1 Stress-laminated timber deck plate (drawing: K. Bell)

Stress-laminated timber decks work as plates due to the lateral stress between the lamellas created by the pre-stressing force. Such force must be able to prevent vertical slips due to concentrate wheel loads (see Figure 1c) and to avoid gaps between the laminations (see Figure 1b). Ritter [2] suggested the necessary pre-stressing force F_p can be evaluated according to Equation (1).

$$F_p \geq 6\frac{M_T}{h} \quad ; \quad F_p \geq \frac{V_T}{\mu} \tag{1}$$

In Equation (1) M_T is the transverse moment given by the loads, h is the height of the timber deck, V_T is the shear acting on the deck and μ is the friction coefficient.

However, the pre-stressing force cannot be higher than the compression strength perpendicular to grain of timber under the anchorage plate.

Moreover, EN 1995-2 [3] prescribes a minimum long term pre-stressing stress of 0.35 MPa. The dimensional change of timber due to long term moisture and load exposure is the reason of the losses of pre-stress in the pre-tensioned rods and therefore in pre-stressed timber decks. Thus, the rods are commonly re-stressed after some months as well as after about 25 years to guarantee the stiffness of the deck.

2. Compression orthogonal to grain tests

Several compression orthogonal to grain tests were performed [4] on timber classified as Norwegian CE L40C. Two different setups had been tested during the experimental campaign: in the first system, the entire top surface of the timber specimen is loaded in compression (Figure 2), while in the second system there is a variable quantity of untouched timber (L_u) aside the loading area (Figure 3). The geometry of the tested specimens is given in Table 1.

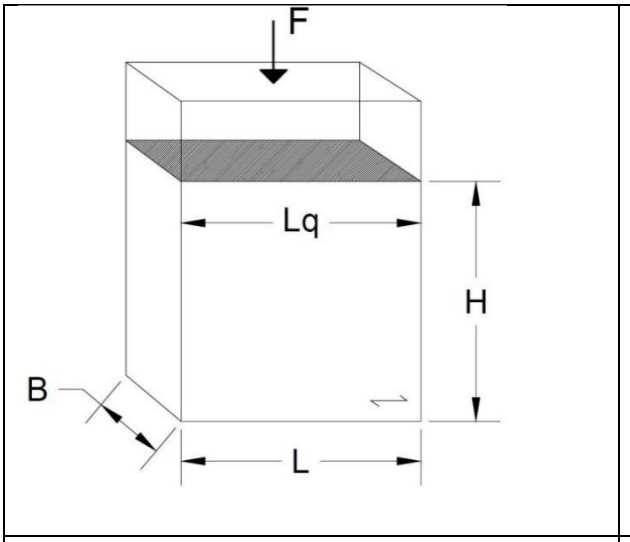

Figure 2 Test system 1: specimen Rxx

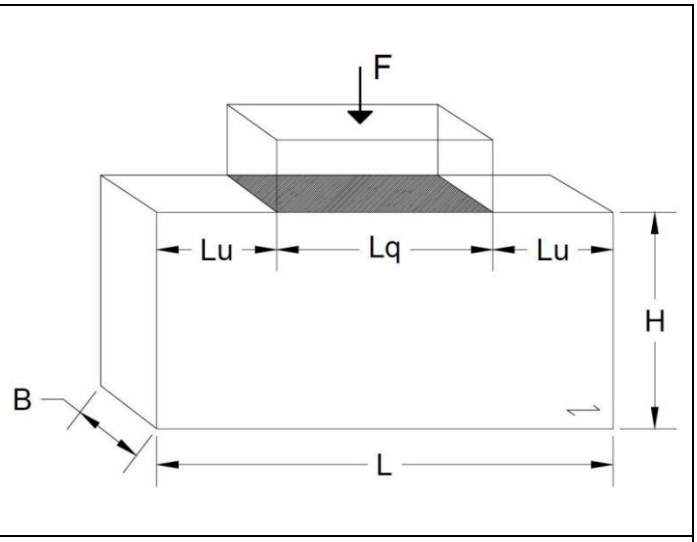

Figure 3 Test system 2: specimen Luxxx

Table 1 Geometry of the tested specimens[4]

Setup	L_q [mm]	B [mm]	L [mm]	H [mm]	L_u [mm]
R90	90	89	90	90	0
R120	90	89	90	120	0
R150	90	89	90	150	0
Lu30	90	89	150	200	30
Lu50	90	89	190	200	50
Lu70	90	89	230	200	70
Lu100	90	89	290	200	100
Lu150	90	89	390	200	150
Lu200	90	89	490	200	200

The tests were performed applying a deformation of 2 mm/min through a compression machine, reaching a final deformation of 20 mm under the loading area. This high deformation allowed getting information on the post-elastic behaviour of the specimens. Finally, the measurements were realized with the use of the system Aramis which combine optical measurements and digital image correlation analysis.

2.1 Post-elastic behaviour

The tested specimens showed a post-elastic behaviour that was analysed with the use of the Tsai-Wu criterion in its orthotropic formulation ([5], [6]).
The strength values of timber used in this study for the evaluation of the Tsai-Wu surface are obtained from [7], with the exception of the compression strength orthogonal to grain.

Table 2 Timber mean strengths (proportionality limits) used in the numerical model [7]

	f_T [MPa]	f_C [MPa]		f_V [MPa]
L	41,4	23,2	LR	6,1
T	3,37	3 [(a)]	LT	4,2
R	1,84	3 [(a)]	RT	1,6
L: longitudinal, T: transversal, R: radial – [(a)] from backward statistical analysis				

The compression strength for both radial and tangential direction was chosen as 3 MPa. This is the mean strength value obtained with a backward analysis from the characteristic compression strength orthogonal to grain of 2.5 MPa given in NS-EN 14080:2013, according to the probabilistic distribution given by the Joint Committee on Structural Safety JCSS [8].

Table 3 Timber stiffness values used in the numerical model (GL30c)

E_L [a] [MPa]	E_R [c] [MPa]	E_T [c] [MPa]	ν_{LR} [b]	ν_{LT} [b]	ν_{RT} [b]	G_{LR} [a] [MPa]	G_{LT} [a] [MPa]	G_{RT} [a] [MPa]
13000	150 - 185	150 - 185	0.501	0.695	0.835	650	650	65

E: normal modulus of elasticity, ν: poisson's ratio, G: shear modulus
[a] mean values from [9] [b] from [7] [c] experimental data fitting

The experimental tests [4] were numerically modelled in the software Abaqus. The used elastic mean properties are shown in Table 3. The elastic modulus parallel to grain E_L and the shear moduli G_{LR}, G_{LT}, G_{RT} were chosen as the mean values provided in [9] for GL32c, which is the class with approximately the same properties as CE L40c, while the Poisson's ratios are obtained from [7]. Finally, the elastic moduli orthogonal to grain E_R and E_T are chosen individually for each test in order to get the best fit in the elastic domain. The reason for this approach is that the pit location in each specimen is not known and hence using fixed values of E_R and E_T is not sufficient in this case.

The results of the numerical analysis and the experimental tests are compared in Figure 4 and Figure 5, where the letter N stands for the numerical results and T for the experimental results.

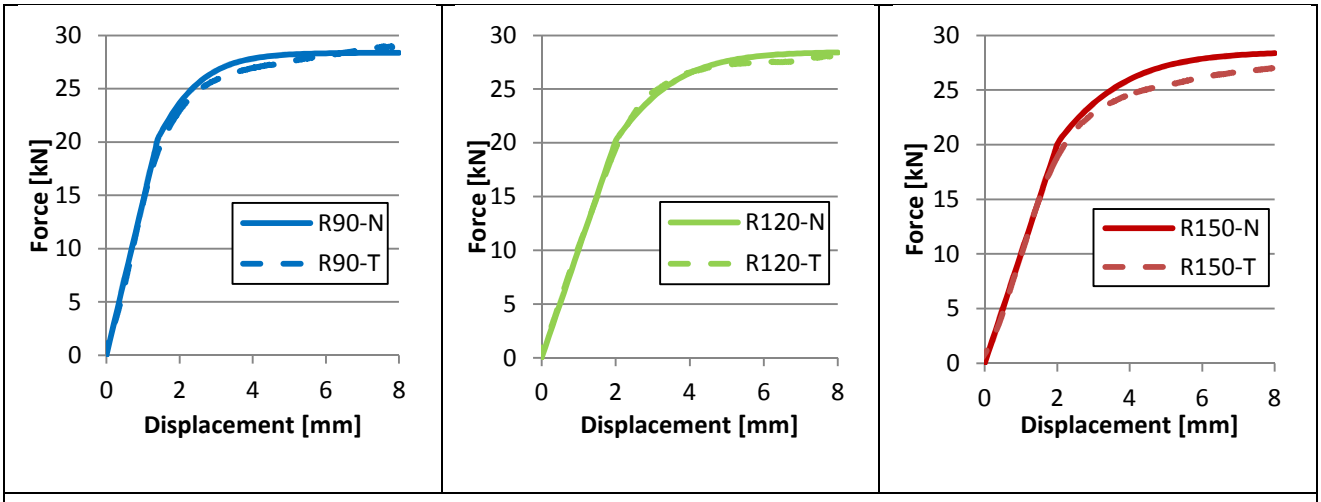

Figure 4 Comparison between experimental (T) and numerical results (N) for Rxx system

The plots showed in Figure 4 and Figure 5 show reasonable good agreement between the numerical results and the experimental measurement for both the systems, with and without unloaded timber outside the loading area. Therefore, these results allow the use of the same numerical approach to analyse other geometrical layouts and mechanical systems than the ones tested during the experimental campaign.

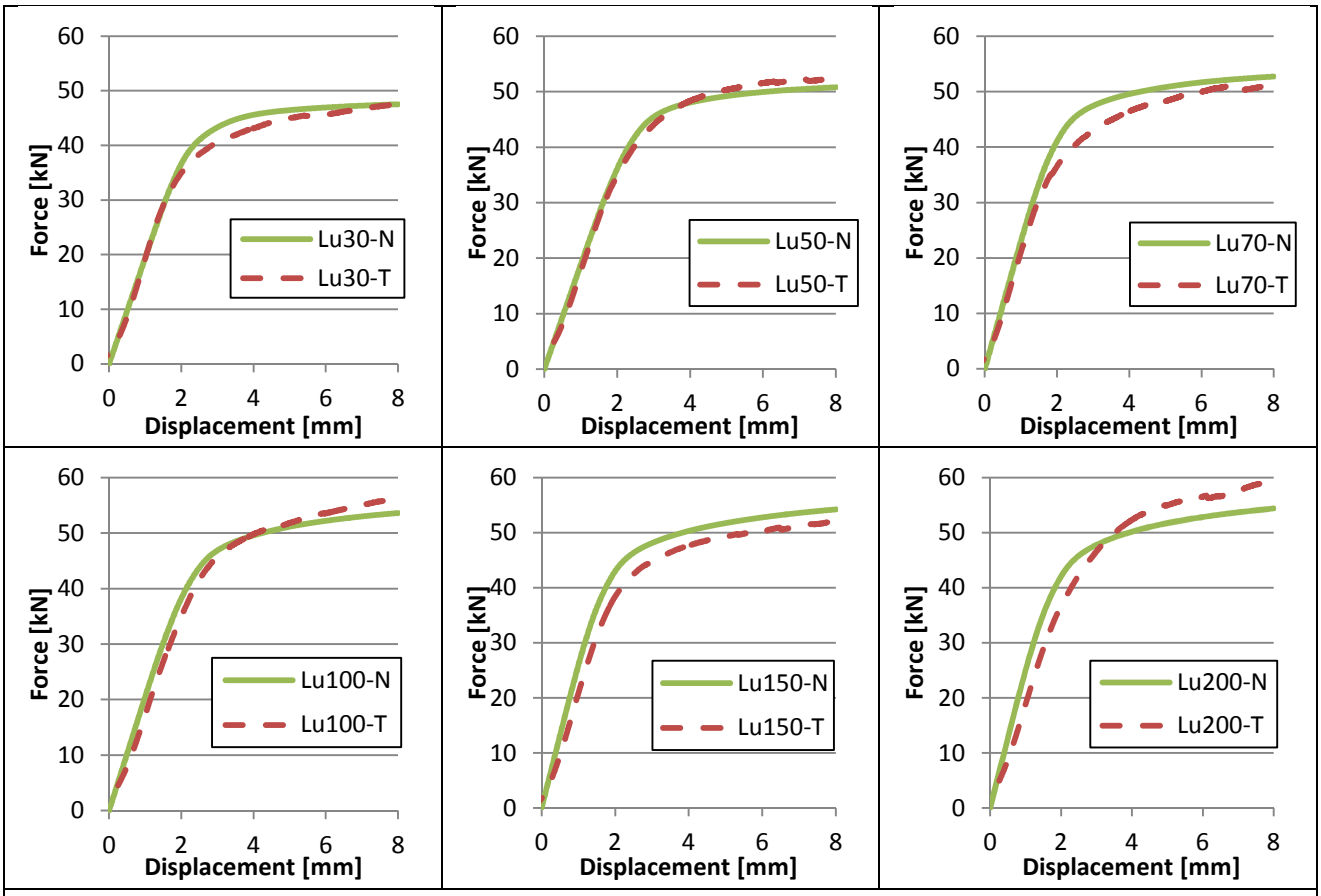

Figure 5 Comparison between experimental (T) and numerical results (N) for Luxx system

3. Compression stresses under anchor plates

Stress laminated timber decks are pre-stressed by means of steel rods as described in paragraph 1. The pre-stressed rods cause a compression stress in the timber deck that is higher in proximity of the edge and become constant after a diffusion length L_d (see Figure 6).

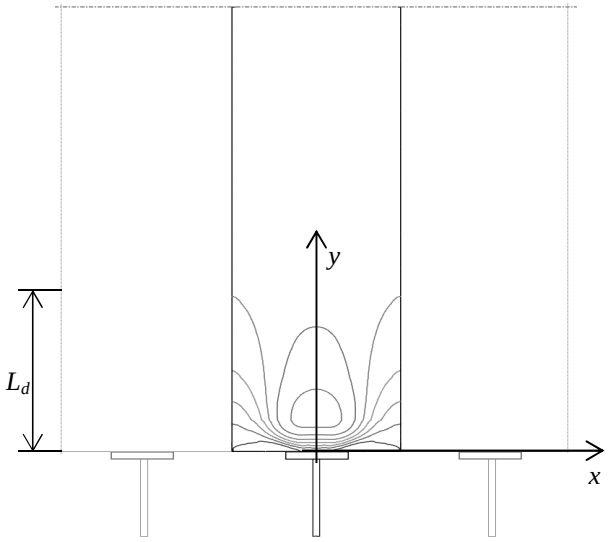

Figure 6 Diffusion of compression stress in section of a pre-stressed deck (plane section of a deck: the x-direction is the longitudinal to grain direction)

Numerical analyses have been performed on a pre-stressed timber deck (Norwegian spruce) with height of 450 mm where the dimensions of the circular anchorage steel plate (radius R and thickness T) have been varied. In the simulations it was applied a pre-stressing force in order to achieve a uniform compression stress of 1 MPa, after the diffusion length L_d. These analysis show that a too small plate can lead to high stresses in proximity of the edge. The results of the analyses using plates with radius R of 150, 175, and 200 mm and with thickness T of 20, 30, and 40 mm are shown from Figure 7 to Figure 11.

It is evident that the use of plates with radius 150 mm achieves a compression stress in proximity of edge that is bigger than the proportionality limit, evaluated to 3 MPa (Table 2). The maximum compression stress decreases with the increase of the radius of plate (see Figure 9 to Figure 11). This trend recurs analysing the effect of different thicknesses. Indeed, the use of the plate with only 20 mm thickness origins compression stresses higher than the proportionality limit, while thicker plates remain under this limit (see Figure 7 and Figure 8).

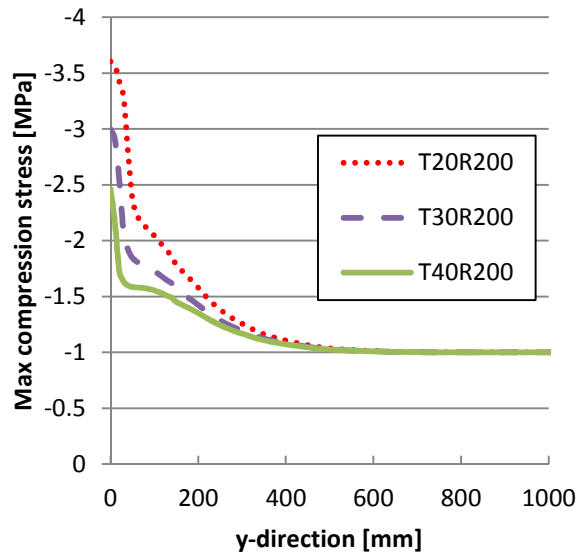

Figure 7 Development of compression stress along the y direction (transversal): anchorage plates radius 200 mm

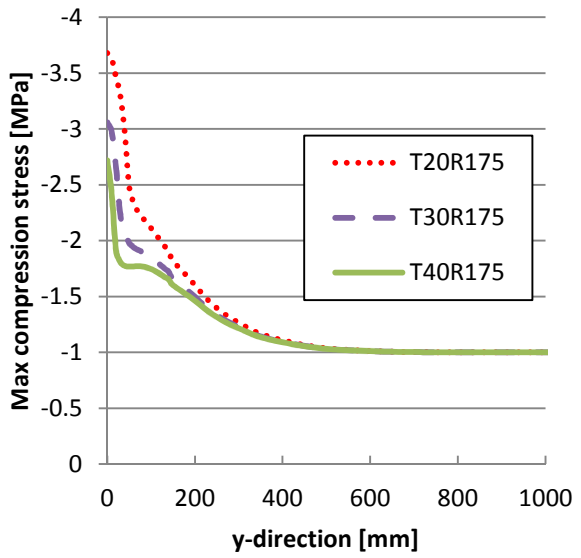

Figure 8 Development of compression stress along the y direction (transversal): anchorage plates radius 175 mm

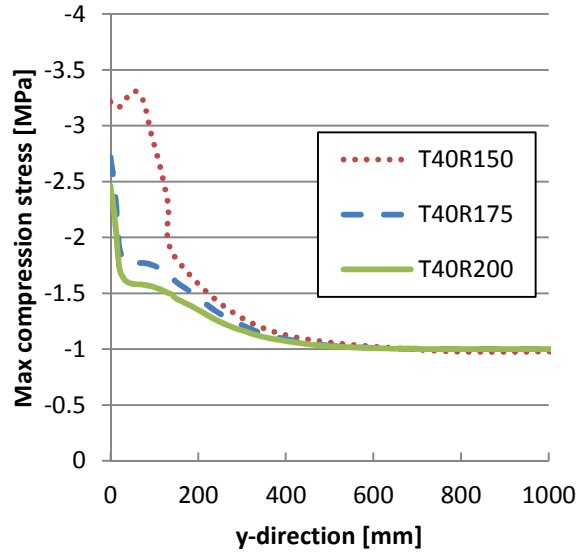

Figure 9 Development of compression stress along the y direction (transversal): anchorage plates thickness 40 mm

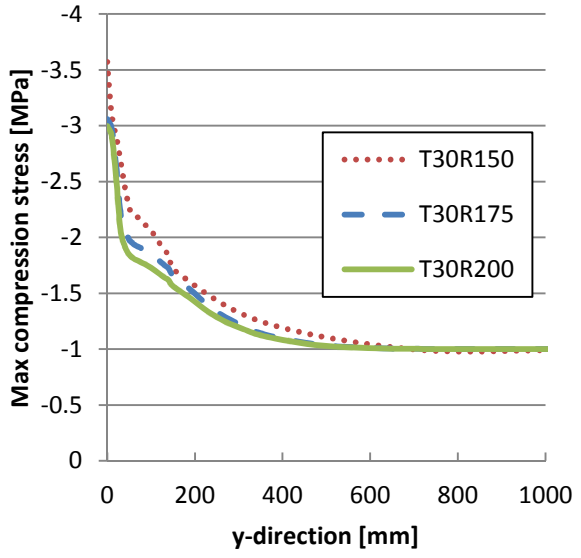

Figure 10 Development of compression stress along the y direction (transversal): anchorage plates thickness 30 mm

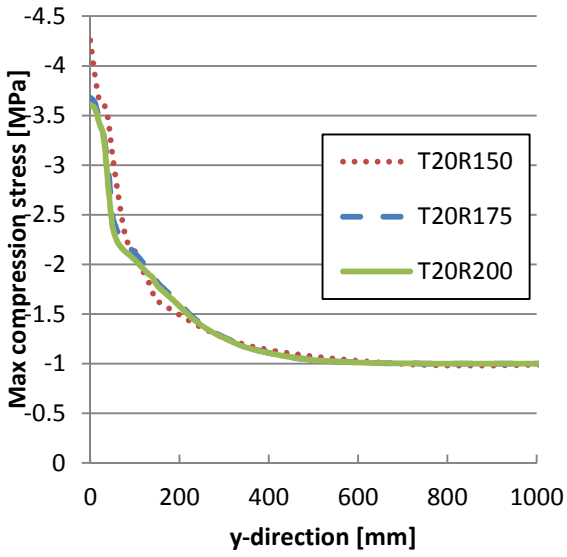

Figure 11 Development of compression stress along the y direction (transversal): anchorage plates thickness 20 mm

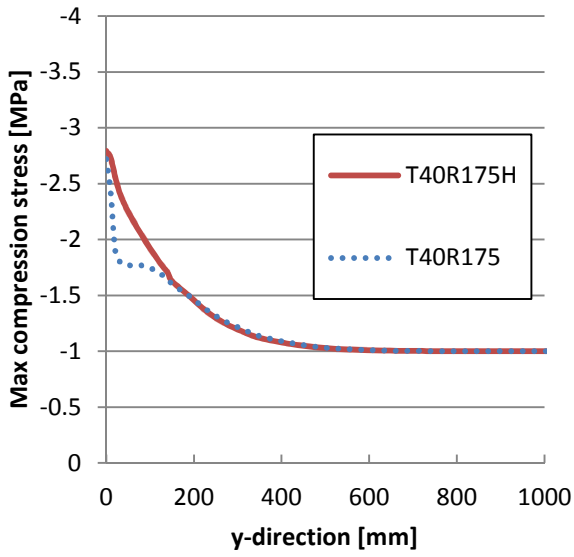

Figure 12 Development of compression stress along the y direction (transversal): anchorage plates radius 175 mm, thickness 40 mm. (H: additional hardwood layer)

3.1 Use of additional layer between anchor plate and deck

Furthermore, it was analysed the effect of a different structural layout wherein a layer made of hardwood (oak) is inserted between the anchor steel plate and the timber deck. Therefore, a 20 mm thick layer, having the properties shown in Table 4, was included in the numerical model. The layout with the additional hardwood layer is illustrated in Figure 13.

Table 4 Timber stiffness values used in the numerical model (D30)

E_L [a] [MPa]	E_R [a] [MPa]	E_T [a] [MPa]	ν_{LR} [b]	ν_{LT} [b]	ν_{RT} [b]	$G_{LR} = G_{LT}$ [a] [MPa]	$G_{RT} = G_{Lx}/10$ [MPa]
11000	730	730	0.350	0.448	0.560	690	69

E: normal modulus of elasticity, ν: poisson's ratio, G: shear modulus
[a] mean values from [10] [b] from [11]

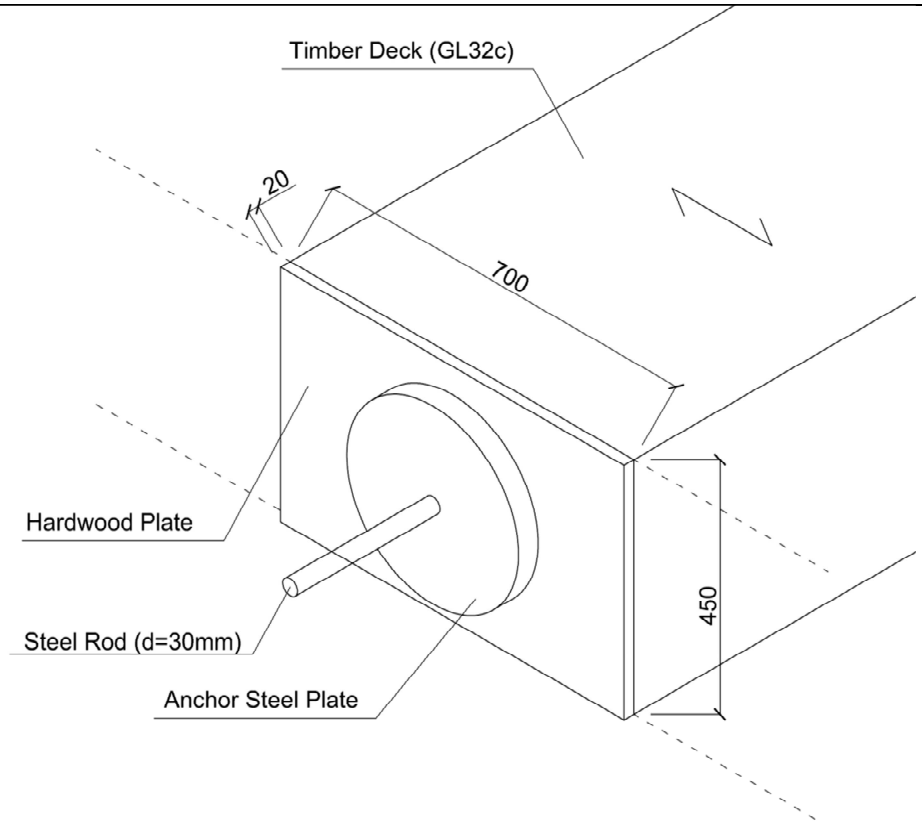

Figure 13 Sketch of the layout with the additional hardwood (D30) layer

The comparison of the results of the model T40R175 with and without the introduction of the hardwood plate show that there is not any evident effect on the maximum value compression reached as shown in Figure 12, where the curve identified with the letter H is relative to the model with the additional hardwood layer. However, even if the peak stress is similar, the compression field shows that a less amount of timber reaches high compression stress (dark blue area in Figure 14 and Figure 15). Furthermore, the maximum tension orthogonal to grain decreases from 0.27 MPa to 0.06 MPa. Additionally, the introduction of the hardwood plate improves the shear distribution reducing the peaks of shear that are present in the model without the hardwood element (Figure 16 and Figure 17).

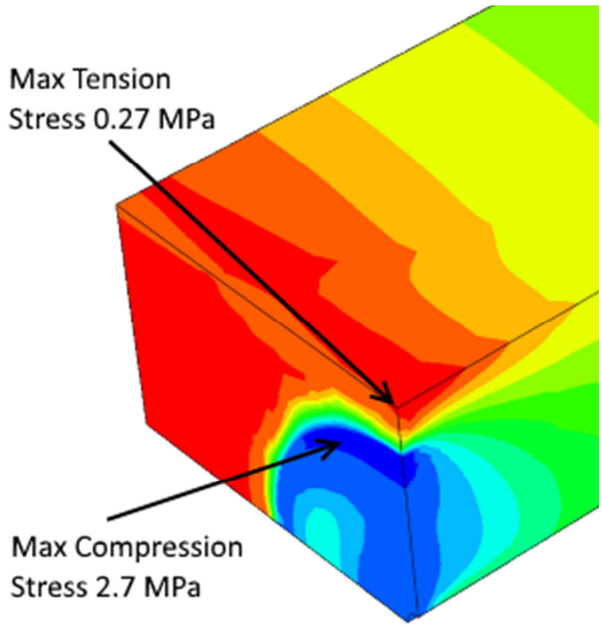

Figure 14 Contour plot of orthogonal to grain stresses (T40R175) – red: tension stresses, from green to blue: compression stresses

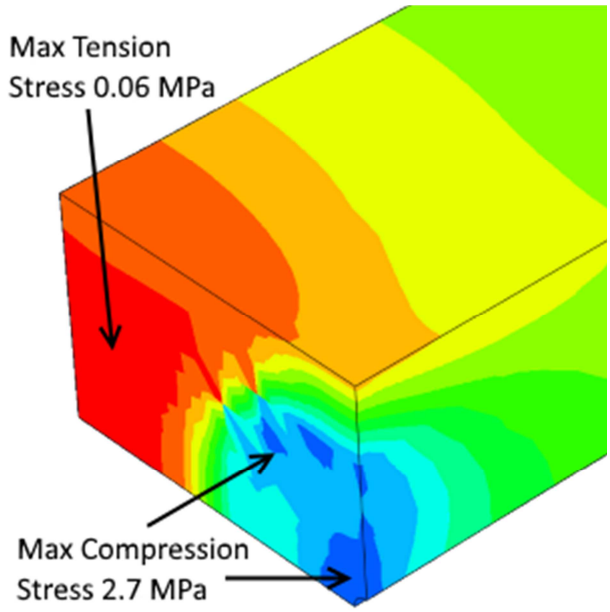

Figure 15 Contour plot of orthogonal to grain stresses (T40R175H) – red: tension stresses, from green to blue: compression stresses

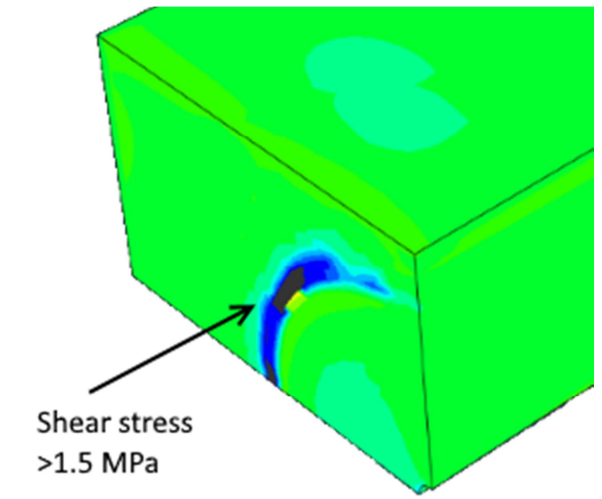

Figure 16 Contour plot of shear stresses (T40R175) – the dark area corresponds to shear stresses > 1.5 MPa

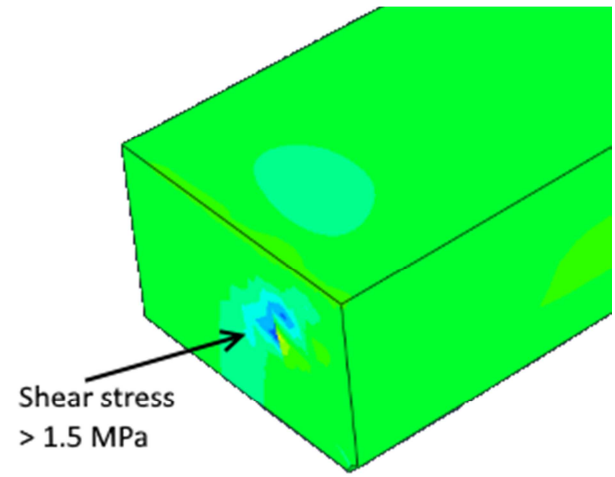

Figure 17 Contour plot of shear stresses (T40R175H) – the dark area corresponds to shear stresses > 1.5 MPa

4. Conclusions

It is important that the anchorage system allows the spread of the compression stresses. Smaller radii of the load plate will lead to higher compression stresses under the plate in order to reach the required pre-stress in the timber deck. The same effect is shown for smaller thicknesses. Therefore it is important to design the load plate with an adequate geometry in order to avoid too high compression stresses that can lead to crushing of fibres. The introduction of an additional layer stiffer than the deck between the load plate and deck does not have a huge effect with regard to the

compression field stress but it helps to avoid high shear stress on the deck lamellas in correspondence of the load plate, redistributing them through the stiffer layer.

5. Acknowledgements

This work was funded by the WoodWisdom-Net+ project DuraTB ("Durable Timber Bridges") and the support from the funding bodies and partners is gratefully acknowledged.

6. References

[1] Malo K. A., "Chapter 11 - Timber Bridges," *Innovative Bridge Design Handbook*, A. Pipinato, ed., Boston: Butterworth-Heinemann, 2016, pp. 273-297.
[2] Ritter M. A.: *Timber Bridges: Design, Construction, Inspection, and Maintenance*, U.S. Department of Agriculture, Forest Service, Washington DC, 1992.
[3] CEN, "Eurocode 5: Design of Timber Structures – Part 2: Bridges," Comité Européen de Normalisation 2004.
[4] Troller J. B., "Compression Capacity of Timber Sills Loaded Perpendicular to the Grain," Master Thesis, Department of Structural Engineering, Norwegian University of Science and Technology, 2014.
[5] Tsai S. W., Wu E. M., A General Theory of Strength for Anisotropic Materials, *Journal of composite materials*, 5 (1): 58-80, 1971.
[6] Clouston P. L., Lam F., Computational Modeling of Strand-Based Wood Composites, *Journal of engineering mechanics*, 127 (8): 844-851, 2001.
[7] Dahl K. B., "Mechanical Properties of Clear Wood from Norway Spruce," PhD Thesis, Department of Structural Engineering, Norwegian University of Science and Technology, 2009.
[8] JCSS, "Jcss Probabilistic Model Code," *Part 3: Resistance Models*, JCSS, 2006, p. 16.
[9] CEN, "En 14080:2013 - Timber Structures - Glued Laminated Timber and Glued Solid Timber - Requirements," Comité Européen de Normalisation 2013.
[10] CEN, "En 338:2016 - Structural Timber - Strength Classes," Comité Européen de Normalisation 2016.
[11] Forest Product Laboratory: *Wood Handbook: Wood as an Engineering Material*, United States Department of Agriculture, 2010.

Mechanical properties of acetylated radiata pine

Ferry Bongers
Product Dev. Manager
Accsys Group
Arnhem, the Netherlands
Ferry.bongers@accsysplc.com

As wood scientist and working more than a decade on product development of acetylated wood Ferry Bongers has been involved in various publications which among several on mechanical properties of acetylated wood.

Summary

The benefits from acetylation of wood to enhance resistance against fungal decay and dimensional stability have been known for many years. Since 2007 Accsys Technologies has been commercial producing Accoya® wood that is based on acetylation of Radiata pine (Pinus radiata D. Don). Accoya® has shown its potential for many applications, including structural uses. Over the years various projects have been realised, and a series of investigations on the mechanical properties of strength graded acetylated radiata pine. A Design Guide for Accoya® structural wood was made on this basis. The research was mostly limited to structural pre-graded radiata pine and to 38 mm thickness. The new work reported in this paper presents a detailed investigation of the mechanical properties of (ungraded) acetylated radiata pine ranging from 25 to 100 mm thickness and widths from 100 to 250 mm by Karlsruhe Institute of Technology (KIT) Germany. In addition duration of load tests were done. Based on this a strength grade has been allocated to Accoya wood.

Keywords: acetylation, mechanical properties, structural design

1. Introduction

The benefits from acetylation of wood to enhance resistance against fungal decay and dimensional stability have been known for many years [1-3]. Since 2007 Accsys Technologies has been commercial producing Accoya® wood that is based on acetylation of Radiata pine (*Pinus radiata* D. Don). Accoya® has shown its potential for many applications, including structural uses. Encouraged by the success of the two heavy load-bearing traffic bridges constructed using Accoya® wood in Sneek the Netherlands [4-5], several pedestrian bridges and various other column type structures situated in wet (Service Class 3) conditions have been completed. A design guide for Accoya® structural wood was made on basis of a series of investigations [6-7]. The Karlsruhe Institute of Technology (KIT) in combination and Schaffitzel + Miebach GmbH conducted an extensive study of manufacturing and testing of Accoya Structural Glulam [8-9]. This research was based on full size 38 x 150/200 mm beams (both defect free and qualities containing knots) of pre-graded radiata pine.

Recently a extensive investigation of the mechanical properties of (ungraded) acetylated radiata pine ranging from 25 to 100 mm thickness and widths from 100 to 250 mm by Karlsruhe University. In addition duration of load tests were conducted. Based on this in combination with quality control processes a strength grade has been allocated to Accoya wood of A1 quality [10-11].

2. Materials and methods

2.1 Sample preparation

Twenty-six bundles (circa 45m^3) of Radiata pine (*Pinus radiata* D. Don), from 10 different sawmills from the typical forest areas in New Zealand on both the North and South Island, ranging from 25 to 100 mm thickness and width varying from 100 to 250 mm were allocated for the test. Most boards were of a defect free quality (A1), but (knots) lower visual appearance grade boards (containing either knots, visible resin pockets or wane) were included as a distinct grade (A2 and A3 as defined by Accsys Technologies [12]). In total 1,289 boards were acetylated in the production facilities of Accsys Technologies in Arnhem, the Netherlands, according the patented process and within the KOMO certification scheme of BRL 0605 [13]. The wood was treated in nine different acetylation batches.

2.2 Brookhuis MTG measurements

Prior to and after acetylation the dynamic Modulus of Elasticity was determined with measurements with a Brookhuis MTG by Accsys Group. The method is based on measuring of a frequency response of an impact. The dynamic modulus of elasticity is calculated [14]. For machine grading settings need to be prepared [15-16]. Of each board prior to acetylation the dimensions, weight and wood moisture content (electric resistance moisture meter) were measured. The Brookhuis MTG was used to determine the natural frequency of the board. The dynamic MOE of each board has been calculated according to Eq. 1. After acetylation the measurements were repeated except for the wood moisture content (this cannot be measured accurately with a non-destructive device for acetylated wood, but overall the wood moisture content is very low after the process (0-3%).

$$MOE_{ViSCAN} = \frac{\rho(2L_m f_e)^2}{10^6} [N/mm^2] \quad (1)$$

With: ρ density in [kg/m^3]
L_m is the board length during the ViSCAN measurements in [m]
f_e a longitudinal frequency measured by the ViSCAN in [Hz]

2.3 Four-point bending tests

A selection of the acetylated wood has been used for 4 point bending tests according to EN 408. The MOR have been corrected for k_h to 150 mm depth in accordance to EN 384. EN 14358 has been used to determine the characteristic bending strength. Most boards have been tested in edgewise position. In addition 25 and 38 mm boards have been loaded flatwise. An overview of the samples is given in Table 1.

Table 1 Test setup of 4 point bending tests

Series	Dimension	Wood quality	Test	# samples
1	25 x 150 mm	A1	Edgewise	30
	25 x 200 mm	A2		20
	25 x 150 mm	A1	Flatwise	31
	25 x 200 mm	A2		20
2	38 x 200 mm	A1	Edgewise	30
	38 x 150 mm	A2		20
	38 x 200 mm	A1	Flatwise	30
	38 x 150 mm	A2		21
3	50 x 150 mm	A1	Edgewise	41
		A3		10

Series	Dimension	Wood quality	Test	# samples
4	50 x 250 mm	A1	Edgewise*	40
5	63 x 100 mm	A1	Edgewise	50
		A2		6
6	75 x 100 mm	A1	Edgewise	41
		A2		5
		A3		4
7	100 x 100 mm	A1	Edgewise	50

2.4 Shear strength test

Twenty samples Accoya and 20 samples Spruce/Fir have been tested according to EN 408 on shear strength. The Accoya samples have been cut from boards of 38 mm thickness and A1 and A2 quality. Dimensions of the samples is 200 x 80 x 38 mm³. The samples have been tested with an angle of 14°.

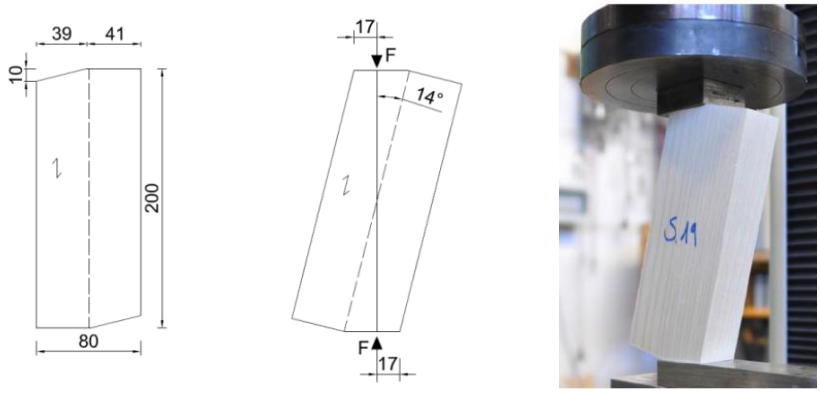

Figure 1 Shear strength set-up at Univeristy of Karlsruhe

2.5 Compression perpendicular to the grain

Forty samples of Accoya were tested according to EN 408 on compression strength perpendicular to the grain. The samples have been cut from Accoya boards of 50, 63, 75 and 100 mm thickness.

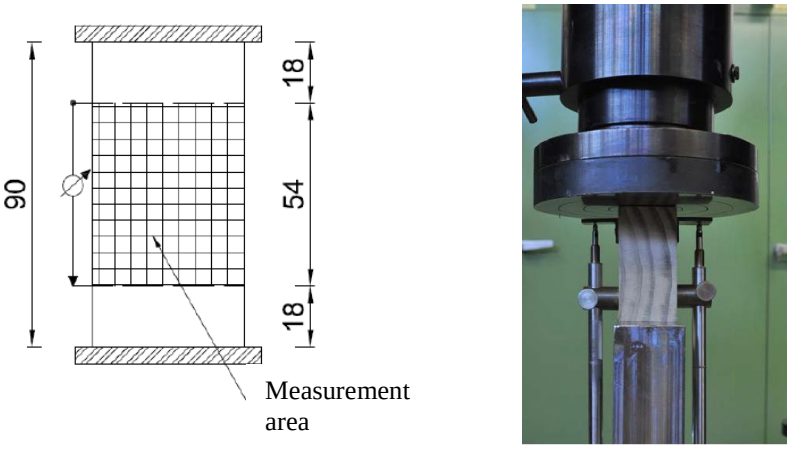

Figure 2 Compression perpendicular to the grain test set-up

3. Results and discussions

3.1 Brookhuis MTG measurements

In Figure 3 and Figure 4 the dynamic MOE, calculated on basis of the Brookhuis MTG measurement, is shown in relation to the results of the static edgewise bending test for local MOE and MOR respectively. For both A1 and A2 Accoya wood quality the Dynamic MOE has a strong correlation with the local (static) MOE. The correlation with the bending strength (MOR) is less as expected since other factors such as slope of grain play a role.

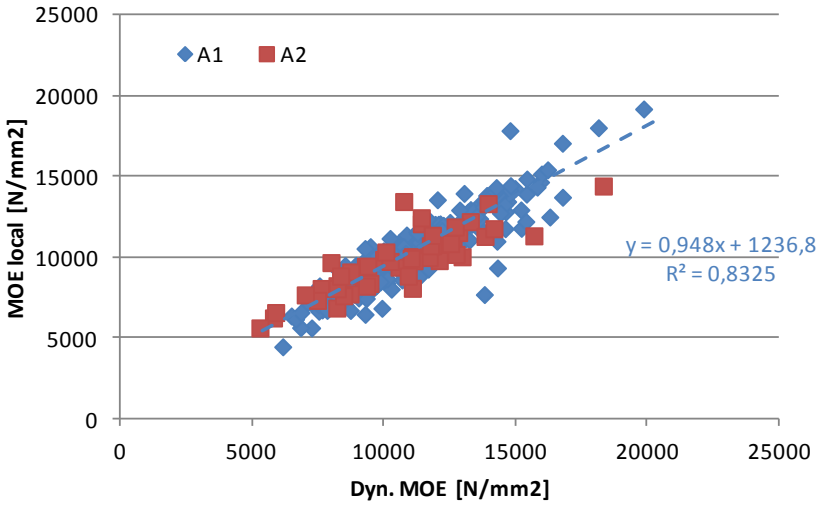

Figure 3 Dynamic MOE in relation to MOE local for edgewise bending test

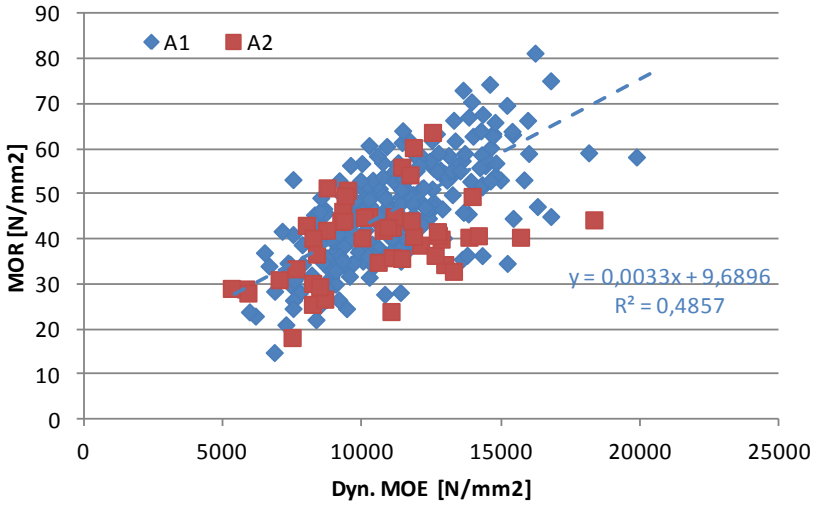

Figure 4 Dynamic MOE in relation to MOR for edgewise bending test

3.2 Four-point bending tests

In Figure 5 and Figure 6 distributions of the bending strength (MOR) and (local) bending stiffness (MOE) respectively per dimension and wood quality are shown. In total the mean bending strength of 449 boards Accoya radiata pine of different dimensions is 48.7 N/mm^2, and the stiffness 10.000 N/mm^2. The average density is 530 kg/m^3. Influence of the knots on the strength properties could not be found.

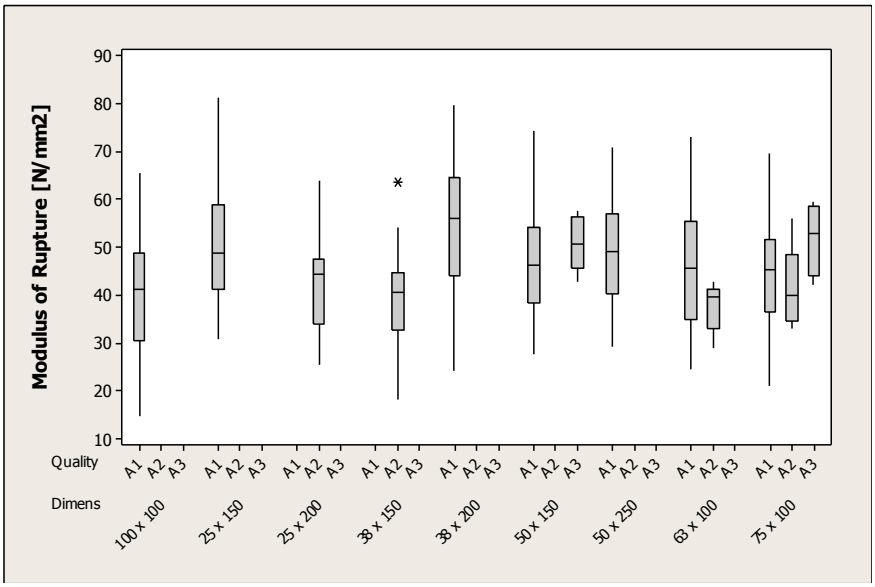

Figure 5 Bending strength distribution per dimension and quality (edgewise bending tests)

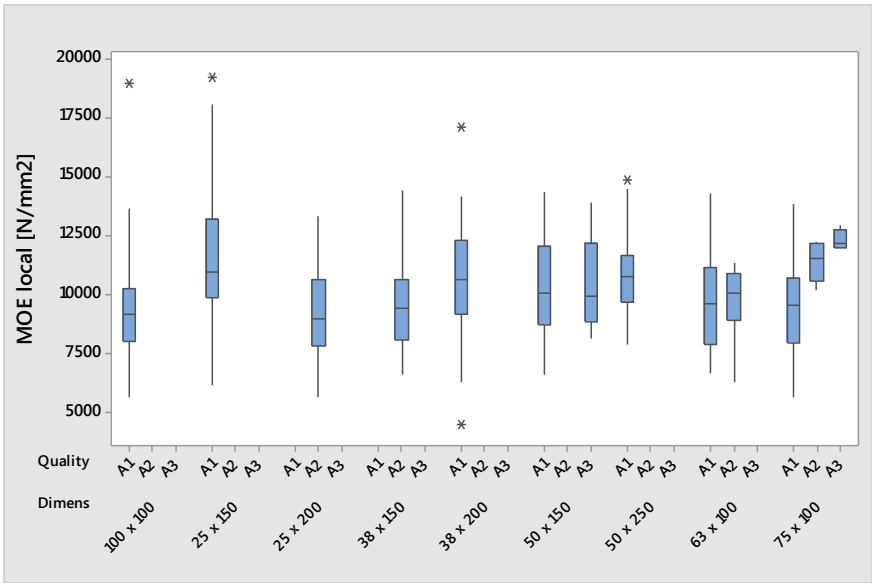

Figure 6 Local bending stiffness distribution per dimension and quality (edgewise bending tests)

3.3 Shear strength tests

The results are summarized in the table below. Evaluation of the breaking behaviour indicated especially for untreated spruce a brittle behaviour.

Table 2 Results of shear strength test

Series	**N**	f_m **in N/mm²**	
		Mean	**STD**
Accoya RP (A1 quality)*	14	8.3	1.3
Accoya RP (A2 quality) *	6	7.8	1.5
Spruce	20	5.5	1.0

* samples cut from 38 x 150 mm boards

3.4 Compression perpendicular to the grain

A summary of the results is given in the table below. Mostly elastic distortions were seen, although some samples had a brittle behaviour.

Table 3 Results of compression strength perpendicular to the grain of Accoya radiata pine

Series	**N**	$F_{c,90}$ **in N/mm²**	
		Mean	**STD**
3.1 (50x150 mm)	10	10.8	2.2
5.1 (63x100 mm)	10	8.3	0.9
6.1 (75x100 mm)	11	8.7	1.9
7.1 s*) (100x100 mm)	10	8.2	1.2
7.1 l*) (100x100 mm)	10	7.6	1.4

**) s = quarter sawn samples, l = plain sawn samples*

3.5 Strength class allocation and other considerations

The characteristic bending strength for the combined wood qualities (A1, A2 and A3) are circa 14% lower than the characteristic value for A1 quality only. A combined grade of A2 and A3 has a circa 26% lower characteristic bending strength compared to A1 quality.

Based upon EN 384 without correction k_h and k_i in combination with the draft EN 14358:2013 the characteristic bending strength fm,k = 22.7 N/mm^2 for all Accoya qualities combined (A1, A2 and A3). This value is conservative for defect free Accoya (A1) quality since for Accoya containing defects (A2 and A3) the characteristic bending strength fm,k = 16.8 N/mm^2 is used.

The characteristic average bending stiffness of Accoya is E0,mean = 9920 N/mm2, the average density ρmean = 526 kg/m^3 and the characteristic density ρ_k = 440 kg/m^3. Based on these results it has been proposed by Blaß (2016) to classify Accoya of A1 quality as C22, and Accoya A2 quality as C16 as defined in EN 338. A comparison between the defined C22 class (EN 384) and the test results (combined A1, A2 and A3 quality grades) is given in Table 4.

Table 4 Comparison of values for C22 declared in EN 338 with the research results for Accoya A1.

Property		**Value for C22 (EN 338)**	**Test results**
Bending strength	$f_{m,k}$	22 N/mm^2	22.7 N/mm^2
Tensile parallel	$f_{t,0,k}$	13 N/mm^2	17.3 N/mm^2
Tensile perpendicular	$f_{t,90,k}$	0.4 N/mm^2	-
Compression parallel	$f_{c,0,k}$	20 N/mm^2	40.2 N/mm^2

Property		**Value for C22 (EN 338)**	**Test results**
Compression perpendicular	$f_{c,90,k}$	2.4 N/mm^2	4.8 N/mm^2
Shear strength	$f_{v,k}$	3.8 N/mm^2	5.4 N/mm^2
Average stiffness parallel	$E_{0,mean}$	10,000 N/mm^2	9,920 N/mm^2
Stiffness parallel	$E_{0,05}$	6,400 N/mm^2	-
Average stiffness perpendicular	$E_{90,mean}$	320 N/mm^2	-
Average shear strength	G_{mean}	630 N/mm^2	-
Density	ρ_k	340 kg/m^3	440 kg/m^3
Average density	ρ_{mean}	410 kg/m^3	526 kg/m^3

4. Conclusions

Based on 4-point bending tests of 449 boards Accoya radiata pine of different dimensions the mean bending strength is 48.7 N/mm^2, and the stiffness 10.000 N/mm^2. The average density is 530 kg/m^3. Influence of the knots on the strength properties could not be determined. The maximum shear strength of the Accoya boards is 8.1 N/mm2 in average and is higher than found for spruce (average 5.5 N/mm^2). Compression strength perpendicular to the grain gave an average of 8.7 N/mm^2 for Accoya radiate pine.

Based on this testing and other studies the following conclusions and considerations were drawn (Blaß 2016):

- The standard safety factors as given in EN 1995-1 may be used, except for k_{mod} for permanent load. It is advised to use a factor of 0.5 (see Table 5) until the duration of load testing with Accoya and untreated spruce at KIT is completed and an appropriate k_{mod} factor is validated.
- For the dimensioning of components and connections with pin-shaped connections in Accoya A1 quality, the characteristic strength, stiffness and bulk density characteristics of the strength class C22 should be applied. For components made of Accoya A2 quality, those belonging to strength class C16 according to EN 338 should be used.
- Accoya wood connections may be made with nails, clamps, wood screws, dowels and bolts. Note for specifiers: Accoya® contains a small amount of residual acetic acid from the modification process. While it is less acidic than oak or several tropical hardwood species, in order to ensure an adequate life for metallic fixings it is recommended to use stainless steel. If discoloration is a concern then grade A4 fixings will be required. If stainless steel is no option other methods may be considered to prevent corrosion by for instance using coated steel or by creating a physical barrier between wood and metal (e.g. glued-in rods).
- For nails and screws in non-pre-drilled holes, ACCOYA is considered to be a brittle (sensitive to splitting) wood species as defined in EN 1995-1-1 8.3.1.2 (6). In this case, the minimum distances should be maintained as for wood with a characteristic raw density ρk of 420 kg / m³ $<\rho_k \leq$ 500 kg / m³.

Table 5 Proposed values for k_{mod}

	Load Duration				
Service class	**Permanent action**	**Long-term action**	**Medium-term action**	**Short-term action**	**Instan-taneous action**
1	0.6	0.7	0.8	0.9	1.1
2	0.6	0.7	0.8	0.9	1.1
3	0.55	0.65	0.7	0.9	1.0

Acknowledgements

The mechanical testing was done at Karlsruhe Institute of Technology (KIT). The pleasant cooperation with Prof. Dr.-Ing. Blaß, Dr.-Ing. Görlacher and Ms. Glattacker (MSc) is very much appreciated.

References

[1] Hill, C.A.S., *Wood modification: chemical, thermal and other processes*. John Wiley & Sons. Chichester, England, 239, 2006..

[2] Rowell, R.M. & Dickerson, J.P., Acetylation of wood. Deterioration and protection of sustainable biomaterials, eds. T.P. Schultz, B. Goodell, D.D. Nicholas, *ACS Symposium series 1158.* American Chemical Society. ISBN 978-0-8412-3004-0, 2014.

[3] Bongers, F., Hague, J., Alexander, J., Roberts, M., Imamura Y. & Suttie, E.,. The resistance of high performance acetylated wood to attack by wood destroying fungi and termites. *Proceedings IRG Annual Meeting*, IRG/WP 13-40621, 2013.

[4] Tjeerdsma, B. & Bongers, F., The making of a traffic timber bridge of acetylated Radiata pine. *Proceedings of the Forth European Conference on Wood Modification*, pp 15-22, 2009.

[5] Jorissen, A. & Lüning, E., Wood modification in relation to bridge design in the Netherlands, *Proceedings of 11th World Conference on Timber Engineering*, 2010.

[6] Bongers, F., Alexander, J., Marcroft, J., Crawford, D. & Hairstans, R., Structural design with Accoya® wood. *International Wood Products Journal* 4(3): 172-176, 2013.

[7] Bongers, F., Marcroft, J., Perez, F., Alexander, J., Roberts, M. & Harrison, I., Structural performance of Accoya® wood under service class 3 conditions. *Proceedings of the World Conference on Timber Engineering*, 2014.

[8] Blaß, H.J., Frese, M., Kunkel, H. & Schädle, P., *Brettschichtholz aus acetylierter Radiata Kiefer*. Karlsruher Berichte zum Ingenieurholzbau / Karlsruher Institut für Technologie, Holzbau und Baukonstruktionen (Band 25). KIT Scientific Publishing, 2013.

[9] Frese, M. & Blaß, H.J., Dauerhaftes Brettschichtholz aus acetylierter Radiata Kiefer. *Bautechnik* 91, Heft 1, 2014.

[10] Karslruhe Institute für Technologie (KIT) report no. 166107 (d.d. 16-09-2016), "*Bestimmung der Tragfähigkeit und Steifigkeit von ACCOYA*".

[11] Univ.-Prof. Dr.-Ing. H.J. Blaß (d.d. 08.09.2016). *Gutachtliche Stellungnahme Acetylierte Pinus Radiata (ACCOYA) für tragende Zwecke*.

[12] Accsys Technologies, *Accoya Lumber Grading Specifications. Grade names & definitions for Accoya® Radiata pine*. Version 9.1. www.accoya.com

[13] BRL 0605:2013. *National Assessment Directive for the KOMO® product certificate Modified Timber*. Certification body SKH, Wageningen, the Netherlands.

[14] Görlacher, R, Sortierung von Brettschichtholzlamellen nach DIN 4074 duch Messung von Longitudinalschwingungnen. *Bauingenieur* vol. 65, 1990.

[15] Ravenshorst, G., Van der Linden, M., Vrouwenvelder, T., 1 and Van de Kuilen, J.W., An economic method to determine the strength class of wood species. *HERON* 49(4), pp. 297-326, 2004.

[16] Ravenshorst, G.J.P. and Van de Kuilen, J.W.G., A new approach for the derivation of settings for machine graded timber. *Wood Material Science & Engineering*, 2014.

Advantages of moisture content monitoring in timber bridges

Andreas MÜLLER[1)]
(Prof. Dipl.-Ing.)
andreas.mueller@bfh.ch
[1)] **Institute for Timber Construction, Structures and Architecture, Bern University of Applied Sciences, Biel, Switzerland**

Head of the Institute and Professor for Timber and Building Construction, Federal expert for preservation of historic buildings, public appointed representative and sworn expert with specialisation in timber construction and timber bridges.

Bettina FRANKE[1)] **(Dr.-Ing.)**
bettina.franke@bfh.ch

Marcus SCHIERE[1)] **(MSc.)**
marcusjacob.schiere@bfh.ch

Steffen FRANKE[1)] **(Prof. Dr.-Ing.)**
steffen.franke@bfh.ch

Summary

Timber road bridges are high performing structures and built worldwide for centuries. Modern timber bridges are designed for operational life cycle of 80 to 100 years. Reliable design and proper planning fundamentals, as well as the right choice of assessment method and monitoring systems, support the planning process and maintenance. The electrical resistance measurement method has proven to be suitable for the moisture content monitoring of timber bridges. The long-term monitoring of moisture content of structural components enables early interventions when discrepancies are detected at an early stage of possible damage. The monitoring results of six timber bridges showed that the wood moisture content in the load bearing cross sections under regular ambient climates was between 12 M% - 22 M%, i.e. continuously below the range for fungi decay. Numerical methods were used to estimate the dependency of moisture content of the cross section on the yearly climatic conditions.

Keywords: Structural assessment methods, moisture content monitoring, large cross sections, service class, timber bridges.

1. Introduction

The timber members for bridges can be supported, connected and protected at a high-quality level. The acceptance of wood increases through safe and reliable design and planning fundamentals. This level of quality must be maintained to further promote acceptance of timber bridges. Timber road bridges have been built worldwide for centuries. In Switzerland, historical pedestrian and road bridges made of timber are still being used. For example, the Kapellbrücke in Lucerne, was built in 1333 and is still used by pedestrians every day. The high efficiency of wood as a load bearing material is proved today through presence of many long spanned constructions. Glued laminated timber members, hybrid cross-sections, and large block glued laminated timber members replace the historic solid cross sections. Still, the durability and safety of timber bridges must be ensured for the life cycle of around 80 to 100 years. Whereas the range of the use of most bridges was from pedestrian to light traffic, a significant increase has been observed in the amount of bridges for

heavy traffic (>20 tons) after 2000 (swisstimberbridges.ch). This has led to an increased width of the main load bearing members from 200 mm to 800 mm or more. The main members of timber bridges are generally protected by construction details, e.g. closed roadway passage or hybrid bridge cross sections (timber concrete composite), against water and wind driven rain.

The daily and seasonal climate changes lead to a variation of air temperature and air humidity. Swiss winter and spring tends to be dryer whereas summer and autumn can be more humid. The timber members of the bridge adapt to the surrounding climate through the hygroscopic nature of wood. As the moisture content changes at the surface an inhomogeneous distribution of moisture content over the cross section follows. The deformations lead to the development of internal stresses perpendicular to the grain. As well, the moisture content also affects the physical and mechanical properties. Hence, the correct estimation of the moisture content is important for the design and life cycle of timber structures. Currently, the planning engineer respects this complex hygroscopic behaviour of wood in the design by the application of service classes. The design standards consider this behaviour by three different service classes (SC) corresponding to the annual average moisture content, EN 1995-1-1:2004, [1].

Modern timber bridges require a different approach to guarantee structural lifetime. As cross sections increase, visual inspection becomes more difficult. In addition to that, with frequent passage of heavy traffic, special attention must be paid to protective measures such as asphalt. Experience shows that imminent damage can be detected in an early stage of its development through moisture content measurements. The paper also discusses what the structures will experience during their lifetime, what appropriate assessment methods could be used, and which inspection periods are recommended.

2. Assessment methods

2.1 Key points in timber bridges and inspection/monitoring methods

The key points of timber bridges are e.g. the structure, cross section, bearing/support, road deck, pedestrian passage, or kerb/handrail. Focus to most detail design is to minimise the risk for development of moisture content just under the fibre saturation point or higher. To ensure the safe operation regular examination of the structure is required. Through visual inspections, minor damage at the structure's surface can be detected and repaired to prevent the need for larger repair measures later. Here, the time intervals and scopes of inspection are essential. A general annual inspection as e.g. required in the new German guideline RI-EBW-PRÜF (2013) [2], requires that wooden bridges over or close to rivers be inspected yearly due to the expected wood moisture content, but this is not necessary or essential for the wooden material. Standardized testing methods as well as guaranteeing the comparability of results of studies that are conducted at different times can considerably reduce the associated amount of effort.

Moisture content at the cross sections' surface will increase during fall and decrease during spring. Where the moisture content shows variations at the surface, it will vary close to the yearly average at the middle of the cross sections [3], [4]. The following hygro-expansion will cause the wood at the surface either to swell or shrink while the center of the cross section will not follow in this process. The different swelling and shrinking cause tension stresses to develop in the cross sections during wetting and on the surface during drying [5], [6], [7]. Stresses can be high enough to exceed tension stress perpendicular to the grain and initiate cracks. The cracks at the surface will best be visible after dry climate. The cracks at the surface of the cross section will then tend to close during wetter periods, making them harder to detect during visual inspections. Furthermore, the prescribed measurement of moisture content at the surface, as done with handheld tools, will not be appropriate for the situation in the center of the cross section. Measured real wood moisture content through installation of monitoring systems is more effective, [5], [16], [17].

2.2 Monitoring campaign of timber bridges

The developments of moisture content variations in cross sections have mainly been investigated under laboratory conditions. However, the Institute for Timber Construction, Structures, and Architecture of the Bern University of Applied Sciences monitored and assessed six timber bridges directly exposed to the climate in several research projects. All monitored timber bridges were in different climate regions of Switzerland, see Figure 1. The main girders comprised: glulam members, block glued glulam members, and timber-concrete composite members. The local climate (temperature and relative humidity) measured at the timber bridges was logged alongside climate (air temperature and relative humidity) of meteorological stations located in the vicinity (MeteoSwiss, www.meteoswiss.admin.ch). Moisture content sensors were placed at two different

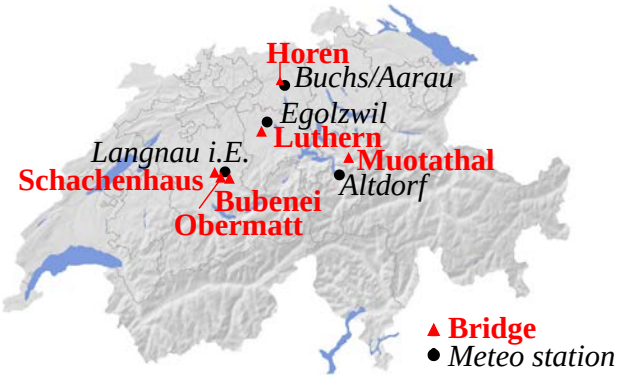

Fig. 1: Location of timber bridges monitored and close by meteorological stations

Fig. 2: Timber road bridge Horen

depths from the surface and at two different cross sections measured from the end grain. Table 1 summarizes the main construction details, monitoring periods, and measured MC values at each timber bridge. Further information and results are given in [5], [8].

Table 1: Monitoring details of the timber road bridges

Bridge/Erection Meteo station	**Characteristics**	**Measuring period/ -rate/ -system**	**Measuring values**
Horen/2008 Buchs/Aarau	Beam bridge Spruce Glulam Block glued	since Oct 2009 every 6 hours local system	20 moisture content sensors 1 air temperature sensor 1 relative air humidity sensor
Muotathal/2009 Altdorf	Arch bridge Spruce Glulam Block glued	Oct 2009 - Dec 2011 every 6 hours local system	16 moisture content sensors 4 wood temperature sensors 2 air temperature sensors 2 relative air humidity sensors
Obermatt /2007-2008 Langnau i. E.	Beam bridge Spruce Glulam	Dec 2010-2014 every 6 hours remote system	16 moisture content sensors 4 wood temperature sensors 2 air temperature sensors 2 relative air humidity sensors
Schachenhaus/2000 Langnau i. E.	Timber-concrete composite bridge	Mar 2011-2013 every 6 hours local system	8 moisture content sensors 2 wood temperature sensors 1 air temperature sensor 1 relative air humidity sensor
Luthern/2010 Egolzwil	Spruce glulam Block glued Deck of Kerto-Q	Nov 2009-Sept. 2011 Every 6 hours local system	18 moisture content sensors 1 air temperature sensor 1 relative air humidity sensor
Bubenei/1988 Langnau i. E.	Arch bridge, Spruce Glulam, Deck of cross pre stressed glulam	since July 2012 every 12 hours local system	24 moisture content sensors 1 air temperature sensor 1 relative air humidity sensor

2.3 Laboratory tests

The observation of the development of moisture content over the cross section, test series were prepared specifically in the three material axes: radial (R), tangential (T) and longitudinal (L), [5]. Two different sizes (200/200/200 mm and 200/ 200/800 mm) per material axes were considered, see Fig. 3. The side faces of the test specimens were sealed, so that the moisture diffusion only could take place in one of the principal material directions. On each specimen, gauges at a depth of 25, 45, 70 and 100 mm from the unsealed surfaces were implemented. For the test series with 200/200/800 mm in size, additional measuring points in a depth of 150, 200, 300 and 400 mm were installed. The specimens were conditioned at 20 °C and 65 %RH before and during the preparation and loaded afterwards with 95 %RH for a period of about 12 months. The electrical resistance method was used for the determination of the moisture content using a pair of insulated stainless steel screws as sensor. A Thermofox and Gigamodul from Scanntronik Mugrauer GmbH were used to log measurements every 6 hours.

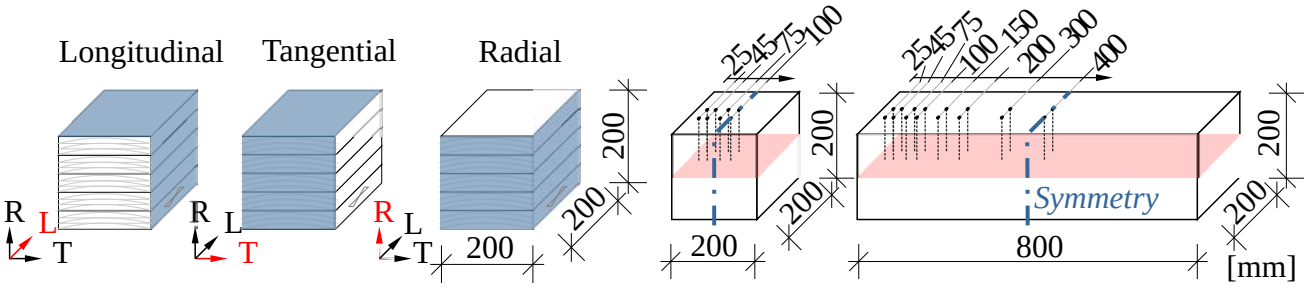

Fig. 3: Test specimens with sealed surfaces in blue (top) and position of measuring points for the 200 mm and 800 mm long specimens (bottom)

2.4 Numerical model for the moisture diffusion transport

The numerical simulations include the moisture diffusion transport in wood as well as the resulting stress strain behaviour of the timber member. These numerical methods can be used to estimate and calculate the cross-sectional dependency on the outer climatic loads. This helps to understand annual moisture content developments in timber cross sections as well as investigate differences between measurements and expectations. The moisture diffusion was modelled by a single phase Fickian law, which is one of the simpler models available. In case of wetting processes, Fickian moisture diffusion is expected to give a good approximation of the actual process. In case of drying, non-Fickian moisture diffusion is often preferred over Fickian diffusion. This means that extra input parameters have to be given to properly simulate the evaporation of moisture from the wood surface. However, the drying process in the simulation was modelled through a Fickian process as well.

In the finite element program ANSYS®, a 2D numerical model was set up to simulate the moisture diffusion. Linear 4-node plate elements with a regular mesh size of 5 mm were used. The time step size in the calculations was set to a constant interval of 0.1 day. This mesh and time step size was determined through a convergence study, which resulted in an uncertainty of less than 0.1 M% compared to automatic time stepping and 1.25 mm mesh size, [9].

The numerical simulations made with the model were compared to experimental values. This was done e.g. for both wetting and drying process by Jönsson (2004), [9] or Angst (2012) [11], [12] as shown in [10]. For the own experiments, the diffusion values for validation of the wetting experiments of the 200 mm wide beams were derived in [10]. The values for longitudinal diffusion was 10.42e-10 m^2/s. The diffusion values for radial moisture diffusion were higher than for tangential diffusion, 2.89e-10 m^2/s and 1.61e-10 m^2/s, respectively. Both were modelled as constant values. The wetting process was simulated from 12 M% to 20 M%, see Fig. 6.

3. Research results

3.1 Timber bridges

The moisture content developments of six timber bridges were monitored continuously for several years. The moisture content adapted to the daily and seasonal surrounding climatic conditions. Whereas the outer parts responded more direct to the ambient climate loads, the inner parts responded slowly and with significant time lag, as shown in e.g. in Fig. 4. The moisture content is shown for sensors close to the surface (MC-S) and sensors at a depth of 200 mm (MC-D). The equilibrium moisture content at the surface was calculated [14] according to the measured ambient climate and temperature and added to the figure as comparison. Theoretically, the equilibrium moisture content is valid for the complete cross section at a constant climate. The moisture content measured in the timber cross section follows the seasonal effective climate changes. The response in the centre of the cross section is delayed along with lower variations for both sensor locations compared to the calculated equilibrium moisture content. The moisture content at the surface gauges varies between about 14 %M and 20 M%. The variation of the moisture content at the surface varies about 5.5 M% around the mean between the summer and winter period.

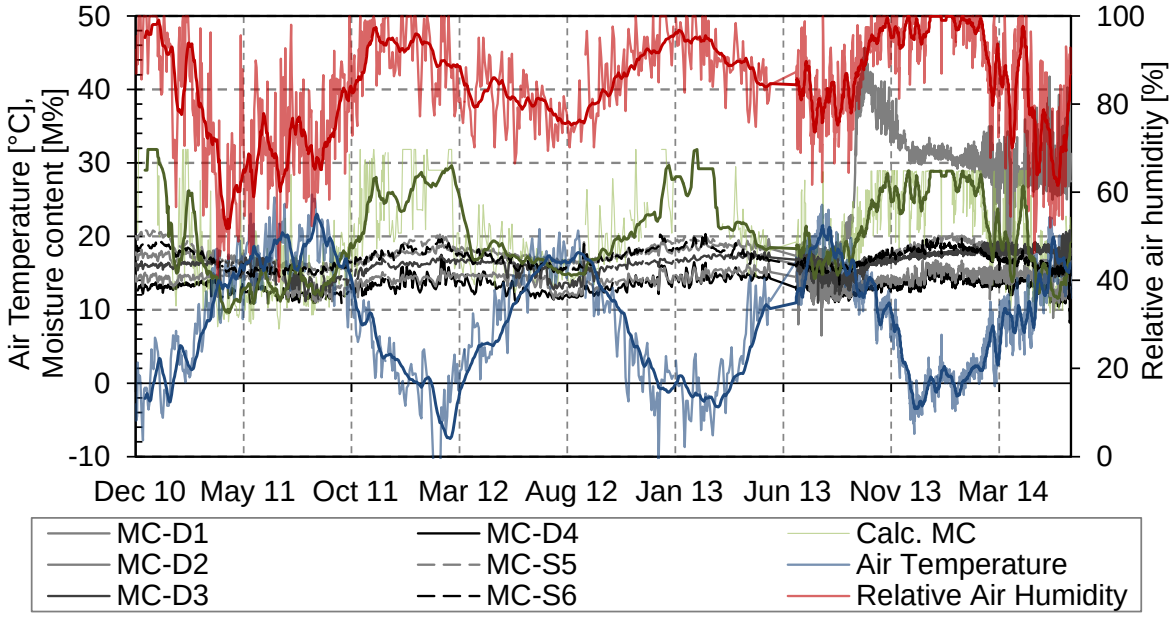

Fig. 4: Timber bridge Obermatt, Measured climate and moisture content and calculated equilibirum moisture content

Table 2: Comparison of the equilibrium moisture content according to meteorological stations and the moisture content measured

Bridge / Meteo station	**Measuring period**	**Moisture content - mean value [M%]**	
		Bridge meas.*	**Meteo calculated**
Mouthatal / Altdorf	15 month	16.6	15.9
Horen / Buchs	12 month	16.4	17.5
Luthern / Egolzwil	14 month	13.5	20.5
Bubenei / Langnau	25 month	22.5	24.7
Obermatt / Langnau	45 month	18.1	20.3
Schachenhausen / Langnau	23 month	17.0	20.5

* Mean value of every measuring point close to the surface

The curves of the moisture content at the inner structure are more stable, with variations of 2.5 M% around their mean. The extra difference of 3 M% observed between the inner and outer moisture content sensors results in internal moisture induced stresses. The phase shift between the theoretical calculated equilibrium and measured moisture content is about 2 to 3 months. Overall, the measurements showed that the wood moisture content in the beam cross-sections under ambient climates was between 12 - 22 M%, which is continuously below the range for fungi decay, [5], [8]. It could, furthermore, be shown that well-planned structures show similar results and are required to guarantee a long service life.

For the planning phase of timber bridges, the analyses of the ambient climate on the bridge and the regional climate by a close by meteorological station were compared. Differences were observed between the two. The comparison with a nearby meteorological station shows differences which reach up to 6 M%, see Table 2. For each case, the same measuring period was used for which the mean values can differ for the same meteorological station. It is concluded that the local effects regarding the location and type of obstacle (e.g. water or road crossing) should not be neglected. Further influences on the ambient climate due to constant shadows, flora, and wind also play a role. A positive result is that the moisture content calculated from climate at the bridges is lower than the one calculated from the meteorological stations in 5 out of 6 cases.

After the erection, the ambient climate will induce a moisture gradient in the cross section starting at a moisture content of 8 M% – 12 M % while coming from the production line and entering ambient climate conditions.

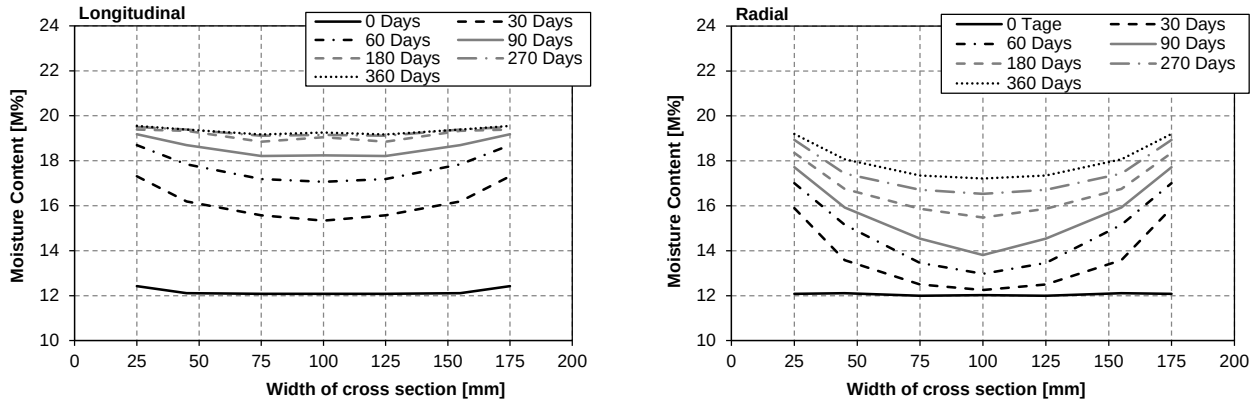

Fig. 5: Results of wetting process of 200/200/200 mm test series in longitudinal and radial direction

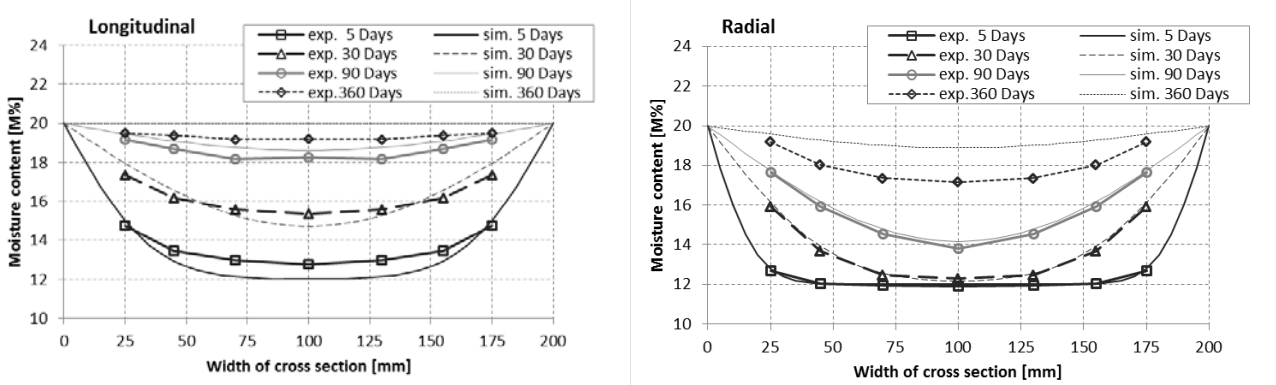

Fig. 6: Comparison of experiments and simulations of wetting process in radial and tangential direction of a 200 mm wide beam

3.2 Laboratory test results and numerical simulations

The moisture distribution in the cross section for the measuring period for the 200/200/200 mm test soon reached a plateau in longitudinal direction, roughly after 90 days. However, in radial and tangential direction, an increase of the moisture content was still present after 360 days, illustrating the slower process of wetting, as shown in Fig. 5, [5]. It must be pointed out, that the plateau reached is at 20 M%, whereas the equilibrium moisture content according to the climate of 20°C/95% is 24 M%. The oven dry method carried out after the tests confirmed a moisture content of 24 M%. After measurements were finished it was observed that, although galvanised, the screws showed corrosion. This may affect the measurement of moisture content. This could be considered by determining an additional time dependent calibration factor. However, the comparison of the measurement with the two numerical simulations should not occur and other materials should be used.

Comparisons between simulations and experiments overlap over at least the first 90 days of the experiments. Afterwards, differences are observed and they become larger over time, although the differences barely exceed 1 M%, as shown in Fig. 6.

This is most likely due to non-Fickian effects taking place as moisture content in the cross-section approaches equilibrium moisture content [13]. This is not accounted for in the numerical model. The measurement might also be affected by corrosion affecting the measured resistance between the gauges.

Discussion

The measured moisture content on timber bridges show a wide variation compared to other structures e.g. agriculture building, ware houses, or halls, but can still be assigned to Service Class 2, as shown in Fig. 7. The timber bridge of Bubenei is the only bridge with higher moisture content. This is related to the monitoring system being was installed after repair of a leaking deck to monitor the drying process. These values are not used for further discussions. Fig. 7 includes the measured moisture content on timber bridges as mean values, minimum and maximum from a gauge close to the surface and the equilibrium moisture content calculated from the local ambient climate. The comparison confirms again that the ambient climate at a bridge needs to be considered carefully and that the simply use of information from nearby meteorological stations can lead to overestimations of the moisture content. The presented results are important guidelines for planning engineers, since recommendation of assignment of timber structures to service classes are not available in the standards.

The distribution of the moisture content over the cross section could be experimentally and numerically determined during an intensive adsorption process by 20 °C and 95 %RH. For two different sizes and three material directions, the distribution over the cross section was determined, as shown in Fig. 8 or [5]. The measured distribution over the cross section was extrapolated to the surface according to the resulting equilibrium moisture content calculated from the climate. The distribution of the moisture content along the radial or tangential direction is not converged after one year of an intensive adsorption process, [5], [6], [7]. Daily or weekly climate changes like experienced by timber bridges result in a change of moisture content in the outer zone of the cross section, which is relatively small for more modern type of cross sections of large timber bridges. Fig. 9 shows a numerical result the moisture content at different material depths on a 200 mm wide cross section subjected to ambient climate.

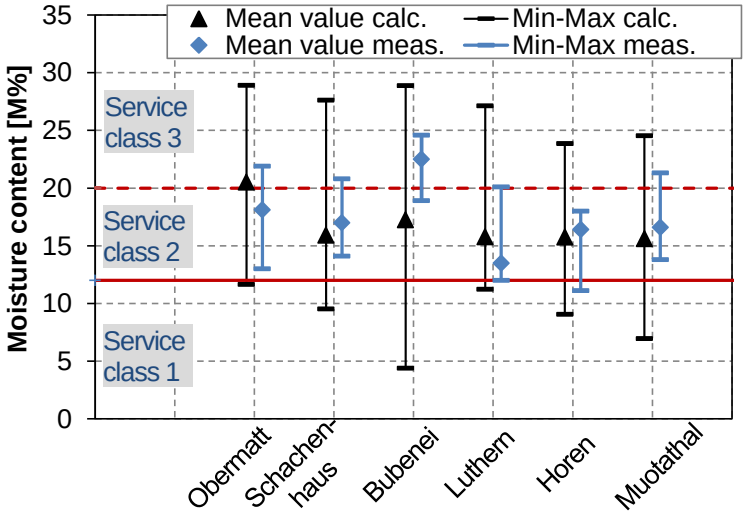

Fig. 7: Average moisture content in typical timber building constructions and relation to service classes according EN1995-1-1:2004

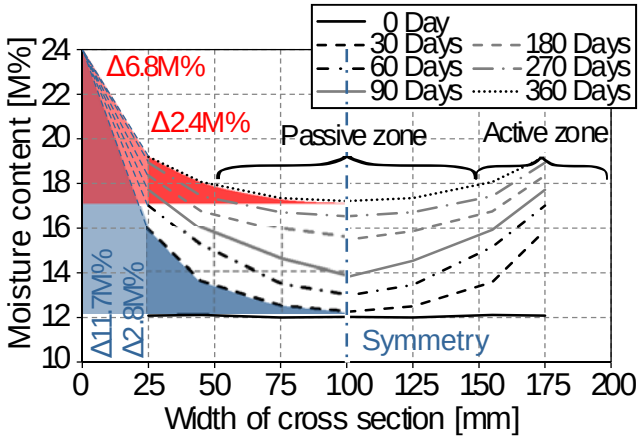

Fig. 8: Experimental results of moisture distribution in radial direction for the adsorption process, 200/200/200 mm

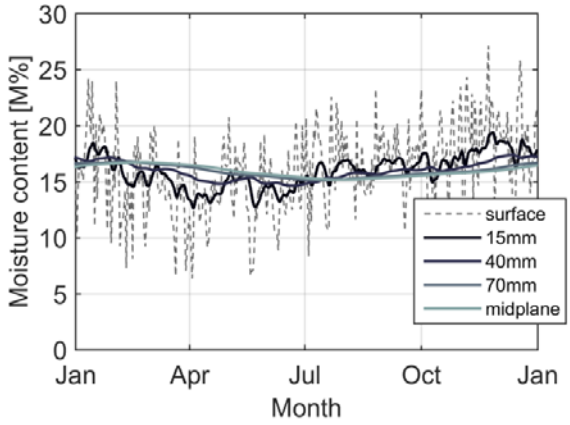

Fig. 9: Seasonal moisture content developments on a bridge on a 200 mm wide beam

The analyses of the experimental and numerical results show that the moisture content distribution over the cross section allows a division in an active and passive zone. Currently, only a constant service class is used for the design. It is suggested to differentiate the service class over the cross section, as shown in Fig. 10. The existing load capacities (active zone = SC 3, passive zone = SC 2) could increase the capacity of the structure, depending on its location and operational conditions. Another suggestion could be to calculate the bridge cross section according to a Service Class 2, and use a margin of active zone as a buffer zone to take the climatic variations. The definition of the active zone can be delicate though. A theoretical analysis using the shrinkage swelling mass show that a difference greater than 1.5 M% is enough to increase allowable stress levels over the tension strength perpendicular to the grain, as shown Table 3.

4. Conclusions and recommendations

Results observed from the long term monitoring of six timber bridges provide first guidelines for designers. High frequent changes in the surrounding ambient climate show little influence on the global distribution of moisture content. Only long wetting phases like in the fall lead to a measurable increase of the moisture content in the timber bridge cross sections. Parameters like the

Table 3: Theoretical limits of the moisture content for the risk of fracture of the cross section, material characteristics according [6].

Material direction	Shrinkage/ Swelling mass for Spruce	Modulus of Elasticity E [MPa]	Tension strength f_t [MPa]	Limit of moisture content
Longitudinal	α_L = 0.01 %/M%	10'000	80	> 80 M%
Radial	α_R = 0.19 %/M%	800	2.7	> 1.8 M%
Tangential	α_T = 0.39 %/M%	450	2.7	> 1.5 M%

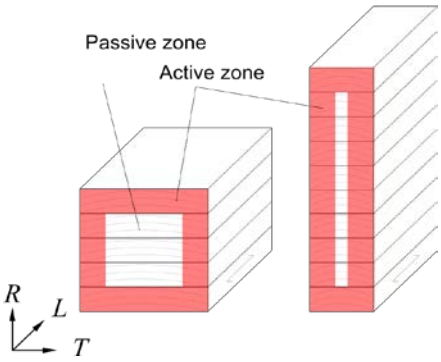

Fig. 10: Differentiation of cross section in active and passive zone

air flow around the bridge, the orientation and location with respect to microclimatic effects influence the developed moisture content distributions.

Through the electrical resistance method, moisture content in structural cross sections can be found in a range of 12 M% - 22 M% under the present climate situations. In all six cases the moisture content was below the critical level for fungi decay. Experience has shown that if adequate measures are taken against leakage of bridge decks, attention is paid to detail design, timber bridges can be appointed a long service life.

The research results provide new guidelines for the planning engineers for the assignment of service classes. The analysis of ambient climate data of timber bridges allows a first characterization according to the service classes. An annual assessment of timber bridges, as e.g. required in the German guideline RI-EBW-PRÜF [2] for timber road bridges over/close to water, can be questioned. The experiences show that the application of monitoring systems is more efficient and insight into structural health of large timber cross sections can be obtained. The monitoring system can track changes in the ambient climate and detect possible leaks in the construction.

Through simulations, insight was gained on moisture content developments on large cross sections. The numerical model was validated on experimental test series and published experimental results. The numerical simulation could successfully be applied to a case study of a timber road bridge. The experimental and numerical results support scientific as well as the planning engineers.

Finally, introduction of an active and passive zone in structures could enhance the load bearing capacity of structures. As shown through simulations, maximum moisture contents for the inner part of the cross section (passive zone) are below 20 M. Service Class 2 could be applied. Daily or weekly climate changes result in a change of moisture content only in the surface of the cross section, which is relatively small for example for the cross section of large timber bridges.

5. Acknowledgements

The research work was proudly supported by the Federal Office for the Environment (FOEN) and the industry partners Roth AG, Makiol and Wiederkehr, and Tiefbauamt des Kanton Bern.

6. References

[1] Eurocode 5, Design of timber structures - Part 1-1: General and rules for buildings. CEN. (EN 1995-1-1), 2004

[2] RI-EBW- PRÜF, Bundesministerium für Verkehr, Bau und Stadtentwicklung: Richtlinie zur einheitlichen Erfassung, Bewertung, Aufzeichnung und Auswertung von Ergebnissen der Bauwerksprüfungen nach DIN 1076 (RI-EBW-PRÜF), 2013

[3] Häglund M., Varying moisture content and eigen-stresses in timber elements. *Wood Materials, Science Engineering*, pp. 38–45, 2008

[4] Fragiacomo M., Fortino S., Tononi D., Usardi I., Toratti T., Moisture-induced stresses perpendicular to grain in cross-sections of timber members exposed to different climates, *Engineering Structures* (33), p. 3071-3078, 2011

[5] Franke B., Müller A., Franke S., Magniere N., Langzeituntersuchung zu den Auswirkungen wechselnder Feuchtegradienten in blockverleimten Brettschichtholzträgern, Research Report, ISBN 978-3-9523787-7-9, 2016.

[6] Franke B., Franke S., Müller A., Schiere M., Long-term behaviour of moisture content in timber constructions – Relation to service classes. INTER, Graz, 2016.

[7] Franke B., Franke S., Schiere M., Müller A., Moisture diffusion in wood – Experimental and numerical investigations, WCTE, Vienna, 2016.

[8] Franke B, Franke S, and Müller A., Case studies: long-term monitoring of timber bridges, *Journal of Civil Structural Health Monitoring* 5, p. 195-202, 2015.

[9] Schiere M., *Moisture diffusion and moisture induced stresses in glulam cross sections*, Master Thesis, Bern University of Applied Sciences, Switzerland, 2016.

[10] Jönsson J., Internal stresses in the cross-grain direction in glulam induced by climate variations, *Holzforschung* 58, pp. 154–159, 2004.

[11] Angst-Nicollier V. (2012), *Moisture induced stresses in glulam - effect of cross section geometry and screw reinforcement.* PhD thesis, NTNU Trondheim, Norway, Doctoral Theses 2012:139.

[12] Angst V. and Malo K. (2010), Moisture induced stresses perpendicular to the grain in glulam: a review and evaluation of the relative importance of models and parameters. *Holzforschung*, 64(5), p. 609–617

[13] Frandsen, H., Damkilde, L., Svensson, S., A revised multi-Fickian moisture transport model to describe non Fickian effects in wood, *Holzforschung* 61, 563-572, 2007

[14] Simpson W., Predicting equilibrium moisture content of wood by mathematical models, *Wood and Fiber*, 5(1), p. 41-49, 1973.

[15] Grosser, D., Zimmer, B., *Einheimische Nutzhölzer und ihre Verwendung*, holzbau handbuch R4/T2/F2, Informationsdienstholz, Düsseldorf, 1989

[16] Dietsch P., Franke S., Franke B., Gamper A., Winter S., Methods to determine wood moisture content and their applicability in monitoring concepts, *Journal of Civil Structural Health Monitoring* 5, 115–127, 2014

[17] Dietsch P., Gamper A., Merk M., and Winter S., Monitoring building climate and timber moisture gradient in large-span timber structures, *Journal of Civil Structural Health Monitoring 5*, p. 153-165, 2015.

Moisture monitoring of nine protected timber bridges in Germany

Johannes KOCH
Research assistant
Fachhochschule Erfurt
University of Applied Sciences
Erfurt, Germany
johannes.koch@fh-erfurt.de

Johannes Koch, born in 1991, received his M.Eng. by Fachhochschule Erfurt - University of Applied Sciences (FHE) in 2015. Since 2016, he is a scientific researcher in the project “Protected Timber Bridges” at FHE.

Ralf W. ARNDT
Prof. Dr.-Ing. Chair for building material science and building diagnostics
Fachhochschule Erfurt
University of Applied Sciences
Erfurt, Germany
ralf.arndt@fh-erfurt.de

Ralf W. Arndt, born in 1970, received his diploma and his doctor’s degree by TU Berlin. After being a PhD student and scientist at the Federal Institute for Materials Research and Testing in Berlin (BAM), he was postdoc at US Federal Highway Adminis-tration and Rutgers University from 2008 to 2012 and assistant professor at FIU in Miami till 2013. Since 2014 he is at FHE.

Antje SIMON
Prof. Dr.-Ing. Chair for timber construction
Fachhochschule Erfurt
University of Applied Sciences
Erfurt, Germany
antje.simon@fh-erfurt.de

Born in 1970,
Civil Engineer since 1994,
Project leader and head of design of civil engineering structures at an engineering office for 10 years,
Thesis in the field of timber-concrete-composite road bridges in 2008,
Professor for timber construction since 2011

Markus G. JAHREIS
Research assistant
Fachhochschule Erfurt
University of Applied Sciences
Erfurt, Germany
markus.jahreis@fh-erfurt.de

Markus Jahreis, born 1975, is a Civil Engineer since 2001 and was seven years employed as engineer and site manager in a company for rehabilitation. For ten years he was a research assistant at the chair of timber and masonry engineering at the University of Weimar and since 2017 at the FH Erfurt.

Summary

Timber bridge construction has a millennia-old tradition in building history. Even though other building materials have become more popular in the last century, timber is still able to compete, especially if it is protected against precipitation and moisture ingress. This is the most important prerequisite for designing durable timber structures because a low moisture content is the key to durability. In fact, load-bearing members of timber bridges should be designed as protected members to prevent the negative influence of precipitation and moisture ingress [1]. To raise the acceptance of timber bridges, the efficiency of structural protective measures is evaluated in field tests under real boundary conditions. Therefore, a monitoring program was initiated to investigate the moisture content and ambient climate conditions of nine protected timber bridges by long-term measurements. This paper describes set-up and application of the monitoring system. First measurement results will be presented.

Keywords: monitoring, moisture monitoring, timber moisture content, protected timber bridges, structural protection, structural protective measures

1. Introduction

Timber bridges have been seldom built in Germany in recent years. Building owners often have considerable reservations to invest in timber bridges. High maintenance costs as well as low durability and a short service life are often their concerns.

However, wood is a great building material because it is the only renewable raw material that can be used for engineering structures. Produced in sustainable forest management, it will be also available in the future. One more big advantage is the ability of carbon storage for the whole service life of a structure. This property can help to counteract the global climate change. Hence, the usage of timber should be increased in general and particular in bridge construction.

Durability should not be a problem for timber bridges if the members are structural-protected. This principle has been established in the German-speaking countries as a modern and ecological method for designing timber bridges without chemical wood protection measures. The German national annex of Eurocode 5 Part 2 [1] requests the protection of load bearing members of timber bridges. Structural timber protection measures are roofs and roof overhangs as well as claddings and coverings, examples of which can be seen in Fig. 1. Hence, low durability, short service life and high maintenance costs should be not an issue if the principle of structural protection is followed. A monitoring program has been initiated to verify this approach and increase the acceptance of the natural building material timber as a real option for new bridge structures.

Fig. 1: Examples of structural protective measures – roof, housing, cladding, metal sheet, roof overhang and timber concrete composite structure

2. Monitoring nine protected timber bridges

2.1 Initiation of a monitoring program

The most important aim of the monitoring program is the demonstration of durability of well-protected timber bridges. Therefore, nine structural protected timber bridges were equipped with a monitoring system for measuring moisture content and ambient climate conditions for a period of two years or more. The concept of the monitoring is to evaluate the durability on basis of the long-time timber moisture level.

This is based on the fact that high moisture content above the fibre saturation point (around 30 mass %) could be dramatically for timber structures because fungal decay could occur. Also, even lower moisture contents of more than 20 mass % over an extended period of time could be problematic, fungal growth and organic destruction could not be ruled out [2]. Hence, if the moisture level is permanently lower than 20 mass %, fungal growth in unlikely and might even be impossible. The bridge would be durable and a long service life should be reached.

Another aim of the monitoring is the investigation of the influence of specified local climates on the timber moisture content. Close distance to waters and spray over roads or waterfalls could be the reason for problematic climate conditions. It is investigated how much the moisture content increases as a result of these influences in contrast to other locations, without those influences.

2.2 Operating principle of the monitoring system

The monitoring system works on the principle of the electrical resistance method and has been used in other research activities before [3], [4], [5]. This method is based on the dependence between electrical resistance and material moisture content. The electrical resistance decreases if the moisture content increases.

To measure the moisture content, electrodes have to be installed in the timber members of the bridges. The electrodes are made of stainless steel screws of different lengths. Preliminary, other types of electrodes were tested. It turned out that screws are more convenient for exact and comprehensible results compared to sharpened threaded rods and glued-in steel cables [6] [7]. The screws are partly insulated with a shrinking tube to measure the moisture content in a well-defined depth of the cross section. The aim is to gain more information about the moisture distribution within the cross section, because there is an active and a passive zone. In the inner passive zone, there is a small variation of the moisture content, while the outer active zone is characterised by a larger range of changing moisture content. As a result of this behaviour strong internal stresses can happen. Therefore, cracks in the members cannot be ruled out [8].

The wood species have an influence on the measuring principle. Therefore, calibration curves are required for each wood species. Seven of the nine bridges that are part of the program were built with glulam made of spruce. Two bridges are made of larch.

Another relevant influencing factor is the temperature of the material [9]. Therefore, additional sensors are required for measuring the timber temperature close to the electrodes. This allows a temperature compensation of the measured timber moisture values to produce more precise results.

Climate sensors were additionally installed to investigate the local climate conditions. These sensors were placed close to the moisture and temperature measurement points at the most measuring areas.

All measured values are saved by data loggers and sent by a remote data transmission device via mobile network, week by week. Only for one of the bridges, this way of data transmission is impossible, because it is located in an area, where no mobile network is available. The data has to be downloaded manually two times a year.

2.3 Bridges of the program

The nine selected bridges are spread out all over Germany, as shown in Fig. 2. Furthermore, different typical structure are taken into consideration, as there are timber concrete composite (TCC) bridges, through bridges, arch bridges, truss bridges and beam bridges. They are also shown in Fig. 2 by different colours.

The bridges in Höngesberg, Schiffarth and Wippra are road bridges. The other bridges are pedestrian bridges and cycle path bridges.

All bridges span over rivers and the truss bridge, which is located in Lörrach, spans additionally over a road. These locations were selected to investigate some specified climate conditions resulting from moisture exposition by waters or spray as a result of the traffic.

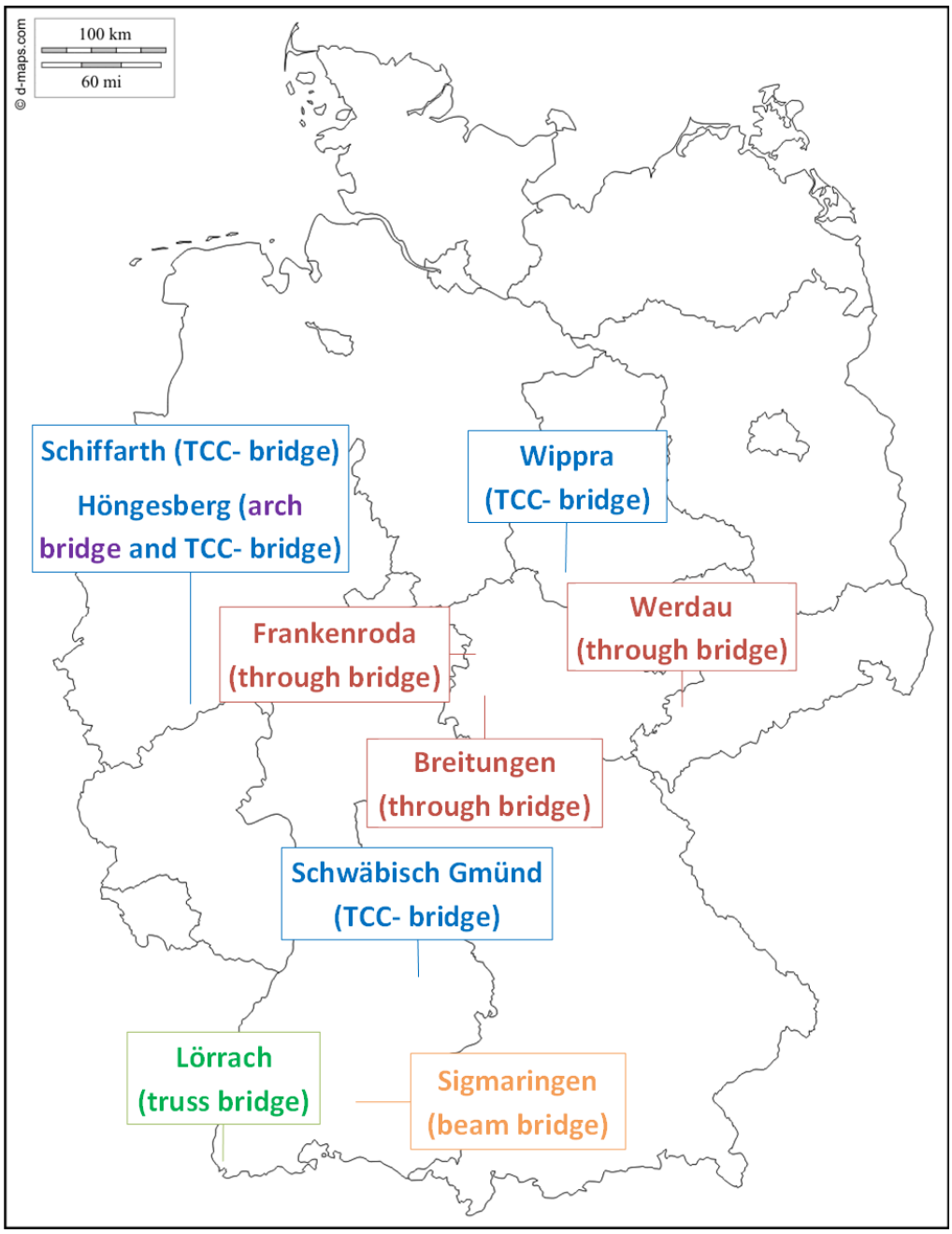

Fig. 2: Location and structure of the monitored bridges

2.4 Implementation of the system

The first bridge, which is located in Höngesberg, has been equipped with a monitoring system in August 2015. The other bridges have been equipped in October and November 2016.

Each bridge contains a minimum of two measuring areas at load bearing members. One measuring area has always been placed above a river. The second one has been placed above the foreland, usually near to the abutment. This arrangement should enable the investigation of influence of close distance to waters on the ambient climate conditions and on the timber moisture content. At a few bridges, a third measuring area has been implemented at points of special interest e.g. at secondary members beneath the bridge deck or above a road in an area of spray exposition.

The measuring areas have been equipped in a similar way as shown in Fig. 3. From two up to four pairs of electrodes were always implemented in several depths. Four pairs of electrodes can be seen in Fig. 3. The measuring depths in this example are 20, 40, 60 and 100 mm. As

shown in the figure, a temperature sensor (red cable) is usually implemented close to the electrodes. That is a necessity for the temperature compensation of the moisture values. Last component is the sensor for measuring the ambient climate conditions, air temperature and relative humidity. Fig. 3 it can be seen as the small black case between the electrodes and the temperature sensor.

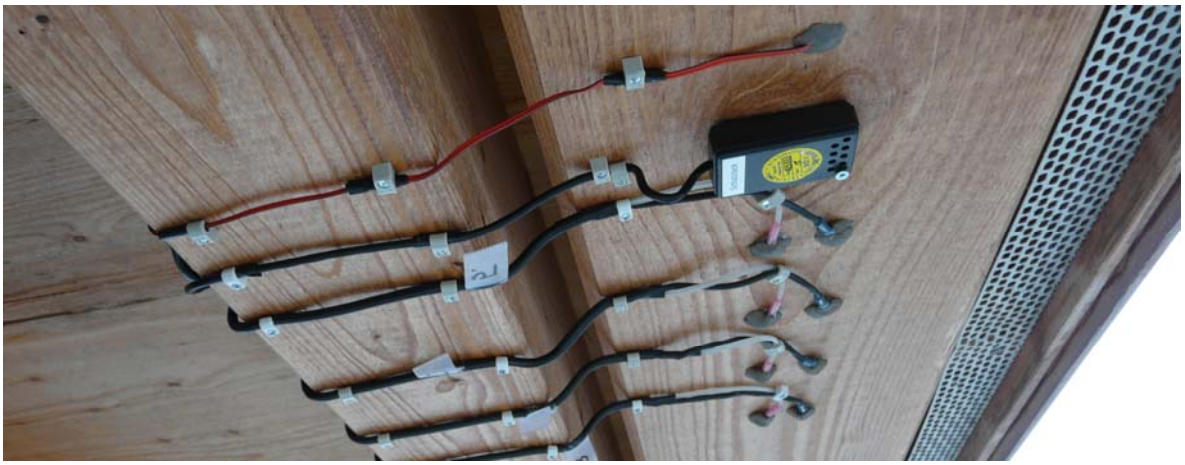

Fig. 3: Example of a measuring area at the cycle path bridge in Frankenroda

2.5 Analysis of the data

The collected data is analysed with the following steps. First, the timber moisture content is calculated from the measured electrical resistance by using the calibration curve for the respective wood species. The second step is the temperature compensation to correct the moisture content.

The climate conditions are displayed as a calculated equilibrium moisture content that would theoretically result on the surface of the members because of the hygroscopic behaviour of wood. The calculation of the equilibrium moisture curve is based on A. J. Hailwood's and S. Horrobin's "two hydrate sorption model" (Equation 1) [10] in combination with the material specific parameters by W. T. Simpson from 1973 (Equations 2 to 5) [11].

$$u = \frac{1800}{M_p} \cdot \left[\frac{K \cdot h}{1 - K \cdot h} + \frac{K_1 \cdot K \cdot h + 2 \cdot K_1 \cdot K_2 \cdot K^2 \cdot h^2}{1 + K_1 \cdot K \cdot h + K_1 \cdot K_2 \cdot K^2 \cdot h^2} \right] \quad (1)$$

$$M_p = 330 + 0{,}452 \cdot T + 0{,}00415 \cdot T^2 \quad (2)$$

$$K = 0{,}791 + 0{,}000463 \cdot T - 0{,}000000844 \cdot T^2 \quad (3)$$

$$K_1 = 6{,}17 + 0{,}00313 \cdot T - 0{,}0000926 \cdot T^2 \quad (4)$$

$$K_2 = 1{,}65 + 0{,}0202 \cdot T - 0{,}0000934 \cdot T^2 \quad (5)$$

where h = relative humidity and T = air temperature

3. First results of the pilot bridge

A road bridge that spans over the little river Agger has been already equipped with a monitoring system in August 2015. The bridge is located in Lohmar Höngesberg near Cologne in North Rhine-Westphalia and was built in 2014. It is a fully protected timber arch bridge with two timber concrete composite foreland bridges. All timber members of the load bearing structure are made of glued laminated spruce.

Fig. 4: Road bridge in Höngesberg

Three measuring areas have been implemented, whereby two of them are close together above the river. The first measuring area has been set up at the tie beam of the arch that is made of glulam. Two pairs of electrodes have been chosen to measure the moisture content in depths of 20 and 100 mm. The same configuration has been chosen at the second measuring area, close to the first one. It has been implemented in the bridge deck, which is completely made of glulam. Furthermore, a temperature measuring point and a climate measuring point have been placed. Both measuring areas can be seen in Fig. 5.

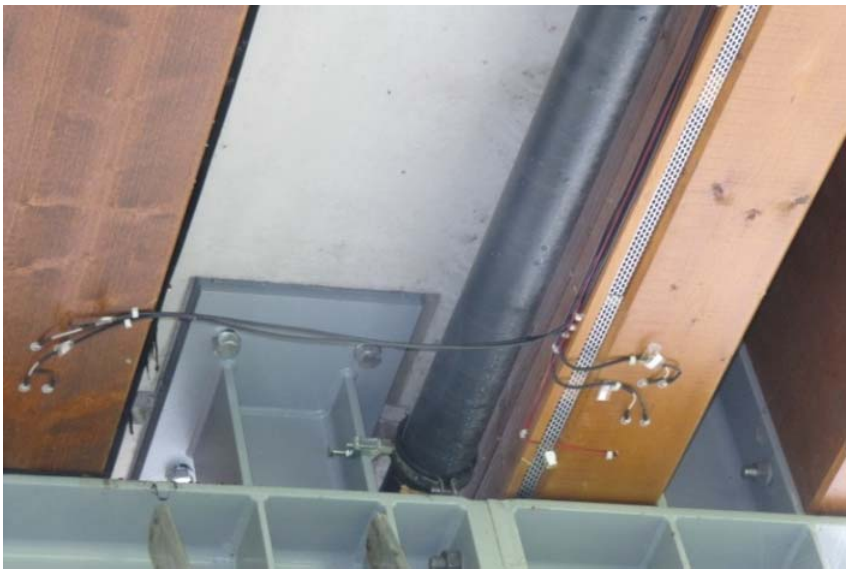

Fig. 5: Two measuring areas above the river at the bridge deck (left) and the tie beam (right)

The third measuring area has been placed above the foreland at the end grain of a main girder. The timber moisture content is measured in depths of 20, 60, 100 and 135 mm, a temperature sensor has been implemented nearby. The measuring area is shown in Fig. 6. A climate sensor was later set up, in October 2016.

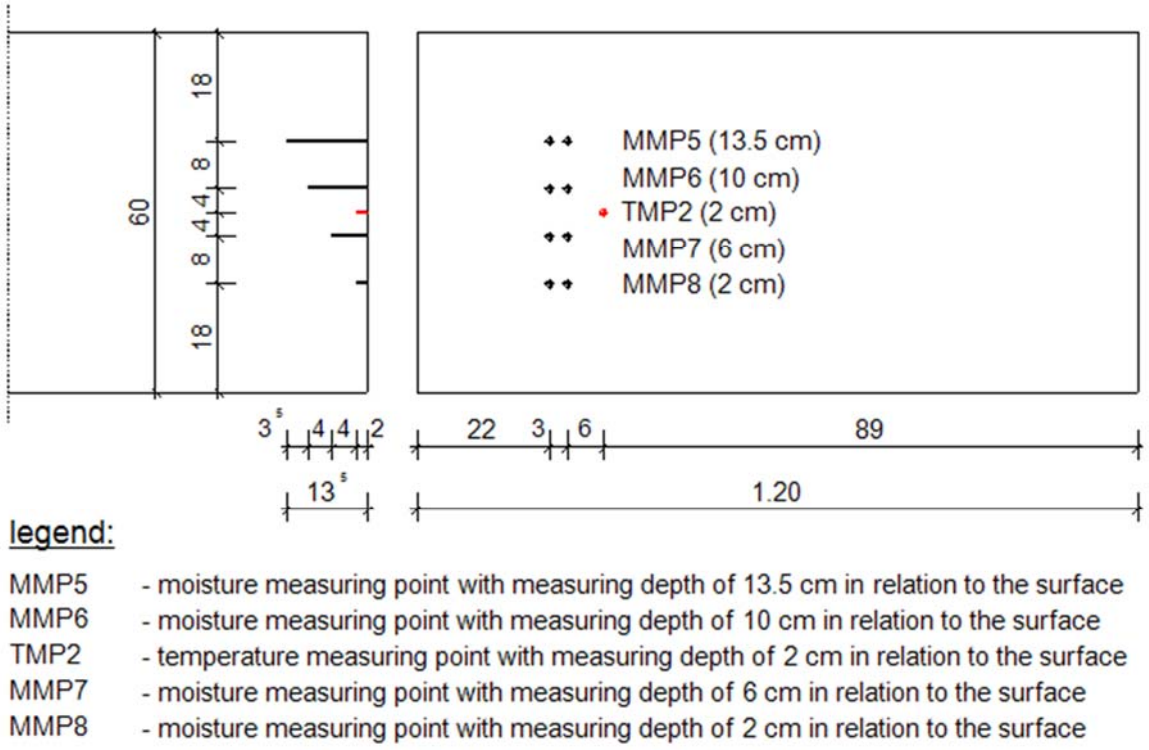

Fig. 6: Measuring area above the foreland at the end grain of a main girder; longitudinal section (left) and view on the end grain (right)

The results of the monitoring are displayed in the diagrams of Fig. 7, Fig. 8 and Fig. 9. The diagrams show the timber moisture content at the different measuring depths and the equilibrium moisture contents, which were calculated from the ambient climate conditions. The diagrams show a three-day moving average of the determined timber moisture content and equilibrium moisture content. On the one hand, the average was chosen to smooth the day and night oscillation and very short periods of extreme climatic conditions, which are not relevant for the long-term view. On the other hand, the period of moving average was chosen as short as possible to display even unexpected peaks, e.g. as a result of penetrating water.

The measurement results of the measuring areas above the river are shown in Fig. 7 and Fig. 8. It turned out that the timber moisture content did not exceed the 20 mass % limit for most of the time of the first 14 months. During the winter 2015/16, a mean increase of 3 mass % has been recognised. In winter 2016/2017 it was much colder than in the year before. As a result, the moisture content increased partly up to 24 mass %. However, for most of the time the moisture content remains around 20 mass %. A similar development was observed at the third measuring area above the foreland in the second winter. This behaviour has to be kept in mind.

The average timber moisture content is around 17.4 mass % for the whole measuring period of both measuring areas and both measuring depths. This is close to the average of the equilibrium moisture content above the river that is around 17.8 mass %. Therefore, in the present stage of knowledge, it can be assumed that the structural protection measures achieve the expectations.

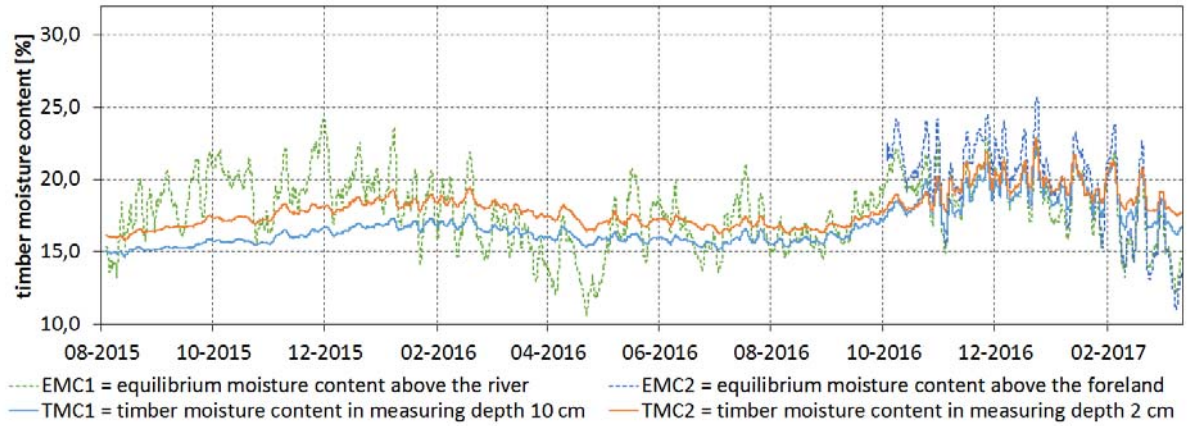

Fig. 7: Measurement results of the measuring area at the tie beam above the river

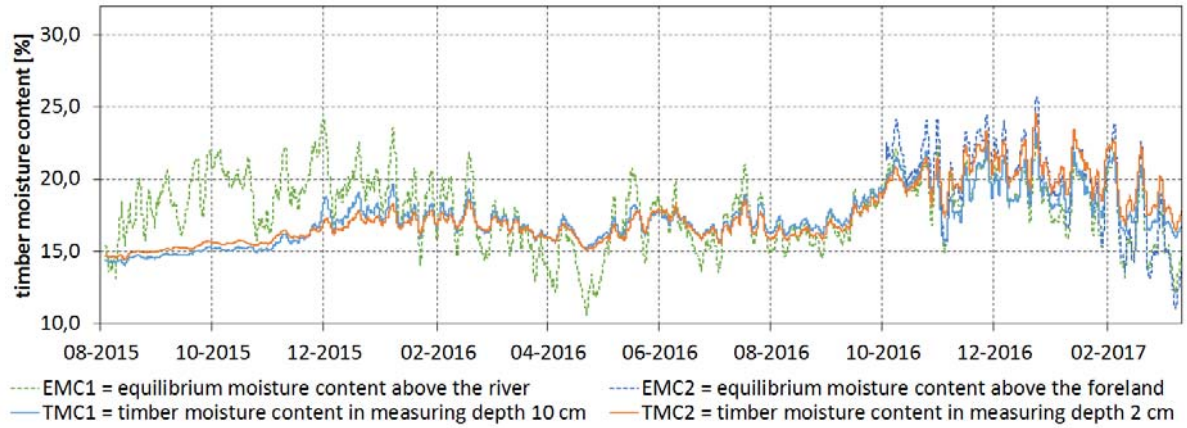

Fig. 8: Measurement results of the measuring area at the bridge deck above the river

Fig. 9 shows the development of the timber moisture content of the measuring point above the foreland. The moisture content increased strongly in November 2015 and in the first quarter of 2016. Moisture values were observed high above the fibre saturation point. An inspection revealed that the expansion joint had a leak, exactly above the measuring area. Hence, rainwater penetrated the structure and ran over the measuring area. A ventilated cladding was installed at the end grain of the beams to protect them against the penetrating water. The work was done in April 2016 and it can be seen that the timber moisture content decreased in summer. This demonstrates the high influence of structural protective measures on the timber moisture content. A simple installation of a cladding improved the situation considerably.

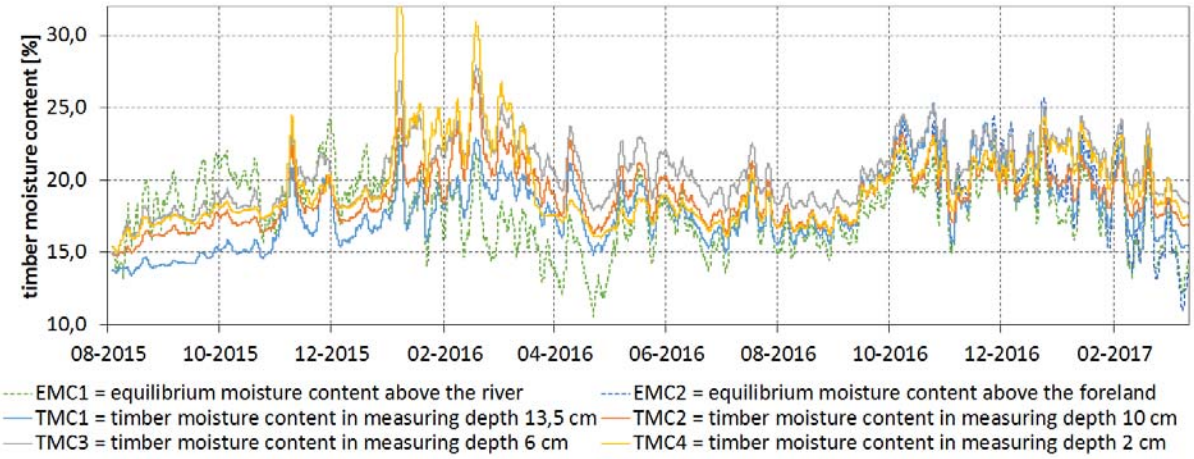

Fig. 9: Measurement results of the measuring area at a main girder above the foreland

4. Further results

Another indicator for the effectiveness of the protective measures can be seen in Tab. 1. It contains the average of the measured timber moisture contents for the different measuring areas at all bridges. The evaluation period of Höngesberg is more than one and half a year from August 2015 to March 2017. The evaluation period of the other bridges is around half a year from October or November 2016 to March 2017.

location of the bridge (structure)	measuring area	average timber moisture content [mass %]
Höngesberg (arch bridge) (TCC bridge)	above foreland	19,2
	above river at tie beam	17,4
	above river at bridge deck	17,4
Schiffarth (TCC bridge)	above foreland	16,4
	above river	16,3
Wippra (TCC bridge)	above foreland	18,9
	above river	18,3
Schwäbisch Gmünd (TCC bridge)	above foreland	16,6
	above river	17,2
Breitungen (through bridge)	above foreland	16,3
	above river	16,9
Sigmaringen (beam bridge)	above foreland	16,6
	above river	17,4
Lörrach (truss bridge)	above foreland	17,5
	above river	18,4
	above road	16,6
Werdau (through bridge)	above foreland at main girder	17,1
	above foreland at secondary girder	17,8
	above river	16,8
Frankenroda (through bridge)	above foreland	18,1
	above river	17,8

Tab. 1: Average timber moisture contents [mass %] at the bridges of the monitoring program

The lowest average value is 16.3 mass % in Schiffarth and Breitungen and the highest one is 19.2 mass % in Höngesberg, whereby the extreme high values are included while the water ran over the measuring area. It can be seen that the timber moisture content is generally lower than the critical 20 mass % limit at all bridges. A relevant difference between the measured timber moisture content above the foreland and the river is not obvious for the current evaluation period.

5. Conclusions and outlook

It is the most important aim of the monitoring program to demonstrate the durability of well-protected timber bridges. Another aim is the investigation of influence of specified local climates on the timber moisture content. To investigate these issues, nine timber bridges have been equipped with monitoring systems to analyse the timber moisture content and ambient climate conditions. Several structures and varying ambient climate conditions characterise the bridges. Eight of them were equipped with a monitoring system in October and November 2016. Results of a longer evaluation period are available for one bridge that was equipped in August 2015. The first results indicate that structural protective measures can guarantee acceptable timber moisture contents. Furthermore, a problem at an expansion joint was detected. A ventilated cladding was installed to protect the affected beams from penetrating

water before secondary damage at the timber structure could evolve. This shows the potential of monitoring systems to prevent costly damages.

Currently, a great quantity of data is collected. The measuring and analysis of the data is ongoing until autumn of 2018, when the research project will be finished.

6. Acknowledgement

For funding ProTimB, many thanks go to the German Federal Ministry of Education and Research (BMBF), the companies of the Qualitätsgemeinschaft Holzbrückenbau e. V. as there are Schaffitzel Holzindustrie GmbH + Co. KG, Schmees & Lühn Holz- und Stahlingenieurbau GmbH and Grossmann Bau GmbH & Co. KG and to Setzpfandt Beratende Ingenieure GmbH & Co. KG.

7. References

[1] DIN EN 1995-2/NA:2011-08, Nationaler Anhang – National festgelegte Parameter – Eurocode 5: Bemessung und Konstruktion von Holzbauten – Teil 2: Brücken.

[2] Graf E., Meili M.: “Holzzerstörende Pilze und Insekten - Analyse, Prognose, Bekämpfung”, Lignum, Schweizerische Arbeitsgemeinschaft für das Holz (Ed.), *Lignatec: Die technischen Informationen der Lignum* EMPA/LIGNUM-Richtlinie 14. CH-Zurich, 2001.

[3] Brischke C., Rapp A. O., “Untersuchung des langfristigen Holzfeuchteverlaufs an ausgewählten Bauteilen der Fußgängerbrücke in Essing”, Arbeitsbericht Nr. 2007/2, Bundesforschungsanstalt für Forst- und Holzwirtschaft, Institut für Holzbiologie und Holzschutz, DE-Hamburg, 2007.

[4] Franke B., Müller A., Vogel M., Tannert T., “Langzeitmessung der Holzfeuchte und Dimensionsänderung an Brücken aus blockverleimtem Brettschichtholz”, Forschungsbericht, Berner Fachhochschule, Architektur Holz und Bau, CH-Biel, 2012.

[5] Gamper A., Dietsch P., Merk M., Winter S., “Building Climate – Long-term measurements to determine the effect on the moisture gradient in timber structures”, Final report, TU München, DE-München, 2014.

[6] Koch J., “Feuchtemonitoring an geschützten Holzbrücken - Planung, Durchführung und Auswertung” Master Thesis, Fachhochschule Erfurt - University of Applied Sciences, DE-Erfurt, 2015.

[7] Koch, J.; Simon, A.; Arndt, R. W.: “Monitoring of moisture content of protected timber bridges”, CD-ROM Proceedings of the World Conference on Timber Engineering (WCTE 2016), AT-Vienna, August 22-25, 2016.

[8] Franke B., Franke S., Schiere M., Müller A., “Moisture diffusion in wood – Experimental and numerical investigations”, CD-ROM Proceedings of the World Conference on Timber Engineering (WCTE 2016), AT-Vienna, August 22-25, 2016.

[9] Keylwerth, R., Noack, D., Über den Einfluß höherer Temperaturen auf die elektrische Holzfeuchtigkeitsmessung nach dem Widerstandsprinzip, *Holz als Roh- und Werkstoff*, Vol. 14, No. 5, 1956, pp. 162-172.

[10] Hailwood A. J., Horrobin S.: “Absorption of water by polymers: analysis in terms of a simple model”, *Transactions of the Faraday Society*, Vol. 42B, 1946, pp. 84-92.

[11] Simpson W. T.: “Prediction equilibrium moisture content of wood by mathematical model”, *Wood and Fiber*, Vol. 5, No. 1, 1973, pp. 41-49.

Moisture Content Monitoring in Glulam by Electrical Methods

Hang LI
PhD Student
Institut Clément Ader
Tarbes, France

Marianne PERRIN
Associate Professor
Institut Clément Ader
Tarbes, France

Florent EYMA
Associate Professor
Institut Clément Ader
Tarbes, France

Xavier JACOB
Associate Professor
PHASE Laboratory
Toulouse, France

Vincent GIBIAT
Professor
PHASE Laboratory
Toulouse, France

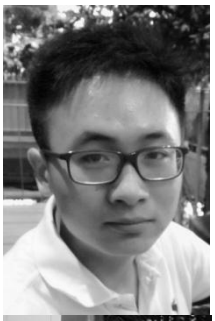

Hang Li is currently on PhD thesis entitled "The use of smart wood materials for the sustainable management of infrastructures" at Laboratory Institut Clément Ader.

Marianne Perrin is associate professor at Laboratory Institut Clément Ader, working mainly on the non-destructive testing of wood and composite materials.

Summary

Today, the development of glulam structures is limited by the durability problems related to excessive moisture content (MC) or wetting/drying cycles. As a result, the development of continuous monitoring techniques of MC in glulam structures becomes essential. Currently, the most used methods are based on electrical measurements (resistive or capacitive). Nevertheless, existing solutions do not allow measurements inside the lamellas of glulam. In the light of these observations, we propose to transform glulam into "smart material" by embedding the MC monitoring system in the lamellas, considering the major constraints of fabrication of this material. To achieve this, we have identified 4 measurement configurations using different types of sensors based on electrical principles. Results show that the selected configurations are operational for the local MC measurement (10-70%) in the lamellas of glulam.

Keywords: Moisture content monitoring, Glulam structures, Electrical measurements, Embedded sensors

1. Introduction

Today, more and more timber structures are used in building and civil engineering due to new challenges imposed by sustainable development and thanks to their competitive costs. In recent years, glulam is gaining popularity in the construction due to not only its higher mechanical strength compared to solid wood, but also the possibility it offers to build large-span structures. However, the problem of durability is a limiting factor for the development of these structures [1]. Pathologies such as cracks, delaminations or slots, as well as fungal or insect attacks have been observed on wooden infrastructures. The majority of them can be attributed either to excessive moisture content (MC) (> 22%) or to the wetting/drying cycles in the material [2]. In order to promote the use of wood in construction, infrastructure supervisors have expressed their need on continuous monitoring techniques of wood MC.

Currently, the most used MC control methods for wood material are based on the electrical measurements [3]. They consist in determining wood MC through resistive or capacitive measurements and are widely used in wood industry in the form of moisture meters [4]. Nevertheless, both types of moisture meters have their limits: the resistive moisture meter requires the insertion of metallic electrodes in the material, which can harm the material integrity; the capacitive moisture meter is sensitive to the surface conditions of the material (roughness, MC…), which means the measured results are strongly influenced by surface condition [4].

In literature, several studies have shown the possibilities using resistive and capacitive methods for the continuous monitoring of wood MC [5,6].

As for the resistive method, it concerns the use of the "pin-type" electrodes by inserting them in wood specimens [7]. Nevertheless, during long-term monitoring, problems in maintaining electrical contact between the electrodes and wood due to dimensional changes of wood had occurred [6]. As a result, several authors proposed improved solutions such as using screws [8] or applying conductive glue between the coated metallic cable and wood [6,7]. In recent years, continuous MC monitoring using resistive sensors (screw-type or nail-type) in wooden buildings or bridges is reported to have been initiated in several European countries [9]. The monitoring results show that it is possible to use these types of electrodes for MC monitoring in timber structures since the sensors generally sent data corresponding to the climate changes although malfunction of sensors happened in several cases.

Regarding the capacitive method, the "surface electrodes" were used for the MC monitoring in wood [5]. This type of electrodes consists in placing two parallel metallic plates on the outer surfaces of the specimen. Although the feasibility of surface-type electrodes for the MC measurement in solid wood specimens has been proven, no information exists involving the application of continuous MC monitoring on wooden structures.

According to the studies cited above, existing solutions of MC monitoring stay in the measurement monitoring near the surface of wooden structures, which is not sufficient to extend the service life of timber structures, especially for those with long spans (glulam structures). In order to extend the service life of glulam structures, it is necessary to realize internal and local MC measurement in the lamellas because it is more precise and furthermore it can provide a link between the MC (or wetting/drying cycles) and the durability of the structures in order to inform the infrastructure supervisors as early as possible with the potential risk of damage so that appropriate maintenance operations can be made in advance. To achieve this, MC sensors should be embedded in the lamellas. Given the industrial fabrication process of glulam beams [10], the major constraints for sensor integration are the small glue line thickness (about 0.3 mm) and the bonding pressure (about 10 bars).

In the light of these observations, we propose to transform the glulam into "smart material" by embedding MC monitoring systems in order to perform internal and local MC measurement in the lamellas. To achieve this, we have identified 4 measurement configurations from low to medium cost (0.9 € to 3 €, material purchasing price), using "pin-type electrodes" or "surface electrodes" in order to conduct electrical measurements (resistive/capacitive). The objectives of this study are: 1) to make sure of the good functionality of the 4 measurement configurations; 2) to verify the feasibility of the 4 measurement configurations in the measurement of MC variation in glulam structures; 3) to investigate the influence of bonding pressure and electrode spacings on the electrical measurements.

2. Material and methods

2.1 Specimen preparation

Four measurement configurations using different electrode set-ups were identified in this study (Fig. 1). The specimens were prepared with Douglas fir because it is extensively used in construction. The Configurations 1 and 3 were proposed since using screws [8] or applying conductive glue between the coated metallic cables and wood [6,7] can help maintaining the electrical contact between the electrodes and wood. The Configuration 2 was equally proposed to be a contrast/intermediary configuration for the Configurations 1 and 3 because it has drilled holes compared to the Configuration 1 and has different type of electrodes compared to the

Configuration 3. On the other hand, the Configuration 4 was proposed since the "surface electrodes" were often used for capacitive measurements [5]. Moreover, the resistive measurements can also be conducted in this configuration.

In order to investigate the influence of bonding pressure on the sensor performance, both solid wood and glulam specimens were prepared for each configuration. The thickness of the lamella (or specimen) is 33 mm because it is the recommended thickness for the construction of large-span structures as it manages better the swelling and shrinking of wood. In order to facilitate the water absorption, the width of the specimens is fixed at 90 mm since it is the smallest width for glulam in industry.

Furthermore, in order to verify the influence of the electrode spacings on MC measurements, specimens were prepared with two different electrode spacings. As for the Configuration 1, 2 and 3, two spacings (20 mm and 40 mm) were achieved on the same specimen (Fig. 1). Regarding the Configuration 4, the two spacings were realized with two different specimens with respective thicknesses 33 mm and 16.5 mm (Fig. 1). In order to distinguish the specimens with different electrode spacings in Configuration 4, we name those with an electrode spacing of 33 mm Configuration 4A and those with an electrode spacing of 16.5 mm Configuration 4B.

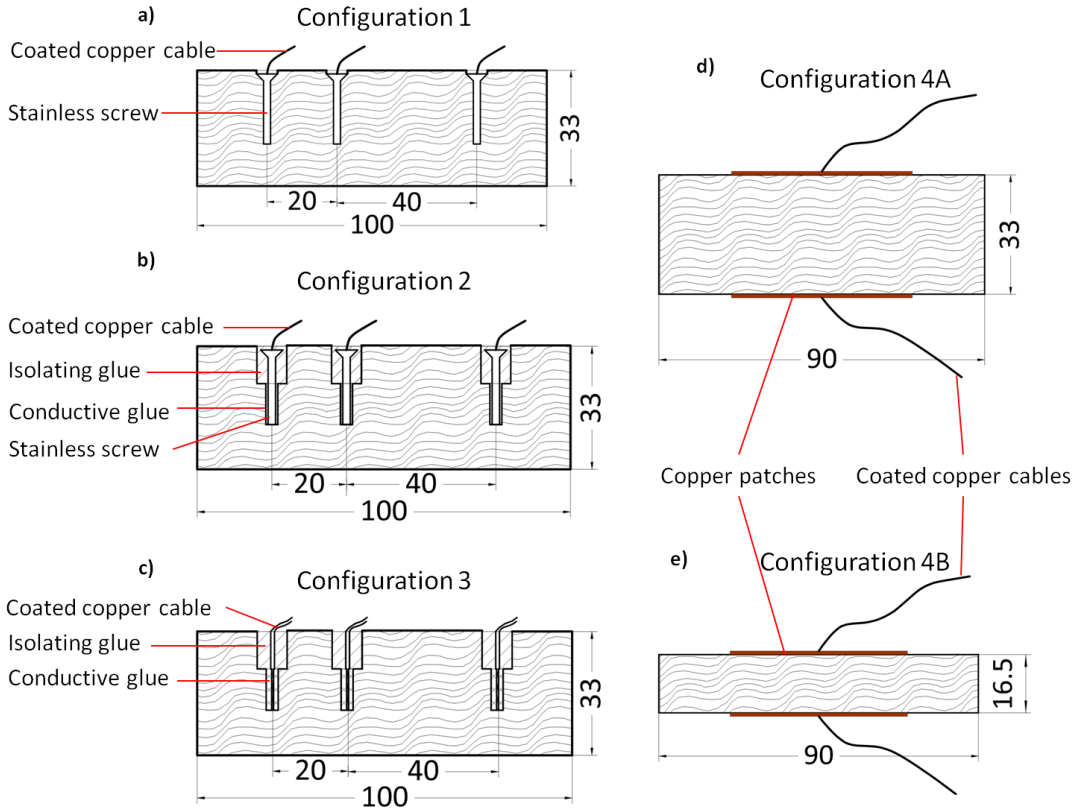

Fig. 1 Measurement configurations: a) Configuration 1; b) Configuration 2; c) Configuration 3; d) Configuration 4A; e) Configuration 4B

The *Configuration 1* uses stainless screws as MC sensors and the screws were driven directly into the wood with a screwdriver. The *Configuration 2* uses also stainless screws as MC sensors but they were placed in the pre-drilled counter-bored holes. The rest space in the bottom holes was filled with conductive glue and the rest void in the top holes was filled with polyurethane glue used for glulam bonding. The *Configuration 3* uses directly the copper cables as the MC sensors. The cables were stripped of 11 mm at the end and were then placed in pre-drilled counter-bored holes with the same dimensions as the Configuration 2. At last, the rest space in the bottom holes was filled with the conductive glue and the rest void in the top holes was filled with the polyurethane glue. The *Configuration 4* uses the copper patches (Ø50 mm) as MC sensors. They were then stuck on the center of the specimen. At last, the coated copper cables were glued to the center of the patches by the conductive glue.

Following the previous steps, solid wood specimens were prepared as described as follows. For the Configurations 1 and 2, the polyurethane glue was applied on and around the screw head in order to create electrical isolation. For the Configuration 4, a thin layer of polyurethane glue was applied on the patches to create electrical isolation and to prevent the patches from peeling off when moistening. On the other hand, the glulam specimens were prepared using a hydraulic press on setting the bonding pressure at 10 bars during 24 h. One more lamella (33 mm in thickness) was glued for the Configurations 1, 2 and 3 on the screwing/drilling side; two more lamellas (16.5 mm in thickness) were glued for the Configuration 4 on the two sides where patches were struck. In the end, it is important to point out that 5 identical specimens (for both solid wood and glulam specimens) were prepared for each configuration.

2.2 Experimental procedures

Two procedures were used to change the MC of the specimens. Concerning the measurements made at the MC below 20%, a climate chamber which allows changing the temperature and the relative air humidity was used. The specimens were considered to have attained the equilibrium MC when the mass was stable. With regard to the MC between 20% and 70%, an immersion in basin was used. The measurements were realized following a schedule fixed according to the results of a study of humidification kinetics conducted before launching the experiment.

At each measurement, the electrical resistances for all specimens were measured with a Giga-Ohmmeter developed at laboratory.

For the Configurations 1, 2 and 3, in order to distinguish the electrical resistances measured between the two pairs of electrodes, we name the resistance measured between the 20 mm spaced electrodes R_{20} and the resistance measured between the 40 mm spaced electrodes R_{40}. Furthermore, in order to verify the influence of electrode spacing, the wood resistance and the contact resistance associated with the wood/electrode interface were also calculated. According to the literature [11], the measured resistance can be considered as a series connection of the wood resistance and the contact resistance. As a result, we can write R_{20} and R_{40} in the following form:

$$R_{20} = R_{w1} + 2R_{c1} \tag{1}$$

$$R_{40} = 2R_{w1} + 2R_{c1} \tag{2}$$

where, R_{w1} represents the wood resistance between the 20 mm spaced electrodes and R_{c1} is the contact resistance. The R_{40} is considered to contain twice the R_{w1} since the length of the conducting path is doubled (according to Eq. 3):

$$R = \rho \frac{l}{A} \tag{3}$$

where R is the electrical resistance (Ω), ρ is the resistivity of material (Ω▪m), l is the length of the material (m) and A is the cross-section area (m²). On solving the Eqs. 1 and 2, we can obtain:

$$R_{w1} = R_{40} - R_{20} \tag{4}$$

$$R_{c1} = \frac{2R_{20} - R_{40}}{2} \tag{5}$$

As for the Configurations 4A and 4B, in order to distinguish the electrical resistances measured on the two types of specimens, we name the resistance measured on the specimens 4A R_{33} and the resistance measured on the specimens 4B $R_{16.5}$. The wood resistance (R_{w2}) and the contact resistance (R_{c2}) are:

$$R_{w2} = R_{33} - R_{16.5} \tag{6}$$

$$R_{c2} = \frac{2R_{16.5} - R_{33}}{2} \tag{7}$$

Regarding the capacitive measurements (Configuration 4), a LCR meter was used. In order to distinguish the capacitances measured on the two types of specimens, we name the capacitance measured on the specimens 4A C_{33} and the capacitance measured on the specimens 4B $C_{16.5}$. Furthermore, if we consider the measured capacitance as a series connection of wood capacitance and contact capacitance, we can write the C_{33} and the $C_{16.5}$ in the following form [12]:

$$\frac{1}{C_{33}} = \frac{1}{C_w} + \frac{2}{C_c} \quad (8)$$

$$\frac{1}{C_{16.5}} = \frac{1}{2C_w} + \frac{2}{C_c} \quad (9)$$

where C_w represents the wood resistance of the specimens 4A and C_c is the contact capacitance associated with the wood/electrode interface. The $C_{16.5}$ is considered to contain twice the C_w since the distance between is halved (according to Eq. 10) [12]:

$$C = \varepsilon_0 \varepsilon_r \frac{A}{d} \quad (10)$$

where C is the capacitance (F), ε_0 is absolute permittivity of vacuum (≈ 8,854*10^{-12} F•m^{-1}), ε_r is the dielectric constant (CD) which determines some kind of ability to store electrical charge, A is the area of the plates (m²) et d is the distance (m) between them. The solutions of Eqs. 8 and 9 are:

$$C_w = \frac{1}{2*(1/C_{33} - 1/C_{16,5})} \quad (17)$$

$$C_c = \frac{2}{2/C_{16,5} - 1/C_{33}} \quad (18)$$

The frequency range of the LCR meter is from 100 Hz to 2 kHz. Several studies have already confirmed the variation of the CD (proportional to the capacitance, cf. Eq. 10) as a function of MC at different frequencies from 0.01 Hz up to the range of GHz [13]. James [14] have realised the measurements of CD at 4 different frequencies (0.2 kHz, 1kHz, 10 kHz, 100 kHz) and he concluded that the sensibility for MC monitoring increases with increasing frequency. As a result, we conducted preliminary tests at 100 Hz and at 2 kHz which are the two extreme values of our measurement device in order to determine the optimal frequency in our case.

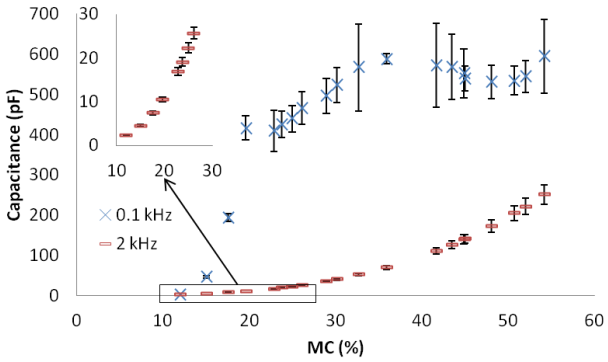

Fig. 2 Capacitance at 0.1 kHz and 2 kHz on wood specimens

Our results showed that 2 kHz allows to better discriminate the different MCs (Fig. 2), which is in accordance with the conclusion of James [14]. As a consequence, the frequency is fixed at 2 kHz in this study.

The specimens were also weighed at each measurement in order to calculate the exact MC by gravimetric method according to the European standard [15].

3. Results and discussion

3.1 Feasibility of electrical measurements in wood

The implementation of the different measurement configurations was firstly achieved on solid wood specimens. The measurements at initial state (10% in MC) on these specimens have shown the possibility to realize electrical measurements in wood (Fig. 3). As for the resistive measurements, it was found that electrical resistance is in the order of 10^9 Ω for the Configurations 1, 2 and 3 and 10^{10} Ω for the Configuration 4. These values are in the same order of magnitude with information available in literature [3,11].

Regarding the capacitive measurements, the values of capacitance found in this study were in the same order of magnitude with information available in literature using similar frequencies [16]. In our study, the capacitance measured on the 33 mm thick specimen is 2.3 pF on average while it is 5.0 pF by extrapolating the results of James at 1 kHz [16]. The difference can be explained by the different frequencies used since our results were measured at 2 kHz.

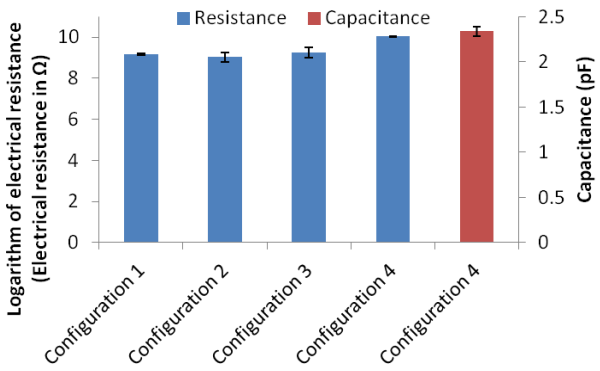

Fig. 3 Electrical resistance and capacitance of solid wood specimens measured at initial state (10% in MC)(Configurations 1, 2 and 3: sensor distance = 40 mm; Configuration 4: sensor distance = 33 mm)

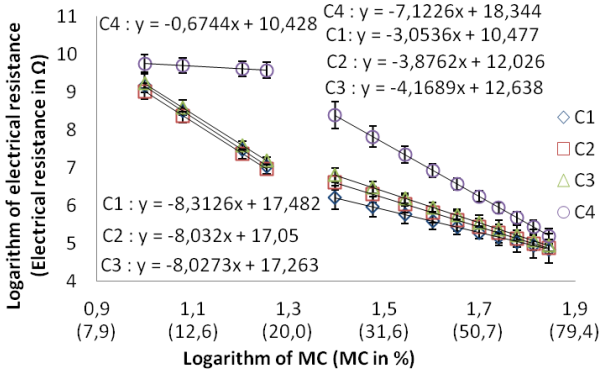

Fig. 4 Logarithm of electric resistance as a function of logarithm of MC for solid wood specimens (Configurations 1, 2 and 3: sensor distance = 40 mm; Configuration 4: sensor distance = 33 mm)

3.2 Feasibility of MC monitoring

Thereafter, the feasibility of these solid wood specimens on the monitoring of MC variation was investigated using the moistening procedures described earlier in this paper. The results of resistive and capacitive measurements are presented relatively in Fig. 4 and Fig. 5. It can be observed that it is possible to monitor MC with all the 4 measurement configurations in the range of our study. The results before and after 20% in MC were analyzed separately since two different trends can be observed. This can be explained by the fact that two different moistening procedures were used in this study.

Before 20% in MC, the water sorption is in the form of water vapor while after 20% in MC, liquid water absorption is involved [17]. This means that only bound water was present in our specimens before 20% in MC and after 20% in MC, free water began to be absorbed in the intercellular cavities of wood. According to the literature, the influence of bound water and free water on the resistive/capacitive properties is different [13,18]. In consequence, results were analyzed separately before and after 20% in MC in our study.

It is interesting to point out that the evolutions of electrical resistance of Configurations 1, 2 and 3 are almost the same while that of Configuration 4 differs from them (Fig. 4). The difference can be explained as follows. Firstly, according to the literature, when surface electrodes are used, the measured resistance tends to be affected by the surface roughness of the specimen [3,19]. Surface roughness can result in a smaller effective contact area than the electrode size (Fig. 6), leading to a higher resistance measured than the theoretical value. When wood MC is below 20%, only bound water is present, so that the characteristics of contact interface are not significantly changed with the MC variation. As a result, the decrease of resistance is not significant from 10% to 20% in MC (Fig. 4). From 20% in MC, free water begins to enter into the free space of wood, including the space between the electrodes and the specimen, which can lead to an improvement in the condition of electrical contact. As a consequence, a significant decline of resistance can be observed from 20% to 70% in MC, and the resistance ends up at values close to Configurations 1, 2 and 3 (Fig. 4).

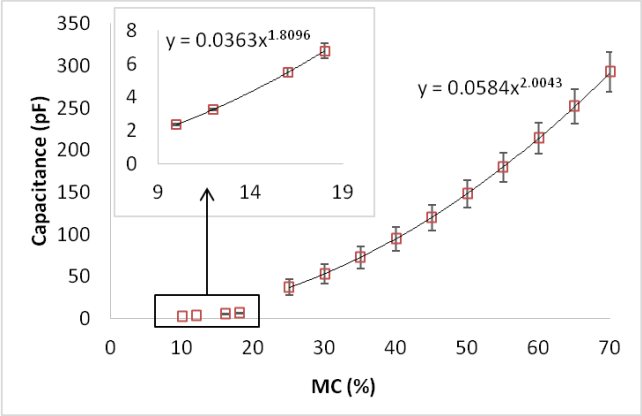

Fig. 5 Capacitance as a function of MC for solid wood specimens (Configuration 4, sensor distance = 33 mm)

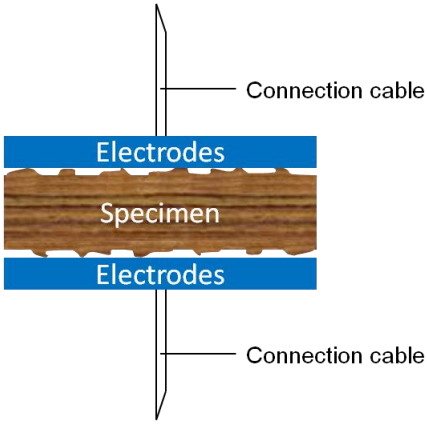

Fig. 6: Illustration of electrical contact on a rough surface

3.3 Influence of bonding pressure

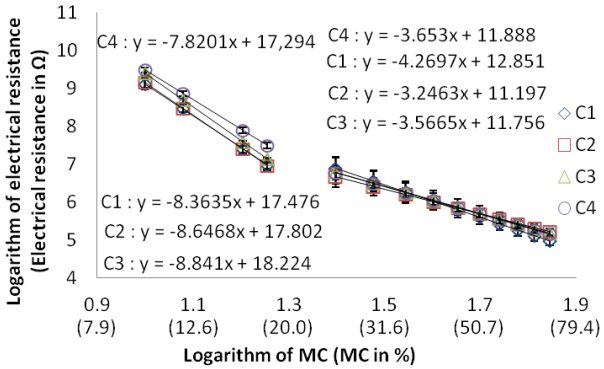

Fig. 7 Logarithm of electric resistance as a function of logarithm of MC for glulam specimens (Configurations 1, 2 and 3: sensor distance = 40 mm; Configuration 4: sensor distance = 33 mm)

The feasibility of MC monitoring using the proposed measurement configurations was also investigated on glulam specimens. The results of resistive and capacitive measurements are presented relatively in Fig. 7 and Fig. 8. It can be observed that it is possible to monitor MC with all the 4 measurement configurations in the range of our study.

Moreover, with respect to the resistive measurements, it can be observed that the 4 configurations have close values and identical tendencies. This observation is different with what can be observed in solid wood specimens, especially for Configuration 4 (cf. Fig. 4 and Fig. 7). This difference can be explained by the application of the bonding pressure on the surface electrodes, leading to an improvement of the contact condition between the electrodes and the specimen.

With respect to the Configurations 1, 2 and 3, similar tendencies were observed on solid wood and glulam specimens (cf. Fig. 9). This can be explained by the fact that the bonding pressure was not applied directly on the sensors so that the condition of electrical connection between the electrodes and wood was not changed by the pressure.

Regarding the capacitive measurements, it was found that the capacitance of the glulam specimens is greater than that of the solid wood specimens (Fig. 8). This can be explained by the application of the bonding pressure, which has improved the contact condition between the electrodes and the specimen, leading to a higher capacitance measured [20]. On the other hand, the difference in capacitance between glulam and solid wood specimens is observed to increase with increasing MC (Fig. 8). A possible explanation is given as follows. The capacitance of wood is contributed by the permanent dipoles (hydroxyl groups, molecule of free or bound water, etc.) in the material [3]. Since the glulam specimens have two more lamellas outside, they have more free space to absorb water. As a result, the dipole components in the two exterior lamellas might have contributed to the measured capacitance, which can explain why the difference in capacitance increases as a function of MC. In order to confirm our hypothesis, we firstly conducted capacitive measurements on solid wood specimens (immersed in water) without wiping the water off the exterior surfaces. We then

wiped the water off the exterior surfaces completely and conducted the same measurements. It turned out that results of capacitance obtained with water on the exterior surfaces are on average 10% higher, which can support our hypothesis.

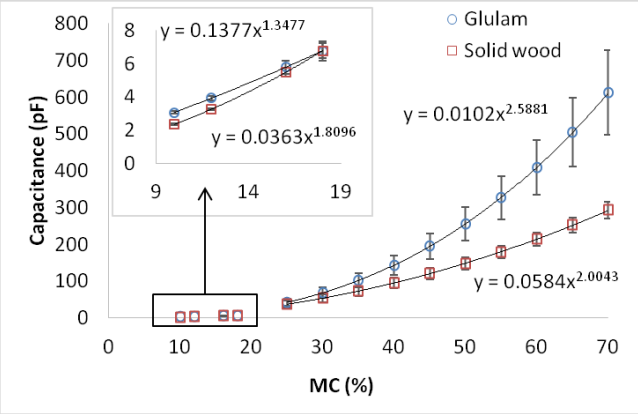

Fig. 8 Capacitance as a function of MC for both solid wood and glulam specimens (Configuration 4, sensor distance = 33 mm)

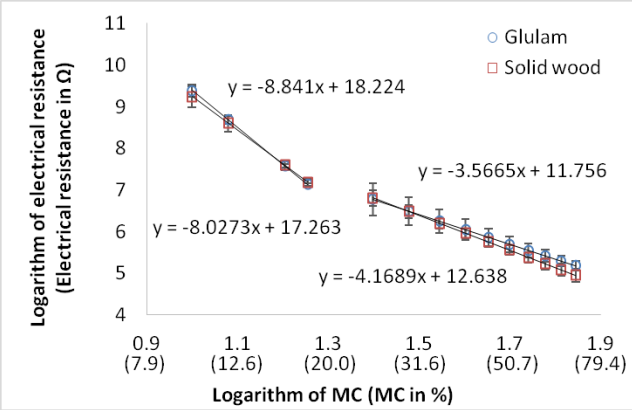

Fig. 9 Logarithm of electric resistance as a function of logarithm of MC (Configuration 3, sensor distance = 40 mm)

3.4 Influence of electrode spacings

In order to investigate the influence of electrode spacings, the results of both electrical resistance and capacitance obtained with different electrode spacings were compared.

Regarding the resistive measurements, it turned out that no difference can be observed in our study (Fig. 10 and Fig. 11). This can be explained by the fact that the contact resistance, which can be calculated with Eq.5 and Eq.7, contributes to the majority (more than 80%, cf. Fig. 12) of the total resistance measured. Similar observation was also made in literature [21].

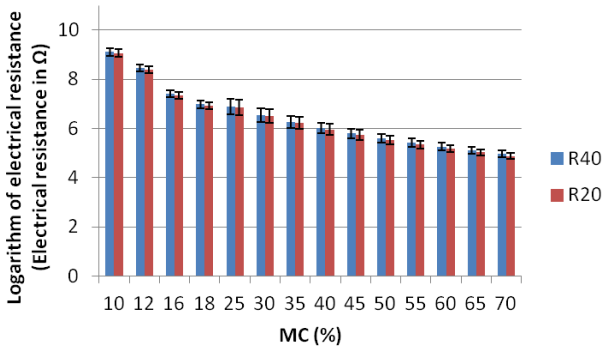

Fig. 10 Comparison between electrical resistance measured with different electrode spacings (Glulam specimens, Configuration 1)

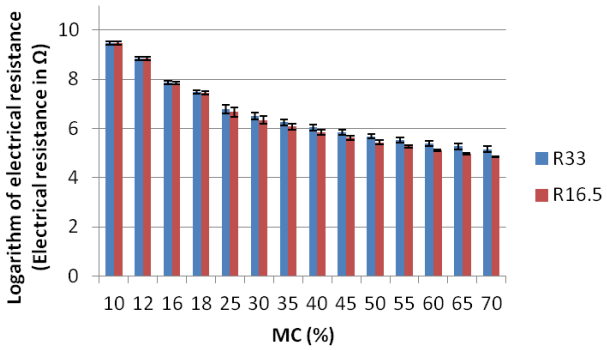

Fig. 11 Comparison between electrical resistance measured with different electrode spacings (Glulam specimens, Configuration 4)

With respect to the capacitive measurements, the capacitance measured on the 16.5 mm thick specimens was observed to be higher than that measured on the 33 mm thick specimens on average (Fig. 13). This observation can be explained by the theoretical equation (Eq.10) which shows that the capacitance will be doubled if the material thickness is halved. However, our results do not show two-fold relationship. For MC below 20%, the results show a 1.8 time' relation and the slight difference can be explained by the contribution of contact capacitance [22], which can be calculated with Eq.18 (Fig. 12). Above 20% in MC, results obtained on specimens with different thickness become close to each other. This can be attributed to the fact that the 2 exterior lamellas of the glulam specimens contribute to the measured capacitance, knowing that the dimensions of the exterior lamellas are the same for specimens of different thickness.

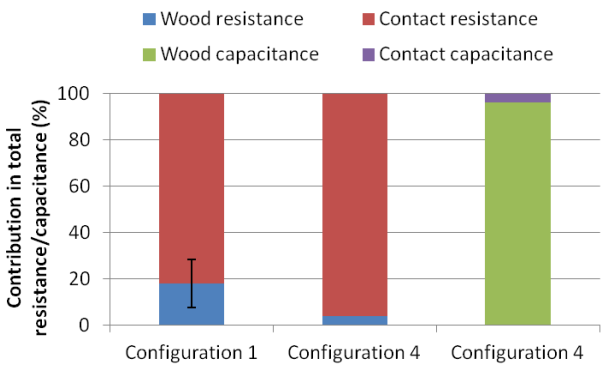

Fig. 12 Contribution of wood resistance/capacitance and contact resistance/capacitance in total resistance/capacitance of Glulam specimens at initial state (10% in MC) (Configuration 1: sensor distance = 40 mm; Configuration 4: sensor distance = 33 mm)

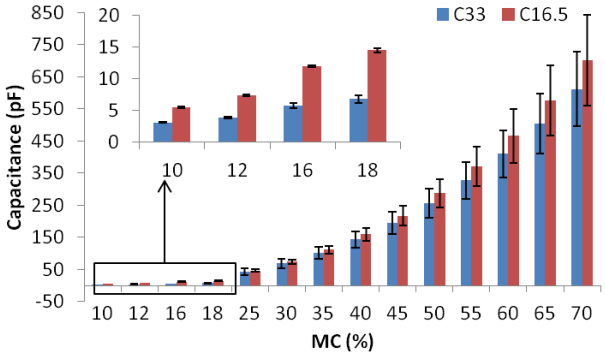

Fig. 13 Comparison between capacitance measured with different electrode spacings (Glulam specimens, Configuration 4)

4. Conclusions

Within the framework to develop embedded MC monitoring systems in the lamellas of glulam structures in order to improve the infrastructure durability, 4 measurement configurations were tested in this study. Results showed that it is possible to monitor the MC in wood specimens in the range of our study with all the 4 configurations. Among them, the Configuration 4 presents the best potential to be applied on glulam structures for in situ monitoring for the reasons below:

1) It is easy to realize in the glulam fabrication line since no extra drilling/machining is needed;
2) It is a more versatile configuration since it is possible to conduct both resistive and capacitive measurements, which can provide complementary information;
3) It has lower cost compared to other configurations (0.9 €, material purchased price, measurement system not included).

On the other hand, the influence of bonding pressure was also investigated in this study. It was observed that it is possible to conduct MC measurements after the application of bonding pressure. Moreover, it was found that compared to solid wood specimens, the glulam specimens exhibit lower electrical resistance and higher capacitance. All this can be associated with the application of bonding pressure since the latter can improve the electrical contact at wood/electrodes interface.

At last, the influence of electrode spacing was also investigated. Regarding the resistive measurements, no influence was observed in our study. This can be attributed to the important contribution of contact resistance in total resistance measured. With respect to the capacitive measurements, influence of the electrode spacing can be observed and it can be associated with the contribution of the exterior lamellas. Nevertheless, this does not influence the feasibility of MC measurements, which can be demonstrated by our results on specimens with standard lamella thickness (33 mm).

Acknowledgment

Authors would like to thank the co-financers of this research project: la Région Midi-Pyrénées, le Conseil Général des Hautes-Pyrénées and le Grand Tarbes. Special thanks should also be addressed to Emannuel Laught for his contribution in developing the Giga-Ohmmeter and to Tommy Vilella and Frédéric Leroy for their help in experimentation.

References

[1] Kasal B., “Assessment, Reinforcement and Monitoring of Timber Structures–COST FP1101”, *Advanced Materials Research*, Vol. 120, 2013, pp. 1037–1040.

[2] Dietsch P., Gamper A., Merk M., and Winter S., "Monitoring Building Climate and Timber Moisture Gradient in Large-Span Timber Structures", *Journal of Civil Structural Health Monitoring*, Vol.5, No. 2, 2014, pp. 153–165.
[3] Skaar C., *Wood-Water Relations*, Springer-Verlag, Berlin Heidelberg, 1988, 304 pp.
[4] Kasal B., and Lear G., "Moisture Measurement", *In Situ Assessment of Structural Timber*, Springer, 2011, pp. 99–104.
[5] Moron C., Garcia-Fuentevilla L., Garcia A., and Moron, A., "Measurement of Moisture in Wood for Application in the Restoration of Old Buildings", *Sensors*, Vol. 16, No. 5, 2016, pp. 697–705.
[6] Brischke C., Rapp A. O., and Bayerbach R., "Measurement System for Long-Term Recording of Wood Moisture Content with Internal Conductively Glued Electrodes", *Building and Environment*, Vol. 43, No. 10, 2008, pp. 1566–1574.
[7] Fredriksson M., Wadso L., and Johansson P., "Small Resistive Wood Moisture Sensors: A Method for Moisture Content Determination in Wood Structures", *European Journal of Wood and Wood Products*, Vol. 71, No. 4, 2013, pp. 515–524.
[8] Norberg P., "Monitoring Wood Moisture Content Using the WETCORR Method Part 2: Calibration and Validation", *Holz Als Roh-Und Werkstoff*, Vol. 58, No. 3, 2000, pp. 129–134.
[9] Dietsch P., Franke S., Franke B., Gamper A., and Winter S., "Methods to Determine Wood Moisture Content and Their Applicability in Monitoring Concepts", *Journal of Civil Structural Health Monitoring*, Vol. 5, No. 2, 2014, pp. 115–127.
[10] AFNOR, 2013, *NF EN 14080, Timber structures - Glued laminated timber and glued solid timber - Requirements*, AFNOR, 2013, 108 pp.
[11] James W. L., *Electric Moisture Meters for Wood*, Dept. of Agriculture, Forest Service, Forest Products Laboratory, Madison, Wisconsin, 1963, 17 pp.
[12] Terzic E., Terzic J., Nagarajah R., and Alamgir M., "Capacitive Sensing Technology" *A Neural Network Approach to Fluid Quantity Measurement in Dynamic Environments*, Springer, London, 2012, pp. 11–37.
[13] Torgovnikov G. I., *Dielectric properties of wood and wood-based materials*, Springer, Berlin Heidelberg, 1993, 196 pp.
[14] James W., "The Interaction of Electrode Design and Moisture Gradients in Dielectric Measurements on Wood", *Wood and Fiber Science*, Vol. 18, No. 2, 1986, pp. 264–275.
[15] AFNOR, *NF EN 13183-1, Moisture content of a piece of sawn timber - Part 1 : determination by oven dry method*, AFNOR, 2002, 5 pp.
[16] Holm R., *Electric Contacts - Theory and Application*, Springer-Verlag, Berlin Heidelberg, 1967, 484 pp.
[17] James W. L., "Dielectric Behavior of Douglas-Fir at Various Combinations of Temperature, Frequency, and Moisture-Content", *Forest Products Journal*, Vol. 27, No. 6, 1977, pp. 44–48.
[18] Siau J. F., *Transport processes in wood*, Springer-Verlag, Berlin Heidelberg, 1984, 245 pp.
[19] Lin R. T., "Review of the Electrical Properties of Wood and Cellulose", *Forest Products Journal*, Vol. 17, No. 7, 1967, pp. 54–60.
[20] Dervos C. T., and Michaelides J. M., "The Effect of Contact Capacitance on Current-Voltage Characteristics of Stationary Metal Contacts", The 43rd IEEE Holm Conference on Electrical Contacts, 20-22 October, Philadelphie, Pennsylvania, 1998, pp. 530–540.
[21] Skaar C., "Some Factors Involved in the Electrical Determination of Moisture Gradients in Wood", *Forest Products Journal*, Vol. 14, No. 6, 1964, pp. 239–243.
[22] Tereshchenko O. V., Buesink F. J. K., and Leferink F. B. J., "An Overview of the Techniques for Measuring the Dielectric Properties of Materials", The 30th General Assembly and Scientific Symposium, 13-20 August, Istanbul, Turkey, 2011, pp. 14-18.

Smart Timber Bridge on Geosynthetic Reinforced Soil (GRS) Abutments

Adam Senalik
Research Engineer
Forest Products Laboratory
Madison, WI, USA
christopherasenalik@fs.fed.us

Adam is a recent graduate of the University of Illinois, Urbana-Champaign, where his PhD thesis focused on nondestructive inspection of glulam beams. He has worked at FPL in timber bridge research for 4 years on a wide variety of projects.

James P. Wacker
Research Engineer
Forest Products Laboratory
Madison, WI, USA
jwacker@fs.fed.us

James completed his Civil and Environmental Engineering studies at the University of Wisconsin – Madison. His FPL research has primarily been focused on timber bridge-related studies for the past 27 years. He is also a registered professional engineer in the state of Wisconsin.

Travis K. Hosteng
Director/Engineer
National Center for Wood Transportation Structures
Ames, IA, USA
kickhos@iastate.edu

Travis earned his MSc degree from Iowa State University. He is the lead engineer for wood bridge projects at ISU's Bridge Engineering Center and Co-Director of the National Center for Wood Transportation Structures. He is a member on the ASCE committee for timber bridges.

John Hermanson
Research Scientist
Forest Products Lab.
Madison, WI, USA
jhermanson@fs.fed.us

John's research focuses on the areas of multifield and multidomain modelling of continuum systems.

Summary

Recently, Buchanan County, Iowa, has cooperated with the U.S. Federal Highway Administration (FHWA), USDA Forest Service, Forest Products Laboratory (FPL), and Iowa State University's Bridge Engineering Center (ISU–BEC) to initiate a project involving the construction and monitoring of a glued-laminated (glulam) timber superstructure on geosynthetic reinforced soil (GRS) integrated bridge system (IBS) abutments. The research team from FPL installed sensors in the substructure as well as in the bearings of the girders. In addition, the research team from ISU–BEC installed sensors on the superstructure that create an autonomous structural health monitoring system for the bridge. Data are collected remotely and transmitted continuously around the clock

every day. Long-term monitoring enables researchers to evaluate GRS–IBS system performance with respect to variables of time, ambient conditions, and loading.

Keywords: Geosynthetic reinforced soil, health monitoring, timber, glulam, substructure, superstructure

1. Introduction

In October 2016, the Catt bridge project was dedicated near the city of Independence in Buchanan County, Iowa, USA (42.475702° N, 91.828430° W) (Fig. 1). Its unique construction techniques were documented through a live webcam, which is accessible from the National Center for Wood Transportation Structures website (www.woodcenter.org). Buchanan County has a long history of constructing timber bridges, and it currently maintains 21 within its mostly rural, agriculture-based roadway network. Within the entire state of Iowa, there are approximately 3,000 timber bridges, the highest state inventory in the United States [1].

(a) (b)

Fig. 1 August 2016 photographs of the completed Catt Bridge: (a) End view (b) Profile view

Because it was one of the first timber bridge superstructures to be installed on geosynthetic reinforced soil (GRS) abutments in the United States, it provided the opportunity to collect key performance data using an array of sensors integrated into a structural health monitoring (SHM) system. The process of monitoring smart timber bridges is described in Phares et al. [2]. This project is a joint effort between the USDA Forest Products Laboratory (FPL), Iowa State University's Bridge Engineering Center (ISU–BEC), and the Federal Highway Administration (FHWA). This paper provides an overview of the design and construction phases, installation of sensors for SHM of the substructure and superstructure systems, and a review of the preliminary monitoring data collected to date.

2. Substructure Design

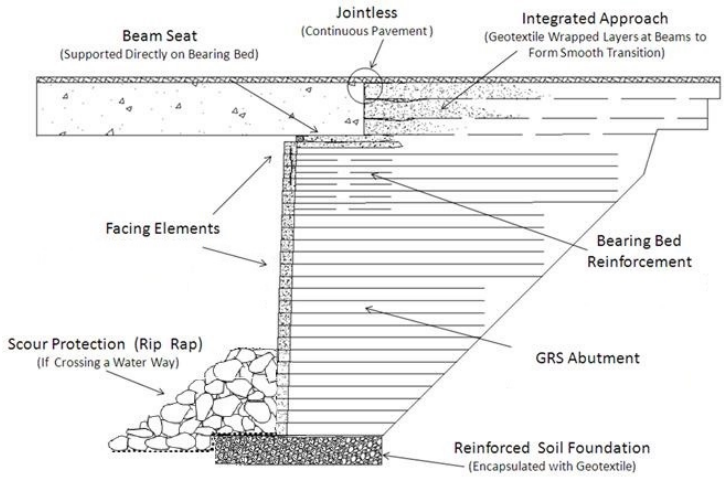

Fig 2. Geotextile reinforced soil integrated bridge system cross section showing typical characteristics (Used with the permission of FHWA)

As part of the Bridge of the Future Initiative, FHWA developed the GRS integrated bridge system (IBS). Geosynthetic reinforced soil walls (originally referred to as Geotextile-reinforced walls) were first constructed by the U.S. Forest Service in 1974. The GRS–IBS uses reinforced soil as part of an economical bridge system. The GRS–IBS was developed to be lower cost, be faster to construct, have improved durability compared with other single-span bridge construction, and have design flexibility allowing for adaptation in the field. Typically, steel and concrete bridge superstructures have been used with GRS–IBS. The bridge superstructure of a GRS-IBS is set

directly on the GRS abutment, which provides a stable foundation without the need for deep foundations or cast-in-place concrete. Prior to the construction of this bridge, only one timber bridge superstructure was known to be built on a GRS–IBS substructure.

A GRS–IBS cross section is shown in Figure 2, with typical characteristics identified. The GRS was built using a layered construction of aggregate wrapped in geotextile fabric. The fill material met Processed Aggregate Size No. 89 [3] and was 13 mm or smaller. The fabric was a woven polypropylene geotextile sold as Geotex® 350ST (Propex, Chattanooga, TN) and met AASHTO M288 standards [4]. Construction is described in Adams et al. [5]. Deciding layer thickness is a part of the design process. For the subject bridge in this study, the deepest layers were the thickest at 200 mm. The layers within the bearing bed reinforcement were 100 mm. The layers beneath the integrated approach were 150 mm. Some key characteristics were the reinforced soil foundation, the GRS abutment, the bearing bed reinforcement on which the beam seat sits, and an integrated approach to the bridge. The bridge superstructure sits directly on the bearing bed and is connected to the roadway by in integrated approach. This construction creates a jointless, continuous pavement between the approach and the bridge. The entire GRS–IBS is designed such that the superstructure and the approach settle at the same rate, avoiding the development of a “bridge bump” where the approach meets the superstructure.

3. Superstructure Design

The bridge superstructure was made up of a traditional glulam stringer and transverse glulam panel deck system, a commonly constructed prefabricated bridge system (Fig. 3). The design was based on the current standards set forth by the American Association of State Highway Transportation Officials–Load and Resistance Factor Design (AASHTO–LRFD) specifications [6]. A total of six glulam bridge girders were spaced at 1.57 m (center-to-center), which were interconnected by 1.35-m-wide and 13-cm-thick diaphragms. The 17.1-cm-thick transverse glulam deck was comprised of 1.22-m-wide panels along the traffic direction. The glulam panels were edge-butted and interconnected with 13.1-cm-deep glulam stiffener beams that were through-bolted to the bottom side of the deck panels. The bridge spans 16.2 m between the GRS–IBS bridge abutments. The roadway measures 8.5 m between glulam bridge railings.

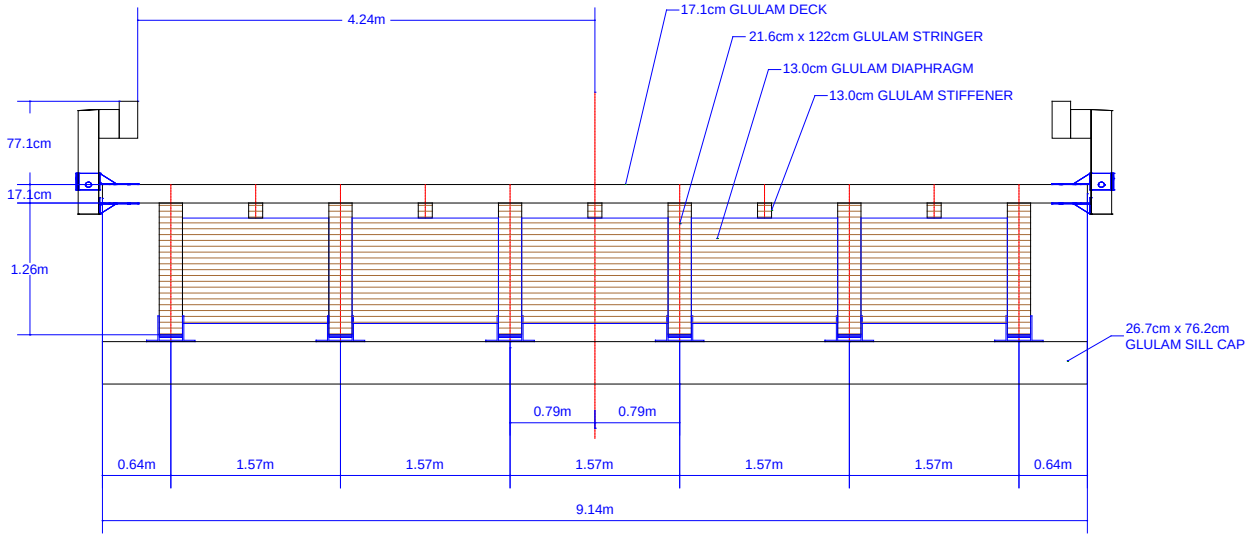

Fig. 3 The bridge cross section showing the configuration of the girders, the deck, and the Test Level 2 crash-tested guardrail system

Design of the GRS timber bridge is a direct reflection of current design practices for timber bridge construction in the United States. Out of the many styles and configurations of timber bridge superstructures, a glulam stringer design with glulam transverse deck panels was selected.

Timber stringers offer economic advantages compared with other design types but require consideration for things such as vertical clearance (that is, hydraulic opening in this case) as timber stringers often require deeper sections than their concrete and steel equivalents. The 16-m length of the GRS–IBS abutment supported superstructure is in an optimal span range for glulam stinger

bridges, and adjustments were made at the roadway approaches to accommodate the superstructure depth.

To minimize possible reflective cracking in the wearing surface, longitudinal timber stiffeners were used at midspan of the stinger spacing. These stiffeners were bolted to the underside of the transverse decking to assist in transferring differential deflections from panel to panel. Using stiffeners in conjunction with a waterproofing wearing surface has proven to maintain the stability of the decking and resist movements that otherwise resulted in the asphalt wearing surface cracking. To meet current safety performance standards, a Test Level 2 crash-tested, bridge railing system was installed that includes glulam posts and glulam railings but without a curb system. A bituminous asphalt wearing surface will be installed on the bridge roadway and approaches in the near future.

4. Structural Health Monitoring

4.1 Substructure Monitoring

The stability of GRS is one of its valuable aspects. Motion of the soil decreases the utility of the GRS structure. To date, monitoring of the movement of GRS–IBS abutments has come from manual surveying of set locations on the exposed side and top of the facing elements, the top of the abutment or the integrated approach, and the superstructure and comparing those points against fixed survey targets away from the bridge and abutments. The surveying data are typically collected manually at intervals of days, weeks, or months. Specific areas of interest within the GRS abutment are targeted for monitoring: movement or tilting of the back wall and wing walls, settlement at the superstructure sill and approach roadway joint, lateral soil movement within the GRS abutment, and soil pressure in high stress areas of the GRS abutment, which are subject to scour.

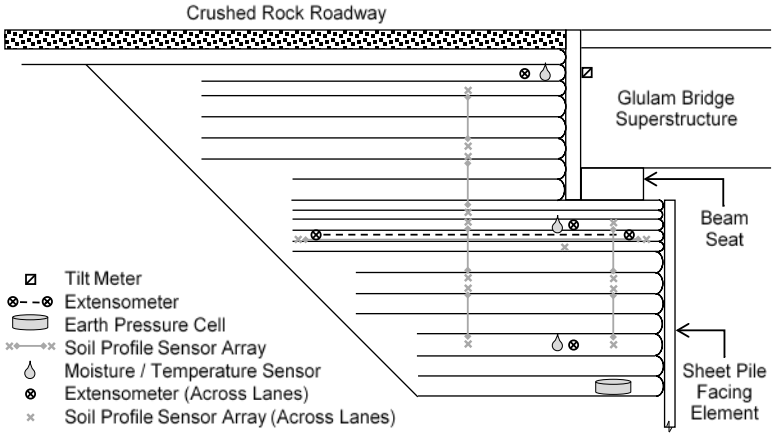

Fig. 4 Sensor placement within GRS abutment. Adapted from site design plans prepared by Buchanan County, Iowa, and used with permission

The monitoring sensors installed within the abutment are shown in Figure 4. The cross section shown in Figure 4 was adapted from the abutment design plans for the site and used with permission from Buchanan County, Iowa. The sensors include tilt meters, moisture and temperature sensors, extensometers, earth pressure cells, and soil profile sensor arrays. The tilt meters measure back wall and wing wall tilt angle. Vertically oriented extensometers (VE), referred to as borehole extensometers, measure abutment settlement. Each VE was approximately 58 cm long prior to installation. There are six sets of VE in the abutment. Four sets of two VE are positioned under the beam seat, 30 cm from the sheet pile facing element. Two sets of four VE are positioned within the roadway approach to the superstructure, 1.88 m from the facing element. Horizontally oriented extensometers (HE), referred to as soil extensometers, measure lateral soil movement. Four HE are used in total. Each HE was approximately 3.35 m long prior to installation. A set of two HE are positioned parallel to the roadway and placed near the midpoints of each of the two driving lanes. A set of two HE are positioned perpendicular to the driving lanes below the interface between the bridge and the approach. Soil profile sensor arrays (SPA), also referred to as shaped accelerometer arrays, and are a series of accelerometers connected by segmented rods. The rods are 0.5 m long. The connection points between the rods are hinged to allow a degree of freedom of motion between the rods. The accelerometers monitor relative movement at each of the connection points, providing internal soil profile information. Two sizes of SPA were used, 3 and 7 m. Two 3-m SPA were placed parallel to the roadway and near the midpoints of each of the two driving lanes. Three 7-m SPA were placed perpendicular to the driving lanes. The first was near the bottom of the abutment, approximately 1.37 m below the level of the beam seat and positioned directly below the interface between the approach and the superstructure. The second was placed at

approximately 25 cm below the level of the beam seat and directly below the interface between the approach and the superstructure. The third was placed near the top of the abutment, approximately 46 cm below the roadway surface and within the approach, 30 cm from the superstructure. Three moisture–temperature sensors were placed at the midpoint of the roadway 15 cm adjacent to each of the 7-m SPA as shown in Figure 4. Two earth pressure cells were placed at the bottom of the abutment, near the midpoints of each of the driving lanes and directly under the beam seat. Two sets of two tilt meters were affixed to the abutment back wall. Tilt meters measure tilt angle in one direction. The tilt meters were mounted in pairs of two and oriented such that the direction of angle measurement was perpendicular within each pair. The pair of tilt meters measure the angle of tilt of the back wall parallel and perpendicular to the driving lanes.

Several ambient condition sensors were mounted in and around the abutment. Wind speed, wind direction, solar radiation, and precipitation are measured on site. Temperature and relative humidity are measured on site, both above the level of the abutment and below the superstructure. The ambient condition sensors and datalogger housing are shown in Figure 5. The abutment and ambient condition sensors are summarized in Table 1. Data are collected from the abutment and ambient conditions sensors every 30 minutes by a CR1000 datalogger (Campbell Scientific, Inc., Logan, UT). The data are transmitted via cellular connection for processing and permanent storage.

1. Vane
2. Anemometer
3. Tipping Bucket Rain Gage
4. Pyranometer
5. Temperature–Relative Humidity Probe
6. Cellular Antenna
7. Datalogger Housing

Fig. 5 Ambient weather condition sensors and datalogger housing

Table 1. GRS abutment and ambient weather condition sensor summary

Measuring	Sensor	Model	Quantity	Buried
Vertical Settlement	Extensometer	Geokon A3 w/ Model 4450 Transducer	16	Y
Back Wall Movement	Tilt Meter	Geokon 6350	4	Y
Soil Pressure	Earth Pressure Cell	Geokon 4800	2	Y
Horizontal Soil Movement	Extensometer	Geokon 4435	4	Y
Moisture–Temperature	Water Content Reflectometer	Campbell Scientific CS655	3	Y
Settlement Profile	Soil Profile Sensor Array	Measurand SAAF	5	Y
Wind Speed	Anemometer	03101 R.M. Young Wind Sentry	1	N
Wind Direction	Vane	03301 R.M. Young Wind Sentry	1	N
Solar Radiation	Pyranometer	Campbell Scientific SP230	1	N
Precipitation	Tipping Bucket Rain Gage	TE525	1	N
Temp–Relative Humidity	Temp–RH Probe	Rotronic HygroClip2	2	N

4.2 Superstructure Monitoring

The bridge superstructure is monitored with two independent SHM systems under dynamic loading, both triggering a 10-second window of data collection. The first system is based on strain measurements; the second system is based on force and displacement measurements.

4.2.1 Strain-Based Measurement Systems

The foundation of the instrumentation plan and monitoring system for the glulam superstructure is a modification of the BECAS monitoring system developed by ISU–BEC [7]. BECAS was initially developed for steel and concrete bridges for long-term, real-time monitoring situations and has been

successfully implemented on four interstate bridges in Iowa and Wisconsin. The system was first modified and tested on a glulam girder superstructure in Delaware County, Iowa, in 2012 [8]. After monitoring and fine-tuning that system for several years, minor changes and improvements were made prior to implementing the system on the bridge of this project.

The two main objectives of the SHM system on this bridge were to (1) collect structural performance data from the bridge and (2) provide real-time, continuous load rating of the superstructure for damage and deterioration detection. The SHM system for the GRS timber bridge consists of 36 strain gages installed on the glulam girders, 6 strain gages installed on the underside of the transverse glulam deck panels, 3 moisture sensors (2 in girders, 1 in deck) [9], and 2 temperature sensors. All 47 of these sensors are connected to and monitored by a CR9000X datalogger (Campbell Scientific). Figure 6 illustrates the instrumentation layout for the GRS timber bridge. An on-site desktop computer collects the data from the data logger and pushes them wirelessly via cell modem and router to the BEC main servers at the home office in Ames, IA. Figure 7 illustrates the logger enclosure mounted on the wingwall of the bridge. After the data are received by the servers, they are filtered and reduced, separating out data files with a detected truck event for further analysis and evaluation.

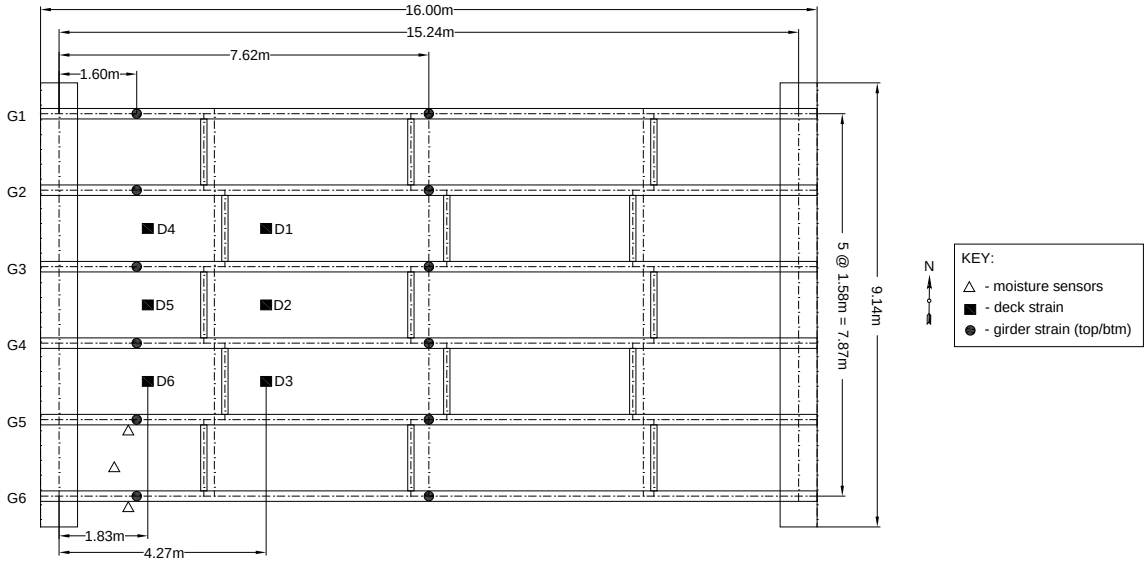

Fig. 6 GRS timber bridge instrumentation layout

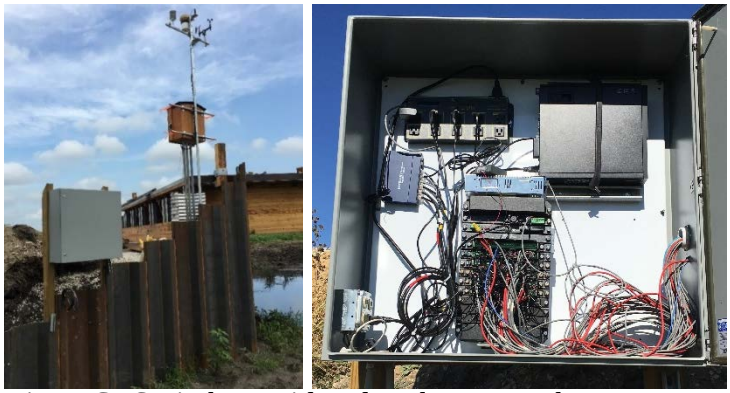

Fig. 7 GRS-Timber Bridge data logger enclosure

Girder strains are being collected at two cross sections: (1) a distance *d*, *d* being the depth of the girders, from the center of bearing of the girders at the west abutment, and (2) at midspan of the bridge as shown in Figure 6. Girder strain gages were installed approximately 5.1 cm below the deck surface and midwidth on the bottom of the girders at each location. As shown in Figure 8, each strain gage is comprised of a foil strain gage affixed to a 2.5- by 20.3-cm. strip of 0.127-mm-thick stainless steel. This strain gage configuration was developed in a previous research project by ISU and is referred to as a shim gage. The shim gage is then attached to the glulam girder using Loctite 426 adhesive (Loctite, Düsseldorf, Germany). Girder strains are used for multiple analyses of the structure, including but not limited to, the neutral axis, peak tensile strain, girder end rotation, transverse load distribution, and various truck detection–evaluation calculations.

Deck strains are collected at key locations, using the same shim gage configuration discussed previously, to obtain vehicle information as well as deck performance measures. The six deck gages

are located in bays 2, 3, and 4 and along two cross sections. As shown in Figure 6, the first cross section is located 1.83 m from the centerline of the girder bearing on the west abutment, and the second is located 2.44 m east of the first line. In each of the three instrumented bays, there is one strain gage per cross section located adjacent to the longitudinal stiffener beams and oriented in the transverse direction. The deck gages allow the BECAS system to not only detect the presence of a vehicle, but determine the speed of the vehicle, the transverse position of the vehicle on the bridge, the number and spacing of axles on the vehicle, as well as assess glulam deck performance.

Fig. 8 Shim gage configuration for measuring strains

The raw strain data collected in the SHM system are continuously stored in the database as 1-minute data files. Each 1-minute data file contains five strain components: (1) creep- and shrinkage-induced strain response; (2) temperature-induced strain response; (3) noise; (4) quasi-static strain response caused by ambient traffic; (5) dynamic strain response caused by ambient traffic and other dynamic loads such as wind. For this study, damage detection and structural capacity evaluation are both based on the quasi-static bridge response caused by truck events, which is a portion of strain component (4). Accordingly, the other four strain components are excluded from the strain data collected for these truck events. Truck events are identified using the deck strains; data files not found to have a truck event are discarded, and only data files representing truck events are further analyzed. A typical strain response to the presence of a three-axle truck crossing a bridge with an SHM system is shown in Figure 9.

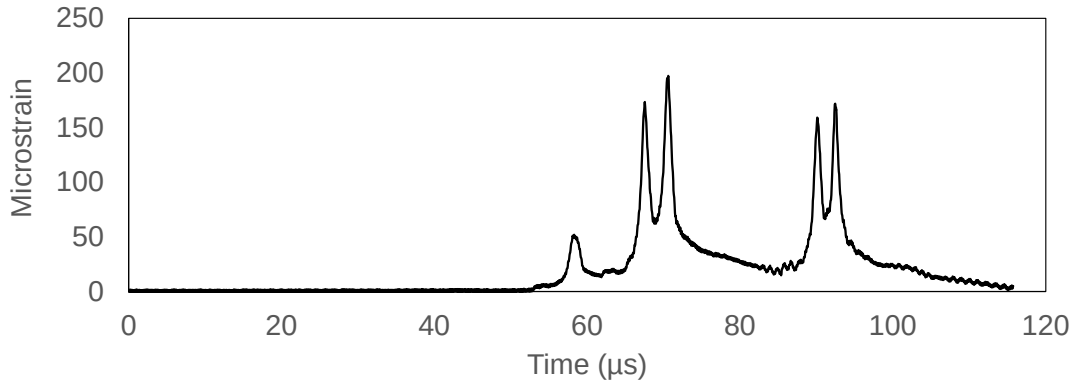

Fig. 9 Typical strain response of a three-axle truck crossing a bridge with an SHM system

The change of the strain response caused by creep, shrinkage, and temperature changes within a 1-minute period are considered negligible and can be neglected during the data process, which was also discussed by Doornink et al. [10] and Lu [7] . However, the strain response caused by creep, shrinkage, and temperature changes, which is almost constant in each data file, needs to be eliminated. To zero the strain response, a constant baseline strain should be determined for each strain sensor. The baseline strain for each sensor can be identified by finding the mode of the sensor data, which represents the value most frequently occurring in the 1-minute data collection [7]. The raw strain data of each sensor can then be zeroed with respect to the baseline strain to eliminate the creep-, shrinkage-, and temperature-induced strain components.

4.2.2 Force and Displacement Measurement Systems

The approach taken for monitoring the superstructure dynamic behavior is to consider that the superstructure is a black box composed of structural governing equations with unknown parameters that takes in first-order inputs in the form of forces and yields displacements as first-order outputs. Forces are measured using LBM-20K load cells (Interface, Inc., Scottsdale, AZ) capable of measuring up to 89.0kN. Two load cells are placed at each end of the six glulam stringers, for a total of 24 force measurements. A welded plate bearing assembly to which the load cells are

mounted and which affixes stringers to the beam seat is shown in Figure 10. The use of two load cells per stringer end ensures static equilibrium and facilitates measuring stringer torsion. Load cell signals are conditioned and digitized using six-input LabJack T7 Pro multifunction DAQ devices; four LabJack devices are utilized in all. Force measurement data is transferred from the LabJack via USB to a Raspberry Pi 2 single-board computer, which transmits the information to the remote server for archiving.

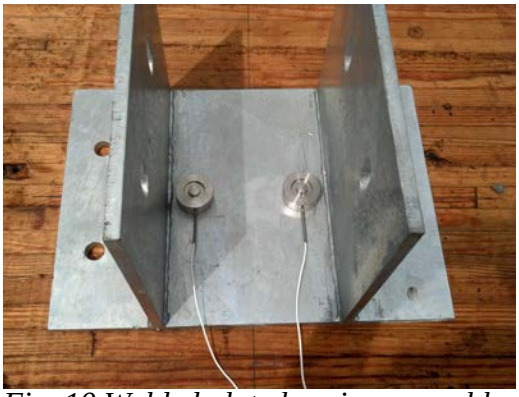

Fig. 10 Welded plate bearing assembly with mounted load cells

The displacement output of the bridge is measured by fixed reference frame cameras monitoring the movement of infrared laser LEDs. The LEDs are to be placed by identifying the locations on the bridge that provide the most robust and unique information to solve for the unknown parameters. The LED locations are determined by simulation of the superstructure behavior. The infrared laser LEDs have a divergence of 2° and are imaged using the camera settings as a white dot in a black background. The centroid of this dot is tracked in real time to monitor the movement of the bridge with subpixel accuracy. Two types of cameras are used to monitor the bridge. A Raspberry Pi NoIR Camera is attached to each of the four Raspberry Pis. The Raspberry Pi converts the image of the LED to a digital coordinate. The other camera system used is the Pixy CMUcam5. The Pixy camera system utilizes an embedded microcontroller to calculate the image to coordinate conversion onboard at 50Hz. The Raspberry Pi reads the coordinates output from the Pixy. The displacement data is sent with the force data to the server. An additional Raspberry Pi is utilized to act as a master to coordinate the timing between the four data acquisition Pis and to serve as a gateway between the locally networked Pis.

The generated force displacement data will be utilized to inversely solve for the unknown superstructure parameters by satisfying the governing system of equations. Each vehicle becomes an excitation to the system that adds to the behavior space for which to characterize the black box and which to subsequently compare against for indications of degradation.

5. Results

5.1 Girder Stiffness Testing

Fig. 11 Girder with weight at midspan during stiffness testing

To obtain a better understanding of the individual strength parameters of the girders for the bridge, and to facilitate more accurate modelling, calibration, and load ratings from the SHM system, all six glulam girders were individually load tested prior to installation at the bridge site. Testing took place at the Buchanan County maintenance shop. Each girder was positioned on temporary supports, set at the same distance as the abutments on the bridge, and braced laterally at each end. Three displacement transducers were then attached to the underside of the girder, one offset from each support approximately 2.5 cm, and another at midspan of the girder. Loading of the girders was achieved using a crane and the steel hammer from a pile-driving apparatus as dead weight. Total weight of the hammer and rigging was approximately 10.14 kN. Once the girders were properly braced, instrumented and data collection was underway, the weight was carefully, without impact, placed at midspan of the girder until full relief of tension in the crane rigging was achieved. Figure 11 illustrates a girder with the weight placed at midspan. Data was collected for approximately 10 sec. and then the weight was removed while data continued to be collected. Data collection was stopped once the weight was completely removed and displacements appeared to balance back to zero. This process was done twice for each

girder to ensure repeatability of the data. Using basic fundamentals from mechanics of materials and the data from the girder load tests, the Young's Modulus of each girder was calculated and is presented below in Table 2.

Table 2. Young's Modulus (GPa) for GRS Timber Bridge Girders

Girder	1	2	3	4	5	6
Test 1	9.03	9.10	8.62	9.51	10.00	11.38
Test 2	10.41	11.38	6.89	10.76	9.93	11.72
Average	9.72	10.27	7.79	10.14	10.00	11.58

5.2 GRS Settlement Measurements

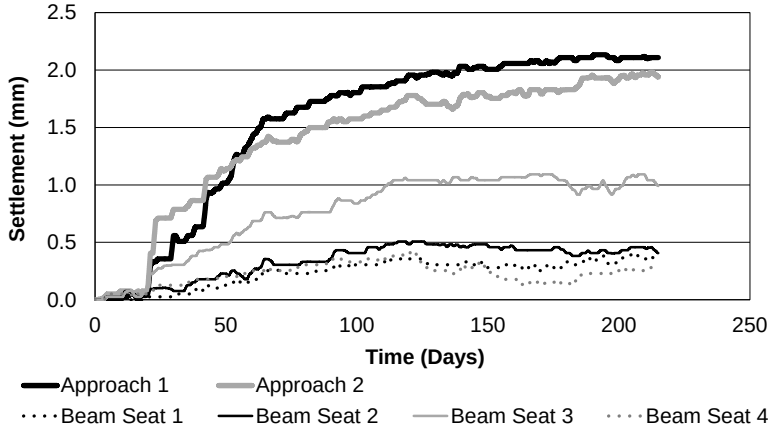

Fig. 12 Monitored settlement measurements from vertical extensometers mounted under the beam seat and within the roadway approach

As previously noted, the main benefit of the GRS-IBS system is the reduction in settlement of the approach roadway adjacent to the bridge ends. Settlement at the site is monitored by vertical extensometers (VE) installed into the abutment. The settlement results for the first 215 days of monitoring are given in Figure 12. The VE in the roadway approach are labelled Approach 1 and 2. The settlement for the approach is approximately 2 mm across a 2.32 m span (4 VE in series). The VE under the beam seat are labelled Beam Seat 1 through 4. The largest of the settlement measurements under the beam seat was Beam Seat 3, which has approximately 1 mm of settlement across a 1.16 m span (2 VE in series). Wahls indicated that a differential settlement of 12 mm would likely require maintenance, but would not be considered intolerable. The differential settlement between the roadway approach and the beam seat after 215 days is between 1 and 1.5 mm, far below the level requiring maintenance [11].

5.3 On-Site Validation Testing

In addition to the long-term structural monitoring being conducted by the SHM system, routine short-term live-load tests are included in the program for this structure. The initial load test will be conducted in the spring of 2017, with subsequent tests to follow every 6 to 12 months for a period of 2 to 3 years. These tests will involve use of a structural testing system and instrumentation from Bridge Diagnostics, Inc. (BDI) (Boulder, CO) and will allow for collection of strain and deflection data in addition to data collected by the on-site SHM system. BDI strain transducers will be installed in the proximity of the existing shim gages. In addition, deflections will be measured at midspan of each of the girders. Loading of the structure will be completed using loaded trucks, of known but varying weights and axle configurations, traveling across the bridge at crawl speed to collect quasi-static response data. Data from the live-load testing will be used to validate strains collected from the SHM system, verify vehicle recognition parameters for the system, and provide additional structural performance information on the structure. In addition to the structural-related measurements, moisture readings will be taken during the live-load testing using typical moisture meters to validate moisture readings collected by the SHM system.

6. Summary and Recommendations

A collaborative bridge design and construction effort culminated with the October 2016 opening of the Catt Bridge in Buchanan County, Iowa. The new bridge is supported by a nontraditional substructure system referred to as a geosynthetic reinforced soil (GRS) bridge abutment. The superstructure spans 16.2 m and is comprised of glulam girders supporting a transverse glulam deck

system. Both the sub- and superstructural systems are being actively monitored with an extensive array of sensors embedded in the GRS abutments or attached to the bridge superstructure. Data collected will be helpful in maintaining the overall health of the bridge by detecting structural deficiencies or triggering timely maintenance actions. This should result in a significant increase in the bridge's life expectancy, which could potentially exceed 100 years.

7. Acknowledgements

The authors thank the following individuals and organizations, who have contributed to the overall success of this project: Federal Highway Administration, Washington, DC; Laminated Concepts, Inc., Big Flats, New York; Alamco Wood Products, Albert Lea, Minnesota; and Brian Keierleber and the Buchanan County Bridge Team, Independence, Iowa. Special thanks are given to FPL electronics and computer engineers, Dave Simpson and Will Kinney, for their assistance with the installation of the field data acquisition system and weather station equipment.

8. References

[1] USDOT, Federal Highway Administration, National Bridge Inventory, January 2017, https://www.fhwa.dot.gov/bridge/nbi.cfm.

[2] Phares B. M., Wipf T. J., Deza U., Wacker J. P., *Development of a Smart Timber Bridge—A Five-Year Plan*, General Technical Report FPL-GTR-195, U.S. Department of Agriculture, Forest Service, Forest Products Laboratory, Madison, WI, 2011, 10 p.

[3] AASHTO, AASHTO M43, *Standard Specification for Sizes of Aggregate for Road and Bridge Construction*. American Association of State Highway and Transportation Officials, Washington, DC, 2005.

[4] AASHTO, AASHTO M288, *Standard Specification for Geotextile Specification for Highway Applications*, American Association of State Highway and Transporation Officials, Washington, DC, 2015.

[5] Adams, M., et al., *Geosynthetic Reinforced Soil Integrated Bridge System, Interim Implementation Guide*, No. FHWA-HRT-11-026, U.S. Federal Highway Administration, 2011.

[6] AASHTO, *Load and Resistance Factor Design (LRFD) Design Specifications for Highway Bridges*. 14th Edition. American Association of State Highway Transportation Officials, Washington, DC, 2014.

[7] Lu P., Wipf T., and Phares B., *A Statistical Based Damage Detection Approach for Highway Bridge Structural Health Monitoring*, Ph.D. Dissertation, Iowa State University, 2008.

[8] Boechler A., Pence T., Hosteng T., and Phares B., *Development of a Smart Timber Bridge – Sensor Evaluation, Algorithm Methods and Identify Changes in Timber Bridge Stiffness, and Developing a Timber Bridge Rail Impact Detection System*, Institute for Transportation, Iowa State University, 2015.

[9] Pence T., Hosteng T., Phares B., and Wacker J., *Investigation of Moisture Sensors for Historic Covered Bridges*, Institute for Transportation, Iowa State University, 2014.

[10] Doornink J., Wipf T., and Phares B., *Monitoring the Structural Condition of Fracture-Critical Bridges Using Fiber Optic Technology*, Ph.D. Dissertation, Iowa State University, 2006.

[11] Wahls, H.E. *NCHRP Synthesis of Highway Practices 159: Design and Construction of Bridge Approaches.* Transportation Research Board, National Research Council, Washington, DC, 1990.

A Robust, Passive Resistance Sensor for Moisture Content Monitoring of Timber Bridges

Niclas Björngrim
PhD student
Luleå university of Technology
Skellefteå, Sweden
niclas.bjorngrim@ltu.se

Niclas research interests are monitoring and inspections of timber bridges and measurement techniques for moisture in wood.

Per-Anders Fjellström
Senior Engineer
RISE
Skellefteå, Sweden
Per-anders.fjellstrom@sp.se

Per-Anders Fjellström has been working with full scale tests, health monitoring, inspection test methods and inspections manuals since 1994.

Olle Hagman
Professor
Luleå university of Technology
Skellefteå, Sweden
olle.hagman@ltu.se

Wood Science and Technology
Luleå University of Technology

research topic: non-destructive calibration, testing and predictions of wood and wooden structures by means of multimodal sensors and multivariate image processing.

Summary
To assure a long service life for a timber bridge the super structure must stay dry. Good design, scheduled inspections and monitoring of the moisture content will help achieve a long service life. Sensors for measuring wood moisture content is not adapted for monitoring of timber bridges. This paper presents moisture content sensor adapted for timber bridges. The sensor can both be installed during the manufacturing and retrofitted. As a result of the monitoring, a design flaw was detected and corrected. The Swedish transport administration demand that this system is installed on all new stress laminated timber bridges that are built.

Keywords: Moisture content, Timber bridge monitoring, Moisture content sensor, Wood moisture content.

1. Introduction

The single most important aspect for a long service life of a timber bridge made of Spruce is the moisture content in the super structure. Dry bridges do not rot and by using wood protection by design, moisture content sensors and scheduled in-depth inspections by qualified inspectors to achieve correct bridge management data dry bridges are attainable. Pousette and Fjellström [1] reported their findings from inspections of 67 stress laminated timber bridges built between 1994 and 2015; 21 of those bridges showed MC over 20%, and eight had started to show decay.

The optimal sensors should be robust, simple, cheap, scalable and should last the service life of the bridge. The sensor output should be reliable, have excellent repeatability and be simple to use to avoid measurement bias. A fixed position for the system for measuring moisture

content is important in order to achieve correct data for bridge management. The goal is to be able to detect the moisture content (MC) in four different classes:

1. 0-20% MC
2. 20-24% MC
3. 24-28% MC
4. 28- % MC

This paper presents an optimized sensor for use on timber bridges. The sensor is based on passive resistance measurements and can be installed during manufacturing as well as a retrofit. Resistance measurements have an accuracy of circa 1,5 percentage points between 6 and 24% MC [2] which fits well in to the goal of four different classes. The sensor is well suited for large cross-sections such as girders, arches and pre-stressed decks. The sensor will measure the moisture content the whole height of the cross-section. This makes it possible to find elevated moisture content under the membrane or close to the pre-stressing rods etc. The sensor uses uninsulated electrodes that are just a few centimeters shorter than the height of the cross-section. Due to parallel resistivity, the resistance is decreasing logarithmically with increased electrode length. The resistance is also increasing with decreasing temperature. The system is installed on twelve timber bridges in Sweden, most notably Sweden's longest timber bridge for heavy-duty traffic.

2. Experimental

Laboratory test was conducted to evaluate how the moisture content (MC), number of glue lines, and the pre-stressing force affect the measured resistance.

2.1 materials

All specimens were made of Norway spruce (*Picea abies (L.) Karst.*) The glulam used is glued with melamine-urea-formaldehyde adhesive and have 45 mm-wide lamellas. Glulam specimens where of two sizes; ten small measuring 270 mm long, 60 mm wide, and 18 mm thick and six large measuring 495 mm long, 65 mm wide, and 55 mm thick. The small specimen is of a thickness typically for pedestrian bridges and the large specimen have a thickness suitable for vehicle traffic. Boards of the same dimension as the small glulam specimens where also used to evaluate how the glue lines affected the resistance measurements. The electrodes where made of stainless steel with a diameter of 0,8 mm.
An Instron 5500 R universal testing machine was used to apply pressure on the specimens to simulate the stress-laminated force.
Two stress laminated mock bridges where also used; the small mock bridge measures 620 mm long, 450 mm high and 270 mm deep and the large mock bridge measures 2000 mm long, 495 mm high and 345 mm deep. Both decks consist of three glulam beams. The small deck is stressed to 0,3 MPa with two steel bars and the large deck is stressed to 0,7 MPa with six steel bars. The small deck has electrodes clamped between the glulam beams and the large deck have electrodes both clamped between the glulam beams and electrodes pushed into drilled holes. The resistance was measured with a Fluke 1507 resistance tester on all specimens and on the small deck. On the large deck an Omnisense S-900-1was attached to the electrodes and the resistance was measured every hour.

2.2 laboratory tests

The glulam specimens where paired and between each pair two electrodes where placed with a 25 mm spacing. The glulam pair with two electrodes where the put under pressure in the

universal testing machine to simulate a stress laminated deck with electrodes clamped between two glulam beams.

The small glulam specimens are made of six lamellas. To test the influence of the number of glue lines the resistance was measured with the electrodes passing the first lamella, and the second and so forth. For each length increment of the electrode three levels of pre-stressing force was tested. The specimens where conditioned to three different MC levels. Two 1485 mm long glulam pieces where constructed by clamping three large glulam samples together, to be able to calibrate the resistance for the largest of bridge decks (see figure 1).
The small mock bridge was put in a climate chamber and the temperature and resistance was measured at every 5°C decrement from 20°C to -10°C. For a more thorough explanation of the tests refer to Björngrim et al. (2017).

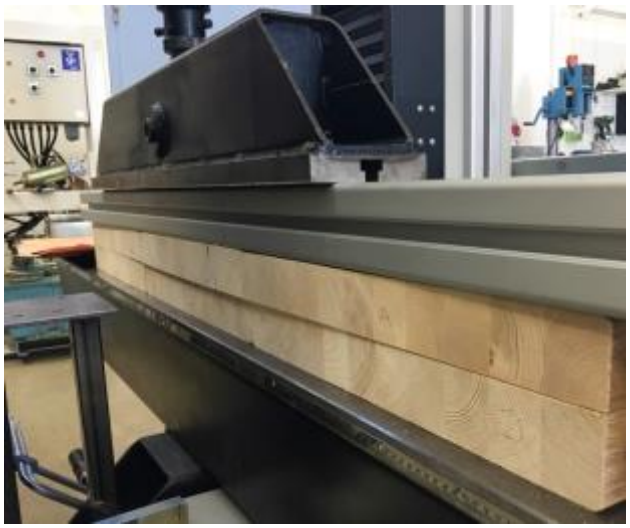

Fig. 1. 1485 mm long glulam with electrode in between is tested in the universal testing machine.

2.3 long term evaluation of the two techniques

The sensor proposed here can either be installed at factory during the manufacturing process or retrofitted later at the bridge site. When installing the system at the factory electrodes of stainless steel wire is clamped between the glulam beams. The diameter of the wire is 0,8 mm. When retrofitting the sensor, the electrodes are pushed in to bore holes. To be able to push in the electrode a larger diameter must be used, here stainless steel pins of diameter 2,4 mm have been used. When drilling the holes for the retrofit sensor there will be some sawdust left in the holes, that together with the larger diameter of the electrode made it necessary to assure that the different methods give the same results. Therefore a long-term study was conducted.

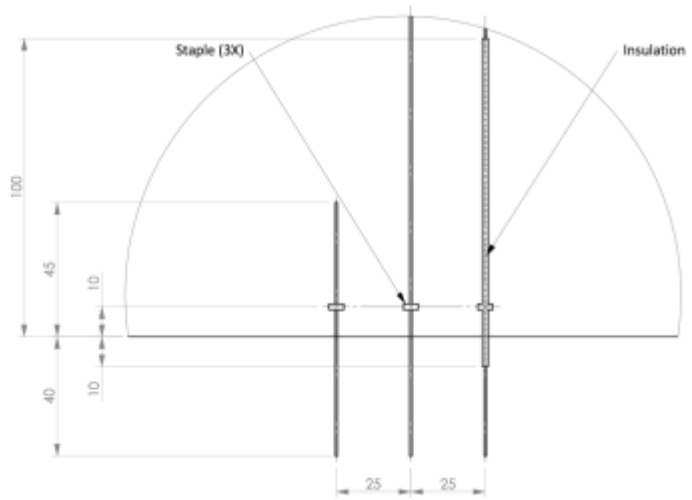

Fig. 2 Schematic figure of the passive resistance sensor.

On the large mock bridge five sensors where attached. Figure 2 show the schematics of the MC sensor. Each sensor consists of one 45 mm long electrode and two 450 mm long electrodes spaced 25 mm. These three electrodes forms one sensor, where the short electrode and one long measure the MC at a depth of up to 50 mm from the bottom. The second long electrode is insulated the first 100 mm and together with the first long electrode the MC is measured between 100 to 450 mm from the bottom.
Sensor 1, 2 and 3 is clamped between two glulam beams and the bridge was stressed, see figure 3. Sensor 4 is retrofitted ca 15 mm towards the mid lamella from sensor 1 and 2. Sensor 5 is retrofitted ca 15 mm towards the mid lamella from sensor 3. At each measuring point a OmniSense S-900 is attached and measure the resistance every hour. After fitting all the sensors, the large mock bridge was painted and a waterproof membrane was attached to the top (figure 4). Lastly a combined roof and sidewall construction is placed on top of the bridge and placed outside (figure 5).

Fig. 3 Stressing the large mock bridge.

Fig. 4 attaching water proof membrane.

Fig. 5 Wood protection by design.

2.4 Experimental results

Shot summary of the results are presented here, for a more thorough explanation of the results refer to [3]. Resistance measurements on all samples specimens showed a logarithmic decrease when the electrode length was increased. The temperature dependency was tested and when the temperature decreases the resistance in the wood increases. The pre-stressing force did not affect the resistance measurements. The experimental data was used to create two models, one for electrodes measuring the surface MC, from 0-50 mm and one from 100 mm to 10-20mm from the top. The model differs no more than 1,5 percentage points for MC up to 28% and electrode lengths up to 635 mm. In figure 6 a clamped sensor, S3, is compared to a retrofitted sensor, S5. The curves are almost identical for the two installation types.

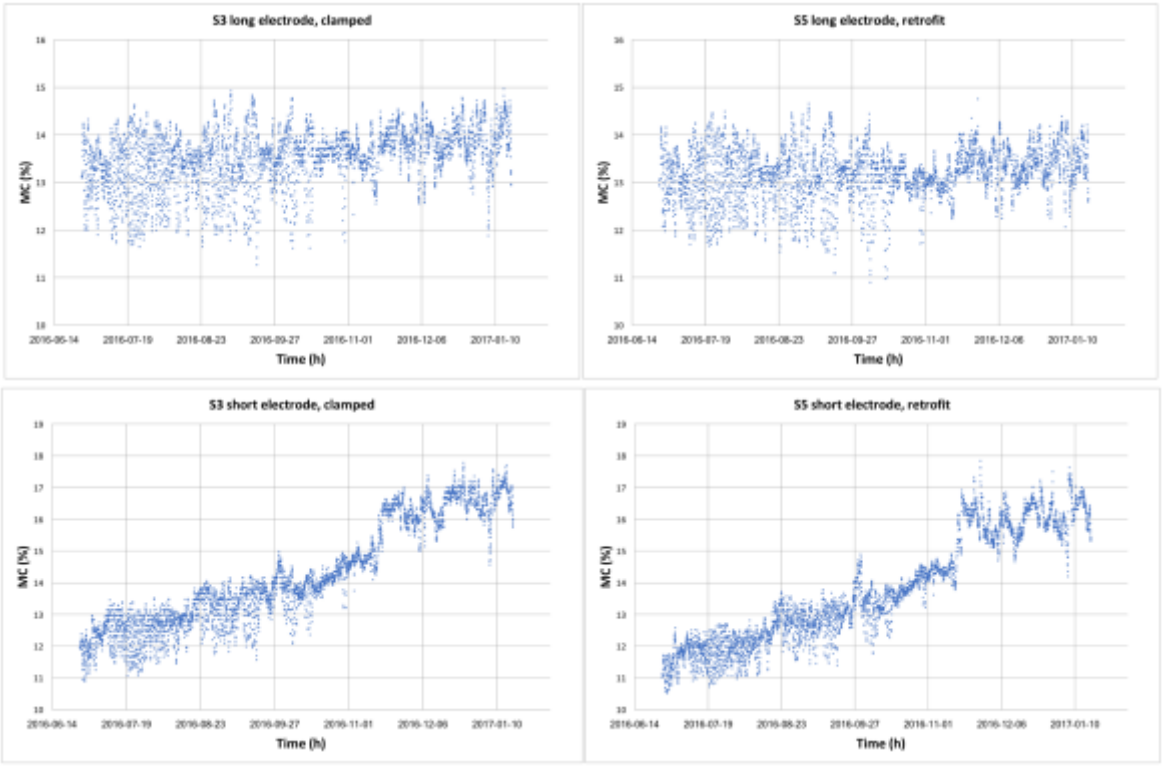

Fig. 6 a, b, c and d. MC variation over seven months for a: long electrode of a clamped sensor, b: long electrode of a retrofitted sensor, c: short electrode of a clamped sensor d: short electrode of a retrofitted sensor.

3. Field test

Two bridges where chosen for this study. Gislaved bridge was retrofitted with the sensor in October 2015. Sundbron was delivered with the sensor installed at the factory.

3.1 Gislaved Bridge

Gislaved Bridge is Sweden's longest timber bridge for full traffic load. The bridge spans 46 meters and the deck is 10.5 meters wide. The deck is made of stress laminated timber and the arches of glulam. The bridge spans the river Nissan, and is the longest bridge for highway traffic in Sweden. The bridge was erected in October 2013. In October 2015 during two days the bridge was retrofitted with 16 MC sensors. Each arch have three sensors, the deck have four on each side and two in the middle of both ends, see figure 7. The MC have been measured three occasions.

Fig. 7 a, b. The sensors marked on a: the north facing side and b: south facing side of Gislaved bridge.

3.2 Sundbron Bridge

Located in Boden, Sundbron is a stress-laminated, one-lane traffic bridge. The bridge is four meters wide and 26 meters long, and was erected in November 2015. The bridge spans a strait between two lakes. The bridge was equipped with seven sensors that was installed at the factory, see figure 8. There are three sensors on the south facing side and four on the north facing side. All seven sensors are clamped between the two outermost glulam beams. The MC have been measured three occasions. During the second measurement, an Omnisense S-1 (Omnisense 2017) logger was installed at measurement point 1, short electrode. That measuring point was then monitored until the beginning of October 2016.

Fig. 8 a, b the sensors marked on a: the north facing side and b: south facing side of Sundbron bridge.

3.3 Results of field tests

Gislaved Bridge

In figure 9 and 10 the MC measurements for the short respectively the long electrode is shown. Short sensor 4 and 11 and long sensor 4, 6 and 10 all show MC values close to or over the fiber saturation point. The high MC was due leakage, the reason for the leakage was found and the design have been changed in early 2017.

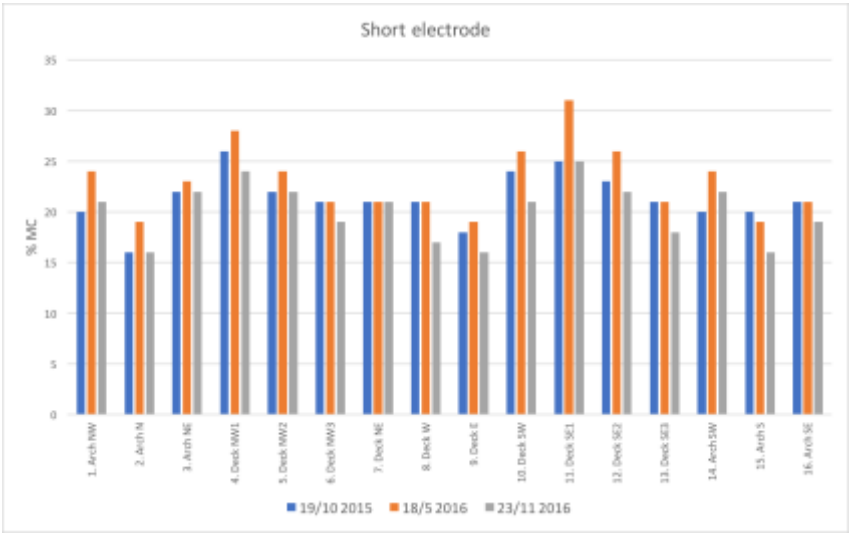

Fig. 9 MC values of the short electrode on Gislaved bridge from three measurement occasions.

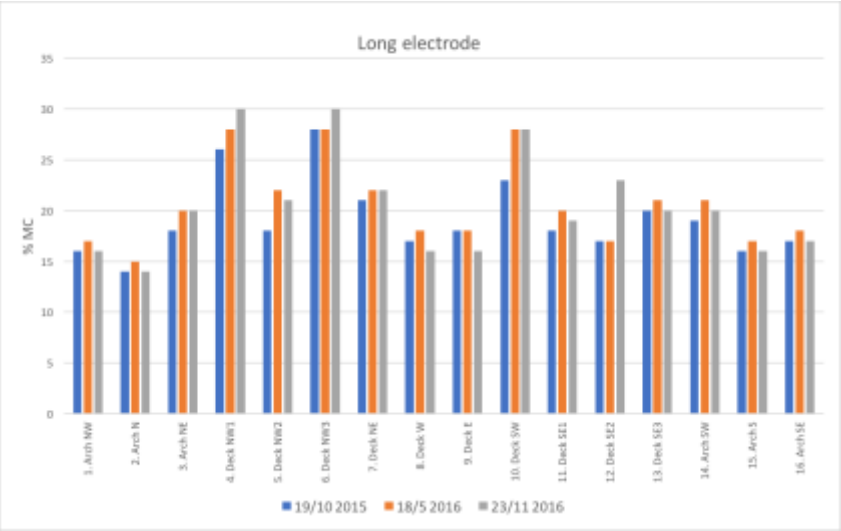

Fig. 10 MC values of the long electrode on Gislaved bridge from three measurement occasions.

Sundbron Bridge

In figure 11 and 12 the MC measurements for the short respectively the long electrode is shown. The bridge was erected in both sleet and rain which explains the very high MC during the first two measurements. In figure 13 the monitoring results of sensor 1, short electrode is shown, the initially high MC dries out during down to a MC of 16-17% during the summer. The missing bar in figure 11, sensor 1 is because of the logger installed.

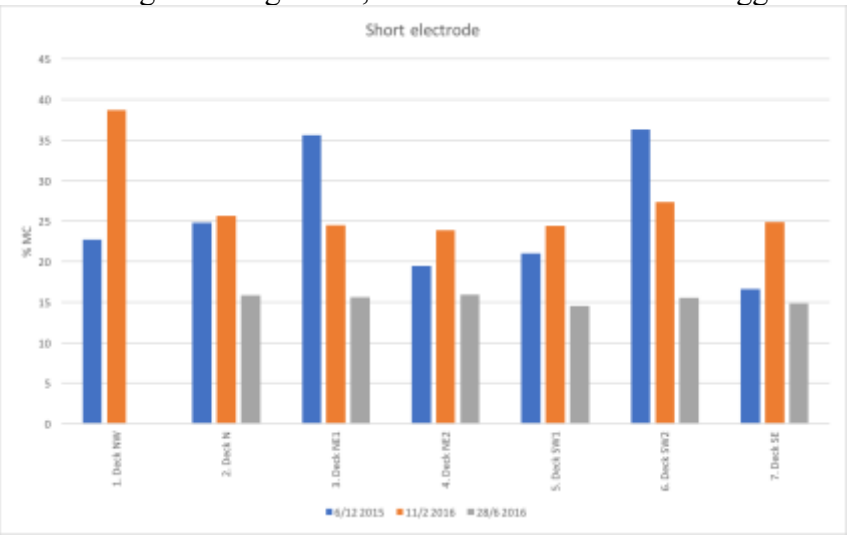

Fig. 11 MC values of the short electrode on Sundbron bridge from three measurement occasions.

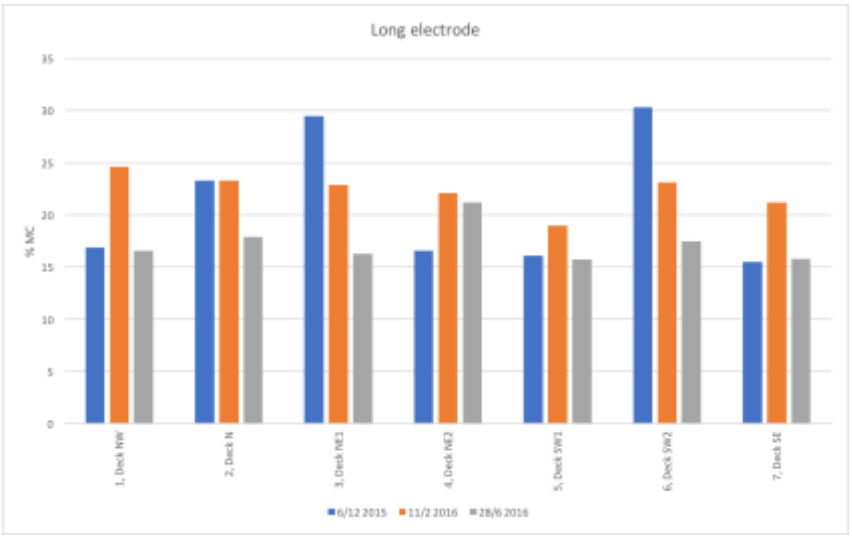

Fig. 12 MC values of the long electrode on Sundbron bridge from three measurement occasions.

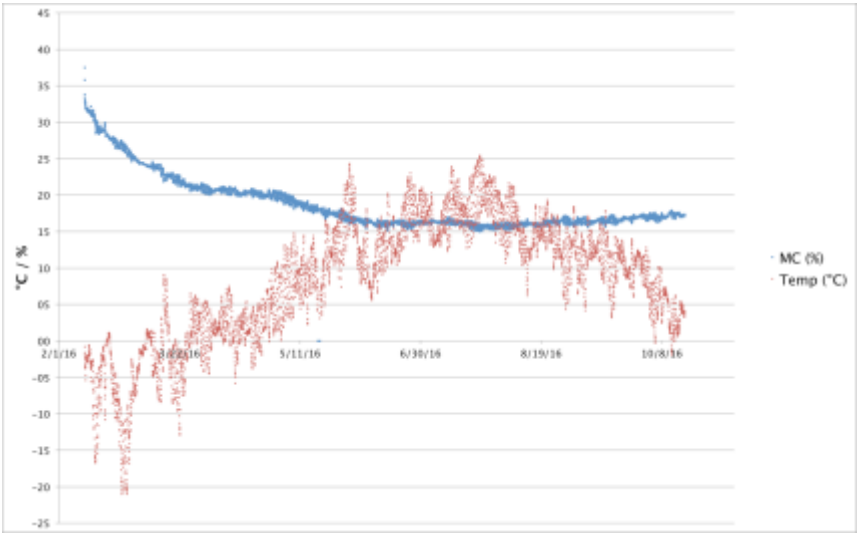

Fig. 13 MC and Temp of sensor 1 at short depth from February to October.

4. Conclusions

- By using uninsulated electrodes and calibrate for the electrode length the MC of timber bridges can be monitored in a very efficient way. The sensor can only find the single highest MC value along the length of the electrode.
- The resistance decreases with an increased electrode length, since the electrodes are uninsulated this is assumed to be because of the parallel resistivity in the wood.
- The sensor is robust, simple, cheap, scalable and should last the service life of the bridge. The sensor uses resistance measurements, a well-proven method of determining MC in wood.
- Our proposed sensor uses two electrode lengths, the first measure 0-50 mm in from the bottom and the second measure 100 mm from the bottom up until 10-20 mm from the top. Due to the uninsulated electrodes, the resistance is very length dependent making

it necessary to use two models to calibrate the MC, one for short and one for long electrodes.

- The model differs no more than 1,5 percentage points up to an electrode length of 635 mm.
- The pre-stressing force does not affect the model, so this system could be used in any solid wood construction where MC monitoring is of interest.
- The long-term evaluation showed no difference between the two installation methods. The MC close to the bottom of the bridge will vary during the year and the MC close to the waterproofing layer will remain stable over the year.
- Gislaved Bridge took two days to retrofit with 16 sensors. Considering that it is a large bridge with tall arches, and the number of sensors that were mounted, the retrofitting was quite fast. For bridges without arches, the retrofitting could be completed even more quickly.
- Sundbron was erected during rain and sleet hence the long-term monitoring showed that after initial high MC the surface moisture on the bottom of the bridge deck dried down to normal MC levels during the spring.
- This research was performed on Norway spruce, and the findings might not be transferable to other species without calibration.
- All timber bridges ordered by the Swedish Transport Administration are required to have the passive resistance sensor installed.

5. Acknowledgments

Financial support from the Swedish Research Council Formas project, Experimental studies of capillary phenomena in bio-based materials 942-2016-64, is greatly acknowledged.

6. References

[1] Pousette, A., and Fjellström, P. A. (2016). *Experiences from timber bridge inspections in Sweden–examples of influence of moisture*. SP Report, ISSN 0284-5172 ; 2016:45

[2] Forsén, H., and Tarvainen, V. (2000). *Accuracy and Functionality of Handheld Wood Moisture Content Meters*, Technical Research Centre of Finland, Espoo, Finland.

[3] Björngrim, N., Fjellström, P. A., & Hagman, O. (2017). Resistance Measurements to Find High Moisture Content Inclusions Adapted for Large Timber Bridge Cross-Sections. *BioResources*, 12(2), 3570-3582.

[4] Omnisense (2017) https://shop.omnisense.com/s-900-1-wireless-t-rh-wme-sensor

Effect of on-site splice joints for timber network arch bridges

Martin CEPELKA
PhD. Candidate
Norwegian University of Science and Technology (NTNU)
Trondheim, Norway
martin.cepelka@ntnu.no

Martin Cepelka received his civil engineering degree from the Czech Technical University in Prague in 2011, worked as a bridge engineer from 2011 to 2014 and is currently pursuing a PhD at NTNU.

Kjell Arne MALO
Professor
Norwegian University of Science and Technology (NTNU)
Trondheim, Norway
kjell.malo@ntnu.no

Kjell Arne Malo is professor of timber structures at NTNU. His research topics are methods for increased strength and stiffness of connections for timber structures and vibrations in timber structures.

Summary

Feasibility studies of glulam arches with network hanger configurations have shown possibilities to achieve large spans of timber bridges. However, the length of timber elements is limited due to production and transportation issues. Long-span arches of full-timber cross sections must thus be spliced at building site. Considering stability and buckling problems of the timber arches, high requirements on flexural rigidity are imposed on the incorporated splice connections. In this paper, a novel timber splice solution using long threaded rods is presented and the effect of rotational stiffness of splice joints on stability of timber network arch bridges with spoked-wheel configuration of hangers is investigated by use of numerical models. The present investigation revealed that application of long threaded rods can provide practical splice joints with sufficient rotational stiffness in order to maintain stability of timber network arch bridges.

Keywords: timber bridge, splice joint, long threaded rod, network arch, rotational stiffness, buckling, finite element analysis

1. Introduction

The development of glued laminated timber (glulam) enables production of timber elements with nearly unlimited cross-sectional dimensions. The fact that glulam has excellent strength to weight ratio compared to steel and concrete, promotes glulam to be used in structures with large spans. However, production and transportation impose limitations on the length of timber elements. In order to obtain large spans, either truss structures or splicing of elements are necessary. Truss structures are characterised by a high number of connections, which are expensive and time consuming. When used in outdoor conditions such as timber bridges, connections have increased risk of decay due to moisture exposure.

Feasibility studies of glulam arches with network hanger configuration have shown that road timber bridges with spans reaching 100-120 m feature excellent stiffness properties and can be designed for full traffic loading [1, 2]. Massive glulam arches of such lengths must be spliced at the building site. In order to maintain stability and reduce buckling problems of the arches, it is crucial to incorporate flexural rigidity in the splice connections. The stability problems of network arch bridges containing splice joints were studied earlier in [3, 4]. These studies were carried out with a

common layout of arch bridges where wind truss between arches is used to stabilize the arches laterally. A new conceptual design of timber network arch bridges presented in [2] introduces a so called spoked-wheel configuration of hangers, where hangers are inclined both in the in-plane and the out-of-plane direction. The wind truss can thus be avoided since the sideway support of the arches is provided through hangers. The out-of-plane stability of the arches can however be expected being a critical design issue and sufficient rotational stiffness of the splice joints is a key prerequisite in order to maintain the stability of the arches. In the present paper, a novel splicing solution by use of long threaded rods is presented and the effect of rotational stiffness of splice joints on stability of timber network arch bridges with spoked-wheel configuration of hangers is investigated by use of numerical models. The necessary rotational stiffness of the splice joints both in the in-plane and the out-of-plane direction is identified and the results are compared to the design possibilities of the presented splicing solution.

2. A novel splicing solution by use of long threaded rods

There are various examples of use of moment resisting splice joints in the building industry. These are mostly placed in planar structures (frames, arches) and indoor conditions. There are fewer examples of splice joints used in timber bridges. Several state-of-the-art connection techniques are presented in [5]. There are, however, no jointing techniques available, fulfilling requirements for a practical and rotationally stiff on-site splicing of large glulam sections of timber bridges.
The recent research at Norwegian University of Science and Technology, NTNU has dealt with application of long threaded rods as fasteners in timber splice connections subjected to a bending moment. The main objective of the research project has been to develop a splice that allows practical and reliable on-site splicing of large timber sections of glulam arch bridges. The dominating internal force in such structures is compression, which can be transferred by direct contact of timber end faces. Shear force can be transferred via shear keys. The design utilizes high withdrawal stiffness and has virtually no initial slip. The use of threaded rods can give rotationally stiff joints that can transfer moderate bending moments. By providing sufficient effective length, the failure mode is yielding of the steel rods. This enables a more reliable prediction of the structural properties and increased ductility of the joint.

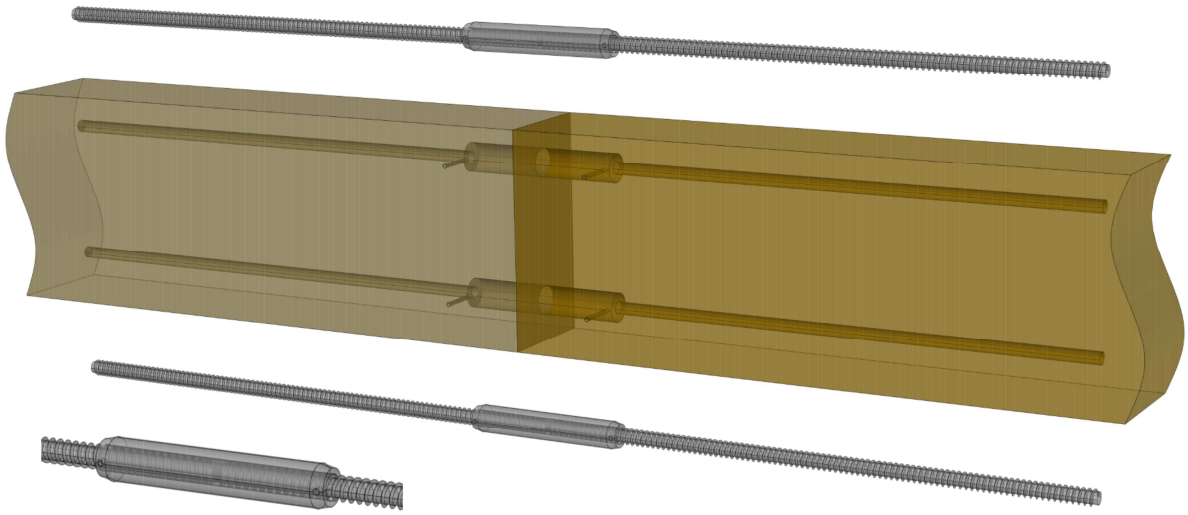

Fig. 1: Layout of splice connection with long threaded rods and grout-filled couplers.

A prototype splice joint using long threaded rods inserted parallel to the grain is shown in Fig. 1. Grout-fill steel couplers (similar to systems used for reinforced pre-cast concrete) were used for a mutual connection of the long threaded rods inserted in the opposed parts of timber beams. The steel couplers were purpose made, and manufactured from common structural steel. Two-component epoxy adhesive was used for grouting. Experimental and numerical investigations were carried out in order to determine the rotational stiffness and the moment capacity of the splice joint. Based on those, analytical relations for determining the rotational stiffness are proposed, and are here briefly summarized in the following. More details can be found in [6].
In the present analytical model, the relative rotation of the end faces of the splice connection is approximated by a relative rotation of the end sections of a beam portion of length $2l_c$. A deformed splice connection with a relative rotation θ of the end faces caused by the bending moment M is shown in Fig. 2. Here h and b are height and width of cross section respectively, a_0 is the height of wood in compression, a_i is a coordinate along z-axis of i-th row of the rods determined from the upper edge of wood in compression, l_c represents equivalent length of compression zone at each side of the connection, σ_x is normal stress in wood, K_{si} is axial stiffness of the i-th row of the rods and u_i is horizontal displacement at the the i-th row of the rods.

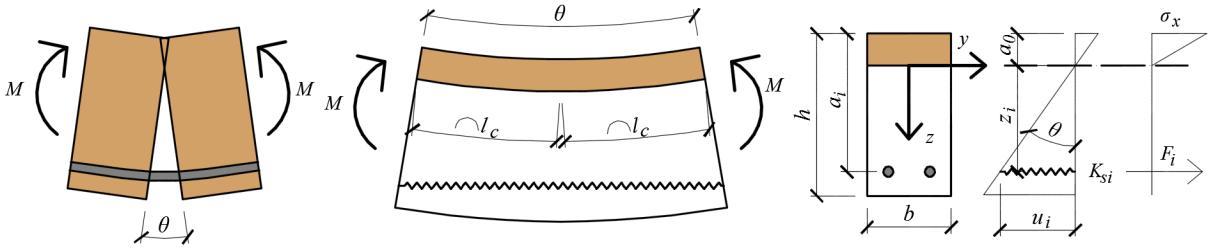

Fig. 2: Characteristics of the analytical model.

The height of wood in compression (position of neutral axis) is obtained by the following equation:

$$a_0 = \frac{-\sum_{i=1}^{n} K_{si} + \sqrt{\left(\sum_{i=1}^{n} K_{si}\right)^2 + \frac{E \cdot b}{l_c} \cdot \sum_{i=1}^{n} K_{si} \cdot a_i}}{\frac{E \cdot b}{2 \cdot l_c}} \tag{1}$$

where E is modulus of elasticity of timber parallel to the grain. The z-coordinate of the the i-th row of steel rods z_i is:

$$z_i = a_i - a_0 \tag{2}$$

The rotational stiffness of the connection k_θ is obtained as:

$$k_\theta = \frac{M}{\theta} = \sum_{i=1}^{n} K_{si} \cdot z_i^2 + \frac{E \cdot b \cdot a_0^3}{6 \cdot l_c} \tag{3}$$

The equivalent length of compression zone, l_c, is given by the following equation:

$$l_c = 0{,}85 \cdot h + l_{cr} \cdot \frac{E}{E_{cr}} \tag{4}$$

where E_{cr} is crushing modulus and l_{cr} is a crushing length.

The axial stiffness of the i-th row of steel rods, K_{si}, corresponding to the layout shown in Fig. 1 is given by Eq. (5). K_{si} is obtained as an effective stiffness of a system of three springs representing the axial withdrawal stiffnesses of the threaded rods at each side of the connection, denoted as K_w,

and the axial stiffness of the joint of threaded rods in the rod coupler, denoted as K_{co}. The number of steel rods in one row is denoted as n_r.

$$K_{si} = n_r \cdot \frac{K_w \cdot K_{co}}{2 \cdot K_{co} + K_w} \tag{5}$$

With reference to the performed experimental work as presented in [6], the following input parameters were determined: K_w=264 kN/mm, K_{co}=299 kN/mm, E_{cr}=114 MPa and l_{cr}=3 mm.

The orientation of the threaded rods in the grain direction enables direct force transfer in the axial direction. It also utilizes the high withdrawal stiffness of rods parallel to the grain. On the other hand, for rods inserted parallel to the grain, the withdrawal failure is rather brittle, something that can lead to a progressive failure of a group of rods. Furthermore, the development of shrinkage cracks (in the grain direction) in close proximity to the threaded rods, can lead to loss of capacity. These shortcomings can be overcome by using long threaded rods with a small inclination to the grain.

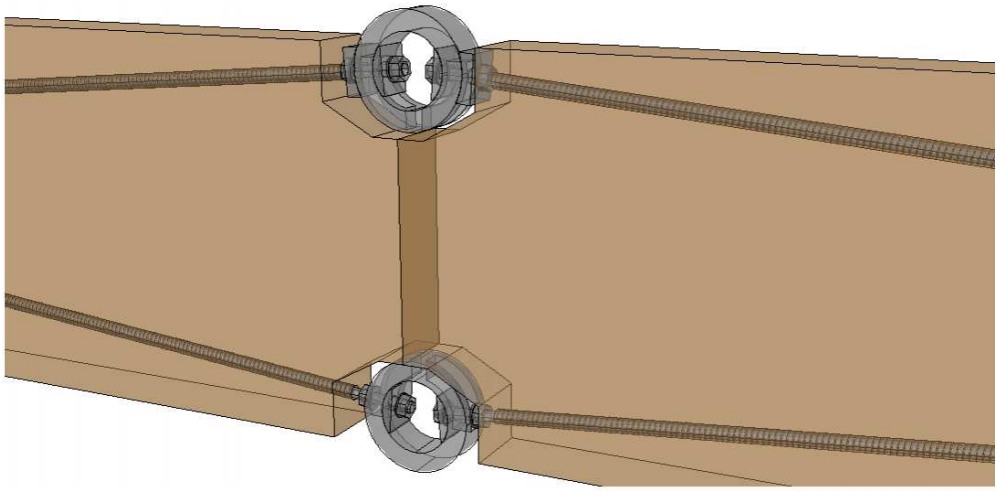

Fig. 3: Splice joint using long threaded rods inserted with an inclination to the grain.

A prototype splice joint using long threaded rods inserted with an inclination to the grain is shown in Fig. 3. Purpose made long threaded rods fabricated with a metric threaded part at the end of the rods furthermore allow easy and fast mounting of the rod coupler. The prototype joint was investigated by use of experiments and numerical models. The inclination of the rods was 5 degrees and effective length of the rods (the length of the rod screwed in the timber) was varied from 1000 mm to 1850 mm. A ductile tensile failure in rods (in the tension side) was achieved for rods of 1200 mm effective length and gross diameter of 22 mm. The experimentally tested splice joints featured large rotational stiffness and no initial slip. It should be noted that the application of the threaded rods with an inclination to the grain imposes a lateral force component at the end of the rods, which must be taken into account in the structural calculations. With reference to the analytical model presented here, Eq. (5) is adjusted for the combined axial and lateral deformations in dependence on the applied boundary conditions at the rod coupler. Detailed description of the performed work and analytical models will be published in the near future.

3. Effect of rotational stiffness of splice joints on stability of timber network arch bridges

3.1 Numerical models

A case-study arch bridge containing 2, 3 or 4 splice joints in each arch was modelled both in 2D and 3D and analysed by use of numerical models. The conceptual design of the bridge is based on the previous work of Bell [3] and Malo et al. [2]. The network configuration of hangers, where hangers cross each other at least twice, was shown to give a significantly lower bending moments and shear forces in the arches, as compared to the vertical arrangement of hangers, since the load is distributed approximately uniformly along the arch. The hangers are furthermore arranged in pairs with an out-of-plane inclination, providing a sideway support to the arches. By this so-called spoked-wheel configuration of hangers, a wind truss in between arches can be avoided, which in turn enhances durability of the arches due to lack of connections at the sides of arches. It is noted that network arch bridges present complex structural systems, for which various input parameters play important role in the distribution of stiffness characteristics and thus affect considerably the structural performance. The current investigation is limited to one particular arrangement, which is believed to be a representative example of a feasible network arch bridge with spoked-wheel configuration of hangers.

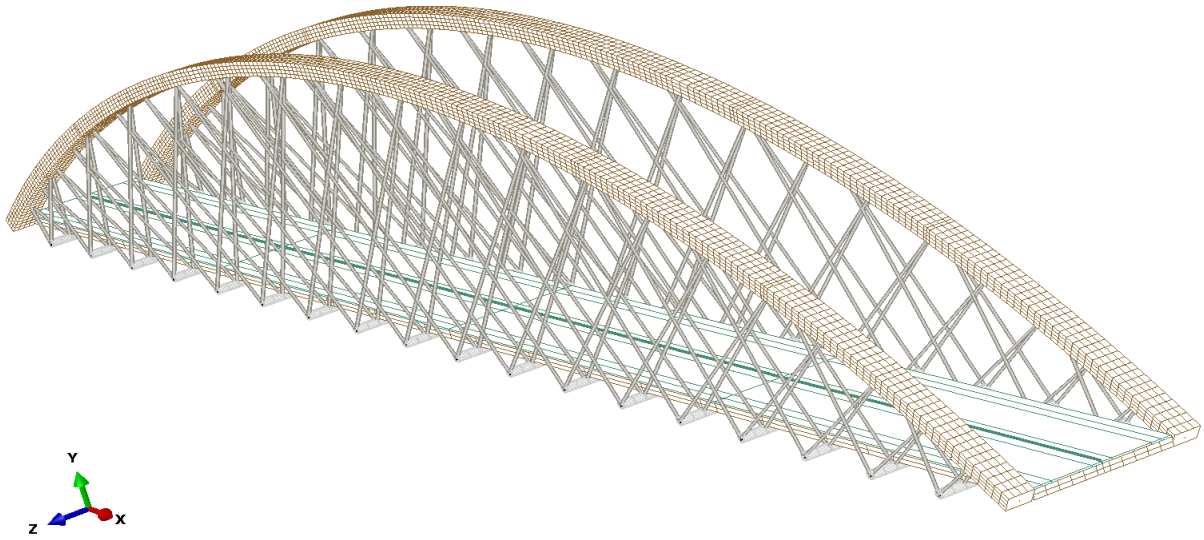

Fig. 4: 3D FEM model of the analysed bridge.

The bridge considered herein is a 2 lane road network arch bridge with a span of 100 m. The clear width of the bridge deck is 7 m, giving a distance between the centres of the arches of 8,3 m. The arch has a circular shape with the arch rise of 16 m, measured from the centre of the deck to the centre of the arch. There are 18 steel cross-beams uniformly distributed along the deck. The lateral distance between the anchor points of hangers at the cross-beams is 1200 mm (2*Z* with reference to Fig. 6). The arches have 1300 mm width and 900 mm height and are of glulam GL30c. The deck is made of a 500 m thick glulam stress-laminated slab of laminations GL24h. The steel hangers are 62 mm in diameter. The bridge parts were pre-designed according to European standards (Eurocodes) in order to assure suitable stiffness characteristics. The arches are supported through hinges in the in-plane direction, while a full rotational restraint is assumed in the out-of-plane direction at the abutments. In reality, the transverse rotational stiffness of the joint at the abutments will not be entirely rigid. However, as will be demonstrated later, the effect of a semi-rigid joint is negligible concerning stability assessments. The horizontal thrust is assumed to be taken by the abutments.

The deck displacements are restrained both in the vertical and the horizontal directions at the abutments.
The numerical analyses on a 3D model were performed by Abaqus [7], see Fig. 4. All structural parts were modelled by beam and bar elements except from the deck, which was modelled as a shell rigidly connected to the cross-beams. The hangers were defined such that they could take only tension. Dead load, traffic load (LM1) and wind load were applied according to Eurocode 1. The traffic load was applied in different configurations as shown in Fig. 5. Design values of loads were assumed in the load combinations (ULS). Static nonlinear analyses and linear (perturbation) buckling analyses were performed. The buckling analyses were in addition carried out on deformed shape of the structure (further referred to as "pre-load" since firstly the deformations by nonlinear analysis are found, and thereafter this deformed geometry is used as a base state in the buckling analysis).

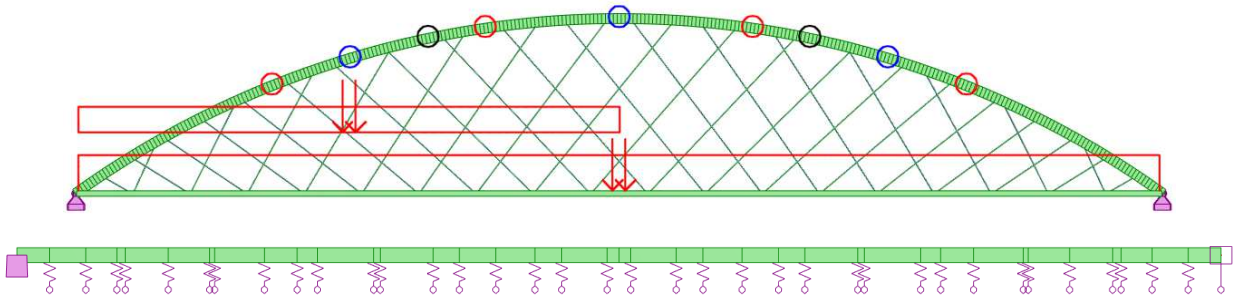

Fig. 5: 2D FEM models for analysis of in-plane (upper figure) and out-of-plane (lower figure) stability; the different configurations of the splice joints are differentiated with colours.

In order to validate the 3D model and to study the effect of the incorporated splice joints on in-plane and out-of-plane stability of the arches separately, complementary 2D analyses by use of RSAPRO [8] were performed, see Fig. 5. The in-plane model consisted of one arch carrying half the deck (modelled as a beam) by hangers which were forced to transfer only tension (with a cross section corresponding to one pair of the hangers). Nonlinear P-Δ analyses and linear buckling analyses were performed. Vertical load by dead load (including self-weight) and traffic load was assumed as shown in Fig. 5. The out-of-plane stability was studied on a simplified model consisting of the arch modelled as a straight beam (of arc length of the arch) supported by linear springs at the locations of the attachment points of the hangers. Linear buckling analyses were performed with the arch loaded by a uniform normal force along its axis. The spring stiffnesses were determined using Eq. (6), which assumes that for the lateral displacement of the arch to take place, one of the hangers in the pair buckles, while the second hanger supports the arch by its elongation component transversal to the arch.

$$K_t = \frac{E_s \cdot A_h}{L_h} \cdot \cos^2 \beta = \frac{E_s \cdot A_h}{L_h} \left(\frac{Z}{L_h} \right)^2 \tag{6}$$

Here E_s is elastic modulus of steel, A_h and L_h are cross-sectional area and length of a hanger, respectively, Z is lateral distance of a hanger anchor point at the deck level measured from the arch axis, and β is the angle between a hanger force and its component lateral to the arch. It is obvious from Eq. (6) that the lateral support of the arch, provided by hangers, decreases considerably with the increasing height of the arch above the deck. The effect is visualized in Fig. 6.

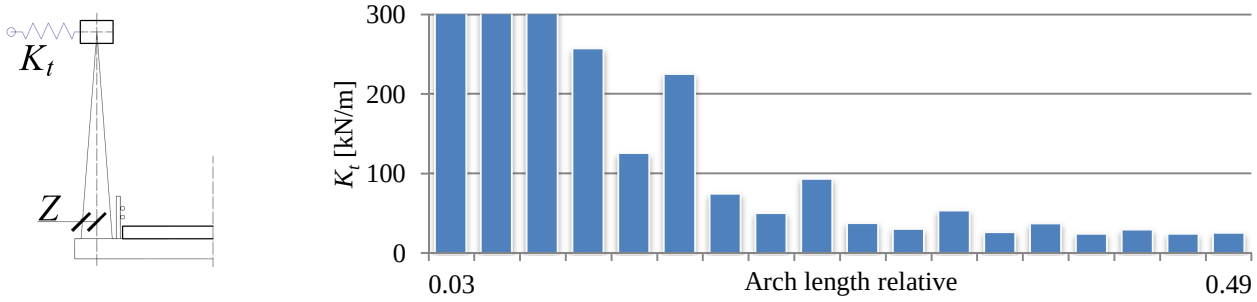

Fig. 6: Lateral elastic support of the arch provided by inclined hangers (K_t of first 3 hangers are 4480, 736 and 1166 kN/m).

3.2 Results and discussion

The results of the buckling analyses for the models without splice joints are summarized in Table 1. Here N is the maximum normal force in the arch, N_{cr} is the critical buckling normal force for which the arch becomes unstable, and $\chi = N_{cr} / N$ is a buckling load factor corresponding to the critical force (denoted as α_{cr} in Eurocode 3 [9]). The coefficient k_c is herein chosen as a measure related to stability verifications since it directly reduces the capacity of the cross section in ULS stability assessments according to Eurocode 5 [10] as shown in Eq. (7).

$$\frac{\sigma_{c,0,d}}{k_{c,y} f_{c,0,d}} + \frac{\sigma_{m,y,d}}{f_{m,y,d}} + k_m \frac{\sigma_{m,z,d}}{f_{m,z,d}} \le 1 \quad \text{and} \quad \frac{\sigma_{c,0,d}}{k_{c,z} f_{c,0,d}} + k_m \frac{\sigma_{m,y,d}}{f_{m,y,d}} + \frac{\sigma_{m,z,d}}{f_{m,z,d}} \le 1 \tag{7}$$

Table 1: Results of buckling analyses for models without splice joints

Model	2D		3D pre-load		3D without pre-load	
Notation	2D-in	2D-out	3D-pl V	3D-pl V+H	3D V	3D V+H
N	6831	6891	6163	6891	6163	6891
N_{cr}	91809	13162	16394	13782	16455	16745
χ	13,44	1,91	2,66	2,00	2,67	2,43
k_c	0,99	0,43	0,52	0,44	0,52	0,53

Note: V=only vertical load; V+H=vertical+horizontal load

The coefficient k_c was obtained by relations in Eurocode 5 [10] for the critical length obtained through the classical Euler's formula $N_{cr} = \pi^2 EI / L_{cr}^2$. By comparing the results from in-plane and out-of-plane 2D models with the results obtained by the 3D model, it becomes clear that buckling load of the arch is governed by the out-of-plane stability. The shape of the first buckling mode (see Fig. 8) obtained by the 3D model is also predominantly characterized by the out-ouf-plane buckling. It is therefore reasonable to calculate the coefficient k_c based on the arch stiffness EI in the out-of-plane direction. It is noted that the results presented herein correspond always to the load combination with the most unfavourable position of the traffic loading. The normal force for the out-of-plane 2D model is set equal to the maximum normal force from the 3D model for easier comparison of the relative values.

The stability of the arches containing splice joints (the locations of the splice joints are shown in Fig. 5) was studied by varying the rotational stiffness of the splice joints both in the in-plane and the out-of-plane directions. The results of the buckling analyses on models containing the splice joints are related to the unspliced models and are shown in Fig. 7. The shapes of the first buckling modes

are shown in Fig. 8. The rotational stiffnesses in-plane and out-of-plane were assumed equal in the 3D models. It is, however, clear from the results that the in-plane stability is large compared to the out-of-plane stability and even for very low values of the in-plane rotational stiffness, the critical load of the arch is governed by the out-of-plane buckling.

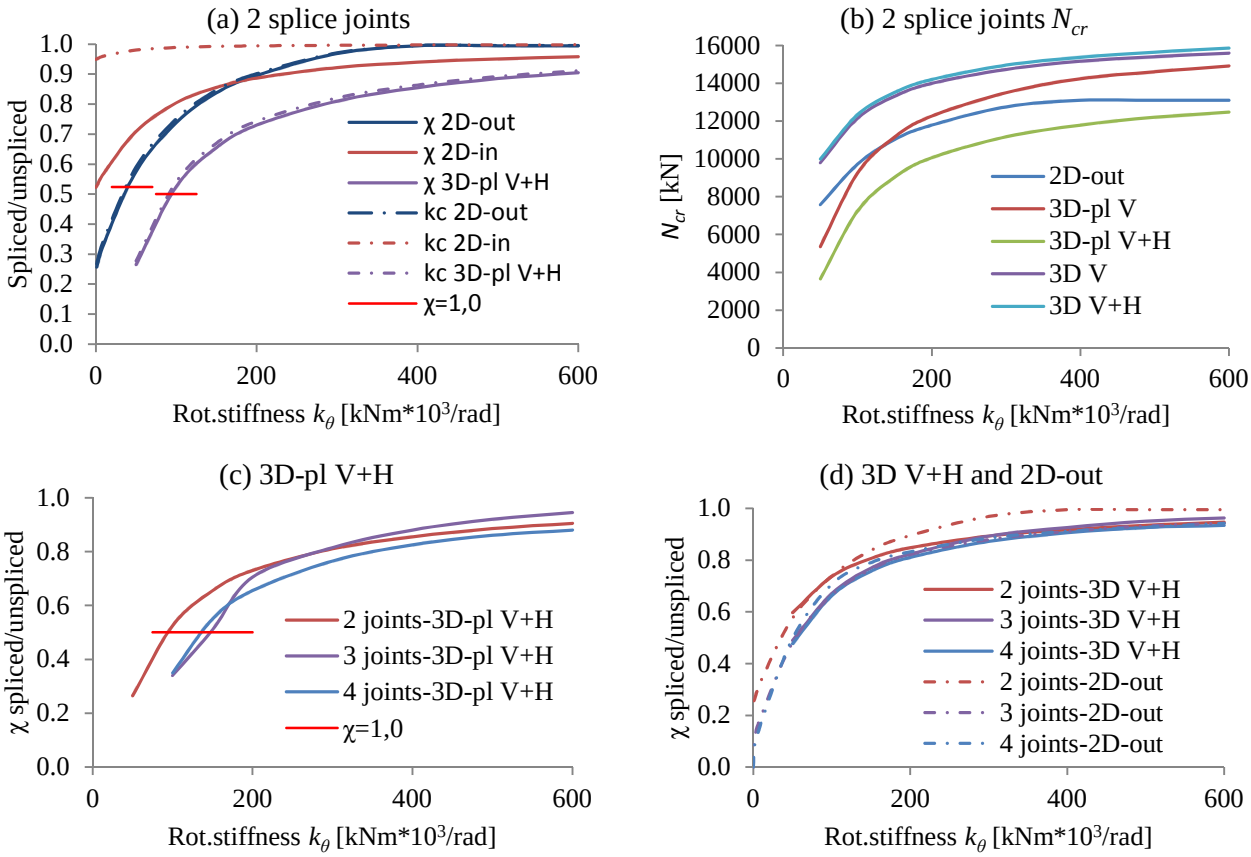

Fig. 7: Results from numerical models containing splice joints; for notation see Table 1.

Comparison of the results for the 2D in-plane, 2D out-of-plane and the 3D model is shown for the case of 2 splice joints in Fig. 7 (a). Same trends are also observed for the cases of 3 and 4 joints and the detailed results are therefore not shown herein. The comparison of cases with 2, 3 and 4 splice joints is shown in Fig. 7 (c). The results from the 3D model are shown for the case with pre-load and both vertical and horizontal loading, since this is the analysis yielding the lowest critical load, see Fig. 7 (b). The critical load obtained by the 3D model is nearly identical for the case of pure vertical loading and the case with vertical and horizontal loading in the analyses without pre-load. However, if the buckling analysis is performed on the deformed (pre-loaded) shape, the effect of the horizontal load becomes significant. From Fig. 7 (d), it is observed that the buckling behaviour of the arches with splice joints predicted by the simplified 2D out-of-plane model is similar to the results obtained by the 3D analyses without pre-load. Finally, no distinct difference is observed comparing the cases with 2, 3 and 4 splice joints. The buckling load is somewhat higher for the models with 2 joints especially for joint stiffnesses smaller than 200 000 kNm/rad. However, the buckling load factor χ is in this range close to a unity, which is the stability limit. The results indicate that for the out-of-plane rotational stiffness larger than approximately 400 000 kNm/rad, a further increase of the rotational stiffness is insignificant.

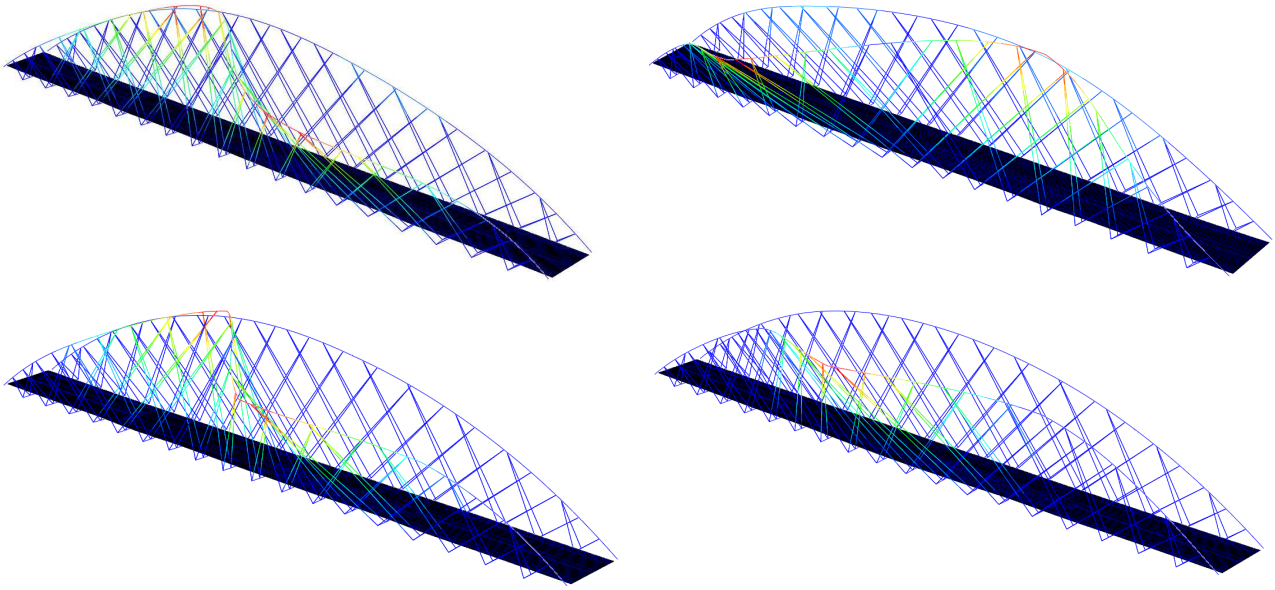

Fig. 8: Shapes of the first buckling mode: clockwise from the upper left corner: unspliced arches; 2 splices; 3 splices; 4 splices in each arch (plotted for models with k_θ=200 000 kNm/rad).

Considering the cross-sectional dimensions of the arch of 1300 mm width (out-of-plane) and 900 mm height (in-plane), the rotational stiffness of the splice joints that can be achieved by use of long threaded rods, as discussed in Section 2, will be approximately 600 000 kNm/rad in the out-of-plane direction and 500 000 kNm/rad in the in-plane direction. Based on the results presented in Fig. 7, this seems to be sufficient in order to prevent stability problems. In consideration of the most critical results, which were obtained by the 3D model with pre-load including horizontal loads (which in fact is a rather conservative approach), the effect of 2 splice joints in each arch is: $k_{c,spl.}/k_{c,unspl.}$=0,88, which means 12% reduction of the capacity. It should, however, be noted that the arch dimensions were not optimized. Consulting the extreme values of the internal forces presented in Fig. 9, a better utilization of the arches, and larger rotational stiffness of the joints, can be obtained by increasing the ratio of the width over the height of the cross section. The precedent statement is based on the assessment by Eqs. (7) which reveals that the capacity of the arch is governed by the out-of-plane buckling.

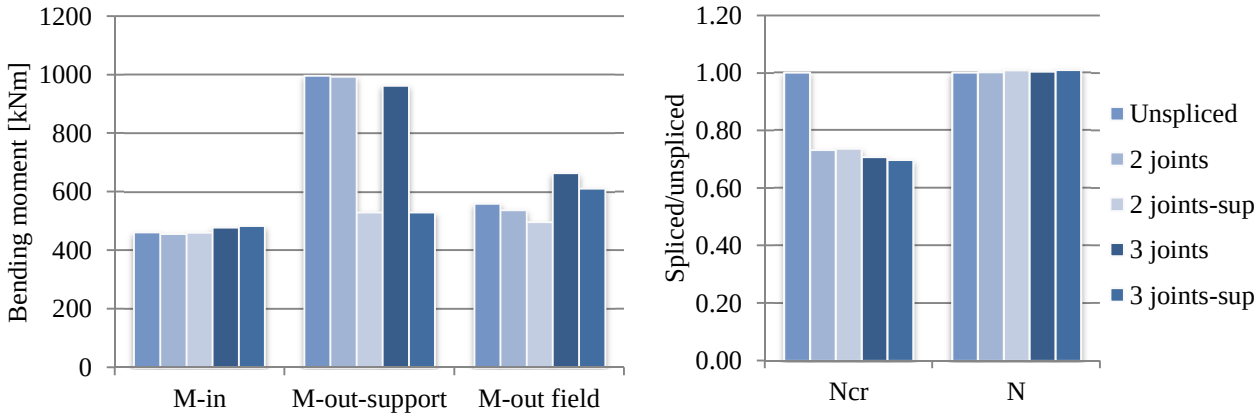

Fig. 9: Extreme values of the internal forces in the arches obtained by 3D models (3D-pl V+H; models with joints: k_θ=200 000 kNm/rad).

From the results in Fig. 9, it is evident that the splice joints have very little impact on the extreme values of the internal forces in the arches. In addition to the splice joints, a rotational stiffness of 100 000 kNm/rad was applied in the out-of-plane direction instead of the fixed rotational degree of freedom at the arch support (results denoted as "-sup"). It is seen that the effect on the critical buckling load is negligible, proving the assumption of the non-uniform distribution of the lateral arch support by hangers as shown in Fig. 6. With additional reference to Fig. 8, it is evident that the critical buckling load is reached due to instability of the central part of the arch. The semi-rigid lateral support furthermore implies that the out-of-plane bending moment at the support drops, but at the same time, the moment in the field remains approximately same, leading to a more uniform utilization of the arch.

4. Concluding remarks

It has earlier been shown that glulam arches with network hanger configuration are a feasible alternative for road bridges with spans reaching 100-120 m. An enhanced durability of the arches can moreover be achieved by avoiding the wind truss between arches and stabilizing the arch laterally through out-of-plane inclination of hangers. Since the timber arches cannot be produced and transported in one piece, rotationally stiff splice joints in arches are a key prerequisite for the viability of the design. The present investigation shows that the stability of timber network arch bridges can be maintained by use of splice joints with long threaded rods.

Acknowledgment

This work was funded by the WoodWisdom-Net+ project DuraTB ("Durable Timber Bridges") and the support from the funding bodies and partners is gratefully acknowledged. The authors would also like to acknowledge Anna Ostrycharczyk for her contribution in building up the 3D numerical model.

References

[1] Bell K., Structural Systems for Glulam Arch Bridges, *International Conference on Timber Bridges (ICTB 2010)*, Lillehammer, Norway, 2010

[2] Malo K.A., Ostrycharczyk A., Barli R., Hakvåg I., On Development of Network Arch Bridges in Timber, *International Conference on Timber Bridges (ICTB 2013)*, Las Vegas, USA, 2013

[3] Bell K., Wollebæk L., Large, Mechanically Joined Glulam Arches, *WCTE 2004*, Lahti, 2004

[4] Wollebæk L., Bell K., Stability of Glulam Arches, *WCTE 2004*, Lahti, 2014

[5] Cepelka M., Malo K.A., Review on on-site Splice Joints in Timber Engineering, *COST-Timber Bridges Conference 2014*, Biel/Bienne, 2014

[6] Cepelka M., Malo K.A., Moment Resisting Splice of Timber Beams Using Long Threaded Rods and Grout-Filled Couplers – Experimental Results and Predictive Models, *Submitted for publication in Construction and Building Materials* (Submitted 01/2017).

[7] Corp. D.S.S., Abaqus Analysis User's Guide, Version 6.14, 2014.

[8] Autodesk, Autodesk Robot Structural Analysis Proffesional (RSAPRO), 2017.

[9] CEN, Eurocode 3: Design of Steel Structures, Part 1-1: General rules and rules for buildings, European Committee for Standardization, Brussels, 2005.

[10] CEN, EN 1995-1-1:2004: Design of Timber Structures. Part 1-1: General-Common Rules and Rules for Buildings, European committee for standarization, Brussels, 2004.

Parallel splitting mode of failure in dowel type connections with chamfered cuts

Katarzyna OSTAPSKA-LUCZKOWSKA
PhD Candidate
Norwegian University of Science and Technology (NTNU)
Trondheim, Norway
katarzyna.ostapska-luczkowska@ntnu.no

Katarzyna Ostapska-Luczkowska received her civil engineering degree from Warsaw University of Technology in 2014 and is currently pursuing a PhD at NTNU

Kjell Arne MALO
Professor
Norwegian University of Science and Technology (NTNU)
Trondheim, Norway
kjell.malo@ntnu.no

Kjell Arne Malo is professor of timber structures at NTNU. His research topics are methods for increased strength and stiffness of connections for timber structures and vibrations in timber structures.

Summary

The results of numerical simulation of fracture in dowel-type connection is presented and discussed. The study investigates the influence of geometry on the splitting failure in the connection. Single dowel connection was simulated to get better insight in the mechanism of failure. Solid elements were applied to capture the influence of width of the connection on the mechanism of the splitting mode of failure and to verify the initial elastic stiffness in the plane stress model. Plane stress elements were utilized for simplification and faster convergence. The qualitative and quantitative influence of the chamfered cuts on the ultimate failure force was observed. The results are related to the European Yield Model predictions used in the design codes. The limitations of the applied numerical model are presented and validation methods for the simulation are proposed.

Keywords: dowel-type connections, cohesive zone model, perpendicular to grain fracture, wood fracture mechanics.

1. Introduction

1.1 Motivation

The empirical character of Eurocode approach to evaluating timber connections renders prediction about structural performance of the design that is outside certain geometrical limits difficult. This is especially pronounced in the nonlinear problems, were both plasticization and fracture are of interest. Geometrical limits imposed on the design to prevent the brittle failure are very rigidly defined and it is not always clear how to interpret them for particulate design. Trusswork timber bridges are an example of structure where connections with elements with chamfered ends are

commonly applied. In this paper the numerical simulation tool is utilized to investigate the phenomenon of parallel to grain splitting in the single dowel-type steel-to-timber connection with a chamfered end.

1.2 Modes of failure in dowel-type connections

1.2.1 European Yield Model

European Yield Model recommended in the Eurocode [3] predicts three failure modes for steel-to-timber connections in double shear with a steel plate as a central member; see Equation (1) and Figure 1. Splitting parallel to grain in the plane along dowel axis is assumed to be prevented by applying minimum spacing and edge and end distances according to the Table 8.5 in [3].

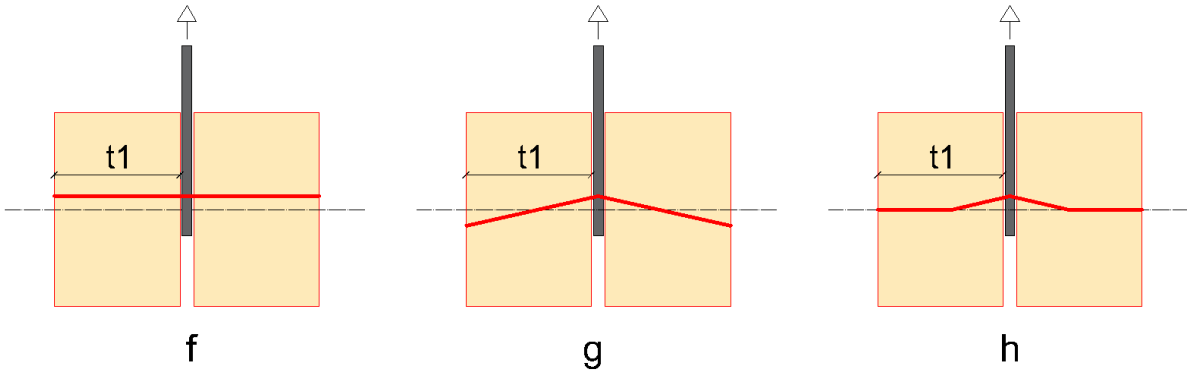

Fig. 1. Failure modes for steel-to-timber connections in double shear: embedement in timber (f), plastic hinge in dowel and embedement in wood (g), plastic hinge in wood (h).

$$F_{v,Rk} = \begin{cases} f_{h,1,k} \cdot t_1 \cdot d & (f) \\ f_{h,1,k} \cdot t_1 \cdot d \left[\sqrt{2 + \frac{4 \cdot M_{y,Rk}}{f_{h,1,k} \cdot d \cdot {t_1}^2}} - 1 \right] & (g) \\ 2.3 \cdot \sqrt{M_{y,Rk} \cdot f_{h,1,k} \cdot d} & (h) \end{cases} \quad (1)$$

1.2.2 Experimental reference

The numerical model was validated against experiments results provided in [1]. In the aforementioned paper, the test for slender connection with one dowel of 12 mm diameter placed in the timber element of cross section 40x72 mm and loaded centrally with steel plate of thickness 8 mm was chosen as most relevant; see Figure 2:

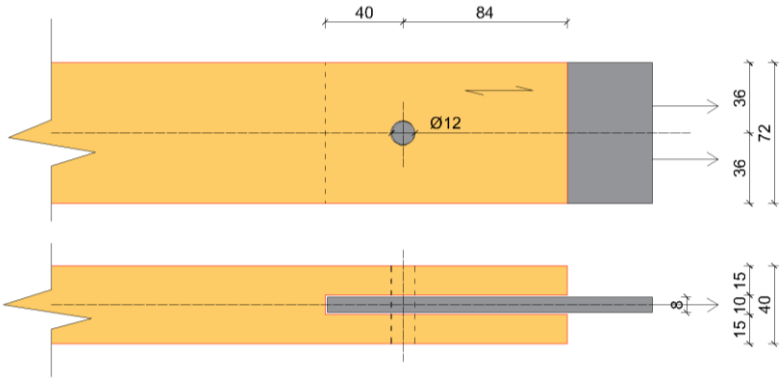

Fig. *2. Scheme of experimental set-up [1] used for validation of numerical simulations.*

Selected test ended in lateral splitting failure delayed by ductile failure in wood compressed parallel to grain. The failure is caused by tensile stresses perpendicular to grain due to the wedge-like behaviour of dowel. The splitting is more pronounced in connections with smooth dowels, where contact area of dowel perimeter and timber is minimal. The values of initial stiffness, according to EC5, depend on density and dowel diameter only; see Equation (2):

$$f_{h,1,k} = 0{,}082 \cdot (1 - 0.01 \cdot d) \cdot \rho_k \quad (2)$$

For the connection above the embedment strength varies from 24,8 to 37,5 MPa depending on the density range from 344 to 519 kg/m^3. Characteristic capacity is 5,44 kN per shear plane. The distances of the dowel to the edge and end are assumed minimum required by EC5.

2. Method

To capture the fracture and plasticisation of timber in compression along the grain, the cohesive zone elements together with plasticity theory were employed. The model was created in Abaqus software. Plastic material was added locally after identifying the proper zone of interest in elastic analysis. Small hardening without densification was considered. The material strength properties were assumed as follows: f_{Lc}=30 MPa, f_{Rt}= f_{Tt} = f_{LR} = f_{LT} =5,0 MPa. Elastic properties of timber used in numerical simulation are presented in Table 1.

E_L	E_R	E_T	G_{LR}	G_{LT}	G_{RT}	ν_{LR}	ν_{RL}	ν_{LT}	ν_{TL}	ν_{RT}	ν_{TR}
9040	790	340	640	580	30	0,5	0,11	0,66	0,06	0,84	0,34

Table 1. Engineering constants for elastic orthotropic material [MPa], based on [2].

2.1 Cohesive zone model

Cohesive elements were applied to model crack initiation and progress. The method was first introduced by Hillerborg in [4]. Cohesive elements are used to model the interface in which fracture takes place and are located in the region of expected crack plane. The crack is modelled through traction-separation law (see Figure 3) defined for each of failure modes separately. In three-dimensional analyses with 3D cohesive elements all three possible modes of failure are present: opening mode and two shearing modes. In plane stress analysis only one shearing mode is relevant. Failure initiation criterion is defined by quadratic law involving three critical stresses for each mode of failure respectively: σ_I ,$\sigma_{II,s}$ and $\sigma_{II,t}$. After damage initiation the element degradation is ruled by linear law with fracture energy as the ultimate failure criterion, defined for single mode in equation below:

$$G_f = \int \sigma_t du, \tag{2}$$

where σ_t is traction and u is length along the crack processing zone. The total fracture energy is a sum of fracture energies for individual failure modes and can be written as: $G_T = G_n + G_s + G_t$ [N/m].

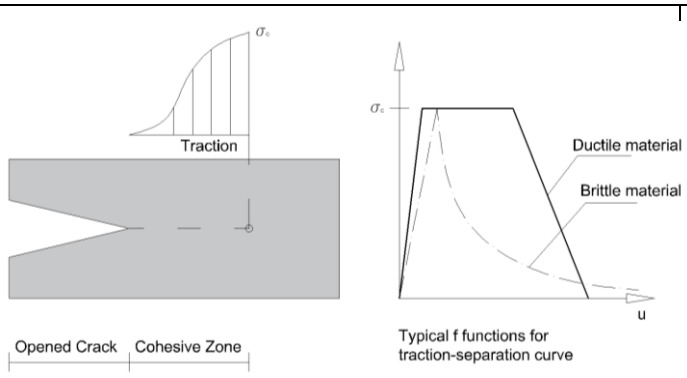

Fig. 3 Traction- separation law: crack processing zone (left) laws for different materials (right).

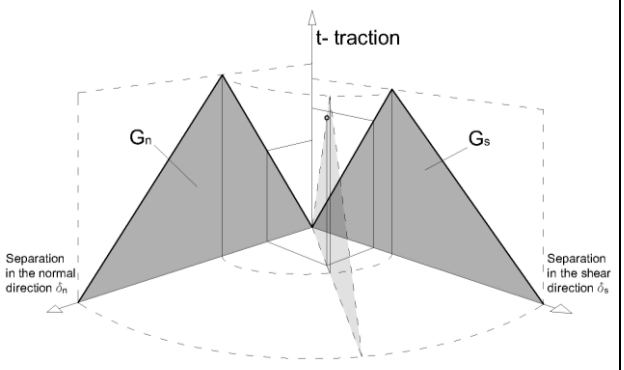

Fig. 4 The mix mode rule for fracture energy criterion evaluation; graphic illustration.

The behaviour of cohesive elements is defined by traction-separation law and has an initial elastic behaviour that affects the model before damage initiation criterion is met. To minimize the added compliance the stiffness is scaled in comparison to the elastic stiffness of the timber material in the respective direction. The mix mode rule for fracture energy criterion is presented graphically in Figure 4. For avoiding convergence problems the small viscosity of 0,0001 was added for cohesive

elements. Element deletion was used for damage level over 0.99.

2.2 Numerical test set-up

Two set-ups were prepared for numerical simulation. Three dimensional analysis with solid elements and symmetry plane was created in Abaqus software. The dowel was modelled with elastic isotropic steel material: E= 210 GPa, ν=0.3. The contact between dowel and timber was assumed frictionless to obtain highest stress concentration zone. Timber was modelled as elastic orthotropic material with coordinate system specified in the Figure 5. The contact area was investigated to substantiate the assumption of plane stresses in the chosen geometrical configuration. The stress distribution is presented in Figures 7 and 8 and can be assumed even enough for plane stress analysis to be applicable. For further parametric studies the geometry types presented in Figure 6 were considered. All models contain cohesive zone both in front and behind the dowel in the central plane parallel to dowel axis.

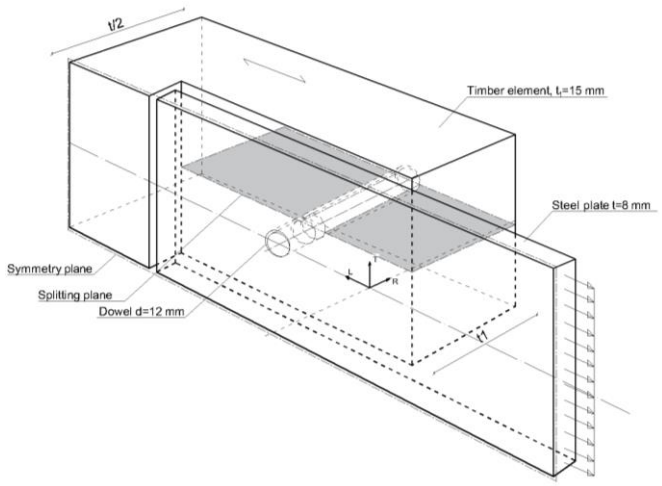

Fig. 5. Schematic set-up for numerical simulation with solid elements. Lateral splitting plane indicates the location of cohesive elements.

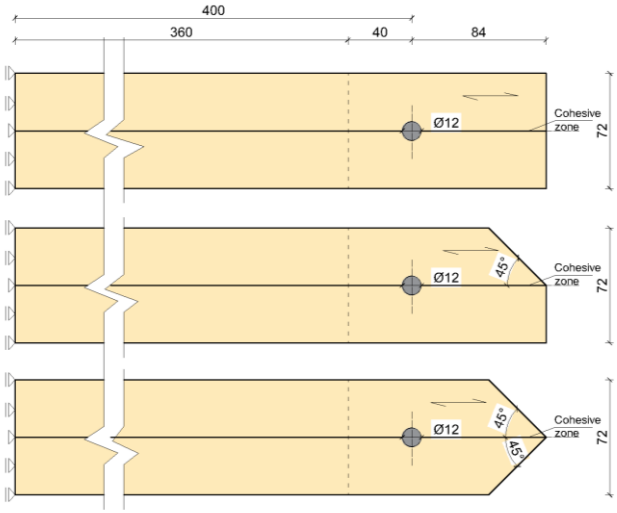

Fig. 6 Configuration of chamfers (middle and bottom) and reference geometry (top) for plane stress simulations.

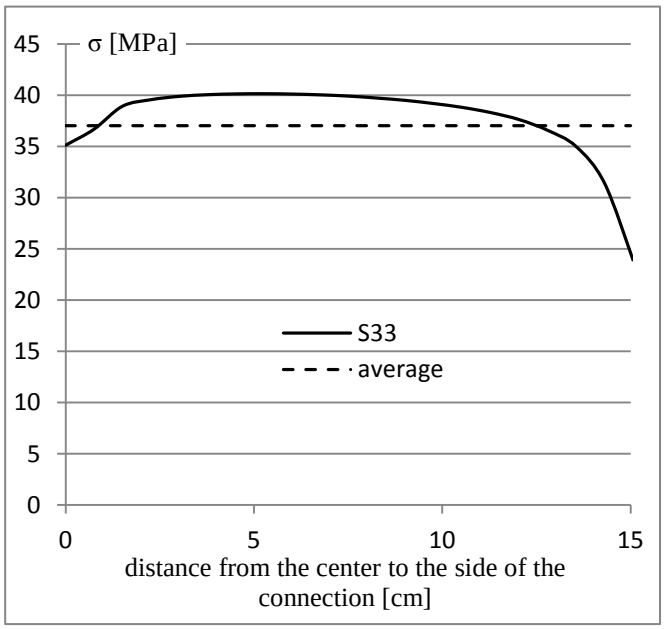

Fig. 7. Compression along the grain stress distribution for timber in dowel-timber contact area.

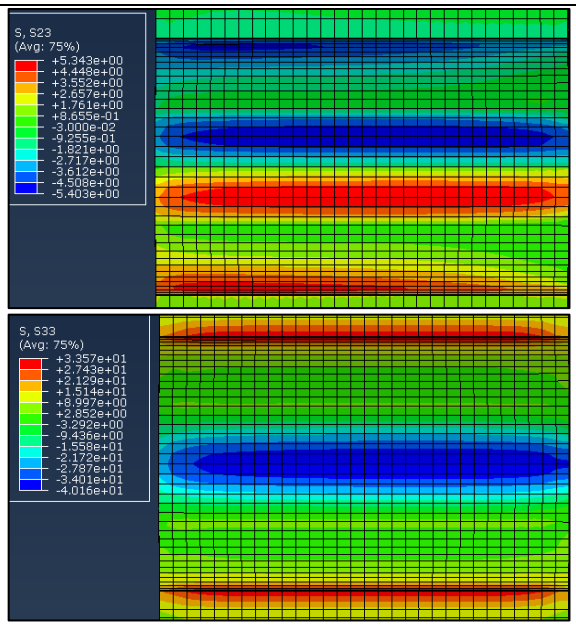

Fig. 8. Compression and shear stress distribution in wood in dowel-timber contact area.

3. Results

Estimated ultimate capacities resulting from simulations for variants of connections from Figure 6 are collected in the Table 2. The numbers indicate expected influence of geometry. Especially single chamfer end connection model is striking with the almost 50% loss of capacity. This is attributed to the much more negative influence of asymmetry for the performance of the connection than simple reduction of the material volume to the end. Frictionless contact has limited the influence of plasticity to the minimum. The plastic strain area can be seen on Fig 11 together with stresses parallel to grain.

End shape	F [kN]	Drop in capacity
regular	2,96	
double cut	2,64	11,04 %
single cut	1,57	46,91 %

Table 2.Ultimate capacity comparison for regular and chamfered ends as shown on Figure 6.

For better fit with experimental data certain friction should be introduced to extend the displacement before failure. Force- displacement relations from simulations are presented in Figure 9. Small hardening before peak of the force can be observed for regular configuration without chamfers. This is caused by very stiff behaviour of cohesive elements and can be remedied by further decreasing cohesive thickness from 0,01 mm while decreasing the cohesive stiffness. It can be observed in Figure 9, that asymmetry in single chamfer causes the connection performance to be not only much lower but also much more brittle.

The influence of the connection thickness is shown in Figure 10. For thickness of 10 mm the brittleness is also clearly observed. Both initial hardened response and post failure hardening are caused by an extrinsic formulation of traction- separation law. The initial, artificially stiff, linear law has an undesirable effect which can be dealt with by either better study of numerical parameters or by introducing an intrinsic law; i.e. activating cohesive elements only after the criterion for damage initiation is met.

The comparison between analysis with solid elements and plane stress elements shows influence of three-dimensionality on the prediction of capacity – see Figure 12.

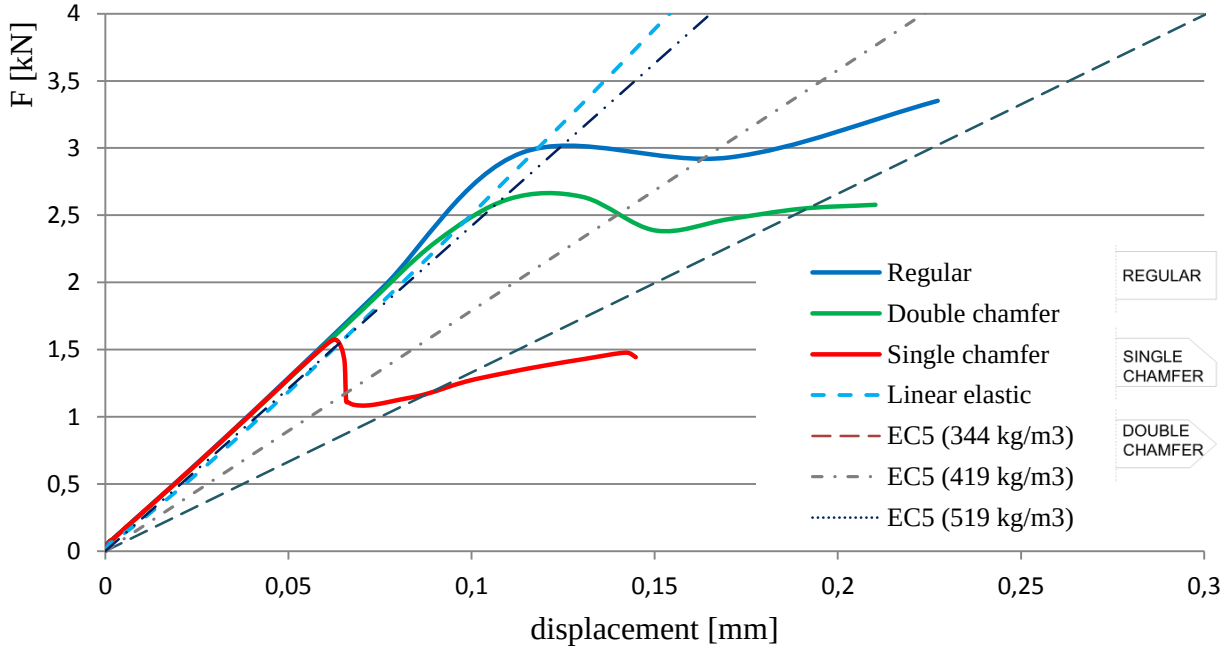

Figure 9. Force displacement curves for variants of chamfered end. Stiffness K_{ser} based on EC5 is presented for a range of densities.

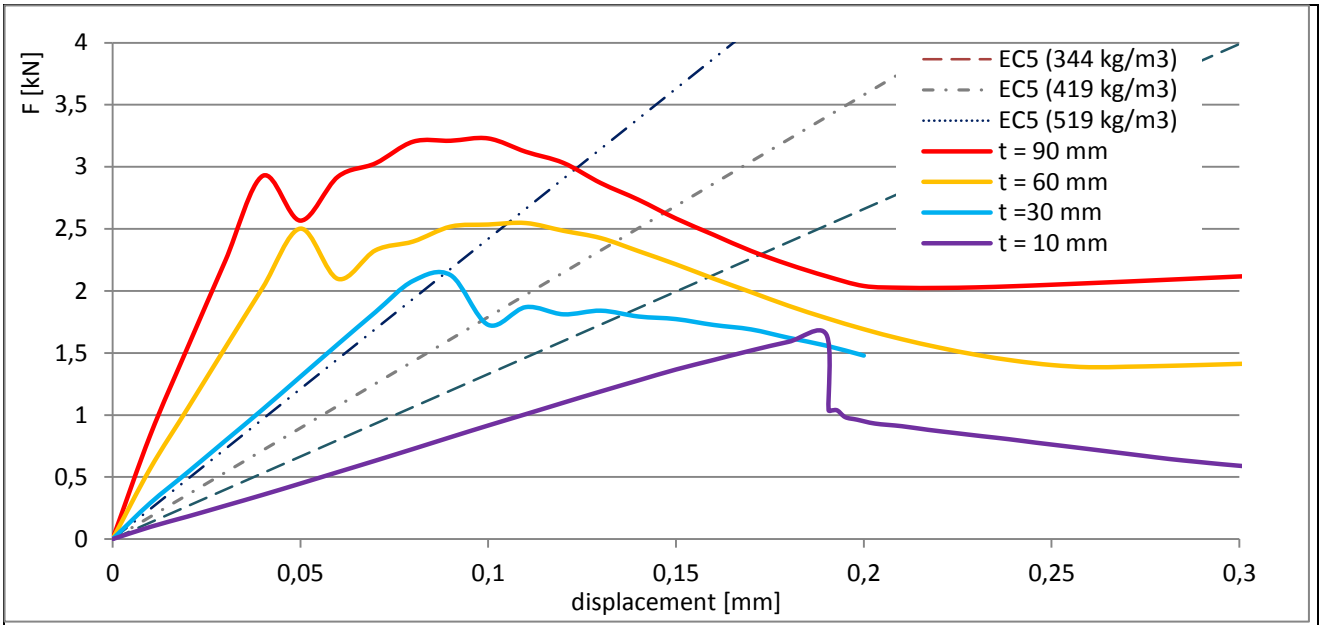

Figure 10. Force-displacement curves for different thicknesses of connection t [mm]. EC5 stiffness is presented for reference for the range of densities tested in [1].

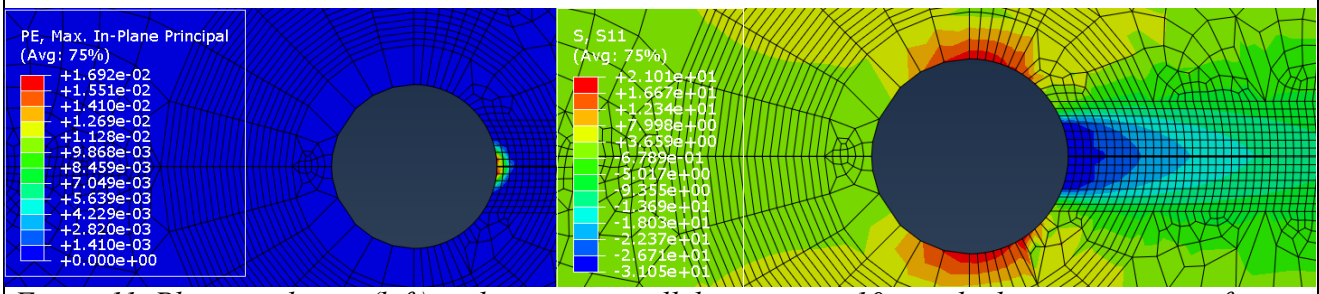

Figure 11. Plasticised area (left) and stresses parallel to grain in 10 mm thickness connection for 0,19 mm displacement .

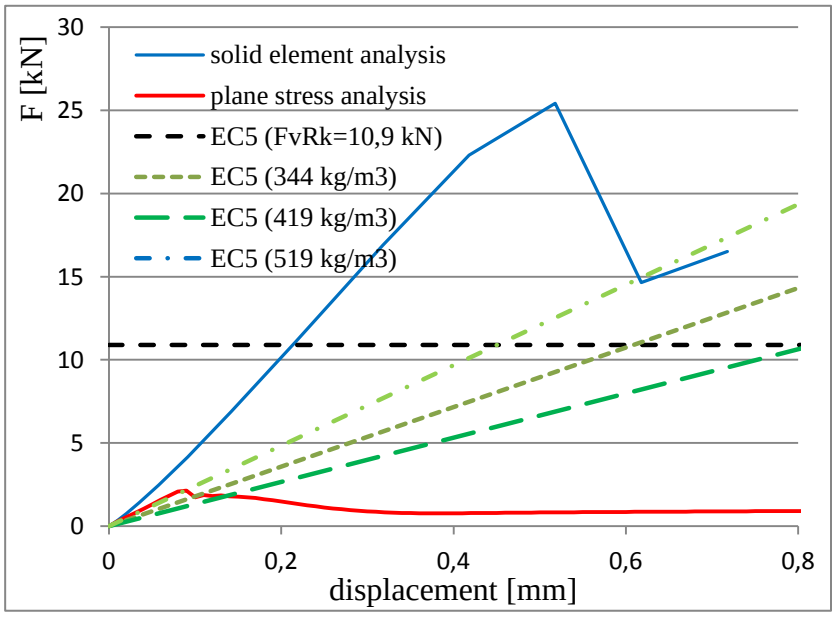

Fig. 12 Traction- separation law: crack processing zone (left) laws for different materials (right).

Solid element analysis was modelled with very rigid boundary conditions and does not provide correct stiffness as obtained from the experiment in [1] but has the stiffness in the range of the unloading and reloading curve (48,5 kN). Thus the ultimate capacity is predicted too high at 25 kN compared to 10,9 kN estimated by Eurocode and even lower experimental value from [1]. The fact of the so much lower capacity in plane stress analysis can be explained by lack of local effects representation in plane stress states. The failure at some point of critical cross-section covers a priori the whole width. Therefore failure propagates faster and is not restricted to the zone with stress concentrations.

4. Discussion

4.1 Limitations of the simulation tool

The cohesive zone model is an artificial concept developed originally for concrete materials. Therefore the model needs extensive validation and verification. The influence of the initial stiffness on the predicted failure has to be investigated. Selective activation of cohesive elements would help to avoid stress concentrations due to stiff elastic traction-separation curve and delay activation of failure criterion. Moreover the proper stiffness of the simulated setup has to be captured for the results to be quantitatively relevant, i.e. predict correct capacity. However qualitative conclusions can be drawn and mechanism of failure is adequately modelled.

4.2 Comparison with Eurocode

It is concluded in paper [1] that Eurocode [3] does not provide adequate evaluation tools for connections outside the typical area of application. Especially slender and thick connections are overestimated and underestimated respectively when it comes to stiffness and capacity. The density based estimation can well be supplemented with numerical analysis to cover the cases that are not addressed in the codes.

4.3 References

[1] Dorn M., de Borst K., Eberhardsteiner J., “Experiments on dowel-type connections”, *ASCE Engineering Structures*, No. 47, 2013, pp. 67-80.

[2] Dahl K.B., “Mechanical properties of clear wood from Norway spruce”, *Doctoral Thesis*- NTNU, Department of Structural Engineering, 2009

[3] EN 1995-1-1. Eurocode 5: Design of timber structures- Part 1-1, European Committee of Standardization (CEN), 2004.

[4] Hillerborg A., Modéer M., Petersson P.E., “Analysis of crack formation and crack growth in concrete by means of fracture mechanics and finite elements”, *Cement Concrete Res*, No. 6, 1976, pp. 773–782

Effects of Notching on Timber Girder Performance

Justin Dewey
PhD student
James Cook University
Townsville, Australia
justin.dewey@my.jcu.edu.au

Rabin Tuladhar
Senior Lecturer
James Cook University
Townsville, Australia
rabin.tuladhar@ jcu.edu.au

Lara Mullamphy
Graduate Engineer
Queensland Rail
Townsville, Australia

Lucy McCormack
Graduate Engineer
Queensland Rail
Townsville, Australia

Summary

With the advent of modern construction materials such as concrete and steel, the use of timber in bridge construction in Australia has significantly decreased. However, many aging timber bridges, with an average age of more than 60 years, are still in operation around the country. Maintenance and repair of these aging timber bridges thus poses a growing challenge for the asset owners. One of the major concerns while managing the existing timber bridges is determining the capacity of the girders with notches. Notching is where a section of a beam is cut to allow for its placement on supports. Notching, however, causes stress concentration at the notch corner, which may initiate crack opening at the notch corner and lead to the ultimate failure of the girder. This research is focused on the experimental study on rectangular and circular timber girders to identify the effect of notch on their shear capacities and determining the critical notch angle. While there are design standards available for notching on rectangular timber beams, there is currently no standardized equations for notching on circular timber breams. Twelve small-scale rectangular and circular timber members with three different types of notch angles were tested under three point bending. Three notch angles tested were 1:0, 1:2 and 1:4. Experimental study showed that a notch angle of 1:0 had the lowest capacity for both rectangular and circular members. For notch angle 1:0, notch crack initiation and notch failure loads were much smaller compared to the ultimate failure load. Whereas for notch angle 1:4, notch crack initiation and crack propagation were very similar to the ultimate failure load, which indicated that full shear capacity of the beam could be achieved with the notch angle of 1:4. The shear capacity of the beams from the experimental study were also compared with the existing Australian design standards for rectangular notched beams. The experimental results showed that the existing design equation for notched beams in the Australian design standards are very conservative. Comparison with design equations found in Australian standards showed that existing design provisions for notched beams are very conservative when applied to round sections.

Keywords: Snipe, Notch, Round Girders, Timber Girdes.

1. Introduction

Many of the timber bridges in Australia uses round or octagonal timber girders. These round members are notched at both ends. Notching (or sniping) of the end support areas of girders is required for seating purposes and to create levelness in the top of the structure. This sniping reduces the strength of the girder in the vicinity of the connection. The concentration of high shear and tensile stresses perpendicular to the grain at the re-entrant corner can cause cracks to propagate along the grain leading to catastrophic brittle failure of the girders.

The behaviour of round timber members is not very well understood in either flexure or shear. A review of the literature shows that most methods used are extensions of design equations used for rectangular members. This ignores the fact that the grain profile in natural round members is completely different. Research related to sniping of circular members is also extremely limited. Department of Transport and Main Roads Queensland, Australia has found that the majority of investigation undertaken on notching of timber beams has been on rectangular shaped softwoods used in regions other than Australia [1].

The principal actions that a timber girder must resist are bending and shear (Fig. 1) [2]. Bending is greatest at the middle of the span due to the dead loads and live loads acting on the structure. Tensile stresses form in the tension region while compression occurs in the fibres above the neutral axis. Shear failure is more likely to occur in spans with short effective lengths and girders that have been sniped. When the timber girders have notches on the tension side, the concentration of shear and tensile stresses perpendicular to the grain can lead to a catastrophic brittle failure which tends to rip girders into a top and bottom section parallel to a fault along the grain [3, 4].

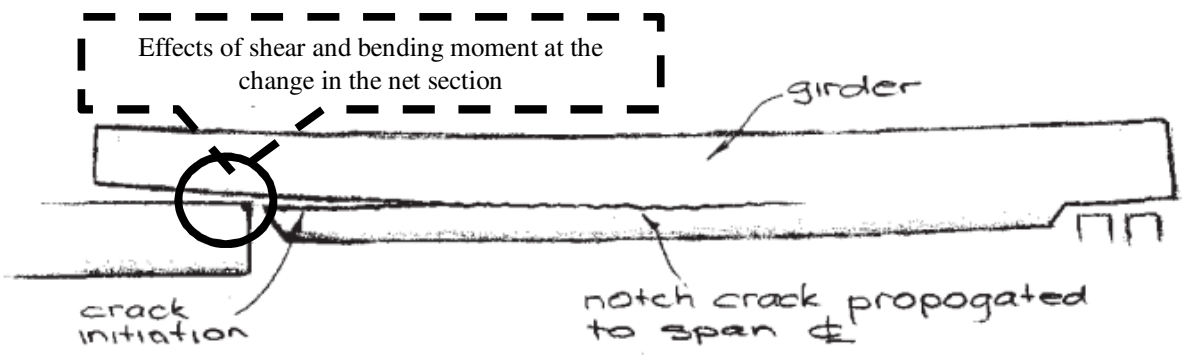

Fig. 1 Effect of shear failure in a timber girder [2].

The maximum recommended loss of depth in a round girders due to sniping is 15% of a residual depth (i.e. after top seating is formed) and an absolute maximum loss of 30%, provided bolted strengthening is applied [5]. This equates to an area percentage loss of 10% and 25% respectively in notched girders.

Some methods to reduce these stress concentrations are to predrill the notch corner creating a curve which reduces the effects of stress. Another option is to taper the cut away from the horizontal at a less severe angle. A gradual tapering of the notch negates the effects of increased stress [6,7]. Keeping the distance between the face of the support and the internal notch corner small will also help to reduce any effects caused by bending [9].

Notch failures can be separated into three distinct failure modes (Fig. 2). Mode 1 occurs due to the tensile stresses perpendicular to the grain. Mode 2 relates to shearing of the grain due to shear stresses parallel to the grain and the less common Mode 3 occurs due to torsion or rolling shear. In AS1720.1 [7] these are represented as characteristic tensile strength perpendicular to the grain (f_t'), and characteristic strength in shear parallel to the grain (f_{sj}'). Mode 1 initially occurs at the centre of the width of the notch before propagating laterally outward towards the surface. Mode 2 has been found to occur when the crack length on the longitudinal surface is half the height of the girder; after this point, shear stresses parallel to the grain become the predominant cause of failure with a sudden brittle rupture. Mode 3 rarely occurs in round sections due to the geometry encountered.

Notching is commonly used in round members particularly for seating purposes, however, there appears to be very little information regarding the design of notched rounds sections. A review of the literature shows that design equations are based on rectangular sections with the assumption that the behaviour of the different cross section and grain profile is similar. Also there are very limited experimental studies on the behaviour of notched round timber girders. This paper presents the experimental study on the behaviour of round and rectangular timber girders with different notch angles.

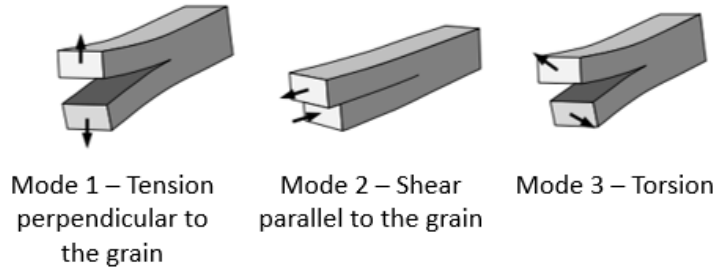

Fig. 2 Modes of failure in timber subjected to shear effects [3]

2. Experimental Program

2.1 Experimental Setup

Load testing were carried out on twelve rectangular and twelve round timber members with notching at angle of 1:0, 1:2, and 1:4 to determine the effect of notch angle on failure patterns in the timber beams. Four timber specimens were tested for each notch angle. For all the specimens, notch was created on one-side of the beam only, this ensured that the failure is concentrated on the end with a notch. The notch depth was kept at a constant 30 % depth in rectangular members and 25 % of the diameter in round members. This equates to an area percentage of 30 % and 19.5 % respectively. Testing was conducted on a MTS machine and load was applied at a rate of 10 *kN/minute*.

Experimental set up consisted of a three point loading (Figure 3). The supports were 600 *mm* apart, the distance of the notch from the support was 100 *mm*. The same set-up was used for the round specimens except a flat face was created on the opposite end to the notch to allow a flat bearing surface. A 25 *mm* thick 40 mm wide steel section with an internal diameter of 100 mm was used as a loading plate (Figure 4). Vertical displacement at the mid-span of the specimen was measured using a LVDT.

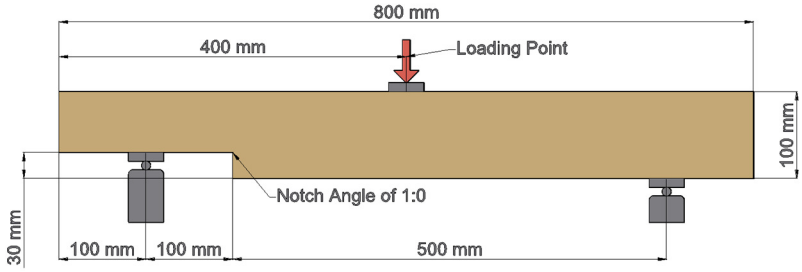

Fig. 3 Experimental test setup

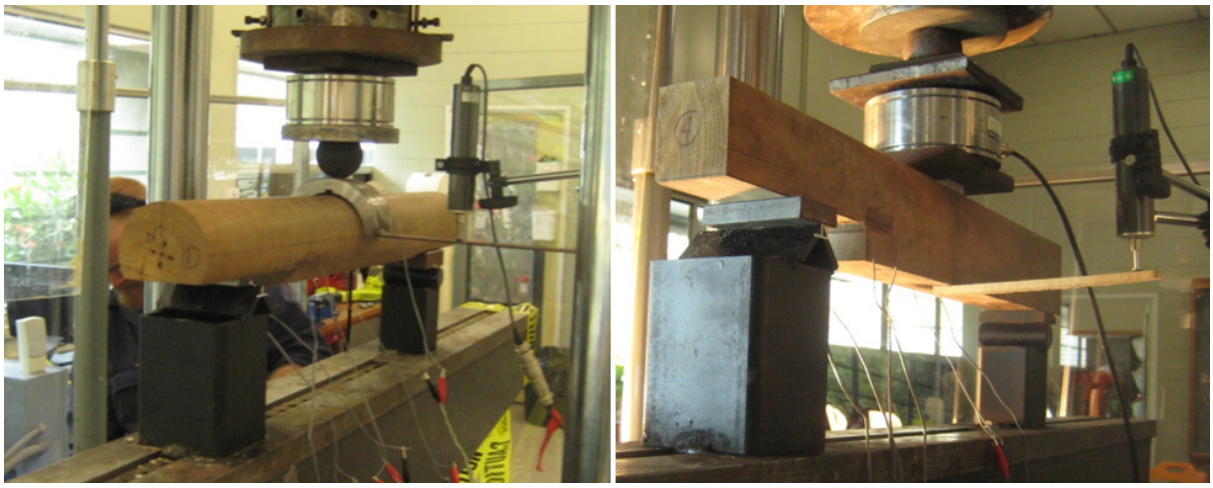

(a) (b)

Fig. 4 Experimental test setup (a) Round timber member (b) Rectangular timber member

Strain gauges were placed in the same locations for all specimens tested. A 2 *mm* (FLA2–11–3L) strain gauge was placed vertically, five millimetres from the notch corner to record strain perpendicular to the grain. A 30 *mm* (PFL–30–11–3L) strain gauge was placed horizontally at the notch corner to measure longitudinal strain. This arrangement was mirrored on both sides of the specimen allowing an average strain to be determined. 30 *mm* strain gauges (PFL–30–11–3L) were placed centrally on the top and bottom surface of the beam at the mid-span to measure longitudinal strain at the mid-span. Strain gauges at the notches were used to determine the crack initiation load and strain gauges at the mid-span were used to determine the ultimate failure load and failure mode.

2.2 Materials

All timbers used were hardwood of the same species - Corymbia Maculata (more commonly known as Spotted Gum). Rectangular specimens were sawn from the outer wood before having the notch cut using a band saw. Rounded specimens were first sawn before being made round using a timber lathe. Notches were created using a milling machine. Attempts were made to cut sections without defects but this proved difficult with regards the round sections as defects that were not initially visible became apparent upon machining.

3. Results and Discussions

The experimental setup worked well with nearly all failures initiating due to tension perpendicular to the grain before shear failure occurred with the crack extending parallel to the grain from the notch to the centre of the member (
Fig.). With sloping notches the failure sometimes occurred lower on the tapered face.

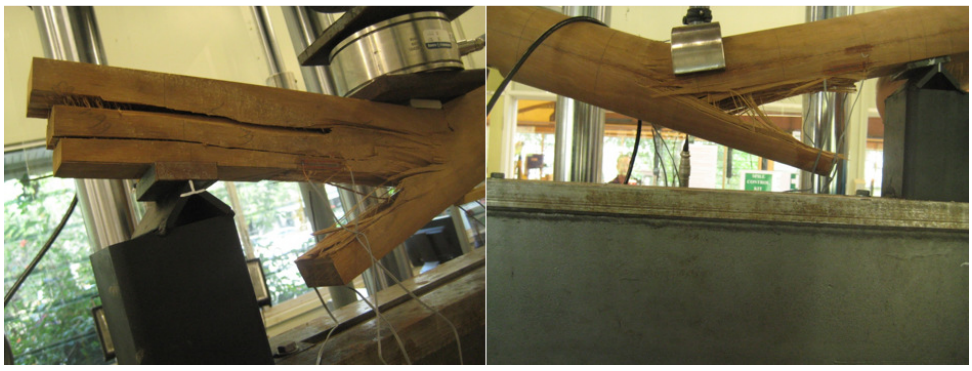

(a) (b)

Fig. 5 Typical failure (a) Rectangular member (b) Round member

The failure pattern observed in both the rectangular and round specimens were comparable. Figure 6 and 7 presents the average results from the tests. In Figure 6 and 7, crack propagation load denotes the initiation of the crack perpendicular to the grain at the notch; and the ultimate failure load denotes the maximum load carried by the beam. From Figure 6 and 7, it is seen that sloping of the notch significantly increases the load at which crack starts to initiate at the notch. The increase in load at which crack initiates at the notch is significantly higher for 1:4 notch slope compared to 1:0 for both rectangular and round members. For specimen with 1:4 notch, crack initiation at notch only occurs very close to the ultimate load capacity of the member which shows that specimens with 1:4 notch slope could exhibit full capacity without premature failure at the notch..

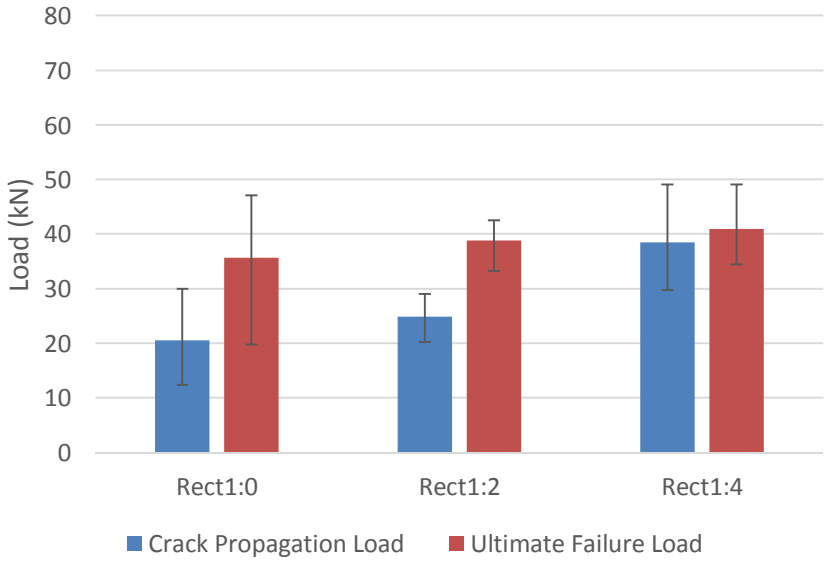

Fig. 6 Crack initiation and ultimate load capacity for rectangular members

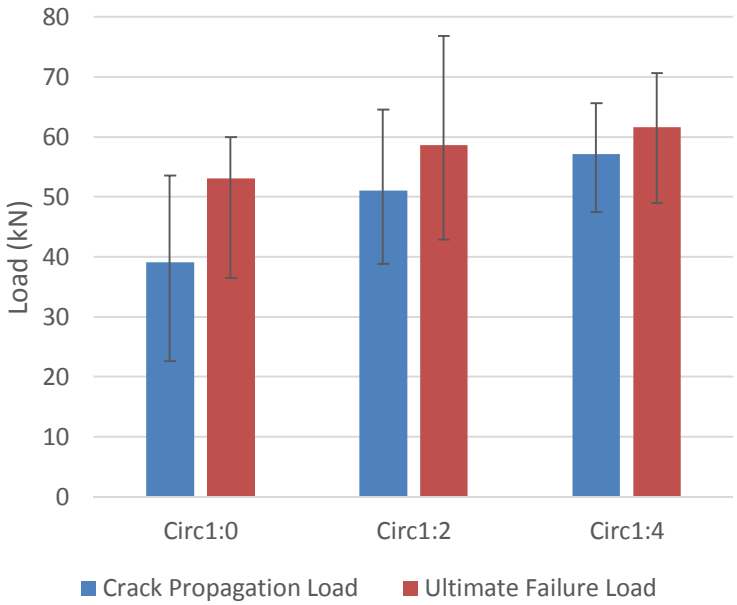

Fig. 7 Crack initiation and ultimate load capacity for circular members

4. Conclusions

A notch slope of 1:2 and 1:4 was found to achieve higher ultimate load capacities for both rectangular and circular members. Notch slope also delayed crack opening at the notch corners. For 1:4 notch angles, crack opening occurred close to the ultimate capacity of the beam which shows that 1:4 notch angle could avoid premature failure due to the failure at the notch.

Notch crack growth was found to be more brittle and sudden in the rectangular specimens than the round which showed a more gradual crack growth. This was assumed to be due to the differing fibre arrangement between the rectangular and round specimens.

The ultimate failure modes differed between the two section members, where the rectangular members consistently failed in shear and the round predominantly failed in flexure. The cause of this was assumed to be due to a combination of the differing fibre arrangement between the two sections, and the round section having a larger net area remaining.

5. References

[1] DTMR, *Bridge Inspection Manual Appendix H.* , Queensland Government Department of Transport Main Roads, Australia, 2004.

[2] DTMR, *Bridge Inspection Manual*, B.A.M.-S. Division, Editor. Queensland Government Department of Transport Main Roads, Australia, 2004.

[3] Steffen F., Bettina F., and Annette, M. H., "Failure modes and reinforcement techniques for timber beams–State of the art", *Construction and Building Materials*, Vol. 97, 2015, pp. 2-13.

[4] Jockwer R., *Structural behaviour of glued laminated timber beams with unreinforced and reinforced notches,* ETH Zurich*,* 2015, 178 pp.

[5] Wilkinson K., *Capacity Evaluation and Retrofitting of Timber Bridge Girders*, in *Civil Engineering*, Queensland University of Technology, Queensland, 2008, 254 pp.

[6] DTMR, *Timber Bridge Manual Part 2 - Component Maintenance*, Queensland Government Department of Transport and Main Roads, Queensland, 2005, 205 pp.

[7] *AS 1720.1—2010 Timber structures Part 1: Design methods*, Standards Australia, 2010.

[8] Ozelton, E. C. and Baird, J. A., *Timber designers' manual*, John Wiley & Sons, 2008.

Fatigue strength of axially loaded threaded rods embedded in glulam at 45º to the grain

Haris STAMATOPOULOS
Postdoctoral Fellow
Norwegian University of Science and Technology (NTNU)
Trondheim, Norway
haris.stamatopoulos@ntnu.no

Haris Stamatopoulos is a postdoctoral fellow at NTNU. He received his Civil Engineering Diploma (2007) and his M.Sc. Degree on Seismic Design of Structures (2010) from the University of Patras, Greece. He received his Ph.D. Degree on Timber Engineering (2016) from NTNU.

Kjell Arne MALO
Professor
Norwegian University of Science and Technology (NTNU)
Trondheim, Norway
kjell.malo@ntnu.no

Kjell Arne Malo is professor of timber structures at NTNU. His research topics are methods for increased strength and stiffness of connections for timber structures and vibrations in timber structures.

Summary

Axially loaded threaded rods feature high withdrawal capacity and stiffness and they can be a convenient, economical and easy-to-apply fastening system to be used in timber bridges. Bridges are subjected to repeated loading and therefore members and connections should have fatigue verification. Several studies have investigated the static properties of axially loaded self-tapping screws and threaded rods. However, there is a significant lack of knowledge with respect to their fatigue properties. In the present paper, a preliminary experimental investigation on the fatigue performance of axially loaded threaded rods is presented. Threaded rods were embedded in glued-laminated timber elements at 45º to the grain direction. Static and fatigue tests with stress ratio 0.1 were carried-out. The experimental results are plotted on a logarithmic scale and compared to the fatigue verification rules given by Eurocode 5.

Keywords: threaded rod, fatigue, glulam

1. Introduction

1.1 Background

Bridges are predominantly subjected to repeated loading and therefore their structural components and connections should be checked for fatigue. Steel-to-timber connections with slotted-in steel plates and numerous dowels are very typical in timber bridges constructed during the last decades. The load-carrying capacity and stiffness of fasteners loaded perpendicular to their axis (e.g. dowels) are limited by the wood embedding strength and stiffness, and the bending capacity and stiffness of the fasteners. As an alternative to laterally loaded fasteners, axially loaded threaded rods may be used. They can be a convenient, economical and easy-to-apply fastening system and contribute to easier and faster assembly on-site. Several studies have investigated the static properties of axially

loaded self-tapping screws and threaded rods; see for example [1, 2]. These fasteners feature high withdrawal capacity and stiffness without initial slip and hence they may be used to develop stiff joints for timber bridges. Stiffer joints at bridge footings can increase the sideways stability of bridges [3]. Moreover, stiff joints can be used for effective splicing of timber members [4]. Another potential application of axially loaded threaded rods could be the fastening of hangers to the timber arch in bridges. In this case, threaded rods are inserted at an angle to the grain direction. An example is a conceptual study of the timber network arch bridge which can be found in [5]. Some conceptual applications of threaded rods are summarized in Figure 1 [6].

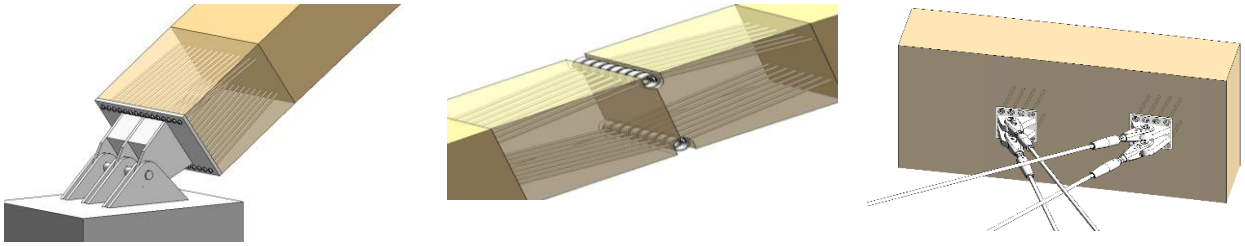

Footing Splicing Hanger fastening

Fig. 1 Conceptual applications of threaded rods in timber bridges [6]

1.2 Fatigue verification according to EN1995-2

EN1995-2 [7] has proposed a simplified design method for the fatigue verification of timber components in bridges. This method is based on equivalent constant amplitude fatigue loading, representing the fatigue effects of the full spectrum of loading events. The stress range is expressed normalized to the corresponding strength in dimensionless form through the ratio κ:

$$\kappa = \frac{\left|\sigma_{\mathrm{d,max}} - \sigma_{\mathrm{d,min}}\right|}{f_{\mathrm{k}} / \gamma_{\mathrm{M,fat}}} \tag{1}$$

where $\sigma_{\mathrm{d.max}}$ and $\sigma_{\mathrm{d.min}}$ are the numerically maximum and minimum design stresses respectively, f_{k} is the corresponding characteristic quasi-static strength and $\gamma_{\mathrm{M,fat}}$ is the material partial factor for fatigue loading. A fatigue verification is not required if the ratio κ does not exceed the values provided in Table 1. These values are therefore assumed to be the endurance limit for the corresponding loading. If the value of κ exceeds the limits provided in Table 1, fatigue verification is required. The fatigue verification criterion is:

$$\sigma_{\mathrm{d,max}} \leq f_{\mathrm{fat,d}} \tag{2}$$

where:

$$f_{\mathrm{fat,d}} = k_{\mathrm{fat}} \cdot \frac{f_{\mathrm{k}}}{\gamma_{\mathrm{M,fat}}} \tag{3}$$

The strength reduction factor k_{fat} takes into account the strength reduction with the number of loading cycles as well as the effect of the stress ratio $R = \sigma_{\mathrm{d,min}} / \sigma_{\mathrm{d,max}}$ and it is given by the following expression:

$$k_{\mathrm{fat}} = 1 - \frac{1-R}{a \cdot (b-R)} \cdot \log_{10}(\beta \cdot N_{\mathrm{obs}} \cdot t_{\mathrm{L}}) \tag{4}$$

where:

- a, b are coefficients representing the type of the fatigue action provided in Table 2;
- β is a factor taking into account the consequences of damage (β= 3.0 for substantial consequences, β= 1.0 for non-substantial consequences);
- t_{L} is the service life of the structure according to EN 1990 [8] and

- N_{obs} is the number of constant amplitude stress cycles per year.

Guidelines with respect to the number of cycles and fatigue load models for bridges are provided by EN1991-2 [9]. Equation (4) specifies a log-linear relationship between the strength reduction factor k_{fat} and the total number of stress cycles. It can be re-written in the following format:

$$k_{fat} = 1 - A \cdot \log_{10} N \tag{5}$$

where A and N have been defined as follows:

$$A = \frac{1-R}{a \cdot (b-R)} \tag{6}$$

$$N = \beta \cdot N_{obs} \cdot t_L \tag{7}$$

Equation (6) provides the slope of the log-linear relationship between the stress level and the number of cycles. This value is an indicator of the fatigue life; increasing values of A indicate decreasing fatigue life and vice versa. The values of the slope A according to Equation (6) for stress ratio R= 0.1 for the corresponding type of loading or joint are also given in Table 2. Finally, guidelines for the fatigue verification of steel fasteners are given in [10].

Table 1 Limit values of ratio κ [7]

Type of loading or joint	**Limit value of ratio κ**
members in compression parallel or perpendicular to grain	0.60
members in bending or tension	0.20
members in shear	0.15
connections with dowels	0.40
connections with nails	0.10
other connections	0.15

Table 2: Values of coefficients a and b [7]

Type of loading or joint	***a***	***b***	***A* (*R*= *0.1*)**
compression parallel or perpendicular to grain	2.0	9.0	0.051
bending or tension	9.5	1.1	0.095
shear	6.7	1.3	0.112
connections with dowels ($d \leq 12$ mm)	6.0	2.0	0.079
connections with nails	6.9	1.2	0.119

1.3 Outline

The present version of EN 1995-2 [7] does not provide guidelines for the fatigue verification of axially loaded fasteners (neither for glued-in nor for screwed-in fasteners). Some studies on the fatigue performance of glued-in rods can be found in the literature [11-19] . On the other hand, there is very limited knowledge about the fatigue performance of screwed-in fasteners. An experimental study on the low-cycle fatigue performance of axially loaded rods embedded in glulam elements can be found here [20]. The high-cycle fatigue behaviour of these fasteners

remains unknown. This paper presents a preliminary experimental study on the fatigue performance of axially loaded threaded rods embedded in glulam element at an angle of 45° to the grain direction.

2. Materials and methods

A preliminary experimental investigation of the fatigue performance of axially loaded threaded rods embedded in glulam elements was carried out at NTNU [21]. A picture of a specimen is presented in Figure 2a. Two quasi-static static tests and six fatigue tests were performed. The static tests were performed according to EN 26891 [22]. For the fatigue tests, a sinusoidal waveform with constant amplitude, stress ratio R= 0.1 and frequency f= 2.5 Hz was applied. This stress ratio is considered as representative of the stress ratio which occur in a bridge. The constant amplitude force level used in the fatigue tests was varied between 0.60 and 0.824 of the capacity obtained in the quasi-static tests. Within the first few cycles, the frequency gradually increased from 0.1 Hz to the final value of 2.5 Hz.

The specimens were cut from glulam beams of strength class GL30c [23], fabricated with 45 mm thick Norway spruce (*picea abies*) laminations. The width of glulam beams was 140 mm. Prior to testing, all specimens were conditioned to standard temperature and relative humidity conditions (20°C / 65% R.H.), leading to approximately 12% moisture content in the wood. The temperature and the moisture content were monitored during the tests. A picture of a threaded rod used in this investigation is presented in Figure 2b. The rods were inserted at 45° angle to the grain direction. Their outer-thread diameter was d= 22 mm and the core diameter was d_c= 16.1 mm. Rods were screwed in pre-drilled holes with diameter equal to the core diameter. At their ends, the rods featured a metric M20 thread. The steel grade of the rods was 8.8. The embedment length of the rods in the static tests was l= 440 mm (i.e. 20·d).

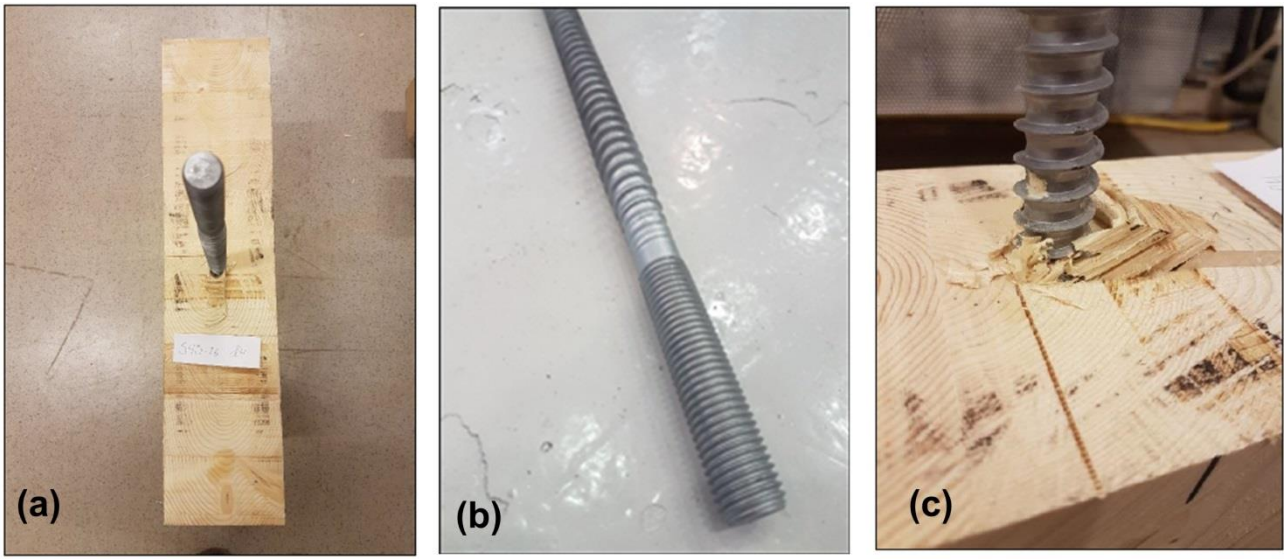

Fig. 2 Specimens for withdrawal tests [21]

The embedment length was reduced in fatigue tests because the high magnitude of withdrawal force resulted in steel fatigue failure instead of withdrawal, as a result of vulnerability of steel to fatigue. Failure was observed in the free length of the threaded rod. The lower forces due to shorter embedment length resulted in withdrawal failure instead of steel failure.

The fatigue withdrawal strength (after N cycles to failure) was quantified by dividing the applied force level by the area of the interface, i.e.:

$$f_{max} = \frac{F_{max}}{\pi \cdot d \cdot l} \tag{8}$$

The withdrawal strength can be expressed in dimensionless form by dividing f_{max} with the corresponding quasi static withdrawal strength f_{ref}:

$$\overline{f}_{max} = \frac{f_{max}}{f_{ref}} \tag{9}$$

$$f_{ref} = \frac{F_{ref}}{\pi \cdot d \cdot l} \tag{10}$$

where F_{ref} is the mean withdrawal capacity obtained in the quasi-static tests.

3. Results and discussion

The specimens failed due to withdrawal as shown in Figure 2c. Steel fatigue failures are not evaluated here. The obtained experimental results together with the properties of the specimens (moisture content and embedment length) are summarized in Table 3. The normalized withdrawal fatigue strength is plotted as function of $\log_{10}N$ in Figure 3. The least squares method was used to fit a line on the acquired experimental results. Note that a static ultimate reference test represents only a 1/4 of a loading cycle, and strictly in a logarithmic base 10 scale this leads to $\log_{10}N$= -0.6 for the static reference. The regression analysis on the experimental results resulted in the following expression:

$$\overline{f}_{max} = 0.976 - 0.059 \cdot \log_{10} N \tag{11}$$

Axially loaded fasteners introduce mainly shear stresses in the timber element they are embedded into. It is therefore reasonable to assume that their fatigue performance depends on the fatigue properties of timber subjected to shear. The prediction of EN 1995-2 [7] for shear is also plotted in Figure 3.

Table 3: Specimen properties and experimental results

Test	**Type**	***l* (mm)**	***MC* (%)**	F_{max} **(kN)**	f_{max} **(MPa)**	$\overline{f}_{max}$	**Cycles to failure, *N***
1	Static	440	12.8	188.0	6.18	1,02	0.25
2	Static	440	12.5	182.2	5.99	0.98	0.25
3	Fatigue	300	12.0	104.0	5.02	0.824	8178
4	Fatigue	330	12.0	104.0	4.56	0.75	15619
5	Fatigue	330	11.8	104.0	4.56	0.75	21994
6	Fatigue	330	11.6	104.0	4.56	0.75	17979
7	Fatigue	330	11.7	90.2	3.95	0.65	75517
8	Fatigue	330	12.1	83.3	3.65	0.60	91289 [a]

F_{ref} = 185.1 kN, f_{ref} = 6.09 MPa

[a] Terminated without failure

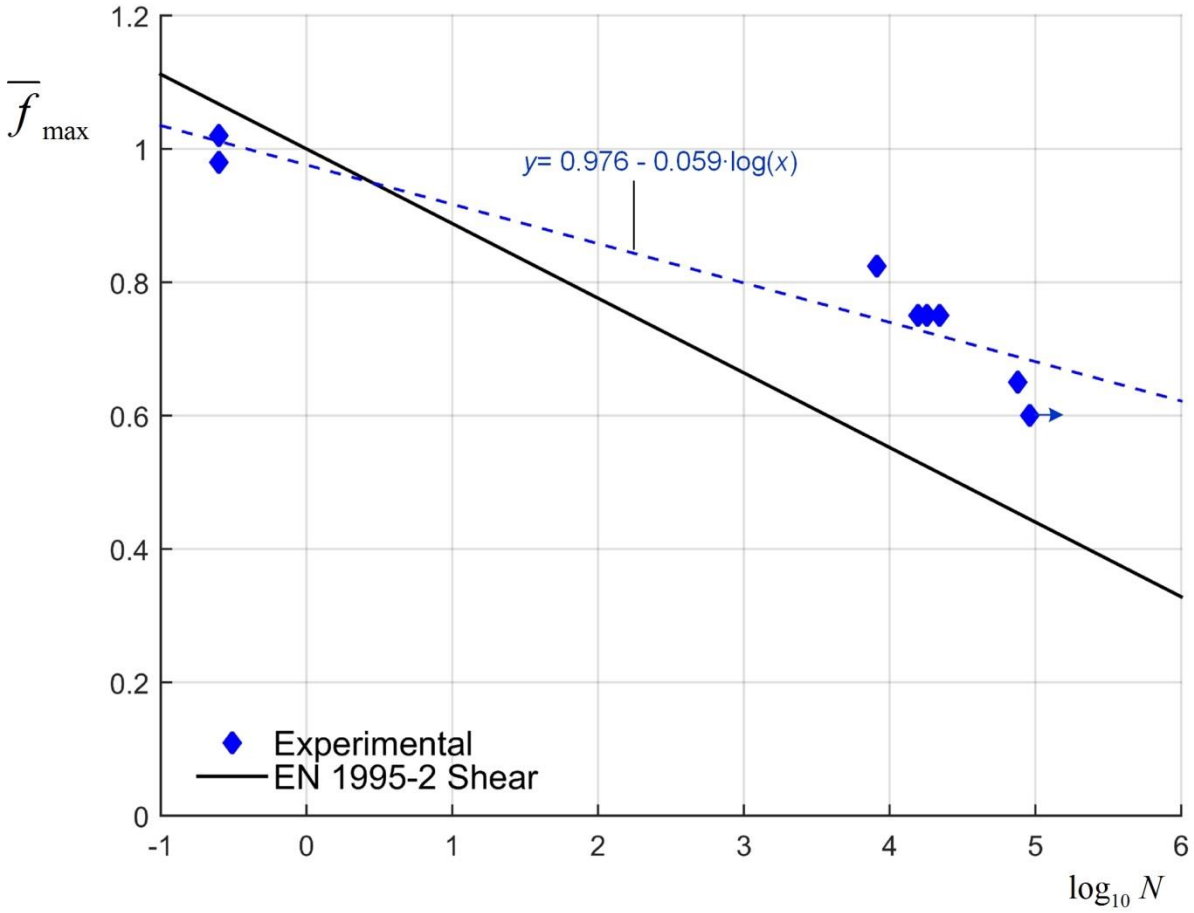

Fig. 3 $\overline{f}_{max}$ - $log_{10}N$ curves for axially loaded threaded rods (R =0.1); experimental results compared to shear loading curve obtained from [7]

The value of the slope of the fitted line (A = 0.059) is much smaller than the corresponding value for shear according to EN1995-2 [7] (A= 0.112) for R= 0.1. Therefore the prediction of EN1995-2 [7] for shear seems to provide a very conservative estimation of the fatigue withdrawal strength, confer also Figure 3. Moreover, the value of A for glued-in fasteners subjected to fatigue loading [11-19] is in the range of 0.08-0.10. Therefore the findings of the present preliminary investigation suggest that the fatigue performance of axially loaded screwed-in fasteners is better than the performance of glued-in fasteners. However, further examination at lower stress levels, different stress ratios R and different angles to grain is required to obtain a better insight of the fatigue performance of these fasteners and obtain well established fatigue properties of screwed-in rods.

4. Conclusive remarks and future work

A preliminary experimental investigation on the fatigue performance of axially loaded threaded rods embedded in glulam elements has been presented. The findings of this investigation indicate better fatigue performance of these fasteners compared to the predictions of EN 1995-2 [7] for shear loading and connections with laterally loaded fasteners. Compared to available results for glued-in rods, screwed-in rods seem to have better fatigue performance. However, further investigation is required to confirm these findings; testing at lower stress levels will provide better insight for high-cycle fatigue behaviour of threaded rods. The influence of the angle to grain should also be investigated as rods may be inserted at different angles in practice. Finally, some connections may exhibit alternating stresses and the effect of the stress ratio R should also be quantified for this case.

Acknowledgement

This work was funded by the WoodWisdom-Net+ project *DuraTB* ("Durable Timber Bridges"). The support from the funding bodies and partners is gratefully acknowledged.

References

[1] H. Stamatopoulos and K. A. Malo, "Withdrawal stiffness of threaded rods embedded in timber elements," *Construction and Building Materials,* vol. 116, pp. 263-272, 2016.

[2] H. Stamatopoulos and K. A. Malo, "Withdrawal capacity of threaded rods embedded in timber elements," *Construction and Building Materials,* vol. 94, pp. 387-397, 2015.

[3] L. Wollebæk, "Analyses of geometrical nonlinearities with applications to timber bridges," Ph.D. Thesis, Department of Structural Engineering, Norwegian University of Science and Technology, Trondheim, Norway, 2005.

[4] M. Cepelka and K. A. Malo, "Moment resisting splice of timber beams using long threaded rods and grout-filled couplers – Experimental results and predictive models," *Submitted for publication in Construction and Building Materials,* Submitted 01/2017.

[5] K. A. Malo, A. Ostrycharczyk, R. Barli, and I. Hakvåg, "On development of network arch bridges in timber," presented at the Proceedings of the 2nd International Conference Timber Bridges (ICTB), Las Vegas, USA, 2013.

[6] M. Eilertsen and D. E. Haddal, "Long span network arch bridges intimber," Master's Thesis, Norwegian University of Science and Technology, Trondheim, Norway, 2016.

[7] CEN, European committee for standardization, "EN 1995-2:2004: Design of timber structures. Part 2: Bridges," ed. Brussels, Belgium, 2004.

[8] CEN, European committee for standardization, "EN 1990:2002: Eurocode - Basis of structural design," ed. Brussels, Belgium, 2002.

[9] CEN, European committee for standardization, "EN 1991-2:2003/AC:2010: Eurocode 1: Actions on structures - Part 2: Traffic loads on bridges," ed. Brussels, Belgium, 2003.

[10] CEN, European committee for standardization, "EN 1993-1-9:2005: Design of steel structures - Part 1-9: Fatigue," ed. Brussels: European Committee for Standardization, 2005.

[11] R. J. Bainbridge, C. J. Mettem, M. P. Ansell, and K. Harvey, "Fatigue performance of bonded-in rods in glulam, using three adhesive types," presented at the Proceedings of the 33th CIB-W18 meeting Delft, Netherlands, 2000.

[12] R. Bainbridge, C. Mettem, K. Harvey, and M. Ansell, "Bonded-in rod connections for timber structures—development of design methods and test observations," *International Journal of Adhesion and Adhesives,* vol. 22, no. 1, pp. 47-59, // 2002.

[13] J. C. Molina, C. Calil Junior, and M. R. Carreira, "Pullout strength of axially loaded steel rods bonded in glulam at a 45º angle to the grain," *Materials Research,* vol. 12, pp. 427-432, 2009.

[14] J. Faddoul, "Improved stud configurations for attaching laminated wood wind turbine blades," in *DOE/NASA/20320-66, NASA TM-871 09*, ed: NASA: National Aeronautics and Space Administration, 1985.

[15] M. Pedersen, C. Clorius, L. Damkilde, and P. Hoffmeyer, "Strength of Glued-In Bolts after Full-Scale Loading," *Journal of Performance of Constructed Facilities,* vol. 13, no. 3, pp. 107-113, 1999/08/01 1999.

[16] T. Tannert, H. Zhu, S. Myslicki, F. Walther, and T. Vallée, "Tensile and fatigue investigations of timber joints with glued-in FRP rods," *Journal of Adhesion,* Article in Press pp. 1-17, 2016.

[17] M. Madhoushi and M. P. Ansell, "Experimental study of static and fatigue strengths of pultruded GFRP rods bonded into LVL and glulam," *International Journal of Adhesion and Adhesives*, vol. 24, no. 4, pp. 319-325, 8// 2004.

[18] M. Madhoushi and M. P. Ansell, "Behaviour of timber connections using glued-in GFRP rods under fatigue loading. Part I: In-line beam to beam connections," *Composites Part B: Engineering*, Article vol. 39, no. 2, pp. 243-248, 2008.

[19] M. Madhoushi and M. P. Ansell, "Behaviour of timber connections using glued-in GFRP rods under fatigue loading. Part II: Moment-resisting connections," *Composites Part B: Engineering*, Article vol. 39, no. 2, pp. 249-257, 2008.

[20] M. Gong and K. Komatsu, "Fatigue Behaviour of Lagscrewbolted Timber Joints," presented at the Proceedings of the 8th World Conference on Timber Engineering, Lahti, Finland, 2004.

[21] N. Løkken, "Fatigue of Threaded Rods Subjected to Axial Load," Master's Thesis, Norwegian University of Science and Technology, Trondheim, Norway, 2016.

[22] CEN, European committee for standardization, "EN 26891:1991 (ISO 6891:1983): Timber structures- Joints made with mechanical fasteners-General principles for the determination of strength and deformation characteristics," ed. Brussels, Belgium, 1991.

[23] CEN, European committee for standardization, "EN 14080-2013: Timber structures- Glued laminated timber and glued solid timber - Requirements," ed. Brussels, Belgium, 2013.

Reinforcement of Sundbyveien bridge

Magne A Bjertnæs
M.Sc. Structural Engineering
Sweco Norway AS
Lillehammer, Norway
Magne.bjertnaes@sweco.no

Head of Sweco Lillehammer office. Responsible for structural design of large timber structures and dynamical analyses.

Trond Arne Stensby
B.Sc. Structural Engineering
Bridge department,
Norwegian Public Roads Administration
Hamar, Norway
Trond.arne.stensby@vegvesen.no

Played an important role in the development of modern timber bridges in Norway since the early 90ies through his work in NPRA.

Summary

This paper deals with the reinforcement of Sundbyveien bridge, a timber truss bridge with a total length of 61,4 m with a mid-span of 42,0 m. During an investigation in February 2016 a deviation of design was found in a tension joint in the bottom girder. The joint had been calculated with the correct number of dowels in the slotted in steel plates, but the work drawings did not show the correct amount. This again led to a reduced capacity of the tension joint. The paper describes the design and work done to reinforce the joint with techniques which also can be applied in other similar cases.

Keywords: Timber bridge, truss bridge, tension joint, reinforcement.

1. Introduction

Sundbyveien bridge is placed south of the lake Mjøsa, Norway. It crosses the road E6 with four lanes. The bridge has a timber truss superstructure with a pre-stressed timber deck, which carries two traffic lanes and one pedestrian lane. The total length of the bridge is 61,4 m with a mid-span of 42,0 m. The bridge was finished in 2010, see Figure 1.

Figure 1 Sundbyveien bridge

After the collapse of Perkolo bridge February 2016, see Figure 2, caused by design failure, investigations of several bridges were conducted.

Figure 2 Perkolo bridge

During the investigations, a deviation of design was found in a tension joint in the bottom girder on Sundbyveien bridge. The joint had been calculated with the correct number of dowels in the slotted in steel plates, but the work drawings did not show the correct amount. This again led to a reduced capacity of the tension joint, see Figure 3, marked with a red circle.

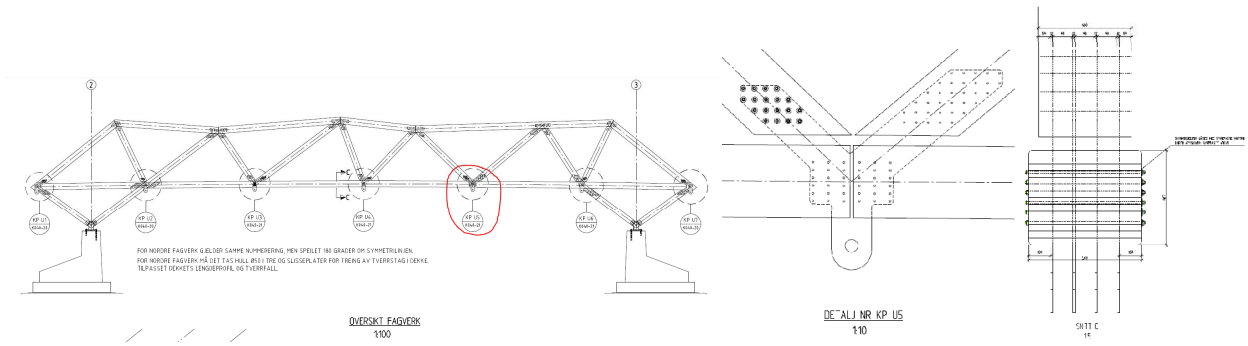

Figure 3 Affected joint

Immediately after this deviation was found, the two traffic lanes over the bridge were reduced to one. It was needed to reinforce the joint so that the bridge could bear the total design loads. Because the trusses are “mirrored” around the center of the bridge, the affected joints are placed diagonal related to each other. The bridge crosses an important main road, E6, so it was important to find a solution to avoid large traffical problems and costs during the construction period for the reinforcement. This paper describes how the design and work was done.

2. Method

2.1 Design

The bridge is design for traffic loads given in [1]. The original design of the joint had the capacity to bear the enhancement of the axial force (delta force) over the joint of 2166 kN by using 4x6 dowels, the two rows close to the edge were not used because of the distance to the edge. One side alone could not bear the maximum tension load of 2325 kN going from bottom girder into the joint. See Figure 4 Forces in the joint. The solution had to handle the force going from side of the bottom girder to the other and be fast and easy to build. The design was done by the rules given in Figure 4.

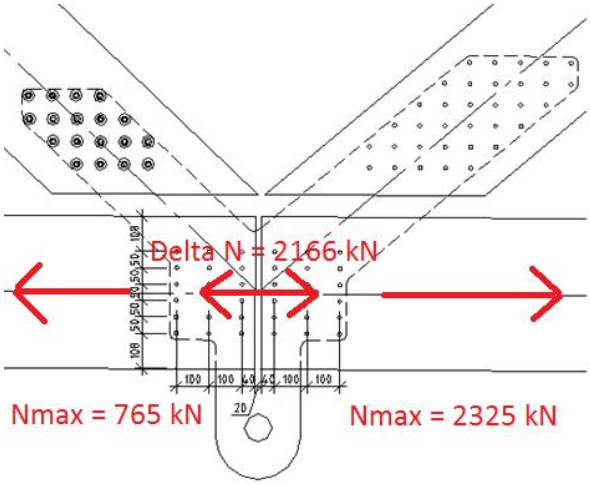

Figure 4 Forces in the joint

To enhance the capacity, it was chosen to add large steel plates with holes for timber screws 16x260 mm. The steel plates and screws has a capacity of 2615 kN, based on [2], and ensures the maximum tension over the joint. The pull out of the timber section was also controlled. See also Figure 5 Chosen solution.

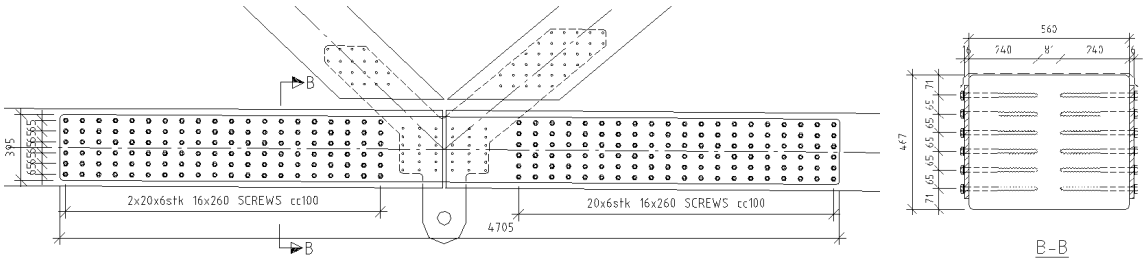

Figure 5 Chosen solution

The dead load of the bridge brings forces into the joint. To ensure that the reinforced solution should start to work together with the original design it was needed to jack up the bridge. By jacking up the bridge by 300 kN under the affected joint it was possible to reduce the forces almost to zero. From the experience from Statsrådveien timber truss bridge, where two diagonals were mounted incorrect, we knew that it was possible to jack up a timber bridge by quite small forces. In this case the bridge was jacked up so it was possible to remove and replace the affected diagonals.

Figure 6 and 7 shows the axial forces in the trusses without and with the jack for Sundbyveien bridge.

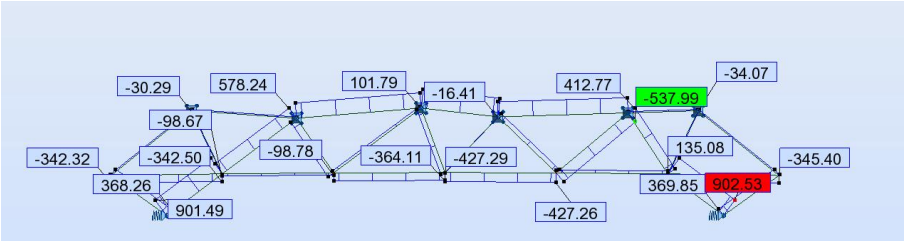

Figure 6 Axial forces from dead load without jacking

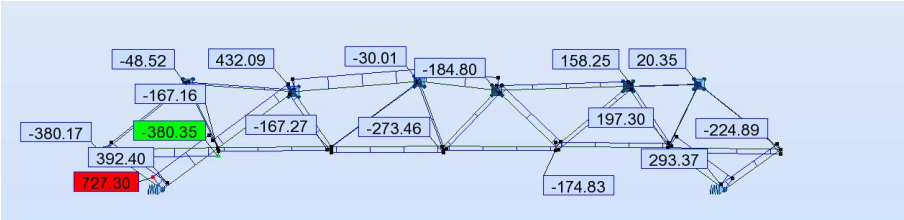

Figure 7 Axial forces from dead load with jacking

To reduce the traffical problems it was also decided that one lane of bridge should be open during all the work. It was decided to design the jacking equipment to also bear the traffic loads given in [3] for Bk10/60, 60-ton traffic load. This meant that the jacking equipment had to be designed for a total load of 840 kN. The traffic had to be led centric over the bridge to ensure areas for the workers. See the section shown in Figure 8.

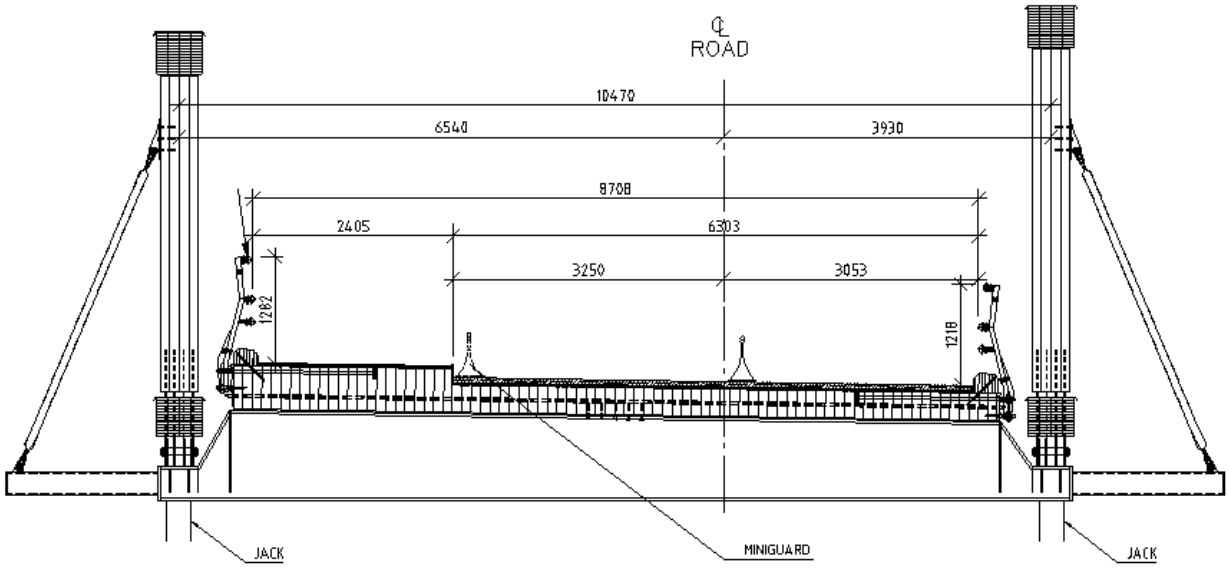

Figure 8 Section of the bridge during reinforcement work

The bridge crosses over the E6 road with four lanes. By shutting down two lanes and send traffic both directions in the two remaining lanes, the jacking towers could be placed under the joint. In this way both the traffic on and under the bridge could go as usual only with a reduced capacity. See the plan view in Figure 9.

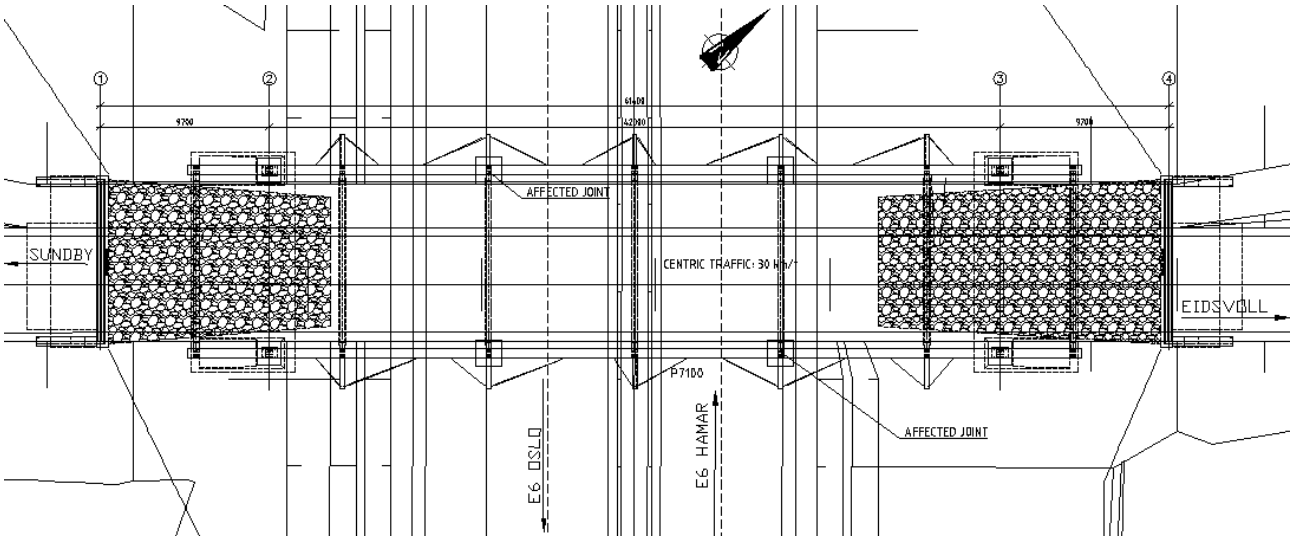

Figure 9 Plan view

After finishing one joint the jacking equipment could be taken down and placed beneath the other joint. The traffic was then led over to the two other lanes.

2.2 Construction

Kruse Smith AS, which built the bridge for The Norwegian Public Road Administration in 2009-2010, was contacted for the reinforcement work. They planned that the work should be finished in seven days. They had prefabricated steel towers stored which could be used as jacking towers. These were placed under crossbeam and the bridge could be jacked up. See Figure 10.

Figure 10 Steel towers

The railing near the joint was then removed so it was possible to access the joint. By using a custom-made drill, made exactly for the timber screws to be used, they were able to reduce the time of predrilling holes, see Figure 11.

Figure 11 Custom-made drill

The steel plates were lifted in position after the bridge was jacked up and mounted as planned. After three days from they got access to the bridge one side was finished and the tower could be placed beneath the other joint and the same work routine was applied there. The finished result is shown in Figure 12, both sides completed in under seven days.

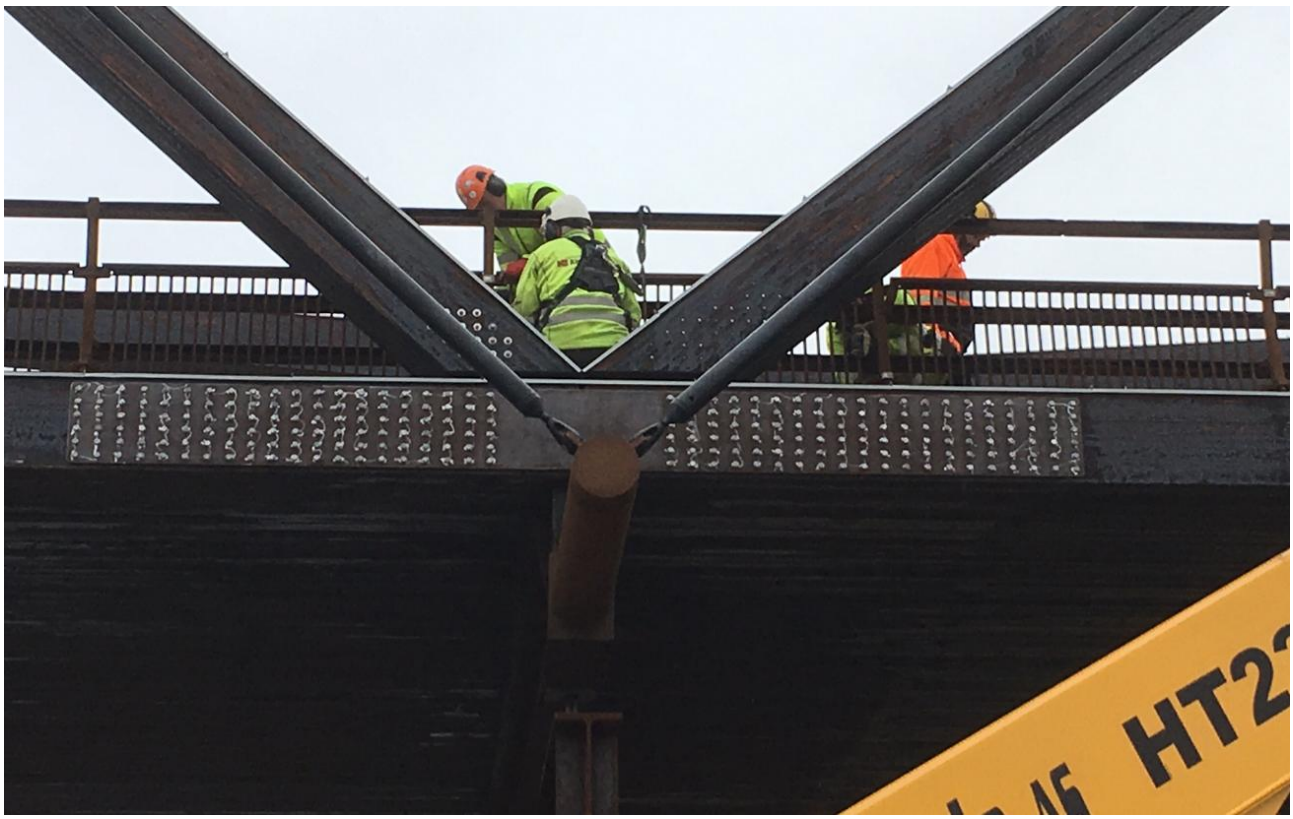

Figure 12 Steel plates mounted in position

3. Discussion

The reinforcement of Sundbyveien bridge was done in an effective way with a small amount of material and relatively low cost. The work was finished in under seven days. Because of the light weight of the bridge it was possible to jack up the bridge with relatively simple steel towers and still have traffic both under and over the bridge through the whole work period. The mounting of the steel plates was done with handheld equipment only. After installation of the reinforcement the bridge now has full load capacity.

4. Conclusion

Even if this was an unfortunate incident, this work shows that timber bridges can quite easily be reinforced. All the work was done with quite accessible light weight tools because it is easy to work with timber compared with other materials. The same technique can also be used for other timber bridges that needs to be reinforced because of changed use, enhanced loads or if some parts needs maintenance etc.

5. Acknowledgements

SWECO

Statens vegvesen

KRUSE SMITH

6. References

[1] Statens vegvesen, *Håndbok 185 Prosjekteringsregler for bruer*, 2006.

[2] NS-EN 1995-1-1, *Prosjektering av trekonstruksjoner*, 2004+A1:2008+NA:2010

[3] Statens vegvesen, *Håndbok 238 Høringsutgave Bruklassifisering*, 2009.

Learning Experiences from Norwegian Timber Bridge Inspections

Hauke Burkart
Senior Engineer
Norwegian Public Roads Administration
Oslo, Norway
hauke.burkart@vegvesen.no

Hauke Burkart has worked with timber bridges in the NPRA for the past 8 years, mostly through bridge maintaining and bridge inspection work.

Otto Kleppe
Senior Principle Engineer
Norwegian Public Roads Administration
Oslo, Norway
otto.kleppe@vegvesen.no

Otto Kleppe is active on timber bridges in the NPRA since the first modern timber bridges in Norway 25 years ago.

Summary

Some learning experience from inspection work on Timber Bridges in Norway is gathered in a publication NPRA Report nr 468 [1]. Inspection have uncovered both successful and unsuccessful technical solutions. Generally having more than one barrier against high moisture content is very important to the robustness of a timber bridge. Different sources for moisture are to be considered when designing with timber, not only rain from above, but also condensation, traffic splashing and more.

Keywords: Bridge Inspection, Timber Inspection, Moisture on Timber

1. Introduction

The NPRA has built modern timber bridges since the mid 1990's. Currently the NPRA is responsible for approximately 200 timber bridges whereof around 125 are built since 1994.

Design has evolved since the first bridges built, but the extent of design considerations when it comes to details vary a lot. Managing timber bridges is still somewhat new as bridges seldom experience problems the first years of service.

Figure 1 Even simple bridges need good detailing

Figure 2 Rainy days easily show the way water runs.

2. Inspecting Timber Bridges

When to inspect a Timber Bridge? When it's raining of course. Normally bridge inspection are carried out in good whether condition. Rainy days are very helpful in understanding structural details; however, rain is not the only source of moisture. Throughout service life a timber bridge has to be able to withstand weathering. Dirt is gathered, cracks will appear, protection might get damaged and moisture levels still need to be low. In addition to this, it is vital to be able to easily check if the bridge is sound and if it has tolerated the loads it has been subjected for.

2.1 Importance of low moisture content and sources of moisture

Evaluating the moisture content is pretty much the only viable way of ensuring the structure stays sound. This depends somewhat on the level of chemical protection, where higher moisture levels might be acceptable. "Might" is probably an important part of the sentence. We do know that creosote is protecting the structure well, but creosote doesn't reach to all of the structure. Hartwood is not as durable as creosote impregnated sapwood.
Evaluating a structure that partly has been subjected to rot is difficult since it demands the whole structure to be checked thoroughly. Assessing the extent of rot and the remaining strength is close to impossible. Thus, low moisture content is important not only due to the length of the service life of the structure, but also for being able to ensure the soundness of the structure.

2.1.1 Precipitation

Figure 3 Dense snow being thrown onto the structure by snow blowing equipment

Direct precipitation can be avoided quite simply in most cases. An overhang with an angle of 30º protects the structure well, but often one has a vertical side needing louvers or other protection measures. Even a simple structure like louvers are to be designed carefully.
One structural part that often hasn't been covered well are columns. A straight vertical structure is very difficult to protect since the exposed area is large and precipitation accumulates on the structure concentrating on the bottom parts.
Snow itself has not proven to be much of a problem and fungi doesn't grow when it's cold, but snow ploughing may damage structural protection and when snow is removed by snow blowers it may be thrown into the structure.

2.1.2 Moisture from traffic

Standing water on the carriage way and, in the case of road crossings, on roads beneath the bridge swirl moisture onto the bridge. This will of course be the case after period of rain, but also snow that is melting may result in a persistent flow of water onto the road which subsequently leading to a longer period of wetting on the bridge. Designing for all of this is very difficult. The designer should keep in mind that the conditions for drying not only depend on the

Figure 4 Standing water on bridge swirled up by each passing car

bridge itself, but also on for example good run-off conditions on the roads, improving the microclimate for the bridge.

2.1.3 Temperature change and condensation

Condensation occurs on cold surfaces. The reason for colder surfaces are many; clear sky and irradiation, quick changes in weather conditions, closeness to other materials with greater heat capacity such as abutments or a combination of these factors for example in combination with a river or stream.

The amount of water created upon surfaces that condensate may not be much. However, when this accumulates the moisture is greater and it appears on surfaces normally well protected, such as the underside of bridge decks or even behind structural protection. The accumulation can be a problem if the moisture is trapped. Areas to think about may be beneath the cladding, into abutments with enclosed area or for example at cross beams.

Figure 5 Rime (white) on the underside of a deck close to a cold abutment

Temperature changes and the temperature difference between timber structures and surrounding might be one more reason for the bridges drying out more than the average equilibrium moisture content would suggest. Instrumentation done by the NPRA shows that at relative shallow depths (1-2 cm) the temperature lag in compared to the surrounding air is quite large and could create a microclimate with larger experienced variation in relative humidity compared to the surrounding. As the relative humidity cannot exceed 100%, an upper cut-off creates a lower experienced average moisture load than the average equilibrium moisture content in the surrounding air. Furthermore, in average for example the deck temperature is greater than the surrounding average temperature, also lowering the moisture content.

2.1.4 Vegetation

Vegetation close to the bridge highten moisture. Not only is it important to avoid vegetation beneath the bridge, but also in the close surroundings of the bridge.

2.1.5 Dirt

Dirt gathers around edges and flat areas without good water run-off. Dirt will keep on moisture and acts much in the same way as vegetation. This has proven not only to be a problem for the timber, but also for steel parts.

Figure 6 Dirt on the side of the deck on onto the cross beam in direct contact with the deck. Note also that the wood is crushed beneath the anchorage plate also leading to higher moisture levels.

2.1.6 Close by hygroscopic materials

Concrete will stay wet for a longer period and may increase humidity around the timber structure. Granite for example is less hygroscopic. Water needs to be shown away from the timber structure and choosing less hygroscopic materials is one way of doing it.

2.2 Learning from older timber structures

One often look at sheltered structures, such as bridges with roofs, when explaining how to build rightly with timber. Such structures seldom cover today's needs and

are rarely build today with the exception of some pedestrian bridges. Successful modern bridges do however have more in common with older still-standing bridges than what meets the eye.

2.2.1 Sheltered structures

A sheltered structure does not need to look like a traditional roof structure. Simple slab bridges or beam bridges with watertight membrane are in some sense great examples of sheltered timber bridges. These bridges seldom fail due to details at other parts than the abutment, the design is robust and traffic influences the structure little. Covered or inclined superstructures is also a sheltered structure much like a multiple roof structure.
Ensuring good drying opportunists is just as important as sheltering the structure. Complicated details where parts are wrapped in not only sometimes fail due to design flaws, they may also fail in service life when damaged and may be impossible to inspect.
Ensuring good microclimate counts for the bridge site as well as for structural details. Connections and abutments may sometimes be so cramped that they do not ensure ventilation around critically parts, especially end-wood.

2.2.2 Inverted pyramid

Older (still standing i.e.) timber structures are often built up like inverted pyramids, with a larger roof covering more than the floors below. Some buildings even have an inclined shape where each floor is narrowed inn and drip noses exist at each floor. Mattew Bronksi made a very good presentation on this matter on a US timber webinar regarding building structures [2].

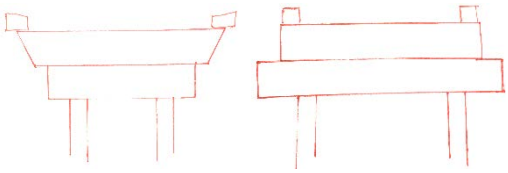

Figure 7 Difference between inverted pyramid design praxis and non-inverted pyramid bridge design.

The idea behind an inverted pyramid design is easy to understand, but how to realise such design in bridges may be difficult. Often only very small details are needed to protect the timber well.
In a cross section it is often quite easy to establish an inverted pyramid design. Designers do however often neglect it in the longitudinal section, which might not be as obvious. When it comes to abutments and bearings such as cross beams bridge designers seem to prefer the non-inverted pyramid design. Such design may have its origin from concrete bridges or just simply without further thought as it is the most “stable” design.

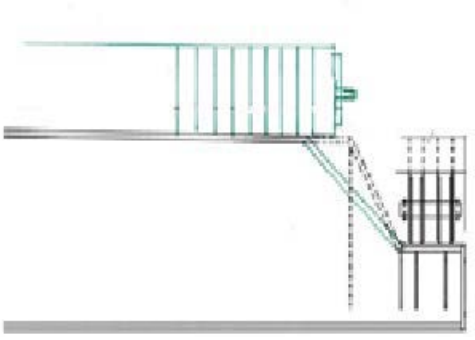

Figure 8 Altering the cross beams to be less wide than the deck is all it takes to achieve better run-off conditions and reduce dirt gathering

The whole bridge might not be able to be designed as an inverted pyramid as it would not allow for hangers and cross beams. Here designers have to be careful on the transition between timber parts and parts of other materials ensuring that the timber isn’t placed on horisontal surfaces that gather up dirt and highten moisture. Elements of the bridge that do not follow the design of an inverted pyramid probably shouldn’t be made of timber.

2.2.3 Examples on modern inverted pyramid design

The inverted pyramid can be found on some timber bridge structures, such as the Leonardo da Vinci Bridge and the timber bridges in Traunreut and Taubersbischofsheim (both in Germany). The bridge doesn't need to have a roofing structure, neither does the bridge need to have a single inverted pyramid. Several structural parts may be connected as inverted pyramids as long as water run-off is ensured on all timber parts.

Figure 9 Example of modern bridges with inverted pyramid design. From left Traunreut, Tauberbischofsheim and Leonardo da Vinci bridge

3. Robustness of protection

In Norway all bridges are to be designed such that they shall last 100 years. Hypothetical this may seem, and especially for timber, it does say something about expectations of the bridge and its design. Not only shall the bridge last long, maintenance should be at a minimum and tear and wear should not reduce expected service life.
Ensuring low moisture content by only one protection might be sufficient if that protection is very robust such as a structural roofing protection or chemical creosote protection. But even with a roofing structure designers have to take details around abutments and transvere beams into consideration, and creosote impregnation doesn't tolerate long-standing water either as has shown to be the case where membrane hasn't been used. Where parts are protected only locally, structural protection has failed due to either design errors or insufficient service life design not taking into account dirt for example.

3.1 Different kind of protections

3.1.1 Chemical protection

Chemical protection consists mostly of creosote or cupper. Creosote has without doubt saved a lot of Norwegian timber bridges from design flaws. To some extent, simple design was done on purpose in order to achieve lower building costs and thereby more competitive timber bridges. Creosote protects the timber in more than one way. It's biocide, it's long lasting, it's hydrophobic and by that not only water repellent, but also protects the cell walls and reduces cracking probably due to lower moisture movements in the timber. Reducing cracking will again increase service life. Leaching of surplus quantity is a problem, more on some bridges than others. No clear reason for this has been found. Some tests on the impregnation process have been conducted [3] as well as some anatomical factors [4] have been investigated.
Cupper impregnation is currently used on most Norwegian bridges. Rot on older (CCA-impregnated timber) bridges without earth contact is found. Protecting only with cupper impregnation without having good structural protection seems insufficient.

3.1.2 Wood stain (paint)

On modern Norwegian bridges wood stain in combination with structural protection was first used on arches that were too big for creosote impregnation. The experience with wood stain is somewhat divided. On the positive side wood stain will reduce moisture transfer considerably [5] and thereby cracking. On the negative side, when cracks appear, moisture can also be to a greater extend trapped inside.
Wood stain protected from weather will probably last very long. As a secondary protection, wood stain may work, but it needs quite good protection itself. Louvers have not proven to protect wood stain from flossing off such that boards or similar probably are needed.

3.1.3 Structural protection

Structural protection is pretty much covered by the principle of the inverted pyramid design. Here some aspects to be taken into consideration are listed:

Cladding: When used as roofing structures voids appear between the cladding and the timber. Condensation may occur and water may be concentrated to one part of the structure and trapped. Therefor it is recommended having a layer that ensures airing between the cladding and the timber. For cupper cladding this has not been done as cupper ions are thought to give a sufficient biocidic effect. Cupper claddings are however pruned to be stolen. In addition, cupper ions dripping on galvanized steel parts have been a problem.

Figure 10 Cupper corrosjon on hot galvanized steel parts from the cladding

Louvers: Rain water will run on the lower side of the louvers. If the fixation is below the lower side of the louver the rain water may be directed onto the timber is should protect.

Larger steel plates: Moisture may be trapped behind the steel plate. Furvthermore condensation and driving rain may concentrate moisture to the bottom part which should be designed with a drip nose or other measures that take care of the moisture locally.

Figure 12 Water runs on the underside of the louvers. If the fixing is beyond the edge of the louvers water may be directed back onto the timber as shown in red line.

Figure 11 Larger steel parts trapping moisture

Enclosing top-down connections: Hangers that are fastened into timber from above is in principle not a wanted design. Protection should be long-lasting such as welded parts and not from a sealant since these have limited service life.

Figure 13 Hangers connected to cladding with broken sealant

Figure 14 Hangers with welded lips covering the connection.

3.2 Multiple protection measurements

Creosote impregnation is in many senses a multiple protection measurement. Also without creosote it is possible to design with multiple protection measurements. Wood stain might be usable behind structural protection in case the structural protection fails if it's well protected, Cu-impregnation may be used even though the structure has a good inclined design. Inclined structural design may also be added with drip edges such that moisture from possible design faults run off earlier. Awareness of the protection measurements is important in order to plan them correctly.

4. Inspection friendly design

Covering parts on all sides with either cladding or louvers makes it difficult or even impossible to inspect timber bridges. Generally connections need to be inspectable and should also be so without the need for lift and removal of parts. Design should also be such that a warning is given when overloaded, as is expected on brides of other materials.

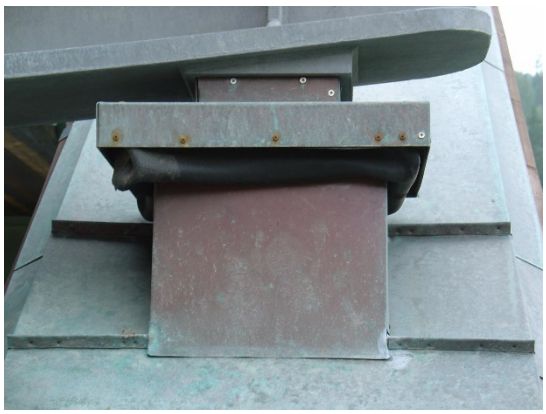

Figure 15 Non-inspectable connection

In many ways timber structures often are complex structures compared to concrete bridges with a lot of details. Complex statical parts come visible whereas they in concrete bridges are molded inside. Having a simpler design is not just desirable for the engineer constructing the bridge, it is also desirable for the bridge managing afterwards. For the case of figure 15, a simpler approach than having a top-down connection for the cross beam on the arch would be to use pillars from ground instead. Complex details are avoided and all parts become inspectable.

5. Design thoughts to timber decks

Despite no registered failures, issues to stress laminated timber decks are raised in Norway. Concerns are especially with the needs for restressing, control over stress level and corrosion on tension bars.

5.1 Stress level

Registering stress level of tension bars is not part of regular inspection, as it requires quite heavy tools to check. The stress level is known to drop for a lot of years [6]. We currently do not really

know what the lowest acceptable level of stress is and some questions remain. For example, is the friction coefficient constant or do the boards somehow interlock after several years? A board cannot move locally, how are the loads distributed? Neither do we know exactly how to combine friction forces in horizontal and vertical direction (some data available in [7]).

5.2 Corrosion on tension bars

Corrosion is found on tension bars around the inner side of the nut. At some bridges this might be related to dripping from the cladding underneath the edge sill, but there are also question raised to whether the tension bars are sufficiently protected when tensioned due to possible cracking of the zinc. Today many bridges are built with wired strands instead that are covered in grease within a plastic tube. Time will show if this is a better solution

5.3 Oblique Interlocked Laminated Timber Decks

A possible new design concept could be to transfer the shear forces not only by friction, but also by direct pressure. The idea has been to glue hexagonal shaped timber elements vertically that when subject to shear force will be restrained by tension bars. The tension bars would not need much pre-tensioning and it would be more favourable to have low-strength steel that would be stiffer than high-strength steel with large elongation. Tests have shown that the shear force is transferred by both friction and direct contact. More will be published in report 420 [8].

Figure 16 By using hexagonal shapes for laminated timber decks, shear forces may be transferred also by pressure instead of friction only

6. Design ideas to abutments

Abutments design was earlier much adopted from concrete bridges with sidewalls covering the sides of the deck. Later these wing walls were taken away and design praxis in Norway today is to move the transition between deck and abutment out away from the abutment such that better ventilation around the end of the deck is ensured together with good run-off capabilities. Rotation of the deck may create cracks in the pavement that act as gutters canalising the water to the sides of the deck near the end-grain. The edge sill should lead the water behind the transition zone as shown by the yellow line in figure 18.

Figure 17 At the transition between timber and concrete, rotation of the deck creates a gutter that leads water towards the end grain of the deck. Over time, dirt is gathered and moisture levels are heightened.

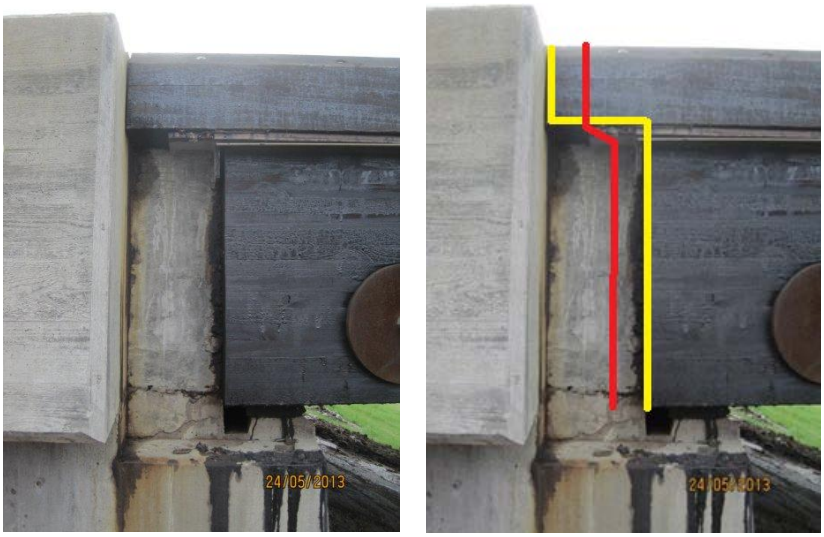

Figure 18 Inverted pyramid design in both longitudinal direction (yellow line) and cross direction (red line)

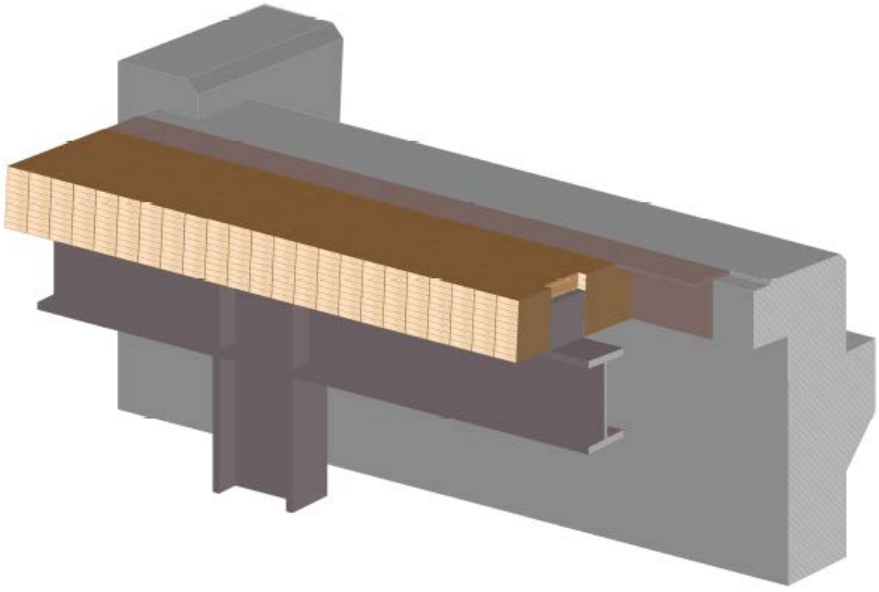

Figure 19 Current design praxis at the NPRA where the transition from concrete to timber is moved away from the abutment. The edge sill is not shown, but should be behind the transition zone as shown in figure 16.

7. References

[1] Burkart H, «Learning Experiences from Timber Bridge Inspections", *NPRA Report nr 468*, January 2016
[2] Bronski M, Durable Design: Lessons from Historic Wood Structures, *Wood Webinar* 14. Januar 2015
[3] Evans F, «Prosessparametrenes innvirkning på inntrengning, opptak og utsvetting av kreosot på limtre», Norwegian Institute for Wood Technology, 2007
[4] Treu A and Zimmer K, "Classification of creosote bleeding from timber bridges by means of wood anatomical factors", International Wood Products Journal 2017
[5] Millstein H, *Fuktighetsinnhold i tre*, Norwegian Institute for Wood Technology, 1985
[6] Horn H, «Monitoring five timber bridges in Norway, results 2012», Norwegian Institute for Wood Technology, 2012
[7] Bekk A, Hangaard L and Ravnås H, «Friksjon tre mot tre», NTNU 2016
[8] Burkart H and Dyken T "*Oblique Interlocked Laminated Decks*", NPRA Report nr 420, June 2017

Rational maintenance of timber bridges

Dániel HONFI
Researcher
RISE
Gothenburg, Sweden
daniel.honfi@ri.se

Dániel Honfi, PhD, has been working with different aspects of performance of various structures and structural systems including aspects of serviceability, robustness and recently resilience.

Thomas LECHNER
Technical specialist
NCC AB
Gothenburg, Sweden
thomas.lechner@ncc.se

Thomas Lechner, PhD, working in the field of structural engineering in various kinds of aspects in both design of infrastructures and in the evaluation of structures and damage using non-destructive testing.

Jochen KÖHLER
Professor
NTNU
Trondheim, Norway
jochen.kohler@ntnu.no

Jochen Köhler, PhD, is a structural engineer with special interest in uncertainty modelling and decision-making in general structural engineering.

Summary

The present paper provides some ideas about how decisions concerning maintenance of timber bridges should be made in a rational way. First, a brief discussion is provided concerning the evolution of maintenance strategies in general and it is suggested that maintenance of timber bridges should follow a risk-based approach. Then the discussion moves on to the condition assessment of timber bridges with a main focus on inspection and monitoring. The use of non-destructive testing methods and structural health monitoring is highlighted with regard to collecting useful information for maintenance decisions. It is argued that the information collected, should be used in a Bayesian decision analysis framework, which is especially useful in quantifying to value of information and thus the worth of various inspection and monitoring alternatives.

Keywords: structural timber, bridge maintenance, condition assessment, decision making.

1. Introduction

1.1 Background

Regular inspection and maintenance of timber bridges is essential due to their susceptibility to various types of deterioration mechanisms. Several inspection methods have been developed and applied to assess structural performance that cause minimum physical intrusion and disturbance of functionality of bridges. Similarly, maintenance is often carried out with as little disruption of traffic as possible. However, both the outcome and the costs of inspection and maintenance involve significant uncertainties [1].

Bridges are often owned by the public and the corresponding authorities manage large portfolios of many bridges. The authorities aim to allocate resources on operation and maintenance in the best possible way. Therefore a balance is needed between the expected benefits of functioning and the expected costs of maintenance including direct and indirect consequences of possible failures.

Rational decisions about maintenance and upgrading require reliable information about the performance of existing structures including exposures, structural response, associated uncertainties and costs of possible consequences. The current paper discusses how a rational decision making framework could be applied in relation to condition assessment of timber bridges with regard to the utilisation of the information collected through inspection and monitoring.

1.2 Rational maintenance approaches

Maintenance in general can be defined as the "combination of all technical, administrative and managerial actions during the life cycle of an item intended to retain it in, or restore it to, a state in which it can perform the required function" (EN 13306:2010 [2]). Determining appropriate maintenance actions require decisions on various issues, namely: how, when, by whom and at what cost an action should be carried out. These decisions should be supported by information about the actual condition and functional importance of the items (i.e. bridges). As such, the decision making process includes also decisions on how to collect and analyse new information.

How these decisions are made can differ depending on the industry in question and the expectations of the operating authority. Furthermore, during the last decades, a significant development has been made on available strategies and techniques to support maintenance. These improvements can be divided into evolving maintenance generations (see Fig. 1). In [3] this process is illustrated by defining three generations: corrective (or breakdown) maintenance, preventive maintenance, and condition-based (or predictive) maintenance. However, since the 2000s, a 4th generation maintenance – the risk/utility-based maintenance – has started to emerge in some industries; especially where maintenance costs are relatively high as, e.g. in oil and gas or off-shore, see e.g. [4] and [5].

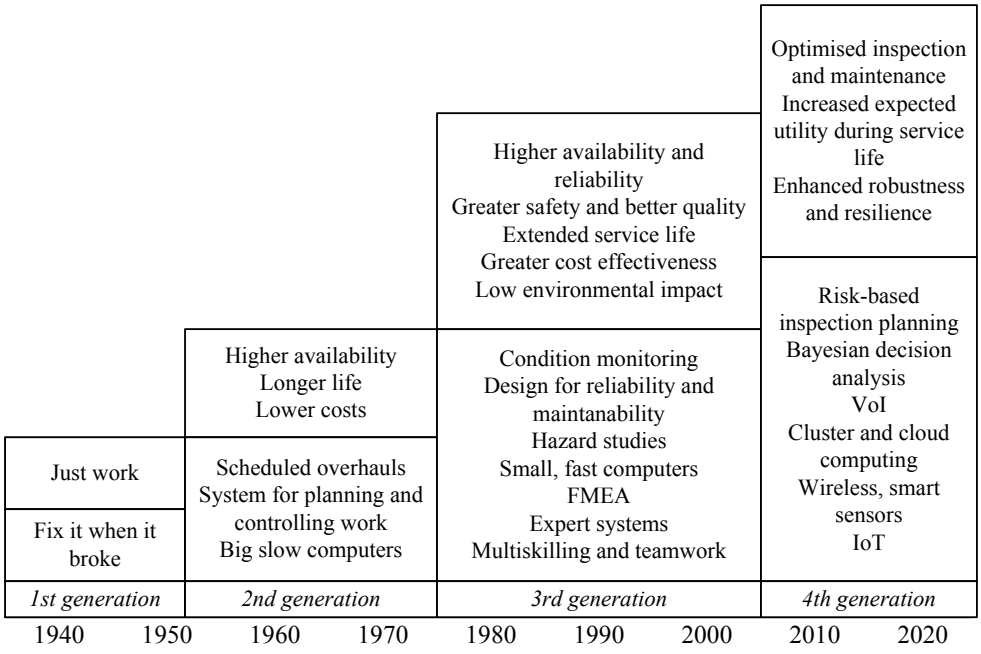

Fig. 1 Evolving maintenance goals and techniques, extended from [3]

The focus of the 4th generation approaches is to provide strategies to optimise inspection and maintenance activities; increase expected utility during service life; and enhance robustness and resilience of the structures and the network of interconnected assets. Techniques utilised to achieve these goals include risk-based inspection planning [4]; Bayesian decision analysis [6]; Value of Information (VoI) theory [7]; high performance computing infrastructures (cluster and cloud computing); wireless, smart sensors; and intelligent infrastructure as part of the Internet of Things (IoT).

Maintenance of transportation infrastructure, including timber bridges, is challenging for several reasons: they are exposed to a wide range of exposures, they are often owned and used by the public, the number of bridges is constantly increasing, consequences of reduced (or non-) functioning can be high, etc. These challenges have led to research projects exploring the possibility of the application of 4th generation maintenance strategies to bridge stocks. However these approaches have not been fully utilized in practice. One particularly interesting and important issue is how the condition assessment procedure of existing bridges can be rationalized given the practically endless methods and techniques available to obtain information on and analyse structural performance. This issue will be further discussed in the subsequent sections focusing on timber bridges.

2. Condition assessment

2.1 Procedure and levels of assessment

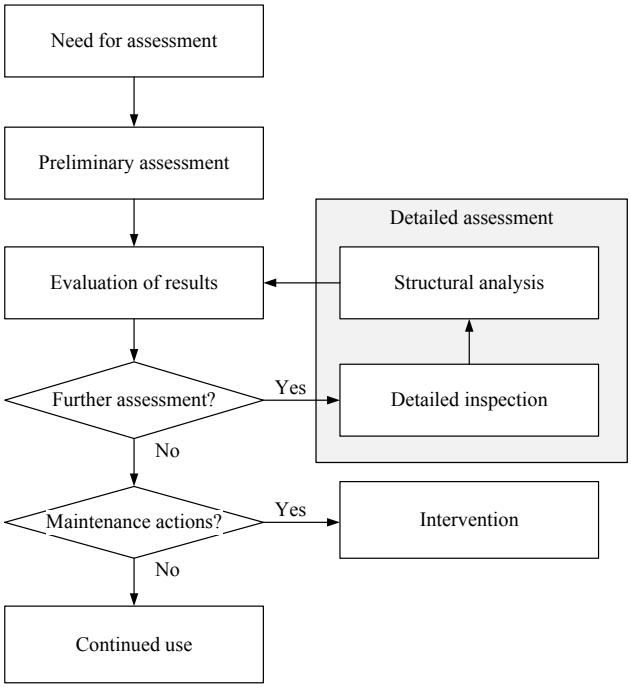

Fig. 2 Assessment procedure of timber bridges

There are several techniques and approaches available for the condition assessment of civil engineering structures. Here a general procedure for the assessment of timber structures is outlined.

The procedure is based on the general assessment framework for existing structures proposed in [8] and [9]; previous research projects on the assessment of existing bridges, e.g. [10] and [11]; ongoing and existing standardisation activities, e.g. ISO13822 (Bases for design of structures – Assessment of existing structures) [12], New European Technical Rules for the Assessment and Retrofitting of Existing Structures [13]; and the strategy suggested for assessment of timber structures in [14].

The methodology comprises the following steps (see also Fig. 2): 1) Identification of the need for assessment due to e.g. regular inspection, doubts about performance, change in requirements; 2) Preliminary assessment (document search, simplified analysis, visual inspection); 3) Evaluation of results; 4) Decision on further assessment; 5) Detailed assessment if needed, including e.g. material testing at critical sections, detailed structural analysis, reliability analysis; and 6) Decision on maintenance actions.

From Fig. 2 it is clear that there might be a loop in the condition assessment process concerning detailed assessment, i.e. the level of detailed assessment is gradually increased if doubts about structural performance continue to exist.

According to [15], the condition assessment of bridges can be performed at different levels. The 1st level is the regular, usually visual, field inspection, also called rating. It provides a qualitative (or semi-quantitative) and rather subjective description about the structural elements and/or the structure itself. The results often provide input data for the bridge management systems and used for prioritisation of actions. Rating based on visual inspection tends to be conservative, i.e. underestimates the capacity and/or remaining service life of damaged elements. On the other hand, some defects remain undetected as a result. The next, 2nd level is a more detailed assessment of the parts which are found problematic at the point of initial inspection. This usually involves some kind of calculation to better quantify the effects of the damage on the structural performance. The final, 3rd level is when the performance of the entire bridge is assessed based on thorough instrumentation and detailed modelling, which in this paper is discussed under monitoring.

There exist other classifications of such levels of condition assessment as described in [16]. These classifications commonly progress from simple to more detailed levels. The increase in the level of

details can either be seen as increasing the level of modelling sophistication, the level of uncertainty/risk consideration, or the level of information incorporated.

2.2 Maintenance actions

If any doubt about the performance of a bridge arises several actions are available to ensure that the bridge fulfils relevant codified requirements related to structural safety and serviceability. The hierarchy of terms related to these actions is given in ISO 13822 [12] and presented in Fig. 3.

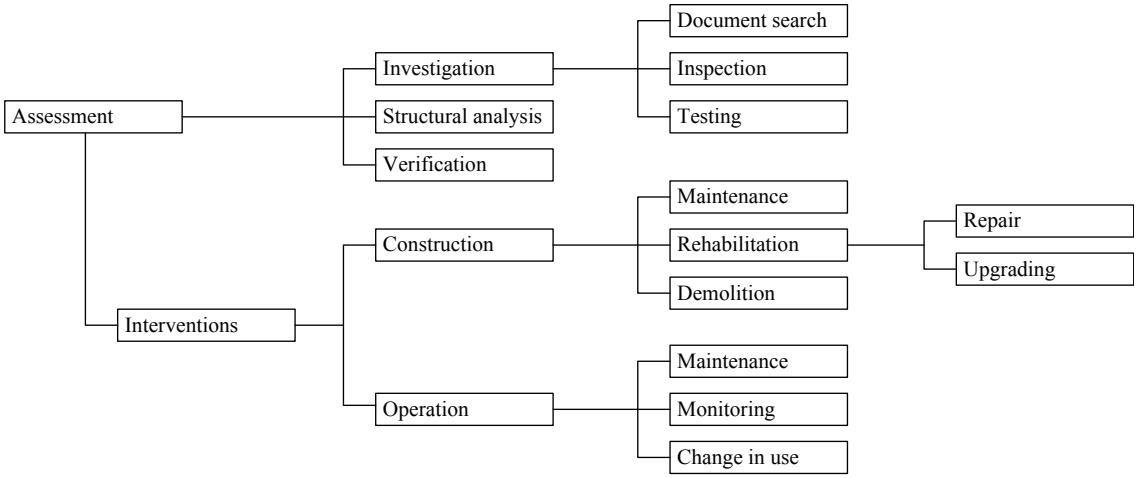

Fig. 3 Hierarchy of terms related to assessment of existing structures form ISO 13822 [12]

The challenge therefore is to select the most appropriate action considering the benefits it may bring to the decision maker, which is usually the public operator taking into consideration the preferences of the society including life-safety, economic and environmental issues.

As described before, the process of condition assessment starts with an initial assessment, i.e. visual inspection. A decision should then be made if: 1) no further actions are required; 2) a more detailed investigation is needed; or 3) interventions should be carried out. Any of these choices will lead to subsequent actions in the near future or the long run, which should optimally be taken into account when making a decision. However, the outcome of the choices can be uncertain; consequences of actions difficult to quantify; relevant information not available directly etc. Thus it is important to utilize a framework, which is able to deal with all these issues in a rational and consistent way.

In the current paper, we focus on inspection and monitoring as two major methods related to collecting information on the structural condition/performance of timber bridges. Various types of inspections include visual inspections, non-destructive and destructive testing typically of structural elements. In monitoring, the focus is on in-situ monitoring using sensors and concerned with the general structural behaviour of the bridge. Measurements of strains, displacements, accelerations, temperature, moisture content etc. are performed.

3. Inspection and monitoring of timber bridges

3.1 Performance of timber bridges

Since timber bridges are often exposed to harsh environments, in most cases this exposure leads to deterioration resulting in biological degradation processes, weathering and mechanical damage which reduces the performance of single structural components as well as the entire system [17]. Therefore it is important to identify the critical details, possible failure modes and deterioration mechanisms in an early stage of the assessment. A wide variety of inspection methods, both non-destructive testing (NDT) and semi-destructive testing (SDT) techniques, can be employed to locate damage and deterioration and obtain relevant characteristics of the structural elements to maintain the structural integrity and continuous functioning of the structure [18]. Often there is a need to combine several inspection techniques using a comprehensive assessment strategy that enables a confident estimation of structural condition and remaining service life.

As wood is an anisotropic material, the characteristics vary between the different directions, but, due to its natural characteristics, which cannot be fully controlled by the production process, the

mechanical properties of new timber structural elements are uncertain and depend mainly on the wood species, moisture content, natural growth defects, load duration and geometry of the elements [19], [20]. For timber structural elements in use these uncertainties can, in principle, be reduced by new information that becomes available by inspection and monitoring.

Wood, if unprotected, is subject to different types of degradation processes. Usually, areas of high moisture content in the decking, girders, abutments and pilings cause appropriate conditions for biological damage such as mould, insects, fungi, bacteria, etc. Also mechanical damage of timber as well as mechanical fasteners (e.g. due to traffic, streams, corrosion) might be observed and are critical, especially since they might give way to further biological damage [21].

3.2 Inspection of timber bridges

Various methods exist and are used in practice to assess structural performance of timber bridges with minimum physical intrusion and disturbance to guarantee the continued function of the structure. Visual inspection, moisture content assessment, mechanical probing, drilling, resistance micro-drilling and stress wave or ultrasound-based technologies may all be used individually or in combination by inspectors. For example stress-wave techniques are used to evaluate the modulus of elasticity of bending members and resistance to drilling is used to gain knowledge of areas of changed density due to insect or moisture induced damages.

The following subsections provide a brief overview about some typical NDT/SDT techniques, which can be employed by an inspector in order to assess the condition of an aging timber bridge.

3.2.1 Enhanced visual inspection

Visual inspection is the starting point for any assessment of existing structures as it is the basis of any form of strength, performance grading on-site. It allows for a rather quick qualitative assessment of the structural integrity of individual structural members. In practice, visual inspections are supported by local NDT/SDT for the detection of damages, internal deterioration and degradation [17].

The standard tool equipment for efficient inspection of timber bridges is composed of a tape measure, a hammer, and an awl for the basic inspections, and a stress wave timer, a resistance micro drill and a moisture meter for the more advanced/detailed investigations [22].

3.2.2 Stress-wave timing

Stress-wave measurement is a simple and effective measurement technique to identify the internal soundness and condition of structural elements and also to estimate the modulus of elasticity (MOE) for structural analysis. In these tests, two piezoelectric probes are used to receive the longitudinal ultrasound wave. One-dimensional stress-wave transmission is the most commonly used technique to measure the time that is required to travel between the piezoelectric sensors [23].

There are several key aspects that influence the travel of the stress waves in timber. These are the effect of wood species, moisture content, temperature, biological and chemical degradation, decay, insect attacks, grain angle and measurement direction [24]. The technique requires an appropriate measurement strategy and approach in order to efficiently determine the structural performance of elements in-situ and successfully detect internal damage, as well as to quantify the extent of both external and internal damage.

3.2.3 Resistance drilling

Resistance drilling can be used to detect and quantify the internal condition and decomposition of the wood in timber structural elements [25].The drilling resistance is proportional to the relative variations in density, i.e. decreasing drilling resistance is followed by reduced torque in the drill. Areas that need less torque are therefore associated with reduced density. One of the main aspects in the use of resistance drilling is to apply appropriate drilling points and drilling direction to evaluate internal condition. The main principle is to drill perpendicularly with respect to the annual rings in order to be able to distinguish between intact wood and incipient decay from the relative density profiles [26]. The interpretation of the density profiles from the drilling-resistance measurements often requires expert knowledge of the composition and the inhomogeneity of wood structures [14].

3.2.4 Moisture meter

Measurements of the moisture content (MC) with resistive moisture meter at critical sections gives a good and fast indication over the risk of biological degradation. A more elaborate measurement method to track the condition of a timber bridge is to continuously measure the moisture content with a remote data transmission system to assess the condition over time, to identify moisture changes, dimensional changes and internal stresses caused by the change of moisture. The main advantage though is that early stage damage can be recognized in order to prevent further deterioration [26].

3.2.5 X-ray investigations

X-rays are short-wave electromagnetic radiation rays that rely on the mass density and the thickness when they penetrate an object. The primary benefit when using X-ray is the opportunity to determine the condition of structures on site without disturbance [27]. A low voltage/energy X-ray powertool can be used for the in-situ investigation of timber bridges for hidden defects and integrity of the structure. An overview of possible applications using X-ray equipment for the evaluation of timber structures is listed e.g. in [27] and [14] including: material loss quantification due to insect attack/decay, corrosion detection, cross section reduction, integrity/failures of mechanical connections, density identification, and mapping damage. As with any other method, X-ray investigations should be combined with other NDT/SDT methods.

3.2.6 Further methods

There exist several further SDT methods for the local condition assessment regarding strength and stiffness properties including e.g.: a) core drilling for internal condition of the timber at suspected deterioration; b) radial core drilling for determination of compressive strength; c) surface hardness test for local indication of the quality of the structural member; d) screw withdrawal resistance test for the indication of the quality of timber; e) thermography to detect voids/defects; f) videoscopy for the internal view of the extent of hidden deterioration; and g) ultrasonic pulse echo to detect e.g. delamination and check structural homogeneity.

3.3 Monitoring of timber bridges

Non-destructive inspection of individual members provides valuable information about the localized condition of bridge elements, but more information is required to assess the condition of a bridge as an entity. Furthermore, since timber bridges often require more frequent maintenance intervals than concrete and steel bridges, monitoring might provide promising opportunities for obtaining information for better decisions on maintenance activities [28].

In the monitoring of the structural condition of timber bridges the main focus is often on relative humidity, temperature and moisture content of the wood at different depths as moisture and temperature conditions are highly relevant for biological deterioration processes. The purpose of the measurements is often to verify models for prediction of long-term durability based on periods of surface wetting, on moisture conditions related to climatic loads, coatings, wood processing etc. [29].

Besides monitoring of deterioration mechanisms, the dynamic performance of some timber bridges, might be highly relevant and worth to monitor. This could be done e.g. to identify signs of damage of bridges with complex structural systems or to verify serviceability performance. Modal analysis is typically used to examine mode shapes of the vibrating structure and compares it either to previous experimental vibrational data on the structure or to data predicted by numerical modelling. Differences in dynamic characteristics can be used to diagnose damage in the structure [17]. Another use of analysing dynamic response could be e.g. to determine dynamic amplification factors for traffic loads [30]. A combination of different sensors in a comprehensive health monitoring system, i.e. continuous measurement of e.g. accelerations, displacements, strains, moisture contents and weather data could be useful to verify the structural design and the long-term behaviour of the timber bridges [31].

It should be noted that even diagnostic static load tests can be seen as a basic type of monitoring, even if a “real” continuous monitoring system is not implemented. Static load applied to a bridge provide valuable insight into the overall stiffness of the structural system and help verifying structural analysis models and thus the load bearing capacity of the bridge [17].

4. Decision making

4.1 Information and structural integrity management

As described e.g. in [32] engineering decision making can be interpreted as playing a game where the decisions aim to optimize the expected utility according to the decision maker's preferences and can be analysed by the game theory [33]. To be successful in the game the rules must be clear, i.e. the constituents of the decision problem must be known. According to [34] this means that information is needed about the system, its surrounding, the possible consequences of actions, the interrelation of different factors that affect system performance etc. Participating in the game is then carried out by "buying" physical changes in the system or "buying" knowledge about the system such that the outcome of the game should be optimized.

In the light of this, the main use of inspection and monitoring techniques concerning timber bridges, or any civil engineering structure in general, is that the information provided by these techniques can be utilized to reduce uncertainties concerning decisions about the structure. Unfortunately, collecting information comes with costs, which might or might not be in balance with the benefits gained by the reduced uncertainties and thus risks. In practical cases, the effectiveness of inspection and/or monitoring often becomes known only after the implementation. However, it is possible to develop a consistent decision procedure for maintenance in general, and for inspection and monitoring in particular, which aims to maximise the utility of the structure over its entire lifetime with due consideration of regulatory constraints (e.g. life safety and environmental requirements).

As it has been mentioned, these decisions usually need to be based on incomplete or uncertain information. To deal with this, Bayesian decision analysis [6] can be utilised where three different types of analysis are generally distinguished, namely, the prior- , the posterior- and the pre-posterior decision analysis. In a prior analysis the optimal action/decision is identified based on probabilistic models on relevant uncertain states of nature using existing information. In a posterior analysis new information (e.g. derived from inspection) are utilized to update the probabilistic models and the optimal action/decision is identified based on the updated models. In a pre-posterior analysis several possible inspection methods are considered as possible sources of information and it is analysed, given their costs, which one is the optimal to use. Based on the pre-posterior analysis it is possible to estimate the effectiveness of inspection and monitoring actions before they are carried out.

4.2 Quantification of the value of new information

Pre-posterior analysis could help quantifying the real benefits of inspection and monitoring and thus help the bridge operator to decide what price should be paid for such services. A decision problem is a choice among courses of action when [6]: 1) the consequence of any course of action will depend upon the state of the bridge structure; 2) the true state of the structure is as yet unknown; and 3) it is possible, at a cost, to obtain additional information about the state.

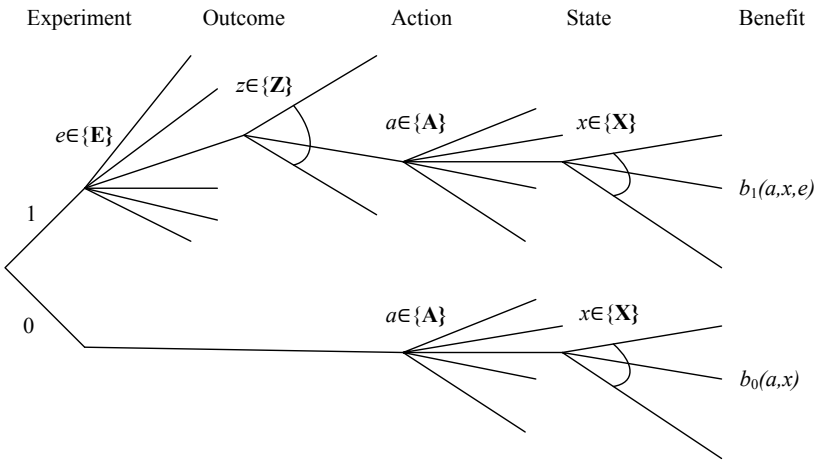

Fig. 4 Decision tree adapted from [35]

In bridge maintenance, the decision problem can be reduced to a limited number of alternatives (e.g. "do nothing", "inspect", "repair", "strengthen" and "reduce loads"). As described e.g. in [35], [36] and [37], the basic concept of pre-posterior analysis and VoI [7] analysis can be illustrated considering a decision tree, see Fig. 4. It is assumed that the the true state of the structure X is random with possible outcomes $x \in \{\mathbf{X}\}$ and various maintenance actions $a \in \{\mathbf{A}\}$ can be chosen, which will affect the probability assignment of the possible states of the structure.

Decision on collecting information about the structure through inspection or monitoring can be seen as the upper branch 1 of the figure, whereas the lower branch 0 can be seen as not collecting information. Considering the lower branch 0 of the decision tree, i.e. not collecting information, the decision analysis consists of choosing the maintenance action a, with maximizing the expected value of the benefit $b_0(a,x)$ resulting in the expected life cycle benefit B_0:

$$B_0 = \max_a E'_X\left[b_0(a,X)\right] \tag{1}$$

For the upper branch 1 in Fig. 4., i.e. opting for collecting information, a further decision has to be taken concerning the choice of the inspection method. This decision could be interpreted as an experiment $e \in \{\mathbf{E}\}$ with an outcome $z \in \{\mathbf{Z}\}$, where Z is a scalar valued random variable.

Applying Bayes' theorem the a-priori probability assignment of the true state of the structure $f'_X(x)$ can then be updated given the outcome of the inspection z:

$$f''_X(x|z) = \frac{L(x|z)f'_X(x)}{\int_{-\infty}^{\infty} L(x|z)f'_X(x)dx} \tag{2}$$

where $L(x|z)$ refers to the likelihood of the true state x given observation z.

The expected value of conducting the experiment e with subsequent optimization actions of the maintenance actions a is evaluated over the possible realisations of Z. Without providing all details here, it is possible to select the experiment e^* that leads to the maximum expected benefit:

$$B_1 = \max_e E_Z\left\{\max_a E''_X\left[b_1(a,X,e)\right]\right\} \tag{3}$$

The expected value of (collecting) information, i.e. the worth of inspection and monitoring, can be calculated as:

$$VoI = B_1 - B_0 \tag{4}$$

The above presented extended form of the pre-posterior decision analysis might, in some cases, be difficult to use and a so called normal form could then be applied. In the normal form of the analysis a decision rule d is defined specifying the action to be taken given the experiment outcome z, more details are given e.g. in [37].

5. Conclusions

Modern maintenance approaches in high-consequence industries are in their 4th generation utilising modern technologies and risk-based methodologies for decision making. It is here argued that these approaches will be used in the future for the maintenance of timber bridges as well.

Modern NDT and monitoring technologies in the condition assessment of timber bridges are already in use and their application is increasing. It is, therefore, expected that the utilization of information for decision making concerning structural integrity management will follow modern approaches as well. That is VoI analysis, which provides a consistent and rational way of making decisions about condition assessment of timber bridges with maximising the expected lifetime benefits of the structure.

The pre-posterior analysis takes into account the uncertainties during the decision making process; however, it might require significant efforts concerning statistical modelling and computation. This could be an obstacle for practical application and need to be further investigated in the context of maintenance of timber bridges.

6. Acknowledgement

The authors acknowledge the support provided by the Swedish Transport Administration (Trafikverket); the strategic innovation programme InfraSweden2030, a joint effort of Sweden's Innovation Agency (Vinnova), the Swedish Research Council (Formas) and the Swedish Energy Agency (Energimyndigheten); and COST Action TU1402.

7. References

[1] Köhler, J., "Risk management and maintenance strategies for timber structures", *Revista Portuguesa de Engenharia de Estruturas*, Vol. 11, pp. 69-78, 2012.

[2] CEN, EN 13306:2010, Maintenance – Maintenance terminology, European Committee for Standardization, Brussels, 2010.

[3] Moubray, J., *Reliability-Centered Maintenance*, 2nd Edition, Industrial Press, New York, 1997.

[4] Faber, M.H., "Risk-Based Inspection: The Framework", *Structural Engineering International*, Volume 12, No. 3, 2002, pp. 186–195.

[5] Sørensen, J.D., "Framework for risk-based planning of operation and maintenance for offshore wind turbines", *Wind Energy*, Vol. 12, Issue 5, 2009, pp. 493-506.

[6] Raiffa, H. and Schlaifer, R., *Applied statistical decision theory*, Harvard University Press, Boston, 1961.

[7] Howard, R.A., "Information value theory", *IEEE Transactions on Systems Science and Cybernetics*, Vol. 2, Issue 1, 1966, pp. 22–26.

[8] Schneider, J., *Introduction to safety and reliability of structures,* Structural Engineering Documents, International Association for Bridge and Structural Engineering, Zürich, 1997.

[9] JCSS, *Probabilistic Assessment of Existing Structures,* A publication of the Joint Committee on Structural Safety (JCSS), RILEM Publications, 2001.

[10] BRIME (Bridge Management in Europe), Deliverable 14, Final report, 2001.

[11] Sustainable Bridges, Guideline for Load and Resistance Assessment of Existing European Railway Bridges, SB-LRA, 2007.

[12] ISO, ISO 13822:2010, Bases for design of structures – Assessment of existing structures. International Organization for Standardization, Geneva, 2010.

[13] JRC, *New European Technical Rules for the Assessment and Retrofitting of Existing Structures*. JRC Science and Policy Report, Publications Office of the European Union, Luxembourg, 2015.

[14] Lechner, T., *In-situ assessment of timber structures - Assessment methods and case studies*, Dissertation, Chalmers University of Technology, Gothenburg, 2013.

[15] Wenzel, H., *Health Monitoring of Bridges*, John Wiley & Sons, 2009.

[16] Honfi, D., Leander, J., and Björnsson, I., "Decision support for bridge condition assessment", The 4th International Conference on Smart Monitoring, Zürich, Switzerland, 2017.

[17] Emerson, R.N., Pollock, D.G., Kainz, J.A., Fridley, K.J., McLean, D., and Ross, R.J., "Nondestructive evaluation techniques for timber bridges", The 5th World Conference on Timber Engineering, Montreux, Switzerland.

[18] Fink, G., Köhler, J., "Quantification of different NDT/SDT methods in respect to estimate the load-bearing capacity", *Construction and Building Materials*, Vol 101, Part 2, pp. 1181-1187, 2015.

[19] Köhler, J., Sørensen, J.D., and Faber, M.H., "Probabilistic modelling of timber structures", *Structural Safety*, Vol. 29, Issue 4, pp. 255-267, 2006.

[20] Köhler, J. and Svensson, S., "Probabilistic representation of duration of load effects in timber structures", *Engineering Structures*, Vol. 33, Issue 2, pp. 462–467, 2011.

[21] Brashaw, B., Wacker, J., and Jalinoos, F., "Field Performance of Timber Bridges: A National Study". The 2nd International Conference of Timber Bridges, Las Vegas, NV, USA, 2013.

[22] Brashaw, B., Wacker, J., and Ross, R.J., *Advanced Timber Bridge Inspection - Field Manual for Inspection of Minnesota Timber Bridges*. University of Minnesota and Minnesota Department of Transportation, 2014.

[23] Wang, X., Divos, F., Pilon, C., Brashaw, B.K., Ross, R.J., and Pellerin, R.F., *Assessment of decay in standing timber using stress wave timing nondestructive evaluation tools : a guide for use and interpretation*. Gen. Tech. Rep. FPL-GTR-147. Madison, WI: U.S. Department of Agriculture, Forest Service, Forest Products Laboratory, 2004.

[24] Dackermann, U., Crews, K., Kasal, B., Li, J., Riggio, M., Rinn, F., and Tannert, T., "In situ assessment of structural timber using stress-wave measurements", *Materials and Structures*, Vol. 47, Issue 5, 2014, pp. 787–803.

[25] Kasal, B. and Anthony, R.W., "Advances in in situ evaluation of timber structures", *Progress in Structural Engineering and Materials*, Vol. 6, Issue 2, 2004, 94-103.

[26] Tannert, T., Anthony, R. W., Kasal, B., Kloiber, M., Piazza, M., Riggio, M., Rinn, F., Widmann, R., and Yamaguchi, N., "In situ assessment of structural timber using semi-destructive techniques", *Materials and Structures*, Vol. 47, Issue 5, pp. 767–785.

[27] Anthony, R. W. "Examination of Connections and Deterioration in Timber Structures Using Digital Radioscopy", The 3rd Forensic Engineering Congress, San Diego, California, United States, 2003.

[28] Gustafsson, A., Pousette, A., and Björngrim, N., "Health monitoring of timber bridges", The 1st International Conference on Timber Bridges, Lillehammer, Norway, 2010.

[29] Sandberg, K., Pousette, A., and Dahlquist, S., "Wireless in situ measurements of moisture content and temperature in timber constructions", The 9th International Conference on Durability of Building Materials and Components, Porto, Portugal, 2011.

[30] Wipf, T.J., Ritter, M.A., and Wood, D.L., "Dynamic evaluation of timber bridges" National conference on wood transportation structures, Madison, WI, USA, 1996.

[31] Björngrim, N., Gustafsson, A., Pousette, A., and Hagman, O., "Health monitoring of a cable-stayed timber footbridge", 1st International Conference on Structural Health Assessment of Timber Structures, Lisbon, Portugal, 2011.

[32] Ditlevsen, O. and Madsen, H.O., *Structural Reliability Methods*, John Wiley & Sons Ltd, Chichester, 1996.

[33] von Neumann, J. and Morgenstern, O., *Theory of Games and Economic Behavior*, Princeton University Press, 1944.

[34] Faber, M.H. and Maes M.A., "On Applied Engineering Decision Making for Society", The 12th IFIP WG7.5 Working Conference on Reliability and Optimization of Structural Systems, Aalborg, Denmark, 2005.

[35] Roldsgaard, J.H., Georgakis, C.T., and Faber, M.H., "On the Value of Forecasting in Cable Ice Risk Management", *Structural Engineering International*, Vol. 25, No. 1, 2015, pp. 61–70.

[36] Faber, M.H., Val, D., and Thöns, S., "Value of information in SHM – Considerations on the theoretical framework", 1st Workshop of COST TU1402, Kongens Lyngby, Denmark, 2015.

[37] Xing, C., Caspeele, R., and Val, D., "Classes of decision analysis", Fact Sheet, COST TU1402: Quantifying the Value of Structural Health Monitoring, 2016.

Investigation of timber bridges in Estonia

Per-Anders Fjellström
Researcher
RISE Research Institutes of Sweden, Skellefteå, Sweden
per-anders.fjellstrom@ri.se

Per-Anders Fjellström has been working with full scale tests, health monitoring, inspection test methods and inspections manuals since 1994, and has inspected many of the Swedish timber bridges.

Alar Just
Associate Professor
Tallinn University of Technology
Tallinn, Estonia
Alar.Just@ttu.ee

Structural engineer with design experience of timber bridges in Sweden, Estonia, Finland and Saudi Arabia. Currently teaches timber structures in Tallinn University of Technology.

Summary

Selected 17 Estonian timber bridges were investigated in terms of durability. The bridges chosen for inspection had different structural types, presence of impregnation and also different character and various building years (1836 to 2013).

Main findings of the study consider the structural protection of the bridges. Detailing of Estonian bridges does not provide the sufficient protection in many cases. Durability of the wooden structural elements can depend on the impregnation, protection by cladding and the wooden specie used. Moisture content and the development of fungal damages were measured during the inspection.

Eigen frequencies and damping of timber bridges with longer span than 24 m were measured in this study.

The results of the investigation of Estonian timber bridges are summarized in this paper and illustrated by examples of the bridges.

Keywords: timber bridge investigation, durability.

1. Introduction

During this research, inspections on 17 timber bridges in Estonia were conducted by authors of this paper in the autumn of 2014. The study was ordered by the Estonian Road Cluster and was performed by SP Technical Research institute of Sweden and Tallinn University of Technology.

Among the examined bridges were 9 beam bridges, 6 arch brides, 1 cable stayed and 1 covered truss bridge. 4 of the bridges were road bridges, 13 pedestrian bridges. Bridges were situated in different locations all over the country. See Fig.1.

Inspection included visual survey of joints, occurrence of rot and measuring of moisture content. All inspections were made according to the guidelines in the Swedish road administrations handbook in Batman and “Bridge Inspector’s Reference Manual” of the US.

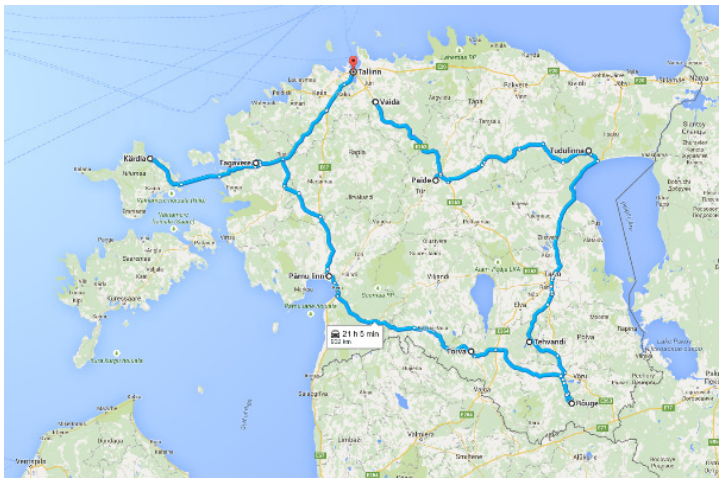

Fig. 1 Location of the investigated bridges

In this paper, the investigation results are described and analysed.

2. Bridge inspections

The most important findings of the investigated bridges are explained by the following examples. The examples are chosen to describe the biggest weaknesses for the purpose of learning from them and avoiding them in the future.

2.1 Vaida footbridge

Year of construction	2008
Total length	124m
Practicable width	4m
Span length	31+62+31m
Type of structure	Cable-stayed bridge
Timber Beams and Deck: Pylons:	 not impregnated Spruce; pressure impregnated Comwood of Spruce
Vertical eigenfrequency	2,4 Hz

Fig 2. Vaida footbridge.

Vaida footbridge is a cable stayed bridge with glulam girders and pylons of Comwood. Main span 62 meters. Main characteristics of the bridge are shown in Fig 2.

The inspection of the glulam in girders and pylons were made with a resistograph and a resistance moisture meter. Each glulam member was tested in at least 3 points. The bridge was inspected on 8th of December 2014. That is roughly six years after the building of this bridge.

Inspection showed that the bridges' superstructure is in fair to poor condition. Six of the glulam members in the girders were in poor condition and should be replaced. The moisture content was very high in the beams below the deck plate. Most of the glulam beams had just minor fungal decay, isolated to the upper 100-300 mm of the beam. Deck was seriously damaged by fungal decay along the edges. Part of the deck was completely rotten and collapsed. See Fig.5.

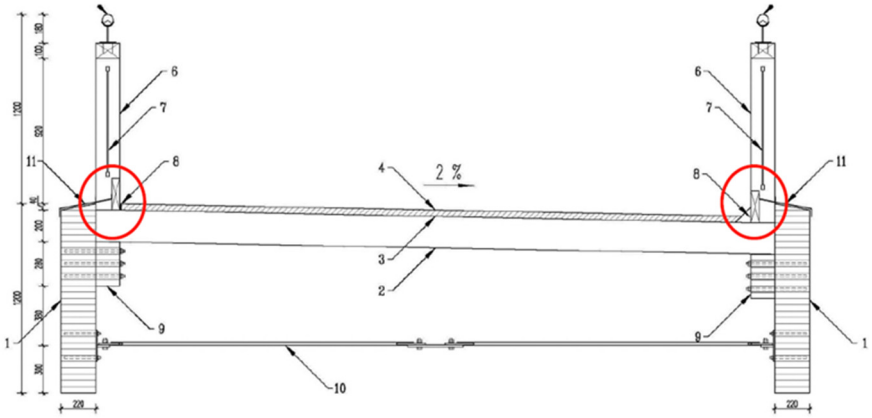

Fig 3. Section of the bridge.

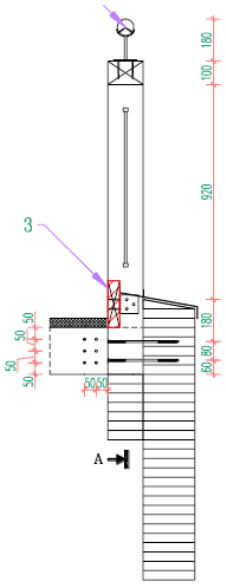

Designed solution

Built solution

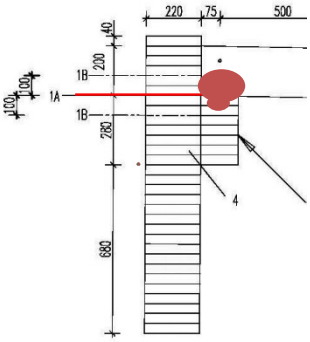

Region of fungal damage

Fig 4. Joint of the deck edge.

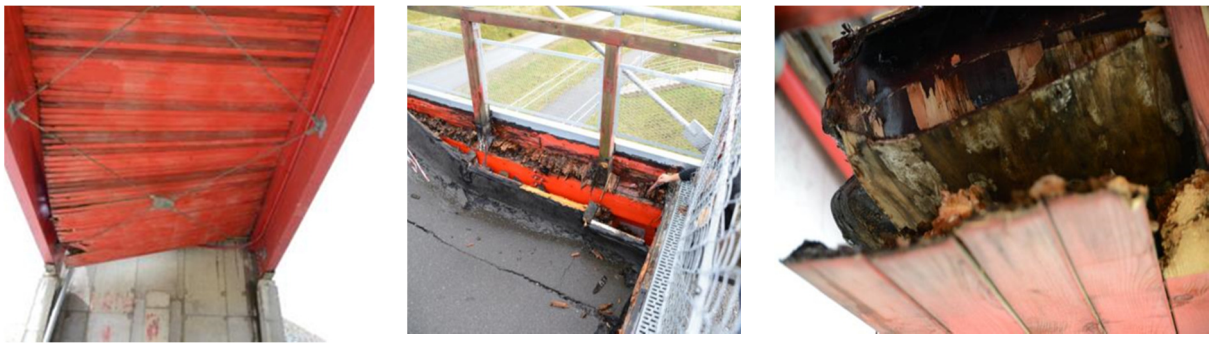

Fig 5. Collapse of the deck in 2014 due to completely rotten deck at supports.

The damage was caused by non-ventilated joints between deck plate and main girder. Deck was covered by water tight layer and asphalt. In contradiction with the designed solution, the support area at the edges of wooden deck plate was also covered by asphalt and the drying of wood of the deck plate at the edges was blocked. The water barrier shown in red in Fig.4. was missing.

Comwood pylons were in satisfactory condition. Moisture content was very high at the pylon foot. Wooden pylon was supported directly on the concrete contrary to designed solution. Pylon was

made of pressure impregnated spruce. The pressure impregnation helped to avoid the destructive fungal damage during the first six years although the moisture content was very high. The transverse beams between the pylons are in satisfactory condition. Very high moisture content in the wood due to lack of water repellent paint system and/or protective cladding was discovered.

All wooden parts of Vaida footbridge except pylons were made of unimpregnated spruce (Picea Abies) instead of chemically treated pine (Pinus Silvestris). Unimpregnated spruce does not have noticeable durability without proper cladding.

The regular bridge inspections made by Estonian Road Office did not discover any damage during these 6 years. Most probably there is no proper system for inspection of timber bridges specifically.

Recovering of damages of the bridge should consist of the replacement of deck structure and replacement of at least two glulam beams (hit by the collapse). The bridge owner - Estonian Road Office – decided to demolish this bridge and build a new steel-concrete bridge instead.

2.2 Merirahu footbridge

Year of construction	2001
Practicable width	3,2m
Length	25,6m
Type of structure	Arch bridge
Timber Arches and Beams: Deck:	 not impregnated Spruce impregnated Spruce (Picea Abies)
Vertical eigenfrequency	7,4 Hz

Fig 6. Merirahu footbridge.

Merirahu footbridge is an arch bridge with span of 24,5 meters. Bridge has a balcony on the sea side. Main structural elements are covered by five layers of alkyd paint. Bridge deck is covered by bitumen emulsion and gravel layer. All the steel elements of this bridge are made of stainless steel. Main characteristics of the bridge are shown in Fig 6.

The bridge was repainted with a dark paint on 2010. Authors of this paper do not have information about the chemical content of the paint.

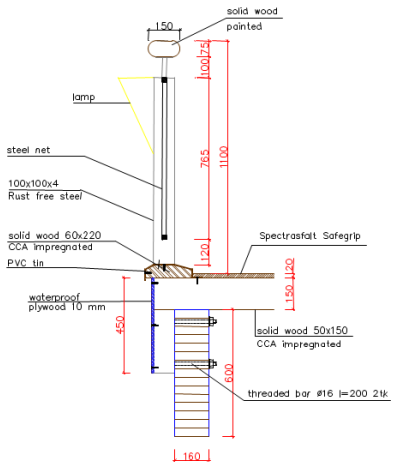

Fig 7. View of the bridge and deck edge detail.

The inspection discovered that the bridges' superstructure was in a serious condition. Probably the dark colour of the new paint led to cracks and allowed the water insertion into the wood. Drying of

wood was blocked and that led to development of fungal damage in the arches and cross-beams.

The most critical damage is severe decay and deformation in one transversal beam. The beam was considered as fracture critical during the inspection. The transversals condition is beyond corrective action due to decay in connecting points and along the upper quarter of all sides. See Fig.8.

Condition of two arches was beyond corrective action due to decay at supports. The arches were in fair to poor condition and the south east side was recommended to be replaced. The moisture content was high, 20-24% and the decay process could continue until the arches are covered with cladding. The arches are made of spruce. These problems could have been avoided with chemically treated arches and/or protective cladding.

The deck was in fair to poor condition. It's a nail laminated deck made of surface treated spruce covered with a thin bitumen layer with washed gravel on top. The deck should have been made of treated pine instead of spruce. The bitumen layer was too thin, and damaged, to protect the deck. Lack of preventive maintenance was also discovered.

The condition of the top followers of the railing was also beyond corrective action due to decay by fungi. The deck had some spots with minor decay. All wood parts were made of spruce (Picea Abies) instead of chemically treated Pine (Pinus Silvestris). The use of spruce instead of a more durable material in weather exposed bridge elements may shorten the service life.

Fungal damage of the transversal beam

Rotten zone and insects in the arch foot

Fig 8. Main fungal damages of the bridge.

Recovering of damages of the bridge should consist of the replacement of two arches and transversal beams. Paint should be removed from the remained structural elements and replaced with the proper protection systems including wooden or steel claddings on the surfaces exposed to direct weathering.

The bridge owner decided to repair the bridge in 2017.

2.3 Tehvandi rollerski bridge

Year of construction	2004
Practicable width	4,5m
Length	24,5m
Type of structure	Arch bridge
Timber Arches and Beams: Deck:	 impregnated Pine not impregnated Spruce

Fig 9. Tehvandi rollerski bridge.

Tehvandi wooden bridge is an arch bridge with length of 24,5 meters. Bridge is built for rollerski track. Main structural elements are made of pressure impregnated pine. Deck is made of solid wood and covered by asphalt pavement. Main characteristics of the bridge are shown in Fig 9.

Inspection showed that the bridges' superstructure was in good condition. The most critical damage was severe decay and lost parts of the railing that was in an imminent failure condition. All parts made of wood needed to be replaced. The railing was noticed to be relatively low 0,98 – 1,06 m. Some railing posts were tilted out from the bridge. Fasteners used in the railing were very small and weak.

Arches were in satisfactory condition and will need a cladding. The moisture content in the glulam, close to the abutments, was very high, 23-37%. The moisture content will remain very high until all weather exposed parts are covered with cladding. Abutments were affected by increased humid environment from plants and earth. See Fig.10.

The deck was in very good condition. It's a nail laminated deck with an asphalt wearing surface on top. The deck was made of spruce.

Arches need re-painting and covering on top

Railing needs replacement

Bridge girders are in contact with ground and need cleaning

Fig 10. Main findings during the inspection.

The bridge should have been re-painted years ago. There is no cladding, sheet metal or other wood protection on the arches or other parts of the super structure. With some preventative maintenance, the bridge should have been in much better condition.

Generally the bridge is in good conditions. The owner of the bridge made maintenance on 2016 consisting re-painting of the bridge and cleaning the abutment areas.

2.4 Tõrva footbridge

Year of construction	1988
Practicable width	2m
Length	38m
Type of structure	Arch bridge
Timber	not impregnated Spruce (Picea Abies)
Vertical eigenfrequency	4,4 Hz

Fig 11. Tõrva footbridge.

Tõrva footbridge is an arch bridge with span of 38 meters. Age of the bridge is about 30 years. Bridge elements are not impregnated nor covered by claddings. The bridge has currently the longest span among timber bridges in Estonia. Main characteristics of the bridge are shown in Fig 11.

The inspection showed that bridges' superstructure was in very poor condition and the bridge should be closed to traffic. The arches have recently been re-painted and some minor repairs have been done. The arches condition was beyond corrective action due to decay in connecting points and along both bottom, top and outer side of the arches.

Deformation and decay in the top of the arch, the hinge is lost.

Decay at the support of the arch.

Fig 12. Main damages of the bridge.

The deck and railing have been replaced and were in good condition. Railings and deck are made of spruce (Picea Abies) instead of chemically treated Pine (Pinus Silvestris).

The abutments had some minor damages, cracks and some efflorescence. It is obvious that there have been no or very little maintenance on the abutments.

The arches are made of pine, not treated, and were in very bad condition. The top of the bridge was approximately 100mm lower at the east side than the west side. See Fig 13 on the right. This tilt was caused by deformation in connecting points. The deformation was a result of decay in the joints of glulam arches.

Moisture content, measured on the bridge was between 15 and 30%. The difference between the moisture content above and below the crack in the paint is shown in Fig 13 on the left. The paint did not allow wood to dry out. Water that entered the crack was collected below the crack and coud lead

to unvisible fungal damage inside the wooden element. The risk is that finally the damaged part of the beam does not have any strength left. The region where the crack can be formed cannot be predicted. The proper paint system that allows wood drying is therefore very important.

Moisture contents measured above and below the crack.

Bridge deck tilted 52mm /m, due to local failure in the arches connection points.

Fig 13. Some examples of the investigation results.

The above mentioned problems could have been avoided with chemically treated arches and/or protective cladding.

The deck and running boards are new and looked good. But there were some things that should have been made different. The crossed layers should have been made of treated pine instead of the used spruce. The floor beams should have been made of treated pine. All fasteners should have been either hot dip galvanized or made of stainless steel. The strips of wood on the running boards were made for indoor use and were not suited for outdoor use on a bridge deck.

The owner of the bridge made a renovation of the bridge at 2016 consisting making new larger steel plates to extend arch top and foot connections to the undamaged wood.

2.5 Ala-Rõuge road bridge

Year of construction	2013
Practicable width	9,4m
Length	7m
Type of structure	Beam bridge
Timber	impregnated Pine (Pinus Silvestris)

Fig 14. Ala-Rõuge road bridge.

Ala-Rõuge road bridge is a timber-concrete beam bridge with length of 7 meters. Bridge is made for road traffic in the South Estonia. Main structural elements are made of pressure impregnated pine and concrete deck. Deck is covered by asphalt pavement. Main characteristics of the bridge are shown in Fig 14.

Inspection showed that the superstructure and abutments of the bridge were in excellent condition. The bolts connecting two glulam beams together in the girders were lose (more than 50%) and need to be tightened. The load distributing washers were too small and had to be replaced. Moisture content in the wood material was 15-18%. This was a result of very good protection by design of details. Timber beams were effectively protected from the direct weathering.

Some minor deficiencies were found from the railing. No protective coating at the cut end of bolts was used. Fasteners for top rail were of indoor quality. Some bolts were loose and too small washers were used.

The bridge did need just some minor repair by changing washers and tightening bolts.

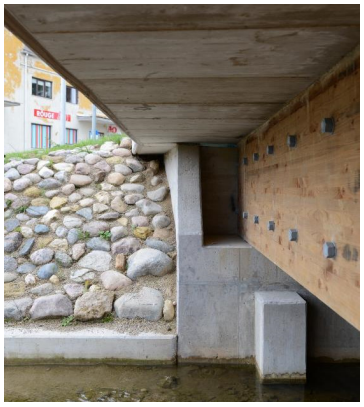

Loose bolts in girders and too small load distributing washers

Too small washers and no steel protective coating at cut off ends.

Fig 15. Some examples of the investigation results.

2.6 Järuska road bridge

Year of construction	2013
Total length	26,4m
Practicable width	3,5m
Type of structure	Truss bridge
Timber	not impregnated Spruce (Picea Abies)
Vertical eigenfrequency	9,5Hz

Fig 11. Järuska covered bridge.

Järuska bridge is the only bridge in Estonia covered by roof. The bridge was made by the community of local enthusiasts to join both sides of the river. Bridge is used by cars and pedestrians.

Inspection showed no damages or weaknesses that could decrease expected durability. From the structural point of view the strength and stiffness was designed with big reserve. Bridge is added here as a very good and unique example of timber bridges in Estonia. To hold these good conditions of the bridge regular inspections and maintenance is needed.

3. Summary

Proper design, careful building according to design, proper inspection and maintenance are the most important aspects to follow when planning and creating timber bridges.The inspection of 17 Estonian timber bridges showed some typical problems that should be dealt with. Overview of the investigations is listed in Table 1 and 2.

Wooden species have different durability. The use of spruce instead of a more durable material in weather exposed bridge elements shortens the service life down to as little as 5 years. Pressure impregnated pine can provide much better durability.

High moisture content is normally caused by wrong design of protection and details. Moisture content that is more than 25% can lead to fungal damage. Almost none of the bridges have steel or wooden cladding on the weather exposed surfaces. This can lead to development of fungal decay.

The inspection of timber bridges by bridge owners was discovered as very poor. Road Office for example does not have proper rules for inspecting timber bridges.

Poor maintenance was discovered on many bridges. Supports were not cleaned from plants, drain systems were blocked. There are simple works that should be done to avoid major problems.

Table 1. Main damages and problems inspected on Estonia's timber bridges.

Bridge	Main problems investigated						Wood specie	Pressure impregnation	Cladding on the load-bearing elements
	Fungal damage	High moisture content >25%	Bad situation of paint	Bad situation of railing	Corrosion of steel	Cleaning of support areas			
Vaida	x	x	x				spruce	No	Upper surface
Reopalu		x			x		pine	Yes	No
Tehvandi	x	x	x	x	x		pine	Yes	No
Ala-Rõuge							pine	Yes	deck
Keisripalu				x		x	pine	Yes	No
Tõrva	x	x			x		spruce	No	No
Angels bridge	x	x	x	x			spruce	No	Yes
Järuska							spruce	No	roof
Varbola		x				x	spruce	Yes	No
Merirahu	x	x	x	x		x	spruce	No	No
Lükati	x	x	x				spruce	No	No
Pärnu						x	spruce	No	No
Tagavere		x				x	pine	Yes	No
Nuutri			x	x		x	spruce	No	No
Pihla			x	x			spruce	No	No
Kõrgessaare			x			x	spruce	No	No
Keila	x	x		x		x	pine	No	No
Total	**7**	**10**	**9**	**7**	**3**	**8**			

Finally, three bridges among the 17 investigated bridges had serious damages – Vaida, Tõrva and Merirahu. The majority of the bridges were in fair or good conditions. Because of the fast damages of Vaida bridge, Estonian Road Office has made a decision to avoid timber bridges in the future.

The main aim of this work is to give knowledge for avoiding the mistakes in the future.

4. References

[1] Just, A., Fjellström, P.A. et al. Wooden bridges in Nordic countries: Resistance research analysis with proposals to use in Estonia. SP report 4P05308. July 2015. Skelleftea.

[2] Gustafsson, A et al. Cluster Wooden Bridges. SP report. May 2014. Skellefteå.

[3] Bridge Inspection Manual Part 2 - Deterioration Mechanisms, Department of transport and main roads, Queensland Government, http://www.tmr.qld.gov.au/business-industry/Technical-standards-publications/Bridge-inspection-manual.aspx

[4] Perv, L., Sinisalu, M. A research of timber constructions based on the Vaida pedestrian bridge. Master thesis at Tallinn University of Technology. Tallinn 2015.

Comparative life cycle assessment of concrete and timber road bridge deck designs

Reyn O'Born
PhD Candidate
University of Agder
Grimstad, Norway
reyn.oborn@uia.no

Mr. O'Born holds an M.Sc. in Industrial Ecology. Currently doing a PhD in cooperation with the Norwegian Public Roads Administration related to life cycle assessment of road infrastructure. Main research interests are sustainable transport systems and infrastructure.

Katalin Vertes
Associate Professor
University of Agder
Grimstad, Norway
katalin.vertes@uia.no

Ms. Katalin Vertes is currently Associate Professor at the University of Agder. She has PhD in Civil Engineering. Main research interests are the behaviour of large scale timber constructions, Ultra High Performance Concrete and steel structures

Summary

As the design of environmentally efficient structures becomes more relevant, conventional structural solutions may be updated to achieve low environmental footprints. Bridge decks represent the largest environmental impacts on short and medium span road bridges due to emissions related to the production of materials, mainly steel and concrete. Emissions can be reduced by constructing decks with less emissions intensive materials, such as timber. This study uses life cycle assessment to determine the environmental impacts of two timber bridge deck solutions with a comparison to conventional concrete deck alternatives. The overall purpose of this study is to determine if timber decks can be implemented on future bridge designs to promote more sustainable road infrastructure. The chosen designs show that it is possible to provide a timber deck with reasonable dimensions while having the same load carrying properties as a conventional bridge deck. The results of this study show that there are environmental benefits of choosing a timber decks over concretes decks. The choice of timber decks are shown to significantly reduce emissions in both new bridge constructions and rehabilitation of existing decks

Keywords: timber deck, life cycle assessment, sustainable infrastructure, deck rehabilitation.

1. Introduction

The use of timber in Norwegian road infrastructure has steadily increased in the last years. An upwards of 200 timber bridges have been built in Norway with more planned in the future [1], [2]. Ambitious projects like the timber Mjøsa Bridge are raising the profile of what timber bridge designs are capable of and challenging conventional bridge building techniques [3], [4]. There are, however, some challenges to wider adoption in industry, especially when using timber in bridge decks and bridge rehabilitation.

Timber has notable sustainability benefits in that it is less emissions intensive than steel and concrete but it is only now being recognized in the construction industry as a material that is equally versatile [5], [6]. Previous life cycle assessment (LCA) studies on timber bridge designs have shown that there is an appreciable benefit to using timber over traditional materials [7] in new road

bridge constructions. Timber bridge decks, however, have received relatively little attention in bridge design despite the fact that standard bridge decks on short and medium road bridges contribute to large amounts of climate emissions from concrete and steel production [8].

An LCA study is one way of better understanding the environmental benefits of infrastructure by comparing lifetime emissions between alternatives. A comparison between traditional concrete bridge decks to timber bridge decks using the framework of LCA allows decision makers to determine which option should be chosen. In this paper, two Norwegian case studies are presented with equivalent concrete and timber deck alternatives. The first case study is a planned network arch bridge that is to be built while the second case is an existing bridge that requires rehabilitation in the form of a new bridge deck. Through this LCA study, it is shown that timber bridge decks can be used for sustainable design of bridge infrastructure.

2. Case studies

2.1 Case study 1: Oppstadåa Bridge (network arch bridge design)

The bridge used in the first case study is based on a previous network arch bridge design done for the Oppstadåa Bridge located in Norway. A typical network arch bridge design is a light-weight steel bridge arch that increases bearing capacity by arranging steel cables in an interwoven network where each cable crosses another at least two times.

Our previous work analyzed the comparative environmental impacts of two optimized network arch bridge designs for the Oppstadåa Bridge; with one design that had a steel arch, and one design that had a timber arch [9]. Our analysis found that the while that building a network arch bridge in timber led to significant CO_2-emission reductions for the arch, but that the main impact in both bridge designs was the concrete bridge deck. It was decided that an additional analysis that looks at a timber deck design could further reduce impacts.

Figure 1. Optimized Oppstadåa network arch bridge designed with timber arch

The Oppstadåa Bridge has a design requirement for 16 500 AADT with a speed requirement of 90 kilometers an hour. The main arch is a timber truss and designed according to Eurocode series and is to be built with a 60 year lifetime. The deck has a driving width of 17 meters and a total width of 21 meters, with a 120 meter span.

2.2 Case study 2: Vippa Bridge (existing bridge with replacement deck)

The bridge in the second case study is the existing Vippa Bridge in Norway. Vippa bridge is a concrete arch bridge, with a concrete deck supported by transversal steel beams connected to the arch by steel hangers. The Vippa Bridge was originally built in 1943 following bridge standards from 1930. The deck has a driving width of 6 meters with a total width of 7.5 meters with a free span of 50 meters. The bridge has a maximum axel

Figure 2. Existing Vippa Bridge [10]

load of 10 tons with a combined total load of 50 tons (bridge class BK10-50). The last time the bridge was rehabilitated was in the 1980s when pedestrian paths were made on each side. The existing bridge deck requires rehabilitation in order to meet greater traffic demands and larger loads for today's road, and to repair damages from use. The main damages on the current bridge deck come from corroded concrete and of reinforcing steel causing the spalling of concrete cover and cracking of the concrete along the bearing structure [11].

The bridge deck will need to be rehabilitated soon and developing a timber deck alternative is one of the objectives of this study. Rehabilitating an existing bridge with a timber deck is rare but not without precedent in Norway. In 2010, the Hundorp Bridge (originally built in 1924) became to the first bridge to receive a rehabilitated timber deck [12]. The 200-meter deck was made with cross-laminated timber and resulted in an increase of load capacity. The Vippa Bridge is much smaller, with a total free span of 50 meters, but has the same load capacity as the Hundorp Bridge.

3. Methods

3.1 Life cycle assessment

This study uses life cycle assessment (LCA) to calculate environmental impacts and loads. Following the ISO14040:2006 Standard for life cycle assessment, LCA is made up of four parts: *goal and scope definition*, *inventory analysis*, *impact assessment* and *interpretation* [13].

The goal of this project was to determine the impacts of utilizing timber in two separate deck designs. The functional unit (a basis of comparison between alternatives) for this study is one bridge deck crossing the Oppstadåa and Vippa bridges. The impacts were determined from material requirements for each bridge design.

The inventory data for the bridge decks are collected from the Vippa design while information on the timber network arch bridge design come from O'Born et al. (2017) based on the Oppstadåa Bridge [9]. Data was collected for the deck support structures, the arch support structures and steel hangers. Additional foundational structures on land and driving surface were the same independent of bridge designs and were thus excluded from the scope of the study. The impact assessment methodology used was the ReCiPe (H) methodology built into the LCA software package SimaPro version 8.2.3.0 [14]. Emissions information came from the EcoInvent 3 database [15].

3.2 Bridge design calculations

Both bridges are designed with an alternative stress laminated timber deck (SLT) solution that has been calculated without detailing (e.g. connections, etc.). The basic consideration of this deck type from construction point of view is the low weight, that can have a relevant effect on the dimensions of the main load bearing structure (in these cases the main arch).

Figure 3. Stress laminated timber deck [21]

The basic layout of a stress laminated timber deck is shown in Figure 3 [21]. SLT decks are made from mostly glulam beams positioned side by side and stressed together using high-strength steel bars. That results in a certain level of force distribution due to the resisting friction caused by the pre-stressing of all beams in the deck.

3.2.1 The Oppstadåa Bridge

As this bridge is a large highway bridge, considering the application of timber as a deck material is important to decrease the loads on the main arch. According to the design results of the previous study [9], the timber arch dimensions are large compared to the steel solution while a relevant load design component was the self-weight of the deck. This indicates that an efficient way to ease the actions on the arch (and obtain a reasonable timber cross-section) could be the application of a lighter SLT deck.

The network arch bridge is by default a favorable solution from the deck design point of view due to the close to uniform supporting effect of the steel hangers. Since this paper offers a solution only for the deck itself, the deck has been modelled independently by applying spring supports and by having the spring properties based on the calculations of [9]. The deck is modelled as a plate with stiffness and strength properties defined according to a possible modelling solution described in [21]. Load conditions were considered according to the relevant Eurocodes [16] [17] [18]. The verification is carried out according to Eurocode 5 [19].

The result of these calculations for the alternative timber bridge deck design has a thickness of 130 cm with GL 32 glue laminated timber beams and pretensioning steel bars in two rows of tension rods of 50 mm diameter and 1030 MPs yield strength. Due to the relatively low stiffness properties of the timber the governing in the design is the serviceability limit state due to displacements.

3.2.2 The Vippa Bridge

The Vippa Bridge is a conventional concrete arch bridge that carries the concrete deck that is supported by transversal steel beams (in a distance of 5m) that are connected to the hangers. Since this bridge is an old structure that has gone over the designed life time, easing the load of the concrete arch by utilizing a light-weight deck can have a beneficial effect on the load bearing capacity in the long run. Due to the degraded condition of the concrete deck, the alternative solution of an SLT deck has been calculated. For the same reasons as the case of the Oppstadåa Bridge, the bridge deck has been considered independently.

In this case, the model of the deck is a continuous girder having supports at the location of the transversal main beams. The deck stiffness has been modelled according to [21]. The verification is carried out according to Eurocode 5 [19]. The relative small distance of the transversal beams allows a thin timber deck of 35 cm thickness (GL 32) together with pretensioning steel bars in one row of tension rods. These tension rods have a diameter of 50 mm and 1030 MPs yield strength. Together with the timber deck alternative a new concrete deck has been also calculated with a resulting a plate thickness of 24 cm (C30/37 concrete quality).The governing in the case of the SLT deck was serviceability limit state again due to displacements.

4. Results

4.1 Life cycle inventory

. The concrete deck based on the original design has a concrete depth of 60 cm and a total volume of 1529 m^3 concrete with an additional 315 tons reinforcing steel. The alternative timber bridge deck design has a thickness of 130 cm with 3276 m^3 glue laminated timber and 64.7 tons of pre-tensioning steel bars. Note that the arch, arch support and steel hangers for each bridge design are identical and unchanged from the previous analysis. The material requirements for the network arch bridge design calculations are summarized for each network arch bridge are summarized below in Table 1.

Table 1: Material requirements for the network arch bridge designs

Element	Concrete deck	Timber deck	Unit
Timber, arch	1425	1425	m^3
Steel, arch support	86.2	86.2	tons
Steel, hangers	44.4	44.4	tons
Timber, deck (GL32)	-	3276	m^3
Concrete, deck (C30)	1529	-	m^3
Reinforcing steel, deck	314.8	75.0	tons

The timber deck uses glue laminated timber strength class GL32 according to Eurocode 5 standards while the pretensioning steel bars used in the timber deck are Macalloy 1030 (50 mm) with a characteristic yield strength of 1030 N/mm^2. The concrete deck uses concrete class C30 while the reinforcing steel used in the concrete is S500B with characteristic yield limit of 500 N/mm^2.

The concrete deck designed for the Vippa Bridge has a total depth of 24 cm which will require 72 m^3 concrete (C30/37) and 5.7 tons of reinforcing steel (S500B). The timber design will have a thickness of 35 cm while requiring 105 m^3 glue laminated timber (GL32) and 4.0 tons of support steel (Macalloy 1030). The material requirements for the Vippa bridge design calculations are summarized for each network arch bridge are summarized below in Table 2.

Table 2: Material requirements for the Vippa bridge deck designs

Element	Concrete deck	Timber deck	Unit
Timber, deck (GL32)	-	105	m^3
Concrete, deck (C30)	72	-	m^3
Reinforcing steel, deck	5.7	4.0	tons

The environmental comparison between each bridge is based on the materials requirements shown in Table 1 and 2.

4.2 Life cycle impact assessment

The results presented for each bridge consider the following seven environmental impact categories:

- *Climate change* measures potential warming of the climate, and is expressed in potential CO_2-equivalents.
- *Ozone depletion* (ODP) measures potential thinning of the ozone layer and is expressed in CFC-11-equivalents.
- *Terrestrial acidification* (TAP) measures potential soil acidification and is expressed in SO_2-equivalents
- *Freshwater eutrophication and marine eutrophication* measures potential excessive nutrient availability in water and is expressed in P-equivalents (freshwater) and N-equivalents (marine)
- *Photochemical oxidation formation* (POF) measures potential tropopherisic ozone damage and is expressed in kg NMVOC equivalents.
- *Particulate matter formation* measures potential particulate matter (particle size 10 µm or less) released to air and is expressed in PM10 equivalents.

4.2.1 Network arch bridge results

The timber deck had lower impacts in all seven impact categories for the network arch bridge design as shown in Figure 4 below.

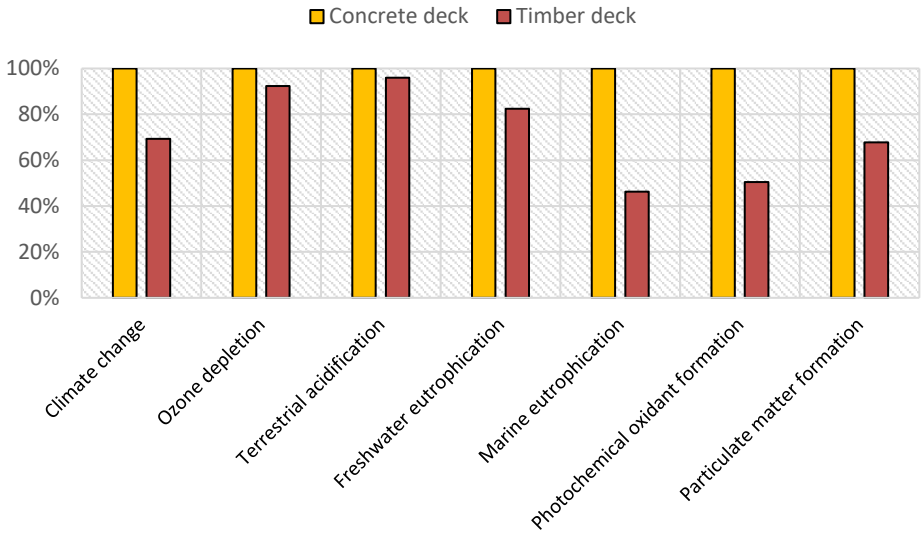

Figure 4. Oppstadåa Bridge comparative life cycle impact results

Perhaps the most useful measure for transport planners is the climate change emissions. The Oppstadåa Bridge timber deck had 31% less total emissions than the concrete deck variant. This is a significant reduction of emissions and is due to the replacement of emissions intensive steel and concrete. Overall, the timber deck bridge had a total of 1410 tons CO_2-equivalents while the concrete deck bridge had a total of 2032 tons CO_2-equivalents. The timber deck bridge also has significant reductions in freshwater and marine eutrophication, photochemical oxidant formation and particulate matter formation.

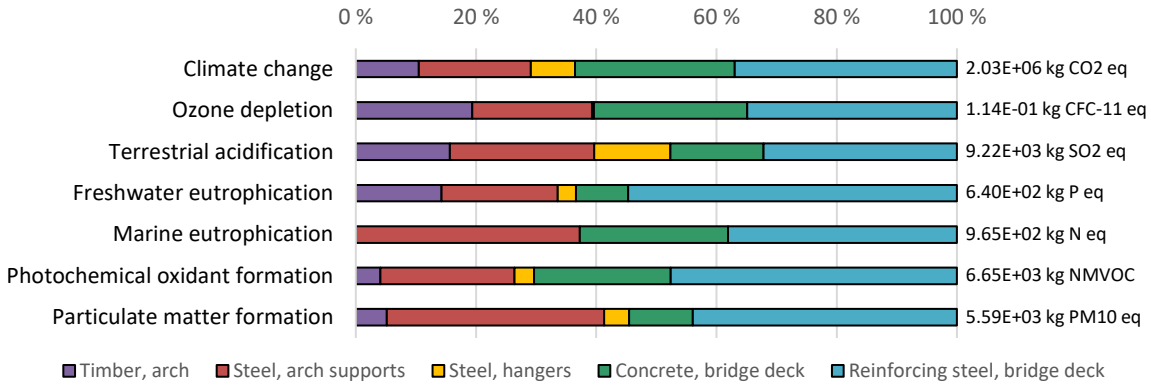

Figure 5. Life cycle impact results for the Oppstadåa concrete deck, by material

Figure 5 shows the overall impacts share for materials in the concrete deck design. The light blue (reinforcing steel) and green (concrete) represent the share of emissions for the concrete deck across the seven impact categories. Reinforcing steel used in the deck is the largest source of emissions in all categories while concrete and steel used in the deck represent the largest share of emissions for the Oppstadåa Bridge. The overall emissions in each impact category is given on the right side of the figure.

Figure 6 shows the same impact share for materials in the timber deck design. The light blue (reinforcing steel) and the green (timber) represent the share of emissions due to the timber deck.

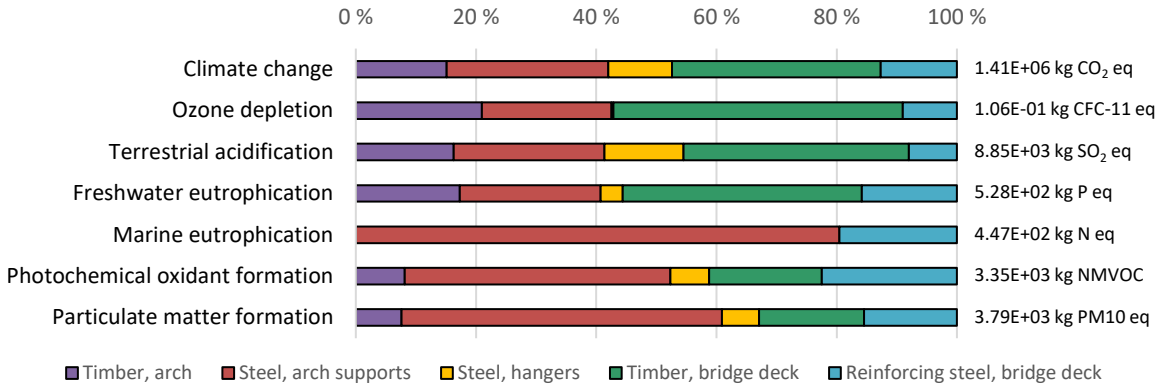

Figure 6. Life cycle impact results for the Oppstadåa timber deck, by material

The overall share of emissions due to the deck are much lower in the timber deck than the concrete deck. This is due to the reduction in steel and the replacement of emissions intensive concrete with less emissions intensive timber. The overall emissions in each impact category is also given on the right side of the figure.

4.2.2 Rehabilitation Vippa Bridge

The assessment of the rehabilitated Vippa Bridge deck showed that the overall environmental benefits of implementing a timber deck were not as uniform as the Oppstadåa Bridge. The results of the impact assessment are shown Figure 7.

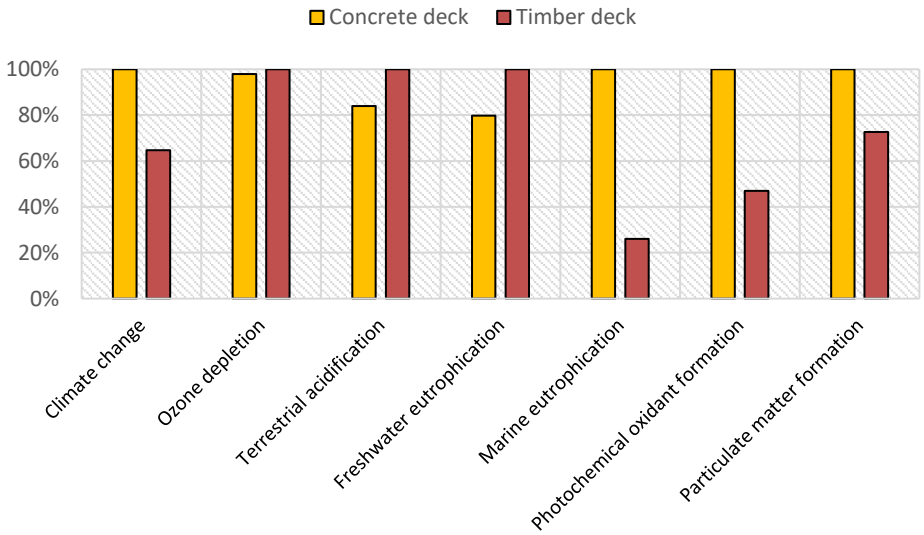

Figure 7. Vippa Bridge comparative life cycle impact results

The timber deck had 65% less impacts overall than the concrete deck in climate change category, and lower impacts in marine eutrophication, photochemical oxidant formation and particulate matter formation categories. The concrete deck performed better in the terrestrial acidification and freshwater eutrophication categories. It should be noted that the overall emissions in each impact category were quite low with the exception of the climate change impacts. The most relevant environmental benefit of constructing a timber bridge deck for the Vippa Bridge comes from the saving of more than 13 tons carbon dioxide compared to the concrete deck.

More information on the overall emissions in each impact category for each deck for the Vippa Bridge are shown in Table 3 below.

Table 3. Characterized life cycle impacts for the concrete and timber deck designs of Vippa Bridge

Impact category	Concrete deck	Timber deck	Unit
Climate change	3,89E+04	2,52E+04	kg CO2 eq
Ozone depletion	2,09E-03	2,13E-03	kg CFC-11 eq
Terrestrial acidification	1,21E+02	1,44E+02	kg SO2 eq
Freshwater eutrophication	8,90E+00	1,12E+01	kg P eq
Marine eutrophication	1,78E+01	4,64E+00	kg N eq
Photochemical oxidant formation	1,28E+02	6,02E+01	kg NMVOC
Particulate matter formation	7,21E+01	5,23E+01	kg PM10 eq

5. Discussion

The overall results of this analysis show that in most impact categories, timber bridge decks provide the most environmental solution for bridge designers. What is perhaps most important to road builders and planners is the CO_2-equivalent emissions reductions. CO_2-equivalent emissions reductions were found to be 31% and 35% for the Oppstadåa and Vippa timber deck designs respectively. Combined with additional savings from the original study by the authors, the Oppstadåa Bridge design with a timber arch and timber deck represents a CO_2-equivalent emissions reduction of more than 61% compared with a similar generic steel bridge design[1]. This suggests that using timber components in bridge design should receive much more attention for road planners in order to reduce climate change impacts in road infrastructure.

The structural calculations showed that the SLT deck is a possible alternative solution from structural point of view even for large span bridges. This can result in a relevant reduction in the dimensions of the main load-bearing structure. However the light weight of the deck can be unfavorable from the hangers' point of view. This requires further investigations [20] as the global behavior of the bridge should include modelling of dynamic effects, such as wind or earthquake. The long term dynamic response of the deck needs also needs to be investigated to get a complete structural behavior of the bridge.

When applying a timber deck solution, the displacements govern the design, which can result in decks with extremely large dimensions (even if the weight is small) specially for large spans. This is the case of the Oppstadåa Bridge and it may not necessarily be a feasible solution. However, for small spans, such as Vippa Bridge, the timber deck provides a reasonable solution with low weight and acceptable dimensions.

6. Conclusion

The overall conclusion of this work is that there are sustainability benefits to building utilizing timber decks over concrete decks. SLT decks seem to be a good alternative if easing of the main load-bearing structure is required or to update old bridges such as the case of the Vippa Bridge. The calculations provided promising results from both a structural and environmental point of view further research is required for the accurate design of timber decks to model accurate behaviour for, among other details, the long term behaviour of the deck itself as well as the whole bridge structures.

[1] A generic steel bridge design of Oppstadåa Bridge was found to emit 3613 tons CO_2-equivalents

7. Acknowledgements

The authors would like to acknowledge the analysis work done by Dennis Memić and Rasmus Solli as part of their master's theses at UiA. Their collection of information and analysis on the current condition of Vippa Bridge provided the basis for the Vippa Bridge deck design.

8. References

[1] M. A. Bjertnæs, G. Veastad, and T. E. Nyløkken, "Timber Bridges," Lillehammer, 2015.
[2] Norwegian Wood Technology Institute, "FOKUS på tre - Broer i tre," 2007.
[3] S. E. Jakobsen, T. A. Stensby, W. Mikkelsen, and P. Meaas, "A timber bridge across Lake Mjøsa in Norway," in *International Conference on Timber Bridges*, 2013, pp. 1–6.
[4] K. Ekholm, *Performance of Stress-Laminated-Timber Bridge Decks*. 2013.
[5] J. N. Rodrigues, A. M. P. G. Dias, and P. Providência, "Timber-concrete composite bridges: State-of-the-art review," *BioResources*, vol. 8, no. 4, pp. 6630–6649, 2013.
[6] J. Hammervold, "Johanne Hammervold Towards greener road infrastructure," no. August, 2014.
[7] J. Hammervold, "Environmental analysis of bridges in a life cycle perspective," in *International Conference on Timber Bridges*, 2010.
[8] J. N. Rodrigues, P. Providência, and A. M. P. G. Dias, "Sustainability and Lifecycle Assessment of Timber-Concrete Composite Bridges," *J. Infrastruct. Syst.*, vol. 4016025, 2016.
[9] R. O'Born, K. Vertes, G. Pytten, L. O. Hortemo, and A. Brændhagen, "Life cycle assessment of an optimized network arch highway bridge utilizing timber," in *Bearing capacity of roads, railways and airfields: proceedings of the Tenth International Conference on the Bearing Capacity of Roads, Railways and Airfields: Athens, Greece*, 2017.
[10] I. H. Guttormsen, "Picture of Vippa Bridge on an beautiful fall day," *Agderposten*, Aust-Agder, 2016.
[11] D. Memić and R. Solli, "Dimensjonering og vurdering av bæreevnen for Vippa bru etter Eurokode," Grimstad, 2016.
[12] A. Rune B and T. E. Nyløkken, "Hundorp Bridge - Bridge deck rehabilitation using cross-laminated timber." Sweco, 2010.
[13] ISO, "ISO14040: Environmental management-life cycle assessment principles and frameworks." British Standards Institution, London, 2006.
[14] M. Goedkoop, R. Heijungs, M. Huijbregts, A. De Schryver, J. Struijs, and R. Van Zelm, "ReCiPe 2008 - Report 1: Characterisation," The Hague, 2009.
[15] G. Wernet, C. Bauer, B. Steubing, J. Reinhard, E. Moreno-Ruiz, and B. Weidema, "The ecoinvent database version 3 (part 1): overview and methodology," *Int. J. Life Cycle Assess.*, vol. 21, no. 9, pp. 1218–1230, 2016.
[16] Standard Norge, "Eurocode 0, NS-EN 1990:2002+A1:2005+NA:2016, Basis of structural design." 2016.
[17] Standard Norge, "Eurocode 1, Part 1, NS-EN 1991-1:2003/AC:2010, Actions on structures - Part 1." 2010.
[18] Standard Norge, "Eurocode 1, Part 2, NS-EN 1991-2:2003/AC:2010, Traffic loads on bridges - Part 2." 2010.
[19] Standard Norge, "Eurocode 5, Part 2, NS-EN 1995-2:2:2004+NA:2019, Design of timber structures - Part 2: Bridges." .
[20] K. Bell, "Structural systems for glulam arch bridges," in *International Conference Timber Bridges*, 2010, pp. 49–60.
[21] M. Ekevad and P. Jacobsson, "Prestressed Timber Bridges: Simulations and experiments of slip," in *International Conference on Timber Bridges*, 2010, pp. 351–358.

Life Cycle Assessment on two design alternatives of the Driva Bridge

Yishu NIU
Doctoral candidate
Aalto University
Espoo, Finland
yishu.niu@aalto.fi

Yishu Niu received her M.Sc. degree from the Aalto University in 2014, Finland. She is working on her PhD in Civil Engineering. Her research is related to life cycle analysis of timber bridges.

Lauri SALOKANGAS
University teacher
Aalto University
Espoo, Finland
lauri.salokangas@aalto.fi

Lauri Salokangas, Dipl.Eng. 1981. 1986-2007 Lab. Man. in Bridge Engineering at Helsinki University of Technology. 2008-2013 Prof. of Bridge Engineering, Infra-structures and Structural Design. From 2014 lecturer at Aalto University.

Gerhard FINK
Assistant professor
Aalto University
Espoo, Finland
gerhard.fink@aalto.fi

Gerhard Fink is Assistant Professor for Wooden Structures at Aalto University. He studied Civil Engineering at the TU Graz, Austria and did his PhD at ETH Zurich.

Summary

Environmental performance of timber bridges during their lifespan has become important in recent years. In this study, two timber design alternatives of the Driva Bridge located in Norway were investigated and compared. The study applied Life Cycle Assessment (LCA) for addressing (1) the distribution of total environmental impact and energy consumption, and (2) the environmental impact and energy consumption variations due to different End-of-Life (EoL) scenarios for timber material. The results relied on five selected midpoint environmental impact indicators. It indicates that different EoL scenarios of timber can largely affect the total environmental impact, and the quantity of steel used significantly influence the total environmental impact as well as total energy consumption.

Keywords: timber bridges, environmental impact, LCA, End-of-Life scenarios.

1. Introduction

With the arising demand on sustainability and environmental-friendliness, Life Cycle Assessment (LCA) has become widely used for assessing and investigating the

environmental effects of products. A full LCA examines the effects of a product within defined goal and scope, from the raw material extraction to the final demolition, often referred as “from cradle to grave”. In this context, a product can be for example a timber bridge.

The outcomes of the LCA are expressed as indicators such as global warming, eutrophication, and ozone depletion, mostly in global scale. The main difficulty of interpreting the LCA output is the variety of indicators. Each indicator has its own emphasis, and the user needs to choose the most important indicators and generate conclusions accordingly.

At present, the construction sector contributes largely in the global environmental burden, for example, it covers about 40% of the total energy consumption in Europe [1]. Therefore, construction sector is a big target for improvement. Bridge, as an important part of construction sector, consumes huge amount of construction materials and energy for construction and use. LCA can be used as an important tool in a Bridge Management System (BMS), although it is not yet a common practice, it gains more and more interest. In order to reduce the environmental impact, wood as a natural material is suggested to be used widely in bridges.

When conducting LCA for a bridge, four life cycle stages may be considered:

1) *Material production stage*: raw material extraction and product manufacturing of the bridge
2) *Construction stage*: transportation of materials and equipment to the construction site, installation of the bridge
3) *Operation and Maintenance (OR&M) stage*: use of the bridge during its service life
4) *End-of-Life (EoL) stage*: starts when the bridge is replaced, dismantled or deconstructed, including demolition, transport, and waste processing.

To estimate the operation and maintenance actions during the use of bridges, many methods and sources can be used. One method is to use historical data about maintenance and repair of bridges from existing databases. Another method is to collect data from LCA calculations made by experienced experts on bridge element degradation and repair. Once maintenance and repair actions and corresponding intervals are obtained or determined, they can be applied to the LCA analysis.

2. Case study

The case study compared two design alternatives for the Driva Bridge along the whole life cycle, by using LCA tool.

2.1 General information

Along with the increasing interest in green materials, the Norwegian Public Road Administration decided to build more timber structures in recent years. Meanwhile, the Norwegian University of Science and Technology (NTNU) has a research project about glulam network arch bridges. The network arch idea of bridges was developed by the Norwegian engineer Per Tveit in the 1950s. They have tied arches with inclined hangers, which have multiple intersections.

Driva Bridge is an existing network arch bridge made of steel and concrete, locates in Norway. It has a single span of 111 m, and the rise of the arch is 18 m. The research project from NTNU includes one Master’s Thesis, which dealt with two design alternatives for the Driva Bridge, by having timber network arch system [2]. It is a pilot endeavour, since so far, the longest span of timber bridges in Norway is less than 90 m [3].

The two design alternatives in [2] considered only the superstructure of the bridge, excluded foundation, end supports, possible settlements, as well as detailed joint on the arches and wind bracing. In addition, connections between the deck and transverse beam were not included. The deck and arches of both design alternatives are fabricated out of glulam, strength class GL 32h [4]. Designed life for the two alternative bridges is 100 years.

Chemical protection such as creosote or Cu-salts is not applied.

The deck is made of stress-laminated timber, with effective width of 11,95 m. The glulam beams are 115 mm wide, with 5,5 m distance. For weather protection, zinc cladding is applied on top of the arches, with louvered timber cladding on the sides. The wearing pavement choice is asphalt, which includes base and wearing layer.

For clarification, two alternatives are named as Network arch Bridge Alternative1 (NBA1) and Network arch Bridge Alternative2 (NBA2). Profile of both alternatives are shown in Fig. 1. NBA1 has no steel wind bracing between the arches, and four sets of hangers are spread out of the arch's plane. The arch has constant glulam cross-section, and is split into four parts with an equal length of 30 m. NBA2 has a similar layout to the existing Driva Bridge, with having K-shaped wind bracings. The arch is also split into four parts of equal length, with varied cross-section of each part.

The steel used in the bridge is assumed to be imported from the same provider as the Driva Bridge, the steel provider locates in Europe. The timber is assumed to be provided from a local supplier in Norway.

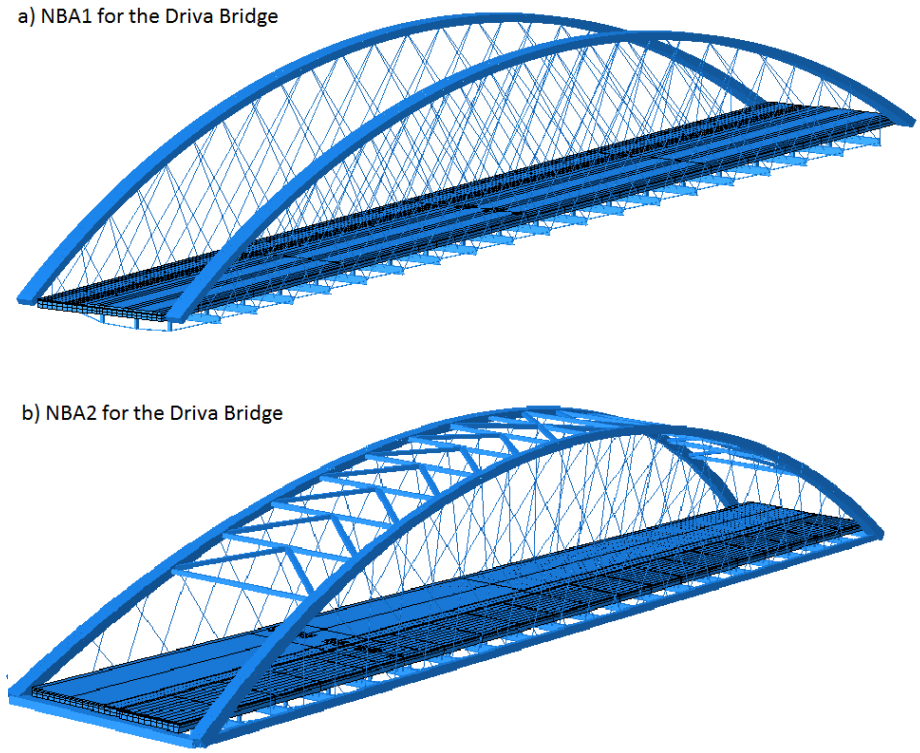

Fig. 1 Two design alternatives for the Driva Bridge [2]

2.2 Specifications of LCA

In this paper, only the superstructure of the bridge during its designed whole life cycle is considered. The goal is to identify how different EoL scenarios of timber contribute to the total environmental impact, and how the EoL of timber influences the energy consumption. The function unit is defined as "bridge effective area within the 100-year service life".

The study utilised *BridgeLCA* tool, in which embedded Ecoinvent database and ReCiPe v1.06 method [5] - [7]. The five selected impact categories were expressed as midpoint indicators: Global Warming Potential (GWP), Ozone Depletion Potential (ODP), Terrestrial Acidification Potential (AP), Freshwater Eutrophication Potential (FEP) and Fossil Depletion Potential (FDP) [8].

2.3 Assumption and simplification of LCA

The study assumed the same erection method, maintenance plan and demolition method for both design alternatives; thus for simplifying the comparison, the diesel and electricity

consumption of equipment during the use stage were not included. Minor materials and activities such as formwork, spikes, weathering of concrete were not considered.

For planning the repair and maintenance actions during the use of the bridge, historical records of existing timber bridges that were extracted from Finnish Bridge Register (Siltarekisteri) [9] and [10] were applied. Quantitative data of the major materials were calculated based on [2].

All materials considered to be replaced during the life cycle of the bridge were assumed to be 100% of the original amount. In the aspect of intervals for replacement actions: asphalt would be replaced every 15 years, and the epoxy would be replaced every 30 years. The guardrails and railings would be replaced every 40 years after the opening of the bridge, and the parapets would be replaced after 60 years of opening the bridge.

For the EoL stage, transportation mode and distance from the bridge site to the EoL site were assumed to be the same as from the material factory to the bridge site. In general, the material recycling in the EoL stage is expected to reduce the environmental impact, thus the assumption for the recycling rate is high. Steel was assumed to be 100% recycled [11]. For timber construction waste, the EoL has not been standardised yet. In order to analyse the influence of different EoL scenarios of timber, two scenarios were investigated in this study: EoL1 as of 100% energy recovered and EoL2 as of 100% put into demolition. Moreover, timber material was assumed as carbon neutral, without considering CO_2 uptakes.

3. Results

Comparison lies between the two design alternatives, for both EoL scenarios of timber. Total results of emissions in each of the five selected impact categories were weighted into one single score in accordance with ISO 14044 [12], in order to consider the impact of the individual indicators correspondingly. The weighting factors were applied according to U.S. Environmental Protection Agency, as shown in Table 1.

Table 1. Weighting factors applied in the study according to [13]

Impact category	GWP	ODP	AP	FEP	FDP
Weighting factors	16	5	5	5	5

In order to find the influence of weighting factors, the study compares the normalised LCIA (Life Cycle Impact Assessment) midpoint results and the weighted LCIA midpoint results. The results reveal that with normalised midpoint, the weighted single score of NBA1 under EoL1 scenario is about 75% of EoL2 scenario, for NBA2 under EoL1 scenario is about 83% of EoL2 scenario.

Fig. 2 shows the comparison for EoL1. It indicates that weighting factors can influence both the proportion and the importance level of each impact category. GWP is the most affected category, in which the proportion is increased into three times from the normalised values to the weighted values. While the proportion changes of ODP, AP, and FDP categories are rather small. For both alternatives, the most dominant category is FEP, which takes over half of the total environmental impact; and the least significant category is ODP, which takes less than 0,5% of the total environmental impact. Moreover, the proportion of each impact category for both NBA1 and NBA2 is nearly the same, except the slight differences of FDP and FEP categories. Similar results of Fig. 2 are found for the EoL2 scenario.

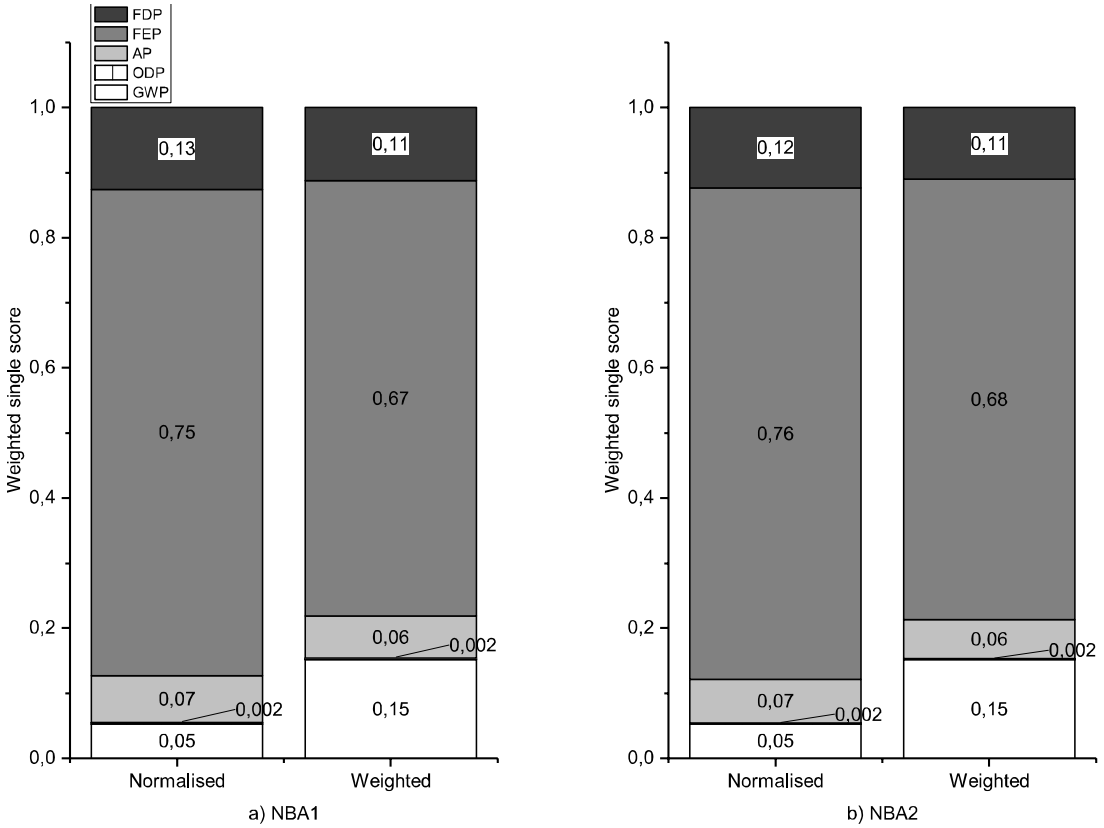

Fig. 2 Normalised and weighted midpoint LCIA results when timber is with EoL1

In the following comparison, for reducing the subjectivity, weighting factors were set equal for the selected five impact categories.

The four life cycle stages introduced in Section 1 were investigated, for addressing the contribution of each stage to the five impact categories. Distribution of all impact categories during each life cycle stage is shown in Fig. 3.

Fig. 3 clearly indicates that, the biggest contributor of all five impact categories is the material production stage, while the least is the construction stage; such result can also be found in [10]. The selection of EoL scenario of timber can largely affects the contribution of life cycle stages to the total environmental impact. The two biggest environmental impact categories induced in the EoL stage are ODP and AP under both EoL1 and EoL2. The contribution of EoL stage for each environmental impact category is much smaller under EoL1 scenario than under EoL2.

As expected, the comparison of different EoL scenarios shows that the bridge with EoL2 has better environmental performance. For example, the environmental impact induced in the EoL stage under EoL2 scenario is nearly one third of each impact category for NBA1, and one fourth of each impact category for NBA2. The midpoint LCIA results change significantly for GWP and FDP categories, where the difference ranges from 8 to 13 times. Under the same EoL scenario, the comparison between NBA1 and NBA2 reveal that, for each impact category, the proportion of EoL stage for NBA1 is bigger than NBA2.

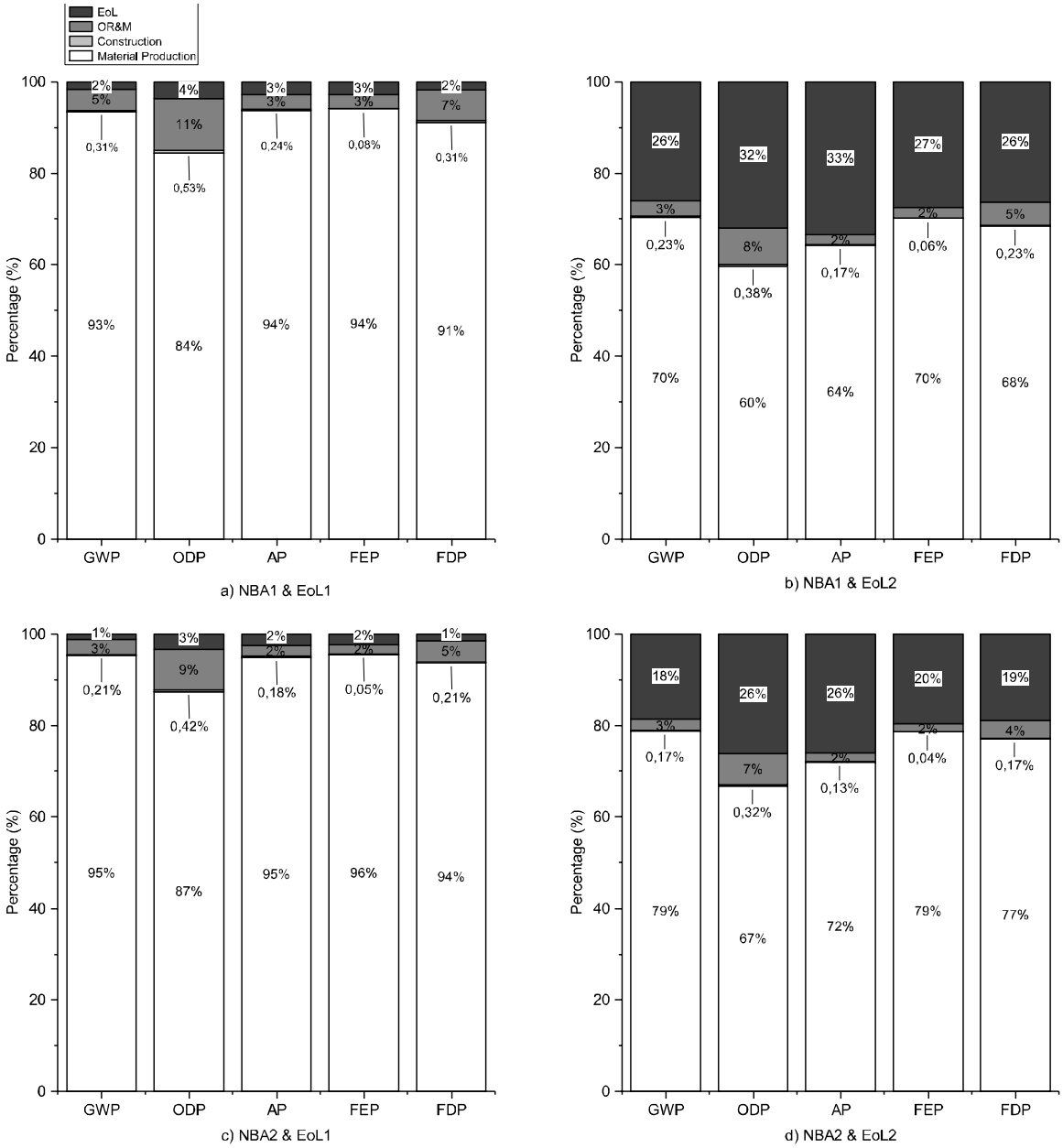

Fig. 3 Distribution of midpoint LCIA results for NBA1 and NBA2

For finding the total energy consumption and its distribution of the two design alternatives, the study compared the results under the two EoL scenarios. When comparing the total energy consumption for both NBA1 and NBA2, no matter the EoL scenario of timber, NBA2 consumed 16% - 18% more energy than NBA1, due to the larger amount of steel used in NBA2. When comparing the energy consumption of each design alternative between EoL1 and EoL2 scenarios, the difference is very small, less than 2%.

Fig. 4 shows the distribution of energy consumption for both NBA1 and NBA2 under the two EoL scenarios. The composition of material quantities and energy consumptions is split into three items: timber, steel, and others. The former two items include the energy consumption caused from material production and corresponding transportation (e.g. transportation due to the import of the material). The major construction materials (here means timber and steel) consumed the most energy, timber as the major material consumed over 50% of the total amount of energy, while steel as the second major material is the second largest of the total energy consumption. Moreover, it shows that increasing the quantity of steel will proportionally increase the addition of energy consumption.

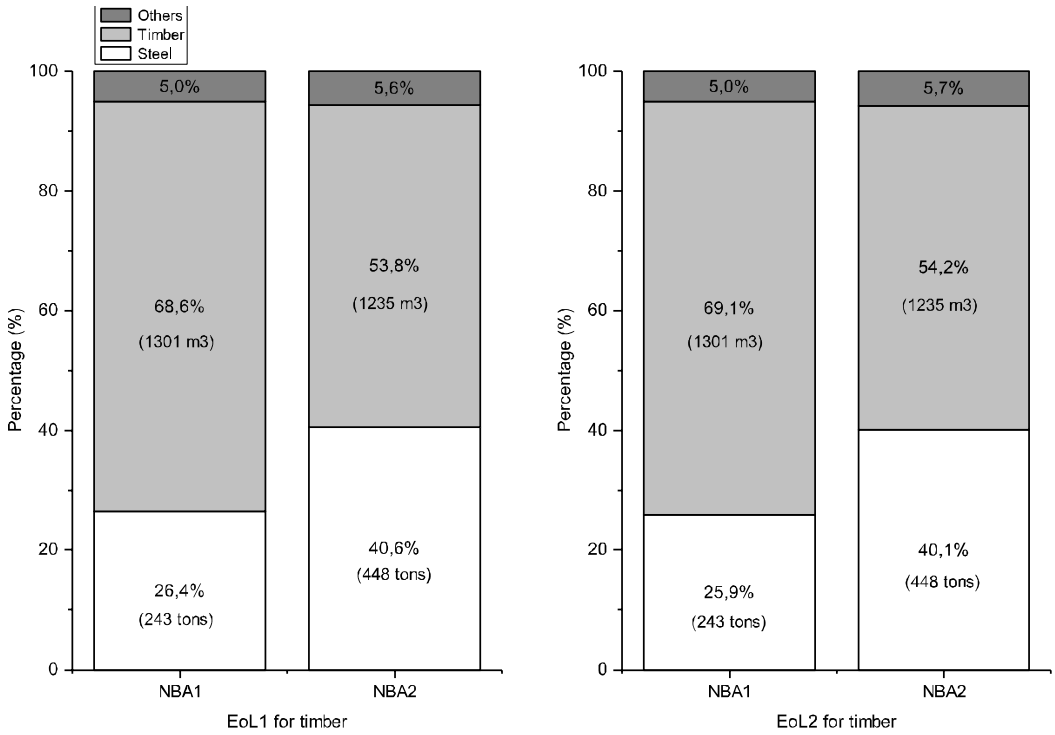

Fig. 4 Energy consumption of construction materials and others

Conclusions

In this study, Freshwater Eutrophication Potential (FEP) and Fossil Depletion Potential (FDP) are the most dominant impact categories, while Ozone Depletion Potential (ODP) is the most insignificant category. However, it may be changed when applying different weighting factors. Different End-of-Life (EoL) scenarios of timber materials largely influence the impact proportion of EoL stage among the life cycle, but insignificantly affect the energy consumption. The preferred EoL of timber is to be 100% energy recovery, which can obviously reduce the total environmental impact; in this study, reducing of the weighted single score of the total environmental impact can be 17% and 25%. The quantity of steel used in timber bridges can significantly change the total environmental impact and proportionally affect the energy consumption. The key factor influencing total environmental impact and energy consumption is the amount of major construction materials used, especially steel.

This study cannot draw general conclusions for all timber bridges. However, the study revealed some key aspects that should be considered carefully, such as EoL scenario of timber and the quantities of other major construction materials than timber.

References

[1] Europa.eu., 2017. EUROPA - European Commission. [online] Available at: https://ec.europa.eu/growth/sectors/construction_en [Accessed 5 Apr. 2017]

[2] Eilertsen M., Haddal D. Network Arch Bridge. Master's thesis. NTNU, Trondheim, Norway, 2016, 104pp.

[3] Veie J. and Abrahamsen R.B., Steien Network Arch Bridge, *2nd International Conference on Timber Bridges*. Las Vegas, Nevada USA, 2013.

[4] EN 14080 Timber structures. Glued laminated timber and glued solid timber. Requirement. European committee for standardization. Brussels, 2013, 103pp.

[5] Salokangas, L. (ed.), ETSI Project Stage III. Bridge Life Cycle Optimisation. Helsinki, 2013, 172pp.

[6] Ecoinvent, 2008. *Ecoinvent Database v 2.01*. Swiss Centre for Life Cycle Inventories.

[7] Goedkoop M., et al. ReCiPe 2008. A life cycle impact assessment method which comprises harmonised category indicators at the midpoint and the endpoint level, 2009, 1.

[8] EUR 24708 EN – Joint Research Centre - Institute for Environment and Sustainability: International Reference Life Cycle Data System (ILCD) Handbook – General guide for Life Cycle Assessment – Detailed guidance. First edition. Publication Office of the European Union. Luxembourg, 2010, 389pp.

[9] Finnish Bridge Register: Siltarekisteri EXT. Non-public confidential system. Helsinki, Finland, 2016.

[10] Niu Y., Salokangas L. "Life Cycle Assessment on timber road bridges: a case study", World Conference on Timber Engineering (WCTE2016), Vienna, Austria, 2016.

[11] International Iron and Steel Institute (IISI), 2005. Steel: the foundation of a sustainable future, sustainability report of the World Steel Industry 2005. Brussels, Belgium, 2005, 51pp.

[12] ISO 14044: 2006. Environmental management – Life Cycle Assessment – Requirements and guidelines. International Organization for Standardization.

[13] U.S. Environmental Protection Agency, 2010. "Environmentally preferable purchasing". [online] Available at: http://www.epa.gov/opptintr/epp/ [Accessed 13 Mar. 2015]

A parametrized process: Design and realization of timber truss bridges

John Haddal Mork

(Marcin Luczkowski, Bendik Manum, Anders Rønnquist)

PHD-candidate ,NTNU

Trondheim, Norway

John.h.mork@ntnu.no

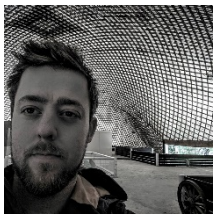

PHD-candidate developing a parametric timber toolkit that aims to simplify the process of designing advanced timber structures.

Summary

Parametric workflows radically change efficiency and methods of designing structures. This study presents the process of designing and building two timber truss pedestrian bridges in Orkdal, Norway. From sketch to fabrication, the design process have been fully parametric. The case project contributes to a long- term research project of developing a parametric timber toolkit. A timber toolkit that simplifies the process of designing and constructing advanced timber structures. The paper ends with discussing the preliminary findings from the parametric design process.

Keywords: Parametric modelling, pedestrian bridge, collaboration, Parametric timber toolkit

Mass customization has been a discussed topic since the early 90s[1].It is mass production, but of components that are individually customized. Potential outcomes are increased profits, bespoke architecture and not least more efficient material usage. The latter consequently influences the environmental impact of architecture. The building industry has also, to some extent, adopted the principles of mass customization. Computer Numerical Control (CNC) [2] machines of different kinds enable manufacturers to produce unique components at the same speed as copies.

However, to make mass customization economically sustainable, not only the manufacturing part, but also the complete process of design and development must allow for efficient and individual customization. Digital parametric workflows represent a dramatically new way of applying digital power while designing our built environment. As we see it, parametrization is key to achieving a mass customized building industry. Instead of drawing geometry, parametric workflows let the user define the design as a series of decisions, systems and relationships. The digital design process has the potential of becoming more streamlined.

Currently, fully parametrized design processes of timber structures are not common. Enormous steel structures, such as Morpheous Hotel [3], had a fully parametrized design process. Millions of unique components were generated by parametric models. Great examples of such methodology can also be seen in advanced timber structures. Shigeru Ban’s famous Nine Bridges Country Club [4] gridshell is realized with the help of DesignToProcution’s use of parameterization and automation of manufacturing processes.

Designing advanced timber structures are especially rule-driven, and therefore well suitable for parametric design processes. Not only are such structures rule-driven, many examples are even based on more or less standardized structural concepts. Despite visual and functional differences, Evenstad Bridge, Tynset Bridge and Treet highrise in Bergen are all using the same connection principle: Dowels and parallel slotted-in steel plates[5]. The more pragmatic rules, the more suitable for automation.

However, there are few good parametric tools specifically tailored for designing timber structures. Some exists, for example, Woodpecker[6] and Beaver[7], but these are developed to tackle the transition from design to manufacturing. Designing parametrically expands the limits of which forms are possible to achieve in design. These designs are trivial to make digitally, but not necessarily designs that are possible, nor rational to build. As the authors see it, the gap is too large from digital parametric design environments to physical reality. Our long-term research goal is thus to develop an interdisciplinary parametric toolkit for designing advanced timber structures. Tools that assists architects, structural engineers and manufacturers to create sophisticated, yet rational structures.

This paper presents a case project of parametrically designing and building two glulam pedestrian bridges. Both bridges are to be completed June 2017. The purpose of the case projects have been to develop a working prototype of the toolkit. Further, such realistic case project gives valuable insights of the needs and challenges in the building industry. These insights are presented in the end of the paper.

1. How: A parametric timber toolkit

The design and construction of the two timber truss bridges investigates the requirements of a flexible, parametric timber toolkit. A timber toolkit that simplifies the process of designing and constructing advanced timber structures. A toolkit that are applicable for most of the member+node based structures, and aims to shorten the distance from sketch to fabrication by automating redundant and repeating design processes. An important value is also improve collaboration between architect, structural engineer and manufacturers by facilitating a shared parametric platform.

From a geometrical and structural point of view, all member+node based structures are principally similar. Although the topology of a gridshell, truss or lightweight wall are drastically different, the relationship between the nodes and the members can geometrically describe both structures. Currently, the core of the toolkit's function is to sort and identify relationships and stream the geometry into different geometrical families. A central database gathers all geometry and meta-data. Additionally, the toolkit also contains a timber materializer and various subtractive timber operations.
The timber materializer attaches metadata to the geometry. Specie, grain-direction, density, structural material properties, manufacturing order, id-tags are relevant examples.
Subtractive timber operations are developed to shorten the distance from design to manufacturing. Instead of using classic 3D-modelling operations, the designer virtually uses operations like cut, drill, pocketing and profiling. An expected outcome is that the designer makes more buildable designs. In addition to digitally visualising the design, the toolkit automatically generates a BTL-code for Computer Aided Manufacturing (CAM)[8].

2. What: The case studies

Orkdal, a municipality in Norway, are refurbishing a park along the river Orkla. A 3-meter wide pedestrian road replaces an existing pedestrian path. Map shown in Fig 1. Snow removal are conducted by a 13-ton wheel-loader and is consequently the dimensioning live load. The research team have been using the pedestrian road's crossing of two side-rivers as case projects. Following was important premises from the municipality:

- Both bridges primarily made of timber
- Similar visual expression on both bridges
- Dimensioning live load: 130 kN wheel-loader + 50 kN gravel in the front loader. 150 kN axle load
- Permanent bridges, but open-minded to experimental solutions
- Universal design, maximum rise: 1:20
- Ice-drift in the rivers, possibly damaging the bridges if placed with too small clearance

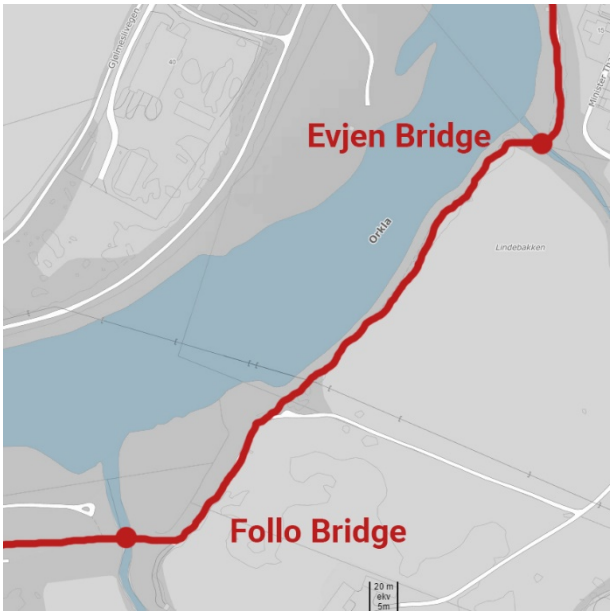

Figure 1: Map of the road and location of the bridges

2.1 Structural concept

A truss bridge with slotted in steel-plates and dowels as nodes were chosen as structural principal. A suspended, steel-based secondary structure were required to fulfil relative large live loads. Longitudinal beams lie on the secondary structure and supports the transverse timber deck. Horizontally, the structure is stiffened by a steel truss placed under the platform.

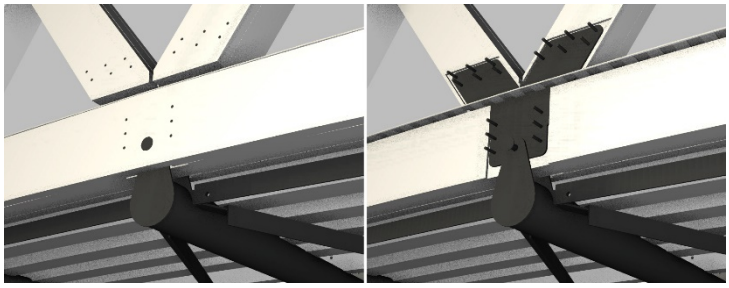

Figure 2: Bottom chord node. Picture on the right shows the detail on the inside

The combination of large live loads and short span challenged the aesthetics of the details. To make the details harmonize with the size of the structure, the nodes had to be as compact as possible. Comparable structural concept suspends the secondary structure from a pinned connection below the bottom chord. In a 50 meter long bridge, the detail harmonizes well. The detail harmonizes well in a bridge like Evenstad Bridge (Figure 3), but becomes too dominant in a 10 meter long bridge. Thus, the pinned connection were integrated in the bottom chord and resulted in a bespoke detail.

Figure 3: Evenstad Bridge

Was this an overdesigned structure? A fair question to ask. An architectural intention was to limit the structural intervention. Thus, a railing height of maximum 1500 mm were chosen. Compared to solid

beams, an open truss structure would blend better with nature. Additionally, such structural concept is more scalable to larger, traffic bridges and better challenges the parametric timber toolkit.

Figure 4: Structural principle seen from below. Picture on the right shows the bottom chord node and the steel truss connection

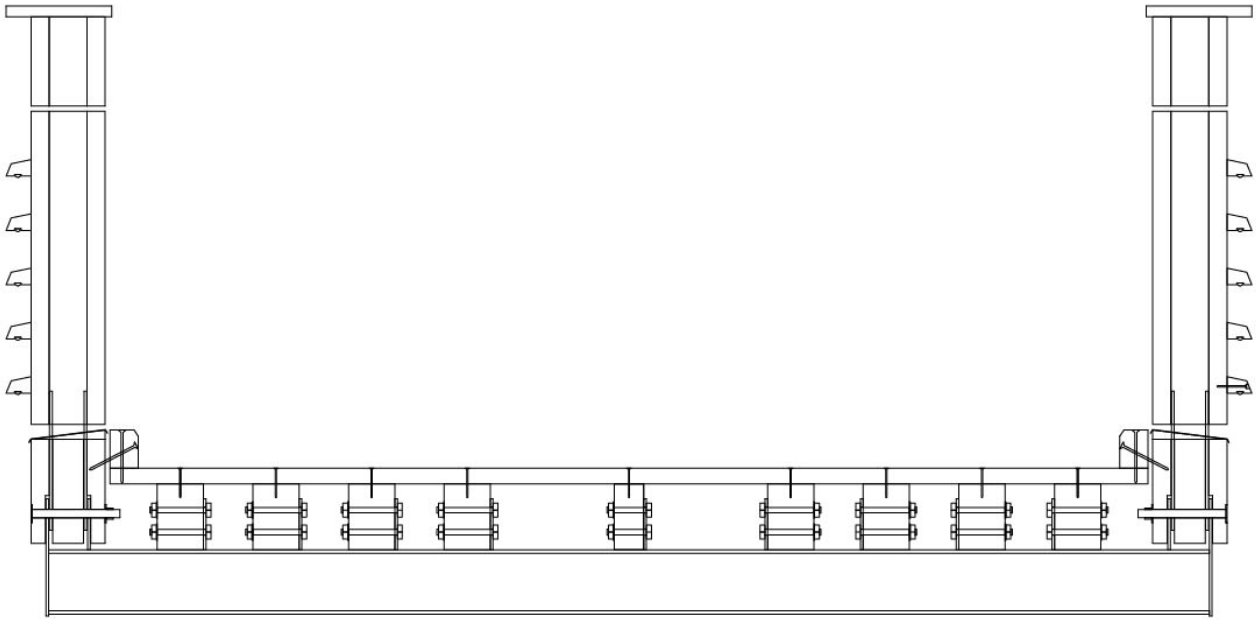

Figure 5: Cross-section of the bridge.

The bottom chord node is indisputably the most complex detail in the project. Two bars are connected to the chord, the secondary structure is connected internally in the chord and the horizontal steel truss is attached. Principally the nodes are similar, but all varies in geometry. What various the geometry, is mainly the angle of the bars, amount of dowels and not least the pattern of the steel truss. Such examples makes a great use of a parametric detail. One logics, many variations. Figure 6 shows one parametric detail, materialized in three variations. While most members required six dowels,

the bars close to the foundations required eight dowels. Further, the figure shows the variations of connecting steel-bars.

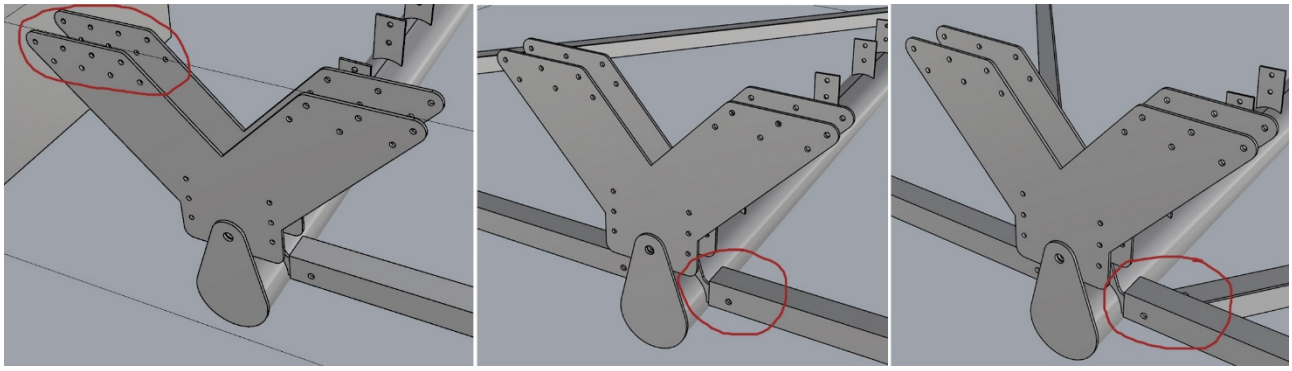

Figure 6: Variations of one parametric detail. Different angles, different connection, different amount of dowels, but similar logic

2.2 Follo Bridge

The Follo River flows through an open, flat area. Where the bridge is placed, the river is surrounded by artificial riverbanks. The span is 10 meters, and due to ice-drift, the vertical bridge clearance from the river is heightened 400mm relative to an existing bridge. For structural reasons, and further height increasing height clearance, the shape of the bridge is arched.

Figure 7: Follo bridge

Figure 8: Details of Follo bridge

2.3 Evjen Bridge

The Evjen river and bridge are located beside a local fireplace and timber shelter. The height difference of the riverbanks is approximately 1.5 meters and due to universal design requirements of maximum 1:20 inclination, the length of the bridge is almost double length of the structure. Furthermore, due to the directions of the connecting paths, the bridge makes two turns. These turns are supported by a concrete foundation. One turn is towards the local fireplace, where small amphitheatre will be built using suitable stones.

Since the railing in the turns is not superstructure of the bridge, the bars are parallel. They have been checked for small vehicle hit and vandalism act according to Eurocode requirements. This adjustment gives the structure an increased visual flow, but retains the architectural expression from the load-bearing structure.

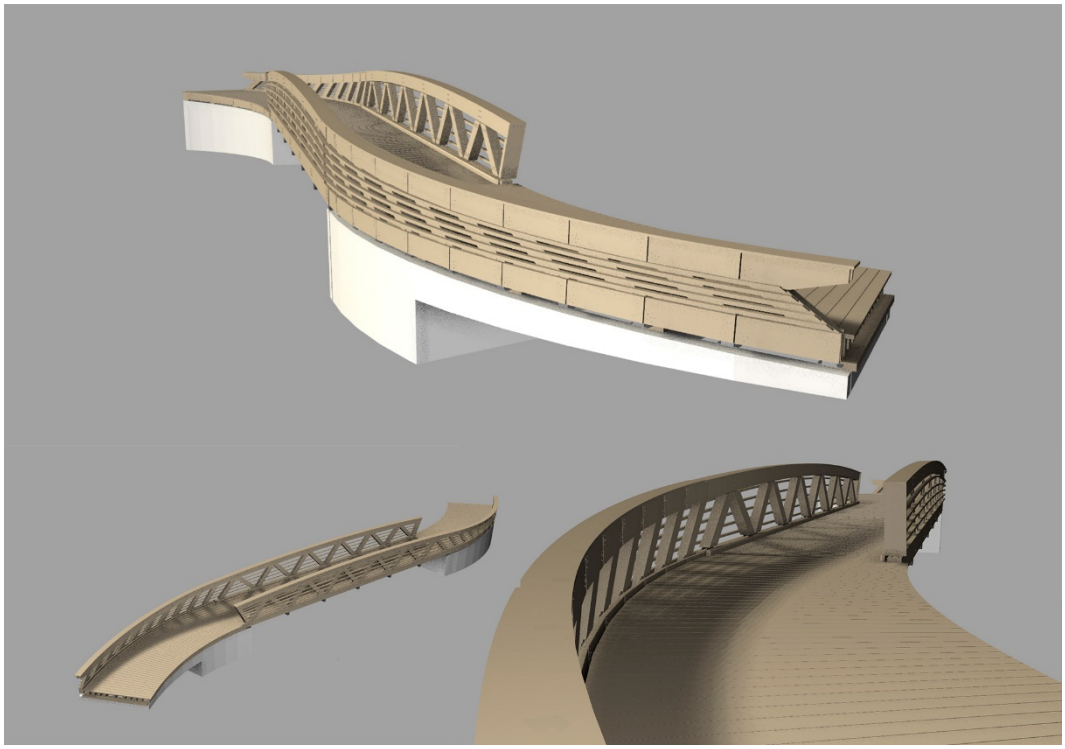

Figure 9: Sketches of Evjen bridge.

3. Learning from the process

The case-project is still on going. Planned opening of the built bridges is mid-June 2017. Both bridges were successfully manufactured and will be finalized April/May 2017. Hence, only preliminary learnings are presented in this paper.

3.1 Speed versus flexibility

Building up a parametric model is an investment. Depending on the complexity of the project, building the model may demand everything from a couple of hours until several months. A flexible parametric model supports a large design-space. However, the more flexible a model is, the more programming effort/time is needed. Thus, a great challenge is to determine how big flexibility is needed to sustain a streamlined design process.

When the core of the parametric model is built up, adjusting a design is very efficient. If changing key parameters like central-path, height or amount of bars, a new, complete model is generated within a 90 seconds. The model then includes structural analysis, geometric representation and a manufacturing code.

The parametric process somehow influences the speed of assembling as well. When modelling parametrically, the chance of making mistakes is decreased. Mistakes done parametrically is logical mistakes and are often more visible in the design. However, drawing manually makes it easy to do small geometrical mistakes that may give large delays on the building site.

Assembling Follo Bridge is reported to be very efficient and lack of errors. Only 5 days were spent from modules and components arrived until the bridge were assembled on site.

3.2 A greater interdisciplinary understanding?

Working on the development of the parametric model from the very beginning can give a greater understanding of other discipline's arguments of possibilities and limitations. The core of proposed platform is parametric model coupled in The real-time with finite element analysis (FEA) using Karamba 3D. Results are real-time checked with EuroCode 5-requirements. While sketching, the designer get real-time visual feedback about strength, capacity, displacement, natural frequency or other structural parameters, both for the single element and global structure. The feasibility appraisal in not only by a true/false indicator, but also by graphically indicating what part of the structure does not full-fill structural requirements. The result is a gamification of the conceptual design phase, making the sophisticated structural design principles understandable for every participant of design process. With limited technical knowledge, an architect can tweak the parametric model until the design is both architectural appealing and structural feasible.

A concrete gamification example from the design process is the final shape of the Evjen Bridge. Two weeks before manufacturing deadline, the shape of the upper chord was linear. Updated structural requirements indicated that the truss height was too small to cope with bending moments. When adjusting the parametric model, a valid solution were easily found. An arched upper chord gave the required midspan height. Consequently, the railing in the turns changed curvature to blend with the truss structure. Comparing the two alternatives (figure 10/11), the final solution visually merges the non-structural and the structural part of the bridge much better. Additionally, it further improves an appearance of motion.

Figure 10: Old version of Evjen bridge. Location and path is similar

3.3 Automation: The end of architects, engineers and manufacturers?

Why do we automate processes? Naturally, there are many motives for automation, such as improved competitiveness and increased profitability. What we see as an important motive is to increase the time spent in the creative process. By applying automation with the purpose of decreasing time spent on redundant processes, increased human power can be spent in the conceptual phase. This attitude towards automation is also supported by Buro Happold's Robert May[9]. In that way, automation does not remove the need of architects, engineers and manufacturers. However, a threat may be that clients do not see the use of conceptual design-phases. Together as a profession, we must protect the conceptual phase in the future, not letting profit-focused clients by-pass the creative process of making architecture.

In this project, the complex railing geometry in the Evjen bridge would not be economically sound applying a conventional CAD-method. However, by parametrization only two different details had to be developed: the upper and lower node. All nodes have different angles, different position of the holes, but have similar geometric logic. Detailing of the railing took about a week of work, adaptable for parameters changes until manufacturing start-up.

3.4 Mainstream or a specialist's design method?

Do we need dedicated team members developing parametric models? Alternatively, should we aim towards a future where every team-member works in a parametric model? The introduction of graphical programming platforms, such as Grasshopper, decreased the threshold of making parametric models. However, it still is a specialist's tool. In described case study, the architect and the structural engineer developed and used the parametric model. The manufacturer fed the model with important parameters, but did not interface directly.

Learning through described and earlier case-projects, we do not believe the key is to make every discipline a parametric specialist. Knowledge needed when completing a building is ever growing and we believe building complex parametric models will be a specialist's tool in the future as well.

What is a key is that the whole design team understands the concept of parametric modelling. Understanding basic limitations and possibilities, and most crucial understanding the speed of generating different iterations of a concept.

3.5 The need of meta-data

One of the greatest learnings from the case-project is the need of meta-data. Parametric geometry crucial, but data like assembly-order, structural properties, timber-quality, assembly position, assembly-vector, manufacturing order and tolerance-requirements are equally important. Currently, the parametric toolkit is not flexible enough to include an arbitrary set of attributes. Next iteration of the tool will focus on building up an accessible and flexible database structure that handles both different geometrical representation, but not least any kind of meta-data.

Such database must also include input-data. Input data may be structural requirements, available glulam-stocks and knowledge-based data like standardized dowel-diameters and minimum distances between dowels. Both input and output data must be accessible and editable for all stakeholders. Even, maybe especially, if not being a parametric specialist.

4. Heading towards a parameterized design process?

This paper have presented the case of two bridges designed solely parametrically. The relevance of a parametric toolkit have been tested through a working prototype. Based on this case project, the authors sees a great potential of fully parametrizing design processes. Especially the efficiency and flexibility achieved while designing the Evjen Bridge demonstrated the power of such method. Additionally, the efficiency and lack of errors while assembling Follo Bridge indicates the power of using a parametric workflow. However, currently the toolkit is in an early development. A considerable effort must be put into further development to make the toolkit accessible and user-friendly.

Acknowledgements

Moelven Gluelam, by former CEO Åge Holmestad, Daniel Barosso and Rune Abrahamsen, has shared their expertise in manufacturing, and thus contributed to improve the understanding of the current workflow and challenges. The authors gratefully acknowledge research funding from Innovation Norway.

[1] Joseph PB. Mass customization: the new frontier in business competition. Harv Bus Sch Press Boston 1993.

[2] Rapp EJ, Johnson GA. Computer numerical control machine tool. Google Patents; 1980.

[3] Hadid Z. The Morpheus Hotel: From Design to Production: Live Webinar on Vimeo n.d. https://vimeo.com/203509846 (accessed April 30, 2017).

[4] Ban S. Nine Bridges Country Club. ArchDaily 2014. http://www.archdaily.com/490241/nine-bridges-country-club-shigeru-ban-architects/ (accessed

January 18, 2017).

[5] Abrahamsen RB, Malo KA. Structural design and assembly of “treet”-a 14-storey timber residential building in norway. World Conf. Timber Eng. 2014, 2014, p. 8.

[6] Stehling H. Woodpecker. n.d.

[7] Petzold F. Beaver. n.d.

[8] Chang T-C, Wysk RA. Computer-aided manufacturing. Prentice Hall PTR; 1997.

[9] May R. Computational Engineering, Bath: IABSE; 2017.

Correct geometry against water damages in Design of Timber Bridges

Tõnis Teppand
Lecturer, PhD student
Est Univ of Life Sciences
Tartu, Estonia
tonis.teppand@emu.ee

Master's degree in civil engineering (rural building) Author's research mainly focuses on long-span shell structures, their modelling and construction technology.

Renno Reitsnik
Lecturer, PhD student
Est Univ of Life Sciences
Tartu, Estonia
renno.reitsnik@emu.ee

Master's degree in civil engineering (rural building) Author's research mainly focuses on determination of residual stresses in different materials, mainly in thin ceramic coatings.

Summary

The concept of the present paper belong to the topic of design aspects and requirements, timber bridge architecture and aesthetics and bridge decks. This paper dissect the reasons of decay timber bridges and make suggestions to avoid them with help of correct geometry. The important part of the paper is description of new type two-curved constructively participating bridge deck and structural members working as leaf springs glued together of concentrically composited lamellas of different species of timber.

Keywords: timber bridge, bridge deck, grid-shell, two-curved surface, carpentry joints.

1. Introduction

Decay of wood because of moisture and freshet damages take lot of timber bridges out-of-use every year all over the world. Lightweight, renewable building materials as wood and reusing old technologies together with possibilities of Computer Age gives to us new opportunities to design and construct timber bridges better and for long-life.

1.1 Water damages of timber structures

One of the most problematic theme of timber bridges is freshet/water and damages because of it. Lot of different solutions as mechanical, physical and chemical has made and issues carried out to keep away the water from timber parts. This is the fighting of consequences. It is not possible to keep off the water 100% but is possible to make the influence of water minimized. Just moistening for a while does not have permanent damages and can avoid with help of treatment technologies. How can it done?

1.2 Expansion of timber because of moistening

The other big problem of timber deck and other structural elements is expansion because of moistening even if it is treated and shrinking after drying. This can lead to extra increasing of inside forces additionally to the loads and plastic deformation of details. The pre-stressing may disappear

even if it was at first and gaps between details will open to let the outside water inside the structure. The rot, mold and fungi start develop. How can it avoid and let the timber part expand without exceeding growth of inside forces?

1.3 Condensate on metallic parts

The last but not least problem of timber structures in the open environment without permanent heating as timber bridges are springing up the condensate on metallic parts because of crossing over saturation of moisture after cold night when the temperature of air rise up very fast and the moisture content in it too. This kind of physical phenomenon at the areas of temperate zone keep the water around the metallic fasteners on exactly contact with timber. The slow decay develop into the timber around the fasteners and therefore reduce the junction slack after what will change the geometry of the whole structure and values of inside forces in it. Is it possible to avoid it at all or decrease the problem?

2. Materials and Methods

2.1 Main features

Timber is anisotropic material and very suggestible of moisture. Moisture has an effect on biological decay, strength and on changing the size of timber structures. All these aspects make quite difficult to design timber structures especially together with other different construction materials of other linear expansion. To avoid exceeding moisture content in timber structures it can covered or treated with other materials but it can´t guaranteed the exact moisture content never as it was been projected and calculated primarily. Especially it apply to the structures as timber bridges, towers etc. standing on open air.

First problem is ordinary non-covered timber structures against precipitation. The second one become of metallic fasteners contact with timber. The condensate growing up and contacting the wood surfaces after fast warming of the air start to decay timber slowly. The third problem is associated with strength. Higher moisture content mean less strength but more elasticity and in the opposite – less moisture content mean more strength but more fragile too. In first case of the structures under the load bend and if they dry the deformation become plastic and the shape does not recur. The last big problem is expansion or shrinkage of timber details because of changing moisture content in it what generate extra inside forces very difficult to take into consideration if the structure itself is not very simple. All these problem can be minimized or avoid with help of correct geometry of constructive members, connection details and timber deck of bridges what does not let the water assemble on them.

2.2 Bridge deck of timber balks

Bridge deck is the most important part of every type of bridge. It carries payload and has fast aging because of foots and wheels. Ordinary the bridge deck does not participate in stiffness of the whole structure what mean that it just add net weight. In divers case the bridge deck has used to give horizontal stiffness for the bridge. Only the structure of arc-bridges use it as constructive element working together with the others.

Simple and short-span timber bridge decks are often made of timber balks laid vertically side-by-side and mounted together horizontally with long bolts. Longitudinal connections of the balks has shifted and in the result different panels of balks will connected to each other to the full deck with butt joints. To avoid the collecting freshet it can made of arc shape too. This will make structure much stiff and even lighter in case of timber bridges instead of concrete bridges. The problem is how to form the bridge deck of balks to the shape of two-curved shell? Is it possible to give the pre-stress to the bridge deck without additional tension details?

2.3 Connections

Most of the connections between the members of timber bridges have to be hinge to avoid the statically indefinite structures. It is very common to use different kind of metallic fasteners more specific or ordinary ones. Mostly for directly carrying loads from one member made of timber to another. There are two main problems in it.

The first one is that there is not enough space for fasteners at the ends of members for needed cross-section in many cases, to carry on the loads even if the cross-section of the member itself has

dimensioned correctly. It lead to over dimensioning of the members themselves. The other problem consist in all kind of issues of moisture condensate and decay of wood because of it. Beside them less important is the increased cost and possible non-long-lasting.

Is it possible to eliminate the problems with the carpentry joints used on new level to carry on the loads together with pins of hardwood if needed counterweight to the metallic fasteners what can decreased minimum in designing and constructing timber bridges?

2.4 Load carrying structure of the bridge

The most effective shape for load carrying purposes is arc in consideration of used amount of materials and useful span. Already Leonardo da Vinci used this phenomenon together with suspending element in its proposal for bridge structure across Bosporus about 500 years ago. The shape of arc is useful even if it will stand vertically as bow working structurally as spring. Is it possible to use these properties together for lightweight timber bridges today?

3. Results and Discussion

As the result of different virtual 3D models and real modelling tests with new type of bridge deck it can be confirmed that light long-span timber bridge with shape that hold of the water, decrease the inside forces at the connections and of minimum metal fasteners is possible to design and construct.

3.1 Two-curved pre-stressed bridge deck

As the result of real modelling tests of routed balks with ambient cross-section of trapezoid-shape may confirm that the two-curved bridge deck is possible to construct. It has several virtues:

Fig. 1 Compressed together balks of variable trapezoid cross-sections (Tõnis Teppand´s photo)

a) Increased strength and stiffness on longitudinal and thwarted direction because of pre-stressed two-curved shape (the supporting ends of the bridge deck will designed and constructed wider than the middle part with help of different cross-sections of the balks);

b) Correct geometry not to let the water assemble on the surface (even if the geometry will change because of expanding under increasing the moisture content);

c) Decreasing the appeared inside compression forces because of increasing the moisture content inside the timber deck in the case (the shell shape let the structure expand up and dissipate the rising forces along the surface without exceeding the critical values.

To construct a two-curved bridge deck of simple balks it is need to change their shape to the one that will form two-curved surface itself. Such shape is of trapezoid cross-section what will done with help of routing balks in the CNC-workstations. The bridge deck at the same time with pre-with the help of long bolts. The real model test has shown on the photo (*Fig. 1*).

The desired shape/geometry appear because of different lengths of edges after routing. The length of upper edges is shorter and the lower one little bit longer. During the mounting of lower parts/edges of balk need to bend until the contact with neighbouring element and will fixed with the screws of hardwood or

steel. It is possible to fix the balks together with jacks at first and after the drilling straight/horizontal holes with long bolts. It generates the pre-stress and rising up the lower surface of the balk what will form both longitudinal and thwarted curved shape.

3.2 Carpentry joints

As the result of different numerical analyses, researches and tests it became clear that together with using old carpentry joints and developing new ones is possible to avoid most of metallic fasteners and if needed change them to the pins of hardwood. To handle the expanding and shrinkage of timber details it can be used different kind of timber mixed softwood and hardwood to keep the constant tolerance in carpentry joints and avoid not eligible extra inside forces.

3.3 Curved or two-curved members

In some elements where we can´t guarantee the designed shape or it has danger to get plastic deformations in it can used curved, two-curved or even twisted GL beams or posts what act as leaf springs. Some details of GL can mounted as pre-stressed to have preventive affect to keep the shape under the carrying loads.

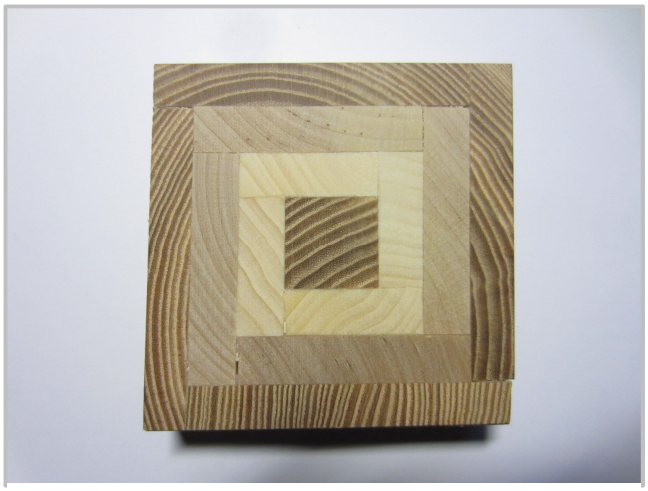

Fig. 2 Specimen description (from inside to out): ash, aspen, birch, ash (Tõnis Teppand´s photo)

There is a possibility to use new type of curved and pre-stressed beams of concentrically glued together lamellas of different species of timber (*Fig. 2*; patent application is submitted). The hardwood vary with softwood in it what gives to the beam extraordinary good properties.

By the results of strength tests in Estonian University of Life Sciences (Tartu, Estonia) and in *Groupe ESB École supérieure du bois* (Nantes, France) with seven different combination the mean bending stress of the best group of specimen was 129 MPa and the mean Elastic Modulus at the same time 16565 MPa. The compression stress was 59 MPa and the Elastic Modulus at the same time 11842 MPa. It mean that such type of beams have much higher bending strength as ordinary GL but retain the very high elasticity. [1]

3.4 The whole timber bridge

A special type of pre-stressed two-curved bridge deck of solid timber balks used to take part in stiffing all structure both as longitudinal and thwart direction. The load carrying two-curved and twisted supporting arc members has used together with suspending members connected to each other with curved and pre-stressed posts and beams carrying the roof structure of two-curved grid-shell. All structure has roof covering made of polycarbonate to avoid freshet as much as possible. The loads and other inside forces between the members will carried over by carpentry joins, mostly by lap joints with half dovetail edge locking under the pre-stress and/or loads.

At finally we will get the expansion of Leonardo´s Bridge (*Fig. 3*). This difficult structure and its details can modelled and analysed by CAD/CAM/FEM-software and produced with CNC-technologies what was impossible only few decades earlier.

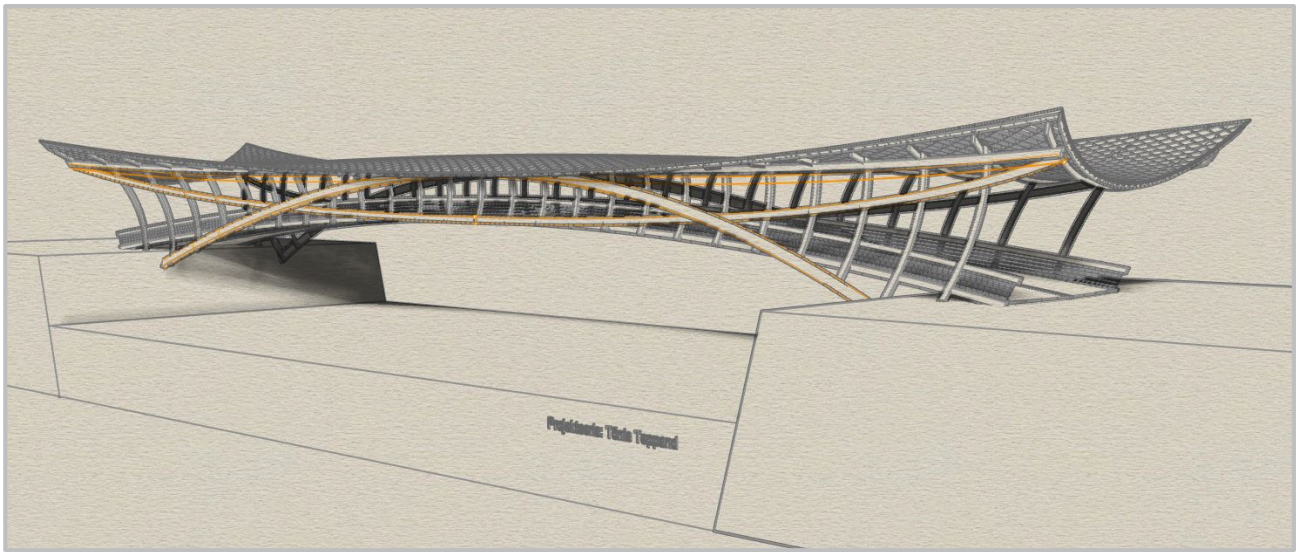

Fig. 3 Expansion of Leonardo´s Bridge (with polycarbonate roof covering on grid-shell; span 67,14m; Tõnis Teppand´s concept design)

4. Conclusions

Using timber in structures of bridges need especially careful handling because of most difficult environmental conditions. To avoid damages and decay of timber elements because of moisture and freshet the first important thing is geometry. It need to consider the correct geometry of the whole structure from general to the smallest detail. After that will come right selection of materials adapted to each other together with needed technical solutions to avoid conflicts between them whatever the reason is.

Right time maintenance works are very important to get desired full-time lifespan of structures what must be schedule already in the design project by the architect-structural engineer. It is not possible or will be very expensive to project every detail last for full-time lifespan (100 years for important landmarks in Estonia), thus designers have to predict/calculate the real lifespan of them. If the result would show that some of the elements does not long-last until the end of total lifespan such of that kind elements have to project for easy(cheap) replacing technology.

5. Acknowledgements

The patent application submitted for producing technology of pre-stressed two-curved bridge decks of balks.

The patent application P20170011 from 28th of February 2017 under process for producing technology of laths glued together of lamellas of different species of wood concentrically and for construction technology of grid-shells built of them.

6. References

[1] Nurme, P., Teppand, T., Teppand, S., Test report: bending and compressing tests of glue-lam laths, Manuscript, Estonian University of Life Sciences, Tartu, Estonia, 2017.

New design guidelines for structural protected timber bridges

Antje SIMON
Chair for timber construction, Prof. Dr.-Ing.
Fachhochschule Erfurt - University of Applied Sciences
Erfurt, Germany
antje.simon@fh-erfurt.de

Markus G. JAHREIS
Research assistant
markus.jahreis@fh-erfurt.de

Johannes KOCH
Research assistant
johannes.koch@fh-erfurt.de

Ralf ARNDT
Chair for building material science and building diagnostics, Prof. Dr.-Ing.
ralf.arndt@fh-erfurt.de

Born in 1970,
Civil Engineer since 1994,
Project leader and head of design of civil engineering structures at an engineering office for 10 years,
Thesis in the field of timber-concrete-composite road bridges in 2008,
Professor for timber construction since 2011

Summary

The strict application of structural timber protection would help to reduce the maintenance costs of timber bridges considerably and could help to increase the acceptance for timber structures in general. Therefore, the research project “Protected timber bridges (ProTimB)” was initiated to review and improve design guidelines of timber bridges and to define standards for the new generation of structural protected timber bridges. Within the paper the necessity of design guidelines is discussed. Furthermore, existing and newly developed detail drawings for structural protected timber bridges are presented.

Keywords: protected timber bridges, structural protection, guidelines, detailing, design

1. Introduction

Timber bridges have a centuries-old tradition. A few very old, but well protected bridges are demonstrating the potential of the natural material timber. However, the specifics of the natural orthotropic material need to be considered for timber structures in general and for bridges in particular. Careful observance is required of the details of construction. Additionally, the material has to be protected against humidity. Timber starts swelling and shrinking with changing moisture content, enforcing internal stresses. Furthermore, a higher moisture content of the material enables insects and fungi to attack and destroy the structure. If the specific requirements are ignored, there is a high risk potential for destruction and the maintenance costs rise. Inspections of several bridges in Germany have confirmed, that the

reasons for most defects are a faulty design in construction as well as missing measures for protection and maintenance.
Within the research project “Protected Timber Bridges (ProTimB)” the state of the art for designing durable timber structures should be reviewed and new design guidelines are being developed and will be published. Additionally, some existing protected timber bridges are monitored to verify the efficiency of the protection [1].

2. Design guidelines for timber bridges

2.1 General requirements for design guidelines

The provision of technical standards representing the current state of the art is a basic requirement for the planning and the building of bridges. Design guidelines standardizing construction details and solutions in principle allow effectivity and economic work in engineering offices. The effort of design and construction is lower if unified standards are available, because it is not necessary to develop new structural details for each regular project. In fact, the most important advantage of unified design guidelines is to prevent serious errors in planning. However, from the architect’s point of view it is desirable to regulate as little as possible because a renunciation of regulation opens creative potentials and a considerable freedom of design.

2.2 Existing design guidelines for timber bridges in Germany

In Germany, comprehensive guidelines are available for the construction of bridges consisting of reinforced concrete, prestressed concrete, steel and steel-concrete-composites. Design, execution, maintenance and inspection are regulated extensively for these structural types. The standards are constantly updated to the state of the art by governmental authorities. As the traffic area of timber bridges is less than 0,04 % of the total traffic area of bridges in federal estate, guidelines for timber bridges are not developed by the government institutions. There is a considerable competitive disadvantage for bridges made of the sustainable material timber, because guidelines for protected timber bridges are missing.

Beside guidelines, there are two standards dealing with timber protection in Germany. In the German National Annex of the Eurocode 5-2 [2], the term “protected” is defined for structural members that *“cannot be exposed to direct weathering by precipitation or moisture ingress”*. All other members are automatically assumed to be unprotected in Germany. The protection should be realized on all exposed sides by claddings or a sufficient roof overhang. Besides the covering against precipitation, it is absolutely necessary to enable the drying of timber being exposed to condensate and rising water. Therefore, a sufficient air ventilation must be provided. Special recommendations are given for details in timber bridges [2]. Furthermore, the standard DIN 68800 [3] regulates principles of structural timber protection and chemical treatment [5]. Some design details for structural protection are also included [4].

Some decades ago, a large number of smaller timber bridges were built disregarding requirements of timber protection. A lot of the bridges were not under frequent maintenance and getting worse over the years. Hence, the bridges were soiled, fungal destruction of the timber started and the bridges lost their load bearing capacity. Now the owners are concerned, blaming on the alleged higher costs and replace the timber constructions by other materials. In 2009, the “Quality association for the construction of timber bridges (QHB)” was founded to improve this bad situation and to share information and experiences in designing durable bridge structures made of timber. They already have started formulating some guidelines and have developed first detail drawings [6]. Furthermore, sample drawings for timber bridges have been developed within a research project in 2006 [7]. Additionally, there is a guideline for timber bridges from the former German association of timber research (DGfH) [8].

In contrast to the specification drawings for concrete and steel bridges, the drawings for timber bridges have not been introduced by the building supervisory authorities of the German federal states. Therefore, the most important objectives within the research project are to define the points of interest for detailing, to merge and update the existing timber drawings and to gain recognition by the supervisory authorities.

3. Development of new design guidelines

3.1 Priority topics for detailing

Design guidelines should help to simplify the planning process by standardization and to avoid fundamental mistakes. Therefore, on one hand it is advisable to define structural points of interest in general for every bridge design project. On the other hand, it is necessary to analyse systematic defects of existing structures before developing new details.

3.2 General structural details

Recurring structural details are for example construction variants for waterproofing systems, joints, bearings, wing walls, bridge-caps, expansion joints, drainage or handrails. In Germany, 173 different specification drawings for engineering structures exist currently [9]. Specification drawings are adaptable for timber bridges only in a few cases. Drawings detailing the surrounding area and the substructure are useable because the substructure of timber bridges mostly consists of concrete. As an important advantage of timber concrete composite bridges, specification drawings could also be used for the superstructure. The concrete deck plate excellently protects the timber main beams arranged below with a sufficient overhang in such composite bridges. All specification drawings developed for concrete superstructures (e. g. for waterproofing, caps, expansion joints and drainage) could be easily used without any adjustment effort. Apart from that, 57 special timber drawings are available from former projects ([6], [7]) containing for instance details for waterproofing systems, bearings and handrails.

In Fig. 1 and Fig. 2 a comparison of the approved specification drawings and the drawings for timber bridges is shown.

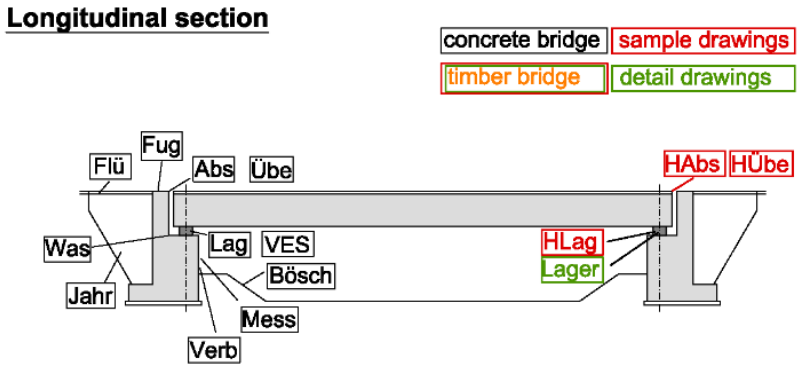

Fig. 1 Longitudinal section of a bridge with details in approved specification drawings for concrete bridges (black) [9], sample drawings (red) [7] and detail drawings (green) [6] for timber bridges

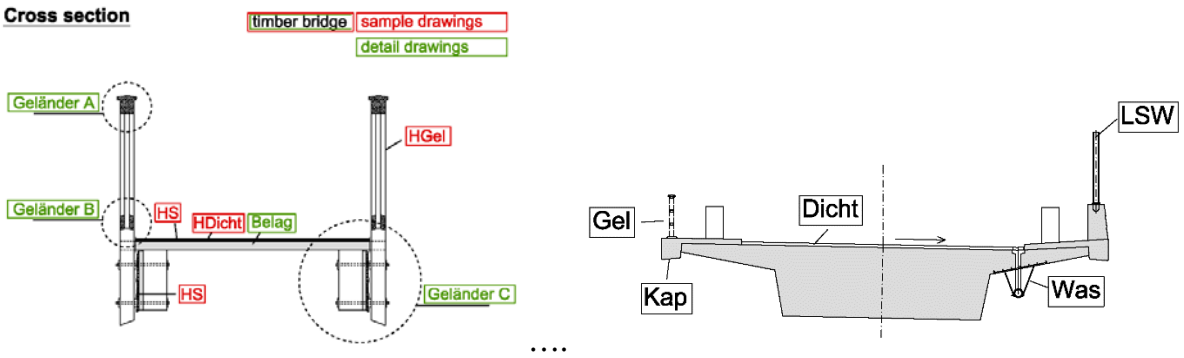

Fig. 2 Cross section of a timber bridge (left side) with details in existing sample drawings (red) [7] and detail drawings (green) [6] and cross section of a concrete bridge with details in approved specification drawings (right side) [9]

3.3 Details of critical points

Systematic defects of existing structures have been identified by inspections of timber bridges. Analysing a large number of inspection results the following typical "problem zones" of timber bridges have been detected by *Aicher* [10]: freely exposed sides and end grain areas of main girders, timber deck boards and connection zones. An increased risk of developing defects occurs in areas where greenery, soil, snow and grit accumulate.

Most defects are caused by ignoring the basic standards of timber protection. One important problem is the missing roofing of the main girders or subcarriers. Another critical point is the bearing area (Fig. 3). Main girders are often situated too close to the soil or the distance to the curtain wall is too small. A spacing of at least 30 cm between timber and the concrete bank is recommended not only for ventilation, but also to keep this area clean. Decks made of timber boards are also problematic. They are extremely exposed to rain and dirt, become slippery and fungi start do colonise the timber (Fig. 4), even if the board is of higher resistance.

Further research is necessary in particular for detailing the "critical" points of timber bridges. Considering the moisture induced damages, the following structural points have to be designed very carefully:

- Waterproofing layers on different surfaces,
- Expansion joints of different superstructure materials with various alternative executions,
- Bearings,
- Handrails and guardrails including their fastenings.

Fig. 3 Closed areas around bearings with dirt, rotting leaves and high humidity

Fig. 4 Fungi attack at a freely exposed deck board

When developing new details the specific orthotropic, hygroscopic and thermal material properties of timber must be considered (Fig. 5). For instance, a variability of moisture content of 4 to 8 % in the outdoor climate could initiate a 1 to 2 %change of the cross section by swelling and shrinkage perpendicular to the grain. This can induce high stress in the joints and it has to be considered at the expansion joints. Furthermore, the corrosive effect of some types of wood has to be considered by selecting the appropriate material or coating for screws, steel plates or covering metal sheets.

Fig. 5 Advanced and double axis elongation at larger timber bridges results in special demand for expansion joints

3.4 Examples

A lot of details could be standardised for road bridges and for foot bridges. As a part of the "ProTimB" project those details will be collected and drawn as construction guidelines in accordance to the German standards. Drawings will be developed for the following details:

> Structural timber protection, deck-plates and planks, end grain zone of main beams, waterproofing systems, handrails, parapets, bearings, expansion joints, drainage.

The following figures show examples of the existing (Fig. 6, Fig. 7) and of the newly developed drawings (Fig. 8, Fig. 9).

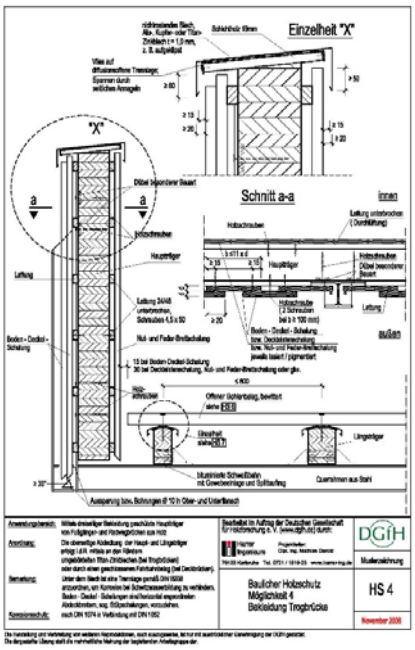

Fig. 6 Sample drawing for structural timber protection [7]

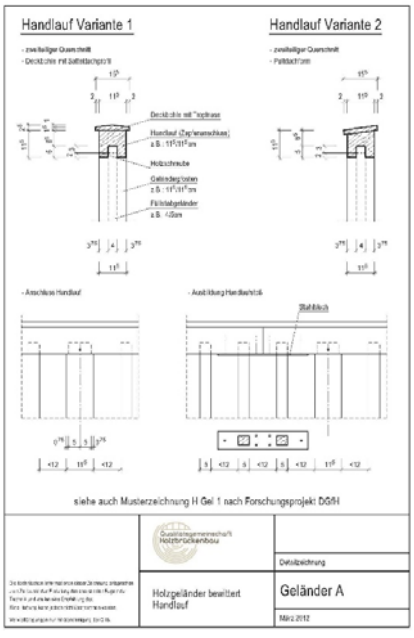

Fig. 7 Detail drawing for handrail [6]

In Fig. 6 some structural protection measures suitable for main girders of through bridges are demonstrated. The drawing gives recommendations for the side cladding, the horizontal covering of the upper surface and the dimensions for gaps that are necessary to avoid accumulation of soil and grit.

Fig. 7 shows some details of the execution of handrails.

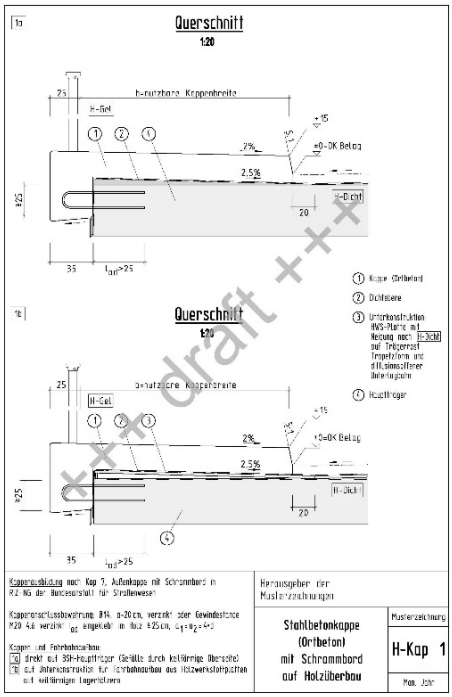

Fig. 8 Example of an cast-in-place bridge-cap for timber bridges (draft)

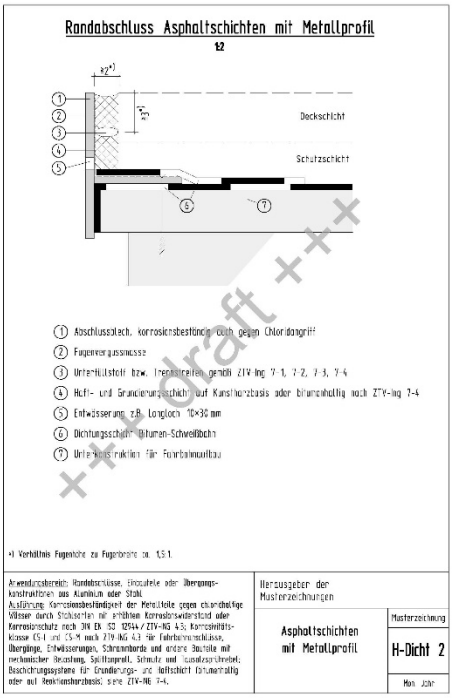

Fig. 9 Example of an edge cover plate for asphalt layers (draft)

Fig. 8 demonstrates the adoption of a special execution of the cantilevered parapets of German concrete bridges. On top of the main construction, over the waterproofing layer, additional concrete elements (called “bridge-caps”) are placed. These elements border the asphalt made traffic lanes. The pedestrian walk, handrail and guardrail are positioned on it. The elements are cast in place and are connected by reinforcement bars at the lateral sites with the main construction. It is important to keep the waterproofing layer faultless without penetration by connecting elements. If the parapets at timber bridges with road traffic should be manufactured on site, they can be joined to the main girder with glued-in rods (Fig. 8). To accelerate the construction progress and decrease the cost, the parapets can be mounted as prefabricated elements and joined with rods and tighteners, for instance.

In Fig. 9 some recommendations for the execution of the edge of the asphalt layer are given. A T-shaped metal plate forms the end of the asphalt layer. To enable temperature expansions a special joint sealing compound is filled in between metal and asphalt. The metal plate has holes for draining water. Special consideration should be given to the correct application of the waterproofing membranes.

4. Conclusion

Protected bridges should be developed as the standard for a new generation of timber bridges. Structural timber protection is essential for a long service life of timber bridges. Timber will only be able to compete with other bridge materials, if structural protection is implemented consequently.

For the design of protected timber bridges, the provision of technical details is necessary. Using standardised drawings increases effectivity and economic work in engineering offices and decreases the danger of serious errors in planning. Existing timber drawings are merged, completed and updated to the state of the art within the research project “ProTimB”. The process is ongoing.

Due to their ecological and sustainable advantages, a significant increase of the market shares for timber bridges will be expected in Germany. Aesthetic, well-protected and durable timber bridges with a high quality standard should characterise our landscape in the future.

5. Acknowledgements

The development of new guidelines for protected timber bridges is the aim of the research project “**Pro**tected **Tim**ber **B**ridges (ProTimB)”. The research work is supported and financed by the Federal Ministry of Education and Research of Germany, the companies of the Qualitätsgemeinschaft Holzbrückenbau e. V. (Schaffitzel Holzindustrie GmbH + Co. KG, Schmees & Lühn Holz- und Stahlingenieurbau GmbH, Grossmann Bau GmbH) and Setzpfandt Beratende Ingenieure GmbH & Co. KG. The authors would like to thank all partners and supporters for their technical and financial support.

6. References

[1] Koch, J.; Arndt, R.; Simon, A.: Moisture monitoring of nine protected timber bridges in Germany. 3rd ICTB Skelleftea, 06/2017, Sweden

[2] DIN EN 1995-2/NA:2011-08: National Annex –Nationally determined parameters - Eurocode 5: Design of timber structures – Part 2: Bridges

[3] DIN 68800-1:2011-10: Wood preservation – Part 1: General

[4] DIN 68800-2:2012-02: Wood preservation – Part 2: Preventive constructional measures in buildings

[5] DIN 68800-3:2012-02: Wood preservation – Part 3: Preventive protection of wood with wood preservatives

[6] Qualitätsgemeinschaft Holzbrückenbau: Detailzeichnungen Holzbrücken, März 2012.

[7] HARRER Ingenieure (im Auftrag der Deutschen Gesellschaft für Holzforschung e.V.): Musterzeichnungen Holzbrücken, 2006.

[8] Holzabsatzfonds, Absatzförderungsfonds der Deutschen Forst- und Holzwirtschaft (Hrsg.) (2005): Brücken - Details für Holzbrücken. holzbau handbuch. Informationsdienst Holz (Reihe 1 Teil 9 Folge 2).

[9] Bundesanstalt für Straßenwesen: Richtzeichnungen für Ingenieurbauwerke (RIZ-ING), Ausgabe 12/2015

[10] Aicher, S.: Dauerhafte Holzbrücken – Schäden, Lösungsansätze, Integrale Bauweisen. 4. Internationale Holzbrückentage IHB 2016

Improved edge design for stress-laminated decks made of spruce

Anna Pousette
Researcher
RISE Research Institutes of Sweden,
Skellefteå, Sweden
anna.pousette@ri.se

Anna Pousette, M.Sc., Lic.Tech, has been working with timber bridges since 1993, with design and construction and also with inspections and inspection methods for timber bridges and other outdoor structures such as facades and decking.

Peter Jacobsson,
Technical Manager
Martinsons Group,
Skellefteå, Sweden
peter.jacobsson@martinsons.se

Peter Jacobsson, M. Sc. Wood Technology, has been working with timber bridges at Martinsons during many years, as a designer and technical manager.

Erik Johansson
Structural Engineer
Moelven Töreboda AB
Töreboda, Sweden
erik.johansson@moelven.se

Erik Johansson, Structural Engineering, has been working as a designer of timber bridges and other timber structures at Moelven during many years.

Lars-Olof Nilsson
M.Sc. Civil Engineering
Swedish Transport Administration
Jönköping, Sweden
lars-olof.nilsson@trafikverket.se

Lars-Olof Nilsson has been working as consultant and client within civil engineering in more than 20 years and today works as bridge specialist in Swedish Transport Administration. Lars-Olof also works with regulations for timber bridges in the authority.

Christine Warg
Bridge Engineer
Swedish Transport Administration
Borlänge, Sweden
christine.warg@trafikverket.se

Christine Warg, M. Sc. Civil Engineering. Has been working with timber bridges at the Swedish Road Administration since 2004. Works today at the Swedish Transport Administration with bridge maintenance issues.

Summary

Stress-laminated bridge decks in Sweden are usually made of glulam beams of spruce and it is therefore crucial to avoid moisture as the wood has no impregnation that can protect it from decay. Typically the protection of the deck consists of a waterproof bitumen sheet under the asphalt layers on the top surface and of claddings along the edges. The aim of this work was to study the risk of damages and how to ensure the function of the deck plates. The adhesion of bitumen sheets and the effect of different primers was studied. The design at the edges was studied and an improved solution with a steel angle along the deck edge was developed and tested. The improved design should be robust and easy to install to always assure a correct performance. The new design has been developed within the European research project DuraTB - Durable Timber Bridges and is now included in general recommendations for timber bridges in Sweden.

Keywords: timber bridge, stress-laminated deck, waterproof bitumen sheet, bitumen primer, edge detail, moisture protection.

1. Introduction

1.1 Stress-laminated timber bridge decks in Sweden

Stress-laminated timber bridge decks are used for many bridges, both road bridges and pedestrian bridges. In Sweden, the stress-laminated bridges are usually made of glulam beams of spruce. The motivation is that impregnated wood should not be used more than necessary in timber bridges due to environmentally concern. The deck plates are completed with a layer of waterproof bitumen sheets and asphalt coating on the upper side as well as wooden claddings on the sides and are thus protected for direct impact of precipitation and can be considered as "under roof", see Fig.1. For timber bridge decks made of spruce it is crucial to avoid moisture and decay and with a good protection the decks can be designed in service class 2 according to Eurocode 5 [1].

Rainwater should be led away as soon as possible from the surface of the bridge. The bitumen sheets should protect so that no water can penetrate into the wood and should be designed so that water is drained away from it. The end of the sealant at the edge of the bridge deck where water should be drained out from the bridge surface is a critical detail to ensure a tight and durable connection. Experiences from inspections of built bridges show that this detail has not always worked, although many bridges work well [2].

The aim of this work was to investigate the risk of damages and how to ensure the function of the decks. First, the properties of the waterproof sheets were studied and the effect of different primers and waterproofing as this must work well to ensure the durability and avoid blistering which can lead to reduced function of this layer. Secondly, the key element is the design at the edge where an improved solution with a steel angle has been developed and tested. The improved design should be robust and easy to install to always assure a correct performance.

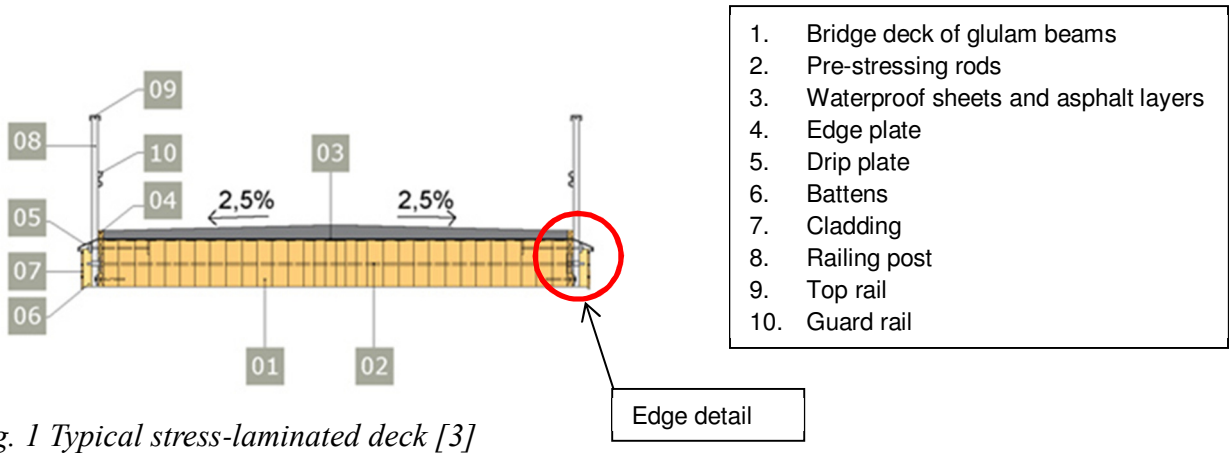

Fig. 1 Typical stress-laminated deck [3]

According to the Swedish Transport Administration's requirements, exposed surfaces of bridges must be provided with an asphalt coating. On wooden deck plates, the watertight layer must consist of waterproof bitumen sheets welded to the wood surface that is treated with a bitumen primer [4].

Primer serves as a pre-treatment to increase adhesion of bitumen sheets to the bridge surface. Solvent-based bitumen primers have been used on timber bridges. There are also water-based bitumen primers, and timber bridge suppliers were interested in using these when it comes to prefabricated timber bridges as a better alternative from a working environment perspective. The waterproof layer on the deck consists of a 5 mm thick polymer modified bituminous sheet according to [5] welded with bitumen to the wood. Along the deck edges there is normally a strip of bitumen sheet to ensure waterproofness at the edges. Asphalt coating is applied in multiple layers. On road bridges, there is a protective layer, binding layer and wear layer.

1.2 Experiences from inspections of stress-laminated decks

The main reason of damages to wooden pre-stressed bridge decks is too high moisture content in the wood. This can cause damage due to deformations when the wood swells and/or shrinks. If the

moisture content is high during a long time this will cause decay, which in the long run affects the strength. Experiences in Sweden from bridge inspections regarding damages to timber bridges is described in [2].

An example of problem at the edge is shown in Fig. 2. The wooden deck was very moist and the outer glulam beams were decayed. They were soft and a knife was easy to insert into the wood. The reason for this moistening was probably bad sealing of the drip plate so that water, instead of flowing out of the edge over the drip plate, went down along the bridge deck, especially at the railing posts.

1.2.1 Experiences of blistering

The coating method with handling, machining etc., may have an effect on adhesion of the bitumen sheet and possible blistering in the asphalt surface. There has occasionally been some blistering on timber bridges. The risk is that the bitumen sheet is raised from the wood surface to form a blister beneath which results in reduced adhesion and consequently deterioration of function. The adhesion between sheet and timber deck takes up braking forces in the use stage, even though reduced to some extent in warm and sunny weather when the bitumen softens. Poor adhesion can affect the formation of blisters, but the blistering problem is often different for timber bridges than for concrete bridges. For concrete bridges, blisters can occur throughout the life cycle, while for timber bridges, most blisters have been reported in connection with the asphalt works of the first layer. Problems with blistering is primarily affected by heat and may be avoided if the first asphalt layer is allowed to cool before the next layer is applied. The blisters will then generally disappear and not return. Blistering problems have occurred on some timber bridges since the 1990s. In the mid-1990s, adhesion tests were used to investigate the impact of different wood surfaces, such as spruce, pine, planed, sawn, impregnated, twig, etc. [6], and the result was no significant difference between them. Blistering was investigated in 2002 [7], where it was found that if blistering occurred, it often took place within about an hour after the first layer was put on. The low heat conductivity of the wood was considered an important factor for the appearance of blisters, as the time to cool the asphalt will be considerably longer for a timber bridge than for a concrete bridge. Because of the high temperature of the asphalt layer, moisture in the wood will form water vapour and blisters beneath the bitumen sheet. Different asphalt systems and blistering was also studied in [8].

A summary of experiences from inspections of stress-laminated decks in Sweden showed that about one third of the more than one hundred bridges had comments about the asphalt surface, but the most common damage was cracking especially at the ends. Very few bridges had blistering or holes in the surface, see Fig. 3. This summary related only to bridges inspected and was not a statistical selection of all wooden bridges in Sweden. The age of the bridges at the inspections varied from 5 to 20 years.

Fig. 2 Moisture damage, decay in outer beams

Fig. 3 Blistering of asphalt surface

2. Tests of waterproofing

2.1 Tests of adhesion with different bitumen primers

Adhesion tests were performed with bitumen sheets applied to wood which was untreated, oiled or treated with solvent-based or water-based bitumen primer to investigate whether there were any differences between treatments. Materials used in the tests were glulam beams of spruce with

moisture content about 12%, and with planed surface. Different types of primers were tested and application of primer was performed according to the supplier's recommendations. The 5 mm bitumen sheet was welded to the substrate.

SP (now RISE) performed tensile tests. Five tensile test samples were taken on each test piece. Steel plates Ø 50 mm were glued to the bitumen sheet. The tensile force was recorded during the test. Most samples had a combination of fracture in wood substrate, between wood and primer, in primer, and between primer and sheet.

Icopal performed tear tests. The first test was carried out on small pieces welded by hand similar to SPs test pieces, but also larger pieces were tested. Uneven welding of the sheets on the small pieces was suspected and therefore burning with a ramp was used on the larger pieces. Also a third test with different treatments of the wood was performed. Tear tests were performed by tearing 50 mm wide strips of sheet from the wood along about 250 mm.

A question that arose was whether primer can protect against moistening on the construction site before the bitumen sheet is mounted. Waterproofing tests were made with specimens of wood with different primers and with a glued frame of a plastic tube Ø 200 mm glued to the surface. The weight of the test piece was measured before the tube was filled with water during one day. After emptying the tube the weight was measured, and also after drying out for 1-14 days.

Table 1. Tested primers

Test piece	**Primer**
1O	Untreated wood surface - (Sheet: DAB/Nord. Waterproofing)
2G	Wood oil Beckers Elit Träolja (040222/040224) (Sheet: DAB/Nord. Waterpr.)
3G	Priming oil Beckers impr.olja art (041136) (Sheet: DAB/Nord. Waterproofing)
4L	Primer, solvent-based, DAB/Nord. Waterproofing / Beta B + Sheet
5L	Primer, solvent-based, Icopal/ Icoflux + Sheet
6V	Primer water-based, DAB/Nord. Waterproofing / Beta M + Sheet
7V	Primer water-based Icopal/ Icopal 2000 + Sheet
8V	Primer water-based Icopal – Elasto-primer + Sheet
9M	Primer MMA, DAB/Nord. Waterproofing/Beta A + Sheet
10FO	Wet untreated wood surface - (Sheet: DAB/Nord. Waterproofing)
11FL	Primer, solvent-based, on wet wood surface, DAB/Nord. Waterproofing / Beta B + Sheet
12DL	Primer, solvent-based, on dusty wood surface, DAB/Nord. Waterpr. / Beta B + Sheet

2.2 Results

The result of the tensile tests showed that there was a large variation between samples from the same test piece. Test pieces that were untreated, treated with priming oil and treated with solvent-based primer had approximately the same adhesion. Water-based primer and MMA primer appeared to have a somewhat lower adhesion. Impact of moisture on the surface without primer (FO) gave the best adhesion. On the other hand, the moisture reduced the adhesion of the solvent based primer (FL). Dust on the wood surface (DL) gave slightly lower adhesion.

The result of the tear tests also showed large variations. Similar results were obtained for both water based and solvent- based primer and untreated surface without primer. The reasons for the wide variation of adhesion are unclear, it may be due to varying amounts of applied primer, different

fiber directions in the wood, surface roughness, surface moisture content or impact on the wood surface of the welding. Different burning techniques and size of the test pieces did not make a clear difference. The adhesion increased with primer but also a surface without primer (1O) gave adhesion. After the tests with the larger specimens, the test pieces were placed outdoors under a roof for approximately 8 months. Complementary tear samples were made with two specimens with Icoflux Primer (4L) and Beta B Primer (5L). The result was higher values and less variation, which means that adhesion had increased after some time.

The result of the waterproofing tests showed that primer had a certain protective effect against water penetration and moistening of the wood surface even if a certain moisture penetration was always present. With primer treatment, water penetration was about 30-60% of the value of untreated wood for both solvent-based and water-based primer. However, drying was faster for untreated wood and after a few days it was about the same moisture level in all samples. After 10-14 days, the elevated moisture was completely dried out for all samples.

3. Tests of edge details

3.1 Tests with steel angle

Basis for details at the edge of a stress-laminated bridge deck where the water is drained over the edge:

- The deck sides where the pre-stressing rods are anchored must be protected against water to avoid deformations and damage that may affect the life and tension forces and thus the function of the deck.
- The sides of the deck are protected with a ventilated wood panel on battens and the transition from the deck surface to the panel should be tight. Drip plate drains the water outside the panel.
- Battens along the edges for screwing edge details have been used to avoid screwing in the upper surface of the deck at the edge.

A new detail with angle of stainless steel at the edge was tested. The function of the steel angle is to support the asphalt layers at the edge and to connect tightly to the waterproof bitumen sheet. Water on the asphalt surface should drain over the edge and not be led in under the sheet. The edge steel angle is mounted on an edge strip of bitumen sheet along the edge of the bridge. The bitumen sheet should then be put over the steel angle so that the angle is attached firmly between the edge strip and the sheet. Because the asphalt layers are not watertight, water that is set down on the bitumen sheet must be stopped from getting underneath the sheet and be drained off. Protruding tubes in the steel angle with centre distances adapted to the bridge dimensions may act as this ground drainage.

Tests with welded edge strips and perforated steel angles at the edge were performed, as shown in Fig. 4-7. Steel angles with a narrow (60 mm) or a wide (150 mm) perforated leg were tested. Primer was put on glulam beams and the edge strip of bitumen sheet was rolled out for welding. The edge strip was welded by hand with burning, which causes the bitumen to melt and attach the strip on to the primer-treated wood surface. Splice pieces under the edge strip was tested to ensure the tightness of spicess. However, splice pieces under the edge strip resulted in an uneven surface that made the mounting of rigid steel angles difficult. To avoid this, the splice piece can instead be lowered into the wooden plate and the edge strip welded on top to obtain a horizontal surface under the steel angle.

The edge strip was heated and the perforated edge steel angle was pressed on to the strip so that melted bitumen penetrated into the holes in the perforated angle leg and secured it. The bitumen sheet was the welded on top of edge strip and steel angle. One problem occurred when welding the sheet on the steel angle. The heat caused the steel to deform and loosen and lift from the substrate. However, it could be pressed back and afterwards attached when it was cooled.

Fig. 4 Edge steel angles with one perforated leg

Fig. 5 Testing with splice pieces under edge strip

Fig. 6 Welding of waterproof bitumen sheet on edge steel angle

Fig. 7 Steel angle was deformed due to heating

3.2 Results

The result was that the larger angle should be used with a width of 150 mm, not the narrower 60 mm wide. The perforation should be performed similar to common proven roofing plates and the steel angle should be attached with two rows of screws. One row of screws will then be in the outer edge batten and the other row will be screwed in the deck plate. This can be avoided by 60 mm width, but the main reason for choosing a wider leg and two rows of screws is that the angles should not risk deformation from heating and risk of lifting if they are pushed outwards for example when rolling the asphalt layers. A disadvantage of screwing in the deck plate itself is the risk of leakage, but the risk is still considered small. It is advantageous if as much as possible of the edge strips, steel angles and bitumen sheets can be prefabricated in controlled conditions.

The results were summarized in the details that were inserted in the new version of AMA [9], the Swedish general recommendations for civil engineering construction works, see Fig. 8-11.

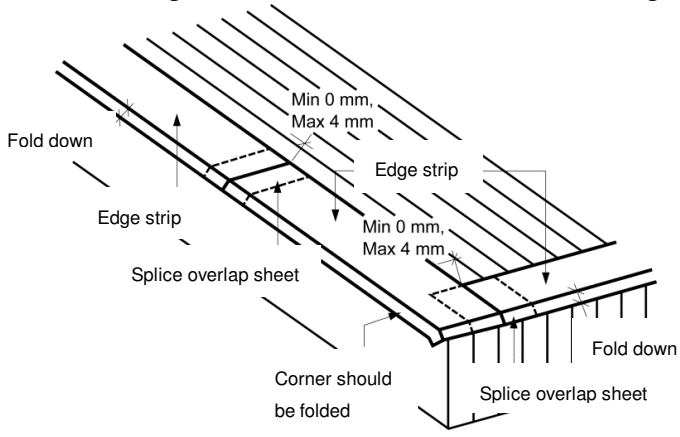

Fig. 8 Edge strip of waterproof bitumen sheet

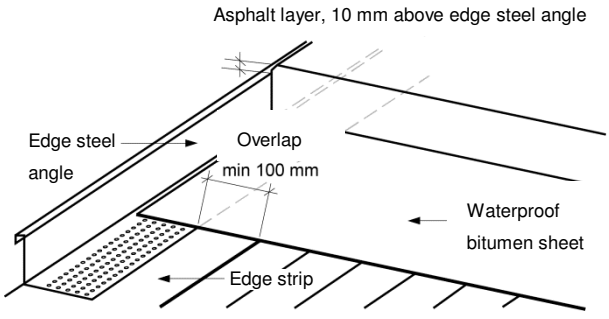

Fig. 9 Edge steel angel and bitumen sheet

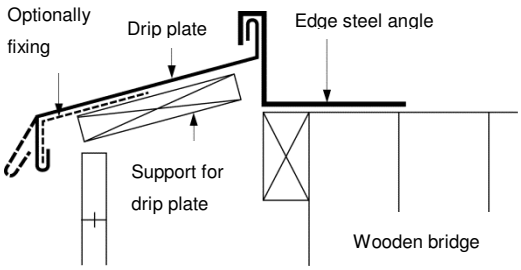

Fig. 10 Edge steel angle and drip plate

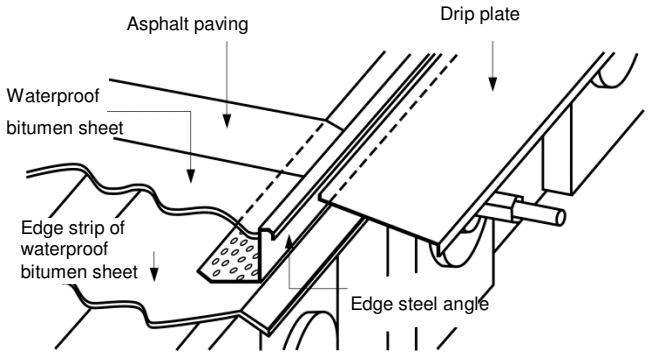

Fig. 11 Edge design

4. Discussion and conclusions

Good and moisture safe solutions are needed, and the Swedish timber bridge suppliers have over the years developed better systems and details at the bridge edge, but sometimes there have been mistakes in the execution.

Several actors are involved in the construction process of a bridge, and clear descriptions are needed for everyone so that the end result will be good. Timber bridge manufacturers make prefabricated bridges or bridge parts. Sometimes they mount the bridge on the building site or the assembly is carried out by another contractor. At the construction site the bridges are then coated by the asphalt contractor. For new actors entering the market, it is also extremely important to have specific instructions on design, so that timber bridges will always be built for long life.

Conclusions from this study are:

- Both water-based and solvent-based primer can be used. Timber bridge manufacturers can use the more environmentally friendly water-based in the factory and the more weather-resistant and quick-drying solvent-based on the construction site.
- Testing of adhesion showed that primer gives slightly increased adhesion, but the variations in the test results were high so it is hard to draw any safe conclusions. This applies to both tensile tests and tear tests. However, there was also adhesion with an untreated wood surface, even if it was damp or dirty.
- Waterproofing tests showed that primer provides a certain moisture protection which is beneficial to the wood. It does not penetrate as much moisture as in untreated wood, but the primer is not totally waterproof. An untreated wood surface becomes moister but on the other hand dries out relatively quickly.
- The edge steel angle showed a tendency to deform when influenced of the heat from welding of the waterproof bitumen sheet. In order to get a robust solution and also withstand the impact of rolling of the asphalt layers, it is recommended also mechanical attachment by nailing or screwing to the bridge deck. The angles should be mounted on top of the edge strip with screws in the perforated leg. The bitumen sheet is placed on top of the steel angle and the perforation contributes to the attachment by melting bitumen penetrating the holes.

The new designs have been included in general recommendations for timber bridges in Sweden.

5. Acknowledgements

This paper is part of the project DuraTB – Durable Timber Bridges. The project has been funded under the WW-net+ Research Programme by the ERA-NET Plus Scheme of the Seventh

Framework Programme (FP7) of the European Commission. The Swedish participation has been funded by Vinnova and industry partners Martinsons Byggsystem, Moelven Töreboda, Limträteknik and Trafikverket.

6. References

[1] EN 1995-1-1, Eurocode 5: Design of timber structures -Part 1-1: General-Common rules and rules for buildings, 2004

[2] Pousette, Anna, Fjellström, Per-Anders, Experiences from timber bridge inspections in Sweden – examples of influence of moisture, SP Rapport 2016:45, ISBN 978-9188349-49-1, 2016

[3] TräGuiden, Skogsindustrierna, www.traguiden.se

[4] TDOK 2016:0204, Krav Brobyggande, Version 1.0, 2016-10-03, Trafikverket, 2016

[5] TDOK 2013:0531, Tätskikt på broar, Version 1.0, 2014-07-01, Trafikverket, 2013

[6] Pousette, Anna, Wearing surfaces for timber bridges, Nordic Timber Bridge Project, 1997, ISBN 91-89002-12-1

[7] Edwars, Ylva, Tätskikt och beläggning på träbroar, Vägverksprojektet ”State of the art 2002”, KTH 2002

[8] Scharmacher Florian, Müller Andreas, Brunner Maurice, Asphalt surfacing on timber bridges, COST Timber Bridges Conference 2014, 25-26 September 2014, Biel, Switzerland, ISBN 978-3-9523787-4-8.

[9] AMA Anläggning 17, Svensk Byggtjänst, https://byggtjanst.se/tjanster/ama/amaanlaggning1/

Investigation of Early Timber–Concrete Composite Bridges in the United States

James P. Wacker Research Engineer USDA Forest Service, Forest Products Laboratory Madison, WI, USA	Alfredo Dias Professor University of Coimbra-Civil Engineering Coimbra, Portugal
Travis K. Hosteng Director/Engineer National Center of Wood Transportation Structures Ames, IA, USA	

Summary

The use of timber–concrete composite (TCC) bridges in the United States dates back to circa 1925. Two different TCC systems were constructed during this early period. The first system included a longitudinal nail-laminated deck composite with a concrete deck top layer. The second system included sawn timber stringers supporting a concrete deck top layer. Records indicate that most of the TCC highway bridges were constructed between 1930 and 1960. The current U.S. National Bridge Inventory (NBI) database indicates that there may be well over 1,000 of this bridge type still in service. This paper will review and discuss the current conditions of several TCC bridges that remain in service today. This will be based on the information given in the NBI and other relevant documents, complemented with information provided by 25 field inspections undertaken during June 2016 in the Pacific Northwest states of Oregon and Washington.

Keywords: timber-concrete, timber bridges, bridge inventory, composite systems, longevity.

1. Introduction

1.1 Historic Background

TCC structures first appeared in the United States in the early 20th century [1, 2]. At that time, the use was for bridges, and this development was motivated by a shortage of steel that urged builders to use other available structural materials or combinations of such materials [3]. The first reported TCC bridge in the United States dates back to circa 1925 [4].

This structural composite bridge solution combining two different materials became more common in the United States in the 1940s [5], and from there, it spread around the world. In the 1950s, TCC structures started to be applied to bridge construction in other locations, such as Australia and New Zealand [6, 7]. However, in other parts of the globe, this structural solution was ignored until quite recently. Since the beginning of the 1990s, TCC bridges have been increasingly used mainly in some northern and western European countries, such as Finland, Switzerland, France, Germany, and Austria [8–12], and also in the South American countries of Brazil [13] and Chile [14].

Records indicate that most of the TCC highway bridges in the United States were constructed between

1930 and 1960. The current USA NBI database indicates that there may be well over 1,000 of this bridge type still in service after many decades. The study presented in this paper provided the opportunity to conduct inspections of more than 25 TCC bridges in the Pacific Northwest states of Oregon and Washington. Analysis of the inspection information revealed that several structures are quite large multiple-span trestle-type bridges, some still carry significant daily traffic counts, and many remain in surprisingly good condition. These findings will be analyzed and discussed in this paper. There will also be a review of the relevant literature, and the current conditions of several TCC bridges that remain in service today will be described.

1.2 Bridge Superstructure Systems

From early times, multiple systems and configurations have been used for bridges. In general, these can be grouped in two categories: T-beam and timber deck (slab). Both TCC systems were constructed during the early period of TCC bridge design. The first system included sawn timber stringers supporting a concrete deck top layer. The second system included a longitudinal timber (nail-laminated) deck composite with a concrete deck top layer (Figure 1) [15].

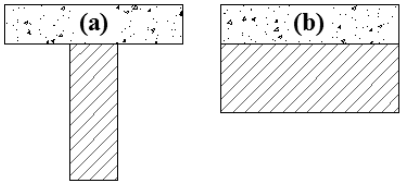

Fig. 1. TCC bridge configuration (a) T-beam; (b) slab [15]

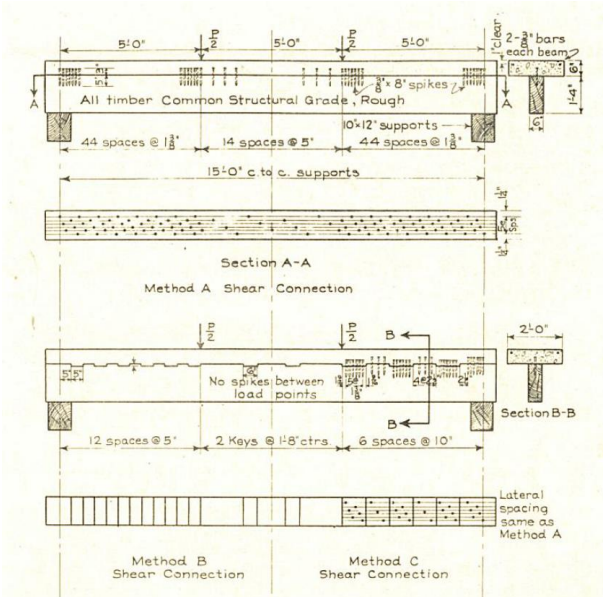

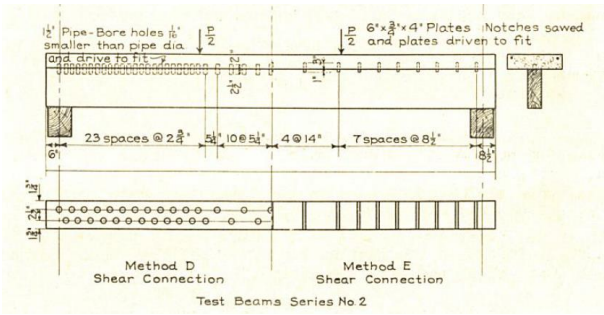

a) T-beam

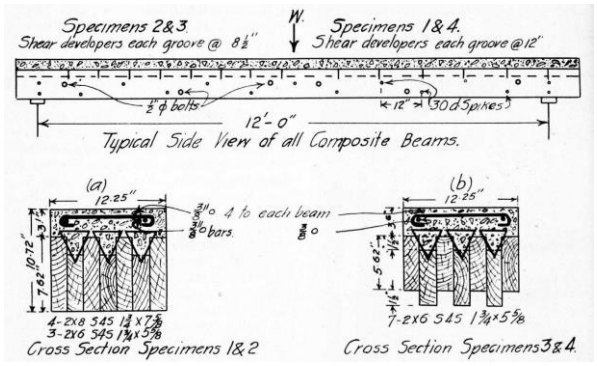

b) slab

Fig. 2 Connection systems tested in the United States in the 1930s: (a) T-beam; (b) slab [16, 17]

In the design and performance of TCC bridges, a key issue is the connection system, which has a direct influence on both the serviceability limit state (SLS) and the ultimate limit state (ULS). From early times, specific connection systems, such as steel spikes or notches, have been tested and used, and some traditional timber connection systems are still used today (Figure 2).

The type of connection used depends on the specific conditions and requirements of the bridge, usually low-demand structures can be designed with simple conventional connection systems, whereas high-demand structures require the use of high performance connections such as notches or notches combined with steel fasteners [18].

1.3 Reasons for Using TCC

The use of TCC for bridges was motivated by different reasons. Among those, some of the most relevant were connected to the need for rehabilitation and improvement of the existing timber bridges to allow their continuation in service or even to upgrade their load capacity because of new load requirements. The deck could be a new composite or a concrete deck overlaid on top of the existing nail-laminated deck, as was done for a large number of bridges in U.S. Route 66 (Figure 3).

Fig. 3 TCC bridge along US Route 66 in California

During the two world wars of the 20th century, large amounts of steel were consumed in the manufacture of armaments, leading to a significant scarcity of reinforcement steel required for a concrete deck superstructure. During that time, TCC systems were seen as an interesting alternative, because a good portion of the steel could be replaced by timber [15]. These motivations are in line with the number of bridges built and research efforts, which had a clear peak in this historic period.

Nowadays, the motivations to use TCC in bridges are slightly different, with aesthetic issues and sustainability considerations becoming increasingly important from the bridge owners perspective [19].

1.4 Research in the United States

The use of TCC bridges started as an upgrade of timber bridges. However, increasing demand for TCC bridges has raised many issues that need to be resolved to allow the wide use of this system for new construction. Timber and concrete have completely different short- and long-term technological behaviors. The basics of the design could be addressed using basic knowledge from the mechanics of

materials, but specific issues, such as the connections (Figure 2) or the long-term performance, could not.

This situation motivated the development of extensive research programs, conducted at different U.S. locations, all focusing on TCC for bridge applications. Among these are three research institutions that have attracted significant resources, which resulted in an important base of knowledge: University of Illinois-Champaign [20], Oregon State Highway Department [17], and George Washington University in Washington, DC, which focused on a patented system [4].

These early research efforts addressed different topics that were critical for the development of TCC systems, such as connection systems, composite effects, cyclic performance, friction between timber and concrete, and long-term performance of the composite. Collectively, these research efforts paved the way for the extensive use of TCC in bridges that has occurred since that time.

2. TCC Bridge Inventory

2.1 Locations

The discussion from this section is based on information provided by NBI from 2016 [21]. The total number of timber bridges still in service and codified as TCC in the United States is 1,644. Some bridges may appear in the database as TCC structures but were originally constructed as narrow timber stringer bridges and were later widened with concrete components to achieve double-lane roadways. These enlarged bridges that combine timber and concrete in a noncomposite manner are sometimes mistaken for true TCC bridges (Figure 4) within the NBI. Additional field bridge studies will help clarify these discrepancies in the future.

Fig. 4 Timber bridge enlarged with concrete members that has been wrongly codified as a TCC bridge

According to NBI, in 2016, TCC bridges were in service all over the United States, in a total of 33 states, from the North to the South as well as from the East to the West coast. The locations of all of these TCC bridges included in the inventory are plotted in Figure 5. It is not clear why these remaining TCC bridges are distributed in such a clustered fashion in so many regions of the United States. These regions may have been where large bridge construction efforts were undertaken to initially build the network of highways during the 20th century (Figure 6).

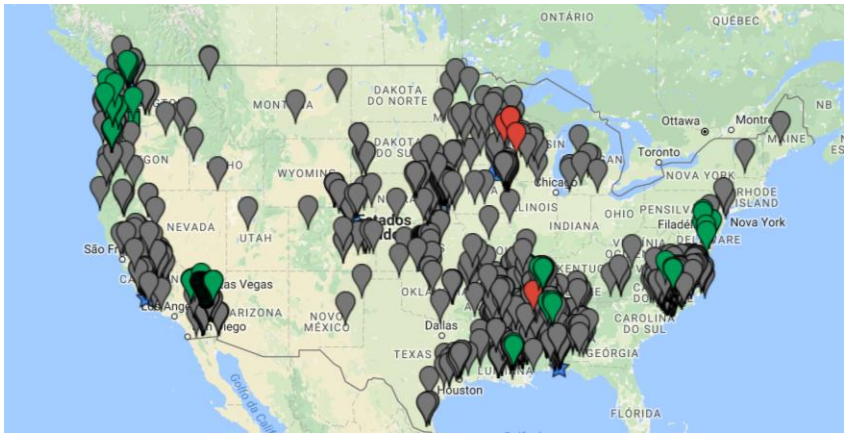

Fig. 5 Location of the timber–concrete composite highway bridges in the United States as reported in NBI (green – confirmed; red – not confirmed; grey – no information)

In addition to data mining of the NBI database, other searches focused on supplemental information from independent sources, such as bridge inspection reports or other relevant bibliographies [22–24]. This provided a method to confirm NBI data for a total of 98 bridges, of which an overwhelming majority (93 percent) were validated as being true TCC bridges.

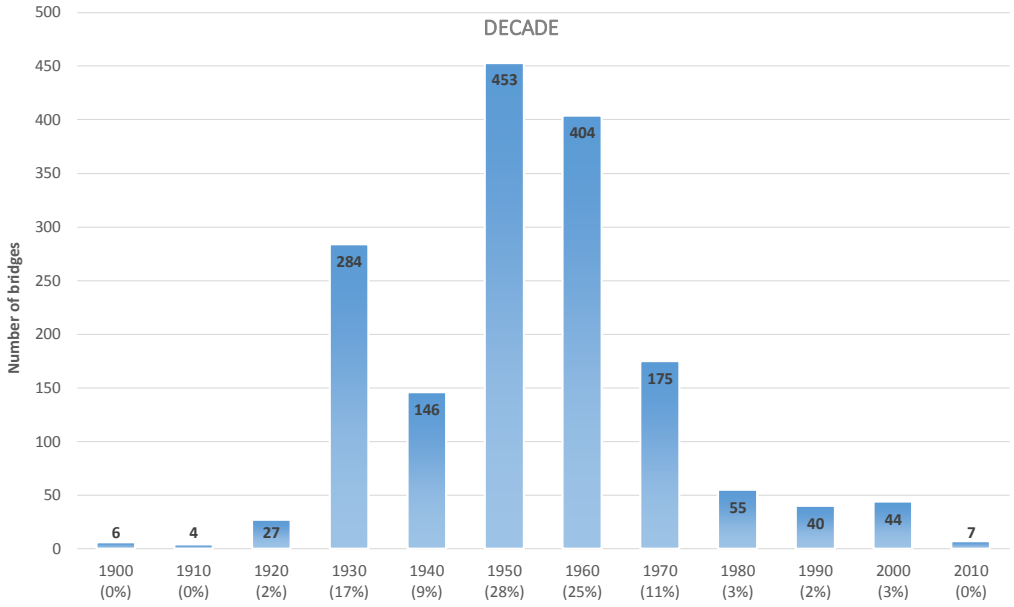

Fig. 6 Number of TCC bridge currently in service by construction decade

Figure 7 shows that in only 6 states, there are more than 100 bridges in service, whereas in 15 states there are less than 10 bridges. The state with a largest number of bridges is clearly North Carolina with close to 400 bridges, almost a quarter of the total number. Despite such a wide distribution of the TCC bridge within the United States, there are only a few hotspots with a high concentration of these structures still in service.

2.2 Date of Building

As previously mentioned, the TCC bridges started to be built in the early 20th century, and the information available indicates 1924 as the year of construction for the oldest TCC bridge. In the NBI, there are a few bridges built before the 1920s decade that were codified as TCC, but these were probably mistakenly entered into the NBI as being true TCC structures. One example is located in Rockford, Illinois, and was reportedly constructed in 1901. This bridge was inspected, and it was indeed a timber bridge but had a small concrete deck extension added later and had no signs of the TCC system (Figure 8).

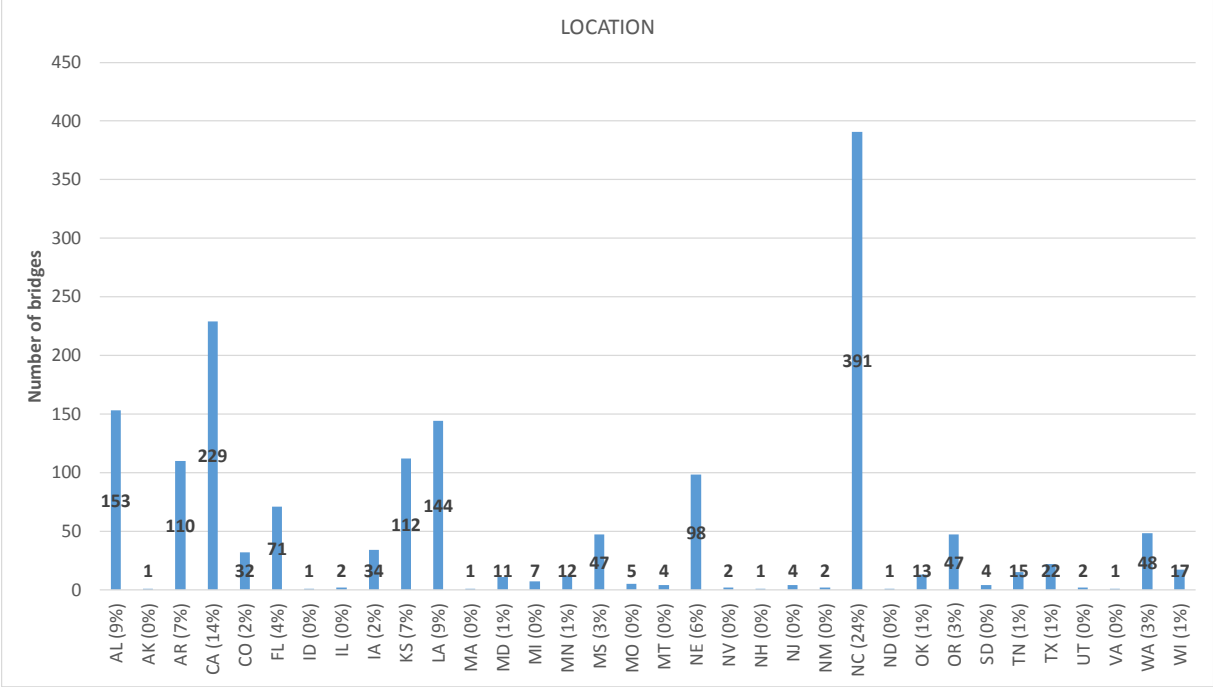

Fig. 7 Number of TCC bridges in service by state

Fig. 8 Bridge in Rockford, Illinois, built in 1901 codified in the NBI as TCC

Fig. 9 Modern TCC bridge built in Singbboet Slough, Washington

Analysis of TCC bridges by construction decade clearly shows that large-scale construction started in the 1930s with the large majority of the bridges being built by the 1970s (92%). In the early years, solid

timber T-beam sections and solid timber decks were primarily constructed. Beginning around 1950, newer engineered wood products (for example, glulam beams) started to be used, which allowed larger spans and new configurations [25].

Although most of the TCC bridges were built between 1930 and 1970, they were still built in more recent decades as well. Modern motivations and bridge characteristics are rather different, but the use of composite systems to improve mechanical performance and durability is still a driving wheel to the adoption of this bridge solution (Figure 9) [15].

2.3 Use and Configuration

Almost all TCC bridges in service are part of national highways, but there is also a small number of highway pedestrian or overpass structures as is shown in Figure 10.

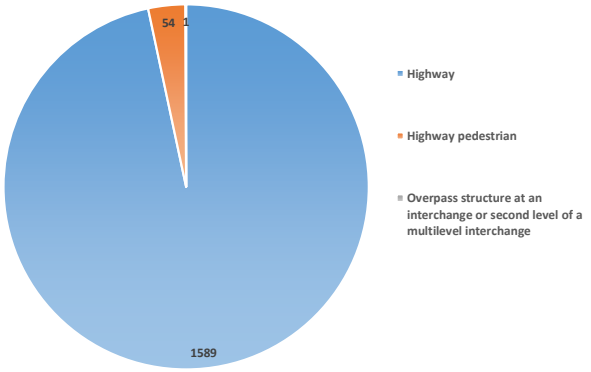

Fig. 10 Number of TCC bridges currently in service by type of use

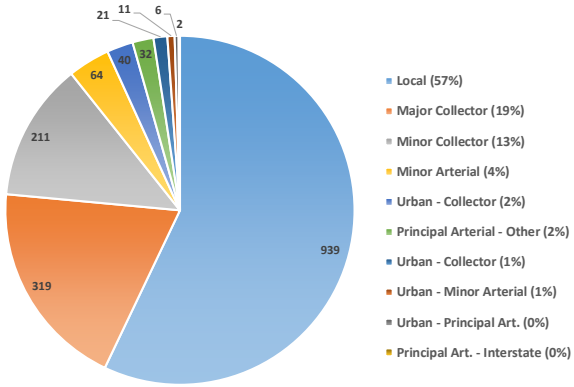

Fig. 11 Number of TCC bridges currently in service by functional class

Among the highway bridges, the large majority are in local, major collectors, and minor collectors (89%), leaving the other types, such as urban arterial and collectors, almost residual (Figure 11). This is well in line with the type of technical solution and motivations for the use of TCC bridges in the early literature. This information is consistent with the annual expected low volume of traffic for these bridges (Figure 12). Indeed, less than 10% of the bridges have an annual traffic count higher than 10 million vehicles.

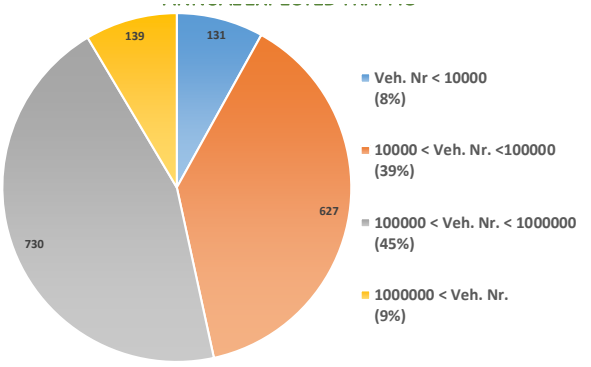

Fig. 12 Number of TCC bridges currently in service by annual traffic

Fig. 13 TCC bridge in a high traffic road, built in 1934 in the city of Portland, Oregon

In spite of this fact, it is important to mention bridges such as the Vermont viaducts in Portland (Figure 13) that carry an average daily traffic of 16,000 vehicles per day, have been in service for 83 years, and

are in good condition without significant intervention. This fact clearly shows that this type of bridge offers a robust and highly durable solution even in highly demanding traffic situations.

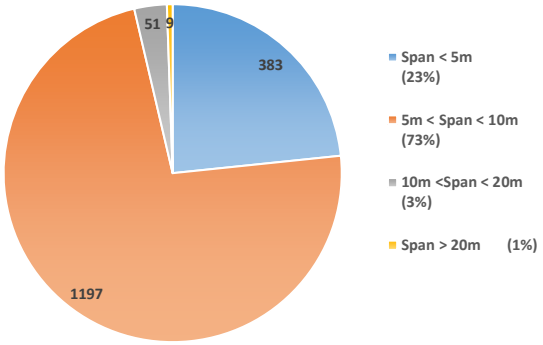

Fig. 14 Number of TCC bridge in service by maximum span length

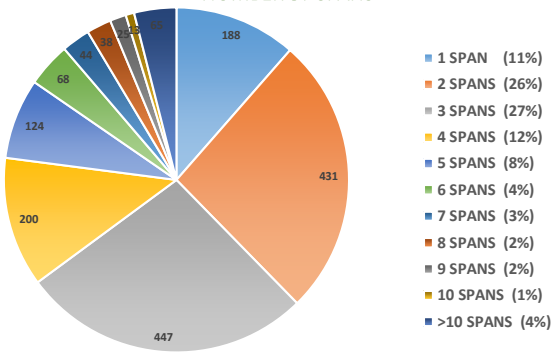

Fig. 15 Number of TCC bridge in service by number of spans

The large majority of the TCC bridges built in the United States are trestle-type bridges, being single spans and relatively short and being in many cases standard spans (around 5 m) (Figure 14). The larger total spans are possible to overcome through the use of multiple standard spans (Figure 15). The NBI indicates that almost two-thirds (65%) of TCC bridges have between 2 and 4 spans. According to the NBI, there are, however, 65 bridges that have more than 10 spans, which necessarily leads to long total span bridges. Indeed, the NBI indicates that there is a total of 80 bridges that have total length longer than 50 m, and the longest total span for a TCC bridge is reported to be 192 m.

3. Condition Rate

In the NBI, the condition of various bridge components must be inspected every 2 years, namely the deck, superstructure, and substructure. Figure 16 gives the TCC bridge conditions for these three components. According to the grading scale (where 1 denotes a failed bridge, and 9 denotes a brand new bridge), a condition rating 5 and above is considered to be good condition, whereas a condition rating of 4 and below indicates that there are structural deficiencies present that can compromise the normal use and safety of the bridge.

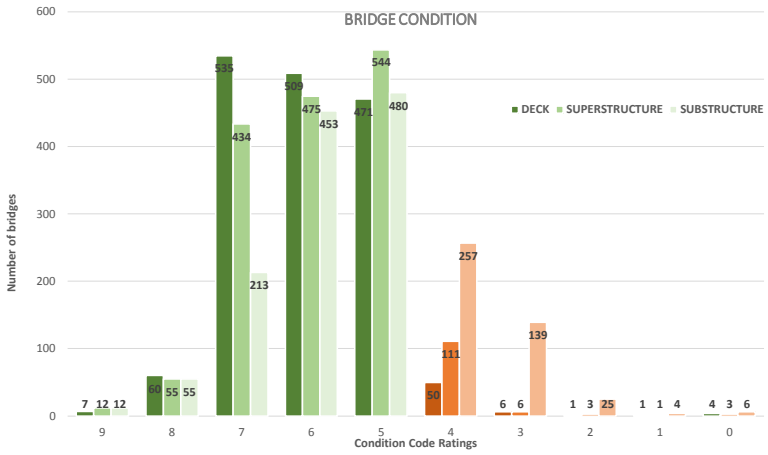

Fig. 16 Condition of TCC bridges in service according to NBI

According to the NBI condition ratings for TCC bridges, the large majority of the bridge superstructures are in good condition. The bridge deck condition ratings, where the composite system is

used, is the component with the highest ratings, whereas the substructure condition ratings are typically lower. This is not surprising because the deck is the component for which using TCC systems provides the largest benefit in durability, while the substructure, because of constant contact with soil and water, is the bridge component for which the TCC solution has the lowest impact in improving the overall bridge structure durability. Only a small percentage of the total number of TCC bridges in service have a deck condition rating lower than 5, indicating the great benefit of a properly designed concrete overhang detail toward the overall durability of a TCC bridge structure.

4. Conclusions

Construction of TCC bridges began in the early 20th century and have been a success story for nearly a century. Indeed, the NBI indicates the existence of a large number of these bridges in service today in the United States, with some in excess of 83 years old and located in in high traffic demand roadways. Evidence indicates that only minor repairs or rehabilitation efforts took place during the many decades in service, which demonstrates the robustness and durability of this structural solution for bridge construction. Many TCC bridges were inspected recently, and the findings confirmed their excellent condition after a long period of satisfactory service under high traffic demands.

On the other hand, it is clear from the inspections that good drainage detailing is critical to achieving a long service life with low maintenance costs. Poor detailing is clearly connected to higher degradation and, in many cases, early replacement of the bridge components.

The total number of TCC bridges that have been built in the United States is unknown. However, the large number of bridges still in service, under completely different service conditions — type of traffic, climatic conditions, daily amount of traffic, technological solutions (for example, connections, wood-based products, spans, and substructures) — constitute a live experimental batch in place for almost a century. The results available from these case studies prove that TCC bridges are a technical solution with great potential for bridge construction. The wide range of examples also prove that this technology was very useful in the past but also has enormous potential for use in the future.

5. Acknowledgements

The authors would like to thank the Fulbright program for the financial support that supported a travel scholarship to FPL during which the field work was carried out.

Valuable assistance in conducting field bridge inspections was provided by Dave Strahl of the U.S. Forest Service and numerous county engineers in the states of Oregon and Washington.

This work was partly financed by FEDER funds through the Competitiveness Factors Operational Programme - COMPETE and by national funds through FST – Foundation for Science and Technology within the scope of the project POCI-01-0145-FEDER-007633.

6. References

[1]. Cook J.P., *Composite Construction Methods*, in *J. Const. Division*. 1976, ASCE. pp. 21-27.

[2]. Richart F.E., and Williams C.B., "Tests of composite timber-concrete beams", *J. American Concrete Inst.* 1943, pp. 253-276.

[3]. Van der Linden M.L.R., *Timber-concrete composite floor systems.* Delft Univ. of Technology, Delft, Netherlands, 1999.

[4]. DelDOT, *Delaware's Historic Bridges.* Delaware Department of Transportation Division of Highways, 2000.

[5]. Duwadi S.R., and Ritter M.A., "Timber Bridges In The United States", in *Public Roads,* Federal Highway Administration, 1997, pp. 32-40.
[6]. Cone C.M., "A Composite Timber-Concrete Bridge", in *TDA Bulletin,* 1963.
[7]. Nolan G., *Experience with Concrete Overlayed Bridges in Tasmania,* http://oak.arch.utas.edu.au/research/bridge/sem2.asp,Nov. 18, 2009.
[8]. Aasheim E., *Development of Timber Bridges in the Nordic Countries*. Vancouver, BC, 2000.
[9]. Natterer J., Herzog T., and Volz M., *Built in Timber 2*. Presses Polytechniques et Universitaires Romandes, Lausanne, Switzerland [in French], 1998.
[10]. Natterer J., *Tendencies in Bridge Construction*, Montreux, Switzerland,1998.
[11]. Flach M., and Frenette C.D., *Wood-Concrete-Composite-Technology in Bridge Construction,* Lahti, Finland, 2004.
[12]. Pischl R., and Schickhofer G., "The Mur River Wooden Bridge, Austria", in *Struct. Eng. Inter.* IABSE, 1993, pp. 217-219.
[13]. Calil Jr. C., *Brazilian Handbook for the Design and Construction of Timber Bridges,* Miyazaki, Japan, 2008.
[14]. Schanack F., *Influence of Concrete Cracking on Wood Concrete Composite Bridges.* Las Vegas, NV, 2013.
[15]. Rodrigues J.N.A., Dias A.M.P.G., and Providência P.M.P., Timber-Concrete Composite Bridges: State-of-the-Art Review, *BioResources*, 2013.
[16]. Seiler J.F., New Type of Composite Beam, *Wood Preserving News*, XI(11), 1933.
[17]. McCullough C.B., Oregon Tests on Composite (Timber-Concrete) Beams, *Journal of the American Concrete Institute*, Vol. 14, No. 5, 1943, pp. 429-440.
[18]. Rodrigues J.N.A., "Pontes com estrutura mista madeira-betão em Portugal: Concepção, construção e sustentabiulidade", in *Universidade de Coimbra*, University of Coimbra, Coimbra, 2015.
[19]. Rodrigues J.N.A., "Pontes Com Estrutura Mista Madeira-Betão Em Portugal: Concepção, Construção E Sustentabilidade", in *Universidade de Coimbra*. Departamento de Engenharia Civil, Coimbra, 2015.
[20]. Richart F.E., and Williams C.B., "Tests of Composite Timber And Concrete Beams", *Universty of Illinois Bulletin,* Vol. 40, No. 38, 1943, p. 62.
[21]. DTFHA, *National Bridge Inventory (BBI)*. DTFHA, 2016.
[22]. SBC. *San Bernardino County (CA) - Department of Public Works*. http://cms.sbcounty.gov/dpw/Transportation.aspx, 2016.
[23]. Wacker J.P., et al., *Service Life Assessment of Timber Highway Bridges in USA Climate Zones,* Quebec City, Canada, 2014.
[24]. MHT, *Inspection Reports: MD-300; K-681, D-724;WI-224; WO-491*, Maryland Historical Trust, 2001.
[25]. Press T., *Rigid Specifications Mark Bridge Jobs for Forest Service.* Portland, Oregon Timber Structures, Inc., Vol. 3, No. 4, 1953.

Design of wood-concrete composite beams under deck bridge – Theoretical developments and construction examples

RENAUDIN Fabien
Head of Bridges Division
Cerema Est
Metz, France
fabien.renaudin@cerema.fr

21 years' professional experience in the field of diagnosis and calculation of structures. Development of methodology on design, diagnosis and management of structures. Award-winning of AFGC price 2015

JANDIN Philippe
Project Director
Cerema ITM
Sourdun, FRANCE
Philippe.jandin@cerema.fr

29 years' professional experience in the field of diagnosis, calculation and bridges management. Development of methodology on the design of structures and new technologies or materials for bridge design.

Summary

Long ago forgotten, wood must find again all its place in the field of construction, especially in bridges. In France, a design guide is being drafting to propose a design of road bridge associating wood and concrete in a composite behaviour, via a mechanical connection. It also constitutes an implementation guide of Eurocode 5 for the justification of the wood sections and the wood/concrete connection. Composite behaviour offers the characteristic to be assured by a connection that, with usually technologies employed, authorizes a relative displacement of materials at their interface. This behaviour is rather atypical in civil engineering structures and it appeared useful to formalize the laws of behaviour that describe this kind of composite beam. Analytical and truss-girder models are made to determine internal efforts in materials, according to the rigidity of connection. At least, three recent constructions inspired by the studies of the working group are described.

Keywords: bridge, composite, concrete, wood, connection, analytical model, examples.

1. New concept: low carbon consumption bridge

1.1 Wood in France

With 16.7 million hectares of forests, in progress of 0.7% per year in the last 30 years, France is the third country in Europe following Sweden and Finland [1]. French forest is majority private-owned (75%) and is mainly deciduous (67%) [1]. Wood industry represents about 440,000 direct and indirect jobs and an annual turnover of 60 billion euros. If wood is more and more used as a construction material for buildings (new or rehabilitation), it is still superseded by concrete or steel in bridges construction.

1.2 Timber bridges in France

In the 1990s and the 2000s, several timber road bridges have been built in France. Some examples are:

- the bridge on the Dore river (Fig. 1), located in Auvergne built in 1994;
- the Merle bridge (Fig. 2), located in Limousin; structure is a timber frame with a non-

connected concrete deck (1999);

- the Crest bridge (Fig. 3), located in Rhônes-Alpes; the longest timber bridge with 92m long (2001);
- the Avoudrey bridge (Fig. 4), located in Franche-Comté, built in 2005.

Fig. 1 Bridge on the Dore river

Fig. 2 Merle bridge

Fig. 3 Crest bridge

Fig. 4 Avoudrey bridge

All these bridges have unique design and contain many fasteners and humidity exposed surfaces. Development of timber bridges in France cannot only lie on such architectural designs that requires heavier ongoing monitoring and maintenance than common structures.

1.3 Presentation of the Cerema concept

At the end of 2000s, Setra created a working group in order to promote the development of timber bridges construction in France by giving to the different actors (building owners, project managers, engineering consultants and building companies) all the necessary tools for a perfect design and sustainable structures. The working group immediately approved the choice of simplicity with wood beams connected to a concrete slab and set the following goals: design a typical wood bridge, completely calculated with Eurocodes and at a competitive cost.

1.3.1 Cross section

The deck is a composite wood/concrete structure made up with longitudinal wood ribs, connected with concrete slab and without any bracing (Fig. 5 & 6).

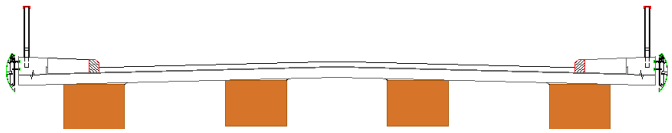

Fig. 5 Cross section

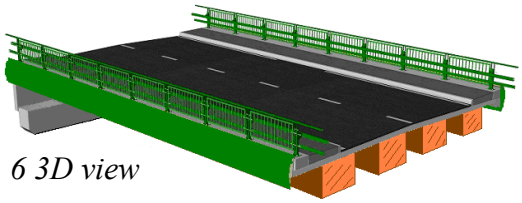

Fig. 6 3D view

The scope of use is one span bridges with a range
from 10 to 20m, for road bridges above rivers or other roads. Bridges of a total length of 35 to 40m with two continuous spans are also achievable. Concrete slab has a good compressive strength and ensure protection of the wood frame from bad weather. The length of the slab's overhangs must be equal or above the height of wood ribs. The slenderness ratio of wood ribs is about 1/15° to 1/18°. Therefore, ribs' height is about 1m to 1.20m. Their number depends on the deck width (from 2 ribs for 6m deck width to 5 ribs for 14m deck width). The ribs are block-glued glulam made with 4 to 5 glued laminated girders according to French standard NF EN 14080:2013 [2], so that perimeter exposed to humidity is divided by 4. This provides high torsion stability, better loads spreading into wood, better impact resistance and no bracing at all.

1.3.2 Deck's end

Deck's end has been designed as a semi-integral abutment (Fig. 7) so that wood ribs are fully protected against water leaking by expansion joints. This design also enables:

- to locally strengthen slab against heavy trucks arriving on bridge;
- to transmit the lateral forces applied on the deck to the bearings (wind and seismic effects);
- to eliminate assemblies between support beams and a potential end cross-beam.

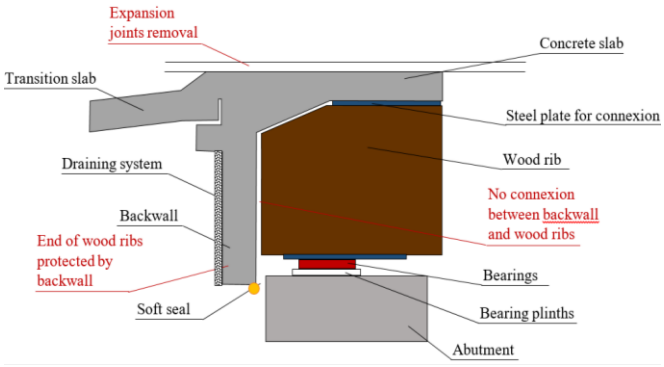

Fig. 7 Semi-integral abutment

1.3.3 Connection

Connection between concrete slab and timber ribs (Fig. 8 & 9) consists in three elements: studs, steel plates and screws. Studs generally have a 16mm diameter and are designed according Eurocode 4 [3]. Studs are welded on a steel plate with a thickness greater than external screws diameter. Screws are designed according to Eurocode 5 [4].

Fig. 8 View of studs welded on steel plate with screws before screwing

Fig. 9 View of connection after screwing

2. New concept: low carbon consumption bridge

2.1 General principles

The justifications for dimensioning this wood/concrete composite bridge concept are based on the formalism of Eurocodes and in particular of Eurocode 5. Because of the choices made for the construction layouts (in particular the protection brought by the overhang and the semi-integral abutment), wood can generally be affected in use class 2 according to standard NF EN 335 [5]. This represents most of cases for bridge built in Metropolitan France. Wood is affected to service class 2 according to standard NF EN 1995-1-1, when its average moisture is stabilized from 13 to 20%.

The principal checks specific to such a bridge concern:

- justifications of the composite sections under positive bending moment (bottom tension fibre) where wood works in bending and traction;
- justifications, if necessary, of composite sections under negative bending moment at support (top tension fibre) where wood works in bending and compression; in these sections, concrete is cracked in the global analysis model and the reinforcement bars contribute to the mechanical resistance;
- justifications under shear force and torsion in wooden beams;
- wood's justification with respect to transverse compression on support; this justification is made either according to the recommendations of technical approvals of the products or in reference to the literature on subject [6];

- justifications of shear connection.

Wood-concrete connection ensured by a mechanical system generally authorizes a relative displacement at the material's interface. It is called a partial connection and its rigidity affects the efforts distribution in materials. So, it must be considered for the justification of connection itself.

Appendix B (informative) of standard NF EN 1995-1-1 [4] suggests a solution (known under the name of Heimeshoff solution) in the case of a load applied to a composite isostatic beam with partial connection generating one moment that varies in a sinusoidal or parabolic way. It nevertheless appeared useful to formalize the constitutive laws for different static diagrams of structures and for more general cases of loading, and then for developing an adapted mechanical model. These developments are successively presented in the following chapters.

2.2 Analytical model of behaviour of a composite section with partial connection

We consider a beam made up of two different materials linked by a partial connection and subjected to load which generate bending (Fig. 10).

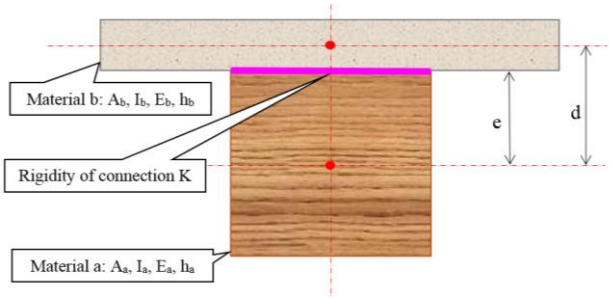

A is the section, I the inertia, E the elasticity module, h the height of each element

d is the distance between the centres of gravity of the two materials;

e is the distance between the centre of gravity of the section of "a" material and the interface between the two sections

Fig. 10 Characteristic parameters of a composite section with a partial connection

This beam undergoes bending moment. We consider a beam section at a distance X from left support (Fig. 11). This section is subject to an internal bending and normal forces in the two materials (Fig. 12).

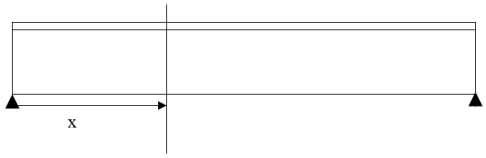

Fig. 11 Location of a section within an isostatic beam subjected to bending

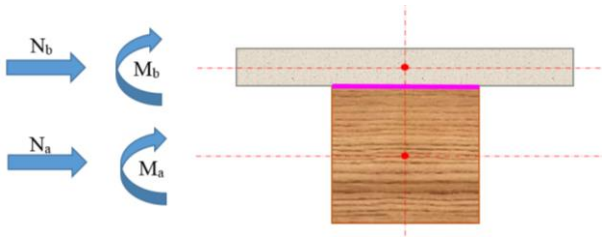

N_a, M_a: respectively normal force and moment interns of material a

N_b, M_b: respectively normal force and moment interns of material b

Fig. 12 Internal forces in the section

With a single external bending moment, the equilibrium conditions of the section are as follows:

- condition 1: zero-sum of forces;
- condition 2: zero-sum of bending moments;
- condition 3: curvature is the same for the two elements (Navier assumption);
- condition 4: at the interface of the two materials, a longitudinal slip appears in link with the stiffness of connection K and the normal force transmitted N by this interface.

Given these conditions, the differential equation (1) governing the normal effort N(x) in the centre of gravity of the "b" element (equal in absolute value to the normal effort in the centre of gravity of "a" element) is written in the following form:

$$\frac{\partial^2 N}{\partial x^2} - AN = -BM \qquad (1)$$

where:

$$A = K\left[\frac{1}{E_a A_a} + \frac{1}{E_b A_b} + \frac{d^2}{(E_a I_a + E_b I_b)}\right] \quad (2)$$

$$B = \frac{Kd}{[E_a I_a + E_b I_b]} \quad (3)$$

and M = M(x), bending moment in the section with X-coordinate x of the beam.

Instead of external moment bending imposed, it is possible to consider the case of a deformation imposed by one of two materials, such as for example concrete's shrinkage or temperature variations effect with materials having different expansion coefficients. The four equilibrium conditions in the section provide following differential equation:

$$\frac{\partial^2 N}{\partial x^2} - AN = K\varepsilon \quad (4)$$

where ε is "b" element internal deformation.

In case of indeterminate structure (continuous spans), restraint deformation of the structure, as a result of imposed deformation, leads to indeterminate support reactions, therefore to one indeterminate bending moment M.

The differential equation (4) becomes:

$$\frac{\partial^2 N}{\partial x^2} - AN = K\varepsilon - BM \quad (5)$$

The table below gives the form of the solution describing the normal effort N(x) in the case of an isostatic beam with one span (Fig. 13) subjected to a load uniformly distributed or an imposed deformation of the material "b".

Uniformly distributed load	Imposed deformation of material "b"
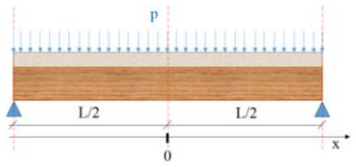	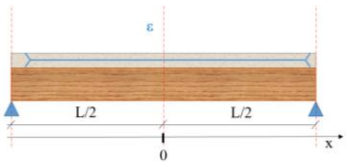
$N(x) = \frac{Bp}{A}\left[-\frac{x^2}{2} + \left(\frac{L^2}{8} - \frac{1}{8}\right) + \frac{ch(\sqrt{A}.x)}{A.ch(\sqrt{A}.\frac{L}{2})}\right]$ (6)	$N(x) = \frac{-K.\varepsilon}{A}\left[1 - \frac{ch(\sqrt{A}.x)}{ch(\sqrt{A}.\frac{L}{2})}\right]$ (7)

Fig. 13 Solutions in the case of one isostatic span

The solutions in the case of two continuous equal spans were also developed.

2.3 Truss-girder model of a composite beam with partial connection

A truss-girder model with vertical stems has been developed to integrate a connection rigidity variation along the beam. It is also possible to modify this rigidity according to the connection load level. This modification involves the definition of a nonlinear constitutive law of the connection (Fig. 14) and a certain ductility of connection (Fig 15). The constitutive law can be given using push-out tests in laboratory [7], [8], [9].

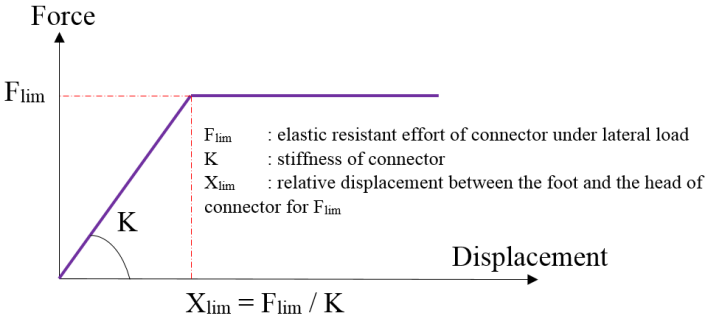

Fig. 14 Nonlinear elastoplastic law modelling the stiffness of connection

Fig. 15 Ductility due to the formation of 2 plastic hinging on the stem of the screws [9]

Concrete slab and wooden beam constitute the two strands of the ladder. The ladder rungs are the connection; their concrete side end is hinged (Fig. 16). To simulate connection stiffness, shear resistant area of the rungs is given the adequate characteristic, normal section and inertia being taken with very large values.

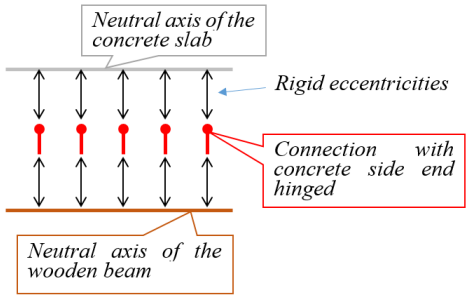

Fig. 16 Principle of the model of the lattice beam

The model takes into account connection rigidity by adapting the shear resistant area of the connection bars. Indeed, the shear strain δ at the top of a beam of length L, embedded at its base and subjected to a force F, is given by:

$$\delta = \frac{F.L}{G.S_y} \tag{8}$$

where G is the shear modulus of material and S_y the shear resistance area.

2.4 Applications to simple cases

The comparison of the two models (analytic and truss-girder) shows a perfect identity of the results on simple cases.

For illustration, we give hereafter the graphic curve of the connection deformations obtained with the truss-girder model of a two continuous spans equal 15 m length. Cracked concrete slab is not considered here. Figure 17 shows section characteristics. Figure 18 gives strains in the case of uniformly distributed load and figure 19 shows strains due to concrete shrinkage.

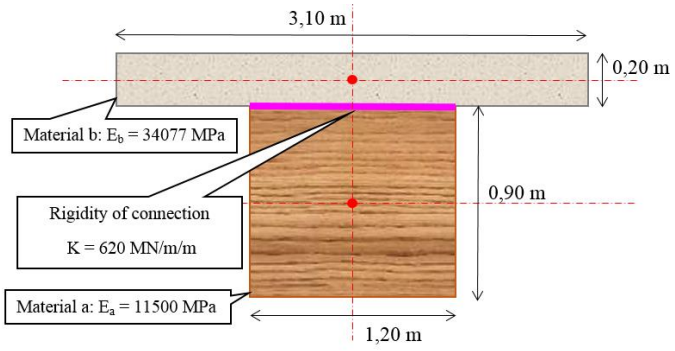

Fig. 17 Characteristic of the studied beam

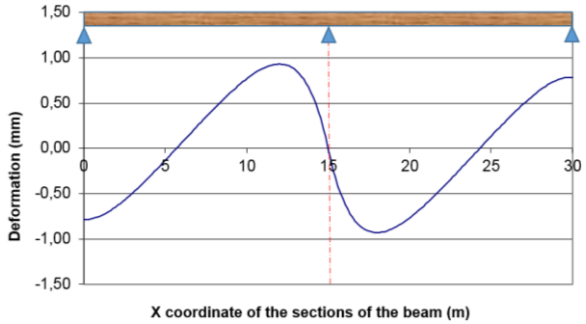

Fig. 18 Deformation of connection – Continued beam on two supports – Uniformly distributed load p=0,1 MN/m

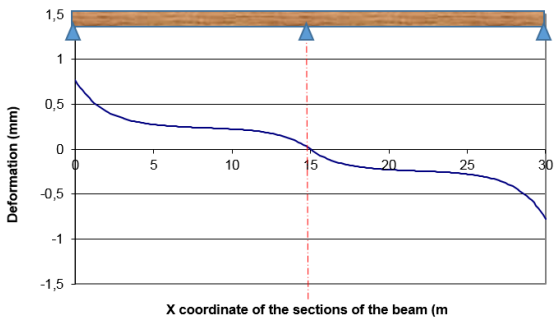

Fig. 19 Deformation of connection – Continued beam on two supports – Shrinkage of concrete $\varepsilon = -3.10^{-4}$

3. Construction examples

We present here three examples of wood-concrete composite bridges, with a mechanical connection, recently built in France, based on the concept presented at the paragraph 1.3. and for which Cerema brought its technical assistance.

3.1 Riou Valley Bridge

The companies Campenon Bernard and Arbonis built the bridge upon the small valley of the Riou near Lantosque in 2015, under the project management of Nice Côte d'Azur Metropole. The bridge carries a metropolitan road with one traffic lane. The deck presents a span of 13 m long for a total width of 6.13 m. It consists of 4 Douglas glulam ribs under the slab (Fig. 20). Each rib has a section of 0.82 m (w) x 0.90 m (h) and is made of 4 glulam beams of 20.5 cm width. Ribs received a protective treatment and a wood stain.

Fig. 20 View of the 4 girders

Connection consists of steel plates 190 mm x 346 mm in plan and 12 mm thick, positioned in reserved spaces dug in beams (Fig. 21). 16 mm diameter studs (6 studs per plate) are welded to superior faces of steel plates, which are bonded to the beams with WURTH VG 12 mm x 140 mm, screws (28 screws per plate). Beams rest on reinforced elastomeric bearings. Beam supports are strengthened with grill of reinforcing screws (SFS WR T 13 500 mm length). A crane placed the ribs on the abutments. There is no bracing at all between ribs. Slab is made of C35 concrete precast segments (Fig. 22), with a thickness of 25 cm. Each segment has four slab connection recesses where studs are concentrated.

Fig. 21 Reserved spaces dug in beam

Fig. 22 Precast segments for the slab

3.2 Cognin bridge

The companies Eiffage and Pierrefeu built the bridge upon the Hyeres River in Cognin in 2015 under the project management of Chambéry Métropole. Bonnard and Gardel design office was project manager for construction works, based on the project designed by the consulting engineer CBS. The bridge carries a secondary road with two traffic lanes and a wide cycle track. The deck presents 3 continuous spans, respectively 9, 19 and 10 m length, for a total width of 12.74 m (Fig. 23). It consists of nine glued laminated ribs in Douglas under the slab (Fig. 24) whose section is 0.54 m (w) x 1.00 m (h). Each rib is made of three glulam beams, 18 cm wide each. Ribs received a protective treatment and a wood stain.

Fig. 23 Lateral view of bridge

Fig. 24 Intrados view of deck

Connection (Fig. 25) is made of steel plates (200 mm x 400 mm in plan and 10 mm thick). Studs 19 mm in diameter (4 or 5 studs per plate depending on areas) are welded to superior faces of steel plates which are bonded to the beams with SFS WR T 13 mm x 400 mm screws (20 to 23 screws per plate depending on the areas). A crane put ribs in place, braced together on every support axis (Fig. 26). They rest on reinforced elastomeric bearings and their support zones are strengthened with grill of reinforcing SFS WR T 13, 500 mm length screws on abutments and 600 mm length on piers.

Fig. 25 Beams with metal plates for connection

Normal concrete class C35 is used for the reinforced slab, 25 cm thick, cast-in-place on sacrificial wood formworks (Fig. 27). The beams are supported by semi-integral abutments with hinged transition slab.

Fig. 26 Bracing on pier

Fig. 27 Casting of the slab

3.3 Large wildlife bridge on RN19

The PS12 over RN19 in Lure was built by the companies Eiffage and Arbonis in 2017 under the project management of "Direction Régionale de l'Environnement de l'Aménagement et du Logement de Bourgogne - Franche-Comté". "Direction Interdépartementale des Routes Est" was project manager for construction works. The bridge spans a forest path and assures ecological continuity for large animals. The deck presents 2 continuous spans 15 m length each for a total width of 12.60 m. It consists of four glued laminated ribs in Douglas under the slab whose section is 1.20 m (w) x 1.00 m (h). Each rib (Fig. 28), 31.40 m length, is made of 6 glulam beams 20 cm wide (Fig. 29). Beams received a protective treatment and a wood stain.

Fig. 28 Beam in workshop

Fig. 29 Gluing of the little beams

Connection (Fig. 30) is made of steel plates (550 mm x 550 mm in plan and 10 mm thick). Studs 16 mm in diameter (9 studs per plate) are welded to superior faces of metal plates which are bonded to the beams with ROTHOBLASS HBS 12 mm x 160 to 320 mm screws (66 screws per plate).

Fig. 30 Girder with connection

Beams are put in place with a crane (Fig. 31), without any bracing. They rest on reinforced elastomeric bearings (Fig. 32) and their support zones are strengthened with grill of reinforcing screws (SFS WR T 13, 600 mm length). Normal concrete class C35 is used for reinforced slab, 20 cm thick, cast-in-place on general shoring supporting wood ribs too. Ribs are supported by semi-integral abutments.

Fig. 31 Beams being put in place with the crane

Fig. 32 Support plates and reinforced elastomeric bearings

4. Conclusions

Wood is a natural material with very interesting mechanical characteristics. It must find in the field of construction all its place, and especially in the field of road bridges.

In this context, Cerema is working on the drafting of a guide for the design of a wood-concrete composite bridge with a mechanical connection. The aim is to help the designer at all stages of the project from the general design to the detailed design. To make reliable the good constructive dispositions that govern a sustainable structure, the guide is based on experiments made during the construction of real works

Beyond allowing a composite behaviour, the advantage of the connection is to ensure the durability at the interface between the two materials. The connection system must be sufficiently flexible and ductile to dampen the anchoring of the imposed deformations and to allow redistributions.

The periodic monitoring of newly constructed structures may, if necessary, lead to proposals for amendments or additions.

5. Acknowledgements

The authors would like to thank the members of the working group (V. Brun and P. Corfdir: Cerema, C. Douthe, Th. Kretz and R. L Roy: Ifsttar, JF. Boquet: Enstib), the contractors and partners (Nice Côte d'Azur Métropole, Chambéry metropole, DREAL Bourgogne Franché-Comté, DIR Est, BG, CBS) and the associated companies (Pierrefeu and Sibsolutions its design office, Arbonis, Eiffage).

6. References

[1] Institut national de l'information géographique et forestière (IGN), *Le Mémento – Inventaire Forestier*, édition 2016, 29 pp.NF EN 14080:2013 – Timber structures – Glued laminated timber and glued solid timber – Requirements.

[2] NF EN 14080:2013 – Timber structures – Glued laminated timber and glued solid timber – Requirements.

[3] Eurocode 4 – Design of composite steel and concrete structures.

[4] Eurocode 5 – Design of timber structures.

[5] NF EN 335 – Durability of wood and wood-based products. Use classes: definitions, application to solid wood and wood-based products

[6] Bejtka I. – Blaß H.J. (August 2006), Lehrstuhl für Ingenieurholzbau und Baukonstruktionen Self-tapping screws as reinforcements in beam supports —– *Meeting thirty-nine – Florence – Italy*.

[7] Blonski A., (2009) Etude de la rigidité de systèmes de connexion pour un pont type bois-béton - *Rapport de PFE, école des Ponts Paris-Tech – Jean Müller International*.

[8] Douthe C. (2013) - Rapport d'essai, essais de fatigue de connexion bois – béton - *Rapport Ifsttar.*

[9] Le Roy R. (2014) - Rapport d'essai, essais de cisaillement sur éprouvette de type push out - *Rapport Ifsttar*.

Short-term analysis of timber-concrete composite bridges

Joonas Jaaranen
Doctoral Candidate
Aalto University
Espoo, Finland
joonas.jaaranen@aalto.fi

Joonas Jaaranen received his M.Sc. degree from Aalto University in 2016. He continues his studies pursuing doctoral degree in Aalto University concentrating in timber structures.

Lauri Salokangas
University Teacher
Aalto University
Espoo, Finland
lauri.salokangas@aalto.fi

Dipl.Eng. 1981. 1986-2007 Lab. Man. in Bridge Engineering at Helsinki University of Technology 2008-2013 Prof. of Bridge Engineering, Infra-structures and Structural Design. From 2014 lecturer at Aalto University.

Gerhard Fink
Assistant Professor
Aalto University
Espoo, Finland
gerhard.fink@aalto.fi

Gerhard Fink is Assistant Professor for Wooden Structures at Aalto University. He studied Civil Engineering at the TU Graz, Austria and did his PhD at ETH Zurich.

Summary

Timber-concrete composite (TCC) structures have been studied intensively during the last decades and some analysis methods has been proposed, but mostly for floor construction. Applicability of different analysis methods for TCC bridge design were evaluated in a parametric study. In the evaluation, the influence of the parameters on the deformation, shear force in the connector, compressive stresses in the concrete deck and tensile stresses in the timber beam were investigated. The study was performed on a simply supported TCC beam, with span of 18 m, and with following parameters: different loads, connector arrangements, connector stiffnesses and cross-sectional dimensions. The results indicate large differences between the evaluated methods, in particular for beams with relatively low connector stiffness.

Keywords: timber-concrete composite, bridges, structural analysis, composite beam.

1. Introduction

Reliable design methods are important for ensuring safety and serviceability of bridges. However, Eurocodes currently do not present guidelines for the design of timber-concrete composite (TCC) buildings or bridges. Some rules of thumb for TCC bridges are given in national guidelines, e.g. Finnish NCCI5 [1], but they are too limited for detailed analysis. TCC bridges were researched in Finland in the 90's, producing new connector types, bridge concepts and some guidelines [2]. Similar research projects on TCC bridges have been carried out in other countries. TCC structures in general have been studied quite intensively in past few decades, thus some validated simplified analysis methods have been proposed, but mainly for floor structures [3]. Purpose of the published study was to investigate applicability of the existing analysis methods for design of TCC beams and the results were used in the paper by Jaaranen et al. [4].

2. Structural behavior of TCC beam

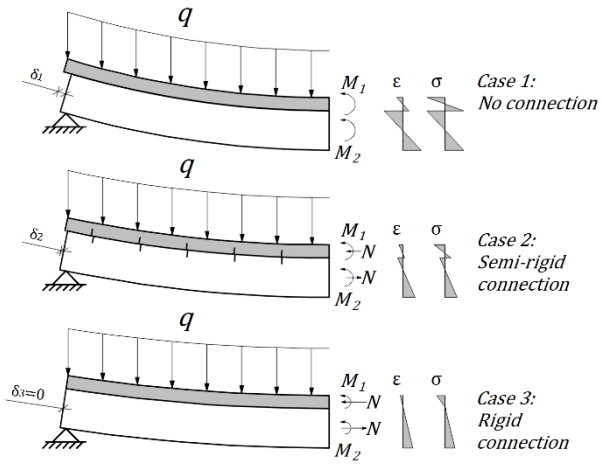

Figure 1. Deformations, internal forces, strains and stresses of a composite beam with different type of shear connection.

A typical TCC beam consists of timber section with concrete slab connected on top by shear connectors. In the case of simple supported beam, timber is in tension and concrete in compression, utilizing the best properties of both materials. Effects of shear connection stiffness on the beam behavior can be illustrated by considering three different Cases (Figure 1):

Case 1. no shear connection
Case 2. flexible shear connection
Case 3. rigid shear connection.

In the Case 1, slip between the components is not resisted by the connection and shear flow will not develop. In the Case 3, the beam is fully composite, with no slip, thus maximum shear flow will develop. In the Case 2, slip can happen, but at the same time shear flow develops due to connectors resisting the slip. Since the connection stiffness can vary between Cases 1 and 3, those Cases present bounds for the bending stiffness and stresses of the beam with flexible connection.

Degree of composite action is defined in this paper by connection efficiency factor γ, as in Eq. (1) [5], where $(EI)_{eff}$, $(EI)_0$ and $(EI)_\infty$ are bending stiffnesses of: a beam with flexible connection, a beam with no shear connection and a beam with rigid connection, respectively.

$$\gamma = \frac{(EI)_{eff} - (EI)_0}{(EI)_\infty - (EI)_0}, \tag{1}$$

3. Analysis methods of TCC beams

In this chapter, four different analysis methods applicable for analysis of TCC beam, namely, (1) fully composite method, (2) continuous flexible connection (CFC) method, (3) γ-method and (4) discrete flexible connection (DFC) method, are introduced.

3.1 Fully composite method

The simplest way to analyze a TCC beam is to assume that the connection is smeared and rigid corresponding to the Case 3. Then the beam can be analyzed by using Euler-Bernoulli (E-B) beam theory.

3.2 Continuous flexible connection method

For more detailed analysis, effects of the shear slip between elements need to be taken into account. One such method, commonly found in literature, is described e.g. in [6, 7]. The model is based on the assumption that the elements are connected by close and equally spaced linearly elastic shear connectors. The connection is treated as smeared connection with constant shear stiffness per unit length. The shear flow in the interlayer is then linearly dependent of the slip between the components along the beam. Individual elements of the beam are assumed to be linearly elastic and behave according to E-B beam theory.

The mathematical model for composite beams is derived by writing static equilibrium of internal and external forces of a beam element and then applying kinematics of E-B beam theory and linear load-slip relation of the connection, leading to a system of three differential equations. The system is then solved by applying boundary and load conditions. However, closed form solution can be found only in special cases. Detailed treatment on the topic can be found in [6, 7, 8]. For this paper, solutions for simply supported beams under uniform and concentrated loads, adopted from Natterer & Hoeft [8], were used.

3.3 γ-method

In the case of sinusoidal load on a simply supported beam, the CFC model has a particularly simple solution, in which bending stiffness is constant along the whole span leading to simple expressions of deformations and stresses. The γ-method is an approximate method, in which effects of other load types are approximated using the bending stiffness derived for the sinusoidal load [7]. Due to the simplifications, the method is exact only under sinusoidal load. In the other cases, the accuracy depends on type of the load, cross-section properties, connection stiffness and the span of the beam.

The method is adopted in EN 1995-1-1, Annex B, where relevant formulas are given. The use is restricted to simply supported, cantilever or continuous beams with components continuous over the whole length and connected by linear elastic connectors, whose spacing is constant or varies according the shear force. This method should be used only for sinusoidal and uniform loads. In the case of varying connector spacing, effective connector spacing s_{ef} according to [7] may be used.

3.4 Discrete flexible connection method

Composite beams can be also analyzed by considering the behavior of individual connectors as in the model proposed in [9, 10]. In both, the authors have treated only simply supported beams. In the [10] it is suggested that the approach can be extended to multi-span systems, and briefly explained how inelastic strains can be included in the analysis. A model with the suggested extensions was derived in this study.

In this method, including the extensions, the composite beam is assumed to consist of two individual beams, connected by arbitrary number of arbitrarily placed shear connectors each with individual slip modulus. Both elements are assumed to follow E-B beam theory and have equal deflections and curvatures.

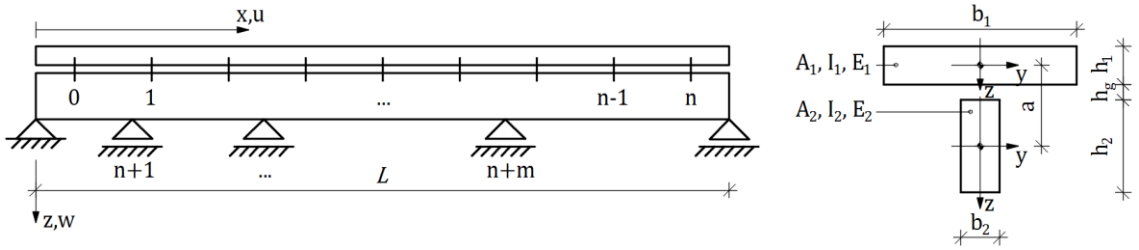

Figure 2. Model and cross-section of a composite beam in the discrete flexible connection method.

The model and the cross-section of the beam is shown in Figure 2. In the general case, the beam is an externally and internally statically indeterminate system. Response to loads is obtained by applying the force method, in which the system is separated into a statically determinate primary system (stage S-1) and a system with redundant connector forces and support reactions (stage S-2). In the stage S-1, connectors $\{1,\ldots, n\}$ and additional supports $\{n+1,\ldots, n+m\}$ are released and the beam is subjected to external loads and inelastic strains. In the stage S-2, effects of unknown redundant connector forces and support reactions are applied on the structure.

Finally, the effects from both stages are superimposed. Applying compatibility conditions for each connector and an intermediate support leads to a system of equations as in Eq. (2), where **B** is a flexibility matrix of the system, **x** is a force vector containing unknown connector forces and support reactions and **u** is a "loading" vector containing elastic and inelastic displacements of redundant connectors and supports in the stage S-1. After solving the redundant forces, the total response of the structure is obtained by superimposing the effects from stages S-1 and S-2. In general cases, the method requires numerical implementation, but since arbitrary loads, connector arrangement and support conditions can be easily implemented without the use of simplifications, this method is advantageous compared to analytical methods.

$$\mathbf{Bx} = \mathbf{u} \tag{2}$$

4. Parametric comparison between the methods

The goal of the parametric comparison was to study differences of the aforementioned methods and evaluate their applicability in design of TCC bridges. Wider range of cases were studied, but only the elementary cases are presented here for clarity.

4.1 Geometric setup and parameters

In the parametric study, a TCC beam with a timber section and a concrete slab connected with spaced shear connectors was considered. The cross-section of the beam is illustrated in Figure 3. Two different connector arrangements; connectors with (1) uniform spacing and (2) spacing varying according to shear force, as illustrated in Figure 3, were considered. In addition, two different load types were considered in the analysis; (a) uniform load and (b) point load at $x = l/2$ as in Figure 4. In the parametric study, four different Cases, which are listed in Table 1, combining different connector arrangements and load types, were considered.

Table 1. Cases in the comparison study.

Case	Connector spacing	Load type
1a	Uniform	Uniform
1b	Uniform	Point
2a	Varying	Uniform
2b	Varying	Point

For each Case, 160 combinations of cross-section dimensions and connector stiffness in total were used. The range of the variables as well as material properties and the span were chosen so that they reflect practical range of values used in TCC bridges. The material properties and variables used in the analysis are shown in Table 2. Effective connector spacing s_{ef} [7]was adopted in both, the γ-method and the CFC method.

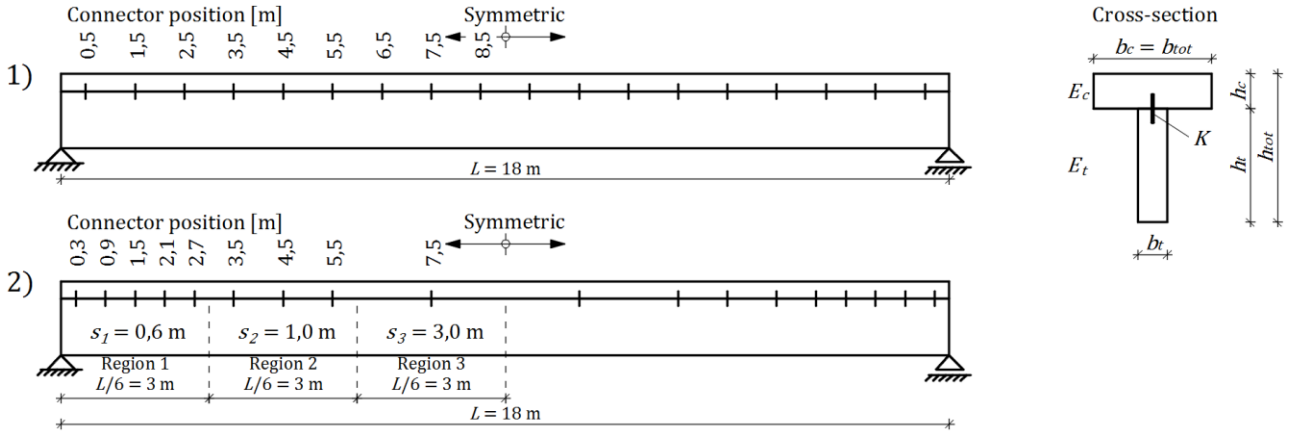

Figure 3. The composite beam and different connector arrangements, 1) uniform and 2) varying, are shown left and cross-section of the beam on right..

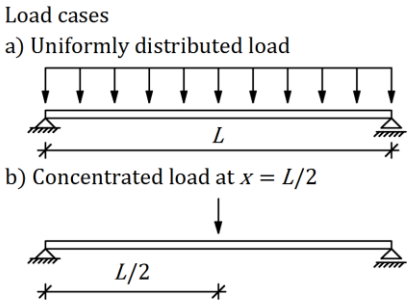

Figure 4. Different load cases.

Table 2. Material properties and dimensions in the parametric study. Number in parenthesis displays total number of parameters for the variable.

Parameter	Value
Span length L [m]	18.0
Concrete elastic modulus E_c [MPa]	30000
Timber elastic modulus E_t [MPa]	13000
Total height h_{tot} [m]	1.5
Total width b_{tot} [m]	1.2
Concrete slab height h_c [m]	0.15, 0.20, 0.25, 0.30 (4)
Timber section width b_t [m]	0.20, 0.25, 0.30, 0.35, 0.40 (5)
Slip modulus K [MN/m]	500, 695, 965, 1341, 1864, 2590, 3598, 5000 (8)

4.2 Presentation of the analysis results

Since the DFC method takes into account individual connector positions, it was considered as the base case for the comparison. Maximum deflection w_{max}, maximum connector force $V_{c,max}$, maximum tensile stress in the bottom fiber of the timber section $\sigma_{b,max}$ and maximum compressive stress in the top fiber of the concrete slab $\sigma_{t,max}$ were calculated for all parametric combinations. In each combination the relative differences of the results from the other methods compared to DFC results were calculated from

$$Diff_i = \frac{S_i - S_{DFC}}{S_{DFC}}, \tag{3}$$

where S_{DFC} is a general effect (w_{max}, $V_{c,max}$, $\sigma_{b,max}$, $\sigma_{t,max}$) using DFC method and S_i is corresponding effect using other method (i = fully composite, CFC, γ-method). The relative differences for each method were plotted against connection efficiency factors γ as in Eq. (1). Bending stiffnesses $(EI)_0$, $(EI)_{eff}$ and $(EI)_\infty$ were determined with the γ-method.

4.3 Limitations of the study

Response of a real composite beam is affected by a number of different phenomena, such as friction between the elements, shear deformations of individual components, cracking of concrete and non-linear behavior of the materials and connectors, some of which are not included in any of the described models. Even though DFC model is assumed to best approximate behavior of TCC beams in the study, in reality the aforementioned effects might significantly affect the accuracy of the methods for individual cases, and therefore the comparison is limited to theory.

5. Results

The results of the comparison are presented in this chapter. The axis scales of all the graphs were unified to allow better comparability between the graphs. In two graphs, where the results were off the scale of the graph, range of the results is marked on the figure with text and arrows.

5.1 Uniform connector spacing - Cases 1a and 1b

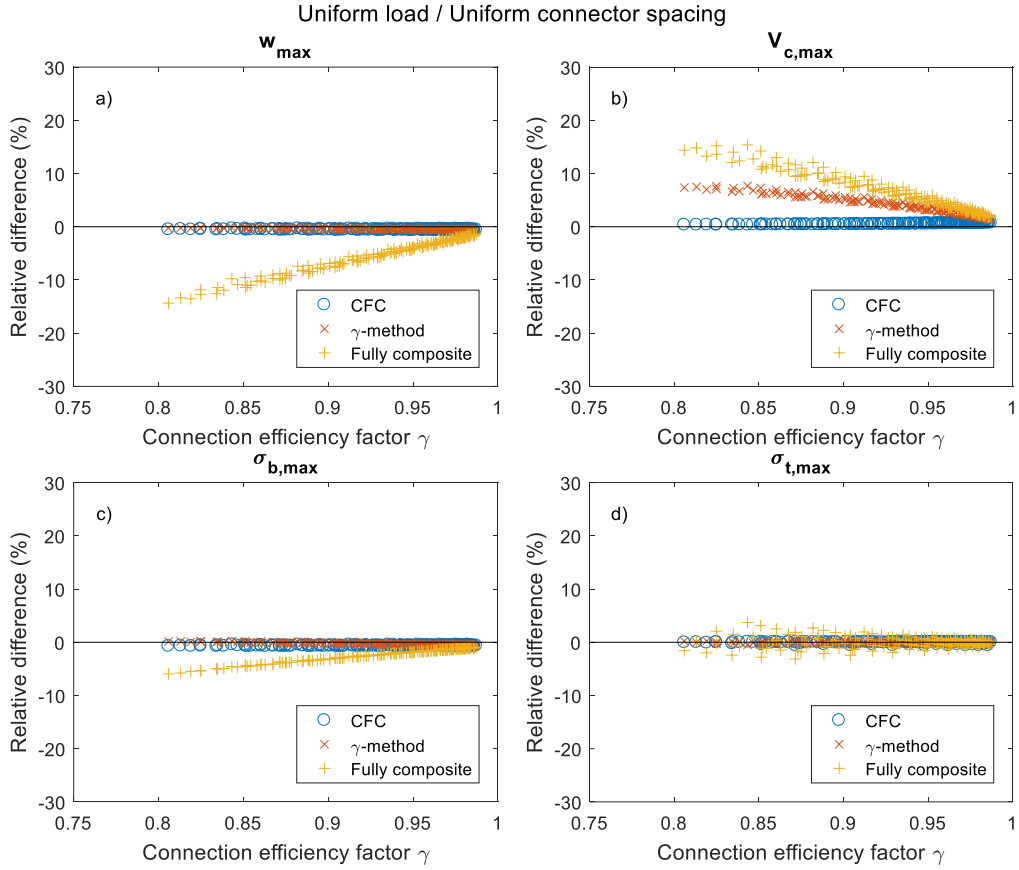

Figure 5. Differences in the Case with uniform connector spacing and uniform load (Case 1a).

The differences in the Cases 1a and 1b were plotted in Figures 5 and 6 functions of connection efficiency factors γ with a range of values, γ = 0.81…0.98.

The CFC method displayed very close agreement with DFC method in both Cases, 1a and 1b. Calculated differences were less than ±1% over the whole range of parameters, thus CFC and DFC methods produce practically identical results.

The γ-method displayed fairly good agreement with DFC method with differences less than ±10%. Differences in deflection were small in the both cases. The connector forces were overestimated in the Case 1a and underestimated in the Case 1b. In the Case 1a the stresses were in close agreement, but in the Case 1b they showed larger differences. Difference of the stress $\sigma_{t,max}$ depended on the ratio h_c/h_t, so that with high h_c/h_t the stress was underestimated and with low h_c/h_t it was overestimated.

The fully composite method displayed largest differences of the three methods overall. The largest differences are around ±15%. The deflection of the beam is generally underestimated, while connector forces are overestimated in the Case 1a and in close agreement in the Case 1b. The stresses had smaller differences in the Case 1a than in the Case 1b. Differences of the stress $\sigma_{t,max}$ depended on the ratio h_c/h_t similarly as with γ-method.

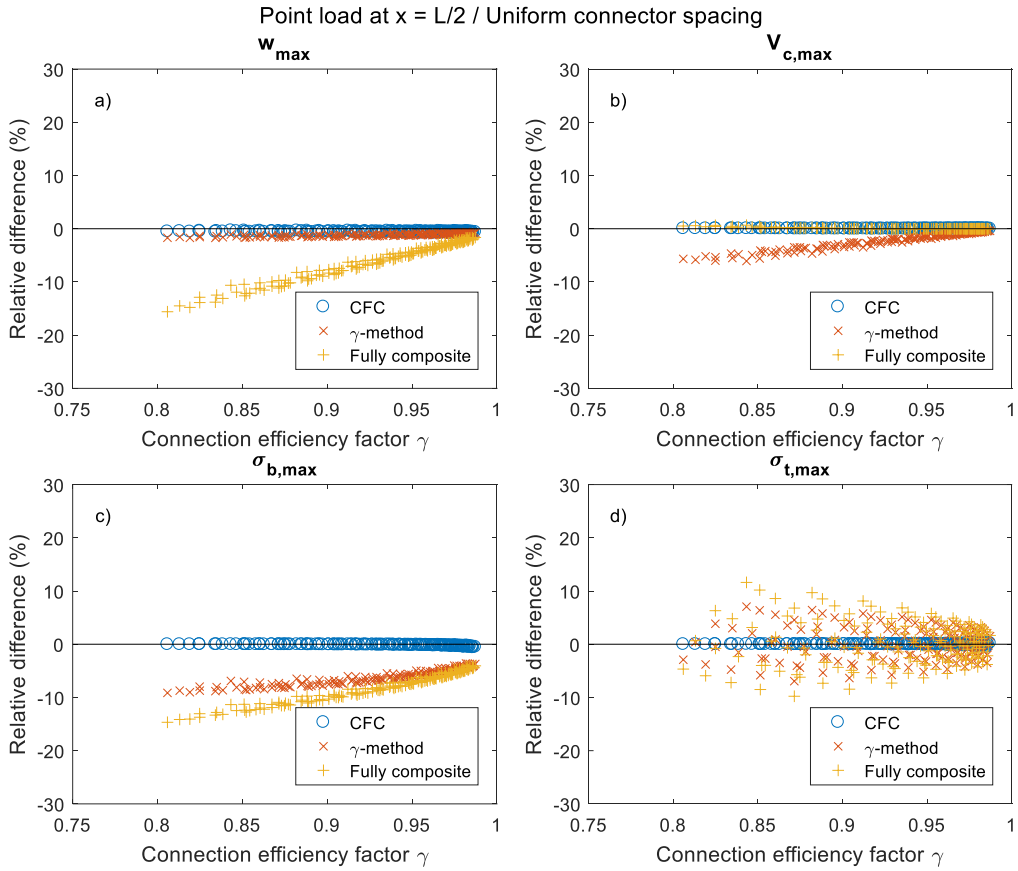

Figure 6. Differences in the Case with uniform connector spacing and point load (Case 1b).

5.2 Variable connector spacing - Cases 2a and 2b

The differences in the Cases 2a and 2b were plotted in Figures 7 and 8 as functions of connection efficiency factors γ with a range of values, γ = 0.78…0.98.

The CFC method had very close agreement in the Cases 1a and 1b, but in the Cases 2a and 2b, the differences were larger. The deflection had a close agreement with DFC, while connector forces displayed very large differences, up to 100% in the Case 2a and around -25…15% in the Case 2b. In the latter Case, connector forces were overestimated with lower γ values and overestimated with higher γ values. The stresses agreed reasonably well with DFC in general, the differences were less than ±5% in all the Cases.

The γ-method had a fair agreement with largest differences around ±10%, excluding the connector forces in the Case 2b, where differences up to 170% could be found. The differences in deflections were less than ±5% in general, while the stresses display larger differences up to ±10%. The stress $\sigma_{c,max}$ is generally underestimated, while difference of $\sigma_{t,max}$ depends on the ratio h_c/h_t as in the Cases 1a and 1b.

The fully composite method displayed largest differences, up to ±20%, excluding connector forces in the Case 2b where differences up to 190% could be found. The deflections were underestimated up to 15%. $\sigma_{c,max}$ is generally underestimated, while difference of $\sigma_{t,max}$ depends on the ratio h_c/h_t as in the Cases 1a and 1b.

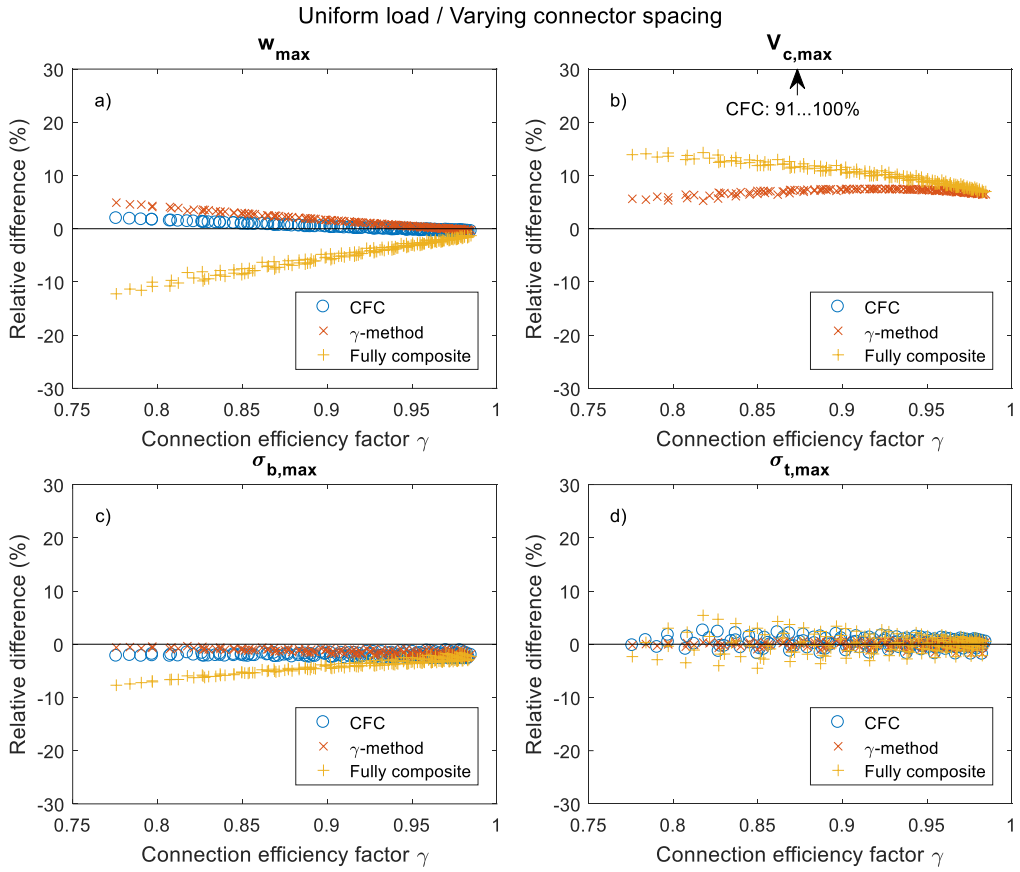

Figure 7. Differences in the Case with varying connector spacing and uniform load (Case 2a).

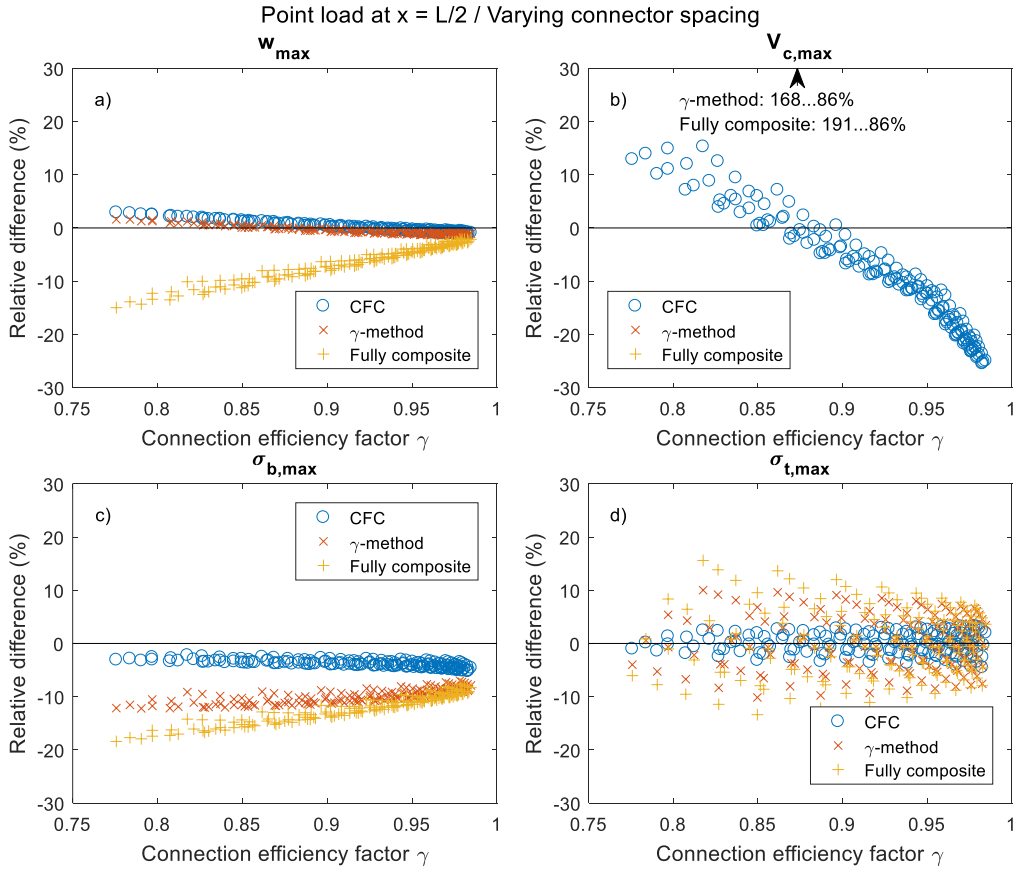

Figure 8. Differences in the Case with varying connector spacing and point load (Case 2b).

5.3 Discussion

Connector forces in the Cases 2a and 2b displayed extremely large differences, so the distributions of the forces were investigated in more detail to understand the reason behind the differences.

In the Case 2a, CFC method displayed up to 100% higher connector forces than DFC method. The connector force distributions in the Case 2a are shown in Figure 9. Increasing connector density towards the supports effectively limits the slip, thus limiting also connector forces, which are linearly dependent of the slip, as may be seen in Figure 9 (DFC curve). In contrast, in CFC method, where varying connector spacing is not taken into account, connector forces are steadily increasing towards the supports. In the fully composite method and the γ-method connector forces are not related to slip, but are estimated fairly well since the connector spacing is accounted for in calculating the forces.

In the Case 2b (Figure 10), connector force distribution of CFC is closer to DCF, but the fully composite method and the γ-method displayed extremely high connector forces near the mid-span. In the DFC method, the slip, as well as the connector forces, develop gradually towards the support. In contrast, the connector forces in the fully composite method and the γ-method were largely overestimated where the connector spacing is wide, since the connector force is proportional to product of total shear force and connector spacing.

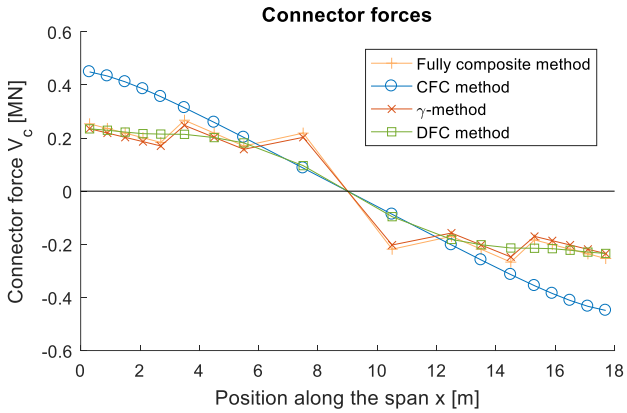

Figure 9. Shear connector force distributions in the Case 2a using different analysis methods.

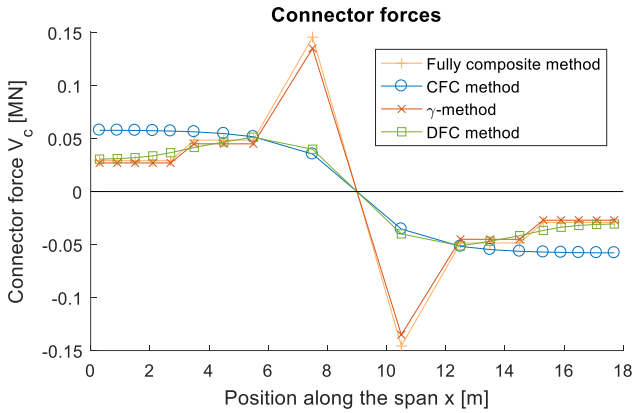

Figure 10. Shear connector force distributions in the Case 2b using different analysis methods.

6. Conclusions

This study showed that within the range of this parametric study, CFC and DFC methods have close agreement, when constant connector spacing is used. Thus, CFC method can be recommended as simpler alternative to DFC method, which generally requires programming a numerical tool for analysis.

Using the CFC method to analyze composite beams with varying connector spacing is not reasonable due to the high differences to DFC in connector forces.

The γ-method displayed lowest differences on average, even though in some cases the differences are higher than by using CFC method. Due to simplicity, the γ-method is best suited for preliminary design stages, when rough estimates are needed, as well as for comparison of effects of different design options.

Using the fully composite method for the analysis is not recommended, unless with very high γ-values, when the results are close the results of the γ-method.

7. References

[1] Liikennevirasto, “Eurokoodin soveltamisohje. Puurakenteiden suunnittelu - NCCI 5.”, Liikennevirasto, Helsinki, 2013.

[2] Jutila A. and Salokangas L., “Wood-Concrete Composite Bridges - Finnish Speciality in the Nordic Countries”, *Proceedings of the International Conference Timber Bridges ICTB2010*, Lillehammer, Norway, 2010.

[3] Yeoh D., Fragiacomo M., De Franceschi M. and Boon K. H., “State of the Art on Timber-Concrete Composite Structures: Literature Review”, *Journal of Structural Engineering,* vol. 137, no. 10, pp. 1085-1095, 2011.

[4] Jaaranen J., Salokangas L. and Fink G., “Long-term analysis of timber concrete composite bridges”, *Proceedings of 3rd International Conference on Timber Bridges (ICTB 2017), 26-29 June, 2017*, Skellefteå, Sweden, 2017.

[5] Lukaszewska E., “Development of prefabricated timber-concrete composite floor”, Luleå tekniska universitat, Luleå, 2009.

[6] Kreuzinger H., “Mechanically jointed beams and columns”, *STEP 1: Timber Engineering, Basis of Design, Material Properties, Structural Components and Joints*, The Nederlands, Centrum Hout, 1995, pp. B11/1-B11/8.

[7] Ceccotti A., “Composite Structures”, *Timber Engineering*, Chichester, Wiley & Sons, 2003, pp. 409-427.

[8] Natterer J. and Hoeft M., “Zum Tragverhalten von Holz-Beton-Verbundkonstruktionen”, Ecole polytechnique fédérale de Lausanne, Lausanne, 1987.

[9] Tommola J. and Jutila A., “Analysis of wood-concrete composite girder with discrete shear connectors”, *IABSE Symposium Report 2001*, 2001.

[10] Fernandez-Cabo J., Díez-Barra R., Fernández-Lavandera J. and Avila-Jalvo J., “The flexibility matrix o timber composite beams with a discrete connection system”, *CIMAD 11, 1º Congresso Ibero-LatinoAmericano da Madeira na Construção*, Coimbra, 2011.

Long-term analysis of timber-concrete composite bridges

Joonas Jaaranen
Doctoral Candidate
Aalto University
Espoo, Finland
joonas.jaaranen@aalto.fi

Joonas Jaaranen received his M.Sc. degree from Aalto University in 2016. He continues his studies pursuing doctoral degree in Aalto University concentrating in timber structures.

Lauri Salokangas
University Teacher
Aalto University
Espoo, Finland
lauri.salokangas@aalto.fi

Dipl.Eng. 1981. 1986-2007 Lab. Man. in Bridge Engineering at Helsinki University of Technology 2008-2013 Prof. of Bridge Engineering, Infra-structures and Structural Design. From 2014 lecturer at Aalto University.

Gerhard Fink
Assistant Professor
Aalto University
Espoo, Finland
gerhard.fink@aalto.fi

Gerhard Fink is Assistant Professor for Wooden Structures at Aalto University. He studied Civil Engineering at the TU Graz, Austria, and did his PhD at ETH Zurich.

Summary

The design of timber-concrete composite bridges is complicated due to time-dependent phenomenon like creep, shrinkage of concrete and effects of the varying temperature and moisture content. Unfortunately, at the moment, Eurocodes include very limited guidelines for designing such bridges. Existing guidelines and methods, time-dependent material models and effects of the environmental variations were studied for the long-term analysis. Based on the findings, a simulation tool for timber-concrete composite beam accounting the time-dependent phenomena was developed. Temperature and moisture content histories of the bridge components based on the existing weather data. The tool was used to simulate the effects over the service life in two cases; a bridge built using un-shored or shored construction method. In overall, wide agreement between the simulation and the approximate model was found.

Keywords: timber-concrete composite, bridges, long-term analysis, composite beam.

1. Introduction

Timber-concrete composite (TCC) bridges are affected by number of time-dependent phenomena, like creep, shrinkage of concrete and effects of varying temperature and moisture content. All these phenomena affect stresses and strains in the structure, and thus affecting deformations and load-carrying capacity of the bridge. At the moment, methods of analyzing the effects of aforementioned phenomena are not covered by the Eurocode standards, which makes long-term analysis of the bridges problematic in design practice. Due to quite intensive research on TCC structures in past few decades, some long-term analysis methods for TCC structures has been proposed, but mainly for building construction. The purpose of this paper was to investigate applicability of these existing methods for design of TCC bridges.

2. Time-dependent behavior of TCC bridges

Long-term behavior of a TCC bridge is affected by multiple time-dependent aspects, such as loads varying over time, different construction stages and time-dependent behavior of the bridge components.

2.1 Loads

A typical TCC bridge is subjected to various loads over the life span. In the construction phase, the structure is loaded gradually by self-weight of bridge components and construction loads like falsework, formwork, equipment, workers and machinery. After the construction is finished, the construction loads are removed. When the bridge is opened for traffic, it is mostly subjected to traffic loads and environmental variations (thermal and moisture content variations) besides the permanent loads (self-weight).

2.2 Construction method

Commonly two different construction methods are used for TCC structures cast on-site, (1) shored and (2) un-shored method. In the shored method, the structure is supported during the construction by intermediate supports, which are removed when the concrete is hardened enough. In the un-shored method, intermediate supports are not used. The clearest difference between the methods is that in the shored construction the self-weight of concrete and other components is transferred to composite section at support removal, while in the un-shored method self-weights are mainly carried by the timber sections. Whereas shored method applies composite section more effectively, un-shored method is particularly attractive due to its simplicity on site. Examples of Finnish TCC bridges built using un-shored method can be found in [1].

2.3 Time-dependent behavior of components

In addition to instantaneous behavior, timber, concrete and connectors display time-dependent behavior. The most notable time-dependent phenomena affecting: (1) timber are creep, mechano-sorptive creep, shrinkage/swelling and thermal strains, (2) concrete are creep, shrinkage and thermal strains and (3) connectors are creep and mechano-sorptive creep [2]. Over time, these phenomena will change stresses and strains [3], which will affect deflections and load-carrying capacity of the TCC beam. In addition, creep in composite structures is non-linear due to interaction between the components, which makes long-term behavior more complex.

3. Existing analysis methods

3.1 Eurocodes

The current version of the Eurocode standards include limited information about design of TCC structures. Only in EN 1995-2 [4] some guidelines for the structural behavior and the connector design are given, however long-term analysis of TCC bridges is not covered.

Nevertheless, the behavior of the individual materials is included in the Eurocodes. The creep in timber components is taken into account by using deformation factors (i.e. creep factors) k_{def} given in EN 1995-1-1 [5] and the effects of the creep on the structure are calculated applying effective modulus method (EMM). The factors are given in different service classes and for different types of wood products. While in the current version only thr final k_{def} values are given, the factors for intermediate duration were given in the earlier version of the standard (1994).

Methods of analyzing the effects of environmental variations in timber (thermal and moisture content) are not considered in EN 1995-1-1 or EN 1995-2. In general, guidelines in the Eurocodes are limited to thermal expansion factors for timber parallel and perpendicular to grain, which are given in EN 1991-1-5 [6].

Long-term behavior of the concrete is defined more explicitly. Standard EN 1992-1-1 [7] defines creep function $\varphi(t,t_0)$ depending on ambient relative humidity, dimensions of the element, strength class of the concrete and concrete age at loading as well as shrinkage $\varepsilon_{cs}(t)$ depending on ambient relative humidity, dimensions of the element, strength class of the concrete and concrete composition. The strains due to thermal variation should be determined by using linear expansion coefficient α_T given in the standard.

3.2 Finnish NCCI1 and NCCI5

Additional rules for timber bridges may be found in the national application documents, like Finnish Transport Agency's NCCI1 [8] or NCCI5 [9]. According to the NCCI5, the creep in TCC bridges may be taken into account by different modular ratios $n = E_c/E_{mean}$, where E_c is concrete modulus of elasticity and E_{mean} is timber mean modulus of elasticity, for short-term (n = 3) and long-term (n = 2) analyses. NCCI5 also gives expansion coefficients due to thermal and moisture content variation along different axes of the timber as well as variation range of timber moisture content for salt and creosote treated wood after the wood has reached its equilibrium moisture content. NCCI1 suggest that the thermal loads on the timber bridges should be defined from temperature distributions given for concrete bridges in EN 1991-1-5.

3.3 Methods proposed in literature

Intensive research on TCC structures has been conducted during the past few decades and some analysis methods has been proposed. Two of these will be discussed in this paper, namely methods proposed by Ceccotti [10, 11] and by Fragiacomo [3].

Ceccotti's approach considers simply supported TCC beam consisting of timber section and concrete slab connected by flexible connectors. Effects of the creep in timber, concrete and connectors is determined by using effective moduli for individual components; however, effects of inelastic strains due to concrete shrinkage and environmental variations are neglected. The total response of the structure is obtained by superimposing effects of individual external loads. It was later noted that Ceccotti's proposal leads to significant errors and un-conservative results due to neglecting inelastic strains in the analysis [12].

An extended version of Ceccotti's approach, a method including effects of the inelastic strains, was later proposed by Fragiacomo. In this approximate method, total effect S is obtained by superimposing effects of external loads, concrete shrinkage and inelastic strains due to environmental variations according to Eq. (1).

Effects of the permanent and imposed loads are obtained by superimposing effects of individual loads, which are calculated by using EMM with effective moduli according to Eq. (2). Effect of concrete shrinkage S_h^s is obtained by calculating effect of concrete shrinkage strain, $\Delta\varepsilon_{cs}(t) = \varepsilon_{cs}(t) - \varepsilon_{cs}(t_0)$, using effective moduli according to Eq. (3). Effects of inelastic strains S_{el}^y and S_{el}^d are both determined by applying elastic moduli according to Eq. (4) and applying yearly and daily inelastic strains according to Eqs. (5) and (6), respectively, as uniform strain loads on corresponding parts of the composite beam [3].

$$S = S_h^{G+Q} + S_h^s + S_{el}^y + S_{el}^d, \tag{1}$$

$$E_{c,eff}(t) = \frac{E_c(t_i)}{1+\phi_c(t,t_i)} \quad E_{t,eff}(t) = \frac{E_t}{1+\phi_t(t,t_i)} \quad K_{f,eff}(t) = \frac{K_f}{1+\phi_f(t,t_i)}, \tag{2}$$

$$E_{c,eff}(t) = \frac{E_c(\bar{t})}{1+\phi_c(t,t_0)} \quad E_{t,eff}(t) = \frac{E_t}{1+\phi_t(t,t_0)} \quad K_{f,eff}(t) = \frac{K_f}{1+\phi_f(t,t_0)}, \tag{3}$$

$$E_{c,eff}(t) = E_c(t_\infty) \quad E_{t,eff}(t) = E_t \quad K_{f,eff}(t) = K_f, \tag{4}$$

$$\Delta\varepsilon^{y}_{t_u}(t) = \alpha_{t_u}\left[u(t) - u(t_0)\right] \quad \Delta\varepsilon^{y}_{t_T}(t) = \alpha_{t_T}\left[T(t) - T(t_0)\right] \quad \Delta\varepsilon^{y}_{c_T}(t) = \alpha_{c_T}\left[T(t) - T(t_0)\right], \tag{5}$$

$$\Delta\varepsilon^{d}_{t_T} = \alpha_{t_T} k \Delta T_{daily} \quad \Delta\varepsilon^{d}_{c_T} = \alpha_{c_T} \Delta T_{daily}\ , \tag{6}$$

where S_h^{G+Q}, S_h^s, S_{el}^y and S_{el}^d are the effects of permanent and imposed loads, concrete shrinkage, yearly inelastic strains and daily inelastic strains, where indices *h* and *el* refer to hydroviscoelastic and elastic analyses. $E_{c,eff}$, $E_{t,eff}$ and $K_{f,eff}$ are effective moduli at time *t* for load applied at t_i, E_c, E_t and K_f are the elastic moduli, ϕ_c, ϕ_t and ϕ_f are the creep factors, where indices *c*, *t* and *f* refer to concrete, timber and connectors, respectively. Times t_0, $\bar{t}$ and t_∞ are the time when the concrete starts curing, the age of the concrete at shore removal and the age of the concrete at the end of the service life, respectively. $\Delta\varepsilon^{y}_{t_u}$, $\Delta\varepsilon^{y}_{t_T}$ and $\Delta\varepsilon^{y}_{c_T}$ are inelastic strains due to yearly moisture variation in timber, yearly temperature variation in timber and yearly temperature variation in concrete, where *u* and *T* are approximate histories of average moisture content and ambient temperature. $\Delta\varepsilon^{d}_{t_T}$ and $\Delta\varepsilon^{d}_{c_T}$ are inelastic strains due to daily temperature variations in timber and in concrete, where T_{daily} is average excursion of ambient temperature during the year and *k* is reduction factor accounting thermal inertia of the timber section.

CEB 90 [13] or B3 are suggested as material models for concrete and creep in timber is suggested to be modelled using Toratti's creep limit model B [14], which includes explicitly effects of mechano-sorptive creep. In the absence of experimental data, creep coefficient $\phi_f = 2\phi_t$ is recommended for the connectors [3].

Fragiacomo's proposal includes all the major time-dependent phenomena affecting TCC structures in outdoor environment, thus it was chosen as possible long-term analysis method for TCC bridges. Its applicability was studied by comparisons presented in the following sections. One drawback of the method is that analysis of structures built using un-shored method is not considered, but treatment of the case is discussed later in this paper.

4. Long-term simulation tool for TCC beams

4.1 General procedure

In the simulation, a time domain $t \in [t_0, t_\infty]$ is discretized into *N*+1 instances $\{t_0, t_1, ..., t_n, ..., t_N\}$, thus having *N* time steps, $\Delta t_n = t_n - t_{n-1}$. During the time step *n*, the structure and its components are subjected to strain increments $\Delta\varepsilon_n$ due to external loads, creep and inelastic strains. Then, general effect increments ΔS_n (strains, deformations, stresses, forces) due to the strain increments during the time step *n* are calculated. Environmental variations are input as discrete domains $\Delta T_n = T_n - T_{n-1}$ and $\Delta u_n = u_n - u_{n-1}$. In the beginning of the analysis, at $t = t_0$, all the effects $S_0 = 0$. Total general effect at time t_n is given by

$$S_n = S_{n-1} + \Delta S_n\,. \tag{7}$$

Depending on the construction stage history of analyzed the bridge, the structure may include only timber sections in the beginning of the simulation before the slab is cast, and may include intermediate supports (shored construction) during the analysis. Before the slab has cured, calculation model consists of timber section only, thus $S_c = S_f = 0$ (*c* = concrete, *f* = connectors). When the slab has cured, analysis model is switched to composite model and effects from the previous step with timber section only are taken as initial values for the composite model.

When the structure is shored, the analysis is carried in two stages, shored and un-shored. In the first stage, the beam is analyzed with intermediate supports. In the second stage, after the supports are removed, the model is switched to model without supports, intermediate support reactions are applied to the beam with opposite sign as external loads and all the effects from the previous step are taken as initial values for the un-shored model.

The calculation tool was implemented in Matlab 2015b and the analysis of stresses and strains during each time step was done by using DFC method [15].

4.2 Rheological models for timber, connectors and concrete

Time-dependent behavior of timber section was modelled in the analysis by using Toratti's creep limit model B [14], with two exceptions: elastic modulus's moisture content dependency and

term $-b\varepsilon(t)$ in $\Delta\varepsilon_{t,u}$ were neglected. The latter change was proposed by Fragiacomo [2] due to bad compliance in TCC models. The strain increments were calculated adopting incremental formulation used by Toratti [14].

The model for the connector slip s_f according to Fragiacomo [2] and time-dependent strain in concrete was modelled according to CEB [13] model. Connector slip increments and concrete strains increments were calculated by adopting similar incremental formulation as presented for timber by Toratti [14].

4.3 Moisture and thermal variations

Moisture content and thermal variations in this study were obtained from time-history analyses based on weather history data. The weather data was compiled of Finnish Meteorological Institute's open data [16] from Kumpula weather station in Helsinki. Since only five full years of data was available, data from 1.5.2010 to 30.4.2015 was used and it was extended up to 50 years by repeating the same data. It is realized that this approximation may exclude peak values, which would exist if actual 50 years data were used. However, response of timber moisture content to ambient variation is slow, thus short peaks have limited effects on the moisture content history, thus having also small effect on the stresses. Effects on the thermal variation-induced stresses are higher due to shorter response time, but the error was considered acceptable for the study. The data included ambient temperature T_{amb} [°C], relative humidity RH [%] and cloud cover N [okta]. Thermal analysis required also data of solar radiation, which was obtained from Copernicus Atmosphere Monitoring Service [17].

Moisture content variation in the timber section were simulated based on Fick's II law using the model presented by Toratti [14]. Thermal variation in the composite section were simulated based on the Fourier's law considering effects of convection, solar radiation as well as radiation exchange with the sky and the environment. Surface structures were not included in the model, since their effect was noted negligible in preliminary studies. The analysis method is mostly adopted from [18], but effective sky temperature T_{sky} was determined from solar radiation and cloud cover data according to [19].

Both, thermal and moisture content analyses, were done as 2D analysis in Comsol Multiphysics (version 5.2.0.220). Thermal and moisture content variations over the section $T(y,z)$ and $u(y,z)$ histories, were transformed to equivalent uniform (T_u, u_u) and difference (T_{My}, u_{My}) component (see 4(3) in [6]) histories for the long-term analyses.

5. Comparison between simulation and existing method

Applicability of the approximate method proposed by Fragiacomo [3] was studied in two cases by comparing the results with results obtained from the simulation.

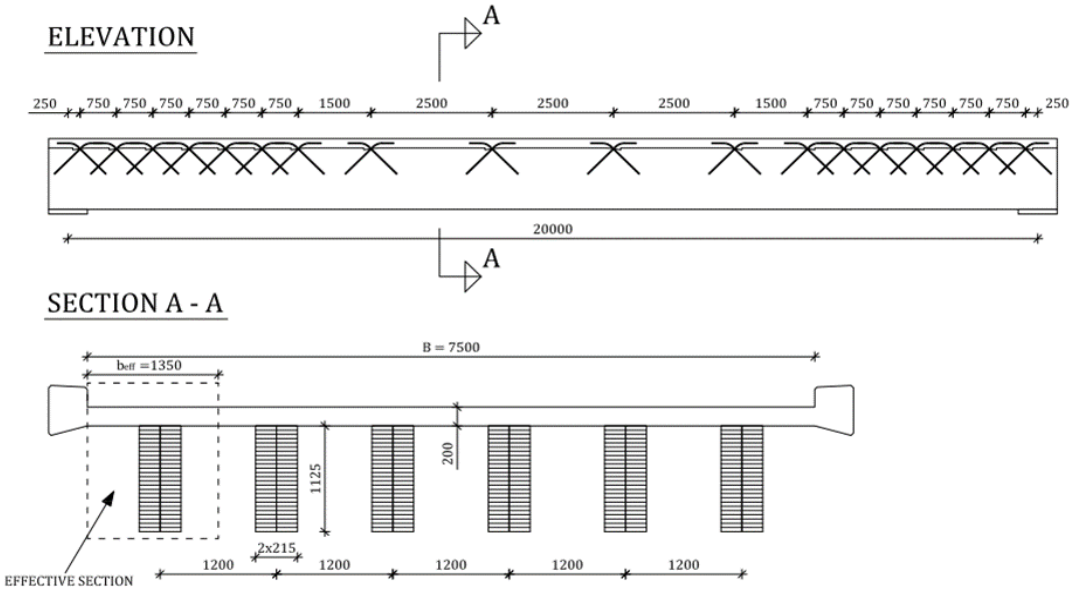

Figure 1. Elevation and cross-section of the case bridge.

5.1 Setup

A case bridge, two-lane road bridge with single span l = 20 m and free width of the deck B = 7.5 m was chosen for the case study. The bridge is illustrated in Figure 1. The dimensions and the material properties are summarized in the Table 1. They were chosen in order to reflect existing TCC bridges in Finland. The service life of the bridge in the comparison studies was 50 years.

Two different analysis cases were considered in the analyses; bridge built using shored or un-shored construction method. In the first case, the structure was supported at 1/3-points during the construction and the supports were removed after a hardening and in the second case, bridge had no intermediate supports during the construction. In the analyses, only effective section shown in Figure 1 was analyzed.

5.2 Loads

The investigated bridge is subjected to (1) external loads, (2) concrete shrinkage and (3) inelastic strains due to thermal and moisture content variations during its life.

The external loads consist of permanent loads (weights of timber sections, concrete slab, surface structures and railings), constructions loads (weight of scaffolding and formwork) and variable loads (traffic loads). The permanent loads were calculated based on the material densities and component geometries. The construction loads were approximated based on typical formwork and falsework structures used in the bridge construction. Traffic loads according to Finnish application document of EN 1991-2, NCCI1 [8], were used. Variability of variable loads were taken into account approximately by including effects of creep for portion $\psi_2 Q_k$ of the load and excluding effects of the creep for $(1 - \psi_2)Q_k$ of the load, where $\psi_2 = 0.3$ is combination factor for long-term loads in NCCI1. This way of accounting creep due to traffic loads is a crude approximation, but it was used due simplicity. The history of loads and construction stages is shown in Table 2. Portion of the total load acting on the effective section were determined by in each case by comparing mid-span deflections of the girders using cantilever rule or FEM model of the bridge depending on the construction stage.

The inelastic strains due to environmental variations were calculated from thermal and moisture content variation histories applying expansion coefficients α given in Table 1. It should be noted, that in this study initial moisture content was u_0 = 20%, while typically glued laminated components are delivered at $u \leq 12\%$. The shrinkage strains were calculated according to CEB.

Table 1. Dimensions and material properties of the case bridge.

Parameter	Value	Parameter	Value
Dimensions		**Timber section**	
Span length l	20 m	Strength class	GL30c
Timber section width b_t	0.43 m	Elastic modulus E_t	13000 MPa
Timber section height h_t	1.125 m	Creep model	Toratti [14]
Concrete slab effective width b_c	1.35 m	Thermal expansion coefficient α_T	5 x 10^{-6} / °C
Concrete slab thickness h_c	0.2 m	Moisture expansion coefficient α_u	5.25 x 10^{-5} / u-%
Concrete slab		**Connectors**	
Strength class	C30/37	Slip modulus K	1500 MN/m
Material model	CEB90 [13]	Creep model	Modified Toratti [1] [14]
Thermal expansion coefficient α_T	10 x 10^{-6} / °C		
(Mean) ambient relative humidity	80%		

1) With c_k = 2, according to [3].

Table 2. History of loads and construction stages in the case studies.

Event	Symbol	Un-shored	Shored
Timber beams installed	t_0	0 days	0 days
Formwork and falsework installed	t_1	3 days	3 days
Concrete slab is cast	t_2	7 days	7 days
Props removed	t_{sr}	- [1]	21 days
Formwork and falsework removed	t_3	28 days	28 days
Surface structures installed	t_4	42 days	42 days
Railings installed	t_5	45 days	45 days
The bridge opened for traffic	t_6	60 days	60 days
End of the service life	t_∞	50 years	50 years

1) No intermediate supports during the construction

5.3 Settings for approximate method

In the approximate method, same load histories, shrinkage and environmental histories as in the simulation were used to allow better comparison, even though Fragiacomo [3] suggest use of simplified moisture content and temperature histories.

Since un-shored construction was not considered in the approximate method, an extended method was used in the un-shored case. In the extended method, effects of the loads applied after the concrete slab has cured, are analyzed as in the shored case. The loads, which are applied before the slab has cured, analyzed using following procedure.

Before curing ($t \leq t_c$), the effect is obtained by applying the load on the timber section only and taking into account the creep by using effective modulus for timber. After curing ($t > t_c$), total effect is obtained by superposing effects of (1) load applied on timber section only, (2) restrained load applied on the timber section and (3) restrained load with opposite sign applied on the composite section. The restrained load is equal to load, which is required to counter the creep deformation after the slab has cured.

The total effect in the latter approach can be calculated by

$$S(t) = \begin{cases} S_t(E^{t_i}_{t,eff}(t)) & ,t \leq t_c \\ S_t(E^{t_i}_{t,eff}(t)) - \left[S_t(E_t) - S_{comp}(E^{t_c}_{c,eff}(t), E^{t_c}_{t,eff}(t), K^{t_c}_{f,eff}(t))\right] \cdot \dfrac{\left[\phi_t(t,t_i) - \phi_t(t_c,t_i)\right]}{1+\phi_t(t,t_i)} & ,t > t_c \end{cases} \quad (8)$$

where $S_t(\bullet)$ and $S_{comp}(\bullet)$ are the effects of the load on non-composite and composite sections, respectively, and values in the parenthesis ($\bullet$) are moduli used to calculate the effects. $E^{t_i}_{t,eff}$ is effective modulus of timber at t for load applied at t_i, E_t is elastic modulus for timber and $E^{t_c}_{c,eff}$, $E^{t_c}_{t,eff}$ and $K^{t_c}_{f,eff}$ are effective moduli for concrete, timber and connectors at t for load applied at t_c (time, when the concrete starts curing).

5.4 Studied cases

The comparison was made for un-shored and shored cases, in which four separate load combinations were considered. The loads in the cases were: (C1) only external loads (permanent, construction and traffic loads), (C2) only concrete shrinkage, (C3) only inelastic strains due to temperature and moisture content variations and (C4) combination of loads from C1 to C3.

6. Results

The mid-span deflection w, stresses in the top fiber of the concrete slab $\sigma_{c,top}$, stresses in the bottom fiber of the timber section $\sigma_{t,bot}$ and connector forces nearest to support V_c were extracted from the analyses in each case. For the comparison, the numerical model results were assumed to be correct.

6.1 Un-shored case

Results from the un-shored case are displayed in Figures 2-5, where num. refers to simulation results and appr. to approximate method. In the case of external loads (C1), good overall agreement was found between the simulation and the approximate method results with differences < 5%. A good agreement (differences < 5%) of effects of the concrete shrinkage (C2) was also found, except for stresses in concrete $\sigma_{c,top}$, which display up to 150% overestimations. Effects of the inelastic strains (C3) had fairly good agreement with differences less than < 10%, except for $\sigma_{c,top}$, which is underestimated up to 50%. In the case including all the loads (C4) deflection w and stresses in timber $\sigma_{t,bot}$ display good agreement with differences < 5%. Stress in concrete $\sigma_{c,top}$ is underestimated by 7% and connector force V_c is overestimated by 11%. In overall, in the case C4 largest differences are around ±10%. Effects of the loads C2 and C4 were small compared to effects of the load C1, which is the reason for good agreement in the combined case.

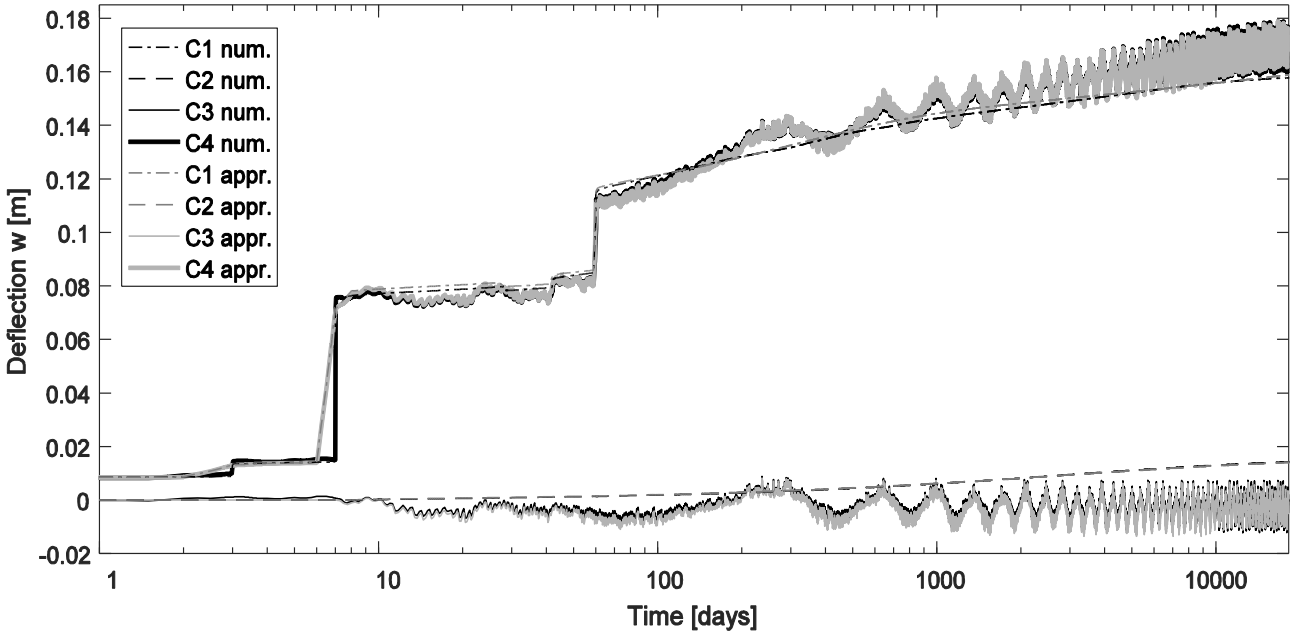

Figure 2. Deflections in the un-shored case.

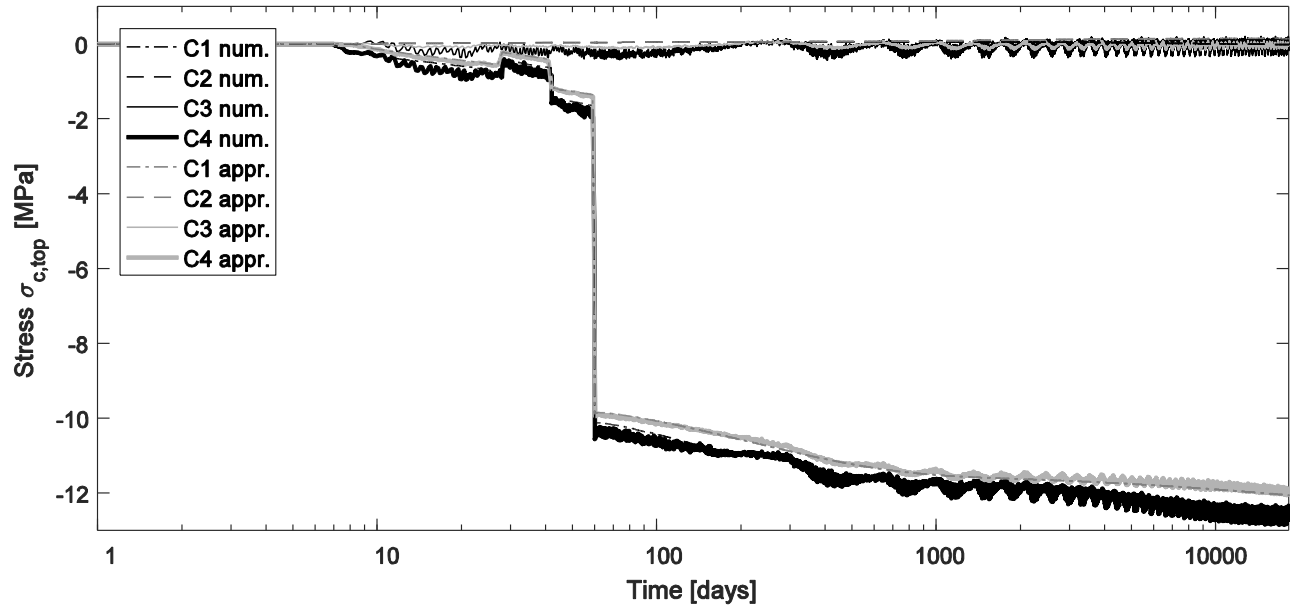

Figure 3. Stresses in top fibre of the concrete slab in the un-shored case.

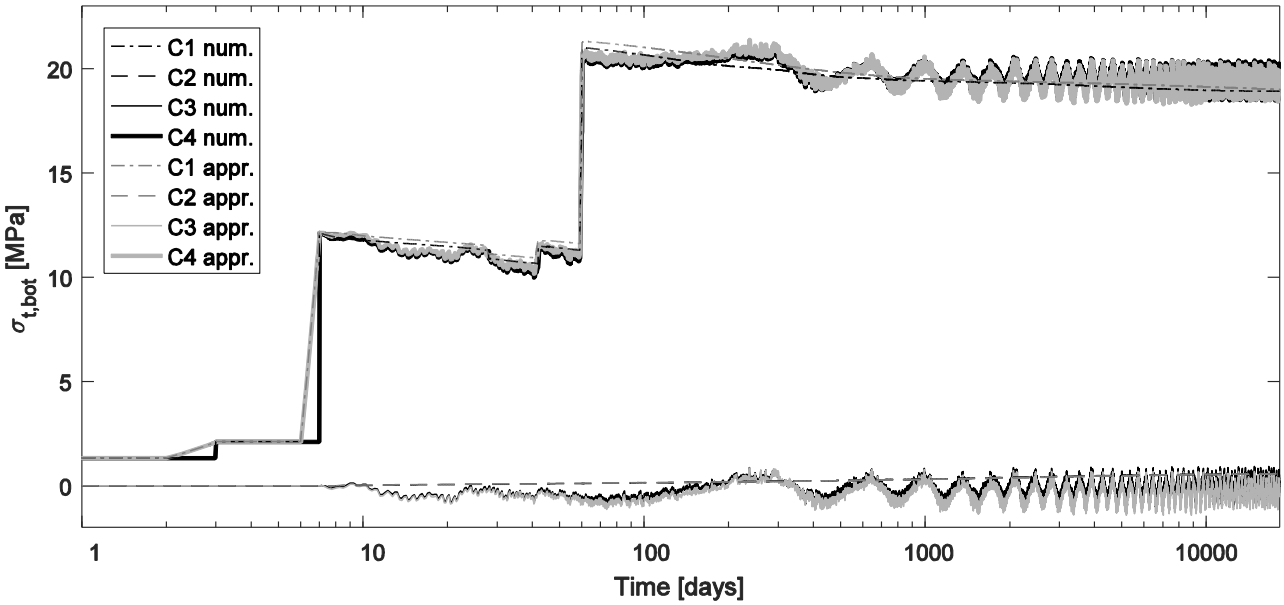

Figure 5. Stresses in bottom fibre of the timber section in the un-shored case.

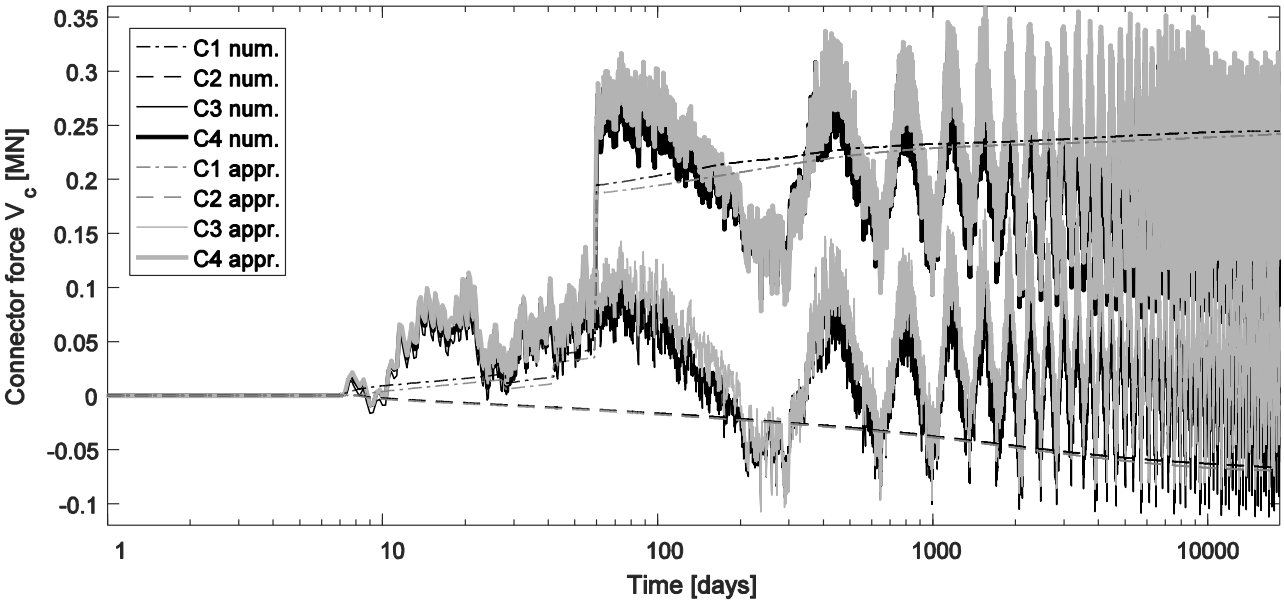

Figure 4. Connector forces in the un-shored case.

6.2 Shored case

Results from the shored case are displayed in Figures 6-9, where num. refers to simulation results and appr. to approximate method. In the case of external loads (C1), good overall agreement was found between simulation and simplified method results with differences < 5%. The effects of the concrete shrinkage (C2) are generally overestimated, displaying differences 5…25%, where highest differences are in concrete stresses and connector forces. The effects of the inelastic strains (C3) displayed poor agreement with the numerical results, except for deflection, which has differences < 5%. The differences in stresses in concrete, stresses in timber and in connector forces were around 20…120%, 25…35% and -5…40%, respectively. In the case including all the loads (C4) good agreement with < 5% differences is displayed, except for connector forces, which are overestimated by 11%. Similarly, as in the un-shored case, effects of the loads in cases C2 and C3 were small compared to effects in case C1, leading to good overall agreement in case C4.

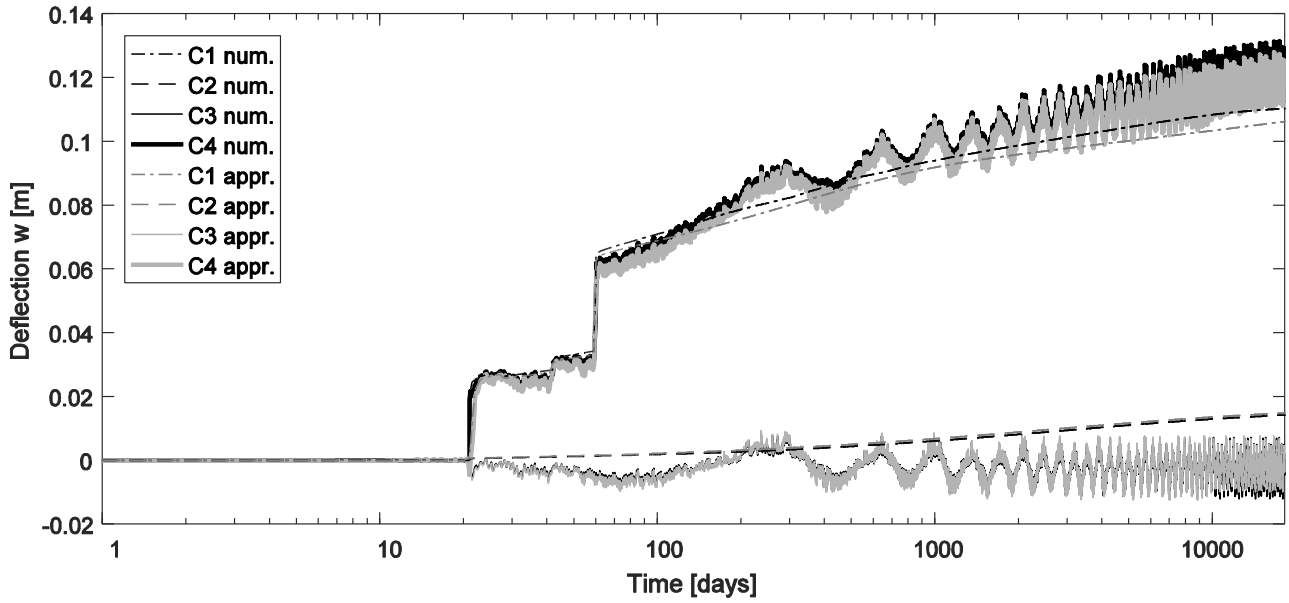

Figure 6. Deflections in the shored case.

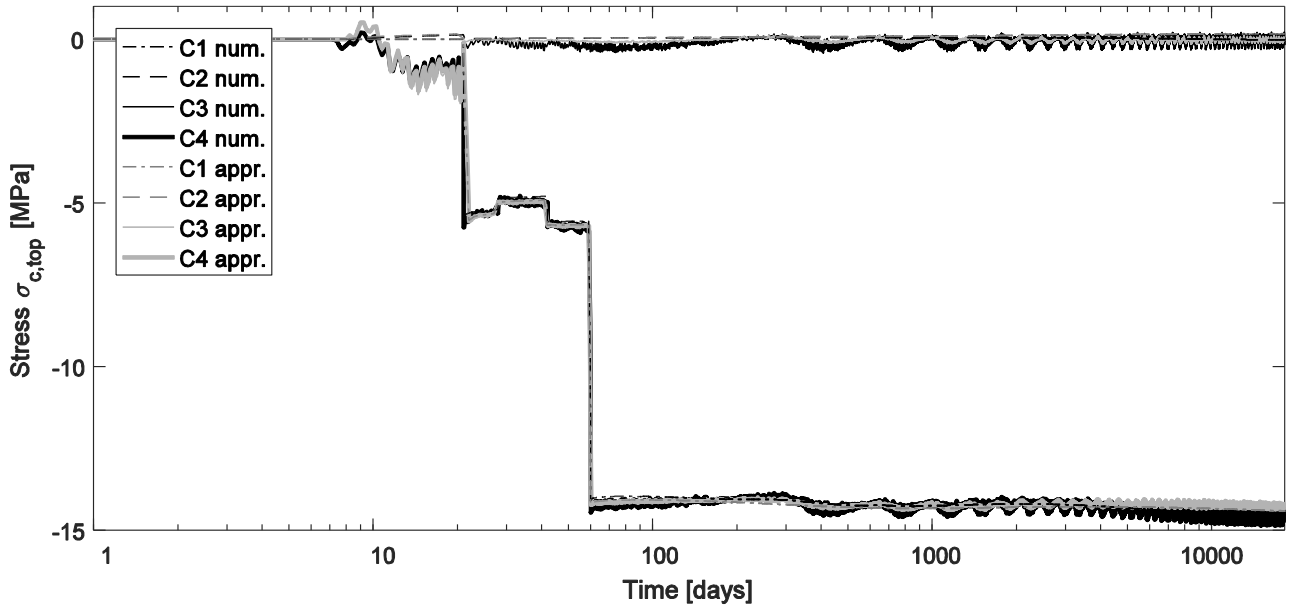

Figure 7. Stresses in top fibre of the concrete slab in the shored case.

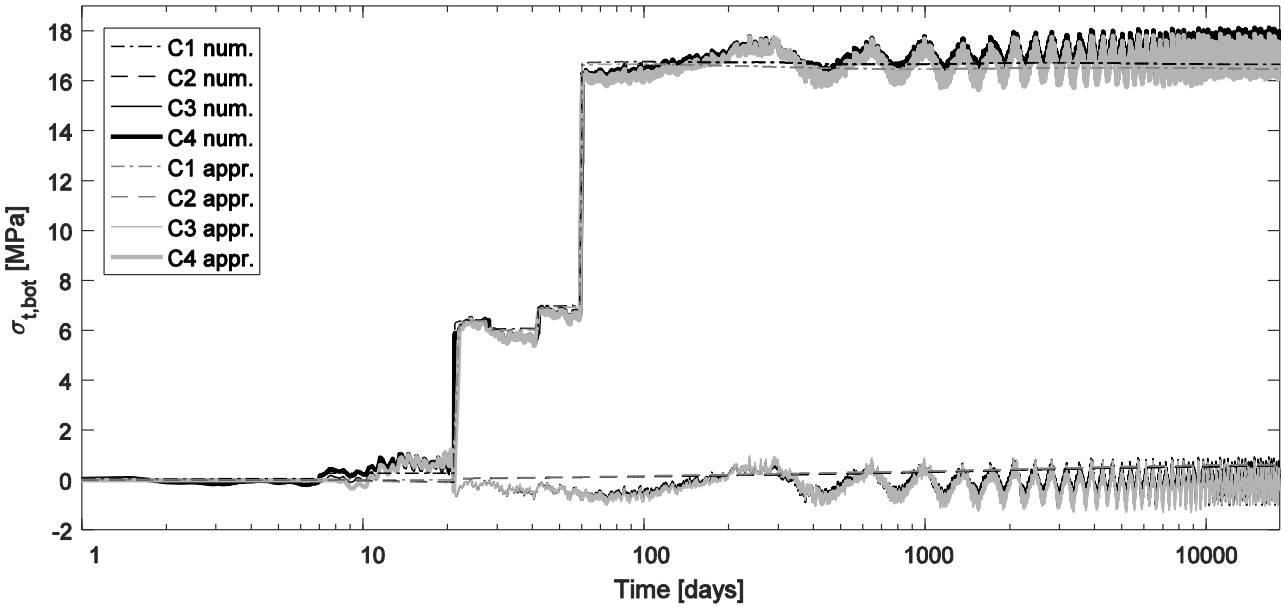

Figure 9. Stresses in bottom fibre of the timber section in the shored case.

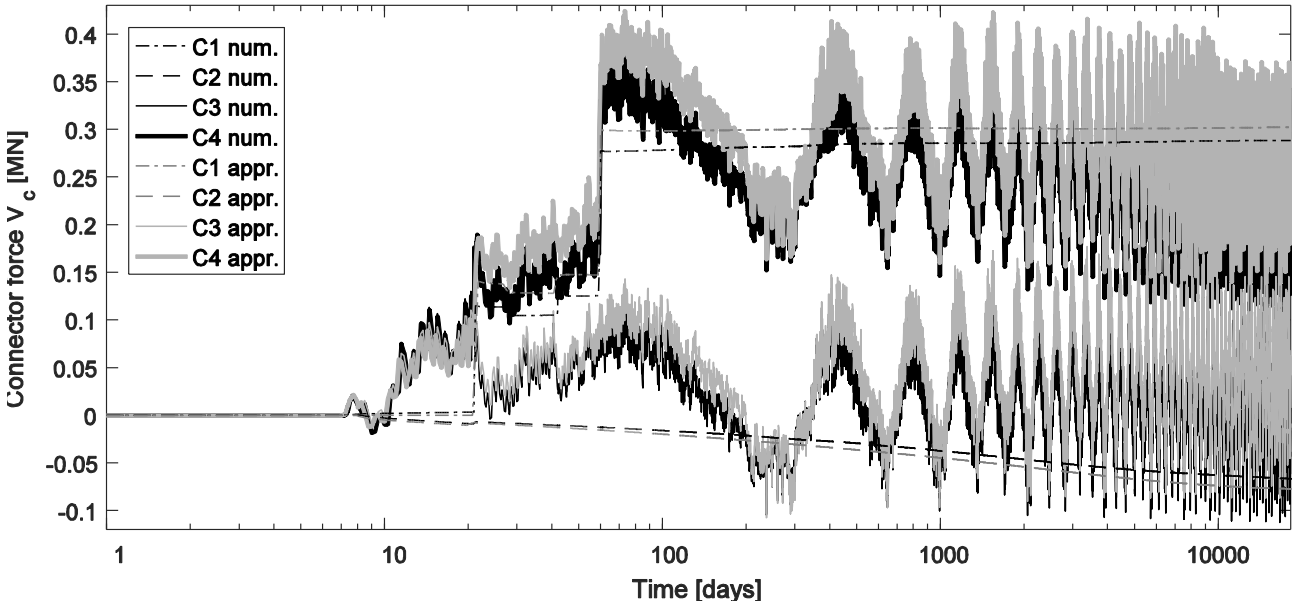

Figure 8. Connector forces in the shored case.

7. Conclusions

Based on the results, the approximate method seems to agree well with the simulation results when considering effects of the external loads in the shored case. Furthermore, the extension for the un-shored case showed a wide agreement. However, results of the extension are based only on this study, thus general applicability is uncertain. Using the simplified method in shored case in design of simple TCC bridges seems feasible for analyzing effects of the external loads. In the un-shored case, further studies should be done to ensure the applicability of the extension.

Weak agreement between the approximate model and the simulation was found, when considering effects of the concrete shrinkage and inelastic strains due to environmental variations. Even though the effects were rather small compared to effects of the total loads, analysis of these loads should be investigated further before applying them widely in the practice due to high differences that were found.

8. References

[1] Noponen S. and Jutila A., "Wood-concrete composite bridges: formwork and falsework construction", Nordic Timber Council, Stockholm, 1999.

[2] Fragiacomo M. and Ceccotti A., "Long-Term Behavior of Timber–Concrete Composite Beams. I: Finite Element Modeling and Validation," *Journal of Structural Engineering,* vol. 132, no. 1, pp. 13-22, 2006.

[3] Fragiacomo M., "Long-Term Behavior of Timber–Concrete Composite Beams. II: Numerical Analysis and Simplified Evaluation", *Journal of Structural Engineering,* vol. 132, no. 1, pp. 23-33, 2006.

[4] SFS-EN 1995-2, "Eurocode 5: Design of timber structures. Part 2: Bridges", Finnish Standards Association, Helsinki, 2004.

[5] SFS-EN 1995-1-1, "Eurocode 5:Design of timber structures. Part 1-1: Genertal, Common rules and rules for buildings", Finnish Standards Association, Helsinki, 2004.

[6] SFS-EN 1991-1-5, "Eurocode 1: Actions on structures. Part 1-5: General actions. Thermal actions", Finnish Standards Association, Helsinki, 2003.

[7] SFS-EN 1992-1-1, "Eurocode 2: Design of concrete structures. Part 1-1: General rules and rules for buildings", Finnish Standards Association, Helsinki, 2004.

[8] Liikennevirasto, "Eurokoodin soveltamisohje. Siltojen kuormat ja suunnitteluperusteet – NCCI1", Liikennevirasto, Helsinki, 2014.

[9] Liikennevirasto, "Eurokoodin soveltamisohje. Puurakenteiden suunnittelu - NCCI 5.", Liikennevirasto, Helsinki, 2013.

[10] Ceccotti A., "Timber-concrete composite structures", *Timber engineering, Step 2: Design, details and structural systems*, 1st ed., H. Blass et al., Eds., The Nederlasnds, Centrum Hout, 1995, pp. E13/1-E13/12.

[11] Ceccotti A., "Composite Structures", *Timber Engineering*, S. Thelandersson and H. J. Larsen, Eds., Chichester, John Wiley & Sons Ltd., 2003, pp. 409-427.

[12] Fragiacomo M. and Ceccotti A., "Simplified approach for the long-term behaviour of timber-concrete composite beams according to the Eurocode 5 provisions," in *Meeting thirty-nine of the working commission W18-timber structures, CIB, International Council for Research and Innovation, Florence (Italy), August 28–31*, Florence, 2006.

[13] Comite Euro-international du béton, CEB-FIB Model Code 1990 Design Code, fib Fédération internationale du béton, 1993.

[14] Toratti T., "Creep of timber beams in a variable environment", Espoo, 1992.

[15] Jaaranen J., Salokangas L. and Fink G., "Short-term analysis of timber-concrete composite bridges", *Proceedings of 3rd International Conference on Timber Bridges (ICTB 2017), 26-29 June, 2017*, Skellefteå, Sweden, 2017.

[16] Finnish Meteorological Institute, "The Finnish Meteorological Institute's open data", Finnish Meteorological Institute, Helsinki, 2015.

[17] Copernicus Atmosphere Monitoring Service, "Time series of solar radiation data from the CAMS radiation service", 2016. [Online]. Available: http://www.soda-pro.com/web-services/radiation/cams-radiation-service. [Accessed 31 Jul 2016].

[18] Larsson O., "Climate related thermal actions for reable design of concrete structures", Lund, 2012.

[19] Hagentoft C., *Introduction to building physics*, Lund: Studentlitteratur, 2001.

Laminated Steel-Timber-Concrete Beams for Bridges

Jeno BALOGH
Professor
Metropolitan State University of Denver
Denver, USA

István SZŰCS
Professor
University of Pecs
Pecs, Hungary

Rose HOLTZMAN
Laboratory Coordinator
Metropolitan State University of Denver
Denver, USA

Summary

This paper deals with adhesive-based laminated steel-timber-concrete composite beam members for bridge applications. In the members studied, the timber-concrete inter-layer connection was achieved by overlaying fresh concrete on top of a timber layer to which moisture tolerant epoxy was applied a short time prior to the concrete placement. Adhesive-based timber-concrete composite beams typically exhibit brittle failure of the timber in tension. Consequently, a steel strip was embedded using adhesives into a groove cut in the timber layer in order to reinforce the tension fibres. This paper presents the results of the laboratory experiments performed on scale specimens with a TT cross-section. The research results indicate that the load capacity and stiffness of the reinforced beams increased significantly, compared to the members without a steel reinforcement. It is concluded that the steel reinforced laminated timber concrete beams could allow for longer spans and higher loads as required in bridge applications.

Keywords: timber-concrete composite beams, laminated structural members, adhesive connection

1. Introduction

While prior studies mostly focused on just timber-concrete bridges with notched shear connections [1], [2], this paper presents a multi-composite, laminated beam configuration with potential applications to bridges. The proposed beam has a TT section consisting of timber webs and a concrete flange interconnected with adhesives at the time the fresh concrete is placed over the top of the timber. The structural performance of such laminated members, including CFRP tension-reinforced members were reported in [3] and [4]. However, these types of laminated beams usually exhibit brittle failure of the timber. Therefore, a steel strip was attached to the tension side of the timber layer in an attempt to induce a ductile behaviour.

2. Experimental Investigation

The load capacity and stiffness performance of four laminated, timber-concrete beams were studied under static conditions on scaled (1:4) specimens at Metropolitan State University of Denver. Two specimens were of laminated timber-concrete (LTC) type, denoted BM1 and BM3, and the other two were of steel-timber-concrete (S-LTC) type, denoted BM4 and BM5. Dayton Superior type Sure Bond J58 adhesive [5] was used throughout.

Fig. 1 Typical test setup of an LTC specimen (BM3 shown)

Fig. 2 Typical test setup of an S-LTC specimen (BM5 shown)

The test configurations of the LTC and S-LTC beam specimens were simply supported with a span of 2337 mm. All beams had a cross-section built up from two nominal 2x6 dimension lumber (38.1 mm x 139.7 mm) Grade 2 Douglas fir and a layer of 50.8 mm of basalt fibre reinforced concrete C40/50, as depicted in Figure 1. The timber was embedded 12.7 mm into the concrete layer to increase the bonding surface. In addition, the S-LTC beams had a 4.76 mm x 38.1 mm cross-section ASTM A36 steel strip embedded into the tension side of the timber on the full length of the beams, as shown in Figure 2.

In a three-point load configuration a mid-span load was applied using MTS hydraulic equipment following a displacement-controlled procedure derived from specification EN-2689 for timber joints [6].

3. Structural Behaviour

The recorded load-displacement diagrams of the four specimens are shown in Figure 3. The load capacity and stiffness increase of the specimens with steel reinforcement are clearly noticeable. The steel strips did not reach yielding during the load tests.

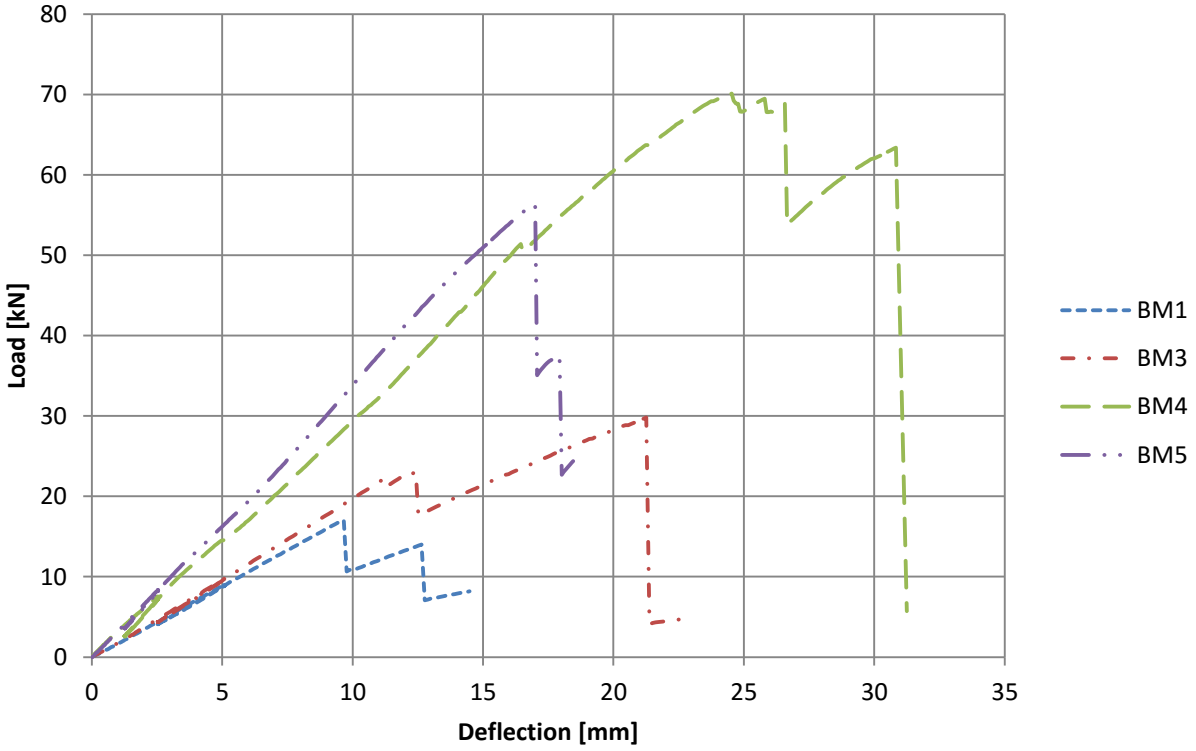

Fig. 3 Failure of the timber in tension (BM3 shown)

4. Failure Mechanisms and Pattern Types

LTC specimens BM1 and BM3 failed in the timber layer in tension, see Figure 4, which is consistent with failures observed on similar specimens in prior studies [3], although they occurred at lower load levels that is attributed to the lower quality of the timber material. The batch of timber used in the specimens for this study was of Grade 2, compared to Grade 2 or better (typically Grade 1 or premium) used in prior studies.

The same adhesive [5] was used for both the timber-concrete and the timber-steel connections. The high moisture tolerant property of the adhesive made it a good fit for the application to the timber-concrete interface, with the bonding strength exceeding the shear strength of the bonded materials [3]. The timber-steel interface, however, showed delamination of the adhesive connection during the failure of the S-LTC specimen BM4, see Figure 5.

Fig. 4 Failure of the timber in tension (LTC specimen BM3 shown)

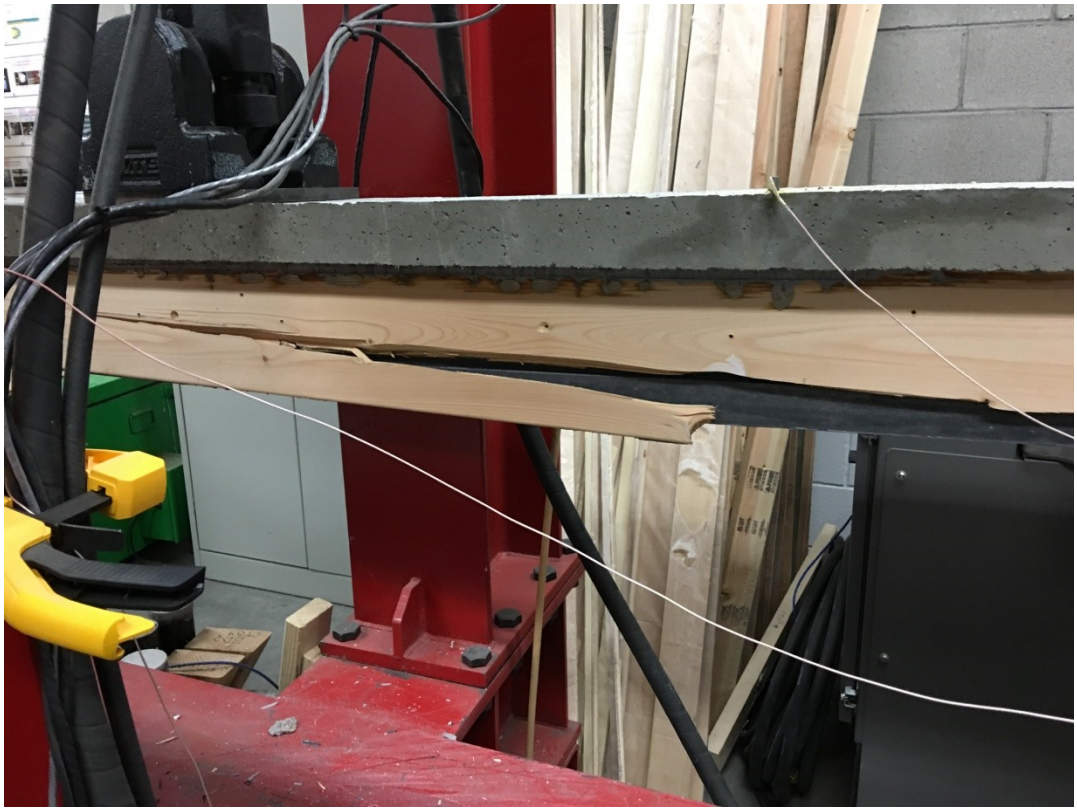

Fig. 5 Failure of the timber in tension and delamination of the timber-steel bonding (S-LTC specimen BM4 shown)

Acoustic emission investigations of the load tests were also performed, and it was reported in detail in [7]. Figure 6 (right) shows a typical acceleration – time function and the relating fast Fourier transformation (FFT) spectrograms (left) of the acoustic emission (AE) activity during the last 25 seconds of a loading test. In the final stage of the failure, the drop of corner frequencies of the succeeding AE signals, representing an inverse proportion to the rupture sizes of their sources, could be directly observed and analysed. The acoustic emissions data is indicative of a defective timber material for BM1 [7], which is consistent with the corresponding measured low load capacity.

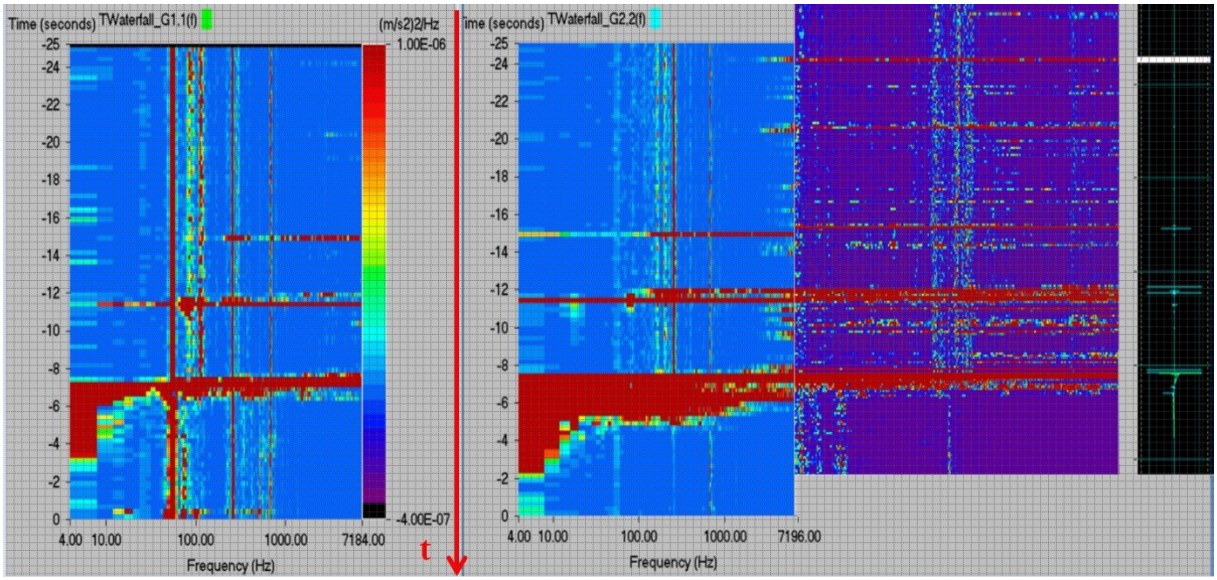

Fig. 6 Typical spectrogram of the AE activity during failure

5. Conclusions

The strength and stiffness behaviour of two LTC and two S-LTC specimens were investigated. The S-LTC specimens showed significant (>100%) increase in load capacity and (> 50%) stiffness over the LTC specimens, enabling larger span and larger load application, such as with bridges. At full scale, glued laminated timber (glulam) beams could be used for the timber layer.

While the two-component epoxy adhesive worked adequately for the timber-concrete connection, during failure, in specimen BM4, the timber-steel layer showed delamination at the adhesive connection, which precluded the timber member to engage the steel strip up to yielding. Therefore, in future tests a different type of adhesive is required for the timber-steel bonding.

A nonlinear, finite element model for the S-LTC type beams is under development for the design of such members and will be presented in a future paper, along with additional test results.

6. Acknowledgements

The research was performed within the framework of the institutional cooperation between the University of Pécs and the Metropolitan State University of Denver. The present scientific contribution is dedicated to the 650th anniversary of the foundation of the University of Pécs, Hungary. The authors are grateful to the MSU Denver students who assisted with the laboratory specimen construction and experimental setup. Dayton Superior (Aurora, CO, USA) donated the adhesive to the project.

7. References

[1] Jutila, A., “Wood Concrete Composite Bridges – Finnish Speciality in the Nordic Countries”, *Proceedings of the International Conference Timber Bridges (ICTB2010)*, Lillehammer, Norway, September 12 -15, 2010, pp. 383-392, 2010.

[2] Rodrigues, J., Providencia, P., Dias, A., "Use of Composite Timber-Concrete Bridges Solutions in Portugal", *Proceedings of the International Conference Timber Bridges (ICTB2010)*, Lillehammer, Norway, September 12 -15, 2010, pp. 67-77, 2010.

[3] Balogh, J., "High Performance CFRP-Timber-Concrete Laminated Composite Members", *Proceedings of the World Conference on Timber Engineering*, Vienna, 2016.

[4] Balogh, J., "Laminated Wood-Concrete Structural Members", *Pollack Periodica, an International Journal for Engineering and Information Sciences*, Vol. 8, No. 3, pp. 79-86, 2013.

[5] Dayton Superior, "Sure Bond J58, Section 1 – Epoxies", Technical Data Sheet, Miamisburg, Ohio, October 9, 2012, pp. 1.35-1.36, 2012.

[6] European Standard, "Timber Structures – Joints made with mechanical fasteners – General principles for the determination of strength and deformation characteristics", EN 26891:1991 (ISO 6891-1983), February 1991.

[7] Szűcs, I., Balogh, J., Holtzman, R., "Acoustic Emission Investigation of Laminated Timber-Concrete Beam Load Tests", Special Issue of the *International Journal of Computational Methods and Experimental Measurements*, (accepted) 2017.

A Century Of A Bridge Of Perfection

Liu Yan
Dr.-Ing
Nanjing University
Nanjing, China
liuyan06seu@hotmail.com

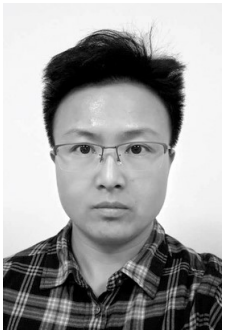

2010-2017 Doctorand in the discipline Bauforschung with Prof. Manfred Schuller, Technical University of Munich.
Since 2017, Associate Researcher in the School of Architecture and Urban Planning, Nanjing University.

Summary

1913, a so-called Full Moon Bridge was erected in the Japanese Garden on the estate of Henry Edward Huntington, the American railroad magnate, in San Marino, California, USA, by a Japanese immigrant carpenter Toichiro Kawai. The curved form of this bridge belongs to traditional Japanese drum bridge, a symbol of Japanese culture and art. While this structure is unique for its woven arch construction, a kind of "reciprocal frame structure" in the modern study.

As an outcome of an archaeological investigation, this paper is going to look through the constructional method and structural problems of this bridge, to unveil the design pursuance of the carpenter master. Through comparison between the current structure and old photos, and with the help of oral history material, an undocumented reconstruction history of the bridge will be revealed.

Keywords: woven arch bridge, reciprocal frame, moon bridge, drum bridge, Japanese architecture, Huntington Library, reconstruction, Bauforschung.

1. From the San Francisco Drum Bridge to the Huntington Moon Bridge

Japanese Landscape in California

In the latter half of nineteen century, Japan went through radical social changes. The Meiji Restoration, started in 1868, broke the old hierarchical order and showed power on all social aspects. Arts and crafts were also greatly influenced. In the mean time, the whole society was attracted by various international expositions, and took them as the opportunity to sell Japanese goods and learn western technologies. Japanese artworks appeared on the Vienna Exposition of 1873 and the Philadelphia Centennial Exposition of 1876 raised an enthusiasm in Japanese art in the western world.

In 1893, the United States went through a heavy economic depression. The California Midwinter International Exposition, opened in 1894 in Golden Gate Park in San Francisco, was held to revive the economy and improve the local neighbourhoods. A most successful part of the Exposition was a Japanese Village, it has been kept in the Golden Gate Park and has been many times rebuilt and enlarged after the Fair and is still welcoming visitors today. The chief administrator of the Japanese Village was George Turner Marsh (1857-1932), the first merchant on Asian art in California[1], who owned a successful Japanese Art Repository in San Francisco. Buildings together with all kinds of supplies were shipped from Japan to California, including a torii, a bell tower and an eye-catching drum bridge. Wooden arched bridge or drum bridge is thanks to its elegant form one of the most influential symbol of Japanese art, witnessed by numerous ukiyo-e (woodblock painting) and by the impressionist artworks at that time. The Drum Bridge in the Golden Gate Park, which was built by a commissioner of the Japanese government[2], as almost a name card of Japanese garden art, has an exaggerated semi-circle shape (Fig.1), much steeper than any bridges ever in Japan.

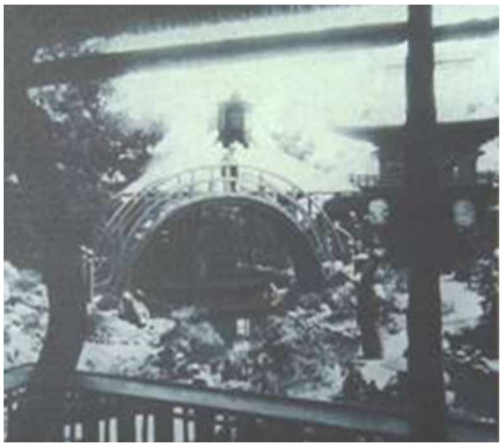

Fig. 1 Drum Bridge in the Japanese Tea Garden, San Francisco, USA, 1894 (From: Huntington Archive)

By the time of the Midwinter Exposition, the railway magnate Henry Edward Huntington (1850-1927) was living in San Francisco. The Japanese Village must have given him a strong impression. In 1911, when Huntington was preparing a new estate in San Marino, a small town at the northeast of Los Angeles, among many botanic gardens he built a Japanese garden on his land. The Huntington estate has been developed and improved during the century and has been opened to the public, with its full name "the Huntington Library, Art Collections and Botanical Gardens" today. Now it takes an area of about 84 hectares (207 acres) and consists of fourteen specialized botanical gardens of various cultures and geographical regions.

On preparing for the Japanese Garden, Huntington hired a Japanese carpenter, Toichiro Kawai, to move a Japanese tea house into his garden. Satisfied with the project, three structures was contracted to the same carpenter later from 1911 to 1913: a torii, a bell tower, and a drum bridge, which is named as the Full Moon Bridge in the early Huntington archive, or more commonly Moon Bridge later. The bell tower and the bridge are still standing in the garden, receiving visitors today.

Toichiro Kawai[3]

In 1898, an American naval vessel travelled from Yokohama, Japan to San Francisco. The Japanese ship carpenter working on board jumped the ship and swam to shore. This is the arrival of Toichiro Kawai (1861-1943) in the USA.

Kawai war born in rural section in Shizuoka-ken, Enshu. Lost his father at age 14, he was sent to a temple in his youth, where he studied reading, writing and among other skills gardening.

He went to Yokosuka to study shipbuilding and worked afterward in Yokohama, the prominent port city of Japan, as a ship carpenter. He learned some simple English on British ships. This language capability and his knowledge on Japanese art introduced him to a Marsh brother, during the buying trips of the latter on Asian art goods in Japan.

After arrival in America, Kawai found the Marsh brothers and worked in their art shops in San Francisco and Pasadena for many years on craftwork repair. The Pasadena shop was in the neighbourhood of the Huntington estate in San Marino. When the Marsh brothers close this shop and sold their collections to Huntington, Kawai was introduced to the latter the move (disassemble and reassemble) of a tea house. He got afterward three additional construction tasks in the Huntington garden: a torii, which has collapsed later, a bell tower, which is still standing in the garden in good condition, and a drum bridge, the Moon Bridge, of our concern in this paper.

2. The Woven Arch Bridge

The Bridge Structure

Located in the central basin of the natural landscape, the moon bridge is a visual focus of the Japanese Garden (Fig.2). Its light and elegant structure is an attraction to the visitors from all directions. The most remarkable feature is its peculiar structure: unlike the drum bridges with curved beams from elsewhere, the Moon Bridge is composed by interlaced timber.

The Moon Bridge has a shape of circular arc, with a structure height of about 3 m, a clear span of some 8 m, and a total width of some 2 m. The under-deck structure is a combination of a woven arch below and a curved wooden arch above it.

The woven arch is made of interlocking longitudinal and cross beams. They are arranged like the lengthwise and crosswise threads of a textile. Neighbouring longitudinal beams are laid alternatively in inner and outer sides. Horizontal beams are clamped at their crossing. By this means each longitudinal beam is supported through the cross beams at its ends by two neighbours, while supporting the same neighbours in the middle. Structures with similar principle are catalogued as

"reciprocal frame" in modern sense of architectural study.

Both the longitudinal and cross beams have the same square section. On their connecting joints, no cutting was made onto the longitudinal beams. All joint-notches are cut on the crossbeams. The notches are triangular in section, following the form of the elements setting inside. This kind of joint could not prevent the moving between the connected two members. Without additional fixing elements, the structure could only rely on frictional force to keep structural integrity, which is obviously far from enough. As a result, nails are applied at the connection of the beams.

Fig. 2 Moon Bridge, Huntington Library, San Marino, USA. 2013. From west side.

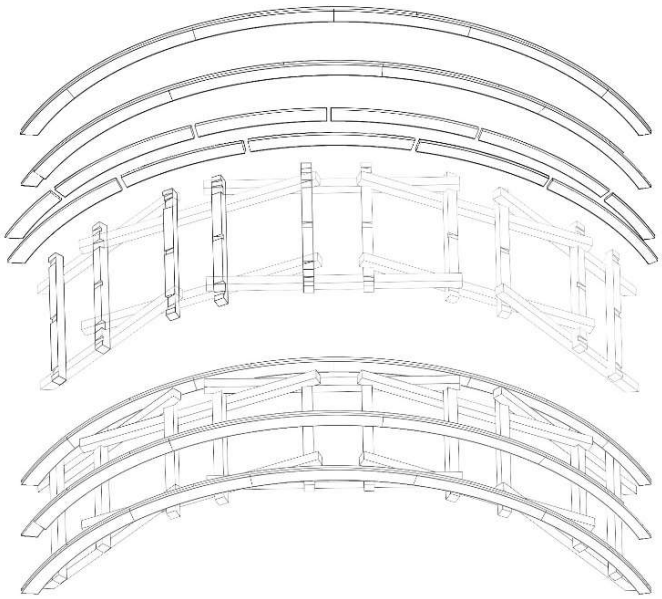

Fig. 3 The curved arch and the woven arch: construction

The curved arch rests on the horizontal beams of the woven arch. This layer of structure has three parallel curved beams, resting at both sides and in the middle of the bridge. Each curved beam is laminated through nails by two layers of boards; each layer of board is composed by four to six short arc-shaped boards, head to head following one another. The division of the boards in two layers is alternate to avoid juxtaposed seams. The boards of the curved beams are nailed separately to the cross beams of the woven arch.

The curved boards are cut from larger woods. This means it will consume larger boards than the its width. When the material is not wide enough, a circular segment is attached along the arc chord with glue.

Deck boards are placed on the curved arch. Steps are made from the same wooden boards as the deck. Width and height of the steps vary according to their position along the arch.

The handrail goes along the curved shape. As the curved beam, the arc-shaped members are cut out of larger wood. The handrail posts are fixed onto the curved arch at their feet with round wooden dowels.

At the feet of the arch are two concrete sills, at their outer sides are huge stone foundations buried deeply in the earth. They serve as the stone steps at the bottom of the bridge steps, and provide steady foundations of the bridge to offset the side thrust of the arch structure.

Hundreds of nails are applied in the bridge structure. According to their position and function, there are three types of nails in the under-deck structure (woven and curved arch): those connecting the longitudinal and cross beams of the woven arch; those connect the two layer of boards of the curved beams; and those connect the curved beams to the woven arch. Among them the most interesting ones are the nails hidden in between the two layers of the curved beams. They indicate that the curved beams are not pre-fixed on the ground and put onto the woven arch as a complete piece, rather, their two layers of boards are nailed onto the cross beams of the woven arch one after another. The position and direction of the nails enable us to track back the process of construction.

The Bridge of Perfection

The full moon has a metaphor for “perfection” in the China-centred East Asian culture, the same as the number 10. In Chinese the word for “circle” has the same meaning with that for “full”, and the word combined by these two characters means exactly “perfect” or “perfection” 圆满, while the combination of the number 10 and the word for “complete” means „complete perfection“ 十全. This is the same in both Chinese and Japanese Kanji (the adopted logographic Chinese characters in Japanese are corresponding 十全, 円満).

This bridge was ordered in the contract under the name “Full Moon Bridge”, and was frequently mentioned with the same name in the earlier documents by the first curator. As mentioned above, it was a production inspired by the semi-circle shaped Drum Bridge in San Francisco, which, with its reflection on the water expressed a perfect circular form, must have given a strong impression to Huntington.

The shape of the Huntington Moon Bridge is, however, not a circular “full moon”. Albeit its designer had other measures to approach the metaphor:

The shape of the structure was elaborately designed. The woven arch is composed by 10 longitudinal beams and 10 horizontal beams, each of these beams are square in section with the width of five cun (Japanese inch, 1 cun = 3.03 cm). For the circular form of the curved beam, the innermost arc line of the curved arch has a radius angle of almost neat 120 degree, and a radius of exact 5 meter, which gives the circular arc a perfect diameter of 10 meter (Fig.4).

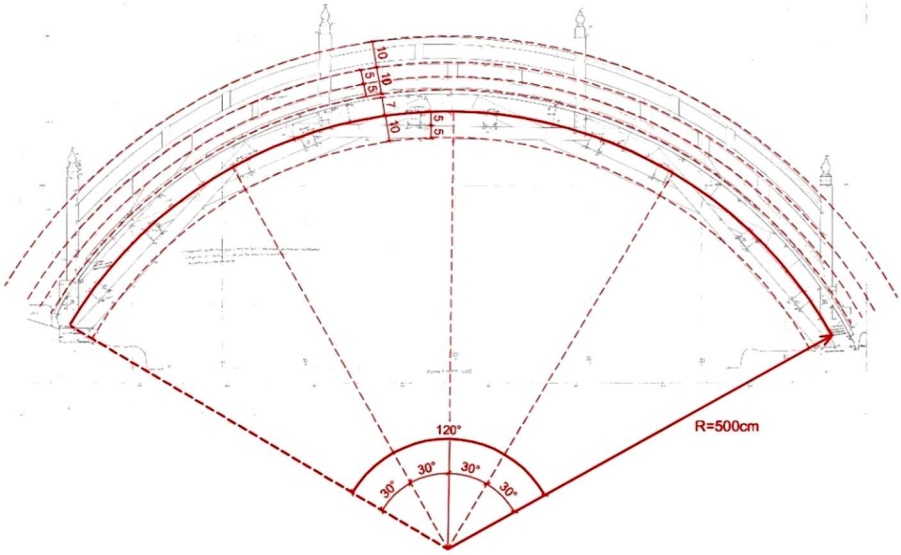

Fig. 4 Geometry analysis of the elevation of the Moon Bridge (unit: cun).

In Kawai’s carpenter career, he had the chance to be familiar with three measurement systems: the traditional Japanese system, the metric system, which had been promoted by the Japanese government in the late 19th century, and the imperial units used in America. When we move on to check other geometry scales, it is clear that the building elements are made according to the traditional Japanese unit, but neither the span nor the rise of the arch are integer numbers in all three measurement systems. In this sense, they could not have been taken as the controlling factor in the design. The initial idea of the design must have been the diameter of the arch: the 10 meter of diameter is too neat to be a coincidence.

The favor of design with integer number has a tradition in Japanese bridge construction. The famous Kintai Bridge takes 60 degrees as the radius angle, making the span equal the radius.

The geometry of the bridge indicates the artful configuration in other aspects. The bridge site has a 23 cm height difference at the northern (lower) and southern (higher) arch feet. If the bridge war designed symmetrically, the centre pair of beams would be inclined. In the current status of the bridge, the centre beams are almost horizontal with only 5 cm height difference, which could hardly be noticed by bare eyes. To achieve this, the length of the lowest longitudinal beams at the arch feet must be unequal. The difference in length is 14 cm.

3. Unwritten History of the Moon Bridge

The reconstruction around 1950

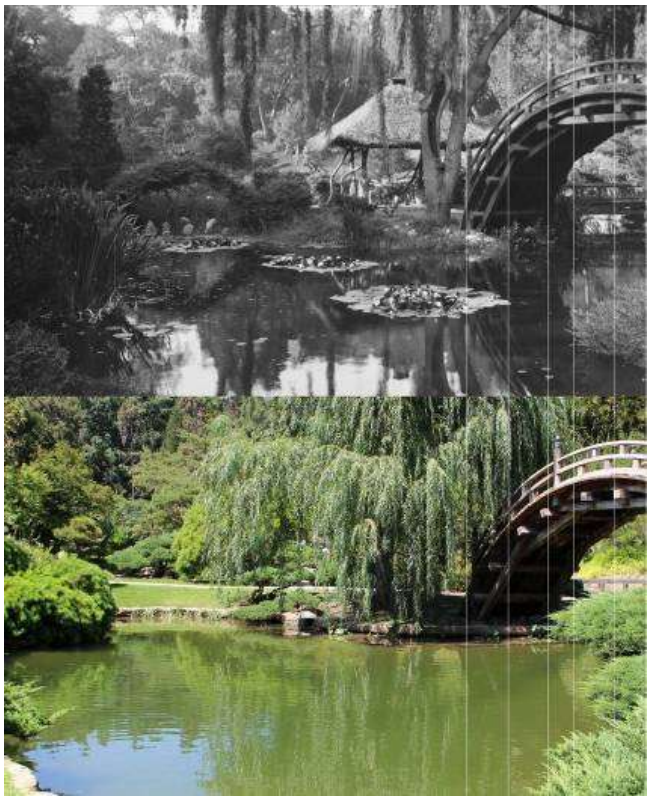

Fig. 5 The Moon Bridge in a century. Huntington Library, San Marino, USA

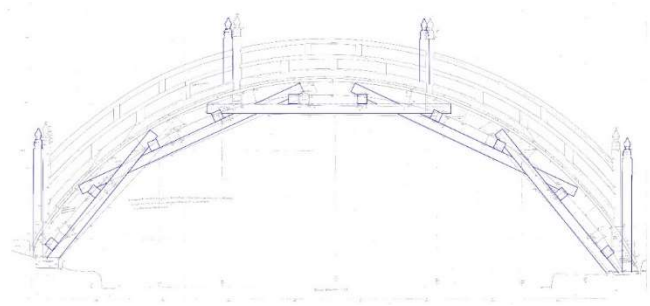

Fig. 6 Proportion of the woven arch, before 1949.

2013 June, when the author arrived at the Huntington Japanese Garden, he could not wait to reproduce an exact viewpoint of a photograph, which is the oldest preserved image of the Moon Bridge, dated between 1913 and 1923[4].

Despite his many attempts, the reproduction was not successful. The new photos from 2013 seem rather close to the old image, but there was always some proportion errors here and there (Fig. 5). The author could only blame the errors on the inaccurate standing point or the optical deformation of the photography.

Soon enough, more photos from the Huntington digital archive[5,6] offer an answer to the inaccuracy problem: The old image of the bridge was not the same one standing in the Japanese Garden today! A group of photos dated around the 1920s demonstrate a different proportion of the woven arch of the earlier structure: the cross beams distribute more uniformly in the old bridge, while they are pairwise closer in the present one.

The latest dated image with the same proportion is taken in January of 1949[6], while the earliest dated photo with the proportion in concordance with the bridge today is dated in 1962[7]. These put the reconstruction of the bridge between 1949 and 1962. With the help of these old photos, the author reconstructed the earlier proportion of the bridge (Fig. 6).

More details in higher resolution images reveal further differences: two photos, both dated around 1925, show out a wave-shaped grain on a central longitudinal beam, which is not found on members of the present bridge; more importantly, in the old photos the notches on the cross beams for adopting the curved beams are much deeper than those today. This indicates all cross beams had been replaced during the reconstruction.

Members of the woven arch could be easily replaced since they need only small timber – comparing with the required wood to replace the handrail, which must be cut out from much larger wood. So it is no surprise, by the comparison of the comparatively fragmentary pieces today and the rather neatly organized seams in the old photos, it's obvious that the old handrail members had been repaired and reused as much as possible during the bridge rebuilding.

The collapse(s) in Nobu Kawai's narration

In the records of the Oral History Project of the Pasadena History Museum, Toichiro Kawai's son, Nobu T. Kawai mentioned a very interesting event, which is not recorded in the Huntington constructional report: Somewhen after their construction, both the Moon Bridge and the torii collapsed. The Moon Bridge was then reconstructed, the torii was not.

The collapse of the Moon Bridge was mentioned by Nobu in three different reports[8,9,10], two of them with a time point, but they contradict each other. In one interview in 1984, Nobu mentioned the collapse "in about 1914", and that the bridge standing there as an "exact duplicate" according to his father's original design[9]:

"He built the tyco bushee (author's note: taiko-bashi)*, which is a drum bridge that is still there and also the bell tower and helped in designing other structures or replacement of stone lanterns and statues throughout the Japanese garden. Now that back in about 1914 and in the meantime the original bridge had rotted through, termites and dryrot and so forth and collapsed. So they have rebuilt that bridge in the exact design that it was built by my father. So the bridge that is standing today is not the one that my father built but it is an exact duplicate of the one that he built at the same location."*

But in another material compiled by Nobu in 1984, he mentioned the time point of the collapse as "several years ago". In all three materials, Nobu imputed the collapse to "age, termites and dry rot". The same reason he gave on the collapse of the torii.

Fig. 7 The bell tower. Japanese Garden, Huntington Library, San Marino, USA.

Kawai established three buildings for the Huntington garden: the Moon Bridge, the torii, and a bell tower. Nobu mentioned how proud his father was for the bell tower (Fig. 7). It was Kawai's favorite work, and stands today in good condition in the garden. In the interview of 1985, Nobu described as follows:

"Dad often quoted Japanese proverbs. one was, 'when a bull dies, it leaves its horns; when a tiger dies, it leaves its hide; when a man dies he leaves his name.' I recall his staying up night after night drawing pages of blueprints. He wanted this to be one with which he would be proud to have his name identified. All his talents were directed to make each joint fit perfectly. That he was satisfied with his work was indicated when he told us he had tacked a plaque, inscribed with his name as the builder and the date of construction, in the attic of the building."

When the author discussed the findings on the reconstruction history with Andrew Mitchell, the architect who take charge of the maintenance of the bridge, he got the information from the latter, that it is "heard, that the bridge has been at least twice rebuilt".

Nobu T. Kawai gave no information on a second reconstruction. Both time points he mentioned (in 1914 and somewhen before 1984) are not reliable. The "several years ago" counting from the 1984 interview might be reluctantly referring to the reconstruction around the 1950s. Anyway the photo archives confirm that the bridge has never been rebuilt but only repaired since 1962. The "1914" is even more confusing. In 1914 Toichiro Kawai was still working in the Huntington Japanese Garden on the bell tower, which was only finished in that December. Could this only be a slip of the tongue during the interview? Or could this be a first collapse accident? Why that Toichiro Kawai, a craftsman with strong professional self-esteem, showed no pride in front of his children on the Moon Bridge, an indeed genius design? Would it therefore be possible, that the bridge had gone through an early accident?

The Homemade Model

In the material compiled by Nobu in 1984, in the same paragraph where he mentioned the collapse, he talked notably about how his father studied the bridge at home[10]:

"He made a model of the bridge which was around the house until it got lost during our wartime evacuation. It was built with interlaced timbers without the use of nails. The more weight placed upon the bridge caused the joints to become tighter and stronger."

We've mentioned it above, without nails or similar fixing mechanics, the woven arch is by no means to be stable. It has two degrees of freedom for motion, that the cross beams could slide along the longitudinal beams under them, and that the longitudinal beams could slide along their axis. To keep the structure stable, the friction force would not be enough.

Toichiro Kawai must have understood this structural problem. The model he made at home, described by his son, is definitely a stable woven structure without the use of nails. Similar structures appear in a large scope of China as a popular folk game, the "chopstick bridge" (Fig. 8). But by aiming at the metaphor of 10 and of perfection, he insist with the 10 members and of an arc form with 10 meters diameter, a beautiful design finally appeared in front of us, by sacrificing the structural stability.

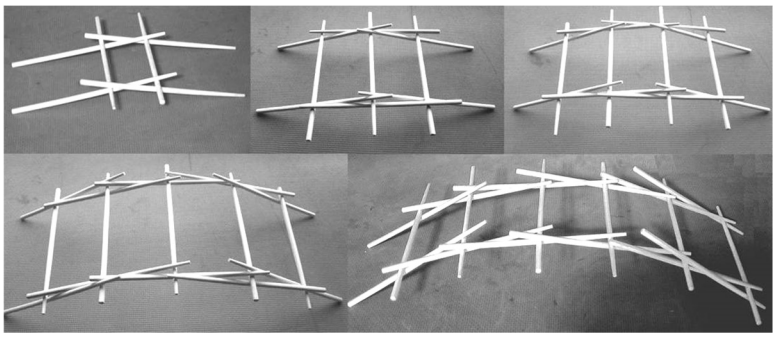

Fig. 8 The traditional Chinese folk game "chopstick bridge".

Kawai must have some means to keep the joints fixed, but probably without the using of nails, as his son proudly recalled. It is also so many times mentioned in the early Huntington archives, that the Japanese carpenters do not use nails, and it was the exact reason that Kawai got his first task (to move the Japanese tea house) from Huntington. Such a belief is still popular in America and even in Asia today. In fact the "without nail construction" is only valid to the main structure of Japanese (and similarly Chinese) architecture; while in the small scaled woodwork, including window, door, ceiling and decking, plenty of nails are involved. In Japan, nails and other iron elements, e.g. iron cramp and iron band, are also common in traditional wooden bridges. It is thus possible, that a proud Japanese carpenter, as Kawai, might be "kidnapped" by the legend of his career tradition, he might therefore avoid the use of iron elements in the main structure, and use other types of joints instead.

There are many means to restrict the motion between the beams. For example wooden dowel between the crossing beam members, or hidden dovetails at the position of present notches – these kind of wood joints will be functional enough for a while, but will also be weak enough to be damaged in a short period of time.

4. A Century of Reconstruction of the Moon Bridge

Now let's put all the information together. If the deduction above is correct, Kawai's inspiration of the Moon Bridge was a model game, which is similar with the Chinese traditional folk game "chopstick bridge". It is an almost self-standing reciprocal structure with interlocking beams and could avoid the use of nails. But for the metaphor of "full moon" and perfection, he sacrificed the inherent constructional logic of this type of structure, but designed the woven arch with 10 cross beams and 10 longitudinal beams in an arch shape with 10 meter of diameter and 120 degree of radius angle. The structure is thus unstable without additional connections.

The Moon Bridge was first finished by Kawai in 1913, and collapsed in about one or two years by the failure of the woven arch. Judging from the quick failure and the quick reconstruction, the original bridge might have been built without nails, but connected only through weak wooden joints. Since the curved arch beams are stable by themselves, the structure from them above could have survived this accident. People – without the involvement of Kawai – reconstructed the woven arch by putting the fallen beams back to their original place, and nailed them together.

The old (and might be damaged) beams caused further structural problems. As a result, a thorough reconstruction was carried out somewhen between 1949 and 1962. In this time both the woven arch and the curved arch are replaced entirely. The curved arch is nailed onto the woven arch piece by

piece. Members of the handrail were repaired and reused as much as possible. The reconstruction has proportion difference in the woven arch with the original structure, since this part of structure is rather sensitive in shape. The arc form of the curved arch should be more loyal to the original design, to fit the curved shape of the original handrail.

Since the 1960s the bridge has never been reconstructed anymore. During the maintain the bridge was repainted, pieces of handrail and deck are repaired and replaced, the main structure stays unchanged.

Acknowledgements

Special gratitude to the curator of the Huntington Japanese Garden Mr. David MacLaren and the architect Mr. Andrew Mitchell, for their kindly help for my investigation there; and to the Pasadena History Museum, for their permission for me to visit the unpublished material of the Oral History Project.

References

[1] Wolf, B., and A. Piercy. "George Turner Marsh and Japanese art in America." Orientations 29.4 (1998): 47-57.

[2] Information from the display board in the Golden Gate Park.

[3] Information of Kawai's life comes from the archive of the Japanese Garden, Huntington Library, and the archive of the oral History Collection of Pasadena History Museum:

Kawai, N. Kawai Family Background. 1985.01. From: Archive of the Japanise Garten, Huntington Library.

Interview with Nobu Kawai. From: Oral History Project. Special Collections on Toichiro Kawai, unpublished manuscript. (Un-edited material). Pasadena History Museum.

Biographical sketch III. From: Archive of the Japanese Garten, Huntington Library.

[4] http://cdm16003.contentdm.oclc.org/cdm/singleitem/collection/p15150coll8/id/313/rec/3

http://cdm16003.contentdm.oclc.org/cdm/singleitem/collection/p15150coll8/id/3807/rec/8

[5] http://hdl.huntington.org/cdm/singleitem/collection/p15150coll8/id/3805/rec/5

http://hdl.huntington.org/cdm/singleitem/collection/p15150coll8/id/3806/rec/5

http://hdl.huntington.org/cdm/ref/collection/p15150coll8/id/3803

http://hdl.huntington.org/cdm/singleitem/collection/p15150coll8/id/3802/rec/1

http://cdm16003.contentdm.oclc.org/cdm/ref/collection/p15150coll8/id/90

[6] http://hdl.huntington.org/cdm/singleitem/collection/p15150coll8/id/3907/rec/13

[7] http://cdm16003.contentdm.oclc.org/cdm/ref/collection/p15150coll8/id/3808

[8] Kawai, N.T. Answers to Questions. unpublished manuscript. From: Oral History Project in Pasadena History Museum: Long, Long ago oral history project.

[9] Interview with Nobu Kawai, 55 Harkness Street, Pasadena, Thu, 27.sep. 1984. 6-7. Unpublished. Oral History Project in Pasadena History Museum

[10] Kawai, N. T. Kawai family background. 1985.01. From: Archive of the Japanese Garden, Huntington Library

Historic Timber Howe Trusses of British Columbia

Murray Johnson
VP & Project Director
COWI North America
North Vancouver, Canada
mmj@cowi.com

B.Sc.(EN), University of Alberta 1980. Buckland & Taylor (now COWI) 1980-1994, M.M. Johnson Ltd. 1995-2007, COWI North America 2007-present. Bridge design, bridge construction engineering, timber bridge specialist incl. inspection and rehabilitation.

Gary Farnden
Sr Bridge Rehab Engineer
BC Min of Transportation & Infrastructure
Victoria, BC, Canada
Gary.Farnden@gov.bc.ca

B.A.Sc., University of British Columbia 1981. BC Ministry of Transportation and Infrastructure, 34 years. Senior Bridge Engineer responsible for bridge evaluation, repair, retrofit policy and procedures. Program Engineer for 2010 Timber bridge program.

Summary

The Province of British Columbia (BC) in Canada is a largely mountainous region with extensive forests and innumerable river and stream crossings. When construction of roads began in the mid-1800's, the bridges needed were built mostly from the most plentiful material available, timber. The construction of timber bridges of many types continued through the 20th century, and timber bridges actually dominated the Province's road bridge inventory until about 1980. The most popular timber bridge type for longer spans was the Howe truss. From relatively small components of sawn timber, and a bare minimum of iron or steel parts, Howe trusses were built with clear spans of up to 55m. Many Howe truss bridges, some nearly a century old, still carry traffic in BC today. The paper describes the history, design, and original construction of the timber Howe trusses, then discusses present-day inspection and assessment methods as well as repairs and rehabilitation techniques.

Keywords: timber bridge, Howe truss, timber Howe truss, Howe truss highway bridge, timber bridge rehabilitation, timber truss bridge, BCMoTI timber bridge, COWI North America timber bridge.

1. Introduction

1.1 Early Road Building in British Columbia, Canada

The province of British Columbia (BC) is about 945,000 square kilometres of mostly-rugged terrain, with extensive mountain ranges, wide interior valleys, steep river canyons, and heavy forests. Travel through this landscape has always been challenging. In the centuries leading up to the early 1800's, the First Nations peoples built trails to facilitate trade between communities, which included some basic bridge structures. When land-based fur traders began to arrive in 1805, they expanded upon these trails and built new routes, but did little in the way of bridge building. Gold miners began pouring into the regions around the Fraser and Thompson Rivers in 1857, spurring the construction of gold trails to access mining areas. While these trails served their purpose well, their usefulness in moving freight was limited, and construction of roads suitable for freight wagons began in the late 1850's. These roads included wooden trestle-type bridges and the first crossing of the Fraser River at Alexandra with a suspension bridge. Late in the 1860's and through the 1870's, the development of trunk roads was government policy in order to encourage development of the economy beyond gold and fur trading. The arrival of the railroads in the 1880's slowed this trunk road development, and the railroad routes even destroyed some existing roads. Road building in the province proceeded slowly through the start of the 20th century, until in 1920 the automobile age came to BC. While it took until after the Second World War for any real work to begin at connecting the various regions of the province with better roads, construction of roads within regions included the building of many bridges between 1920 and the 1950's [1].

1.2 Timber Road Bridges in BC

In a province covered in forests, much of it large Douglas Fir, with its excellent structural properties, the obvious material choice for bridge-building was timber. In fact, up until about 1980, timber bridges dominated the Province's road bridge inventory [2]. Many simple beam and trestle-type structures were built, but for longer spans to cross steep-sided canyons, larger streams, and for multiple spans crossing wide rivers, another option was needed. The solution for this became the timber Howe truss. Invented in 1840 by William Howe of Massachusetts, the Howe truss, with timber chords and diagonal members and iron (later steel) vertical rods and connection blocks, was the most popular bridge design in the United States during the last half of the 19th century, and is the structure within many of the covered bridges remaining within the USA today. In BC, the timber readily available near most bridge sites, and the small amount of steel required to build a Howe truss bridge, made this a very practical choice. Stories are recalled within the BCMoTI of the early days of Howe truss bridge building, in locations not yet accessible by built roads. Crews would cut and hand-saw timber at the bridge site in advance of the construction season, while the small amount of iron and steel needed for the bridge was brought in by pack animal. Tensions rods were heated at their midpoint over a fire, bent in half, and packed into the site, where they were heated again over the campfire and straightened back out.

Researching the total number of timber Howe truss bridges that were built in BC is beyond the scope of this paper, however it is believed that the number was in the hundreds. It should be noted that while there were also many timber Howe truss bridges built for the railroads, especially in the early days, it is not known if any survive, and this paper focusses on the road structures, being within the realm of both authors' experience.

1.3 The Howe Truss

The truss developed by William Howe featured heavy timber diagonal members in compression and lighter, vertical iron (later steel) members in tension, with parallel timber chords. The use of threaded, adjustable iron tension members, secured by nuts, was the feature that made Howe the first bridge designer to devise a method of adjusting a timber truss to keep joints tight. Other versions of timber trusses, which included vertical tension members of wood, were difficult to detail in an efficient manner that would keep joints tight, and Howe's simple, elegant solution of replacing these timber verticals with iron rods resulted in a truss that was not only easy to erect, but could be adjusted and parts replaced while remaining in service [3].

Howe based his design on the limited stress analysis information available at that time. The statically-determinate form meant that real forces and stresses could be accurately computed and efficiency achieved while creating a safe structure. The popularity of the Howe truss also resulted, in part, from its comparatively simple erection, as the design eliminated the need for skilled carpenters notching and pegging wooden joints.

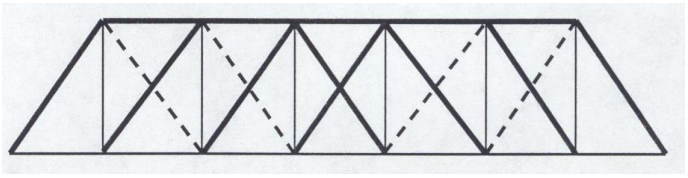

Fig. 1 *The General Form of a Howe Truss*

Bridge historian Eric DeLony wrote, "The Howe truss may be the closest that wooden-bridge design ever came to perfection. For simplicity of construction, rapidity of erection, and ease of replacing parts, it stands without rival." [4].

2. The Timber Howe Truss Bridge in BC

2.1 General

The discussion in this paper is focussed mainly on the timber Howe truss road bridges that still remain in service in BC, with some mention of bridges that have been removed or have failed in recent history. The remaining bridges represent the legacy of over five decades of bridge building, with the oldest remaining example built in 1907, and the newest built in 1961. While earlier truss designs likely had some different details, the design details, inspections, condition, and repairs discussed here all relate to these remaining bridges.

The BC government entity responsible for the construction of bridges on the provincial highway network at the time was the Department of Public Works. Through the years there have been several government reorganizations and department name changes, and the entity currently responsible for these bridges is the BC Ministry of Transportation and Infrastructure (BCMoTI). The BCMoTI currently maintains a total of approximately 2800 bridges on the numbered highway and secondary road system.

2.2 Standard Truss Designs

Timber Howe trusses for bridges built in BC in the 20th century typically were constructed following one of many standard designs for the truss span(s), including the bridge deck and railings. For a particular bridge project, site-specific designs and drawings would be prepared for the layout, substructures, and shorter timber-stringer approach spans, and the appropriate standard drawings for the truss spans added to the drawing set.

In the older drawing records of the BCMoTI there is a register showing nearly fifty such standard truss designs. While Canada now uses the SI system of units, at the time the Imperial system was in use, and bridge spans and widths were shown in feet and inches. The increment in bridge span used for the standard designs was 10 ft (3.05m), with spans ranging from 80 ft (24.4m) to 200 ft (61.0m), and bridge deck widths from 10.5 ft (3.2m) to 20 ft (6.1m). Rough-sawn timber sizes were shown in inches. Henceforth in this paper dimensions will be shown in SI units, in keeping with the standards of the conference.

The standard truss designs were prepared in both through-truss and deck-truss configurations. The designs typically divide the truss span bearing-to-bearing into an even number of panels with a constant length. Panel lengths typically vary from 3.81m to 4.57m, for example, a 150 ft (45.7m) span would be divided into ten panels at 15 ft (4.57m) long. The depth of the parallel-chord trusses varies from about 6.0m to 8.0m, with aspect ratios for the truss panels (height/length) varying from about 1.4 to 1.9.

The standard design drawings for the trusses are very compact compared to what we would typically see today, with almost all of the information clearly and efficiently contained on a single drawing, as shown in Fig. 3. Two additional drawings showed the details of the cast-steel angle blocks at panel points and the chord assemblies.

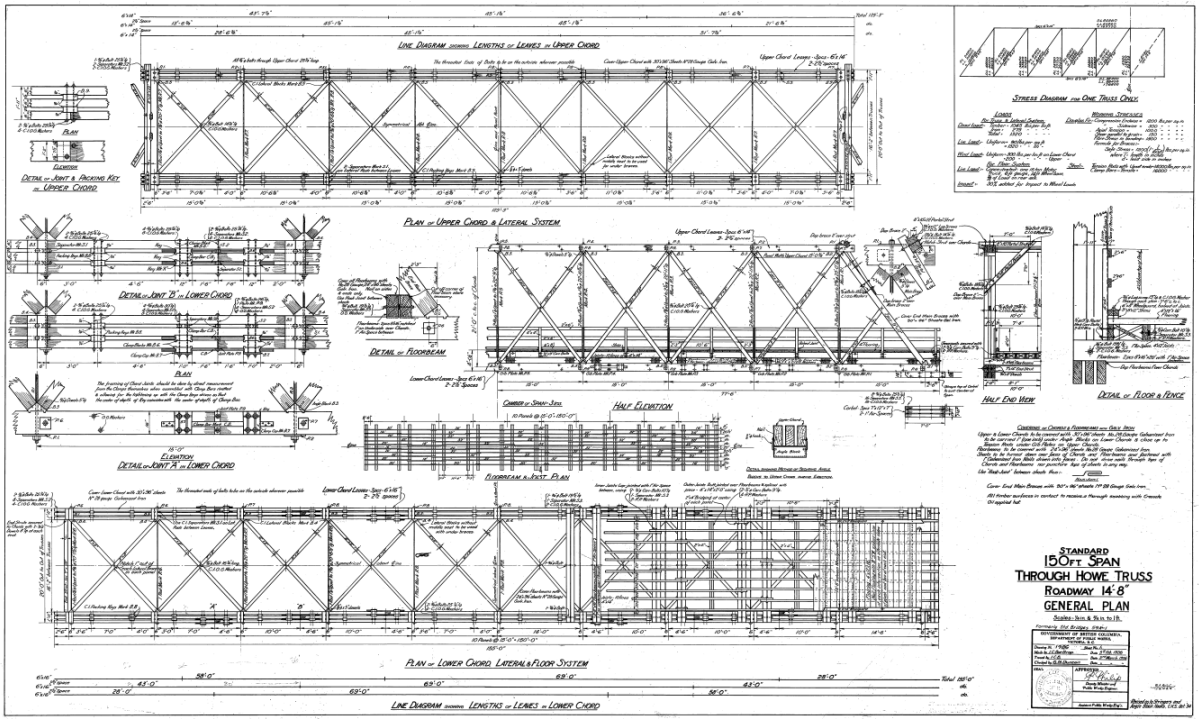

Fig. 3 *Typical Standard Drawing for a Timber Howe Truss, from 1926*

2.3 Remaining Timber Howe Truss Road Bridges in BC

Over the years, many of the timber Howe truss bridges in BC have been replaced with newer bridge types, usually of concrete deck slabs on concrete or steel girders. Functional limitations of the Howe trusses with respect to the needs of modern traffic include limited vertical clearance in through-truss configurations, narrow widths often resulting in effectively single-lane bridges, lack of shoulders, and traffic load restrictions. In addition, as the timber bridges age, the cost of maintaining them in a safe condition rises.

Fig. 4 *Collapsed Howe Truss Bridge, Struck By Heavy Equipment on a Crossing Truck*

Narrow width, low vertical clearance, and lack of redundancy of the timber Howe truss bridges also makes them vulnerable to damage and even collapse by being impacted by heavy vehicles, often carrying heavy equipment or logs.

Today, the BCMoTI maintains a total of 23 water crossings that include timber Howe truss spans. Within these bridges there are a total of 31 truss spans, with 6 deck-trusses and 25 through-trusses. In addition, two Howe truss bridges remain in use that the BCMoTI has divested to other entities: a single span roadway through-truss and a 5-span through-truss over the Fraser River that has been converted to a pedestrian/cycle bridge.

Few of the timber Howe truss bridges remain on numbered highways in BC, most are on secondary roads serving smaller communities with primarily local traffic, relatively low traffic volumes, and available alternate routes for heavy or oversize vehicles.

Fig. 5 *Quick Bridge*

The oldest remaining timber Howe truss bridge still in service in BC is the Ashnola Bridge near Keremeos. This bridge was built in 1907 by a railway company, and later converted to road use. It is also the only covered Howe truss bridge in the province, and its painted enclosure has given it the nickname of "Red Bridge".

The oldest timber Howe truss bridge actually built for road use is Quick Bridge, built in 1921 at Quick Station over the Bulkley River in northern BC to connect farmers on one side of the river with the railway on the other side.

This bridge comprises two – 45.7m spans supported on mass concrete piers in the river with a short approach span at each end. The bridge currently has a vehicle load limit of 8 tonnes.

The most recently-constructed timber Howe truss bridge in BC is the Moose Mouth Bridge, built in 1961 over Moose Creek in northern BC. This bridge has a single 39.6m Howe truss span supported on a concrete pier and a timber-pile pier, with a short approach span at each end.

2.4 Truss Details

2.4.1 General

The timber Howe truss road bridges built in BC from 1920 through 1961 share many common details. The Howe trusses were built generally from Douglas Fir sawn timbers, cut from large trees and of a high grade. Most chord members were pressure preservative treated, while diagonal and

bracing members, being more easily replaced, were mostly treated but sometimes not. Many of the bridges have metal flashings covering top and bottom chords, and sometimes diagonals, to protect against the elements; some have tar-and-gravel protective coating on the top surfaces of chords.

Fig. 6 *Bottom Chord Panel Point, Deck Truss*

Fig. 7 *Top Chord Panel Point, Through-Truss*

2.4.2 Bottom (Tension) Chords

Bottom chords are built-up, with timbers used generally varying in smaller dimension between 90mm to 150mm and in larger dimension between 360mm and 400mm. Being tension members, with attendant problems in splicing, the timber lengths used were maximized and are up to 21m long. The oldest of the remaining structures, the Quick Bridge (1921) described above, has bottom chords made up of three separate large timbers with a gap between, and an elaborate system of steel connectors at splices set into notches in the timber to transfer tension between the lengths of timber. All the other remaining bridges built since 1929 are built to newer standard designs and have bottom chords consisting of 5 to 7 plies of timber bolted tight together, with splices along the length staggered such that only one ply is ever interrupted at one location. Since the bolts in shear transfer load between plies as tension splices are passed, bearing area of the bolts is critical. The majority of bottom chord connectors are pipe-bolts, lengths of pipe threaded at each end for nuts, which increases the bearing area while minimizing the steel content.

2.4.3 Top (Compression) Chords

Top chords are built-up, with the individual timbers used generally varying in smaller dimension between 100mm to 150mm and in larger dimension between 300mm and 360mm. Again, the older structure, Quick Bridge, has three separate large timbers with gaps between. All other remaining spans have top chords of several plies bolted tight together, with joints between lengths of timber butted together in compression.

2.4.4 Timber Diagonals

Main diagonal members are arranged in pairs, with dimensions ranging between 200mm and 300mm. The pair of timbers has a space between them, through which the counter-diagonal in the panel, a single timber with dimensions of 150 to 200mm, passes in the opposite orientation. These counter-diagonals, in addition to resisting reversing live load shear effects in the panels towards midspan, also control geometry of the truss; as the vertical tension rods are tightened, the counter-diagonals are brought into compression and the system is slightly pre-stressed against these, leaving the truss in the cambered shape it was detailed to. The counter-diagonals, bolted to the main diagonals at the crossing point, also provide significant bracing to the main diagonals in the plane direction. Within a given truss span, the size of the diagonal timbers used varies for efficiency of material use. The end diagonals (end posts) are typically a pair of 300mm x 300mm timbers, while towards midspan, the timber sizes are reduced down to as small as 180mm x 180mm.

2.4.5 Steel Vertical Tension Rods

The steel vertical tension members are upset rods, that is, the ends have been forged to a larger diameter, so that once threaded, the net area at the threads is not less than that of the body of the

rod, for efficient use of steel. The diameter of the rods varies from 25mm to 54mm; within a given truss, the rods will be larger towards the ends of the bridge, where panel shear is higher, and smaller towards midspan, where shear is lower, again for efficiency of material use. Depending upon the span of the truss, there are either two or three vertical tension rods at each panel point in each truss line.

2.4.6 Truss Connection Points

The connections at the truss panel points are at the heart of the success of the Howe truss design. The detail at both the top and bottom chords employs a cast iron "angle block" which is made with bearing surfaces at the correct angle to allow diagonal members with a square-cut end to bear against it (see Figs. 6 & 7). The angle block is cast with two projecting ribs that are notched into the chord to transfer the net horizontal shear between truss panels. In a truss with two vertical tension rods (as in Figs. 6 & 7), the angle block has two holes through it to allow the rods to pass, while in a truss with three vertical rods, the angle block has a single hole for the middle rod, and the two outer rods pass outside the block and the chord. The holes in the angle blocks are often sealed around the rods with a hot-poured tar sealant. Tension rods are anchored against the bottom chord, and the top of the top chord, by nuts bearing on a steel "gib plate" which bears against the timber. There is no connection between the timber diagonals and the angle block, other than a very small centring pin to locate the timber while the truss is being constructed; in service, this whole joint assembly is kept tight together by the dead load of the bridge itself and the pre-loading of the counter-diagonals resulting from tightening the tension rods.

2.4.7 Bracing Systems

The two Howe trusses in a span are braced against each other with top and bottom lateral bracing systems and sway bracing. The top and bottom lateral bracing systems employ another set of cast iron angle blocks, against the inside face of the chords. A single horizontal tension rod between the two trusses passes through this bracing angle block and the chord member (see Figs. 6 & 7) and a crossed pair of timber braces in each panel abut the angle blocks. Sway bracing in a deck-truss configuration typically consists of crossed timber braces between the trusses at each panel point, butting against the bracing angle block (see Fig. 6). Sway bracing in a through-truss configuration uses a knee-brace arrangement at the top of the trusses (see Fig. 8), at the end top panel points and sometimes at two intermediate panel points along the bridge for longer spans. The knee braces were originally all installed inboard of the trusses, however on some bridges they have been relocated outboard of the trusses to reduce their vulnerability to impact from overheight vehicles.

2.4.8 Decks

The deck configurations of the remaining timber Howe truss bridges vary somewhat. In some cases this is just differences in the original design, but in many cases it is because the deck assemblies are the most likely elements of the bridge to have been replaced due to wear and tear, and the replacement design has varied from the original.

Fig. 8 *Typical View on Deck, Through-Truss With Portal Bracing*

The most common deck configuration comprises sawn timber floorbeams with dimensions up to 200mm x 460mm spanning between the trusses. In a deck-truss, a pair of floorbeams bears on the top chord close to the panel point and creates little chord bending. In a through-truss a pair of floorbeams bears on the bottom chord to each side of the angle block and the geometry of the diagonals pushes the floorbeams far enough from the panel point to create significant chord bending. On top of the floorbeams, sawn timber stringers span longitudinally and support a deck of timber planks laid transversely. In some instances there is an additional wearing surface of planks laid longitudinally.

Fig. 8 shows the typical deck appearance on the bridges.

Variations found in the current deck designs include floorbeams that are regularly-spaced along the bottom chords with the deck planks spanning longitudinally, nail-laminated timber decks spanning longitudinally instead of stringers and planks, and stringer-transverse tie-longitudinal plank arrangements.

Railings on the bridges are of various configurations, some original and many not, but will not be examined in this paper.

3. Inspection

3.1 General

The BCMoTI conducts regular (annual or more frequent) inspections of all the timber Howe truss bridges using their own bridge inspectors. Periodically, they will assign an Enhanced Inspection task to a specialized bridge consulting firm with suitable experience in timber Howe trusses, which will provide a more thorough site inspection, sometimes a load rating assessment, comprehensive condition report, recommendations for short and long-term repairs and rehabilitation works, and estimated costs. For these inspections, qualified bridge engineers undertake the site work as well as the follow-up office tasks.

3.2 Inspection Access and Techniques

Effective inspection of a timber truss bridge requires arm's-length access to as much of the timber surfaces as possible, in order to employ inspection techniques intended to detect hidden deterioration. The few timber Howe deck-trusses remaining in BC can generally be inspected using an under-bridge inspection vehicle (UBIV), although there can be load capacity issues and one of the lighter units available may have to be used. Another option is ladder access from temporary decking laid on the bottom lateral bracing system. For the Howe through-trusses, however, which make up the majority of the spans, the UBIV has limited usefulness as it is not feasible to manoeuvre the platform through the openings between truss web members. The UBIV may be set up at the ends of the bridge and the inspection platform arm extended outside the bridge as far as possible along the bottom chords for close access, but this will not reach the middle portions of the span. Upper portions of the trusses along with top lateral bracing systems are effectively inspected from articulated manlifts. Lower portions of trusses are inspected by walking along decks and crawling over railings with fall protection. Access to the underside of bottom chords or decks may be achieved using movable scaffolding or rope access techniques. For the latter, a specialized team of two or three rope access technicians is employed to safely position the inspecting engineers in the locations that they need to access. Since the steps required for this positioning are fairly time-consuming, locations for inspection may be pre-screened using a remote video camera, enabling inspectors to focus on areas with visual clues of deterioration and limit the number of trips over the edge of the bridge on ropes.

The primary source of deterioration in timber bridge members is fungal decay. This is most dangerous when hidden from view in the interior of a timber member, and so much of the effort in timber bridge inspection focuses around finding such hidden decay. The main components of this inspection work for the Howe trusses are visual, probing, sounding, and exploratory drilling. Visual inspection of timber surfaces provides an experienced inspecting engineer with details of surface deterioration (surficial decay, weathering, checking, mechanical damage, twisting) as well as potential indications of internal decay (crushing, staining, moisture, vegetation growth, and flora indicative of decay organisms). Probing timber surfaces with a pointed awl, especially at checks, joints, ends, and open holes, often provides additional information as to what is occurring within the member. In some extreme cases, the exterior of the member may look intact, but an awl may be easily pushed up to its hilt into the timber, indicating extensive internal decay. Sounding timber members by striking them with a hammer provides an experienced ear with clues of potential internal decay; a solid timber returns a sharper, higher-pitched sound, while a timber hollowed out by decay will return a dull, low-pitched "thud", with varying degrees of sound for cases in between. Exploratory drilling, using a battery-powered drill and a small, sharp auger bit, is used to further investigate areas suspected of having internal decay. Resistance of the wood to drilling is gauged by the inspector, along with collection of the drill shavings, which are inspected for moisture, colour, soundness and consistency. Drill holes are filled with treated wooden plugs, or with caulking.

Inspection of steel and iron components is visual, with section-loss measurements taken when

tension rods begin to show significant corrosion. A portion of the tension rods is hidden within each of the timber chords (both rods in a two-rod truss but only the middle rod in a three-rod truss), in a potentially-wet area where corrosion could occur. In order to inspect these vulnerable areas, the rods may be loosened one at a time and lowered by about a metre in order to inspect the normally-hidden portion. Tension rods are also inspected for uniform tightness, usually by shaking the rod by hand. Counter-diagonals found not to be bearing on their angle blocks also indicate the need for rods to be tightened.

3.3 Typical Inspection Findings

Described below are some of the more significant defects and deterioration found during inspections, focussing on the Howe trusses themselves, as the primary structure.

3.3.1 Fungal Decay in Timbers

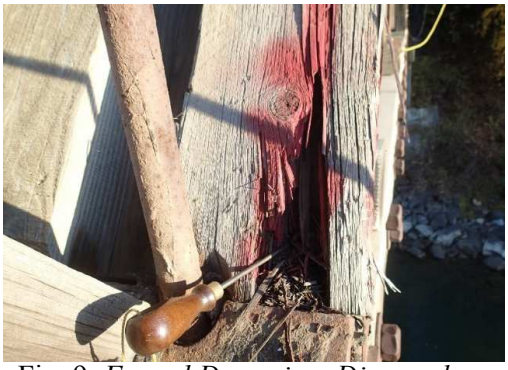

Fig. 9 *Fungal Decay in a Diagonal*

Treated timbers are generally protected against fungal decay, however the treatment may be compromised by penetrations to the untreated interior wood, such as by checking and open bolt holes. Moisture condensing on angle blocks may be drawn up into the end grain of diagonals and promote decay. Horizontal bracing members with checking are particularly susceptible since moisture will not drain away. Untreated timbers are of course more susceptible to decay. Chord members built up from multiple plies of timber that has been treated before assembly are found to perform very well, however, it is very difficult to effectively inspect the interior plies of timber.

In general, timber Howe truss members have been observed to be less susceptible to decay in the colder, drier interior and northern regions of the province than in wetter, warmer coastal regions.

3.3.2 Weathering, Checking, and Distortion of Timbers

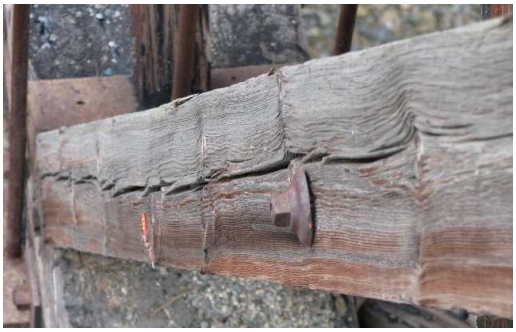

Fig. 10 *Weathering and Checking in a Diagonal With a Noticeable Bow*

Timber members in the Howe trusses, especially the diagonal and bracing members that are unprotected by metal flashing, are often found to show considerable weathering effects. In addition to degradation of the timber faces, heavy checking from the wood seasoning often occurs, as well as twisting of members. Twisting will sometimes rotate the end of the diagonal or brace to a state of partial contact with the angle block. In a timber with a spiral grain orientation, diagonal checking is sometimes quite severe. On occasion, bowing over the length of the member may occur, which may have structural strength implications for a compression member.

3.3.3 Cracking of Angle Blocks

Fig. 11 Cracking in a Top Angle Block

The cast iron angle blocks provide the geometry of the truss connections and the means of connecting tension verticals to compression diagonals. The hollow castings also transfer the net horizontal shear at a panel point into the chord. This load transfer is made through two projecting iron ribs bearing on notches in the chord. Pressure against the rib, particularly the one being pushed away from the angle block, results in tension across a narrow portion of the cast iron, and cracks have been found here in a number of the blocks, as shown in Fig. 11.

3.3.4 Steel Tension Rods

Fig. 12 Tension Rod Corrosion at Base

Steel tension rods are generally unprotected, and the rods usually show some degree of surface corrosion. Over the length of the rods, where moisture does not remain, section loss due to corrosion is generally not severe; measurements are taken with calipers during inspections to monitor this. Where the rods pass through the timber chords, moisture may be trapped and there may be significant corrosion, especially at the bottom chord, where dirt, road salt, and moisture can build up in the rod holes in the angle block and contribute to accelerated corrosion. Fig. 12 shows a rod "necked down" from corrosion at the bottom angle block. Tensions are sometimes found to be uneven between rods at a panel point, especially in a three-rod system, less determinate than the two-rod case.

3.3.5 Mechanical Damage

Mechanical damage to timber members may be found, usually consisting of a section of the member torn away, or a gash across the member. This is most often seen on diagonals or overhead bracing as a result of vehicular impact. If severe enough, these may reduce the strength of the member. Since this damage indicates that moving loads are too close, also of concern is the fact that a marginally more severe hit could potentially collapse the span. Howe through-trusses are less resilient than steel trusses for impact damage. Major damage to end posts, portals, and tension rods from impact is significantly more likely to cause span failure. Mechanical damage has also been observed at the bottom of spans due to debris impact during floods and from poor handling of replacement timbers, such as wire rope crush marks and accidental chain saw kerfs.

4. Assessment, Repairs and Rehabilitation

4.1 Assessments and Load Ratings

Enhanced Inspections of the timber Howe trusses are followed by engineering assessment to determine required repairs, rehabilitation, or loading restrictions needed to maintain the bridge in safe service. If a current accurate live load rating exists for a span, and deteriorated members are found, the safe capacity may be downgraded in a simple way by pro-rating using reduced member capacity. When a new load rating assessment is needed, this is done in accordance with the Canadian Highway Bridge Code, Section 14, Evaluation. This approach considers the required safety level, the behaviour of individual elements, the behaviour of the structural system, and the degree of inspection of the bridge undertaken for the evaluation.

While the basic analysis of a Howe truss is straightforward, being statically determinate, when member capacities are being assessed it has been found that there are some special aspects of structural behaviour that require special attention. Bending moments that occur in the continuous laminated bottom chords, due to the position of the floorbeams transferring deck loads to the trusses, will add to the tensile stress in the chords. The transfer of loads between bottom chord plies via numerous pipe bolts over long distances creates many non-standard "tension" failure modes to be investigated. The end restraint assumptions for timber diagonals on the effective length of these compression members affect capacity calculations and need careful consideration. The common assumption of pin-ended for these members proves to be too conservative given the level of restraint afforded by the end of the relatively squat timbers bearing against the angle blocks.

4.2 Periodic Repairs

One of the valuable attributes of the Howe trusses is the relative ease of replacement of most of the individual members, other than the top and bottom chords. Most bracing members and tension rods can be removed and replaced with minimal precautions, usually just closing the span to traffic loads during the work. Heavily corroded tension rods are replaced new with larger roads or higher strength threadrods (the original upsetting methods no longer being readily available).The paired diagonal members of interior truss panels can be removed and replaced one at a time, with

loosening of adjacent tension rods. The timbers in the paired end diagonals (end posts), with larger loads and less system redundancy, require more engineering and preparation work to temporarily accommodate the member load, typically by using jacking struts or by temporarily bracing or stiffening the member remaining in place. Bridge work crews experienced on the Howe trusses often help develop practical and innovative methods for efficient repair work. Another common adjustment to the Howe trusses is tightening the tension rods to restore lost camber due to creep and shrinkage effects in the timber over time; this technique properly starts by tightening rods at midspan and works outwards towards the ends. When member replacement is not feasible, typically for the chords, then local reinforcement may be undertaken by adding material, either as a permanent repair or as a temporary measure until rehabilitation work is undertaken.

Areas of timber with early or potential decay (open holes, checks) may be fortified against deterioration by inserting and sealing in borate rods, which are activated in the presence of water and inhibit fungal growth.

4.3 Rehabilitation

When an assessment indicates the need for rehabilitation work beyond basic repairs, or an increase in live load rating is desired, more significant rehabilitation work may be undertaken. Rehabilitation work often includes replacement of the stringer and plank bridge decks. Stress-laminated timber decks have been built on several bridges. Strengthening of timber diagonals is a common rehabilitation need. With the controlling failure mode being out-of-plane buckling, the addition of solid timber blocking bolted between the spaced timbers to stiffen a diagonal is often being used to increase capacity significantly. Fitting this blocking tightly between older timbers that have twisted and warped somewhat can prove to be a challenge requiring creative chainsaw work. The most difficult element to strengthen or restore in the timber Howe trusses, as well as being one of the most critical, is the bottom (tension) chords. It is extremely difficult to replace any section of a deteriorated bottom chord, especially as the through-laminate bolting is critical to load transfer, and so the most common approach is to strengthen the chord by the addition of external post-tensioning using high-strength steel rods, which has been undertaken on several bridges to date. It is somewhat easier to replace portions of a deteriorated compression chord. With end-butted splices it does not rely as much on the bolting of the laminates for load transfer, and parts of the outer plies of top chords have been replaced with new material while the bridge supports itself.

5. Conclusion

5.1 Timber Howe Truss Bridges in BC

The timber Howe truss bridge, invented in 1840 by William Howe, was a crucial element in the building of the highway network in British Columbia. Those familiar with the history call it "the bridge that built BC". Those that have them in their community's road network and rely upon them for connection to the rest of the world tend to love them for their history and aesthetics, but dislike them when they are closed for repairs or reduced in posted capacity.

From the glory years of timber Howe truss building in BC, ending in 1961, some 37 spans still remain in service, from 56 to 110 years old. Many Howe truss bridges have been replaced over the decades due to functional obsolescence as the needs of highway users have grown. None remain on the main highway system. Some of the bridges have undergone significant rehabilitation work and should be in use for many more years. Some of the other spans are requiring more frequent maintenance, have shortcomings in vertical clearance or load capacity that affect commercial traffic, or have deteriorating substructures that may hasten the need for bridge replacement. Meanwhile many of these bridges continue to serve as a testament to the inventor, engineers, builders, and maintenance crews that created them and keep them working.

References

[1] *Frontier to Freeway,* British Columbia Ministry of Transportation and Highways, 2000.

[2] Farnden Gary, *Bridge Timbers*, CWPA Conference, 2010.

[3] Parsons Brinkerhoff & Engineering and Industrial Heritage, *A Context for Common Historic Bridge Types*, NCHRP Project 25-25, Task 15, 2005.

[4] DeLony, Eric. "*The Golden Age of the Iron Bridge*." I&T: Invention and Technology, 1994.

The Cloak Bridge in Český Krumlov – construction history research

Jiří BLÁHA
Dipl. Eng., Ph.D.
CET ITAM AS CR, v. v. i.
Telč, Czech Republic
blaha@itam.cas.cz

Educated in construction engineering (1994) and history of architecture (2003) at the CTU in Prague. Dealing mostly with material science and research of historical development of buildings and construction techniques.

Summary

Among numerous building objects of the Castle and Chateau of Český Krumlov a distinctive multi-storey timber bridge connecting the main palace with the Baroque Theatre is probably the most spectacular one. The space, hidden between two formerly independent timber framed galleries, offers a unique chance to study its bearing construction. During the first fifty years of its existence, the bridge underwent several major alterations. In the last 250 years its appearance has not changed. The imprints of former roofing visible on walls as well as other details helped to reveal the sequence of changes. The survey results were verified by dendrochronological analysis.

Keywords: covered bridge, Baroque chateau, chateau theatre, dendrochronology, timber

1. Introduction

1.1 Historical background

The town of Český Krumlov, a significant Czech UNESCO World Heritage Site, is situated in southern Bohemia on the upper Vltava River, not far from the meeting point of the Austrian, German and Czech borders. In the 2nd half of the 16th century, at the time the town was ruled by Wilhelm von Rosenberg, a unique system of covered bridges and hidden corridors was built there connecting the castle premises with the Convent of the Order of Saint Claire, the adjacent gardens and also the Church of St. Joyce. As a private communication link between important sites connected with the Renaissance castle, these corridors were used exclusively by representatives of the noble family. An ingenious system combined masoned corridors supported by vaulted arches, covered timber framed bridges and galleries with passages sheathed with planks crossing through the attics of civic houses. The probable inspiration was the so-called "Corridoio Vasariano", a similar complex of overhead covered passageways built in Florence in 1565 by order of Duke Cosimo I de' Medici with the purpose of connecting the Palazzo Vecchio, Ufizzi, Santa Felicita Church, Boboli Garden and Palazzo Pitti. The entire length of each system was more than 750 m. In the period influenced by Italian Mannerism, similar corridors proliferated around Europe but none of them achieved such a degree of interdependence with the town's urban structure as these two singular examples. [1]

Later, at the end of the 17th century, similar covered bridges began to appear on the opposite side of the Krumlov castle complex, built to connect the wing housing representative halls with the newly built theatrical building and the Upper Ornamental Garden. These corridors not only served the immediate family but were also designed to be used by noble guests invited to enjoy the festive events of the Chateau Theatre, the Masquerade Hall and the gardens. The timber bridges, traditionally named "na plášti" or in literal translation "on the cloak", span the moats protecting the Upper Castle from the western side. The name derives from the mighty fortifications originally situated on the site of today's theatre building.

Fig. 1 The Cloak Bridge as seen from the southwest

After its completion, the bridge connecting the Upper Castle with the theatre has undoubtedly been the most intensively used section of the whole Krumlov system of private corridors. Such an uncommon function demanded an exceptional technical and architectural design. Above the stone arched bridge, connecting the castle courtyards, there are three other levels with two timber framed corridors placed on pillars made of brick masonry. The diversity of building materials was intentionally suppressed, so that the facades are unified in their exterior decoration with a neighboring theatre building remodeled between 1765-1766. From a distance the resultant bridge looks outwardly like one of the castle wings.

1.2 The Cloak Bridge in written and pictorial resources

The building contract between Johann Christian, Prince of Eggenberg and architect Giovanni Giacomo de Maggi, signed on 24th of November 1682 is the oldest known archival document explicitly mentioning a covered timber bridge („Gang auf einem Bundwerkh“). The next existing record is dated 20th March 1686 and refers to the commitment of the local carpenter Andreas Mayer to build „… a timber bridge leading to upper garden crossing 'the coat'.“ [2] The situation plan of the Upper Garden from about 1702 shows the construction of a covered bridge connecting the theatre and garden. In 1706 it was decided to build main supporting pillars for both bridges from stone masonry. Between 1707 and 1708 the covered timber passageway was built above the old timber bridge between the castle and “comedy house” and linked the Masquerade Hall, situated in the main palace of the castle, with the theatre auditorium balcony. Soon after, another covered bridge was added above the previous one, leading from the Painting Gallery directly to the gardens (Fig. 2). Finally, during the 1760's, the arduous project of remodelling the system of bridges took place. The lowest part was replaced by a vaulted stone bridge connecting the courtyard levels. The upper constructions of covered timber framed bridges were integrated into one structure, imitating solid exteriors and interiors with painted stucco plaster fixed onto wooden boarding. The corridor leading to the theatre was widened so that it could be arranged into small lounges during special occasions.

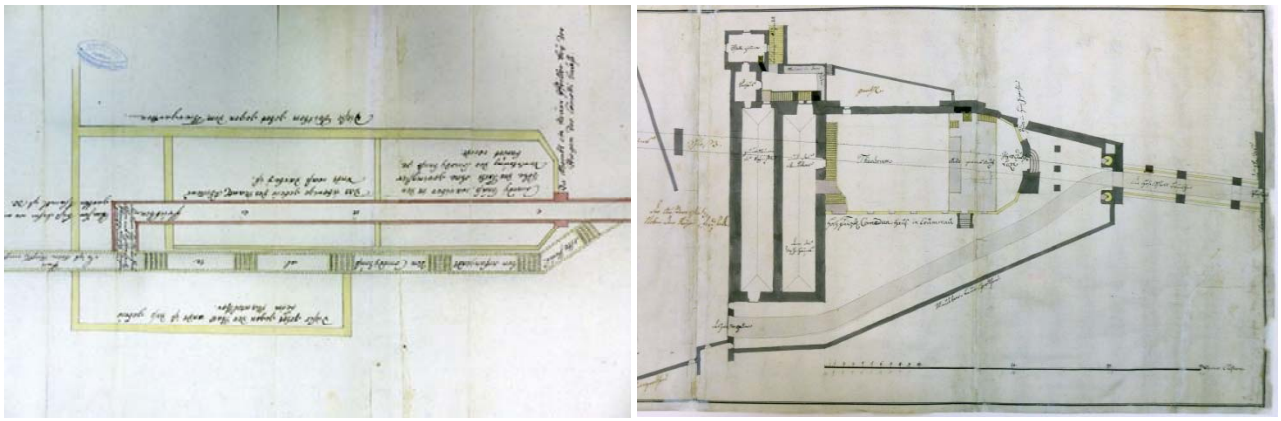

Fig. 2 Plan from the beginning of the 18th century (left) shows linking of a new upper corridor with the already existing western bridge leading into the garden. It is clear that the old bridge had a long staircase rising along the southern wall of the theatre building. Another plan (right) shows the situation circa 1750 when both corridors were already aligned.

Fig. 3 Inlaid tabletop from the Krumlov Chateau collections (left) shows the situation in the early 18th century with the rear bridge leading to the garden built at the level of the theatre roof and with the simple timber bridge crossing a deep gorge by the main palace. Another view (right) from a picture dated 1743 shows that both corridors are of the same width and sheathed with planks.

Among the old iconographic sources several reliably accurate pictures have been preserved which were created in the first half of the 18th century. They documented how the appearance of the bridges was gradually changing. It is clear that individual alterations were directly related to the transformations that the Baroque theatre building underwent. Initially there was no overhead connection between the castle and the first theatre house, built by Johann Christian I. von Eggenberg in 1680-1682. As we know from historical sources, a high timber bridge was built in 1686 leading to the upper garden. It is still uncertain whether it was covered or just an ordinary footbridge (Fig. 3 left). After 1706 the outward appearance of the two separate corridors is documented by several paintings (Fig. 3 right, Fig. 4 left). The distance between their floors was determined by the height of the Masquerade Hall. The side boarding of both corridors, made from vertical planks, and their roofs, covered by wooden shingles, are the same features as seen on covered bridges over the rivers at this time. A modest design was chosen which matched relatively well with the timber walls of the first theatre house. From the 1740s demands for a more fashionably elaborate look grew. For that reason, firstly the lower corridor was made more comfortable and fitted with stucco plaster (Fig. 4 right). Baroque sculptures were placed on the parapet walls including a statue of the recently canonized St. John of Nepomuk. The next modifications had to wait until the remodeling of the theatre building which was completed in the middle of the 1760s. Since the second half of the 18th century the appearance of the bridge has remained the same until today. [3]

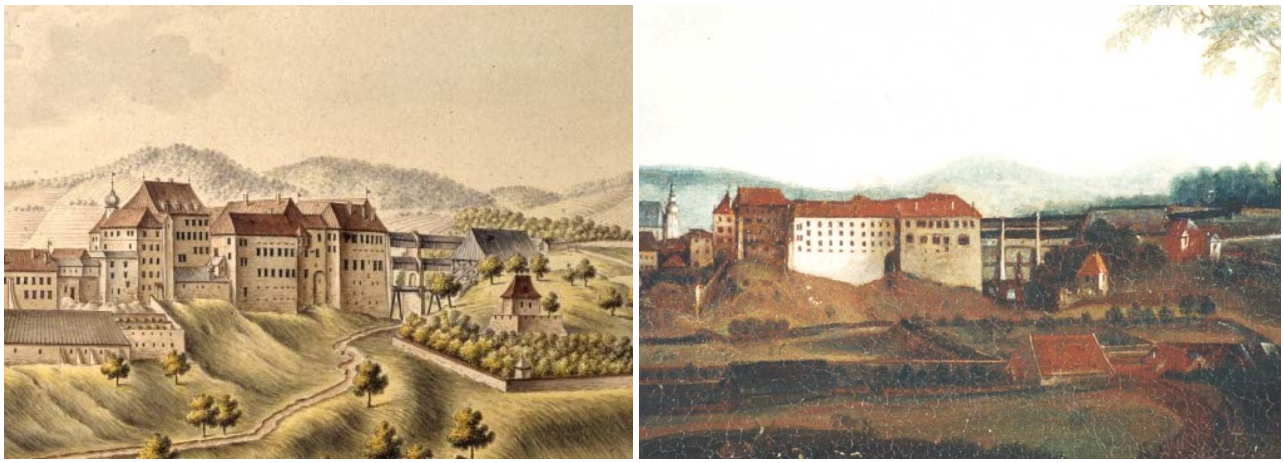

Fig. 4 Two views of the castle area from the north show the difference between the year 1724 (left) when the timber material of bridges and theatre building was apparent and after 1747 (right) when the lower corridor was widened and its wall cladding was plastered and painted.

2. New investigations

2.1 Timber structure

Taking advantage of an opportunity that arose during the preparation of a detailed monograph focusing on the history of the Baroque Chateau Theatre in Český Krumlov, it was possible to explore more thoroughly the space between the two passageways of the Cloak Bridge. It is, in fact, a kind of separated technical storey allowing access to load-bearing timber elements during regular control inspections. The inner space is illuminated by three windows looking southward. Inside it is easy to see the structural arrangement of individual timber elements, their real dimensions and to witness how the beams are settled on supporting pillars. The massive girders carrying the floor of the upper corridor had to be laid on the tops of brick pillars during the last modification of the bridge, which can be seen from the fact that the previous girders had to be of a slightly smaller profile.

Clearly visible is also the way the wooden sheathing is attached to the supporting frame. There are numerous inscriptions on the internal surfaces of the wooden planks, mostly names of craftsmen, sometimes accompanied also by dates. The minor maintenance actions and repairs recorded there took place during the 19th and 20th centuries. Surprisingly there are seemingly no visible traces of more extensive repairs or interventions.

Fig. 5 The space inside the technical storey is divided into three sections, each one illuminated by a single window. In the most westerly section the transversal timber frame (in the background of the right picture) was placed above the pair of slender pillars standing on the terrace in front of the theatre building.

When joining the two corridors into one unit in the 1760s, the rafters and collars that formed the roof structure of the lower corridor were partially cut off. Their remaining parts were used to attach the stiffening elements of the vertical boarding (Fig. 5). Due to this, the original assembly marking of single transversal trusses was preserved and could be properly documented. The carpenters obviously used separate numbering within each section. They made notches with various tools of a code using the Roman “V” symbol for number 5 except in the middle section. The northern side marks of each truss were distinguished by red chalk. The assembly marks in the western part of the bridge have no sequential order. This discrepancy can be most easily explained by some of the later repairs.

Only the imprints on the walls and pillars prove that the lower corridor was originally as narrow as the upper one is now (Fig. 3 right, Fig. 4 left). The roofing in both periods was probably made of wooden shingles but, in the case of the wider roof, the shingles in direct contact with the wall were cut under the level of plastered surface for waterproofing purposes.

Fig. 6 The imprints of pitched roofs from both previous construction phases are still clearly recognizable. The best situation has survived on the outside wall of the castle palace (left) and on the exterior plaster of one of the brick pillars (right).

2.2 Dendrochronological dating

Timber elements were made from very carefully selected wood distinguished by their very dense tree rings. From both construction phases, revealed by the on-site survey, specimens for dendrochronological dating were collected in an effort to compare their results with available archival records. The first necessity was to identify the age of the cut-off rafters and collars shortened for more comfortable access inside the technical storey. Trees for their fabrication were cut down in the winter felling seasons 1744/45, 1745/46 and 1746/47. Mostly a spruce wood was used together with a lesser amount of fir. The few oak and pine wood elements found have not yet been successfully dated. These harder woods were used to reinforce the masonry of pillars. The beams of the massive profiles carrying the upper corridor are of younger origin. Their dating to 1761 (summer felling), 1762/63, 1763/64 and 1764/65 proved that the last restoration of the Cloak Bridge came soon after the reconstruction of the theatre building. From the younger periods only one bigger repair of the wooden casing was determined by the date of felling 1880/81, which corresponds well to most of the graphite pencil inscriptions on the wooden boarding. [4]

2.3 Colour rendering of facades

Fig. 7 Detail picture of two different colour variants giving a tectonic accent to the corners. It is clear that paint was applied before covering the roof.

To understand details of the gradual changes to the exterior view of the Cloak Bridge, the remnants of the older colors of plasters are of great importance. Inside the technical storey, they were well protected from weather effects. The findings show that in the oldest phase, with the narrow lower corridor, the yellowish ochre illusive lesenes highlighted the corners, separated from the white facade area by a darker line representing a shadow. In the period when the lower corridor was enlarged but still independent, in the years 1747-1765, the pillar edges were blue-gray and the wall area white. It was only after the completion of the new theatre building that this combination of colours was abandoned and replaced by its present-day appearance with white corners and blue-gray suppressed areas.

3. Conclusion

The multi-storey Cloak Bridge in Český Krumlov is a unique cultural heritage monument allowing us to really get the feel of the living standard achieved by higher nobility in the Baroque period. The degree of its authenticity is genuinely surprising. For several reasons, it is difficult to find something comparable even in worldwide terms. First of all, it is a terrain configuration, where a medieval castle was built in a well protected situation on the top of a rocky ridge. Moreover the place was so comfortable and spacious that even in the later periods, after the adaptations which changed the mediaeval castle to a luxurious chateau; there was enough space for Masquerade and Mirror Halls and a picture gallery.

Demand for a comfortable connection between the representative wings and extensive gardens and the Castle Riding School building, which were situated on terraces above the castle, required specific technical solutions. The last significant decision was to build a permanent theatre stage on the site between the castle and the garden at a time when the former fortifications had lost their effectiveness. Today the Český Krumlov Chateau Theatre is one of the best preserved monuments of its kind. Besides still having the original stage machinery, it also boasts an extensive collection of period scenic decorations and other accessories.

Acknowledgements

The research result was gained by means of the project LO1219 with the financial contribution of the Ministry of Education, Youth and Sports of the Czech Republic within the framework of the specific support of the "National Sustainability Program I".

References

[1] Bláha, J., "Českokrumlovské kryté chodby. Spojení rezidence, zahrad, Latránu a Nového Města", *Český Krumlov: Od rezidenčního města k památce světového kulturního dědictví* (Český Krumlov: From the residence town to the world heritage site) NPÚ ÚOP v Českých Budějovicích 2010, pp. 191-216. ISBN 978-80-85033-26-7

[2] Muk, J., Lanciger, L, Český Krumlov. *Stavebně-historický průzkum zámku* (Construction history research report), SÚRPMO, Praha, 1991.

[3] Müller, J., "Město bělalo se… Poznámky k ikonografii Českého Krumlova", *Český Krumlov: Od rezidenčního města k památce světového kulturního dědictví* (Český Krumlov: From the residence town to the world heritage site), NPÚ ÚOP v Českých Budějovicích 2010, pp. 843-876. ISBN 978-80-85033-26-7

[4] Kyncl, T., *Český Krumlov – Latrán č.p. 59, Plášťový most. Zpráva o dendrochronologickém datování* (Report on dendrochronological dating), DendroLab Brno, 2017.

Structural Evolution of Woven Arched Covered Timber Bridges in China

Yaxin LI
M.Arch
Illinois School of Architecture, University of Illinois at Urbana-Champaign
117 Temple Buell Hall, 611 Lorado Taft Dr., Champaign IL 61820, USA.
Email: yaxinli4@illinois.edu

Sudarshan KRISHNAN
Ph.D.
Assistant Professor of Structures
Illinois School of Architecture, University of Illinois at Urbana-Champaign
117 Temple Buell Hall, 611 Lorado Taft Dr., Champaign IL 61820, USA.
Email: skrishnn@illinois.edu

Yaxin Li recently graduated with a M.Arch degree from the University of Illinois at Urbana-Champaign where she would be a doctoral student starting August 2017. She holds a B.Arch from Xiamen University in China.

Sudarshan Krishnan is an architect, structural engineer and Assistant Professor of Structures in the School of Architecture, University of Illinois at Urbana-Champaign. His current research focusses on lightweight structures and transformable architecture.

Abstract

Of the many timber bridge types found from China, one of the most expressive forms is the woven arched covered bridge with spans over 40m. The origin of the woven arched bridges can be traced to the Hongqiao or rainbow bridge. The ingenuity lied in their capability for long spans using short and stiff members which helped to standardize the members and facilitate their transportation and erection. China fir was the most suitable species for covered timber bridges because of its natural oil that helped prevent decay. The indigenous craftsmanship and carpentry helped create elegant bridges whose joints relied on friction between the members and not on nails and glue. The mortise and tenon joints allowed for some flexibility without compromising the overall structural stiffness and load-carrying capacity. This paper describes the historical evolution of segmental arch form structure in the covered bridges of China describing the various configurations, spans, indigenous materials, carpentry and construction methods used.

Keywords: China, covered bridge, segmental arch, structure, timber, wood.

1. Introduction

Till date, more than 100 covered bridges have stood over rivers for over hundred years and are still serviceable [1]. Ninety percent of the covered bridges are in the southern part of China, mainly in the Zhejiang and Fujian provinces. One reason for this concentration is the subtropical monsoons that provided an abundance of variety of wood species. The bridge forms and tectonics are strikingly unique when compared to the covered bridges in the West.

The primary purpose of covered bridges was to protect villages as per *Fengshui* prescriptions [2]. Many covered bridges therefore served as temples for local people to worship the deities and perform

religious rites. Contributing to the construction of a covered bridge was considered a philanthropic activity that would bring good fortune to future generations. Thus, people in villages would donate money depending on their financial capacity. The bridges provided shelter from heat and rain and in turn protected the wood from deterioration. The roof over the bridge facilitated social and leisure activities. This prompted retail shops and tea-stalls to be housed within many bridges. Of all the different purposes, transportation seems to be the least important in Chinese covered bridges.

The history of covered bridges can be traced back to approximately thousand years. Hongqiao (Rainbow-like bridge), found in the ancient painting "Riverside Scene at Qingming Festival" (Early Song Dynasty, 960A.D.-1127A.D.), is the prototype of the timber arch bridges that exist today. Timber covered bridges originated and developed fully during 581 A.D. to 1279 A.D. (Sui Dynasty – Song Dynasty), then reached their golden age from 1281 A.D. to 1912 A.D. (Yuan Dynasty – Qing Dynasty) [3]. After 1912 during The Republic of China era, wars and influence of the West hampered construction of timber covered bridges. Fewer than twenty bridges were built. Moreover, many of the older bridges were destroyed by natural disasters, lack of maintenance and other reasons. As a result, only over hundred timber covered bridges exist today and most of them are in urgent need of repairs. Also, the craft of building bridges was passed down verbally from generation to generation. Without paper documentation, some knowledge and skills were lost. This has made the repair and restoration of traditional covered bridges difficult.

2. Chronology of Woven Arched Covered Bridges in China

Hongqiao or the rainbow bridge (Fig. 1) is understood to be the origin of covered timber bridges. Hongqiao is not in existence and there is no other ancient bridge of this form. According to Mao [4], the Hongqiao in "Riverside Scene at Qingming Festival" painting would have spanned approximately 19.2m. This he estimated based on the size of the handrail, the number of people on the bridge, and the width of the river. Note that one must climb up to the top and go down following the arch geometry of Hongqiao.

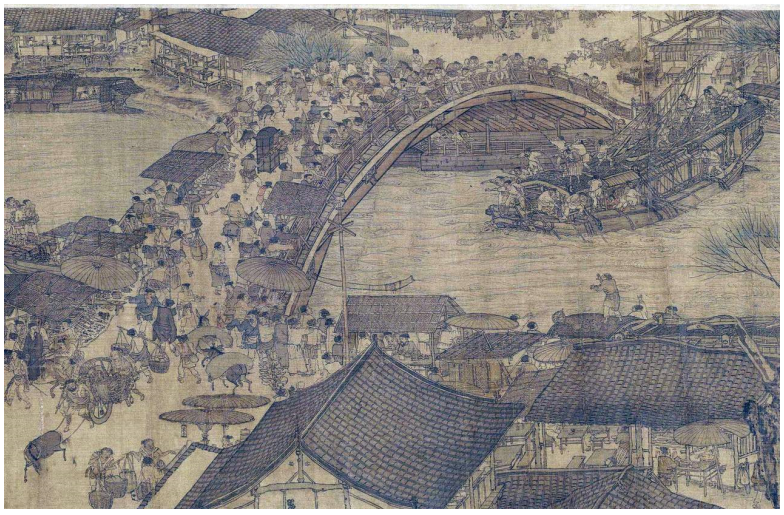

Fig. 1 Hongqiao in "Riverside Scene at Qingming Festival"

The oldest recorded bridge still in existence is the Santiao bridge, first built in 1137 and later rebuilt in 1843. Most of the existing covered bridges in China were rebuilt because they were either destroyed or they had deteriorated to an unserviceable state. Xidong bridge (Fig. 2a) was first built in 1570 with clear span of 25.7m. The bridge is known for its unique roof style, typical of Song dynasty. The roof

has a rise significantly greater than those built in future. As seen in Figure 2, the ends of the roof have a graceful curve to make the large roofs look lighter and to allow sunlight through the clearstories. The roof form also allows proper drainage of rain water and protects the main structure of the bridge from decay. The Rulong bridge (Fig. 2b) is the oldest among all the existing covered bridges and has been serviceable for almost four centuries. A three-storied building rests on top of the arched bridge. Rulong bridge with a clear span of 19.2 m. is in the best possible condition of all the existing bridges. This may be owed to the fact that the bridge has been well-maintained out of respect for Maolin Wu [5], the acclaimed scholar who set rules for maintenance of this bridge. The Wanan bridge (Fig. 2c) is one of the longest covered bridges with the greatest number of arches along the main span. The six arches range from 10.6m to 15.2m each in span with a total length of approximately 98.2m. To reach the bridge deck of the Wanan bridge, one must climb thirty-six steps at the northeast end and ten steps at the southwest end [6]. This ascent is meant to be symbolic of entering a temple. The piers are shaped the mitigate the effect of wave forces generated during floods.

Fig. 2 Views of (a) Xidong Bridge; (b) Rulong Bridge; (c) Wanan Bridge

Table-1 lists the various dynasties during which covered bridges were constructed along with their geometries, spans and notable examples. Approximately half of the existing covered timber bridges were built in Qing Dynasty. The crafts of building covered timber bridge were standardized by the rulers to prevent further innovation. Thus, there were no developments in bridge spans and design during Qing period. Also, seldom were covered timber bridges built after Qing Dynasty, see Table 1. There may be two possible reasons; firstly, being a war-prone region during that period, covered bridges were not in demand and artisans had to give up their careers in bridge construction for other forms of livelihood. Secondly, influence of the West made concrete and steel more popular materials for bridge building in China.

Table 1. A Brief History of Chinese Covered Bridges

	No. of existing timber arch bridges	Approx. percentage of total existing timber arch bridges	Span range for single arch (m)	Notable bridge	Number of arches		Width of bridge (m)	Rise of arch (m)	Span of arch (m)	Rise-to-span ratio	Province	Construction Year
					Three segment arch	Five segment arch						
Song Dynasty (宋) 962-1279	8	9%	9.5 - 27.5	Qiansheng Bridge (千乘桥)	9	8	4.9	5	27.5	0.182	Fujian	Early Song dynasty
				Santiao Bridge (三条桥)	7	6	4	3.5	21.3	0.159	Zhejiang	1137
Yuan Dynasty (元) 1281-1368	6	7%	12 - 28.2	Mengyu Bridge (濛淤桥)	7	6	4.5	4.84	28.2	0.172	Zhejiang	Early Yuan dynasty
				Guangfu Bridge (广福桥)	-	-	5	4.63	26	0.178	Fujian	1333
Ming Dynasty (明) 1368-1644	13	15%	7.5 - 36.8	Lanxi Bridge (兰溪桥)	9	8	5	6.62	36.8	0.180	Zhejiang	1574
				Rulong Bridge (如龙桥)	7	6	6	2.64	19.5	0.135	Zhejiang	1625
Qing Dynasty (清) 1645-1912	43	49%	12.4 - 35.7	Houkeng Bridge (后坑桥)	9	8	5.45	4.8	28.5	0.168	Zhejiang	1671
				Yangmeizhou Bridge (杨梅州桥)	9	8	4.2	5.74	35.7	0.161	Zhejiang	1741
The Republic of China (民国) 1911-1949	3	3%	12.2 - 38	Tangbei Bridge (汤北桥)	-	-	4	5.1	28	0.182	Zhejiang	1915
				Hexing Bridge (合兴桥)	-	-	4	2.9	12.2	0.238	Zhejiang	1928

The table shows that several parameters remained the same during the evolution of the arch structure. Based on the data from existing bridges, the depth-to-span ratios are in the range of 0.14 - 0.20. For smaller spans, the depth-to-span ratio of some bridges is found to be 0.25. The typical width of the bridges is found to be 4m to 6m. However, this depended mainly on the use of the covered bridge, whether it is for transportation, religious activities, social gatherings, entertainment, refreshments, among others.

3. Elements of a typical covered bridge

The typical arched timber bridge is the woven three-and-five segmental arch system, where the three-segment arches and five-segment arches behave as reciprocal structures. Reciprocal structures have several advantages, the foremost being a significant reduction in dead-weight and member lengths due to their self-supporting characteristic. The latter enhances the stiffness of the members and the resulting structure has a high load carrying capacity. The mortise and tenon joints eliminate the need for glue and nails. The stiffness of the joints relies much on the frictional forces between the members. This flexibility helps structural resistance and resilience during earthquakes and other large loads. The demerit of a reciprocal structure is the interdependency of members on other members for its own survival. As such, failure of one member may lead to a progressive collapse of a structure. The covered bridges are therefore made of seven to eleven arches to introduce sufficient redundancy.

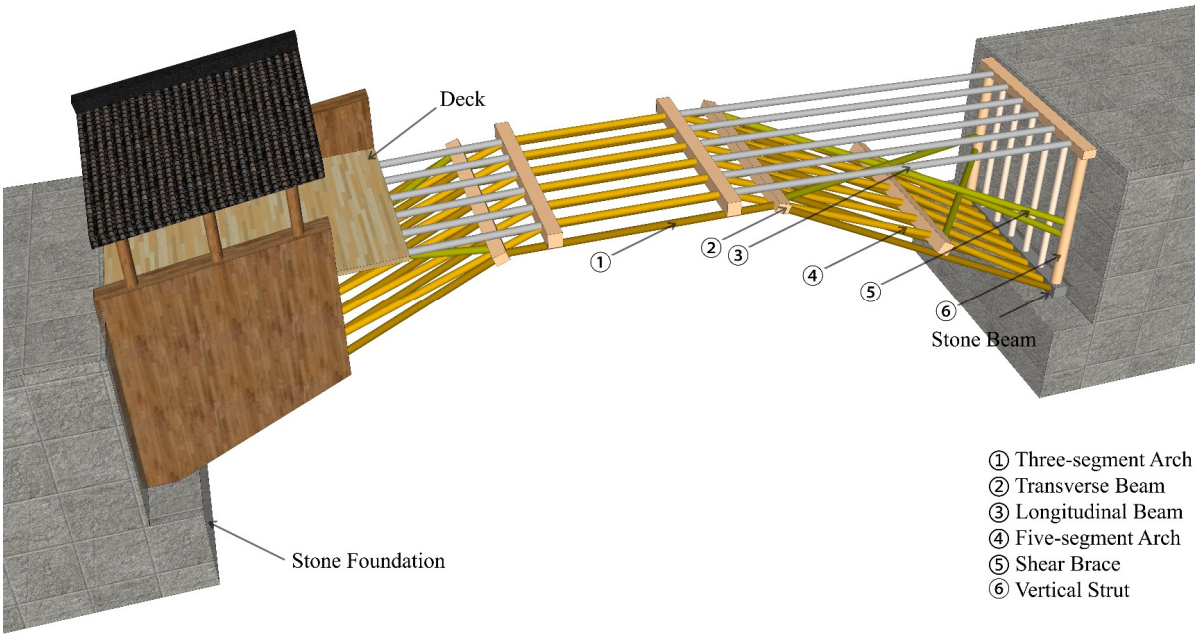

Fig. 3 Elements of a woven arched covered timber bridge

In the existing Chinese timber bridges, one of the most elegant forms is the woven arch-supported timber bridge. A typical bridge comprises the main arches, longitudinal and transverse beams, shear braces, vertical struts, decking system, and stone foundations. The arches are the most important and complex part of the whole system, and it evolved into different types to achieve longer spans. With reference to Fig. 3, the most intricate of the covered bridge arch types consists of: (1) *Three-segment arch system*: A three-segment arch is made from three timber members pin-jointed to formed an arch;

(2) *Five-segment arch system*: A five-segment arch is a variation of the three-segment arch; a joint is added to the outermost segments of a three-segment arch. The reciprocal three and five-segment arches allows the covered bridge to be self-supported without the need for intermediate piers; (3) *Transverse beams*: Multiple beams in the transverse direction keep the arches together and helps to stabilize them; (4) *Longitudinal beams*: horizontal beams extending from the flat portion of the arch on either sides to support the deck; (5) *Shear brace*: There are two sets of X-braces: the first connects the horizontal brace of the three-segment arch and the horizontal brace of the five-segment arch; the second X-brace connects the horizontal brace of the three-segment arch to the vertical struts; (6) *Vertical struts*: Sets of columns at each bridge end connecting the longitudinal beams with the arches. The resulting triangulation enhances the stiffness of the system. Additional struts may be added to support the deck, especially for long spans.

The joints are formed by notching members; no nails and glue are utilized for for forming the connections. The stiffness of the structure as such relies on the frictional force developed between the notched members. Thus, the dead weight of the bridge structure and the architectural components enhance the frictional forces and stabilizes a bridge against lateral and wind uplift forces. The covered part primarily serves to protect the wood in the bridge structure from decay. The bridge deck, independent from the main arch structure, is supported by struts bearing directly onto the nodes at main arch and the horizontally brace. Stone foundations provides resistance to the horizontal thrust from the main arches. Also, stone foundation isolates the timber bridge from the wet soil at the river banks, thus protecting the main structure from decay. Several bridges have a multi-story structure, much like a regular wooden house, in place of a simple deck.

4. Materials and Structure

China fir is the most popular species for buildings in southern China used in covered timber bridge because of their abundant growth in the warm and humid climate of southern China. China fir has clear straight trunk reaching heights of 40m. The fir has a relatively short life cycle of 15 to 20 years which makes them sustainable for construction. China fir can resist corrosion by natural oil present within it. Cedrol found in China fir helps to expel pests. This low-density fir yields lightweight wood which makes it easy for carpentry and construction. At 12% moisture content, China fir has density of 0.357 g/cm3, Young's Modulus of 9804 MPa, compression strength of 40.3 MPa and bending strength of 76.9 MPa [7]. The arch segments of a typical bridge are made of China fir logs 25cm in diameter. Elmwood is typically used for the horizontal braces because of its hardness and anti-corrosion properties [8].

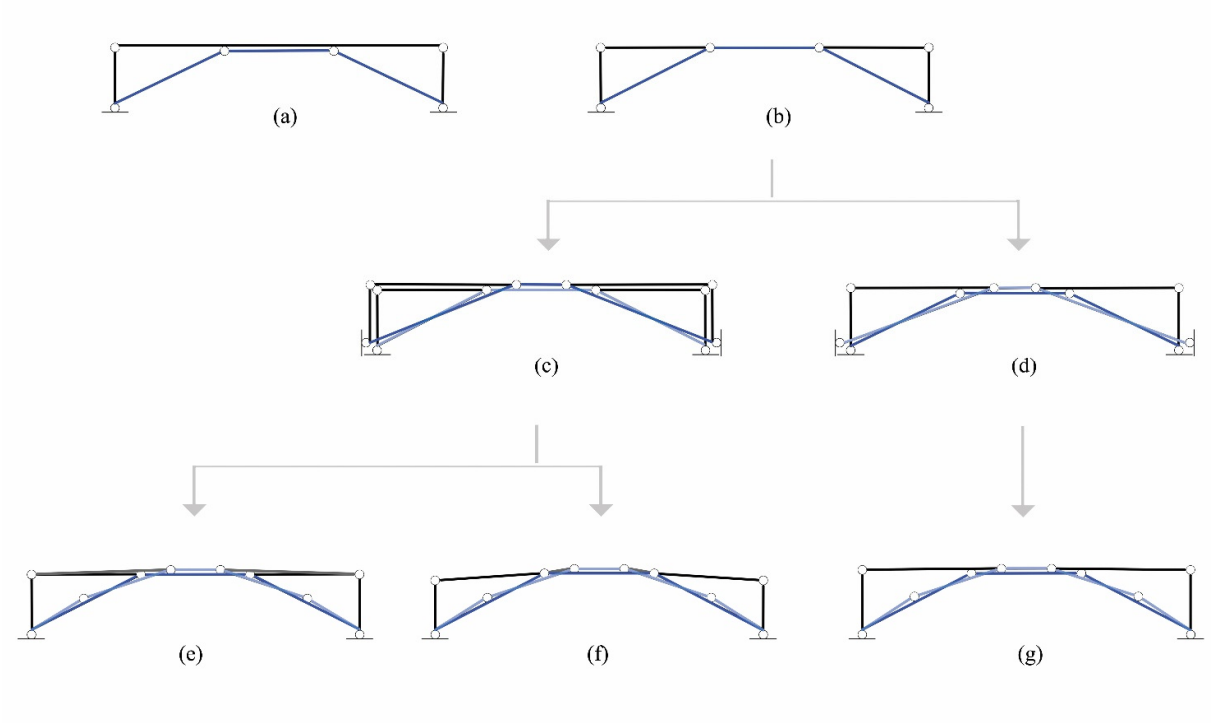

Fig. 4 Arch configurations

Based on the existing literature on timber bridges, the woven arch types may be classified as: Woven three-and-three segmental arch and woven three-and-five segmental arch [9]. The bridge arches in Fig. 4a are made of three-segmental arches stacked together and braced by transverse beams. The battered members act as props for the long-span beam. Fig. 4b shows a modification of the arch in Fig. 4a in that the longitudinal beams supporting the bridge deck is segmented into three pieces. This is more like two truss panels connected by a link beam. The introduction of hinges makes the longitudinal members more flexible and the system behaves more like a truss. The three-segmental arch system evolved to a stiffer system by weaving them with either three or five-segmental arches.

4.1 Woven Three-and-Three segmental arch

Two types of three-and-three segmental arch systems evolved from the arch in Fig. 4b. The first type is formed with two of diagonal braced arches combined (Fig. 4c) but with a variation in the member lengths and inclinations in one of the arches. The base of the two arches are at different elevations which resulted in many support points. Fig. 4d shows the second variation where the arches in Fig. 4a and 4b are placed alternately and secured by transverse beams. In this system, when the applied load causes displacement in one arch, the adjoining arches help is resisting the load by the developing shear forces in the transverse beams. There are few existing bridges using the three-and-three segmental arches and they can only be studied from past literature and photographs.

4.2 Woven Three-and-Five segmental arch

One of the drawbacks of the three-and-three segmental arch system was the two support points at each end formed by two sets of arches. This was resolved in the three-and-five segmental arch system where a joint was introduced in the end diagonals of one of the arches, thus forming the five-segment arch (Fig. 5). This allows for the support point of the three-segment arch and the five-segment arch to be at the same elevation.

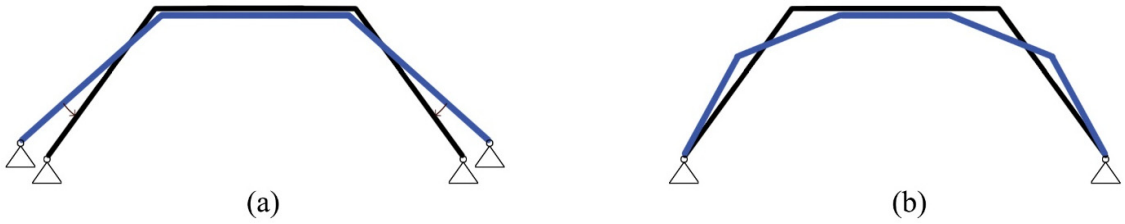

Fig. 5 Transformation of (a) three-and-three segmental arch to (b) three-and-five segmental arch

The five-segment arches have shorter and thus stiffer members. However, the introduction of more joints increases the flexibility of the structure. This is compensated by the reciprocal behavior of the three and five-segmental arches. Three types of three-and-five segmental arch systems evolved. The system in Fig. 4e evolved from the Fig. 4c, where one of the two sets of three-segment arches is broken into five segments. The arch system in Fig. 4f is a modification of that in Fig. 4e where the horizontal beams are split at one of the transverse beams thereby creating two new link beams. Similarly, the arch system in Fig. 4g which evolved from the system in Fig. 4d is the pinnacle in the evolutionary stages and has been extensively used in the design of covered timber bridges. This three-and-five segmental arch system was also the dominant form in the covered bridges built during the Song Dynasty (962-1279), including the Lanxi Bridge that has the longest span among the existing covered bridges.

5. Construction of a Typical Covered Bridge

Construction of covered timber bridges is an intricate process. There is a strong belief that the performance of a covered bridge is indicative of the fate it brings to the people around. The covered timber bridge is typically located at the downstream of the river; the symbolic meaning is to prevent the "fortune" from drifting with the flow. Renowned experts in Fengshui are invited to select the appropriate location for a bridge. Strict rituals are followed to prevent any bad luck from entering their lives. The folloowing steps are customary [9]: 1) Select an auspicious day to start construction. 2) Prepare the Xiliang or fortune beam, which is the top segment of the three-segmental arch. 3) Offer sacrifices to the river and prepare for ground-breaking. 4) The Xiliang is placed first with a bag of coins tied to it. 5) After all the arches have been constructed, craftsmen will take off the bag of coins and share them among the craftsmen. 6) One person who is widely respected in the village as most fortunate, takes the first step and walks on the bridge to cross the river. 7) A celebration is held on the bridge after decking has been placed. 8) After completion of the covered bridge, the villagers show their gratitude to all the craftsmen before they part.

Traditional construction begins with stone abutments built on banks of streams or rivers. The abutments are notched such that the main arch system bears on the notches and thus prevented from contact with water. The elevation of the flat segment of the arch is decided and bamboo scaffolding is constructed from the river bed up to that elevation. In order to bear the weight of the mid-span of the bridge, heavy timber framework is constructed around the scaffolding. Three-segment arches are first erected followed by the five-segment arches. The joints between the two sets of arches are secured. Transverse beams are used at appropriate locations to stabilize the system. Several wedges are driven into gaps between the three-segment arches and five-segment arches along the transverse beams. This increases the frictional forces significantly thus enhancing the joint stiffness. Vertical struts and X-braces are placed to further stabilize the system. For long spans, more layers of intermediate vertical struts may be added along the span.

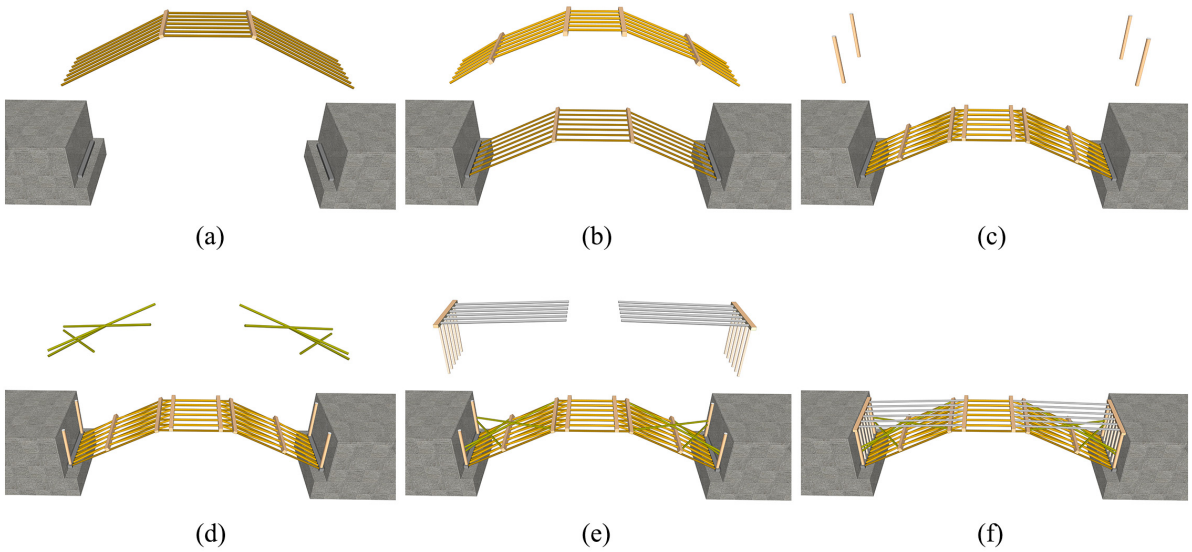

Fig. 6 Modern construction of woven arch system

Modern construction of covered bridges allow for more efficient erection. As an example, the leveling of the bridge deck is done using advanced techniques without the need for extensive scaffolding. The erection procedure is shown in Fig. 6. Although modern technology has enabled more efficient ways of construction, the age-old craftsmanship has only four masters remaining who are determined to pass down the knowledge through apprentices.

6. Observations and Conclusions

1. Covered timber bridges were considered the most important architectural icon for protection of a village prescribed by the Fengshui principles. Construction follows an austere set of guidelines and rituals in order to bring good fortune to a village.
2. Woven segmental arches evolved to overcome the shortcomings of earlier arch types. A salient feature of the woven arches was that even as the bridge spans became long, their member lengths could be kept short as the arches formed a system of reciprocal structures.
3. Progressive collapse may be an issue as the systems of three and five-segmental arches rely on each other for their structural integrity and stability. Failure of a single member may result in premature demise of the entire structure.
4. Compared to the Hongqiao, the future covered timber bridges were superior in their load bearing capacity and ease of pedestrian use. Many of the characteristics such as width, and rise-to-span ratio remained the same even as bridges evolved.
5. China fir provided a lightweight option and its natural oil helped repel pests and resist decay.
6. The three-segmental and five-segmental arches represent the pinnacle in the evolution of covered bridge structure. Present day covered bridges are constructed using a combination of the two sets to form a reciprocal system of arches.
7. Modern covered bridges are built using more sophisticated techniques and it is feared that traditional craftsmanship and carpentry may become extinct. Efforts are underway to preserve the knowledge and pass it down to future generations through apprentices who work under the supervision of master builders.

References

[1] Chen Y., "Discussion on Origins and Structure Types of Covered Timber Bridges in Southern Zhejiang Province", *Southeast Culture*, 2002, pp. 66-71. (In Chinese)

[2] Bi S., Zhao C. "Cultural Heritage of Covered Timber Bridges in Zhejiang and Fujian Provinces", *Southeast Culture*, 2003, pp. 52-56. (In Chinese)

[3] Jiang Y., "Architecture and Cultural Studies of Chinese Covered Bridges", *Doctoral Dissertation*, 2010, 317 pages. (In Chinese)

[4] Mao Y., "Technological History of China's Ancient Bridges", *Beijing Press,* 1986, 315 pages. (In Chinese)

[5] Wu Y., "Ancient Chinese Bridges", *Esphere Media,* 2009, 129 pages.

[6] Knapp R. G., "Chinese Bridges: Living Architecture from China's Past", *Tuttle Publishing*, 2008, 272 pages.

[7] Zhao B., "The Protection Measures of the Timber Arch Lounge Bridge Based on the Properties of Chinese Fir (Cunninghamia Lanceolata)", *Journal of Shanxi Datong University (Natural Science)*, Vol.31, No.2, 2015, pp. 94-96. (In Chinese)

[8] Zhao C., Feng J., et al. "Re-evaluation on The Wooden Arched Bridges as The Subject of Mountainous Human Settlement Culture, *ISSDMHSE' 2001*, Kunming, China, 2001, pp 406-412. (In Chinese)

[9] Zhang G., "Lounge Bridges' Local Context in Min-zhe Province", *Journal of Wenzhou University (Natural Science)*, Vol.31, No.3, 2010, pp. 55-60. (In Chinese)

Mechanics of Stress-Laminated Timber Bridges with Butt End Joints

Mats EKEVAD
Ph.D. Professor
Luleå University of Technology
Skellefteå
Sweden
mats.ekevad@ltu.se

Focus is on finite element simulations of wood material and engineered wood products behaviour during loading.

Johannes A. J. HUBER
M.Sc. Ph.D. student
Luleå University of Technology
Skellefteå
Sweden
johannes.huber@ltu.se

Focus on engineered wood and timber structures.

Peter JACOBSSON
M.Sc. R&D Manager
Martinsons Träbroar AB
Skellefteå
Sweden
peter.jacobsson@martinsons.se

Focus is on increasing competiveness for timber structures and especially bridges.

Summary

A number of variants of single span and three-span stress-laminated timber bridge decks have been studied via finite element simulations and experiments. Glulam beams in the decks were in general shorter than the total length of span which means that there were butt end joints in the decks. The butt end of each beam in a joint was not connected to the other beam which means that each butt end joint reduced the strength and stiffness of the whole of the deck. Results for deflection and stresses were examined for the studied variants in the form of reduction factors for strength and stiffness relative to a deck without butt end joints.

Factors are shown in diagrams as function of ratio butt end distance/beam width and also butt end distance/span width. Comparison of achieved results with existing Eurocode rules shows that Eurocode rules are not totally appropriate.

Keywords: timber bridges, stress laminated, butt end joints, finite element simulations, Eurocode.

1. Introduction

Stress laminated timber bridge decks are made up of glulam beams which are held together side by side by pre-stressed steel bars, see [1] for general information of this timber bridge type. If the decks are longer than the length of single beams the beams are simply put together in length direction and this is called butt jointing. The butt joints have no joining mechanism such as glue and

a gap is assumed to exist in the butt joints so that no lengthwise contact appears. The locations of the butt joints are distributed all over the deck.

Today there are three criteria in Eurocode [2] which provide the minimum requirements for the necessary butt end distance between butt joints of two neighbouring beams. The assumption is that a butt joint in the same lengthwise position in a deck is allowed only for every fourth beam. For a group of 4 neighbouring beams the distance between butt end joints must be sufficiently large. For the fifth beam a butt end joint is allowed in the same lengthwise position as the first beam. The smallest allowed butt end distance is one out of 2d, 30t and 1.2 m where d is the lengthwise distance between prestressing bars and t is the beam width. Reasonably, the most conservative of these 3 conditions should be chosen although this is not stated clearly in the text. As an example, for d=0.9 m and t=90 mm, the three conditions give 1.8 m, 2.7 m and 1.2 m. From these values 2.7 m should be chosen since this gives the most conservative design for this example. The requirements may be used together with a reduction factor of 0.75 for strength according to Eurocode. No reduction factor for stiffness is specified. For the design of a bridge deck the correction factor plays a vital role. A more refined description of the reduction factor is therefore desired to reduce uncertainty.

The goal of this paper is to investigate the relationship between butt end distance and strength and stiffness of a bridge deck. A short butt end distance is expected to yield a greater reduction of stiffness and strength than a long butt end distance. The method used in this paper was to model stress laminated bridge decks with different spans, widths and thicknesses with the finite element software ABAQUS [3]. The decks were modelled as glulam beams which were held together by lateral pre-stress and resulting friction between neighbouring beams. The individual beams which build up the bridge decks were shorter than the total deck span widths. Therefore, the decks contained butt joints which were distributed in a specific pattern in the deck. The butt joints were not considered to transfer longitudinal forces between the beams.

In a first step simulations of three variants of the bridge decks (named F22, F25, F28) were conducted in order to validate the calculation method by comparing to existing experimental results. Then, FEM (finite element method) simulations of several deck variants were performed and the results were analysed without comparisons to experimental results. In [4], [5] and [6] descriptions of FEM models for bridge simulations are described and discussed.

2. Material and Methods

The simulated deck variants are listed in Table 1. First, the variants F22, F25 and F28 which were taken from an experimental study [7] were simulated to calibrate and verify the calculation method. In the next step variants 1-5 were calculated. These variants were 3-span decks with two different butt end distances and two different beam widths. Three-span decks are usually manufactured with butt joints and the chosen dimensions for the variants are common in industry. Variant 1 was a deck without butt joints and was thus taken as a reference case. Variants 6 and 7 with twice the span widths of variants 1-5 were calculated in a next step in order to get a clearer relationship between reduction factors and ratio butt end distance/beam width. The rest of the variants Ext1A to Ext4B were similar to variants 1-5 but with other butt end distances.

Reduction factors for stiffness were calculated as ratio between maximum deflections for variants divided by maximum deflection for reference variant. Reduction factors for strength were calculated as ratio between maximum stresses for variants divided by maximum stress for reference variant. Stresses in positions in the middle of spans and above supports were considered.

Table 1: Variants of bridge decks

Name	# Spans	Span-width (m)	Thick-ness (mm)	Beam width (mm)	# Beams	Deck width (m)	Butt end dist-ance (m)	Pre-stress (MPa)	Dist / Beam width
F22	1	5.2	270	90	9	0.81	0.9	0.3	10.0
F25	1	5.2	270	42	19	0.798	0.9	0.3	21.4
F28	1	5.2	270	90	9	0.81	1.35	0.3	15.0
1 (ref)	3	8-10-8	495	90	40	3.6	-	0.35	-
2	3	8-10-8	495	90	40	3.6	1.2	0.35	13.3
3	3	8-10-8	495	90	40	3.6	2.7	0.35	30.0
4	3	8-10-8	495	180	20	3.6	1.2	0.35	6.7
5	3	8-10-8	495	180	20	3.6	2.7	0.35	15.0
6	3	16-20-16	495	180	20	3.6	2.7	0.35	15.0
7 (ref)	3	16-20-16	495	180	20	3.6	-	0.35	-
Ext1A	3	8-10-8	495	180	20	3.6	1.8	0.35	10.0
Ext1B	3	8-10-8	495	90	40	3.6	1.8	0.35	20.0
Ext2A	3	8-10-8	495	180	20	3.6	3.6	0.35	20.0
Ext2B	3	8-10-8	495	90	40	3.6	3.6	0.35	40.0
Ext3A	3	8-10-8	495	180	20	3.6	0.9	0.35	5.0
Ext3B	3	8-10-8	495	90	40	3.6	0.9	0.35	10.0
Ext4A	3	8-10-8	495	180	20	3.6	3.2	0.35	17.8
Ext4B	3	8-10-8	495	90	40	3.6	3.2	0.35	35.6

The calculation method required solutions of contact problems between the beams as sliding with friction occurred locally or on large surfaces. See [4], [5] and [6] for descriptions of methods for simulating contact and slip between beams. The calculations were performed in the FEM software ABAQUS 6.14, [3], with 3-dimensional elements. The material data used was following recommendations in Eurocode, [2]. Material was assumed linearly elastic and orthotropic with elastic moduli 12000 MPa in longitudinal direction along fibres and 240 MPa in cross directions. Shear moduli for two shear planes (bending shear and inplane shear) were assumed to be 720 MPa and shear modulus for rolling shear was assumed to be 72 MPa. All Poisson's rations were set to 0. The coefficients of frictions were assumed to be 0.29 and 0.34 in longitudinal direction and transverse direction, respectively. The used elements were parabolic (i.e. of quadratic order) and examples of mesh density are visible in Figs. 2 and 3. Contact between beams was described by an exponential pressure-overclosure model with pressure 0.35 MPa and clearance 0.01 mm. Prestress on side edges of the deck was modelled by a constant distributed load on surfaces 0.27m x 0.20m at every position of the prestress bars (every 900 mm) for variants F22, F25, F28, 1, 2 and 3. This resulted in the average prestress indicated in Table 1 but with locally varying pressure close to the edge beams. The prestress on all other variants was modelled with a constant distributed load on the side edges of the deck corresponding to the average prestress because of small differences in the results compared to using discrete prestress locations. Loading and unloading were applied in three steps; first the prestress was applied, followed by the vertical net load and finally the removal of the net load. The vertical displacement of the support surfaces under the deck was assumed to be zero or was modelled by contact conditions against a fixed support.

The vertical net load for the variants F22, F25 and F28 were the point loads used during testing [7]. For the other variants, a distributed vertical load on the entire upper bridge deck surface was applied. The distributed load was specified as a load per length in the lengthwise, span direction and is visible in figures. Loading was stopped if instability developed or if the deformations became considerably large. Self-weight of the bridge deck was disregarded. The models of the bridge decks were not perfectly symmetrical due to the distribution of the butt joints. However, symmetry in both longitudinal and transversal direction was assumed for all variants except for F22, F25 and F28.

3. Results

3.1 F22, F25 and F28

Load-deflection curve, stress along fibres, contact pressure and displacements for variant F25 is shown in Fig. 1, Fig. 2 and Fig. 3, respectively. Results for F22 and F28 are not shown here but their curves show a similar behaviour as variant F25.

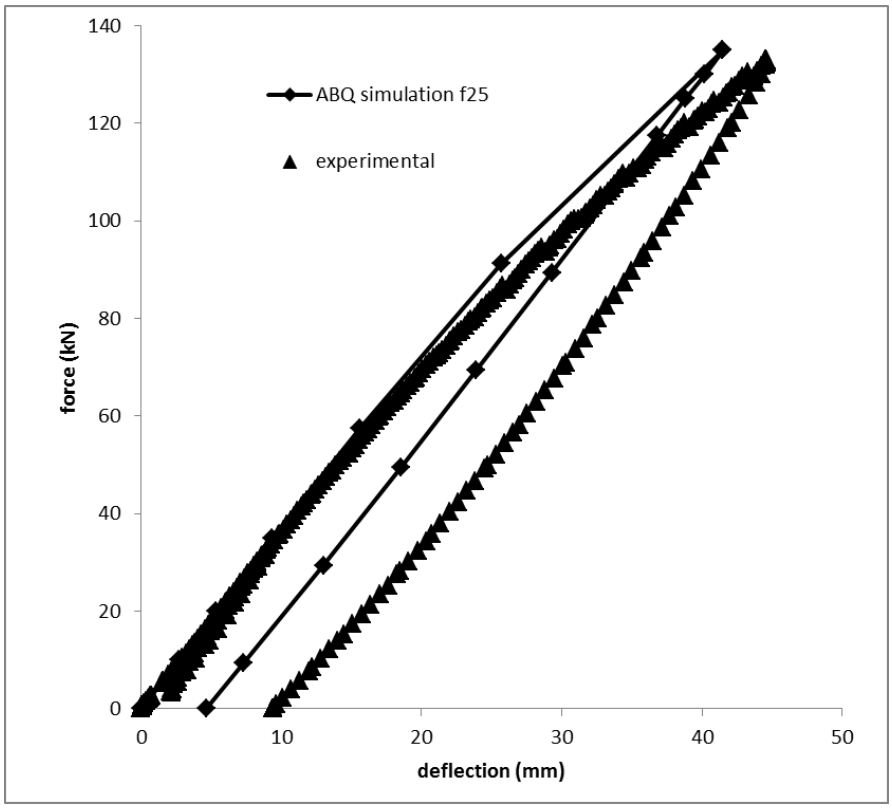

Fig. 1: Load versus deflection for variant F25

3.2 Variants 1-7 and Ext1A to Ext4B

Variant 1 and 7 were references, i.e. they had no butt joints. Variants were loaded up to 200 kN/m and then unloaded. However, loading was stopped for variant Ext3A at 150 kN/m due to instability (collapse). Variants 6 and 7 which had larger span lengths than variants 1-5 were loaded up to 100 kN/m and then unloaded. Figs. 5-8 show examples of how deformations and stresses looked like in the models.

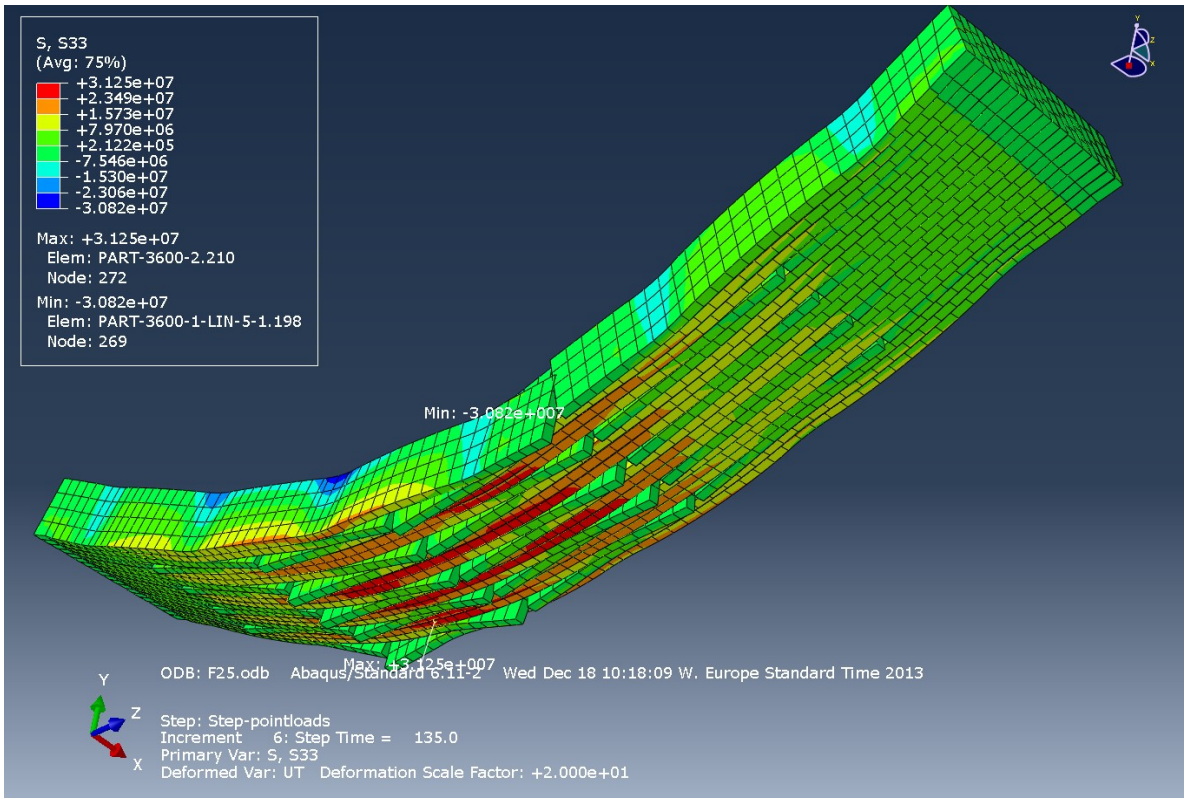

Fig. 2: Variant F25; load 125 kN, stress S33 along fibres, max 31 MPa. Scale factor 20 for deformation.

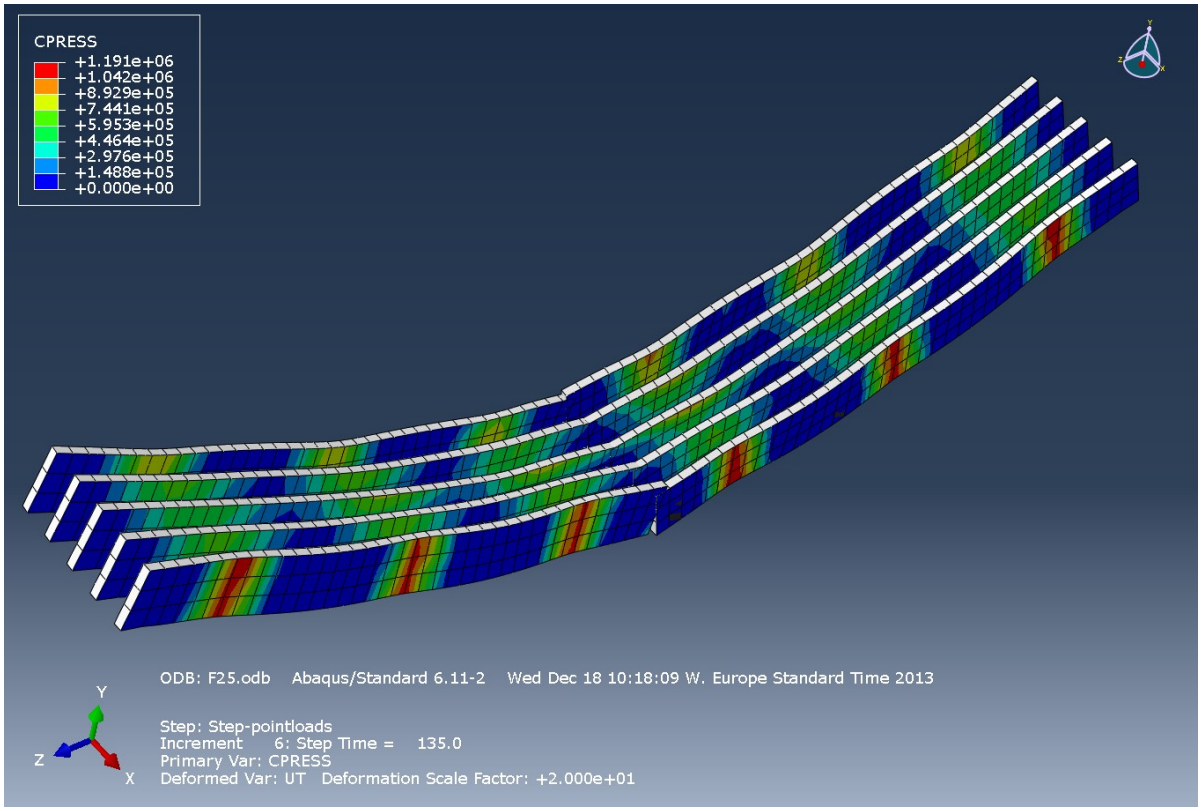

Fig. 3: Variant F25; load 135 kN, contact pressure on every fourth beam, max 1.19 MPa. Scale factor 20 for deformation.

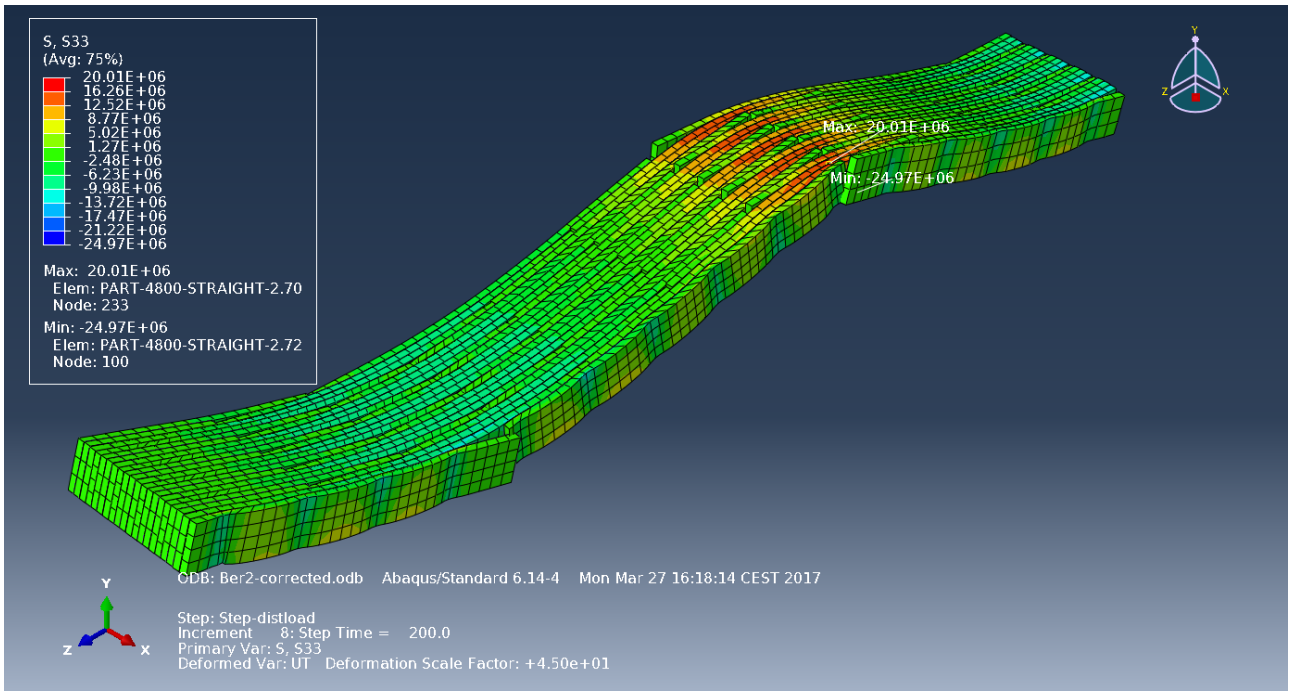

Fig. 5: Deformation and stress along fibres for variant 2 at 200 kN/m. Scale factor 45, maximum fibre stress 20 MPa.

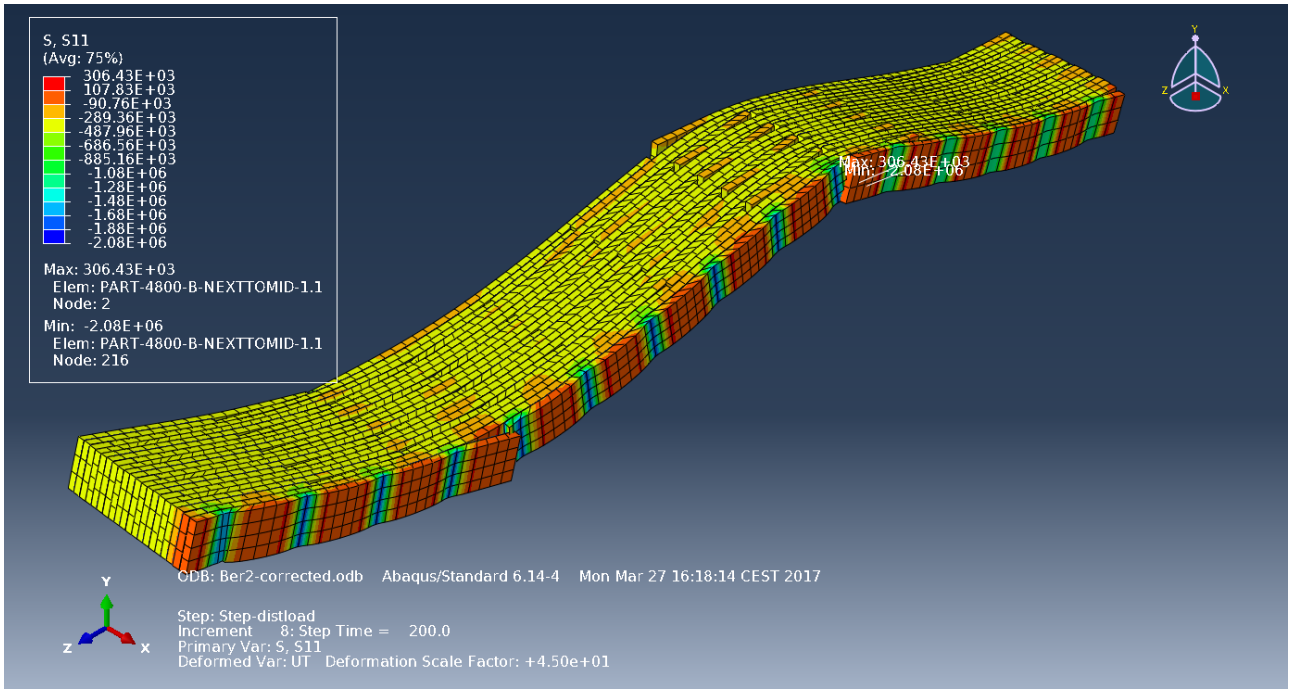

Fig. 6: Deformation and lateral normal stress (average is prestress -0.35 MPa) for variant 2 at 200 kN/m. Scale factor 45.

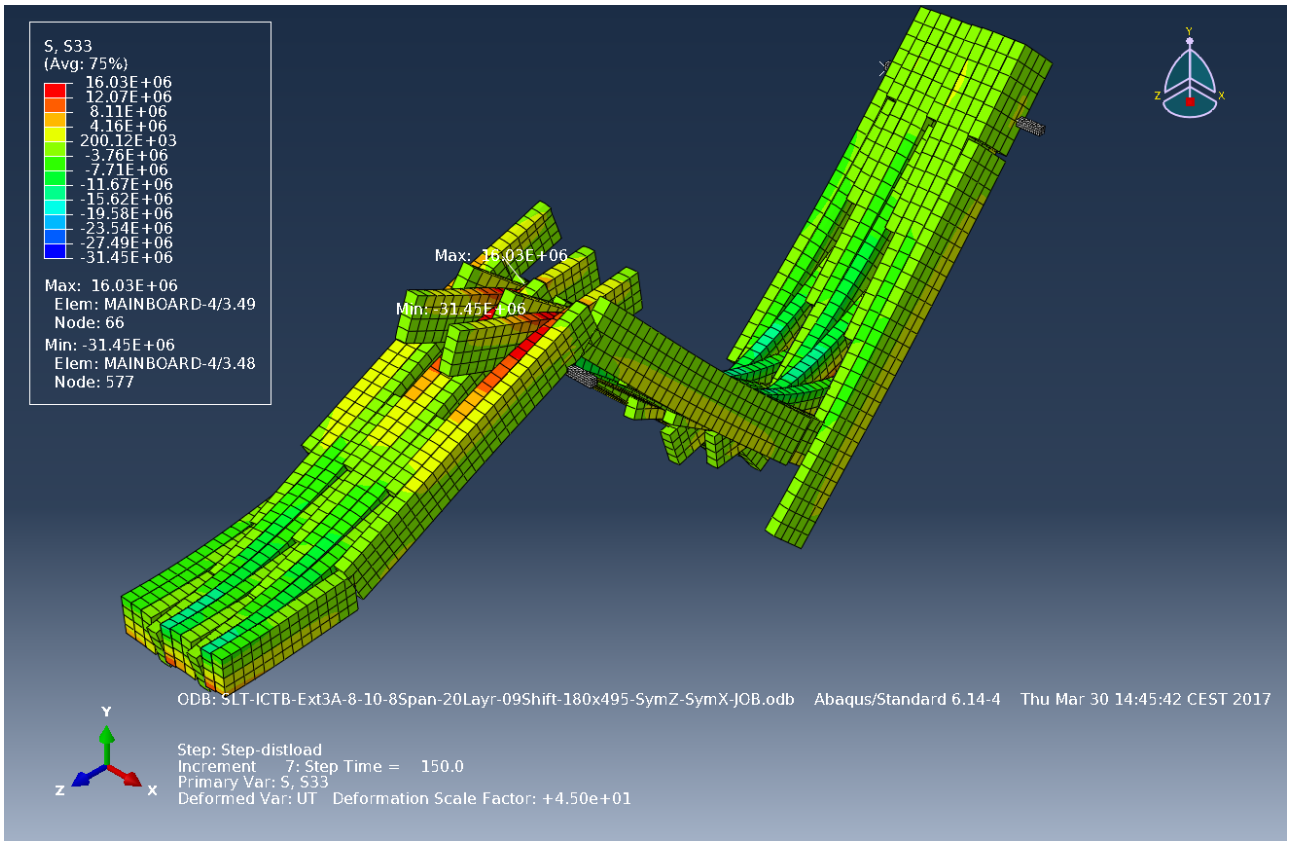

Fig. 7: Deformation and stress along fibres for variant Ext3A at 150 kN/m. Scale factor of 45, max stress 16 MPa.

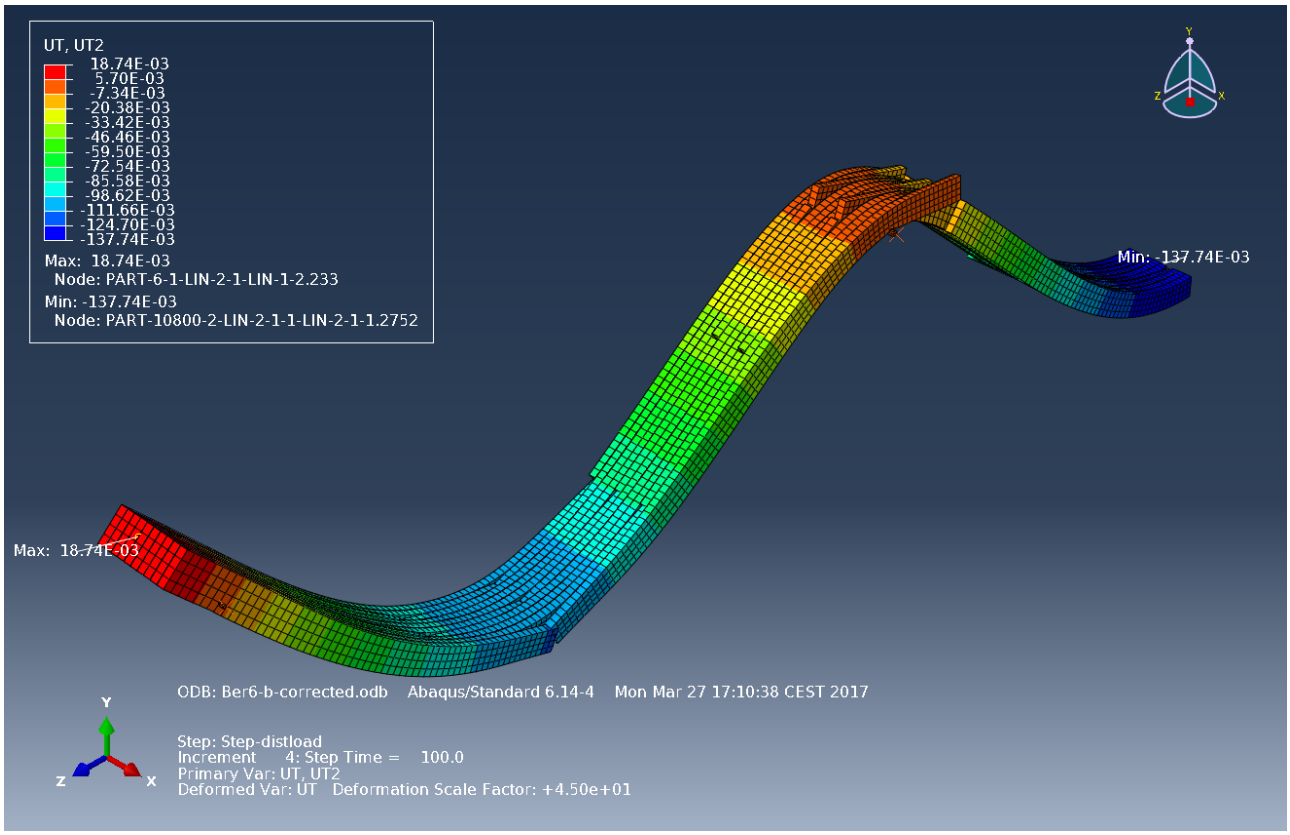

Fig. 8: Deformation for variant 6 at 100 kN/m. Scale factor 45, max vertical deformation 138 mm.

Fig. 9 and Fig. 10 show reduction factors for stiffness and strength plotted against butt end distance divided by beam width. The reduction factors were calculated by recording the maximum deflection and maximum stresses along the fibres and dividing by the corresponding values for the reference cases without butt joints. Results at two load levels are shown in order to show influence of nonlinear slip effects.

Fig. 9: Reduction factor for stiffness as a function of ratio butt end distance/ beam width. Calculated from the deflections measured at two load levels.

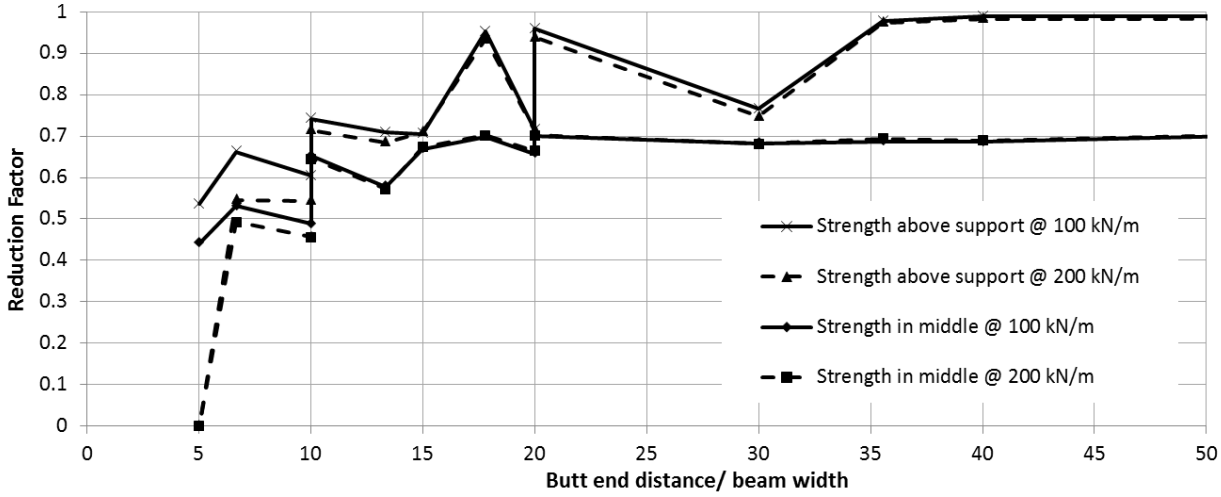

Fig. 10: Reduction factor for strength as a function of butt end distance/ beam width. Calculated from the maximum stresses along the fibres measured at two load levels.

Fig. 11 and Fig. 12 show another way of presenting the reduction factor as a function of butt end length divided by span width.

4. Discussion

4.1 F22, F25, F28

The simulation model worked well compared to the physical tests regarding the load-deflection curve (Fig. 1). Certain deviations exist but are negligible and corrections of the models were thus not deemed necessary. Sliding started at relatively low loading and yielded a non-linear loading curve and a differing curve at unloading, i.e. hysteresis occured. In variant F25 (Fig.1) the hysteresis in the model was less pronounced than in the physical tests. However, in F22 and F28 the

modelled and the physical hysteresis were more alike. Fig. 2 and Fig. 3 show displacements, stresses along fibres and contact pressure which all seem to be realistic.

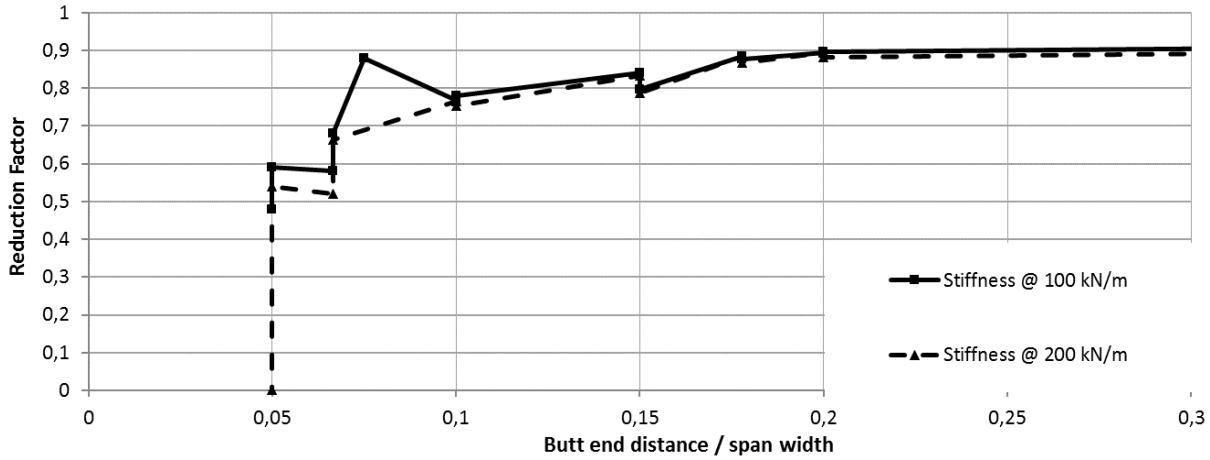

Fig. 11: Reduction factor for stiffness as a function of butt end distance/ span width. Calculated from the deflections measured at two load levels.

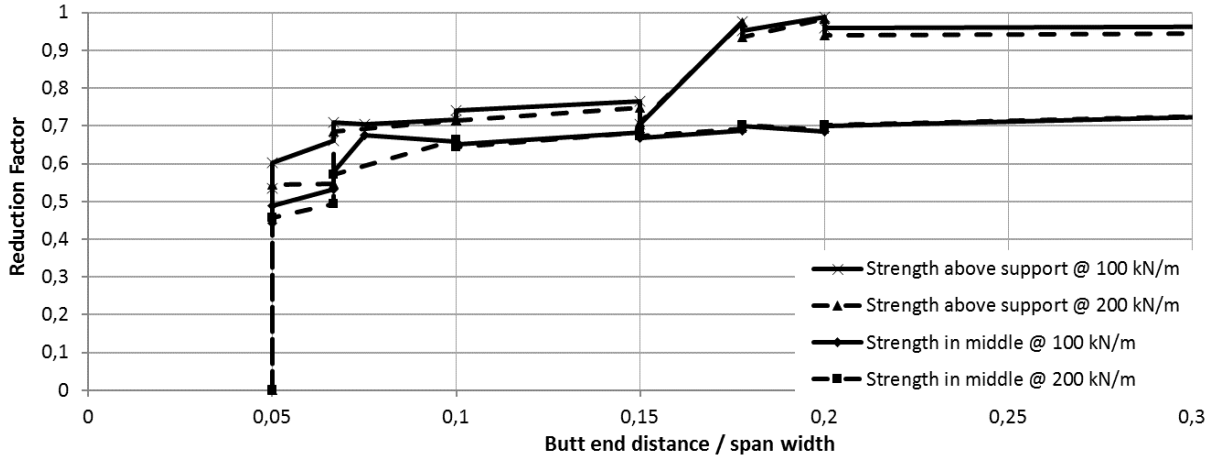

Fig. 12: Reduction factor for strength as a function of butt end distance/ span width. Calculated from the stresses along the fibres measured at two load levels.

4.2 Variants 1-7 and Ext1A to Ext4B

Since variant 1 and 7 were references, i.e. they did not incorporate any butt joints, they resulted in linear loading curves without hysteresis. All other variants resulted in varying degrees of sliding between beams and therefore hysteresis appeared when unloading. Variant Ext3A with a short butt end (0.9 m) and wide beams (180 mm) gave considerably large sliding and simulation was stopped at 150 kN/m due to instability (collapse). Sliding between beams in vertical direction was largest close to the butt joints. Sliding vertically was also large close to regions of large bending moments (middle of span width and above supports). Sliding also occurred in horizontal direction due to torsional moment in the deck.

Reduction factors shown in Figs. 9 and 10 do not give a satisfying picture of the results since curves are not very smooth. Using butt end distance/span width as a descripting variable instead gave a slightly more comprehensive picture (Figs. 11 and 12). However, also this representation is not

perfect. Narrower beams (variants 1-3, Ext1B, Ext2B, Ext3B, and Ext4B) gave other results than wider beams. Larger span widths (variants 6 and 7) gave different results than smaller span widths.

Reduction factors for stiffness and strength were not the same and were lower for strength. Reduction factor for strength was lower when judging stress in middle of span than when judging stress above supports. Reduction factors for both stiffness and strength were slightly lower when using a higher load level (due to increased slip at high load level).

Eurocode specifies a minimum threshold value of 30 for butt end distance/beam width and specifies a reduction factor of 0.75 for strength. Here, from Fig. 10 the reduction value was roughly 0.70 for butt end length/beam widths greater than 20. The reduction factor for stiffness was higher according to Fig. 9, about 0.85 for butt end length/beam widths greater than 20.

5. Conclusions

- Finite element simulations worked well and gave realistic behaviours which correspond well to the experimental results.
- Calculations of reduction factors as a function of only one variable, e.g. as in Eurocode butt end distance/beam width, did not give a comprehensive picture probably because other variables were involved such as span width and/or deck width.
- Confining butt end distance/beam widths > 20 resulted in reduction factors closer to each other for simulated variants, than for butt end distance/beam widths < 20.
- The reduction factors for stiffness and strength were not the same. The factor was higher for stiffness than for strength.

6. References

[1] Ritter, M. A. (2005). *Timber bridges: design, construction, inspection and maintenance (Part one).* University Press of the Pacific, ISBN1410221911.

[2] Anonymous, Eurocode 5: Design of timber structures-Part 2: Bridges. SS-EN 1995-2:2004.

[3] Anonymous, Abaqus 6.14 (2014) Users manual. Dassault Systemes Simulia Corp. Rising Sun Mills, 166 Valley Street, Providence, RI 02909-2499, USA. 2011.

[4] Ekevad M.; Jacobsson P.; Forsberg G.. ”Slip between glulam beams in stress-laminated timber bridges: finite element model and full-scale destructive test”. *ASCE Journal of Bridge Engineering* 16:188-196. 2011.

[5] Ekholm K.; Ekevad M.; Kliger R. (2014). Modelling slip in stress-laminated timber bridges: comparison of two FEM approaches and test values. *ASCE Journal of Bridge Engineering 19(9) 04014029.*

[6] Ekevad M.; Jacobsson P.; Kliger R. (2013). Stress-Laminated Timber Bridge Decks: Non-linear Effects in Ultimate and Serviceability Limit States. International Conference on Timber Bridges 2013 (ICTB2013). Arranged by USDA Forest Products Laboratory. Las Vegas, USA, September 30-October 2, 2013.

[7] Vertikalt glidbrott och stumskarvars inverkan på tvärspända träplattor. Provningsrapport (in Swedish). Kristoffer Ekholm, Chalmers Tekniska Högskola, Konstruktionsteknik, Rapport 2012:06.

Simulation of moisture diffusion in timber bridges exposed to rain

Petr Hradil
Senior Scientist
VTT
Espoo, Finland

Senior Scientist at VTT technical Research Centre of Finland Ltd, PhD in timber structures. Main expertise in structural performance of wood and steel, numerical analysis, structural optimization, standardization and sustainability.

Stefania Fortino
Senior Scientist
VTT
Espoo, Finland

Senior Scientist at VTT technical Research Centre of Finland Ltd, PhD in computational mechanics. Main expertise in hygro-thermo-mechanical analysis of wood-based products and biomaterials. Management of WW-Net projects and participation in Cost actions related to timber structures.

Giovanni Metelli,
Professor at University of Brescia, Italy

Alessandro Musci,
Civil Engineer at University of Brescia, Italy

Jakub Dohnal,
PhD candidate at Brno University of Technology, Czech Republic

Maria Fredriksson,
Senior Researcher at Lund University, Sweden

Summary

The paper presents a modified single-phase numerical model of timber exposed to the outdoor climate. The previous studies by some of the authors showed that finite element method (FEM) with the single-Fickian theory of moisture diffusion is an efficient tool to simulate the moisture gradients in timber structures sheltered from rain. An extension of this approach that takes into account the effect of water due to rain or water traps is proposed in this paper and the numerical model is verified by comparisons with laboratory tests of Norway spruce joints exposed to artificial rain in the laboratory of Lund University. The model is then used to simulate moisture diffusion in selected details of timber bridge elements monitored within the DuraTB project.

Keywords: timber bridges, moisture content, effect of rain, single-phase models, FEM

1. Introduction

Moisture traps in timber bridges exposed to Northern European climates should be carefully avoided in order to improve the durability and performance of these structures. In the WoodWisdom-Net+ project Durable Timber Bridges (DuraTB), the choices of design concepts are made on the basis of minimal moisture trapping and on the results from hygro-thermal, mechanical and life-cycle analyses of existing timber bridges. The relative performance of different details with respect to potential moisture trapping is also studied in order to quantify the risk of decay for different structural typologies. In this context, the moisture monitoring by sensors-based techniques could be assisted by numerical methods aimed to simulate the moisture distribution in timber bridge elements under outdoor climates also in the direct contact with the water caused by exposure to rain or by water leakage.

In previous studies by some of the authors, a simplified numerical approach based on the finite element method (FEM) and on the single-Fickian theory of moisture diffusion, was found useful to simulate the moisture gradients in timber structures sheltered from rain. An extension of this approach that takes into account the effect of water due to rain or water traps is proposed in this paper. The numerical model is verified by comparisons with laboratory tests of Norway spruce joints exposed to artificial rain in the laboratory of Lund University within a previous research by one of the authors. The model is then used to simulate moisture diffusion in selected details of timber bridge elements monitored within the DuraTB project.

2. Moisture diffusion and wood permeability

The transport of water vapour and bound water in wood members is typically simulated in the FEM software as heat conduction when the single-phase models are used. Then the conductivity parameter of the numerical model is equal to the diffusivity l of moisture in wood, the product of diffusion coefficient D and wood density r. The diffusion normal to the grain of wood was experimentally studied by Nilsson [1] and presented as upper and lower bounds of D up until 80% moisture content u. Its calculation until the fibre saturation point (FSP) was later proposed by Toratti [2] (Eq. (1)) and fitted to Jönsson's experiments [3] in Eq. (2). The diffusion along the grain was reported for instance by Sjödin [3]. The single-phase model using Toratti's diffusion coefficients in the wood direction perpendicular to grain combined with Sjödin experimental diffusion in the grain direction was proposed by Fortino et al. in [5] and tested for cases of timber structures with moisture contents below the fibre saturation point.

$$D = 3.6\times10^{-7} e^{2.28u} \ [\mathrm{m^2h^{-1}}] \tag{1}$$

$$D = 8.64\times10^{-7} e^{4u} \ [\mathrm{m^2h^{-1}}] \tag{2}$$

The simulation of timber members exposed to weather is, however, more challenging, because it has to take into account the presence of the free water in wood. The permeability of wood for free water was expressed as free water flux J_f by Younsi et al. [6] as in Eq. (3):

$$J_f = -\frac{abK_l r_l (u_{\max} - u_{FSP})^b}{m_l (u - u_{FSP})^{1+b}} \nabla u \text{, where } u_{\max} = e_d \frac{r_l}{r} + u_{FSP} \tag{3}$$

with dry wood void space e_d = 71%, liquid water density r_l = 1000 kgm^{-3}, and parameters a = 1000, b = 0.61, $K_l = 5\cdot10^{-16}$ and m_l = 1.002.

It would be possible to extend the existing multi-Fickian model for water vapour and bound water transport [7], but single-phase definition was more computationally effective for this study. Here, the diffusion curve joins the permeability as described in Fig. 1. This figure shows the diffusivity of the wood with density r = 450 kgm^{-3}, u_{FSP} = 28% and temperature T = 293.15 K. The transition zone between FSP and u = 50% was proposed by Musci [8].

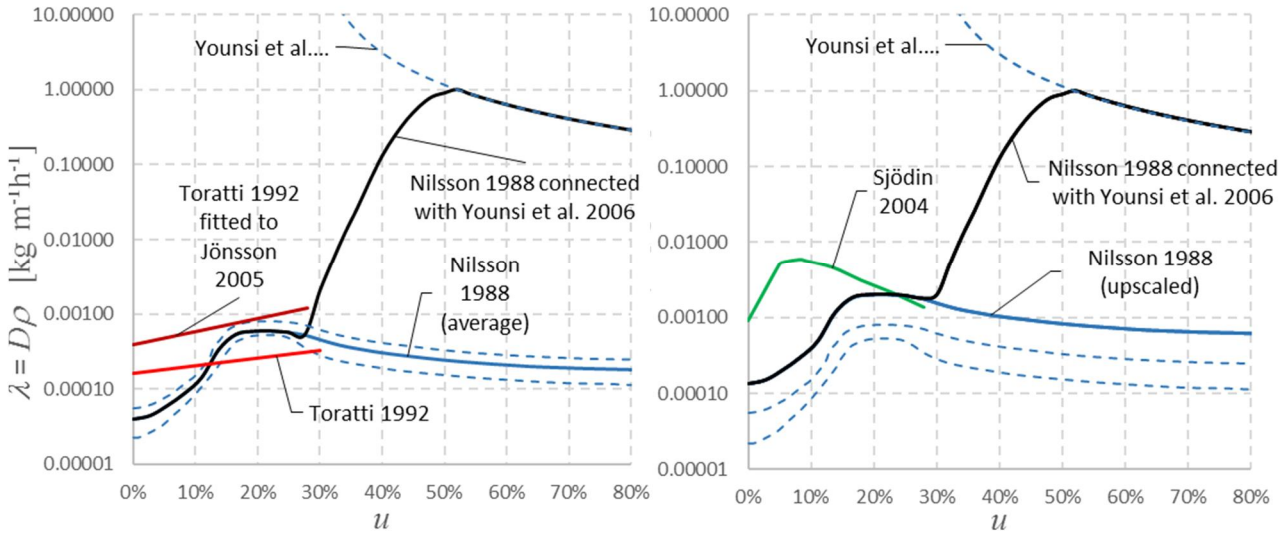

Fig. 1 Diffusion and permeability models perpendicular to the grain (left) and parallel to the grain (right)

Due to the lack of suitable information about the material behaviour along the grain, the model is assuming the same permeability of wood as in the transverse and radial directions and elevated diffusion (see Fig. 1). The prediction of the moisture transport in the longitudinal direction may be less reliable, and therefore most of the design situations in this study are with the dominant diffusion normal to the grain of wood.

3. Surface emission and the effect of rain

The mass flux q from air to the surface layers of wood is modelled by Cauchy's boundary condition in Eq. (4). It depends on the surface emissivity S, dry wood density r and the difference between surface moisture u_{surf} and equilibrium moisture u_{air} of the wood corresponding to the relative humidity h and temperature T of the circulating air.

$$q = rS\left(u_{air} - u_{surf}\right), \text{ where } u_{air} = 0.01\left[\frac{-T\ln(1-h)}{0.13(1-T/647.1)^{-6.46}}\right]^{1/110T^{-0.75}} \tag{4}$$

The positive flux is created when the external humidity corresponds to a higher moisture than on the surface and vice versa. It should be noted that the relative humidity of the air h must be lower than one and its maximum value defines the maximum moisture content u of wood in the numerical model. For instance if the maximum moisture content is limited by the FSP, the corresponding maximum relative humidity h_{max} is approximately 98.65%.

This definition can be used to take into account higher moisture content caused by free water absorption from the surface by a simple replacement of measured relative humidity of the air with the h_{max} value higher than 98.65%. Such temporary elevation of the relative humidity is then able to emulate the effect of rain or leaking water. As can be seen on Fig. 2, the selection of the artificial relative humidity level h_{max} is very sensitive and can produce maximum moisture content only up to about 110% with single precision floating-point numbers. Even though the real upper limit of moisture content u_{max} can be above 186% (from Eq. (3)), the measured moisture of timber elements exposed to external climate was always below 100%. Therefore, this simplified model could be applied in the present study.

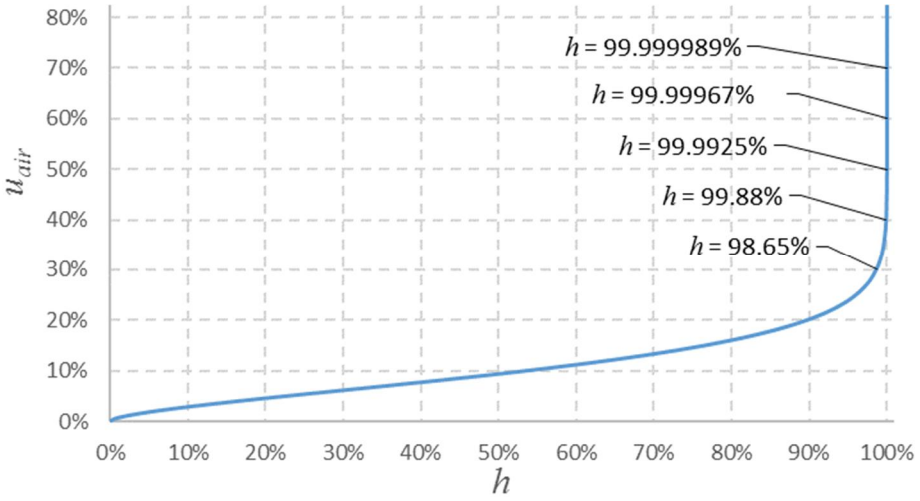

Fig. 2 Model of equilibrium moisture content of wood corresponding to the temperature 293.15 K.

The surface emissivity S depends on the surface treatment and affects greatly the rate of the moisture intake. Even though the mechanism of surface water adsorption is different from the emission of water vapour, the calculation of S is consistent for the whole range of moisture content in our study. It is calculated according to Eq. (5):

$$S = \frac{1}{\frac{1}{S_{surf}} + \frac{1}{S_{paint}}} \tag{5}$$

where $S_{surf} = 3.2 \cdot 10^{-8} e^{4u}$ and S_{paint} is the surface emissivity of the paint. In the case of untreated wood, the reference surface emissivity $S = S_{surf}$ is used. This simplification leads to only two parameters to be calibrated; the maximum level of relative humidity h_{max} (corresponding to the maximum moisture content u_{max}) and the initial moisture content of wood u_{ini}. This initial moisture content was assumed uniform in the whole model whenever there was no detailed knowledge about its distribution. Such assumption results in lower accuracy of the predicted moisture in the initial phase of the calculation. However, this period of inaccurate results can be greatly reduced if the initial level of uniform moisture is carefully selected. It is usually shorter than six months, depending on the size of the cross-section.

4. Numerical models

The following section introduces four different case studies, where the improved numerical model was tested and calibrated. The calculations were performed in Abaqus/Standard as heat transfer analysis, where the heat conductivity was replaced by diffusion defined in Fig. 1. The surface mass flux was defined as user subroutine DFLUX. This subroutine has been updated for the purpose of this study to be able to take into account different external weather parameters on each surface.

The model of combined moisture diffusion and wood permeability was validated by Musci [8] against the experiments on untreated Norway spruce joints by Fredriksson [9]. Joints with side grain surface facing side grain surface (Fig. 3, left) and three different gap sizes (0, 2 and 5 mm) were submitted to a wetting period of 6.5 hours using a water spray gun and the moisture content was measured by resistive method every 5 minutes. Unfortunately, this method does not provide accurate levels of absolute moisture content, but can only detect changes of moisture content over 50%. The same experiments were previously used to calibrate simple one-dimensional single-Fickian numerical model in COMSOL Multiphysics [10] without the effect of wood permeability. In the Abaqus model, the moisture fluxes are applied on the gap and on the right side of the board, where the mesh is denser. The models presented in this paper are from the simulation of 5 mm gap, but the interested reader can refer to [8] for the full set of results.

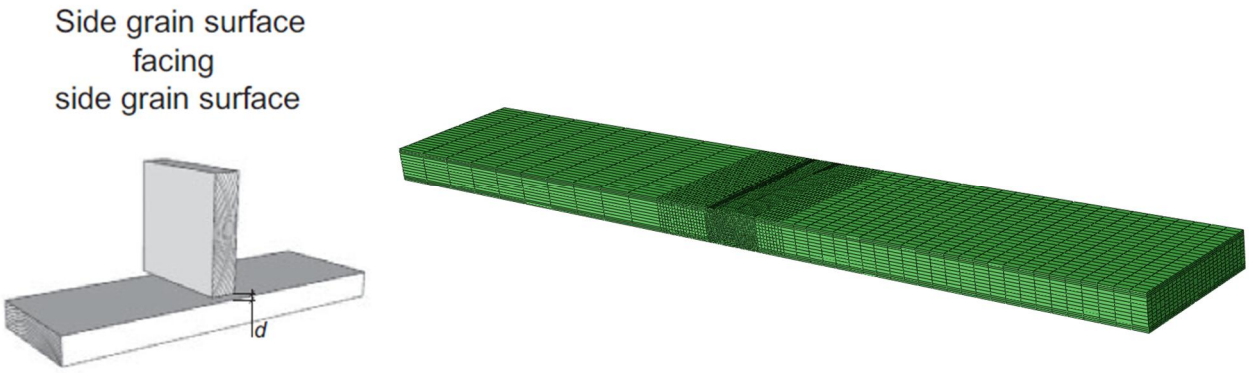

Fig. 3 Drawing of the laboratory test [9] (left) and its FEM model [8] (right)

The ability of the model to calculate results in a real environment was then tested by the simulation of experiments by Isaksson and Thelandersson [11, 12] on the untreated horizontal board 22×95 mm made of spruce (*Picea abies*). Moisture content at the mid thickness was measured by resistive moisture gauges for 3 years in a row. This experiment was also verified by one-dimensional COMSOL model described in [10].

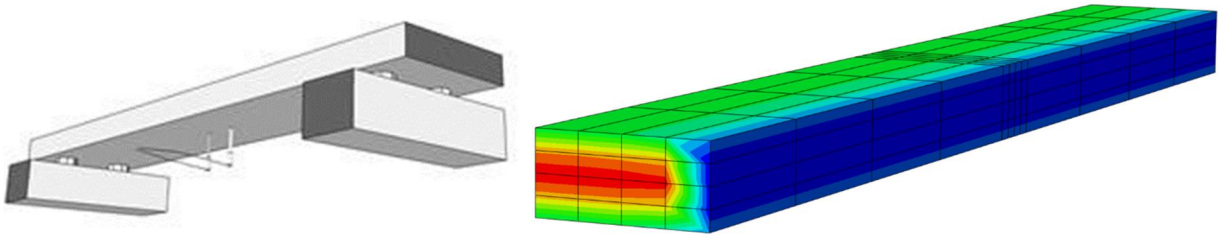

Fig. 4 Drawing of the thin board exposed to climate [10] (left)
and moisture distribution in FEM model (right)

Later experiments by Niklewski [13] studied larger beams exposed fully or partly to the rain. Fig. 5 (right) shows, how the rain affects the moisture content of the wood near to the upper surface in the unsheltered case.

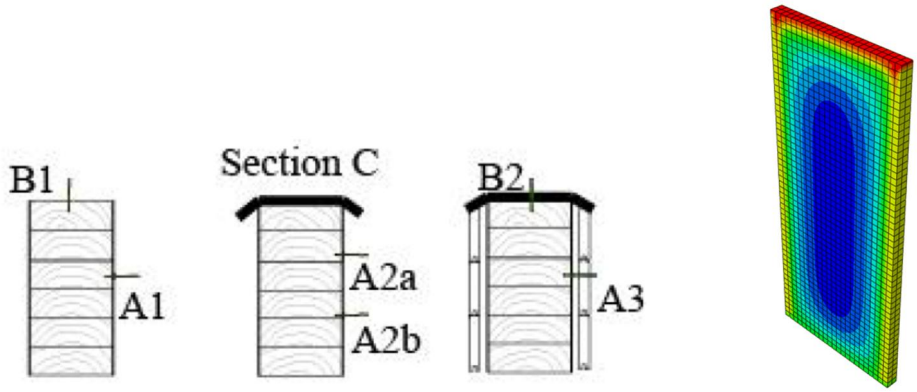

Fig. 5 Drawing of the structural beam exposed to climate [13] (left)
and moisture distribution in FEM model (right)

The same experimental programme also included connections with external steel plates and dowel-type fasteners (see Fig. 6). The moisture content was measured under the plate at 10 mm depth.

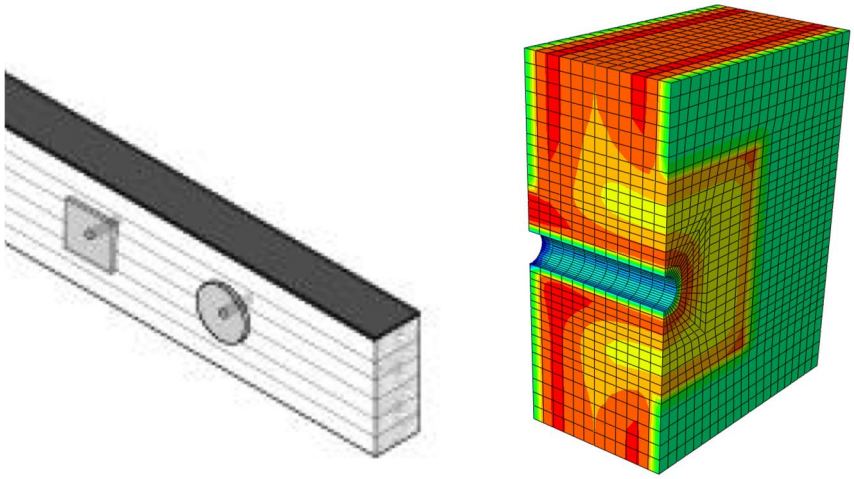

Fig. 6 Drawing of the joint exposed to climate [13] (left) and moisture distribution in one of its FEM models (right)

As a result, a comprehensive collection of experimental data was available for the verification of the improved finite element models. The basic parameters of the four numerical models presented in this paper are summarized in Table 1.

Table 1 Numerical models parameters

	Duration	r [kgm^{-3}]	u_{ini}	u_{max}	Measuring depth from the surface
Laboratory tests	150 hours	382	12%	83%	3, 11 and 19 mm
Thin board	3 years	450	11%	70%	11 mm
Structural beam	10 months	450	18%	70%	10 mm
Steel-to-timber joint	10 months	450	18%	70%	10 mm

5. Results and discussion

5.1 Laboratory tests

In Fig. 7, the comparisons between experimental data and numerical results are shown for the case of 5 mm gap. The results obtained by the coupled diffusion-permeability model using the Nilsson's diffusion from Fig. 1 (model named as "Nilsson, Sandberg and Younsi" in Fig. 7) are also compared with the ones obtained by coupling the diffusion model proposed by Fortino et al. [7] with Younsi's permeability (model named as "Toratti, Sjödin and Younsi" in Fig. 7). For both models the surface emission $S_{surf} = 1.28 \cdot 10^{-7}\ e^{4u}$ ms^{-1} proposed in [2] was used. It can be observed that the moisture content in points at 11 mm and 19 mm from the top surface provide better results than the ones at 3 mm from surface where very high levels of moisture are experimentally measured.

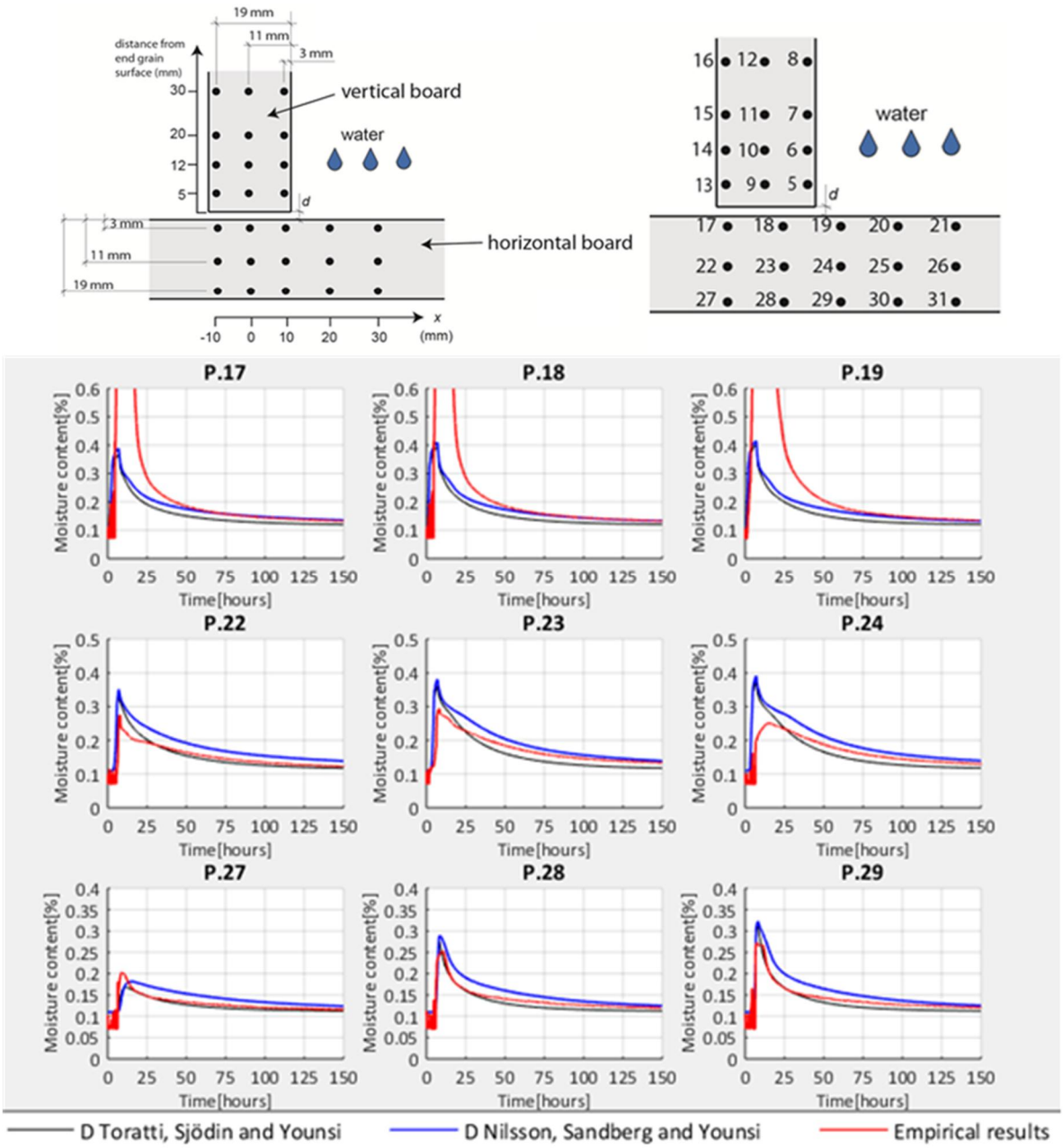

Fig. 7 Example results of simulation of 5 mm gap at the selected points below the gap; comparison between experimental data and numerical results from 2 different diffusion-permeability models

5.2 Thin board

The board was exposed to weather without the possibility of moisture trapping. The rain was affecting top surface and sides, but as can be seen from Fig. 8, the level of moisture in 11 mm depth remained below FSP. This was confirmed by the measurements and numerical model as well.

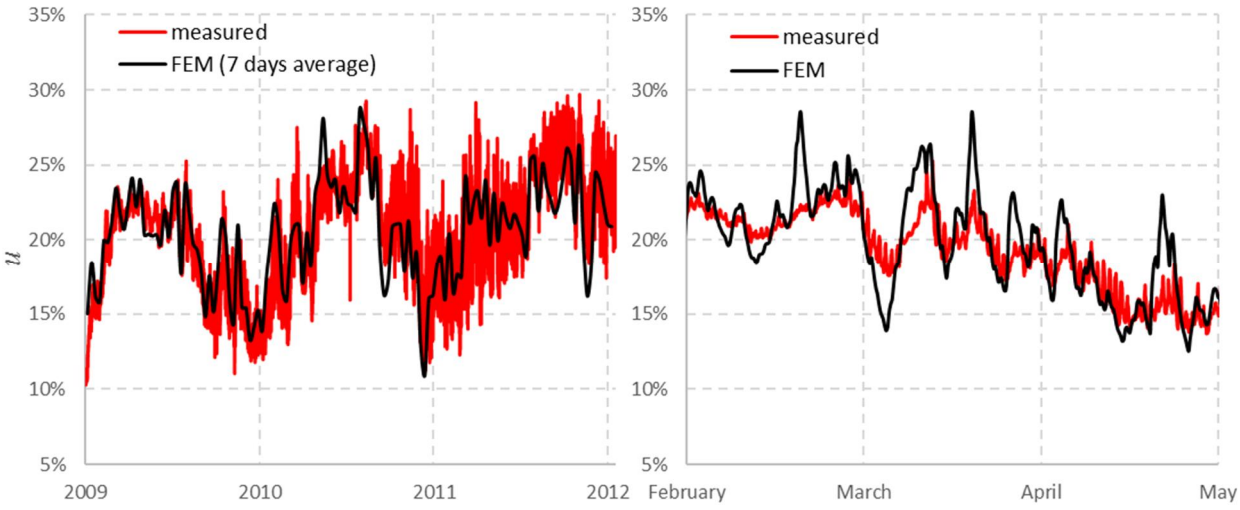

Fig. 8 Predicted moisture content in the middle of the board in the period of 3 years (left) and 3 months (right)

5.3 Structural beam

The similar behaviour with moisture content below FSP at 10 mm depth was observed in the experiments from Lund University [13] with larger beam exposed fully or partly to the rain. Fig. 9 shows the initial period of inaccurate results from September 2014 to March 2015 caused by the assumption of uniform initial moisture distribution. On the other hand, the results from March to July 2015 show a very good agreement with the measurements.

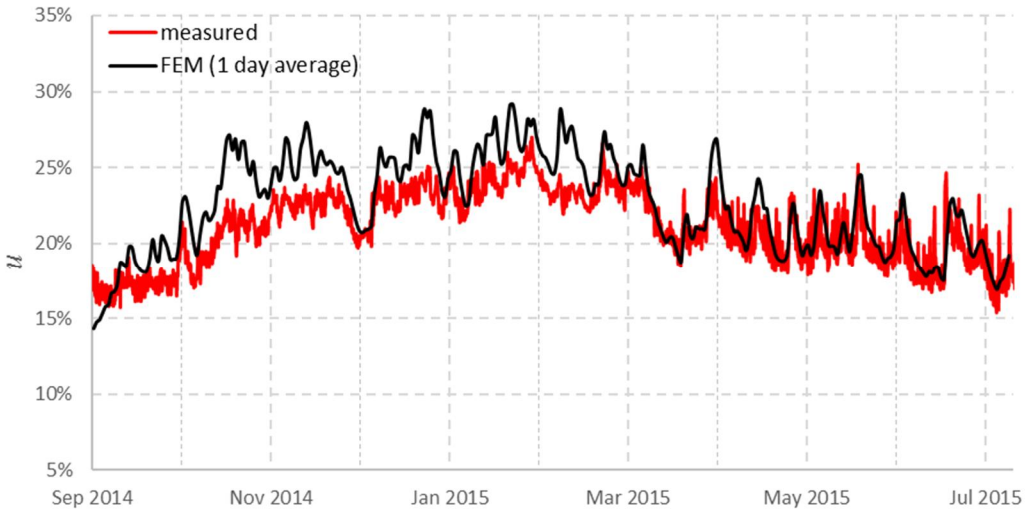

Fig. 9 Predicted moisture content 10 mm from the surface of the beam

5.4 Steel-to-timber joint

The simulation of leaking water behind the steel plate is always problematic. As can be seen from Fig. 10, three major leaking events were observed in the monitoring period. Moreover, the drying process after the third leakage was significantly slower than in the previous two cases, and the measured moisture content was about 5% higher than the prediction since January 2015. This may indicate that the geometry of the specimen has changed either by opening the gap between the plate

and wood or the crack in wood itself. Numerical models cannot naturally predict the time of such random event, and therefore the leaking accidents were inserted in the model inputs manually. The results in Fig. 10 show that the moisture content has recovered according to the measurements in the first case and partly after the second leakage.

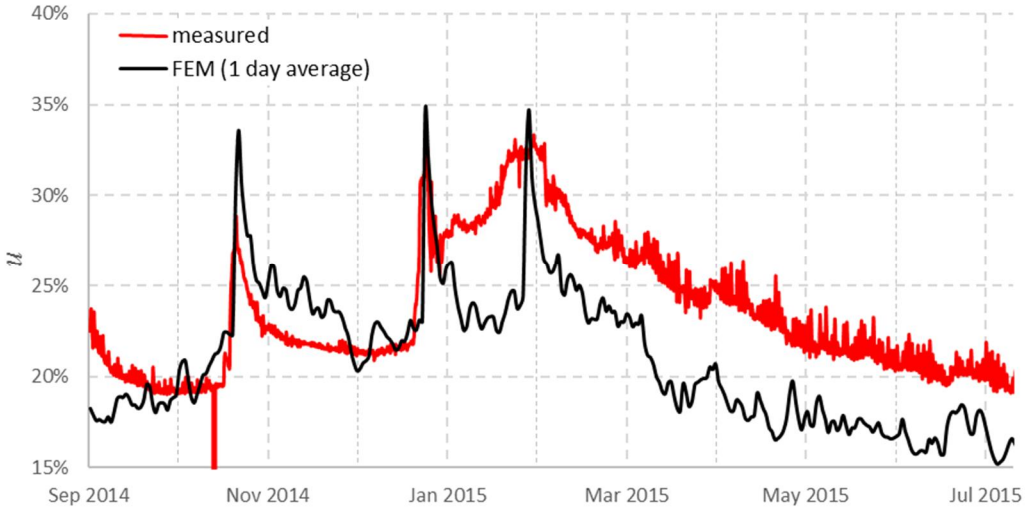

Fig. 10 Predicted moisture content 10 mm from the surface under the external plate

6. Conclusions

The demonstration of improved finite element models showed that the numerical prediction of moisture in wood members exposed to the external climate is possible. It can be a useful indicator of the length of the periods with moisture higher than fibre saturation point (FSP) or any other level indicating the risk of biotic degradation of timber bridge deck or structural elements.

Single-phase (single-Fickian) models are more computationally efficient than multi-phase (multi-Fickian) models. However, they cannot model precisely the combined effect of free water transport, bound water and vapour diffusion, and therefore such models are not suitable for details with very long periods of elevated moisture content. The simulation results may be further improved when the water adsorption of the surface is included in the calculation of the surface mass flux.

Acknowledgements

The research leading to the presented results was supported by WoodWisdom-NET+ project DuraTB (Durable Timber Bridges) which is greatly acknowledged. We would like to thank Jonas Niklewski and Tord Isaksson for the experimental data used in this paper.

References

[1] Nilsson L.-O. “Moisture transport properties of wood and wood-based boards – an inventory and analysis of knowledge and required knowledge” (in Swedish), Report P-88:4, dept. Of building materials, Chalmers University of Technology, Göteborg, Sweden, 1988.

[2] Toratti T. “Modelling the Creep of Timber Beams”, *Rakentieden Mekaniikka*, Vol. 25, No. 1, 1992, pp. 12-35.

[3] Jönsson J (2005) Moisture induced stresses in timber structures, Technical Report TVBK-1031, Dissertation, Division of Structural Engineering, Lund University of Technology.

[4] Sjödin J. “Moisture transport in glulam during the construction phase” (in Swedish), *KTH TRITA-BYMA*, No.3, 2004.

[5] Fortino S., Mirianon F. and Toratti T. “A 3D moisture-stress FEM analysis for time dependent problems in timber structures” *Mechanics of Time-Dependent Materials*, Vol. 13, No. 4, 2009, pp. 333–356.

[6] Younsi R., Kocaefe D., Poncsak S. and Kocaefe Y. “Transient Multiphase Model for the High-Temperature Thermal Treatment of Wood”, *AIChE Journal*, Vol. 52, No. 7, 2006, pp. 2340-2349.

[7] Fortino S., Genoese A., Genoese A., Nunes L. and Palma P. “Numerical modelling of the hygro-thermal response of timber bridges during their service life: A monitoring case-study”, *Construction and Building Materials*, Vol. 47, 2013, pp. 1225-1234.

[8] Musci A. “Effects of Moisture Content on Timber Structural Elements; Case Study: Vihantasalmi Bridge”, Master Thesis, DICATAM, University of Brescia, Italy, 2015.

[9] Fredriksson M., Wadsö L., Johansson P. and Ulvcrona T. “Microclimate and moisture content profile measurments in rain exposed Norway spruce (Picea abies (L.) Karst.) joints.”, *Wood material Science & Engineering*, Vol. 11, 2006, pp. 189-200.

[10] Niklewski J., Fredriksson M. and Isaksson T. “Moisture content prediction of rain-exposed wood: Test and evaluation of a simple numerical model for durability applications”, *Building and Environment*, Vol. 97, 2016, pp. 126-136.

[11] Isaksson T. and Thelandersson S. “Experimental investigation on the effect of detail design on wood moisture content in outdoor above ground applications”, *Building and Environment*, Vol. 59, 2013, pp. 239-249.

[12] Thelandersson S., Isaksson T., Suttie E., Frühwald E., Toratti T., Grüll G., Viitanen H. and Jermer J. “Service life of wood in outdoor above ground applications: Engineering design guideline; Background document”, Report TVBK-3061, Lund University, Sweden, 2011.

[13] Niklewski J. “Effects of climate exposure on the (moisture) performance of structural details in timber bridges”, Performance and maintenance of bio-based building materials influencing the life cycle and LCA, Kranjska Gora, Slovenia, 2014.

Updating of numerical timber bridges models by experimental modal analysis

Julio Vivas
Structural Engineer
MEDIA MADERA
Asturias, Spain
julio@mediamadera.com

Soledad Rodríguez
Laboratory Engineer
CETEMAS
Asturias, Spain
srodriguez@cetemas.es

Juan Carlos Santos
Industrial Engineer
MEDIA MADERA
Asturias, Spain
carlos@mediamadera.com

Summary

Development and updating of numerical models using data obtained from test on prototypes has become significant in civil engineering structures. The comparison between measurements of the real structures and the results with analytical procedures can generate better numerical models that can simulate faithfully the actual behavior of the structures. Experimental Modal Analysis is a useful tool to validate at first, and improve later, the numerical model of a structural system because one of its advantages is the high accuracy in the determination of natural frequencies of a structure. The results show numerical models of different structural types of timber bridges which have been developed, compared and updated using the modal parameters of actual prototypes tested with experimental modal analysis.

Keywords: Model updating; Modal testing; Dynamics; Footbridge; Modal shapes

1. Introduction

The objective of this work is to develope representative numerical models of various structural typologies of modern timber footbridges. These models are updated using data obtained through experimental modal analysis on real prototypes. The dynamic properties of the numerical model should be as similar as possible to the real prototypes and should be general enough so that the models can be adapted and modified to predict the dynamic properties of different sized footbridge in same typology.

In order to achieve this objective, first, dynamic tests were carried out on four real footbridges that correspond to common different typologies: simply-supported beam bridge, two hinged arch bridge, bow-string bridge and tide-bow bridge. Thus, through experimental modal testing, the eigenfrequencies, dampening and vibration shapes were identified. The determination of the natural frequencies in timber bridges has been studied by several authors [1,2].The numerical modeling of the different typologies was developed in a MEF software capable of reproducing a modal analysis, in order to replicate a model with the same dynamic properties as the prototypes tested.

2. Methodology

2.1 Starting numerical models

The structural analysis software *Robot* was used to create the models of the footbridges. This structural engineering software is versatile enough for simple frame sizing and design calculation or complex finite element analysis and allows to carry out the structural dynamic analysis of the bridges.

So, four different models of pedestrian timber bridges were designed and calculated according to Eurocode 5 [3] using this software, and were defined by bars and nodes, assigning cross section and mechanical properties corresponding to strength class GL24h to the main girders, archs or secondary elements of the bridges.

2.1.1 Simply-supported beam bridge

It's the structural typology most frequently used, suitable for lights up to 20-30 meters. It is based on two main beams working at simple bending.

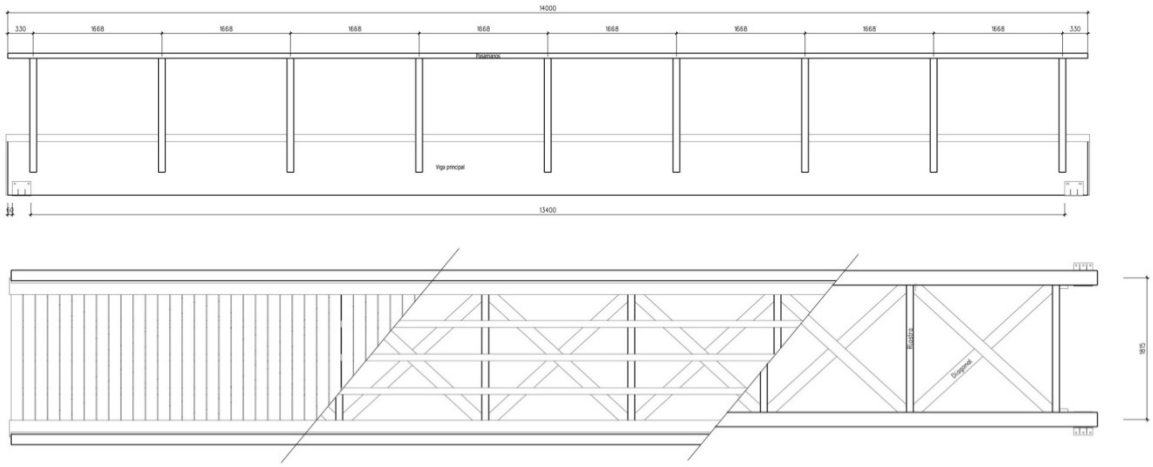

Fig. 1 Manufacuring plan 14 meters span and 2 meters width simply-supported beam bridge

2.1.2 Two hinged arch bridge

It is another of the most common structural typologies for pedestrian timber bridges between 20 and 50 meters span. Characteristic distribution of the efforts with predominance of the axillary component, is especially appropriate for a material such as timber, with high resistance in a direction parallel to the fiber and low capacity in perpendicular.

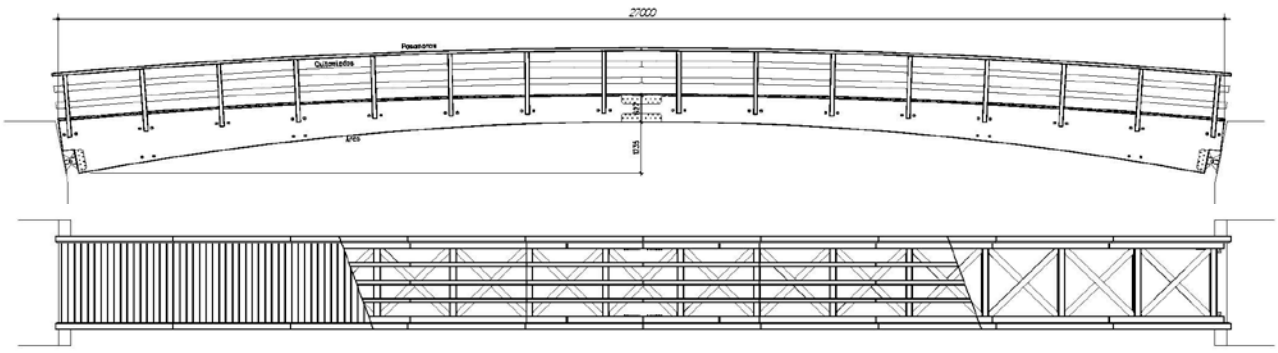

Fig. 2 The 27 meters span two hinged arch bridge plan

2.1.3 Bow-string bridge

Suitable from 30-35 meters span, allows more efficient arches with greater curvature than the previous typology, the board is hanged of the arches

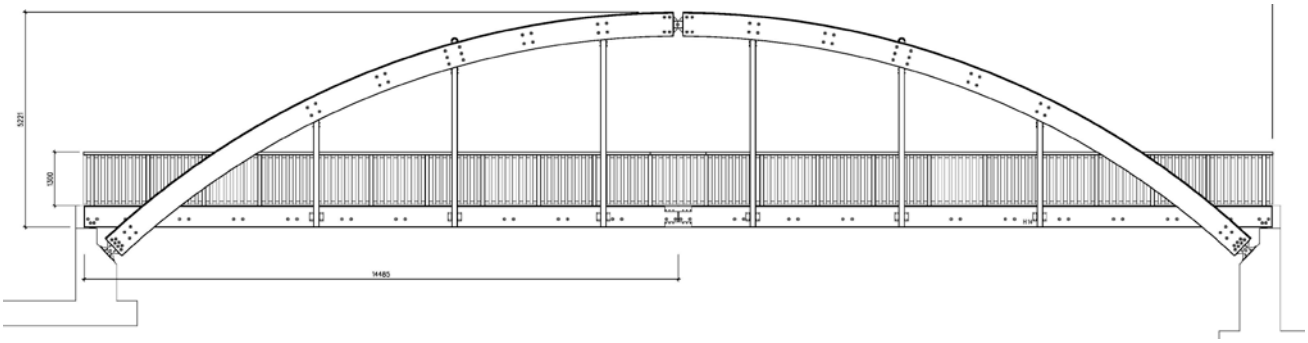

Fig. 3 Bow-string bridge 30 meters, 2,5 m width

2.1.4 Tide-bow bridge

A tied-bow bridge is another kind of bow-bridge in which the outward-directed horizontal forces of the arch are borne as tension by the deck itself, rather than by the ground or the bridge foundations.

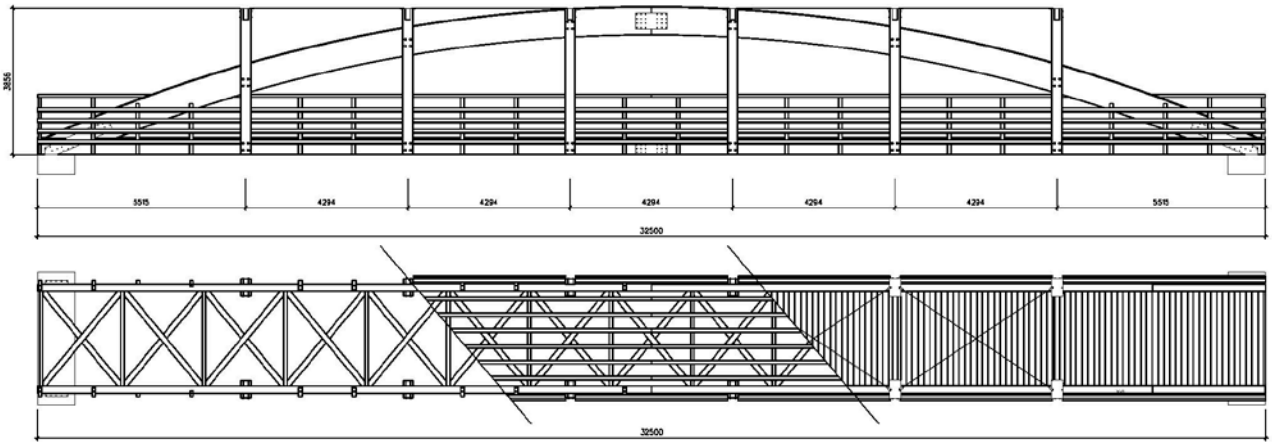

Fig. 4 Plan of the tide-bow bridge 32,5 m span and 3 m width

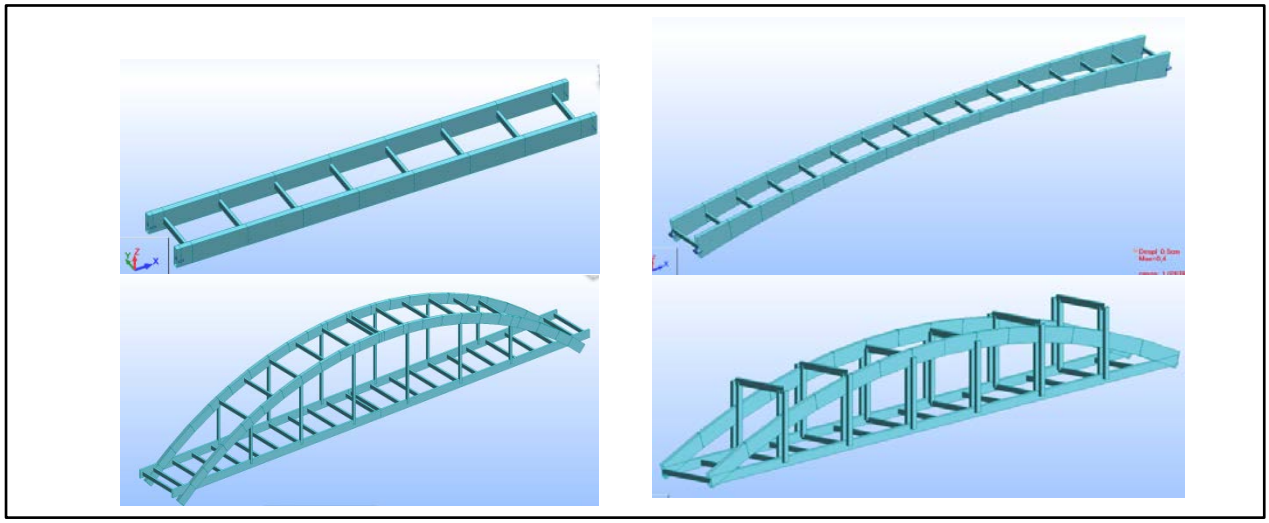

Fig. 5 Numerical models in Robot Structural Analysis

2.2 Dynamic testing

The four bridges calculated through the starting models were built, and they could be tested. Isostatic typologies, tide-bow and simply supported beam bridge could be tested in the facilities where they were manufactured, but the hyperstatic ones, two hinged arch and bow-string bridges, had to be tested in their definitive location.

Dynamic tests were made in order to obtain frequency of vibration of the structure and its associated characteristic modes under external excitation. The methodology has already been used for experimental analysis of the vertical vibrations on timber footbridges [4] and was based on works developed by Crews et al. in Australia on non-destructive evaluation of old timber bridges using Dynamic Frequency Analysis to determine global stiffness [5]

2.2.1 Instrumentation

Six model PCB 3711B112G accelerometers with a sensibility of 1000 mV/g and a measurement range of ±2 g were used to determine the accelerations of the main girders of the bridges. For the bridge excitation an impulse force test hammer, model PCB 086D20, was used.

To register the data of the impact hammer and the accelerations response during the dynamic test mobile measurement system from IMC with eight channel recording was used which allowed a real time monitoring of the entire data acquisition process. The processing of the data from the test was conducted using the software IMC Famos and LMS Test.Lab.

2.2.2 Dynamic Test Configuration

Fig. 6 Accelerometer attached under bridge girder

To measure vibrational response and natural frequency it was necessary to attach accelerometers underneath the bridge girders and to hit on the bridge with an impact hammer. Five accelerometers were placed on the lower edge of the two main girders using magnets and metal plates installed on the bridge.

The tests were conducted in two phases due to the limited number of digital inputs available on the signal acquisition system. In the first phase the accelerometers were placed in positions 1, 2, 3, 4, 5 and 6 of the structure as shown in Figure 2. In the second phase they were placed in the points of impact to achieve the excitation of the structure 6.

2.2.3 Test procedure

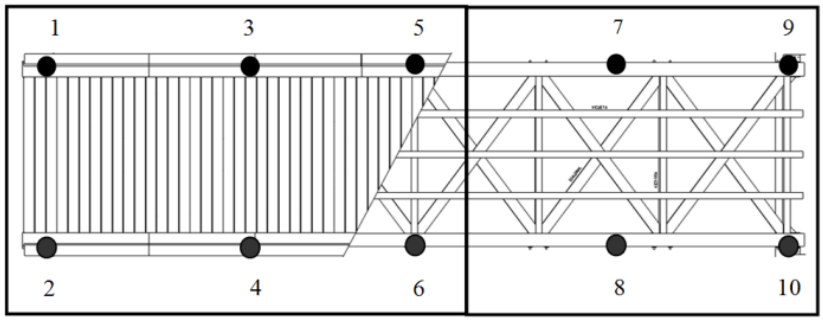

Fig. 7 Locations of accelerometers in the two phases of the test

Acceleration responses generated by the structure during the dynamic test were recorded on a laptop through the IMC Devices software. The configuration of the program was determined according to the characteristics of the structure, based mainly on the adjustment of characteristic values of the accelerometers and the impact hammer (sensitivity, measuring range, number of samples collected during each part of the excitement, etc.). Use of the software allowed us to visualize the behaviour of each individual accelerometer, and to confirm that the structure had been excited correctly, through its faithful monitoring of the impact hammer, Figure 8

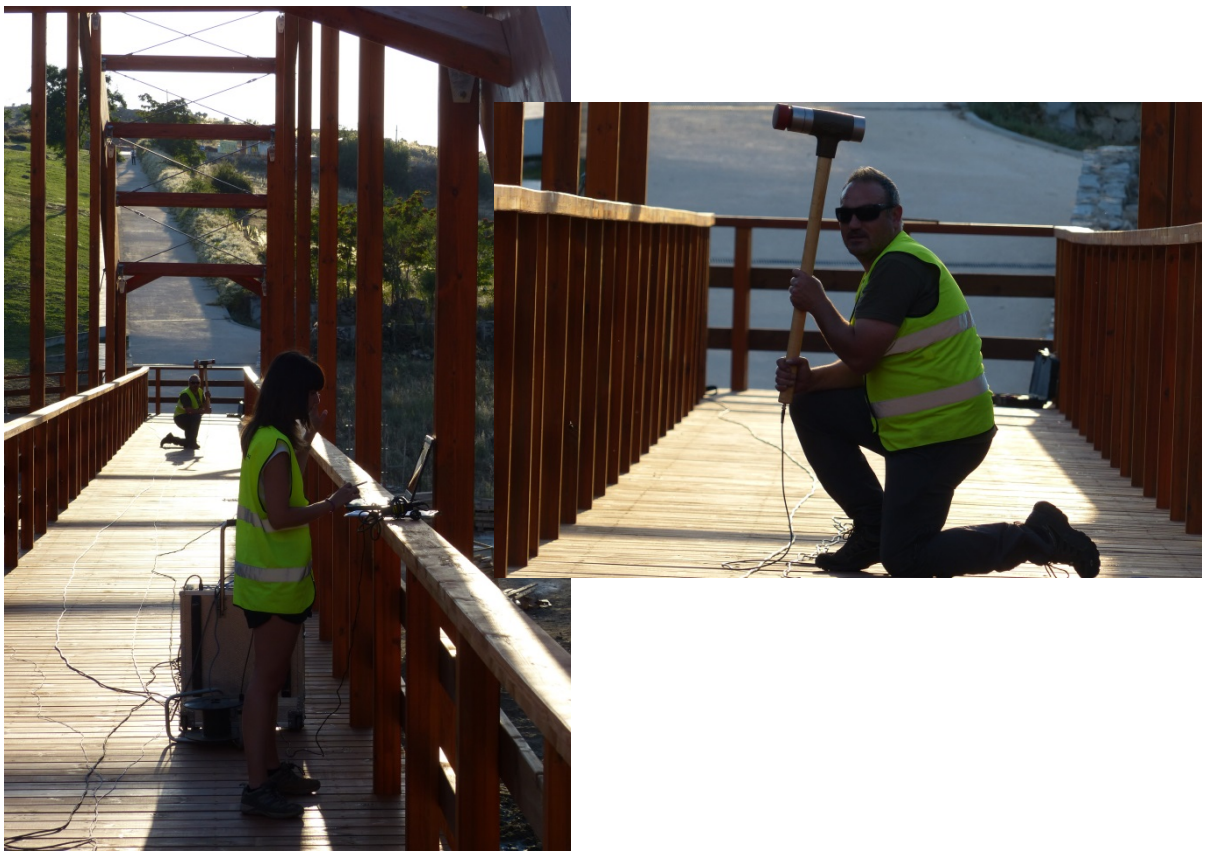

Fig. 8 Dynamic test on bow-string bridge

2.2.4 Processing of vibration data and analysis of the FRF

The IMC Famos software confirmed that all the excitement impacts on the bridges were applied correctly and that there were no anomalies during the recording of responses. Also, this software enable the Frequency Response Function (FRF) to be determined from the Frequency Time Function (FFT). Processing was carried out using LMS Test.Lab software which synthesizes the FRF's of the tested bridges and dynamic responses was evaluated.

2.2.5 Tests results

		Modal shapes		
Typologie	**Span**	**1st flexion mode**	**1st torsion mode**	**2nd flexion mode**
Simply-supported	*14 m*	*6.665 Hz*	*8.349 Hz*	*22.285 Hz*
Two hinged arch	*27 m*	*6.442 Hz*	*6.919 Hz*	*7.548 Hz*
Bow-string	*30 m*	*5.994 Hz*	*6.634 Hz*	*No data*
Tide-bow	*32,5 m*	*6.98 Hz*	*9.476 Hz*	*No data*

Table 1 Dynamic test results

2.3 Updating of numerical models

First, it is studied the correlation between the eigenfrequencies obtained numerically and those obtained experimentally.

If it is observed that the numerical model does not respond in a similar way to the prototype it is necessary to look for the design parameters that must be modified. Differences could be due to the considered boundary conditions, joints or supports

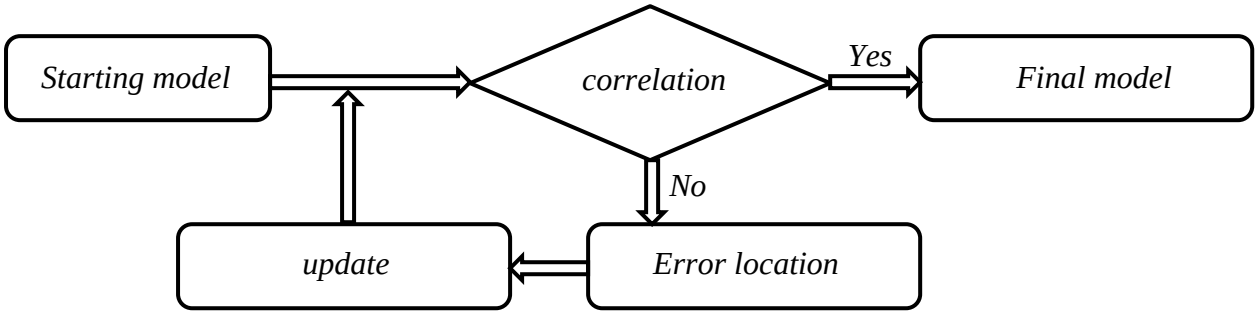

Fig. 9 Update process

It is very important to select the parameters appropriately, either locally (for each element) or grouping them, because the convergence or not of the update depends heavily on it. As important as this is the control of variation of the parameters, imposing limit values (lower, upper or both) depending on the physical sense of such variation.

3. Conclusions and discussion

The Despite having focused only on the vertical direction of dynamic behaviour, the main objective of the work have been achieved and the four numerical models are presented as a good tool.

The results of the dynamic tests showed at least three modes of interest, with a reasonably good correlation with the results of the modal analysis of the numerical models developed, in which up to six modes of interest could be identified. The good results obtained from the simply-supported and two hinged arch models are possible because these two typologies respond to the simpler structural systems.

Comparison of the results of the first mode of flexion				
Typologie	**Span**	**Dynamic test**	**Updated model**	**Diference**
Simply-supported	*14 m*	*6.665 Hz*	*6.74 Hz*	*1.01%*
Two hinged arch	*27 m*	*6.442 Hz*	*6.63 Hz*	*1.02%*
Bow-string	*30 m*	*5.994 Hz*	*5.48 Hz*	*-8.57%*
Tide-bow	*32,5 m*	*6.98 Hz*	*7.51 Hz*	*7.59%*

Table 2 Comparison of the results

Although are presented the data corresponding to the current state of the work, a deeper updating for the other two typologies would be advisable.

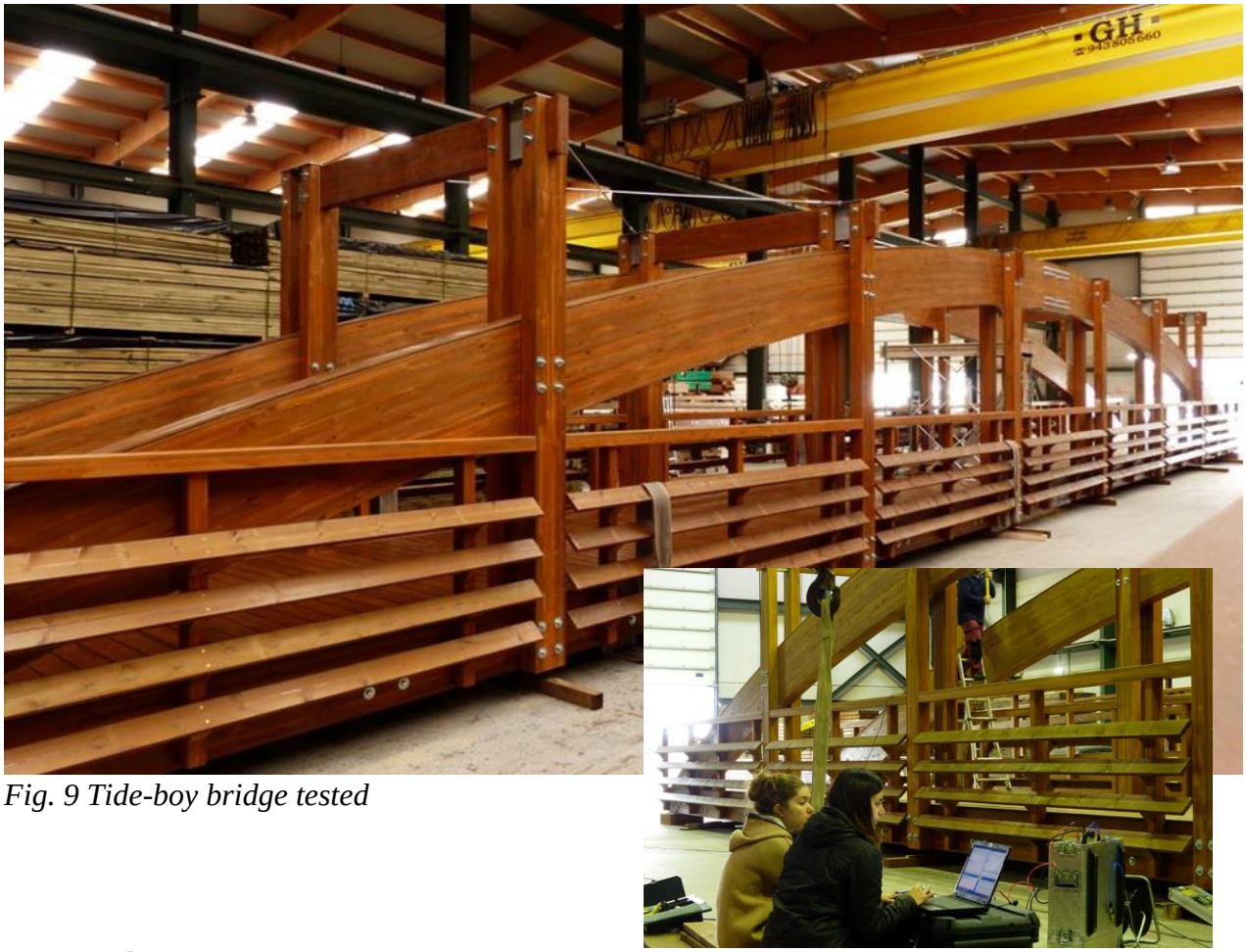

Fig. 9 Tide-boy bridge tested

4. References

[1] Feltrin, G., Steiger, R., Gsell, D., Gülzow, A. and Wilson, W. Serviceability assessment of a wooden trough bridge by static and dynamic tests". Proceedings of WCTE, World Conference on Timber Engineering. Trentino, Italy. 2010.

[2] Wang, X., Wacker, J., Morison, A. M., Forsman, J. W., Erickson, J. R., Ross, R. J. Nondestructive assessment of single-span timber bridges using a vibration-based method. Research paper FPL-RP-627. Forest Products Laboratory. Forest Service. USDA, United States Department of Agriculture. 2005.

[3] CEN(1997) Eurocódigo 5. proycto de estructuras de madera. Pate 1-1: Reglas generales y reglas para edificación. AENOR. Madrid. UNE-ENV 1995-1-1 110 pp.

[4] Baño, V., Santos, J.C., Vivas, J., Rodríguez, S., Vega, A. and Crews K. A study of the influence of different types of timber footbridges on the vibrational natural frequency. 17th International Nondestructive Testing and Evaluation of Wood Symposium. Sopron, Hungary. 2011

[5] Crews, K., Samali, B., Li, J., Bakoss, S. and Champion C. Testing and assessment procedures to facilitate the management of timber bridge assets. 3rd CECAR- Civil Engineering Conference in the Asian Region. Seoul, Korea. 2004

Comparison of Cross- and Stress-Laminated Timber Bridge Decks

Jonas TURESSON
Ph.D. Student
Luleå University of Technology
Skellefteå, Sweden
jonas.turesson@ltu.se

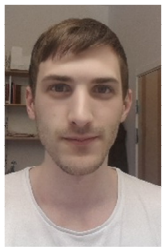

Studying the behaviour of timber constructions with use of finite element simulations.

Mats EKEVAD
Ph.D., Professor
Luleå University of Technology
Skellefteå, Sweden
mats.ekevad@ltu.se

Research focus is on finite element simulations of wood material and engineered wood products behaviour during loading.

Sven BERG
Ph.D., Senior Lecturer
Luleå University of Technology
Skellefteå, Sweden
sven.berg@ltu.se

Research focus is on finite element simulations of wood material and engineered wood products behaviour during loading.

Summary

Simply supported bridge decks made of cross-laminated timber (CLT) and stress-laminated timber (SLT) are compared. The decks have a constant axle load and varying span and thickness. CLT in the form of a plate is built up from an uneven number of layers of boards with crosswise varying fibre directions. SLT is built up from glulam beams with the same fibre direction placed side by side to form a plate. Both CLT and SLT have homogenised mechanical and physical properties and can be produced as large elements. This study was conducted by comparing results from finite element simulations of bridge decks made up from SLT and CLT for various bridge spans. The ratio of timber volume needed to fulfil deflection limits for CLT and SLT increased as the bridge span increased. The ratio was 1.3 for 24 m span and width 3.2 m. The transverse displacement curve was flatter for CLT compared to SLT. Longitudinal displacement curves were similar for CLT and SLT.

Keywords: stress-laminated, cross-laminated, timber bridge deck, FEM, finite element method

1. Introduction

Timber bridges today are mainly constructed using stress-laminated timber (SLT). SLT is constructed of multiple glue-laminated (glulam) beams placed side by side. SLT decks are pre-stressed using steel bars fitted in transversely drilled holes in the deck. The purpose of the frictional forces created between the beams is to hold the beams together in the transverse direction and transfer load between beams. Another way to construct a deck is to use cross-laminated timber (CLT). The use of CLT in construction, e.g. for floors, walls and beams has been increasing recently because CLT has several advantages compared to glue laminated timber and solid wood. For example, a beam designed in CLT has the major advantage of a high tensile strength perpendicular to the beam axis and it is less susceptible to cracks [1].

CLT panels are designed by an odd number of crosswise layers of wooden boards. Each layer is glued to each other. Some manufactories also use glue on the side edges between the individual boards. The thickness of the cross-section and individual layer should not exceed 500 mm and 45 mm, respectively [2]. An illustration of SLT and CLT can be seen in Fig. 1.

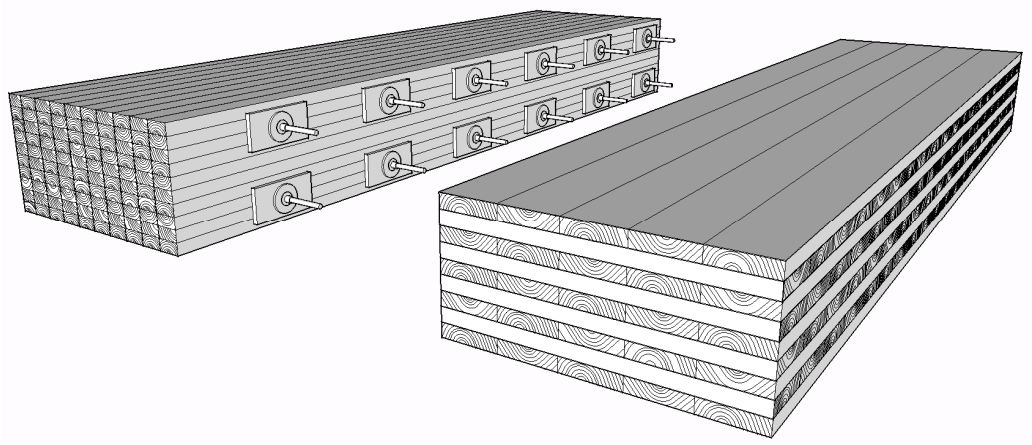

Fig. 1 Stress-laminated timber and cross-laminated timber

Timber is a structurally efficient material, judging strength in relation to self-weight [3]. This is important for a bridge. CLT bridge decks can be fully constructed in a factory and transported to the construction site. Compared to SLT bridge decks, which are mainly built on site, prefabricated CLT bridge decks are constructed in a controlled environment. Bridge decks designed in CLT can also lead to shorter construction time on site.

A timber bridge designed according to Eurocode is frequently limited by bending and shear strength rather than deflection according to [4]. This result was based on hand calculations rather than finite element (FE) calculations. In earlier studies a comparison between linear and non-linear FE simulations for SLT bridge decks was made. It showed that non-linear effects may be important for thin bridge decks in the ultimate limit state [5]. Other studies of SLT bridge decks are [6], [7] and [8]. Only one earlier studies have been found on bridge decks made of CLT [9].

In this paper, FE-modelling was used to compare three different CLT decks designs to corresponding SLT decks. This was done for different spans from 6 to 24 m. The models were constructed to meet the same deflection criteria. The objective of this paper was to investigate the necessary volume ratio of CLT compared to SLT for bridge decks. Also to describe differences in deflection behaviour in the same way as in a similar earlier study [10]. In that study, a SLT bridge deck with an eccentric load was analysed.

2. Method

The bridge span was varied from 6 to 24 m in steps by 6 m with a fixed width of 3.2 m for all models. Symmetry was used in two directions, marked with triangles in Fig. 2. The boundary condition was applied on the lowest edge and is illustrated by circle symbols. This condition restricted the nodes from movement in *y*-direction. The displacement was measured underneath the deck at the edges marked with a dash dotted line.

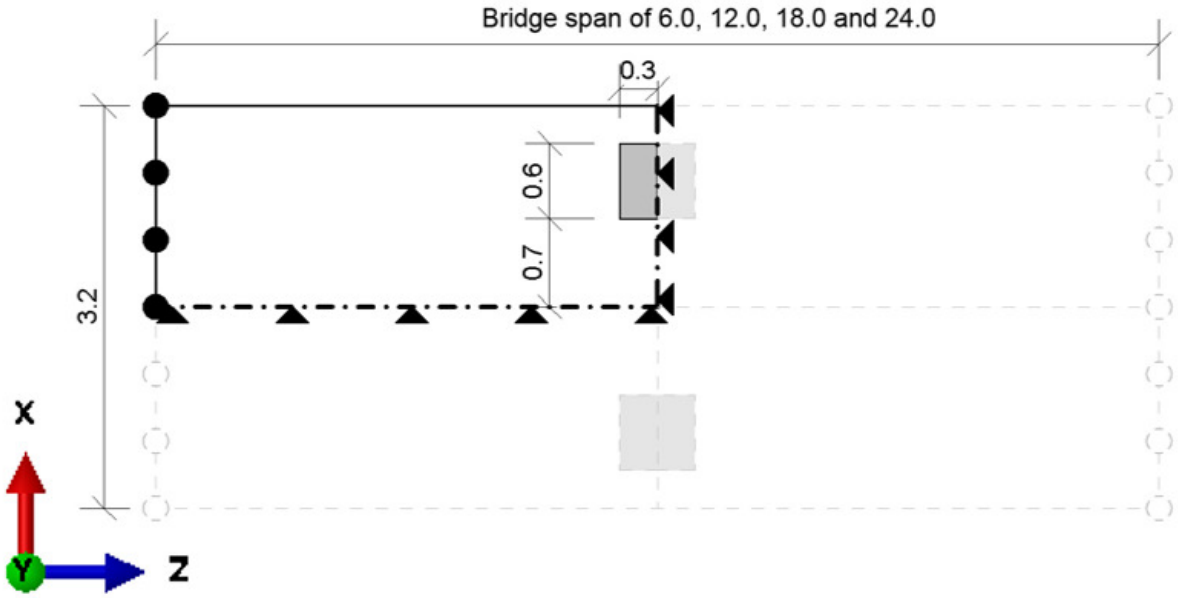

Fig. 2 Loading arrangement used in all simulations. Grey area illustrates the position of the load. Circles show the lowest edge that was locked for displacement in y-direction. Triangles illustrate the positions of the two symmetry conditions. Dash dotted lines show the lowest edges where the displacement was measured. Dashed lines and foggy area illustrates the full size of the simulated bridge deck. [m]

The loading case was chosen to load model (LM) 2 in Eurocode 5 [11]. The contact surface area for the wheel load was designed according to LM 1 [12]. Fig. 2 is showing the wheel load position and the dimension of the bridge deck. The design wheel load was calculated to 360 kN with a β_Q factor set to 0.9 [11], [12]. An efficient loading surface was calculated to 0.6 x 0.6 m [13], [11]. The deflection limit was set to span/400. This limit followed the recommendation in Eurocode 5 and TRVFS [11], [12]. The maximum absolute displacement in *y*-direction was chosen to be the maximum deflection.

Two volumes of the bridge deck were calculated for each loading case, one as an over designed volume and the second as an under designed volume. The first volume was designed to meet the deflection limit with smallest possible margin. The second volume was for CLT taken as the first volume minus two layers and for SLT the first volume minus 45 mm. The exact volume fulfilling the deflection limit was estimated by linear interpolation between the first and second volume. Volume ratios between interpolated volumes of CLT and interpolated volumes of SLT show volume effectiveness for the specific bridge span. Deflection curves in the longitudinal and transverse directions were estimated as linear interpolations between the over- and under-design models. A linear interpolation was used to determinate the exact percentage of each laminate direction which exactly fulfilled the deflection limit. The calculated result was mirrored to illustrate the result of the whole width and span of the bridge deck.

3. FE-models

FE models of the deck geometries were analysed with the commercial FE code ABAQUS [14]. Material data was chosen from Eurocode 5 for SLT plates made of planed timber [11]. The same values were used for the CLT models. Table 1 is showing the used material properties. A Cartesian coordinate system was used to specify material directions. A C3D20r element type was used in all models.

Table 1 Material properties for SLT and CLT models [MPa].

$E_{0,\,mean}$	$E_{90,\,mean}/E_{0,\,mean}$	$G_{0,\,mean}/E_{0,\,mean}$	$G_{90,\,mean}/G_{0,\,mean}$
13000.	0.020	0.06	0.10

3.1 CLT

The CLT models had an odd number of layers. Three different types of CLT models were used, see Table 2 for a definition of name of models.

Table 2 Layer thicknesses in the three CLT models. L = longitudinal grain direction, T = transverse grain direction. [mm]

Name	**CLT40** (L-T-…L)	**CLT90** (L-T-…L)	**CLTVar** (L-T-…L)
Minimum size	40-40-40	90-90-90	80-40-80
∞ **size**	40-40-40-40-…-40	90-90-90-90…-90	80-40-80-40-…-80

Each layer was modelled as one plate. By representing each layer in this way, the boards became edge glued. The thickness of the panel was adjusted by adding or removing one longitudinal and one transverse layer. By using this method, the panel would always be odd numbered with a longitudinal layer on top and bottom. A biased mesh size of 40-150 mm was used in the longitudinal direction, see typical mesh in Fig. 3. The smallest element size was applied in the middle of the bridge span. A fixed mesh size of 75 mm was set in transverse direction. The global mesh size was set to 20 mm for all layers. All layers except the top layer had a structured mesh pattern. The top layer had a sweep mesh pattern of size 20 mm. A tied contact condition was set between each layer.

3.2 SLT

The SLT models were modelled as massive blocks, hence treated as a continuum. To find the over- and under-design volumes, the thickness was adjusted in steps of 45 mm. A fixed global mesh size of 50 mm was used in all SLT models. The mesh was assigned as a sweep mesh pattern.

4. Result and discussion

By using symmetry, simulation times could be shortened. This also made the construction of the models simpler. Fig. 3 shows the element size and mesh pattern for the over-designed volume of CLTVar at a bridge span of 6 m.

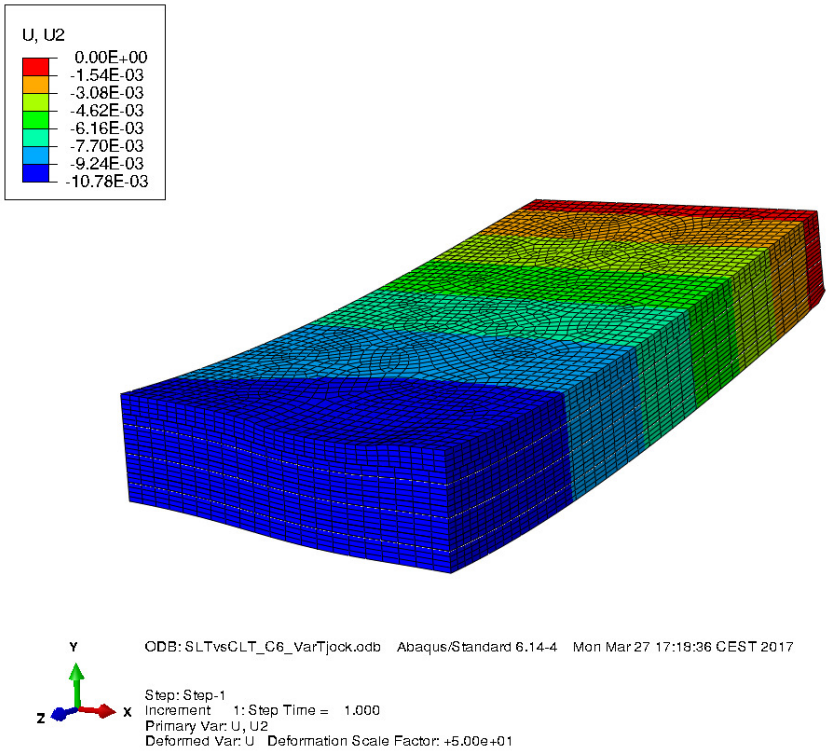

Fig. 3 Element size and mesh pattern used for the over-designed volume of CLTVar at bridge span of 6 m. The result is scaled 50 times and the colours indicate displacement in y-direction. [m]

The CLT/SLT volume ratios for different bridge spans are shown in Fig. 4. The CLT/SLT volume ratios decreased for shorter bridge spans, increased laminate thicknesses and for higher proportion of laminate layers in the longitudinal direction.

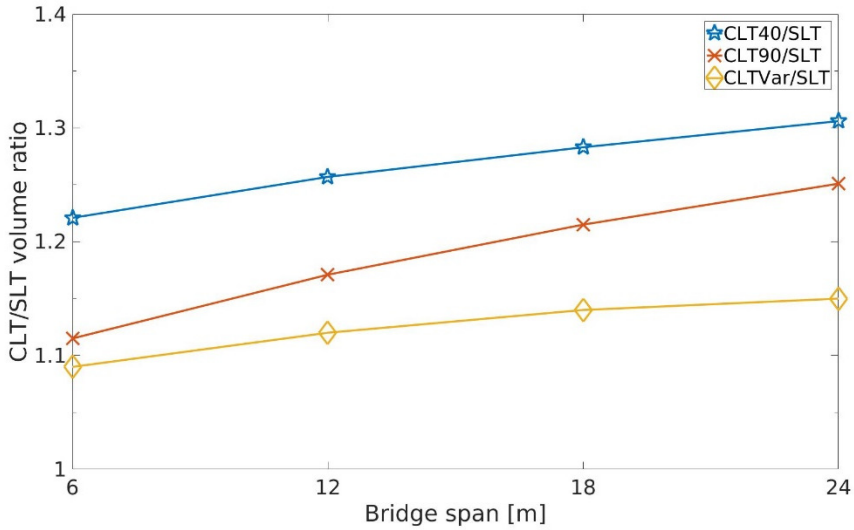

Fig. 4 CLT/SLT volume ratio for a deflection of span/400 for different bridge spans. A value equal to 1 shows that the same volume is needed for both SLT and CLT.

Largest change in CLT/SLT volume ratio between 6 m and 24 m was seen for model CLT90. Approximately the same CLT/SLT volume ratio change was seen for models CLT40 and CLTVar. For CLT40 with a proportion of laminate layers in the longitudinal direction of 45-50%, the CLT/SLT volume ratio became 1.22-1.31. This shows that the CLT/SLT volume ratio depends on the percentage of laminate layers directed in the longitudinal direction. A CLT with 100% of the laminate layers directed in the longitudinal direction, would be a SLT.

Table 3 shows the linear interpolated number of layers, thickness and proportion of longitudinal directed laminate layers for different bridge spans. Fig. 5 shows the interpolate thickness illustrated as a graph. The proportion of longitudinal directed laminate layers decreased for longer bridge spans due to thicker bridge decks. CLT40 had 1.05 and 1.21 times higher proportion of transverse directed laminate layers than CLT90 in the 24 m and 6 m loading case, respectively.

Table 3 Linear interpolated number of layers, thickness and proportion of longitudinal directed laminate layers (PoLD) at different bridge spans for the models.

Bridge span [m]		**6**	**12**	**18**	**24**
CLT40	Layers	10.4	16.9	23.5	30.5
	Thickness [mm]	414	677	939	1220
	PoLD [%]	55	53	52	52
CLT90	Layers	4.2	7.0	9.9	13.0
	Thickness [mm]	378	631	889	1169
	PoLD [%]	63	57	55	54
CLTVar	Layers	5.9	9.7	13.6	17.6
	Thickness [mm]	368	601	832	1076
	PoLD [%]	74	71	70	69
SLT	Thickness [mm]	339	539	732	934
	PoLD [%]	100	100	100	100

CLT40 had 1.74 and 1.57 times higher proportion of transverse directed laminate layers than CLTVar in the 24 m and 6 m loading case, respectively. These geometrical facts explain the difference between the results for the different models shown in Fig. 4

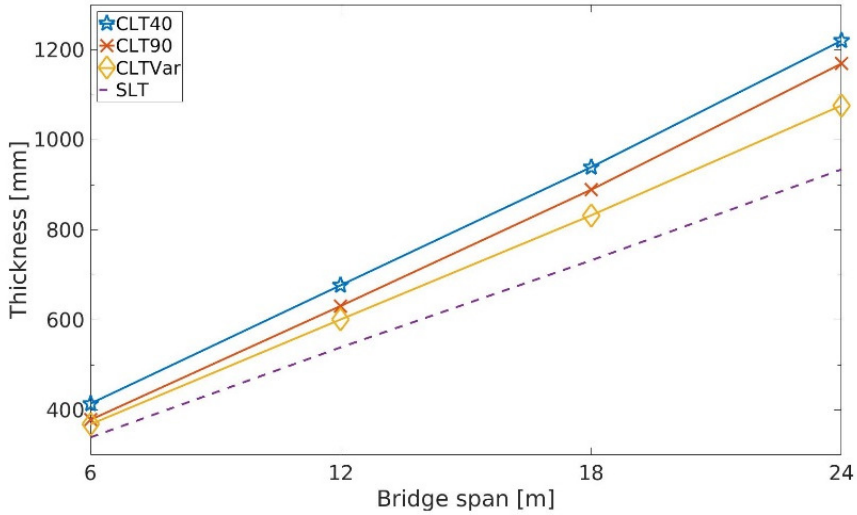

Fig. 5 Thickness of bridge deck at respectively bridge span.

Fig. 6 shows the vertical displacement for the bridge decks for 6 and 24 m span. The transverse displacement curves show that CLT had more even deflection than SLT. The displacement was also affected by the proportion of laminate layers in the longitudinal direction. A higher proportion of

transverse directed laminate layers, gave a more even transverse displacement. The transverse displacement curve for CLT90 was closer to the corresponding curve for CLT40 in the case of a bridge span of 24 m compared to 6 m. This comparison shows the influence of the changed proportions of transverse layers.

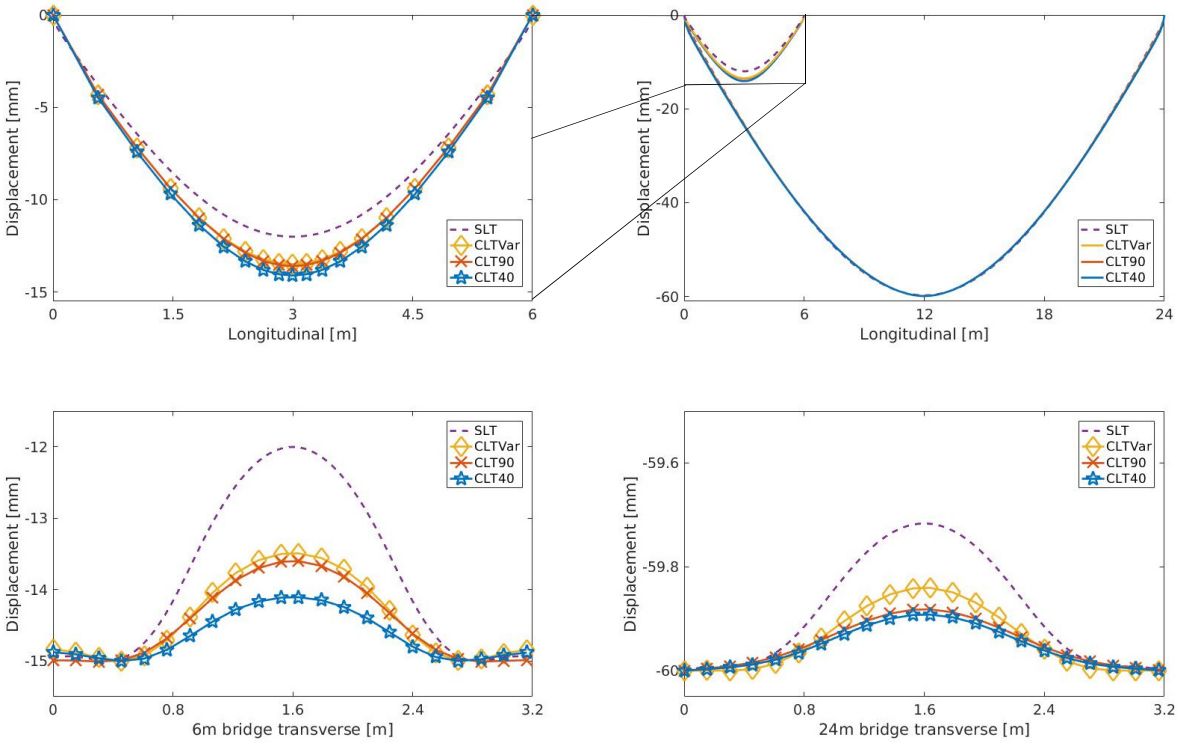

Fig. 6 Displacement in longitudinal (upper row) and transverse (lower row) direction for a bridge span of 6 m (left column) and 24 m (right column) for SLT and the three CLT models. All curves are interpolated to fit the maximum deflection limit span/400.

No difference between models could be seen for displacement distribution in longitudinal direction for 6 m and 24 m bridge span.

In this study the maximum deflection was used as control value. In a real case application, it may be more relevant to use the average deflection in width direction. As a result, a slightly thinner plate would be sufficient. The restriction of the cross section and layers' thicknesses from [2] makes it difficult to use CLT for longer bridge spans. In this study the interpolated thickness of the bridge deck was 414 mm in 10.4 layers for a span of 6 m and 1220 mm in 30.5 layers for a span of 24 m. Because of the restriction for maximum layer thickness many layers would be needed for long bridge spans.

5. Conclusions

- The CLT/SLT volume ratio increased from 1.1 to 1.3 as the bridge span increased from 6 m to 24 m for all studied variants.
- The transverse deflection curve was flatter for CLT than for SLT.
- No difference in longitudinal deflection distribution between CLT and SLT was found.

6. Acknowledgements

The authors are indebted to the European Interreg Nord programme for their support.

7. References

[1] Flaig M., and Blaβ H.J., "Shear strength and shear stiffness of CLT-beams loaded in plane", Conference CIB-W18/46-12-3, Vancouver, Canada.

[2] Anonymous, Timber structures – Cross laminated timber – Requirements. SS-EN 16351:2015.

[3] Ramage M., Burridge H., Busse-Wicher M et al., "The wood from the trees: The use of timber in construction", *Renewable and Sustainable Energy Reviews*, Vol. 68, Part 1, 2017, pp. 333-359.

[4] Wacker J., and Groenier J., "Comparative Analysis of Design Codes for Timber Bridges in Canada, the United States, and Europe". Transportation Research Record 2200. Transportation Research Board, Washington, DC, 2010.

[5] Ekevad M., Jacobsson P., and Kliger R., "Stress-Laminated Timber Bridge Decks: Non-linear Effects in Ultimate and Serviceability Limit States". International Conference on Timber Bridges, Las Vegas, Nevada USA, 2013.

[6] Olivia M., Dimakis A., "Behaviour of stress-laminated timber highway bridges", *ASCE Journal of Structural Engineering*, Vol. 114, No. 8, 1988, pp. 1850-1869.

[7] Ekevad M., Jacobsson P., and Forsberg G., "Slip between Glued-Laminated beams in Stress-Laminated Timber Bridges: Finite-Element Model and Full-Scale Destructive Test". *ASCE Journal of Bridge Engineering*, Vol. 16, No. 2, 2014, pp. 188-196.

[8] Sarisley Jr E., Accorsi M., "Prestress level in stress-laminated timber bridges", *ASCE Journal of Structural Engineering"*, Vol. 116, No. 11, 1990, pp. 3003-3019.

[9] Abrahamsen R.B,, Nyløkken T.E., "Bridge deck rehabilitation using cross-laminated timber". International Conference of Timber Bridges, Lillehammer, Norway, 2010.

[10] Ekholm K., Ekevad M., and Kliger R., "Modeling Slip in Stress-Laminated Timber Bridges: Comparison of Two Finite-Element-Method Approaches and Test Values". *ASCE Journal of Bridge Engineering*, Vol. 19, No. 9, 2014.

[11] Anonymous, Eurocode 5: Design of timber structures-Part 2: Bridges. SS-EN 1995-2:2004.

[12] Anonymous, Trafikverkets författningssamling (TRVFS) 2011:12. Chap. 6, 35.

[13] Anonymous, Eurocode 1: Actions on structures-Part 2: Traffic loads on bridges. SS-EN 1991-2.

[14] Anonymous, Simulia Abaqus 6.14-4, Abaqus/CAE User's Guide.

Inspection of a cable-stayed bridge by 3D scanner

Balázs Major
PhD student
József Bódig Wood NDT Laboratory, University of Sopron – Simonyi Karoly Faculty of Engineering, Wood Sciences and Applied Arts Sopron, Hungary
balazs.major@student.nyme.hu

Wood Industrial Technical Secondary School in Szolnok, Bachelor and Master studies in wood science in University of West Hungary. Currently a PhD. student in University of Sopron, Hungary; research topic: non-destructive testing of wooden structures.

Olle Hagman
Professor
Wood Products Engineering - Luleå University of Technology
Skellefteå, Sweden
olle.hagman@ltu.se

Wood Science and Technology Luleå University of Technology Research topic: non-destructive calibration, testing and predictions of wood and wooden structures by means of multimodal sensors and multivariate image processing.

Summary

The number of wooden bridges increased in Sweden in the past years. These structures require some periodic health control. The 3D scanning is a good method to check for displacements of the structure. Skellefteås Älvsbacka Bridge was investigated in the spring of 2016. Four scans were executed from one specific side of the bridge and other 2 scans were used from earlier scanning procedures. The point cloud had to be cleaned by FARO SCENE program and compared to an original one CloudCompare program. The results show some displacements in every case. Of course we have to consider the climatic and other effects, which were affected the results. We can see the movement of the bridge structure with the help of the color bar on the resulted pictures.

Keywords: Timber bridge, 3D scanning of a bridge, 3D scanner, laser scanning, FARO, SCENE, point cloud, NDT

1. Introduction

According to RISE Research Institutes of Sweden (the former SP Technical Research Institute of Sweden) the number of wooden bridges increased a lot in Sweden in the past years. [1] The timber structures have lots of benefits including the fact that wood is a natural, renewable and sustainable resource. By the effect of the temperature, fungus and insects the wood is prone to deterioration. Therefore, it is important to conduct frequent inspections of timber bridges with modern inspection equipment. This is why the SP Technical Research Institute of Sweden also worked on the

investigation and monitoring techniques for bridges and other wooden structures. These techniques are important for the maintenance and monitoring of the bridges to make the service life longer. [2]

GUSTAFSSON et al. [2] writes that deformations of the structures are often good indicators to characterise or describe the actual condition of a bridge. 3D scanning is a computer aided technique to make accurate 3D models from real objects, also good for inspect the condition and the displacements of timber structures. There are some examples for usage of 3D scanning technology on structures, nowadays architect's offices use drones and 3D scanners condition assessment of old buildings. There is a work from the U.S., about 3D scanning of covered historical bridges. Their main goal was to preserve their structure built up and shape, in case of vandalism or natural disaster (like floods) [3]. While our goal was a condition assessment.

The Älvsbacka bridge of Skellefteå was investigated, 3 scans were taken in different temperature conditions, furthermore some more than 4-year-old scans were used to check the differences.

2. Goals of the research project

In this research project the primary goal was to identify the movements and displacements of the cable-stayed timber footbridge due to different temperature conditions. The main load-bearing elements are steel cables, which can change due to temperature changes. The secondary goal was to investigate the bridge for changes during the past 4 years. These deformations could cause by the dead load of the structure, the dynamic effects like the hundreds of people who use it every day [4] and the cyclic, climatic effects (e.g. snow load, temperature and humidity changes or wind load).

3. Materials and methods

3.1 The timber bridge

Gustafsson et al. [2] describes the structural parameters of the Älvsbacka Bridge very precisely (*Fig. 1*). The bridge was manufactured by the Martinsons Träbroar AB and it connects Älvsbacka and Anderstorp across the Skellefteå River.

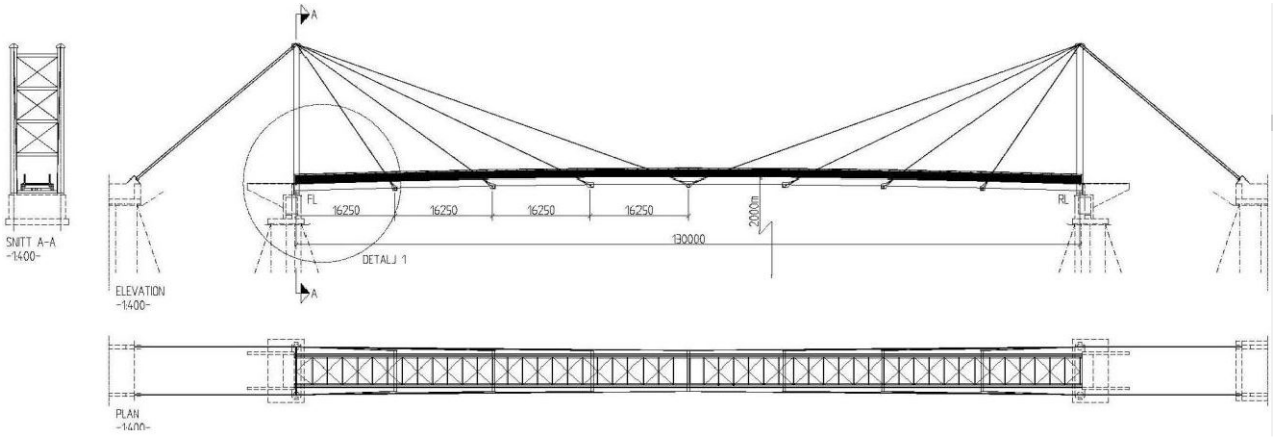

Fig. 1 The technical drawing of the Älvsbacka Bridge, illustration: Martinsons Träbroar AB [2]

This cable-stayed footbridge has a span of 130 meter. Each pylon is made of 900x900 mm^2, square, homogenous, glulam sections. The 4 pieces, 23 m tall pylons are made of untreated European whitewood [Norway spruce *(Picea abies (L.) H.Karst)*]. The distance between the neighbouring pylons is 8.7 m. Each pylon is connected to the main beams by 4 steel cables with a diameter of 45 and 63 mm. The main pillars are anchored in pairs to concrete supports and with cables to concrete anchors on both banks of the river. The distance between the main beams is 4.8 m which gives a clear distance between the beams of 4.40 meter. The main beams are made of glued laminated timber with the cross section of 645x 1100 mm^2. The span consists of a horizontal truss that carries the deck and wind forces acting on the structure. The bridge deck is made of 45 mm open plank deck on longitudinal beams. The bridge is designed for a uniformly distributed load of 4 kN/m^2 or alternatively two axle loads, 20 and 40 kN of a maintenance vehicle. The designed maximum allowable deflection is l/400.

3.2 3D scanning

The 3D scanning methods can be classified into 3 different groups, stereo, active triangulation and laser time of flight measurement [5]. The FARO® Laser Scanner Focus^{3D} is a high-speed three-dimensional, phase shift type laser scanner. The scanner can be controlled with the built in touchscreen display or with the WLAN remote control. The device can make colored 3D point clouds, due to the integrated color camera. The main principle is that the scanner sends infrared laser beams into the centre of its rotating mirror. The mirror deflects these laser beams on a vertical rotation around the environment being scanned; scattered light beams from surrounding objects are then reflected back into the scanner. The phase shift technology means that the constant waves of infrared light of varying length are projected outward from the scanner. Upon contact with an object, some of them are reflected back to the scanner. The distance between the scanner and the object is accurately determined by measuring the phase shifts in the waves of the reflected infrared light compared to the known frequency. The measuring range of the scanner is a 360°x 305° field of view. [6]

The unambiguity interval is 153.49 m, the ranging error is up to ±2 mm at 10 m, the range focus is from 0.6 m up to 120 m. [7]

5 scans were taken from the same side of the Älvsbacka Bridge and approximately from the same scanner position. Only one point cloud was scanned from the same side, but from the ice of the frozen river, with 3 positioning spheres, in different temperature conditions.

3.3 Point cloud programs

The raw point cloud files provided by the scanner can be processed, modified and converted to other formats with the FARO SCENE program [6]. The FARO SCENE supports 8 types of file formats [8]. In SCENE users can cut out the unnecessary or confusing parts of the point cloud, than the cloud can be exported to the xyz file format used by the CloudCompare program [9]. This file contains the information of the points (x, y, z and color coordinates).

For the comparison the user should have to choose a reference scan. The program calculates the distances of the points from the reference scan. In all cases the selected reference scan was scanned on the 29th of May in 2016 and 4-point alignment were used to put together the pictures. It should be mentioned, that the 4 point picking tool has its own error, for e.g. in those cases when the reference scan has a higher resolution the users can not pick the same points from the point cloud. The most stable part on all of the scans was the concrete support under the main pillars. Therefore, the concrete supports were chosen as a base points to the execution of the surface comparison.

The CloudCompare does not handle units, it loads the coordinates as they were stored in the xyz file. Then all values (distances, angles, etc.) are expressed in the same units. This is what called 'implicit units'. The 3D scanner scans are in scale 1:1, it means that the calculated distances of the comparison are in meter. To show the changes of the point cloud a color scale were created (*Fig. 2*).

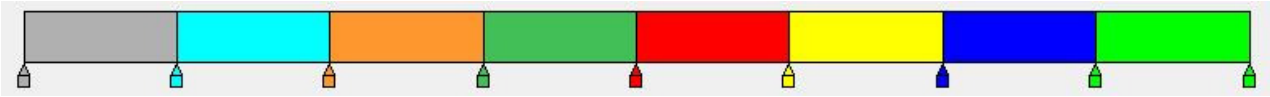

Fig. 2 The created CloudCompare color scale, the white bar is between the green and red bars

On the color scale the approximately zero distance between two points is the white color, which starts at 49.95 % and ends at 50.05 % of the scale. The white color signs the completely similar surface points, any other color will count as a positive or negative distance compared to the original surface.

The final displacement results were calculated in x and y directions, then the total displacements were calculated Pythagorean theorem from the two coordinates.

3.4 Weather conditions

The bridge has its own weather station which is connected to the former SP Technical Research Institute of Sweden (now it is RISE Research Institutes of Sweden) [2][10], it measures

temperature, wind speed, wind direction and humidity, but during the measurements it did not work. There is reliable temperature data from the local weather stations (*Table 1*) and we also measured 2 days the temperatures by our self.

Table 1 Temperature data of Skellefteå from different online sources [11], [12]

Measurement date and time		Number of measurement	rl.se		temperatur.nu	Our
			Temperature [°C]	Wind direction and speed [m/s]	Temperature [°C]	Temperature [°C]
2016	29. 05; 16:50	1.	21	SSE 3	20.4	
	01. 04; 05:30	2.	-5	Calm	-5	-5
	29. 03; 14:30	3.; 4.	9	SSE 5	9.4	11
2012	03. 04; 09:50	5.	-5	WSW 2	-5.8	
	13. 03; 09:50	6.	1	NW 8 (14)	1.2	

4. Conclusions

The *Table 2* shows a chart about the calculated displacement results in cm, the temperature differences and the elapsed time between the compared measurements.

Table 2 The temperature differences between the data of Skellefteå from different online sources

Reference scan: 29. 05. 2016 (1.)							
Date		Number of the scan	Temperature difference compared to the reference scan [°C]	The maximum deviation compared to the ref. scan [cm]			The elapsed time between the two measurements (year, month, day)
				x	y	Resulted displacement	
2016	01. 04.	2.	26	≈0	+3.9	3.9	1m 29d
	29. 03., 1st	3.	11	-16	+1.2	16.04	2m 1d
	29. 03., 2nd	4.	11	-8.9	+4.6	10.02	2m 1d
2012	03. 04.	5.	26	-6	+3	6.71	4y 1m 27d
	13. 03.	6.	20	-29.8			4y 2m 17d

Summarizing the conclusions, the 3D scanning can be used to identify bigger displacements of a wooden structure such as bridges. The biggest displacement of the Älvsbacka Bridge appears on the 6. scan (*Fig. 4*), according to the wind data sources, that day was the highest wind speed among the measured data and also that time there was snow load on the bridge. That could be a reason of the big difference.

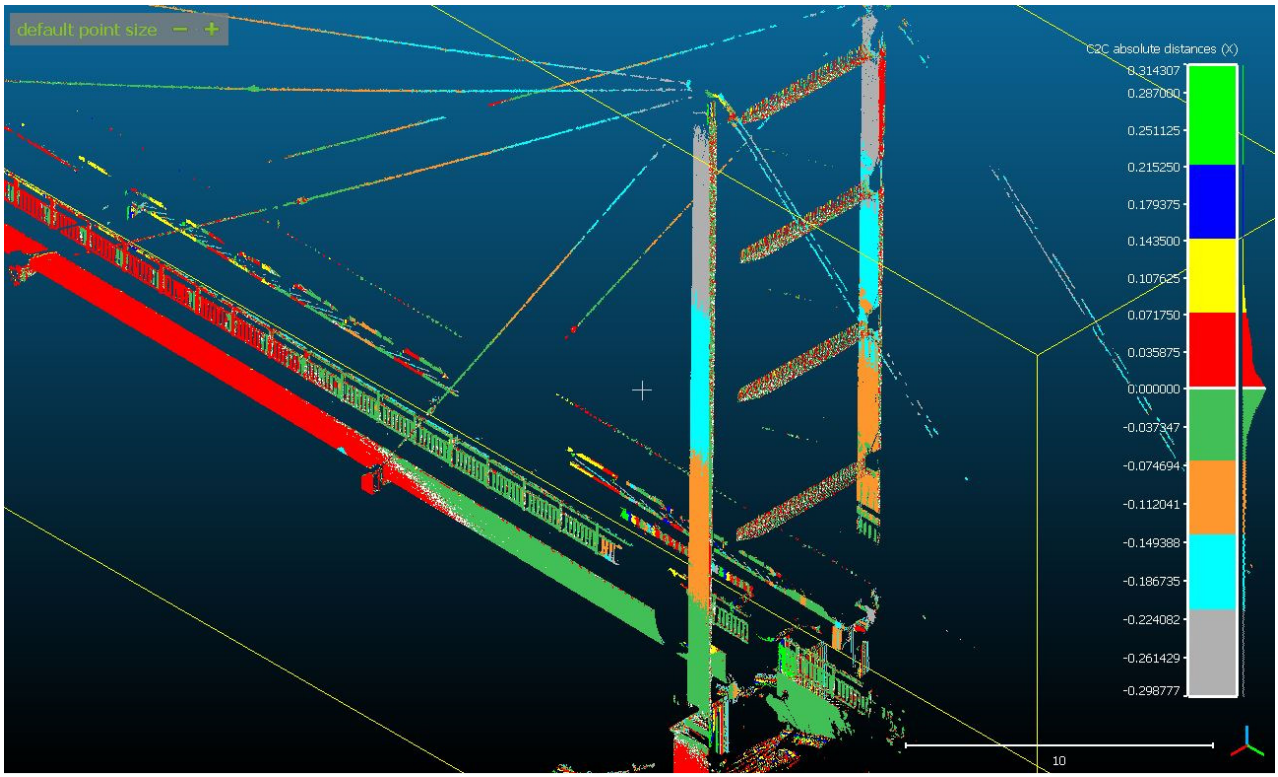

Fig. 4 The results of the scan No. 6

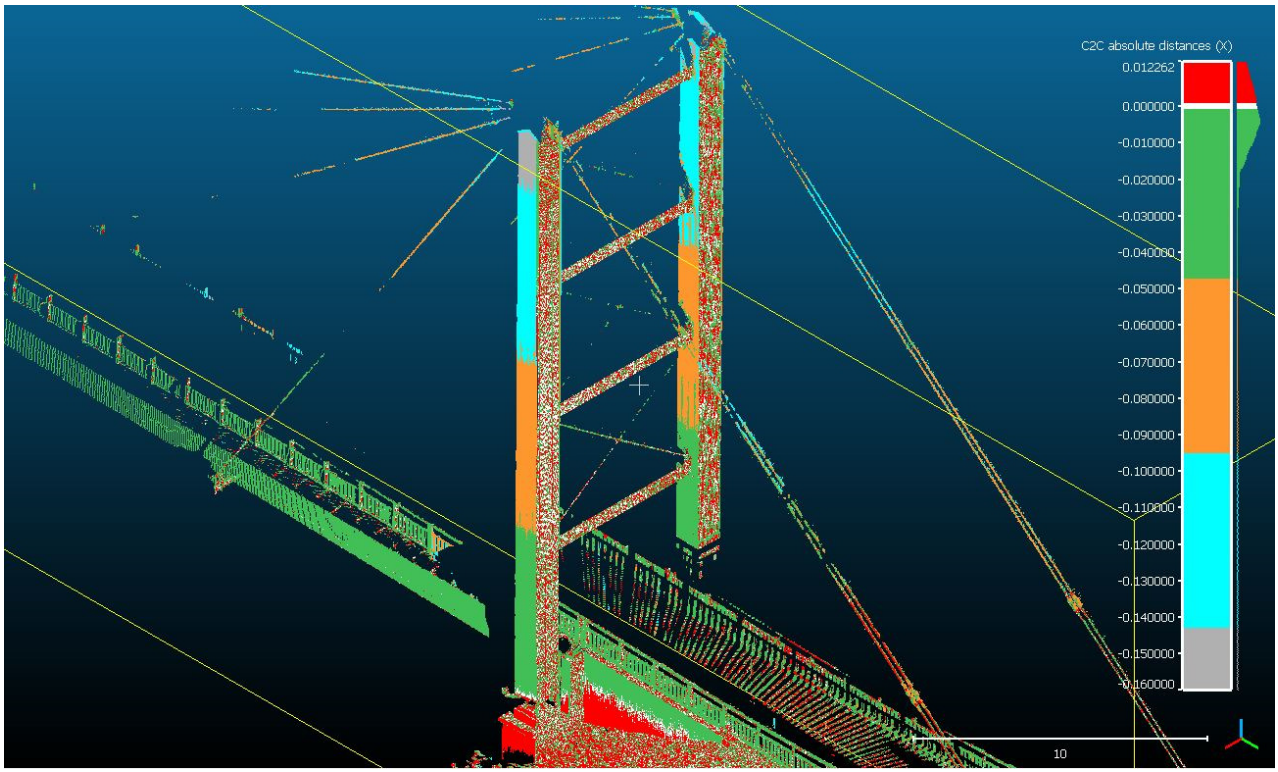

Fig. 5 The second largest displacement shown in the picture, 16.04

On Due to the position of the scanner there are no results for z coordinates (*Table 2*). In the case of the 6th measurement there are no y coordinates, due to the position of the scanner (it was on the ice of the river).

There are lots of factors which can affect the measurement results, like the wind load, especially if the bridge has big surfaces, snow load in winter time what is very common in north Sweden. Furthermore, the inaccuracy of the 3D scanner, the moisture content and the steel cables length changes in result of climatic effects (e.g. because of seasons and/or the weather).

5. Acknowledgements

I would like to say thank you to Prof. Olle Hagman, that he supervised me in the Skellefteå campus of LTU, in the frame of the Erasmus+ programme.

6. References

[1] RISE Research Institutes of Sweden "Timber bridges", *RISE homage*, < https://www.sp.se/en/index/services/woodenbridge/Sidor/default.aspx >, Viewed: 6th of April 2017, 18:31

[2] Gustafsson A., Pousette A., Björgrim N. "Health Monitoring of timber bridges" In: *Proceedings International Conference Timber Bridges: ICTB 2010*, Postmyr, L. (ed.). Trondheim: Tapir Academic Press, 2010, pp. 213-222.

[3] Brashow B., Vatalaro R., Anderson S., Anstey P., Krueger W., Ross R. J., Wang X. "Use of laser scanning technology to obtain as-built records of historic covered bridges" In: *Proc. 17th International Nondestructive Testing and Evaluation of Wood Symposium*, Divós f. ed., Sopron, Hungary, September 14-16, 2011, Vol. 2, ISBN 978-963-9883-83-3, pp. 523-530.

[4] Johannson H., Svensson I. "Vibrations in timber bridges due to pedestrian induced forces", *Master's Thesis 2012:96*, Department of Civil and Environmental Engineering, Division of Structural Engineering, Steel and Timber Structures, CHALMERS UNIVERSITY OF TECHNOLOGY, Göteborg, Sweden, 2012, pp. 4-8.

[5] Wulf O., Wagner B. "Fast 3D scanning methods for laser measurement systems", In: *International conference on control systems and computer science (CSCS14)*, 2003, pp. 2-5.

[6] FARO "FARO® Laser Scanner Focus3D" *Manual*, October 2011, Chapter 1, pp. 1-4. < https://doarch332.files.wordpress.com/2013/11/e866_faro_laser_scanner_focus3d_manual_en.pdf >, Viewed: 10th of April 2017, 15:51

[7] Jiang K. "3D Modeling of Älvsbacka Bridge using Laser Scanner", *Master thesis*, LTU Skellefteå, January, 2013, Chapter 1.3, pp. 2-4.

[8] FARO "FARO SCENE", *SCENE 5.4 user manual*, February 2015, Chapter 9., pp. 184-194.

[9] CloudCompare (Version 2.6) "CloudCompare-Open Source project", [GPL software], OpenSource Project, 2016, < http://www.cloudcompare.org/ >, Viewed: 10th of April 2017, 16:15

[10] Saracoglue E., Bergstrand S. "Continuous monitoring of a long-span cable-stayed timber bridge", *Journal of Civil Structural Health Monitoring*, 2015, Springer Berlin Heidelberg, DOI 10.1007/s13349-014-0088-1, Online ISSN 2190-5479, Vol. 5, Issue 2, pp. 183-194.

[11] RL.se (2015) *RL.SE Weather forecast webpage* < http://rl.se/vadret/historik.php >, Viewed: 10th of April 2017, 16:54

[12] Temperatur.nu *Temperature.hu weather data and forecast webpage*, < http://www.temperatur.nu/skelleftea-egen_graf.html?datum=2016-05-29&datum2=2016-05-29&tid1=16&tid2=17&saved >, Viewed: 13 June 2016, 18:03

The Potential of Acoustic Emission for Timber Damage Assessment

Imen YAHYAOUI
PhD student
Institut Clément Ader
Tarbes, France
imen.yahyaoui@iut-tarbes .fr

Marianne PERRIN
Assistant Professor
Institut Clément Ader
Tarbes, France
marianne.perrin@iut-tarbes .fr

Xiaojing GONG
Professor of university
Institut Clément Ader
Tarbes, France
xiaojing.gong@iut-tarbes .fr

Imen Yahyaoui is currently on PhD thesis entitled "Damage monitoring of wood material using acoustic emission technique"at Laboratory Institut Clément Ader.

Marianne Perrin is associate professor at Laboratory Institut Clément Ader, working mainly on the non-destructive testing of wood and composite materials.

Xiaojing Gong is professor of University at Laboratory Institut Clément Ader, working mainly on fracture mechanics of composite materials

Summary

Considerable development can be observed within recent years in timber bridges. Nevertheless, the damage progress in timber is complex and hardly traceable because it involves several length scales of the wooden hierarchical structures. To avoid critical situations, continuous monitoring should be conducted to estimate the health condition of timber structures. In this context, the acoustic emission (AE) is an efficient method for real time monitoring and for damage identification in structural components as well as in laboratory specimen. In this study, tensile tests in axial direction were performed on standardized wood specimens and monitored by AE and infrared thermography. Thermograms and parametric study using cumulative counts allowed damage discrimination at different levels of loading. Then, the acoustic signature of different failure modes and their typical waveforms were be established by the use of an unsupervised pattern recognition method.

Keywords: Wood, Acoustic Emission, Damage mechanisms, Unsupervised-pattern recognition, Waveforms.

1. Introduction

Today, wood material is extensively used in civil engineering structures such as timber bridges. These structures are susceptible to various damages due to their exposition to severe environmental conditions. In fact this exposure can lead to deterioration resulting from decay, insect attack, weathering. In this case, assessment and evaluation of timber bridges are crucial to identify the severity of the damage. Thus, it is interesting to use a non-destructive method for identifying and locating the damage within the wood structure. Such method should determine the temporal-spatial occurrence of damage mechanisms and their interactions at different length scales since wood

material is distributed across multiple spatial scales, from microscopic to macroscopic. A promising technique being able to address this challenge is acoustic emission (AE). This method is defined as a transient energy generated by incremental crack growth within a material. It is suitable for detecting damage events in wood at both the microscopic and macroscopic scale [1-3]. Besides, AE technique provides unique advantages such as the early detection of crack growth and the recognition of the occurrence of crack within wood material [4].

This paper analyses the damage process of Douglas fir wood, species hardly used in construction purposes due to their excellent strength properties and their natural durability. Damage process observed under tensile loading is studied with acoustic emission signals parameters. Parametric study is performed for tracking damage initiation and accumulation at various stages of loading using AE cumulative hits. In order to obtain additional information, infrared thermography measurements are conducted simultaneously with tensile tests and AE monitoring. In fact, thermograms can display the damage progress of wood specimens [5-6]. In order to identify the acoustic signatures of failure modes, an unsupervised pattern recognition technique was performed via k-means algorithm using Noesis software. Moreover, AE waveforms related to the damage mechanisms are identified after an investigation of the clustered AE data and parametric analysis.

2. Experimental details

2.1 Raw material and specimens

The specimens tested under tensile loading in this study were prepared with Douglas fir. These species are extensively used for structures in large dimensions like building and timber bridges due to its excellent strength properties and durability.
Tensile specimens with dog-bone shape were prepared with nominal dimensions according to NF B51-017 (350 mm overall length, 100 mm in length, 20 mm in width and 20 mm in thickness in grip section, 90 mm in length, 20 mm in width and 4 mm in thickness in the calibrated section) (Fig. 1). All specimens have the length in longitudinal direction and the width in radial direction. To prevent crushing on the specimen by the grips, four tabs in steel of 60 mm in length were glued to the ends of the specimen using bicomponent epoxy resin (ESK-48).

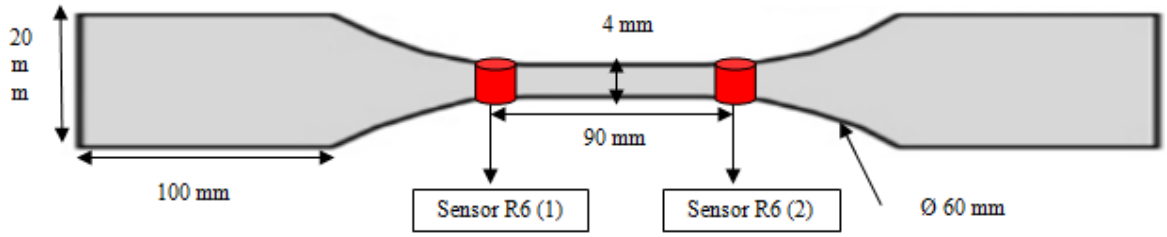

Fig.1 Tensile specimen and sensors position

2.2 Test conditions

Five specimens were tested. They were conditioned and stored at 20°C and 65% relative humidity before testing. Tensile tests were performed by using universal test machine MTS© 20M with a load cell calibrated in the load range of 100kN. The load was applied parallelly to the grain of wood sample and under displacement control with a constant cross-head speed 2.5mm/min until the failure of specimens.

2.3 Acoustic emission equipments

Wood is a very heterogeneous and highly attenuative material. For these reasons, a preliminary study was done to select the suitable AE sensors for wood materials. In the literature the sensors used to monitor damage of wood have resonant frequencies between 150 kHz and 300 kHz [2-4]. Nevertheless, a recent study [1] indicated that during the damage process in wood structures the maximum Power Spectral Density (PSD) (defined as the distribution of energy over the frequency) resided in a low frequency area around 60 kHz. In order to properly assess the frequency portion of the signal, resonant frequency of the sensor is a determinant factor. In this context, four types of

piezoelectric sensors were tested to select the most suitable one: three resonant sensors R15α, R6α and R3α with resonant frequency respectively at 150 kHz, 60 kHz and 30 kHz and one wideband sensor (WD) with frequency band-width between 100 kHz and 1 MHz. Results of wideband sensor showed that the frequency of damage in wood is situated between 30 kHz and 50 kHz (Fig. 2). Consequently, the R3α and the R6α sensors are the most appropriate for wood damage monitoring. Both of them were so used in this work. After analyses of the signals recorded by these sensors, it was found that the R6α sensors gives better results concerning the event localization. Therefore we will limit our analyses on the results recorded by R6α sensor in the next parts of this paper.

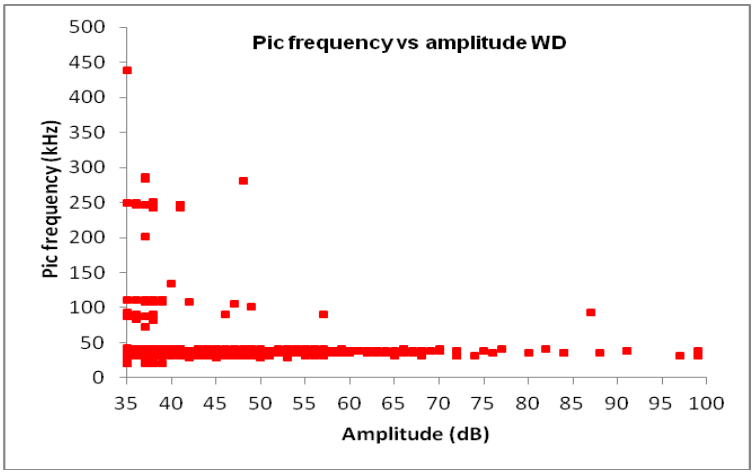

Fig.2 Pic frequency vs. amplitude of WD sensor showing the concentration of AE hits in a frequency range between 30 kHz and 50 kHz.

The positions of AE sensors on the tested specimen can be found in Fig.1. In order to locate AE events, two R6α sensors were placed on the front side of the tensile specimen: one on the top and the other on the bottom of the calibrated section. Moreover, sensors were fixed with clamps to assure good acoustic coupling. In order to avoid any loss of acoustic signal at the transducer-sample interface, silicone-free vacuum grease was used to couple the sensors to the surface of specimens. The AE data are recorded with the help of an Euro Physical Acoustics system composed by a PCI8 board. The acquisition is computed by using AEwin/SAMOS software. The analog filter frequency is set up between 20 and 400 kHz and the acquired signals are preamplified at 40 dB. The environmental noise was filtered using a threshold of 35 dB. The timing parameters, peak definition time (PDT), hit definition time (HDT) and hit lockout time (HLT) are set at 40, 200 and 300 µs, respectively [7].These parameters are verified by Pencil-lead breaks (Hsu-Nielsen source) [8] before the tests. The same sources are used to calculate the wave velocity. It was found to be 4747 m/s (± 560).

2.4 Thermal acquisition

A thermal FLIR Titanium SC7000 retrofitted infrared camera was used to monitor damages during tensile loading. The camera resolution is 640 x 480 pixels. It was positioned at a distance of 0.6 m from the surface of the wood specimen. The sensitivity of the camera is 20 mk at 50° C and the sampling frequency is 50 Hz. Moreover, the software Altair was used to assure the automatic calibration, control of the camera and data recording. In order to take into account the influence of the surrounding environment, post-processing was achieved to eliminate the temperature variations fields $\Delta T = T - T_0$ of the specimen, with T the temperature field at time t and T_0 the temperature field in the initial state t = 0. As a result, the most disturbing effects (environmental ones, highlights the thermal events induced in the material) were removed. Based on the study of the reference [9] the emissivity of wood was set at 0.9.

3. Results and discussions

3.1 Damage characterization

The evolution of the load and AE parameters in terms of cumulative AE hits as a function of the elapsed time for a representative sample is shown in Fig. 3. For more details, characteristic points are illustrated with post-mortem observations and corresponding thermograms (Fig. 4).

In general, the load/time curve could be decomposed in three stages based on cumulative AE hits. In the linear deformation part, some emissions have been observed. The corresponding thermogram (Fig. 4- Point A) doesn't give particular information at this stage. In the study of Raczkowski and Molinski [10] it is suggested that the random AE signals observed in the elastic deformation stage are the result of the non-uniform stress field resulting from the non-homogeneity of wood structure. Actually, reorientations in wood structure are observed leading to adaptation for new conditions of loading [10]. When the curve enters into the non-linear deformation part (part II), the rate of cumulated AE hits increased. Moreover, corresponding thermogram (Figure 4-Point B) shows that there is more thermal energy radiating from the earlywood (EW) part of growth ring than in the latewood (LW). This observation agrees with the study of Zheng et al [5]. This rapid increase of cumulative AE hits and the dissipating thermal energy in EW could be attributed to the inter-laminar shear damage in planes of weakness like EW/LW interfaces [11]. In this stage micro-cracks parallel-to grain in EW/LW transition zones are developed. Finally, the specimen enters into the fracture stage (part III) where a sharp increase in cumulative AE hits is observed. As damage in the specimen intensified, macro-cracking take place and the first visible crack is found at t= 31.44 s, herein a sharp drop of the load can be observed (Figure 5- Point C). The post-mortem observation conduces to suppose that a transverse crack in the EW appeared, followed by a transverse crack in the LW and then the crack propagated in an inclined direction in both EW and LW. Also, a crack parallel-to-grain in the EW/LW interface can be observed in the specimen. The corresponding thermogram (Fig. 4- Point C) visualises the same development of damage. Then, a second visible crack across LW occurred at t=35.11s (Figure 4 - Point D), it is accompanied by a longitudinal crack at the EW/LW interface. Thermogram at point D (Fig. 4) presents the process of second damage initiation and the development of failure is like the post-mortem observation at point D.

In conclusion, a typical damage process in Douglas specimen can be observed. Under tensile load, the different stiffness between earlywood EW and LW generates a shear stress at the EW/LW interfaces, which is the weakest layer because the density of wood between EW and LW changes abruptly [12]. Micro-cracks can initiate at EW/LW interfaces or in EW, where the strength is much lower than that in LW. Their growth and coalescence conduce to longitudinal crack propagation. This process is sometimes accompanied by the fibre breaking in EW [13]. The transverse fracture in EW generates a tensile/flexion coupling effect, which accentuates even more the fibre breaking in EW. When the crack growth attains EW/LW interfaces levels, under shear stress (mode II) and peel stress (mode I), the longitudinal crack propagation (parallel-to-grain) along EW/LW interfaces will occur. And then, one of the latewood layers breaks, the rest of specimen cannot support the higher strength and final fracture occurs [13].

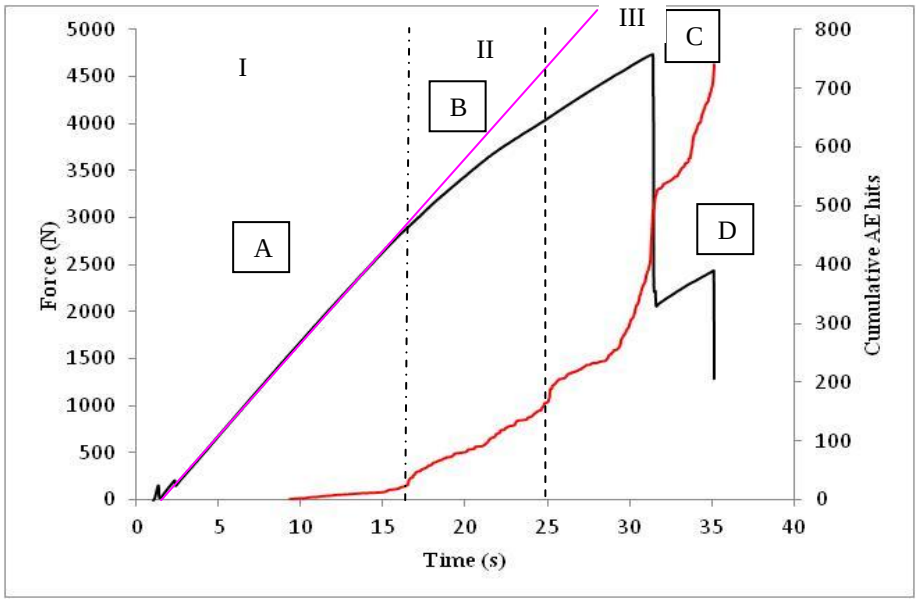

Fig.3 Load vs time, cumulative hits vs time for a representative Douglas fir specimen under tensile loading

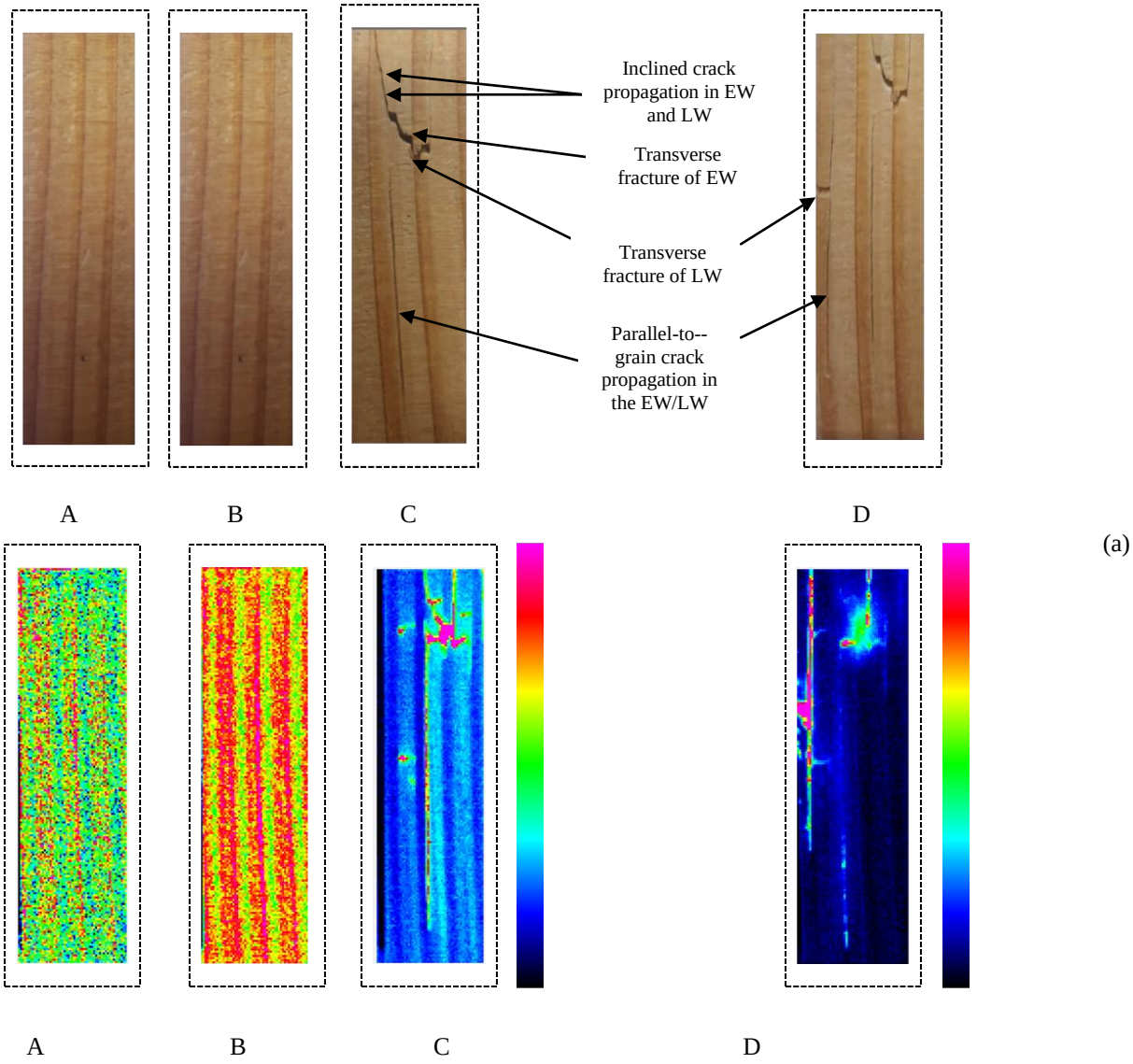

Fig.4 Damage in Douglas fir specimen under tensile loading: post-mortem observations and thermograms

3.2 Analysis of the acoustic signature during wood failure process

An unsupervised pattern-recognition technique was applied in order to discriminate the different damage mechanisms according to their AE patterns. For this purpose, Noesis software was used for recording of AE data and post-processing [14]. The first step consists in selecting the relevant descriptors. The AE descriptors selected in this study are the rise time, the counts to peak, the counts, the duration, the amplitude, the absolute energy, the average frequency, the reverberation frequency, the initiation frequency, the frequency centroid and the peak frequency. The features values were then normalized in the range [0, 1] in order to obtain comparable scales between all the descriptors. Then, k-means algorithm, a popular clustering method [15-18] was used to split the AE signals into three clusters. The number of classes was chosen according to the previous analysis. If we classify the principal damage mechanisms into three categories: cracking parallel-to-grain in EW/LW interfaces, transverse crack propagation in EW and in LW and fiber breaking, it is interesting to establish the relationship between these cluster and the damage mechanisms.

Figures.5-7 show the three classes of AE signals recorded during the test on wood specimen under tensile loading. These figures display the distribution of amplitude versus time (Fig. 5) and of cumulative AE hits versus time (Fig 6). In order to visualize the results in a two-dimensional sub space, a Principle Component Analyses (PCA) was carried out (Fig.7).

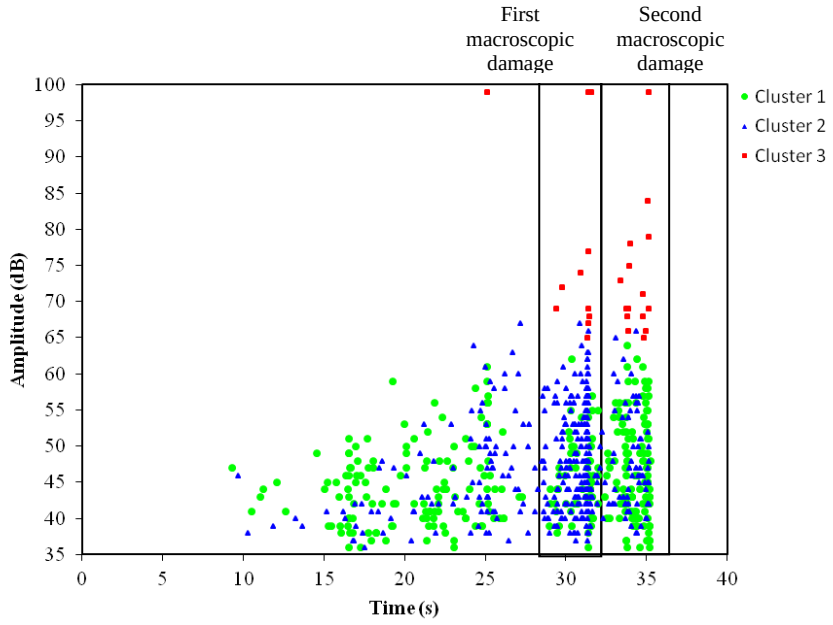

Fig.5 Cluster results: amplitude versus time

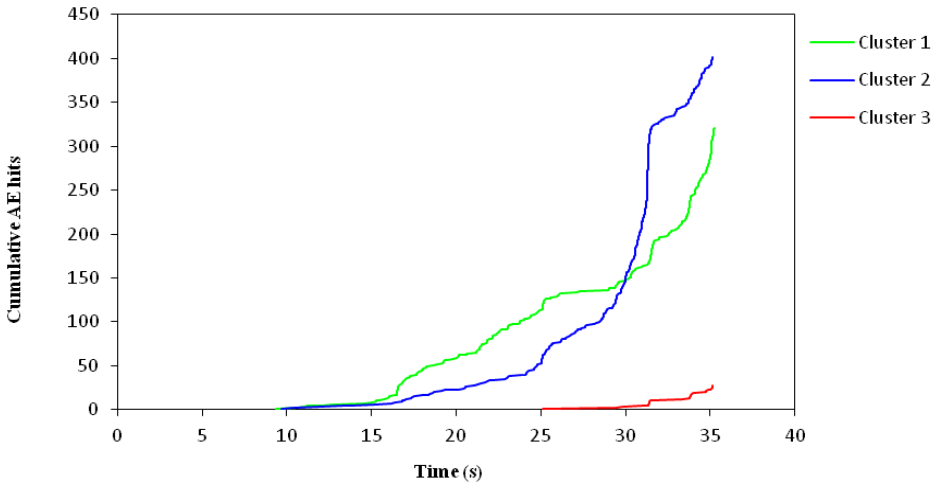

Fig.6 Cluster results: Cumulative AE hits versus time

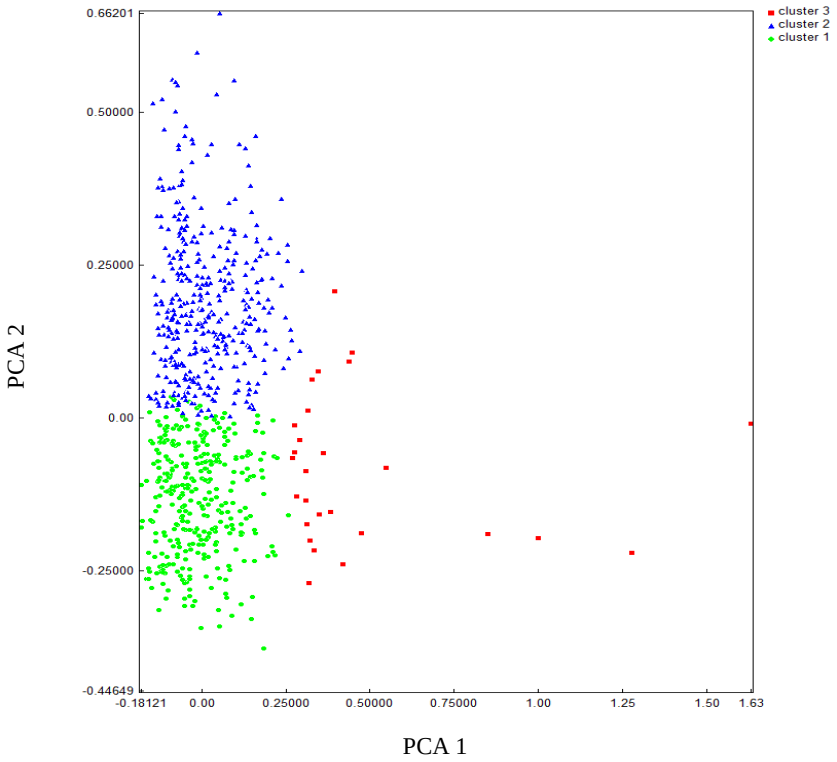

Fig.7 PCA visualization of the AE signals clusters

The first class (cluster 1) includes 52% of the total signals with low to medium amplitude (between 36 and 64 dB). The signals have also long duration and low absolute energy. The cluster 1 occurred during the entire test (Fig.6) and the amplitude increased with the load increase. The second class (cluster 2) contains 45% of the total signals with amplitude close to the cluster 1 signals' amplitude (between 36-67 dB). These signals are characterized by a moderate duration and a low absolute energy. Cluster 2 appears a few seconds after cluster 1 until the end of the test and the amplitude increased also with the load increase. Finally, the third class (cluster 3) represents only 3% of the total signals. They are characterized by a medium to high amplitudes (between 65-99 dB), a high absolute energy. These signals appeared later just before the specimen fracture (Fig. 5-6). Moreover, the three clusters appeared clearly in the first macroscopic damage while in the second one, cluster 1 and cluster 3 are mostly observed (Fig.5). These results correlate well with the post-mortem observations in part 3-1. In fact, more damage mechanisms were observed at point C than at point D (Fig.4). At a first analysis, cluster 3 and cluster 1 can be attributed respectively to fiber breaking and cracking parallel-to-grain in EW/LW interfaces as the two damage mechanisms are mainly occurred at point D. Moreover the signals of cluster 3 are more energetic then the signals of cluster 1, which correlates with the well-known fact the fibre breaking is more energetic than the cracking parallel-to-grain in EW/LW interfaces. In this context, cluster 2 can be attributed to the other mechanisms occurred mainly at point C like inclined crack propagation in EW and LW. Typical AE waveforms related to different AE clusters are shown in Fig. 8(a)-10 (a). The associated Fast Fourier Transforms (FFT) is shown in Fig. 8(b)-10(b). Cluster 1 displays mainly a peak-frequency around 30 kHz, cluster 2 exhibits chiefly a peak-frequency around 100 kHz but cluster 3 displays two peak frequencies at 30 kHz and at 100 kHz . If the values of the peak frequency of 3 clusters are compared in Figure 11, there is no possible classification. This signifies that the three damage mechanisms in wood material cannot be distinguished based only on frequency analysis.

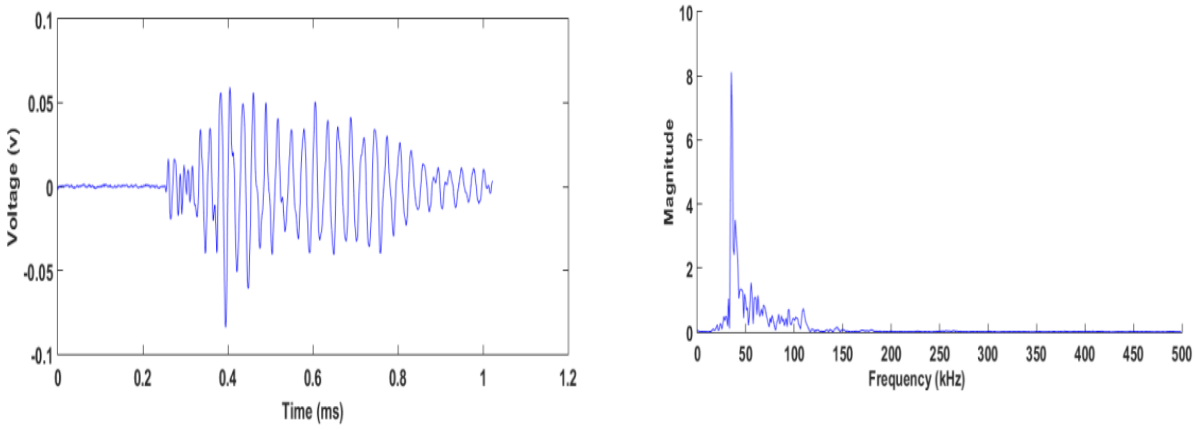

(a) (b)

Fig.8 Cluster 1 results (a) typical AE waveform (b) TTF

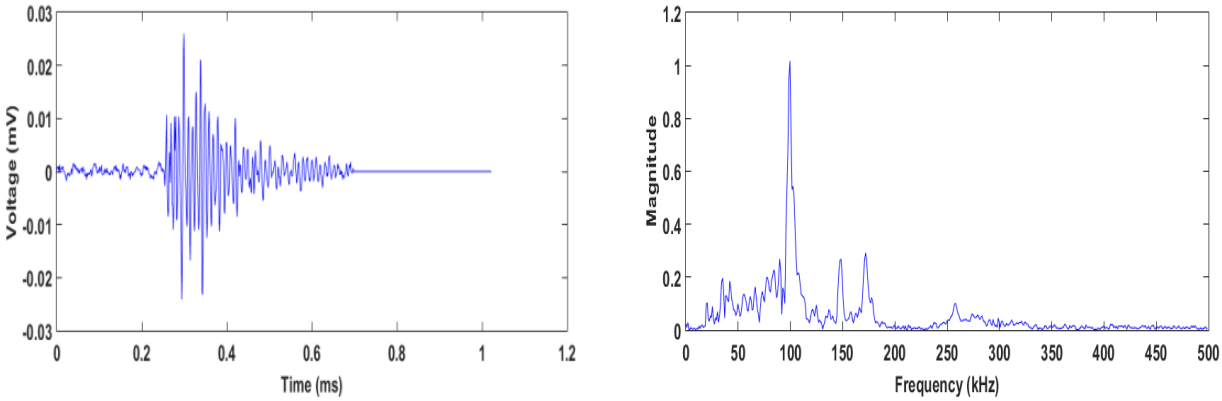

(a) (b)

Fig.9 Cluster 2 results (a) typical AE waveform (b) TTF

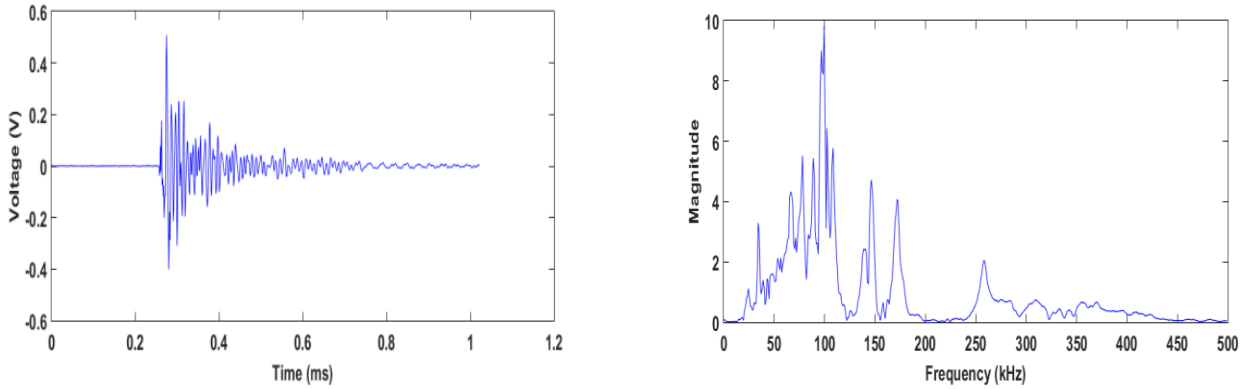

(a) (b)

Fig.10 Cluster 3 results (a) typical AE waveform (b) TTF

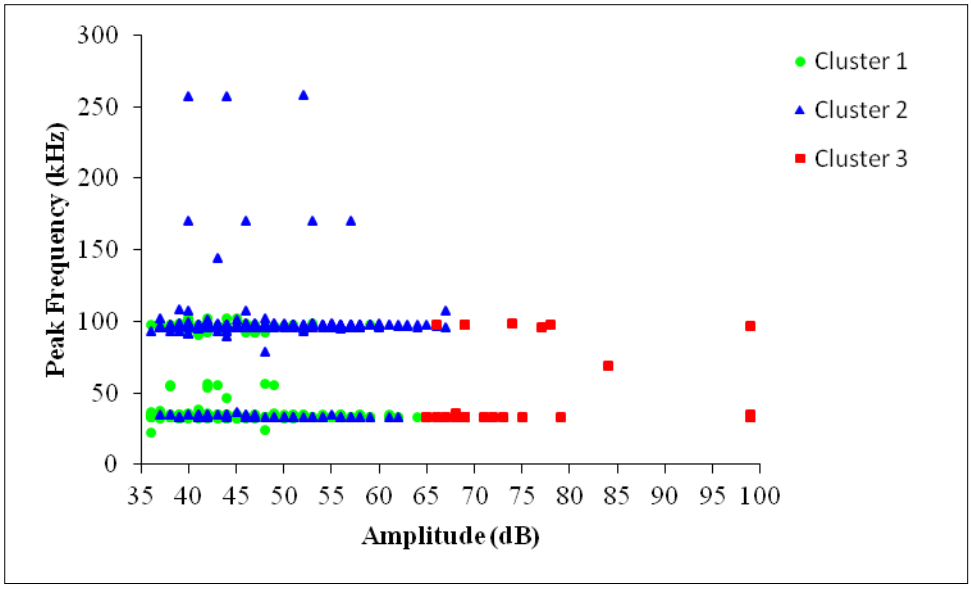

Fig.11 Cluster results: Amplitude vs. peak frequentiel

4. Conclusions

The development of damage in timber bridges may cause catastrophic results. Therefore, continuous monitoring should be conducted to estimate the health condition of these structures. In this study, damage evolution in Douglas fir wood specimens under tensile loading was monitored by AE and infrared thermography. The acoustic signals collected during tensile tests were analyzed using an unsupervised pattern-recognition technique in order to discriminate different damage mechanisms according to their AE patterns. The following conclusions can be stated:

- AE is a promising technique for the health monitoring of timber structures and for a rapid detection of the onset of micro and macro cracking. In fact, the AE data of tensile tests on Douglas fir wood specimens indicate clearly different scenarios from damage initiation and accumulation up to final macroscopic failure. Therefore, it is possible to associate AE responses to the damage mechanisms and the damage level in wood structures, so as to predict the service life or/and service safety for a timber structure.

-AE multiparameters analyses improve the identification of damage mechanisms in wood structures. In fact, the real time analysis of AE parameters can give information about the occurrence of serious damage within a wooden structure. However, more often, only a multi-parameter analysis enables the final reliable evaluation.

- In order to validate clusters labelling, stopped tests at a certain load will be done and tomographic observations of the calibrated section will be performed.

Acknowledgements

The authors gratefully acknowledge Marie-Laetitia PASTOR, assistant professor in Clement Ader Institute in Tarbes-France, for her contribution in the elaboration of infrared thermography tests.

References

[1] Varner D., “Acoustic emission during static bending of wood specimens”. PhD the- sis. Mendel University in Brno, 2012.

[2] Ritschel F., Brunner J.A., and Niemz P., “Nondestructive evolution of damage accumulation in tensile test specimens made from solid wood and layered wood materials”, *J. Composite Structures*, No.95, 2013, pp. 44-52.

[3] Wu Y., Shao ZP., and Wang F., "Acoustic emission characteristics and felicity effect of wood fracture perpendicular to the grain". *J. of Tropical Forest Science*, Vol.4, No.26, 2014, pp. 522- 531.

[4] Kowalski, S.J., and Smoczkiewicz, A., «Identification of wood destruction during drying", *Maderas.Ciencia y Tecnologia*, Vol. 2, No.6, 2004, pp. 133-143.

[5] Zheng C., Gabbitas B., and Hunt D., "A thermal imaging technique for studying crack development in wood under torsional loading", *Journal of Materials Science*, No. 40, 2005, pp. 1929-1935.

[6] Sandak J., Sandak A., and Negri M., "Mechanical testing of wood assisted by infrared spectroscopy and thermal imaging", the 8th World Conference on Timber Engineering, Riva del grada, Italy, 2010.

[7] Lamy F., Takarli M., Angellier N., and Dubois F., "Acoustic emission technique for fracture analysis in wood materials", *Int. J. Fract*, No. 192, 2015, pp. 57-70.

[8] Nilson A., "Acoustic emission source based on pencil lead breaking", *Svejsecntralen*, No. 80, 1980.

[9] Lopez G., Basterra L.A., Acuna L., and Casado M., "Determination of the emissivity of wood for inspection by infrared thermography*", J. Nondestruct. Eval.* , Vol. 32, No. 2, 2013, pp. 172-176.

[10] Raczkowski J., and Molinski W., "Acoustic emission in fracture machanics of wood", *J. of theoretical and applied mechanics*, Vol. 32, No. 2, 1994, pp. 299-322.

[11] Bucur V., "Acoustics of wood", *Springer Series in Wood Science*. Second Edition Germany 2006.

[12] Kollmann F.P., and Coté W.A., "Principles of wood science and technology I: solid wood", *Springer-Verlag New York Inc*, 1968.

[13] Sipolla M., and Fruhmann K.,"In situ longitudinal tensile tests of pine wood in ESEM". Holzforshung, No. 56, 2001, pp. 669-675.

[14] NOESIS software, Advanced acoustic emission data analysis pattern recognition and neural networks software, 2004.

[15] Likas A., Valassis N., and Verbeek J., "The global k-means clustering algorithm", *Pattern Recogn*ition, Vol. 36, No.2, 2003, pp. 451-461.

[16] Godin N., Huguet S., Gaertner R., and Salmon L., " Clustering of acoustic emission signals collected during tensile tests on unidirectional glass/polyester composite using supervised and unsupervised classifiers", *NDT&E International*, No. 37, 2004, pp.253-264.

[17] Munoz V., Vales B., Perrin M., Pastor M.L., Welemane H., Cantarel A., and Karama M., "Damage detection in CFRP by coupling acoustic emission and infrared thermography", *Composites Part B: engineering*, Vol. 85, 2016, pp. 68-75.

[18] Diakhate M., Bastidas E., Moutou-Pitti R., and Schoefs F., "Probabilistic improvement of crack propagation monitoring by using acoustic emission", *Fracture, Fatigue, Failure and Damage Evolution*, Vol.8, 2017, pp. 111-118.

Analysis of Mini-jack technique for in situ measurement of strength

Michal Kloiber
Jan Tippner
Jiří Kunecký
Václav Sebera
Jaromír Milch
Jaroslav Hrivnák

Research Assistant at Mendel University in Brno. Focusing on wood mechanics, finite element analysis and optical strain measurement techniques.

Researchers
Institute of Applied and Theoretical Mechanics ASCR
Mendel University in Brno
Brno, Czech Republic
seberav@gmail.com

Summary

The paper presents a recently developed diagnostic technique for in situ determination of modulus of deformability (MOD_L) and conventional strength (CS_L) parallel to the grain using the mini-jack inserted in bored hole. The mini-jack compression technique simulates the standard compression test, it is compared to that to examine its prediction strength (correlation coefficients). The paper shows an influence of moisture content of wood on experimental measurements using this technique. The measurement was carried out at spruce samples at three moisture contents of 12, 18 and 24%. The results of the tests prove a very good correlation of the strength determined by the proposed technique and wood density and strength determined at universal testing machine in compression parallel to the grain. The effect of the moisture content on the measurement by the mini-jack technique was proved to be significant. Beside that, the newly-developed instrument was also studied using digital image correlation (DIC) technique to analyze induced strains around the bored hole. This was studied on halved spruce samples. The DIC revealed symmetric character of the loading and significant differences between strains induced in tangential and longitudinal directions.

Keywords: non-destructive testing, mini-jack technique, wood, in-situ testing, compression strength

1. Introduction

Historical timber constructions often belonging to valuable architectural heritage are sensitive to a damage caused by biotic factors – wood-destroying insect and fungi. Before their reconstruction, careful inspection and localization of material properties of particular timber members is necessary to be included in the sanation plan. Recently, there has been published a few guidelines and methodologies for investigation of material properties of timber constructional members, many of them were supported by several international committees such as RILEM, COST E55, COST IE0601 (Kasal and Tannert 2011, Cruz et al. 2015). The commonly used and fundamental diagnostic method is a visual inspection that provides a general information and certain qualitative data about timber members' surfaces (Calderoni et al. 2010). Visual inspection can be enhanced by various imaging techniques, for instance using the infrared thermography (Lopez et al. 2014), although the visual inspection is not capable to provide information about inner structure of timber elements. This disadvantage may be overcome by using X-ray techniques (Kruglowa 2012). Nonetheless, both was approaches do not provide any mechanical properties as strength class or elastic modulus (Kloiber et al. 2015). Another approaches to investigate elastic moduli and, consequently, wood deterioration and defects, is to use vibration behavior of wood and stress wave techniques (Ross et al. 1991; Hasenstab et al., 2004).

Disadvantages of many techniques commonly used stem from the fact that their results correlate better with physical properties such as density than mechanical ones such strength and stiffness. Moreover, it is often needed to make samples *in situ* and test them in a laboratory, which increases both time and financial means. Accuracy of determination of the mechanical properties determine the ways of reconstruction design. If exact information about strength and stiffness of the particular construction members is known, it is often possible to preserve majority of historical timber, which is one of the goals in preservation of the culture heritage. The global aim of this work was initiated by rapidly increasing requirements of structural engineers that asses historical timber constructions in the Czech Republic and call for accurate and fast (in situ) mechanical properties of structural timber elements. Therefore, the specific objectives of this work are: a) to present newly-developed semi-destructive instrument for in-situ measurement of mechanical properties of timber; b) to determine the conventional strength and modulus of deformability with use of the instrument at three moisture level; c) to verify the instrument data based on compression tests in laboratory providing the strength and stiffness parallel to fiber and using optical technique based on digital image correlation.

2. Materials and Methods

The first sets of measurement within this study were carried out using a recently developed devices for semi-destructive *in situ* assessment of timber properties. The first device is based on insertion of small size mini jack into a pre-drilled hole and performing compression test along the fiber inside the tested element. The device was presented already in Kloiber et al (2015), so its broader description is omitted here. The device provides the data about deformation process induced by jaws inside the hole with 12 mm in diameter (Fig. 1b). Simultaneously, the force needed for the deformation is being recorded, so the force-deformation diagram can be constructed.

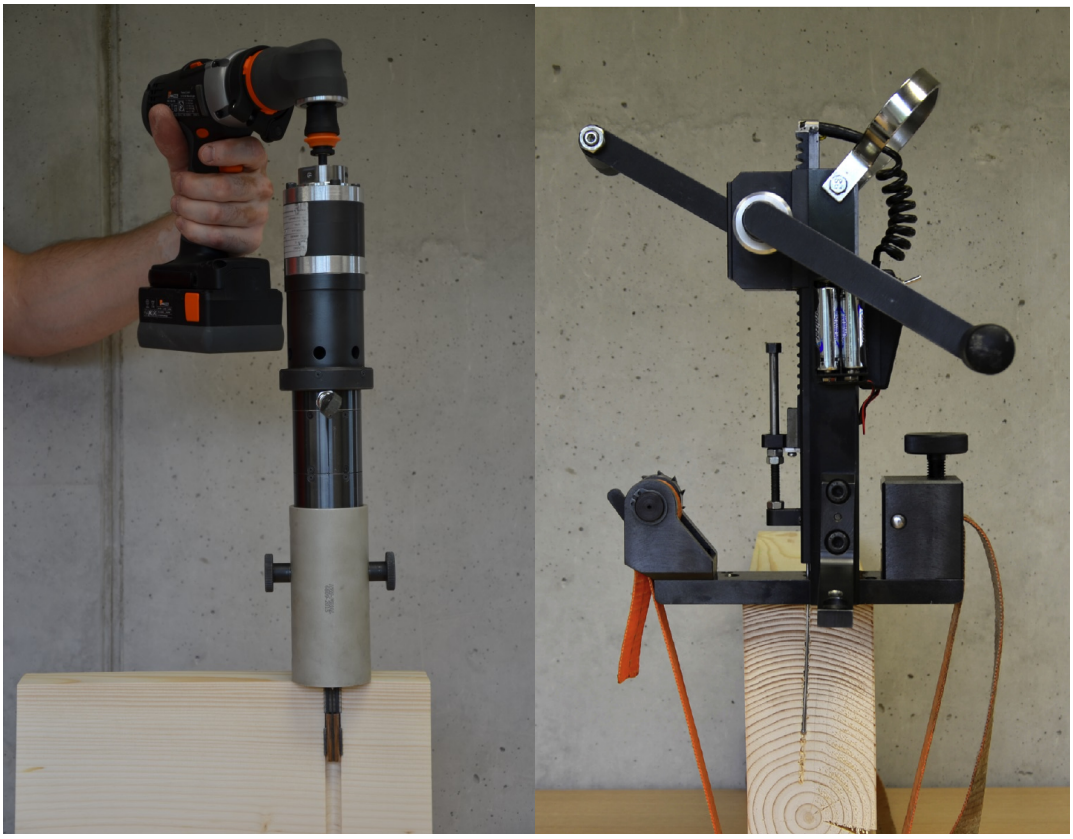

Fig. 1 left – overall view of the mini jack device during measurement, right – view on the pin pushing technique during the measurement

2.1 Experiments

The experimental work consisted of measurement of 96 samples using mini-jack technique. The samples were divided into three sets according to moisture content (MC) levels – 12%, 18% and 24%. Consequently, each MC set had 32 samples. At each sample 4 measurements at different depths (5–25 mm, 35–55 mm, 65–85 mm, and 95–115 mm) along the radial direction were carried out. All the samples were made of Norway spruce (*Picea abies* L. Karst.) since it is commonly used wood in historical constructions in the Czech Republic. For the comparison and verification of the mini jack technique, the standard laboratory testing and another semi-destructive technique (pin pushing) was employed. The mini-jack technique provided the conventional compressive strength (CS_L) and modulus of deformability MOD_L that is analogical to elastic modulus known from standard compression tests, ie. it is calculated from linear part of force-displacement diagram. The (CS_L) values were obtained by finding a yield point produced from intersection of tangents of elastic and plastic parts of the working diagram.

The laboratory destructive testing was based on compression tests along the fiber following European norms (ČSN EN 490110). The samples used had size 20x20x30 mm^3 and were taken at individual positions adjacent to places of measuring by the mini jack device. Only samples at 12% moisture content level were measured and correlated to measurements using semi-destructive devices. The measurements were carried out at universal testing machine Zwick Z050 controlled by TestXpert v 11.01 software. The laboratory measurement provided: wood density (ρ), wood strength in compression parallel to the grain (S_L), and the elastic modulus in compression parallel to the grain (E_L).

Another technique employed to be compared to was pin pushing (Fig. 1 right). The pin pushing technique was described in Kloiber et al. (2012) and consisted in pushing of metal pin with 2,5 mm in diameter and 120 mm in length into a wood in a radial direction. The measurement was carried out at adjacent place to the mini jack techniques. Basic characteristics obtained was average

force (F_{AVG}) that was calculated the quotient of work S and length of displacement L, which best correlates with mechanical properties.

Independently from measurements described, optical measurement using stereoscopic set up was performed. The setup provided pairs of images acquired during the mini-jack technique measurement (Fig. 2). The images were subsequently used for calculation of displacements and strains using Digital image correlation (DIC) implemented in Vic-2010 Software (Correlated Solutions Ltd.). 20 samples made of Norway spruce were tested using this setup. The samples were different from the sample sets in previous measurements due to a fact, that samples had to be cut into halves to enable optical measurement around the pre-drilled hole in radial direction, see Fig. 2. The samples were applied a stochastic and black-white pattern to enable digital image correlation. To enhance contrast and field of view of the cameras, the samples were lit by 500 W LED chip lights.

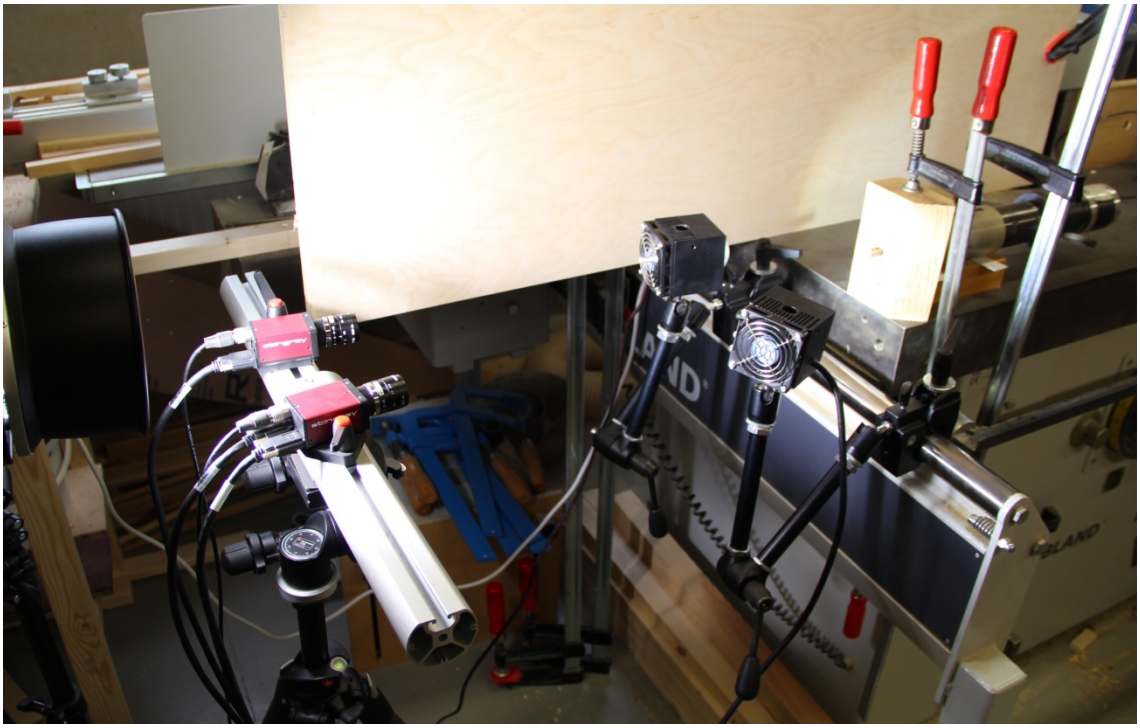

Fig. 2 left – overall view on stereoscopic measurement of deformation process for subsequent DIC analysis

3. Results

The goal of the work was to measure and investigate influence of the moisture content on mechanical properties measured by recently developed technique based on mini-jack inserted in pre-drilled hole. Three groups of samples with different moisture content level (12%, 18% and 24%) were tested using one-way Analysis of Variance (ANOVA) at level of significance $\alpha = 0.01$. The null hypotheses in ANOVA test was that mean values of three groups statistically equal one another. The ANOVA revealed that there is a statistical difference of mean values of these three groups and null hypotheses was consequently rejected. We may state that the mini-jack technique is sensitive to moisture contect changes since it was capable to detect differences in mechanical properties of wood. The three groups of measuerment for conventional strength CS_L and modulus of deformability MOD_L are plotted in Fig. 3

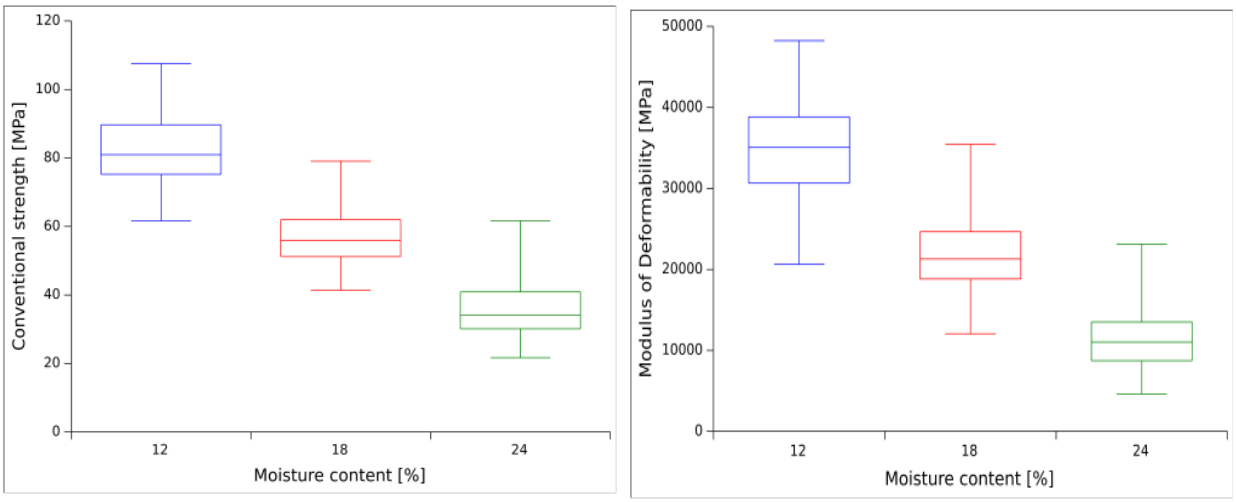

Figure 3 – Variability of Conventional strength (left) and Modulus of deformability (right) at 3 different moisture contents

Descriptive statistics of three groups is showed in Table 1. We clearly see the effect of moisture content on measurement using mini-jack technique. The variability (CoV) of CS_L and MOD_L has increased with moisture content too.

Table 1 – Descriptive statistics of measurements using mini jack technique at three levels of moisture content (12%, 18%, 24%).

	CS_L			MOD_L		
	12	*18*	*24*	*12*	18	24
Mean	82.29	57.05	35.94	*34701*	21634	11147
Median	80.97	55.89	34.14	*35061*	21290	11030
Standard deviation	10.35	8.19	7.85	5835	4289	3529
CoV [%]	12.58	14.36	21.85	16.81	19.83	31.66

3.1 DIC analysis

Fig. 4 illustrates the distribution of strains in vertical direction (ε_{yy}) during the time – beginning of measurement, at maximal force and after reaching maximal force. Despite the small contact area of jaws, there is a large theoretical area of impacted material, which suggests a good potential for estimation of non-local properties. The strain fields are symmetric on both sides of puschin jawas that suggests correct functioning of pressing into wood. The statistical analysis of strains revealed there is no difference between strains induced in radial and tangential direction.

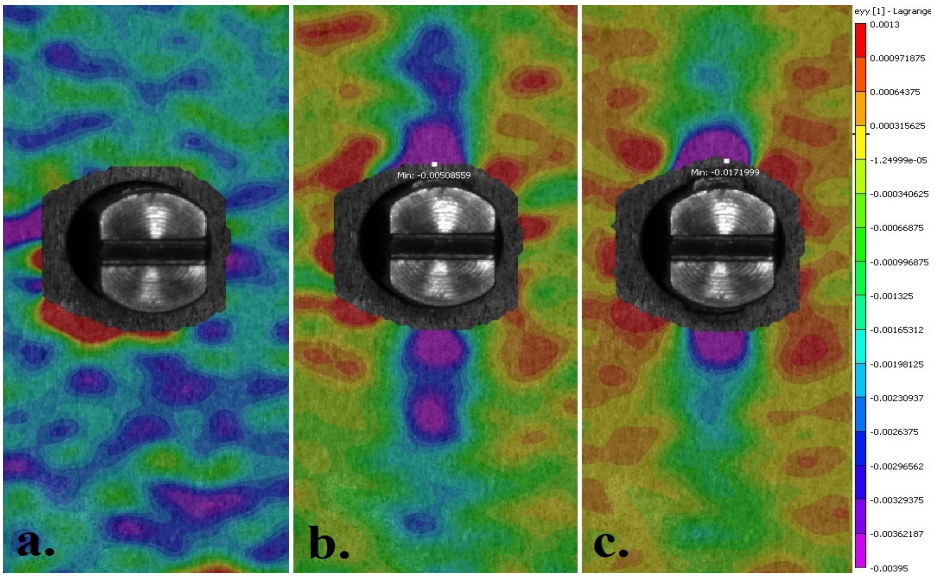

Fig. 4 left – vertical strain (ε_{yy}) during measurement using mini-jack technique computed by DIC analysis

4. References

[1] Kasal B, Tannert T (2011) *In situ Assessment of Structural Timber*. State of the Art reports. Springer, 124 pp.

[2] Cruz H, Yeomans D, Tsakanika E, Macchioni N, Jorissen A, Touza M, Mannucci M, Lourenço P. B. Guidelines for On-Site Assessment of Historic Timber Structures. *International Journal of Architectural Heritage* 9(3), 2015, pp. 277-289

[3] Calderoni C., De Matteis G., Giubileo C., Mazzolani F. M. Experimental Correlations between Destructive and Non-destructive Tests on Ancient Timber Elements *Engineering Structures* 32(2):2010, pp. 442-448

[4] López G., Basterra L. A. , Gemma R. C. de Diego A. Detection of Singularities and Subsurface Defects in Wood by Infrared Thermography *International Journal of Architectural Heritage* 8, 2014, pp. 517-536

[5] Kruglowa T. In-Situ Determination of Density in Timber structures using X- ray: A Guideline. ISSN 1652-9162, *Chalmers Report No.* 2012:03

[6] Kloiber M., Drdácký M., Machado J. S., Piazza M., Yamaguchi N. Prediction of Mechanical Properties by Means of Semi-destructive Methods: A review. *Construction and Building Materials* Vol. 101(2):30, 2015, pp. 1215–1234

[7] Ross R., et al. Transverse Vibration Nondestructive Testing Using a Personal Computer. USDA, Forest Service, Forest Products Laboratory, *FPL-RP-502*, 1991. 17 p.

[8] Hasenstab A., et al Materialuntersuchung an Holz mit niederfrequenter Ultraschall-*Echotechnik*. 2004, pp. 07-10

[9] Kloiber M., Tippner J., Praus L., Hrivnak J. Experimental Verification of a New Tool for Wood Mechanical Resistance Measurement. *Wood Research* 57(3), 2012, pp.383-398

The Cloak Bridge in Český Krumlov – measuring of mechanical properties

Michal Kloiber Researcher Institute of Theoretical and Applied Mechanics, v.v.i., Centre of Excellence ARCchip Telč Batelovská 485, Telč, 588 56 Czech Republic *kloiber@itam.cas.cz*	**Václav Sebera** Research assistant Mendel University in Brno, Faculty of Forestry and Wood Technology, Department of Wood Science Zemědělská 3, Brno 619 00 Czech Republic *vaclav.sebera@mendelu.cz*
Jaroslav Hrivnák Researcher Institute of Theoretical and Applied Mechanics, v.v.i., Centre of Excellence ARCchip Telč Batelovská 485, Telč, 588 56 Czech Republic *hrivnak@itam.cas.cz*	**Jan Tippner** Research assistant Mendel University in Brno, Faculty of Forestry and Wood Technology, Department of Wood Science Zemědělská 3, Brno 619 00 Czech Republic *jan.tippner@mendelu.cz*
Jiří Kunecký Researcher Institute of Theoretical and Applied Mechanics, v.v.i., Prosecká 809, Prague, 190 00 Czech Republic *kunecky@itam.cas.cz*	

Summary

Timber bridges are often exposed to harsh conditions of the environment. The exposure of the timber structure often leads to its deterioration. Standard test procedures to determine typical properties of wood cannot be used as there is the requirement of the minimum interference with the structure. Several non-destructive testing (NDT) methods for the determination of timber condition have been developed and are used. However, the results of NDT can be used to predict mechanical properties of timber elements only to a limited degree. Semi-destructive testing (SDT) methods are a compromise. In the paper a functional model of a device that allows for the measurement of conventional strength and modulus of deformation of timber in compression parallel to the grain is presented. The device is inserted to a bored hole and pushes the jaws apart with a small test jack loading the bore walls. This paper presents possible use of the device for surveys of timber bridges.

Keywords: model of device, mechanical properties

1. Introduction

When designing repairs and maintenance of the existing timber structures, it is possible to evaluate the mechanical properties of integrated elements, which often the so-called characteristic values. If the use or any other modification affecting the loading of the individual elements changes, it is necessary to take into account the loading relevant for these changes. Historic timber structures are generally more flexible than modern constructions; however, their repairs need to be designed with the best possible knowledge of the material and structural properties. Therefore, it is not appropriate

to use modern designs of limit states without further consideration as it may lead to a partial or even complete destruction of the structure. Especially in protected buildings, a sufficient number of probes need to be performed. The designer should make a request for the analysis of strength characteristics of selected timber elements using sophisticated methods, presented e.g. in [1,2,3]. Furthermore, the overall stability of the structure and the behavior of individual parts or elements should be assessed [4].

In critical areas of the structure, where higher load or element damage is expected, the actual strength of the integrated timber must be evaluated. This can be done either by a visual inspection of properties and defects of the wood (visual classification), or using non-destructive measurement of one or more physical, mostly mechanical properties, or an appropriate combination of the two methods [5].The information necessary for the assignment of the species and origin of the structural timber by the visual degree of the strength class is provided in [6]. In order to assign a class, it is necessary that all of the appropriate strengths, growth characteristics or defects fall within the limits laid down for the class.

In the case of historical structures the practice is more complex: what matters is the location and the conditions of loading, which determine the evaluation of the significance of defects in relation to the actual loading of the timber. A simple example would be a short strut that is loaded only in compression so there is no need to evaluate defects affecting the ability of the element to withstand the bending load [4].

When applying the classification used for new timber structures, the evaluator must cope with the fact that: 1. Typical dimensions of the traditional prisms differ from the dimensions used for the evaluation of the defects in the valid standard. 2. The valid standards for the visual classification do not include the size of beams and methods of their working. 3. Current standard [7] for strength classes has not yet been recognised valid for historic timber.

The most important natural defects of wood are knots and grain deviation from the element's longitudinal axis. However, the negative effect of knots and the grain deviation can be eliminated within the production process, which in the past was done during the manual working and precise selection of the material. The deflection limits specified in the Eurocode may not be suitable for historic structures - some have satisfactory load carrying capacity, despite the permanent deformation in deflection.

In order to obtain the characteristic values of strength, the evaluated element may be classified visually by size and position of natural defects. In the absence of the actual strength values for each element, it is necessary to obtain the characteristic values of the wood strength, so that the structure itself could be assessed according to the principles of [8]. This is a conservative approach, in which the timber engineer classifies the strength based on visual inspections as stipulated in [7].

The visual classification must be carried out by an experienced timber specialist. The following principles apply [5]: If necessary, it is possible to identify each of the critical zones separately in order to classify the entire element. If the number of visible sides of the timber element is lower than three or it is not possible to check at least one front of the element, this fact must be stated in the final report. If some parts are affected by mechanical damage or local biological damage (mold, fungi, pests), the classification only applies to the undamaged parts. If some areas of the timber are affected by wood-destroying insects, which have spread across all sides of the element, the classification needs to take into account the loss of density throughout the cross section.

Due to not entirely convincing results of the visual strength classification, one or more instrumental methods for the determination of physical or mechanical properties have been increasingly used recently, as they better correlate with the strengths determined in destructive samples evaluated based on the valid standards. The material characteristics are determined using the methods stipulated in standards when the entire element or a large part of undamaged material need to be sampled. The main wood property tested by destructive methods is the modulus of elasticity, which expresses the stress ratio and the induced deformation. Another property tested destructively is

static strength, which is dependent on the direction of loading with respect to the orientation of the grain because wood is a significantly anisotropic material. Destructive tests determining the mechanical properties shall be carried out in compliance with [9]; the relations between the physical and mechanical quantities are presented in [10]. Destructive material testing methods are standardized for the detection of the quality of new timber. As regards historical buildings, usually it is not possible to sample material for the test specimens of standard size, and the methodology must be modified. In the evaluation of the modified tests, the values of the property tested are converted by correlations, which need to be established [11].
The paper presents selected test methods verified in the practice that can be used to assess the quality and determine material characteristics. The methods include resistance drilling into a timber element and the latest method, which is loading the timber inside a borehole by opening jaws of a small test jack.

2. Materials and Metodology

2.1 Description of the new device

The device (Fig. 1) is designed to measure mechanical properties of wood using semi-destructive investigation of its behaviour when loaded by a small size jack inserted in a pre-drilled hole. The device can be used both in a laboratory and in the field to determine the condition and quality of timber. The device provides the dependence of deformation on the tension (Fig. 2) brought about by pushing symmetrically placed jaws apart in a pre-drilled radial hole with 12 mm in diameter.

Fig. 1 Overall view of the newly designed device

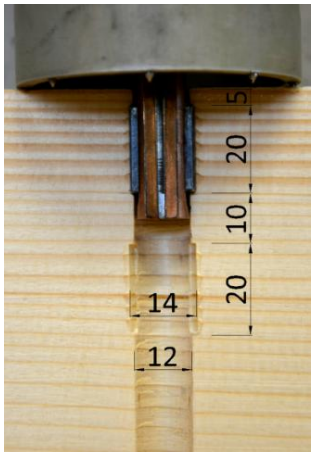

Fig. 2 Detail of the drawbar with the wedge and rounded jaws

The device is laid on the tested sample by means of a cylindrical shell, which allows measuring in four positions of the pre-drilled hole. The maximal absolute deformation that can be reached on both sides is 1,5 mm. The rounded jaws are 5 mm wide and 20 mm long. The jaws also include flexible arms whose movement during pushing is provided by a push-apart bronze wedge fitted to the lower end of the drawbar by means of a pin and screw. The apex angle of the wedge is 15°. This angle is not self-locking and to release the jaws it is sufficient to release the push-apart force [12]. The force of the drawbar drawing is continually recorded. It is calibrated to the real force of the loading jack and simultaneously related to the measured distance of movement of the jaws (Fig. 3). The signals are wireless transmitted to a computer where they are processed. More information about the device can be found in [13].

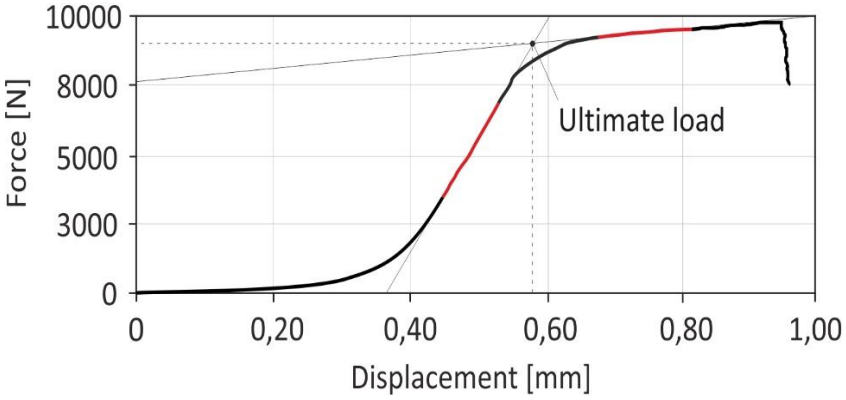

Fig. 3 An example of the device output: a record of the force needed to push the jaws apart in relation to the measured shift (displament) of the jaws

2.2 The other used devices

Other semi-destructive methods used were the measuring of mechanical resistance of wood against microdrilling. Microdrilling was carried out using Resistograph that examines the resistance of the material against the penetration of a small borer with 1.5–3.0 mm in diameter. Because the Resistograph is well known, the readers are referred to important literature such as [14,15,16].

2.3 The Cloak Bridge

Measurement of mechanical properties by semi-destructive equipment was carried out on six beams of Norway spruce (*Picea abies*) and one beam of Scots pine (*Pinus sylvestris*). The measured beams are parts of the structure of the Český Krumlov Cloak Bridge, which is listed in the UNESCO World Heritage list. The bridge "On the Cloak" or the Cloak Bridge spans the moat on the western side of the Upper Castle, where a fortification called the Cloak used to stand. This gave the name to the bridge. The bridge stands on stone piers with arches (Fig. 4). The three main piers expand over the bridge path linking the fourth and the fifth courtyard of the Český Krumlov Castle and they support two corridors, one above another. The lower one connects the Masquerade Hall with the castle theatre and the upper one connects the castle picture gallery with the castle garden. The path through the upper corridor continues through the castle trusses up to the Minorite Monastery on the Latrán. Unfortunately, it is impassable today.

The Cloak Bridge was first mentioned as early as in the 15th century. At that time, it was probably only a timber bridge. Rudolf II's inventory speaks about a "drawbridge On the Cloak with a gate". The new owner of the estate, Jan Kristian I of Eggenberg, began building a new timber bridge into the upper castle garden in 1686. In 1706, the first timber model of the covered corridor to the upper garden, resting on stone piers, was under construction. It was entered from the gallery on the second floor of the castle, and this position of the corridor has been preserved until today. At that time, the castle theatre was linked with the corridor via staircases. In 1707–1708, the second timber corridor, one floor below, was built, leading from the Masquerade Hall to the duke's loge in the castle theatre. Toilets have been preserved near the duke's loge in the piers of the cloak corridor. During the military invasion in Český Krumlov in 1741, when the castle was occupied by the French, the timber corridor over the Cloak Bridge was allegedly destroyed. The lower corridor was broken in 1748–1749 and a new, slightly higher one was built. Other references come from the year 1764, when the bridge started to be reconstructed. The reconstruction took several years. Mainly, a stone bridge from the fourth to the fifth courtyard was constructed and the lower corridor was repaired. In 1777 the corridors were joined into a single unit by cutting off the truss of the lower corridor and its linking with the upper corridor. This gave the bridge its current form (Fig. 5). For more information on the construction and development of the Cloak Bridge, see [17].

Fig. 4 The Cloak Bridge on stone piers

Fig. 5 Top timber part of the bridge with the cloak

The measured beams come from the period of the large reconstruction in the years 1748–1764. From the first stage of the bridge reconstruction (1744–1747) after its demolition, two girders were selected, cross section (170 × 200 and 240 x 210 mm), 5000 mm long. From the second stage (1762–1765) three upper corridor floor beams were selected, their cross section (310 x 330 x 340, 350 and 360 × 390 mm) and length 16000 mm, and one strut beam with a cross section of 270 × 260 mm and a length of 16000 mm. The representation of the species corresponds to the most commonly used material composition of historic structures in the Czech Republic.
After selecting the appropriate elements, a drill of 12 mm diameter was used purely in the radial direction at the places where the beam ends were laid. The depth of the borehole was 130 mm, allowing the measuring by the jaw pushing apart method, in total in four layers: 1st layer (5–25 mm), 2nd layer (35–55 mm), 3rd layer (65–85 mm), and 4th layer (95–115 mm). In total, eight measurements were performed for each element assessed. The total number of positions measured using the new device was 48.

2.4 Preparation of measurment

The surface of the timber must not be boarded, covered in rubble, dirt or dust before the measurement. Wood surface must be cleaned by dry processes (e.g., fine brushing, air pressure or by using an industrial vacuum cleaner) to prevent the surface deterioration of the historic timber. The hole needed for the test is created by a milling bit with an outer diameter of 12 mm (Fig. 6), which is fixed in a cordless drill. To prevent sideways motion of the bit during drilling, the drill is fitted to a special stand (Fig. 7) which fixes it to the element.

Fig. 6 Detail of the milling bit for the preparation of drilling, diameter of 12 mm

Fig. 7 Special stand to fix the drill with the bit and its fixation to the element

The stand can be fixed to the element directly or to a supporting scaffolding. This needs an area of 150×150 mm. It is recommended to control the drilling speed, especially the progress of the bit into the hole, to ensure a good quality of drilling. For the same reason, the bit must be kept sharp and clean. Blunt or dirty bits can cause fibres tearing out of the hole walls, which can distort the results of the measuring.
The hole should be drilled in undamaged parts of the element without visible defects and damage. The measurement is only accurate if the drilling is oriented normally to the grain, as in this direction earlywood and latewood alternate regularly within a tree ring, and if the grips are pushed apart parallel to the grain - in structural elements it is generally parallel to the element axis. In the tangential direction, measuring is affected by a higher proportion of earlywood or latewood, which leads to distorted results.
The minimum number of boreholes necessary for each element is two. In the case that the data from the two measurements differ significantly from each other, it is necessary to perform additional drilling and use the data from the two boreholes that are similar. A higher number of holes improperly placed can affect the mechanical resistance of the element assessed.
Like other on-site methods used for the diagnostics of integrated timber, the presented method for the measurement of strength and modulus of deformability in compression parallel to the grain manifests a considerable dependence on the water content in the investigated material. Increased moisture is therefore an undesirable factor, which negatively affects the strength properties of wood. Therefore, the choice of the drilling location is an essential part of the test. The location must be without obvious signs of increased moisture content.

2.5 Measurment

The measurement itself was carried out by inserting the measuring part into the radial hole (Fig. 8) and the device was attached to the tested element using a cylindrical shell. The jaws were pushed apart in the direction parallel to the grain by pulling up the drawbar with a push-apart wedge, along which the jaws moved. The drawbar pulling was powered by a screw with nut using a cordless drill with epicyclic gearing. The prints of the jaws in the timber can be seen in Fig. 9, which also presents the distance between the layers of measurement across the element.

Fig. 8 Detail of the measuring part of the device before insertion in the borehole, diameter of 12 mm

Fig. 9 Prints of the jaws in borehole no. 12

Further, measurement using a resistance microdrill was carried out at places adjacent to the boreholes made for the new device. Resistograph 4453-S recorded the amount of energy needed to keep constant drilling speed. The output is the profile of power consumption, or relative resistance, including the elimination of energy consumption of friction in deeper layers. To compare this with mechanical properties, it was necessary to assess the graphical output explicitly; therefore, a script was designed in MATLAB to calculate a parameter marked as Resistance Measure *RM*,

i.e., a resistance feature corresponding to the area under the curve divided by the width of the measured section.

2.6 Result

The mechanical properties were determined from the record of the data measured in the form of stress-strain diagram with a record of the force of drawbar pulling. An example of the stress-strain diagram is presented in Fig. 3. The x axis shows the displacement when pushing the jaws apart and the y axis manifests the force required for the jaws pushing. The maximum force (F_{max}), depicted as the "Ultimate load", was established from the intersection of the lines - tangents to the elastic and plastic parts of the stress-strain diagram progress. Conventional strength in compression parallel to the grain ($CS_{C\,(L)}$) was determined from the ratio of the ultimate load and the area of the jaws. Modulus of elasticity cannot be calculated from the stress-strain diagram directly; however, the modulus of deformability ($MOD_{C\,(L)}$) was determined based on the line fitted to the direct part of the force and deformation record. The measurement results were put in a table (Tab. 1).

Tab. 1 Results of the jaw pushing apart in a borehole for 6 selected elements after two drillings

Číslo vrtu	Vrstva měření	$CS_{C\,(L)}$ MPa	$CS_{C\,(L)}$ MPa	$MOD_{C\,(L)}$ MPa	$MOD_{C\,(L)}$ MPa	Vrt číslo	Vrstva měření	$CS_{C\,(L)}$ MPa	$CS_{C\,(L)}$ MPa	$MOD_{C\,(L)}$ MPa	$MOD_{C\,(L)}$ MPa
1	1	70,3		20200,1		**7**	1	62,9		12717,8	
1	2	61,5		16450,1		**7**	2	55,3		8470,2	
1	3	57,2		11535,5		**7**	3	56,1		10158,4	
1	4	55,5	61,2	10156,8	14585,6	**7**	4	57,3	57,9	8643,4	9997,4
2	1	69,1		17115,0		**8**	1	67,5		13217,7	
2	2	54,2		13548,4		**8**	2	64,9		8775,8	
2	3	53,0		9714,8		**8**	3	64,9		10007,4	
2	4	56,2	58,1	9775,2	12538,3	**8**	4	69,1	66,6	9342,9	10336,0
3	1	64,8		14760,6		**9**	1	69,0		11980,6	
3	2	57,5		15537,0		**9**	2	57,0		7444,3	
3	3	58,3		15597,6		**9**	3	51,4		7134,9	
3	4	59,4	60,0	10430,9	14081,5	**9**	4	53,4	57,7	8171,2	8682,7
4	1	69,9		18946,1		**10**	1	61,5		9990,3	
4	2	53,9		14094,9		**10**	2	59,1		9509,2	
4	3	54,9		12593,7		**10**	3	58,8		9022,3	
4	4	62,4	60,3	14606,7	15060,3	**10**	4	56,8	59,1	8732,7	9313,6
5	1	69,3		16447,3		**11**	1	65,2		15598,7	
5	2	63,4		12692,7		**11**	2	75,5		14779,9	
5	3	58,2		9947,2		**11**	3	72,8		12347,9	
5	4	52,5	60,9	9168,1	12063,8	**11**	4	75,2	72,2	15286,6	14503,3
6	1	66,7		18209,7		**12**	1	65,4		13145,0	
6	2	59,8		10901,0		**12**	2	61,6		11549,4	
6	3	52,0		7992,9		**12**	3	69,2		10825,5	
6	4	58,1	59,2	7480,0	11145,9	**12**	4	68,7	66,2	14768,2	12572,0

Conventional compression strength parallel to the grain ($CS_{C\,(L)}$) and the modulus of deformability ($MOD_{C\,(L)}$) had to be converted to the actual strength ($S_{C\,(L)}$), and modulus of elasticity ($E_{C\,(L)}$) in compression parallel to the grain based on correlations. The strength ($S_{C\,(L)}$) determination based on the conversion equation presented in [18] was used as a reference measurement. The equation includes the correction of mechanical properties on the basis of wood moisture content, which was 21% when measuring the structural elements of the Cloak Bridge. The real strength ($S_{C\,(L)}$) and modulus of elasticity ($E_{C\,(L)}$) in compression parallel to the grain specified in the resulting table (Tab. 2) are converted to wood moisture content of 12%. The results indicate that the mechanical properties as measured correspond to the highest strength class.

Tab. 2 The resulting material properties

Číslo vrtu	Název prvku	Dendro. datování	Šířka	Výška	RM	$CS_{C(L)}$	$MOD_{C(L)}$	$S_{C(L)}$	$E_{C(L)}$	ρ
			mm	mm		MPa	MPa	MPa	MPa	kg.m^{-1}
1-2	**Podlahový nosník**	**1762 - 65**	310	340	145	59,6	13562,0	51,7	12521,0	528,0
3-4	**Podlahový nosník**	**1762 - 65**	330	350	161	59,1	13309,9	51,3	12335,0	524,2
5-6	**Rozpěrný trám**	**1762 - 65**	270	260	142	60,1	14570,9	52,0	13265,6	531,2
7-8	**Vazný trám**	**1744 - 47**	240	190	146	60,6	13562,1	52,3	12521,1	534,1
9-10	**Vazný trám**	**1744 - 47**	170	200	136	60,0	11604,9	52,0	11076,8	530,4
11-12	**Podlahový nosník**	**1762 - 65**	360	390	172	58,5	10571,7	50,9	10314,3	520,9
					150,3	**59,7**	**12863,6**	**51,7**	**12005,6**	**528,1**

The results of the mechanical properties, strength ($S_{C(L)}$) and modulus of elasticity ($E_{C(L)}$) in compression parallel to the grain, but also the density (ρ) proved totally negligible differences among the measured elements. In contrast, the resistance measure (*RM*) calculated from the measurements by the Resistograph slightly differed among the individual elements. This can be explained by the variability of the individual measurements within a single element. The greatest variance of measured values within a single element was observed in a floor beam with the measurement number 1-2: the difference of RM was approximately 10%. In the case of conventional compression strength parallel to the grain ($CS_{C(L)}$) and the modulus of deformability ($MOD_{C(L)}$) measured by the jaws pushing apart method, the differences within one element were smaller, up to 5%. The similarity of mechanical properties of assessed elements can be explained by the same location of the timber harvest, as regards both the first stage of the bridge construction and the second stage with a phase offset of about 20 years.
The distribution of the values of conventional compression strength parallel to the grain ($CS_{C(L)}$) and the modulus of deformability ($MOD_{C(L)}$) measured by the jaws pushing apart in a borehole across an element is presented in Tab. 1. The differences in the values of the individual elements are significant and they correspond to the distribution of density and mechanical properties. The distribution of the measured values $CS_{C(L)}$ must be taken into account. The measurement of $CS_{C(L)}$ performed by the method of jaw pushing apart in a borehole can be used to assess the distribution of wood properties across the element in integrated timber. The distribution may overlap with biotic damage in an on-site survey. Such a situation occurs when the measured values decrease by 1/4, which is the difference assessed as a timber defect by the surveyor in the field. The distribution of the values across the element as measured by the Resistograph (RM) was negligible for all measurement points.
The relationship between conventional compression strength parallel to the grain $CS_{C(L)}$ and the selected evaluation parameters is described by linear regression, as presented in Sebera [18]. The coefficients of determination R^2 demonstrate that the dependencies are very close, especially in the establishment of the compression strength parallel to the grain ($S_{C(L)}$). The modulus of elasticity in compression parallel to the grain ($E_{C(L)}$) and the density (ρ) can be derived with similar results.

3. Conclusion

The advantages of the method presented include the high accuracy of mechanical properties established (strength and modulus of deformability in compression parallel to the grain) of timber assessed directly in the field. The device is sufficiently sensitive to the natural differences among the elements of the historic timber as well as natural variation of properties (distribution along the width and the length of the elements, the occurrence of defects).

The testing hole is prepared by a milling bit with an outer diameter of 12 mm. It is recommended to keep the bit sharp and clean continuously to ensure a good quality of drilling. Blunt or dirty bits can cause fibres tearing out of the hole walls, which can distort the results of the measuring. The hole should be drilled in undamaged parts of the element without visible defects. The measurement is only accurate if the drilling is oriented normally to the grain, as in this direction earlywood and latewood alternate regularly within a tree ring, and if the grips are pushed apart parallel to the grain - in structural elements it is generally parallel to the element axis. In the tangential direction, measuring is affected by a higher proportion of earlywood or latewood, which leads to distorted results. A higher number of holes improperly placed can affect the mechanical resistance of the element assessed. The higher the number of holes in a single element is prepared, the more reliable the estimate of mechanical properties will be. The minimum necessary number of boreholes in each element is two. In the case that the data from the two measurements differ significantly, it is necessary to make one more borehole and use the data from the two boreholes that are similar.
Like other on-site methods used for the diagnostics of integrated timber, the described method for the measurement of strength and modulus of deformability in compression parallel to the grain manifests a considerable dependence on the water content in the investigated material. The conventional strength and modulus of deformability in compression parallel to the grain decrease with increasing moisture content. The effect of moisture content is the biggest around the fibre saturation point, when the values of measured mechanical properties are about half lower than when the moisture content is 12%. Increased moisture is therefore an undesirable factor, which negatively affects the strength properties of wood. Therefore, the measurement of the moisture content at the place of testing is essential. If possible it should be performed by indentation probes, which better record moisture changes after the section through the element.
Strong correlations were mainly found for conventional strength in compression parallel to the grain ($CS_{C\,(L)}$) and strength of standard samples ($S_{C\,(L)}$) (correlation coefficient 0.7–0.95). The conventional compression strength parallel to the grain also correlates with the other investigated timber parameters, e.g. density (correlation coefficient 0.7–0.95), and ($H_{\,(L)}$) hardness parallel to the grain (0.7–0.9). The new device helps estimate mechanical properties in pure wood and it is, therefore, necessary to perform the visual correction in which the effect of natural defects is taken into account [3,15].
An essential feature of the field testing is the fact that the measuring is conducted in a loaded element with unknown internal forces present. It was assessed and approved by means of image digital correlations that the tension releases after drilling into a distance of about 2 mm from the hole edge. The measuring is thus not affected by the inner tension of the constructional element unless the element was permanently damaged (occurrence of plastic deformation). The above mentioned assertion has been verified by tests of a bended timber console [19].

Acknowledgenemt

This paper was created with a financial support from grant project DG16P02M026 “Historical Timber Structures: Typology, Diagnostics and Traditional Wood Working”, NAKI program II, provided by the Ministry of Culture and research supported by the project CZ 1.05/1.1.00/02.0060 from the European Regional Development Fund and the Czech Ministry for Education, Youth and Sports and project No. LO1219 under the Ministry of Education, Youth and Sports National sustainability programme I.

References

[1] Tannert, T, Anthony, R., Kasal, B., Kloiber, M., Piazza, M., Riggio, M., Rinn, F., Widmann, R., Yamaguchi, N.: Recommendation of RILEM TC 215-AST: In-situ assessment of structural timber using semi-destructive techniques. In: Materials and Structures 47(5): 2014, Netherlands. ISSN: 1359-5997, pp. 767–785.

[2] Riggio, M., Anthony, R.W., AuUgelli, F., Kasal, B., Lechner, T., Muller, W., Tannert, T.: In situ assessment of structural timber using non-destructive techniques. Materials and Structures, 47: 2014, Netherlands. ISSN: 1359-5997, pp. 749-766.
[3] Kloiber, M., Drdácký, M., Tippner, J., Hrivnák, J.: Conventional compressive strength parallel to the grain and mechanical resistance of wood against pin penetration and microdrilling established by in-situ semidestructive devices. In: Materials and Structures, 48(10): 2015, Netherlands. ISSN: 1359-5997, pp. 3217–3229.
[4] Cruz, H., Yeomans, D., Tsakanika, E., Macchioni, N., Jorissen, A., Touza, M., Mannucci, M., Lourenço, P.B.: Guidelines for the On-Site Assessment of Historic Timber Structures. In: International Journal of Architectural Heritage: Conservation, Analysis, and Restoration, 9(3): 2015, ISSN: 1558-3058, pp. 277-289.
[5] UNI 11119: Cultural Heritage – Wooden artefacts, Load-bearing structures. On-site inspections for the diagnosis of timber members, 2004.
[6] EN 1912: Structural timber – Strength classes, Assignment of visual grades and species, 2012.
[7] EN 338: Structural timber – Strength classes, 2009.
[8] EN 1995-1-1: Eurocode 5: Design of timber structures – Part 1-1: General – Common rules and rules for buildings, 2004.
[9] Bláha, J.: The Cloak Bridge in Český Krumlov – construction history research. In: 3rd International Conference on Timber Bridges Skellefteå, Sweden, 2017.
[10] Drdácký, M., Kloiber, M.: In-situ compression stress-deformation measurements along the timber depth profile. In: Structural Health Assessment of Timber Structures, Book Series: Advanced Materials Research 778: 2013, Trans Tech Publications, Switzerland. ISSN: 1022-6680, pp. 209-216.
[11] EN 384: Structural timber – Determination of characteristic values of mechanical properties and density, 2010.
[12] EN 408: Timber structures – Structural timber and glued laminated timber – Determination of some physical and mechanical properties, 2010.
[13] Kloiber, M., Drdácký, M., Machado, J.S., Piazza, M. Yamaguchi, N.: Prediction of mechanical properties by means of semi-destructive methods: A review. In: Construction and Building Materials, 2015. ISSN: 0950-0618, pp. 1215–1234.
[14] Kloiber, M., Tippner, J., Hrivnák, J.: Mechanical properties of wood examined by semi-destructive devices. In: Materials and Structures 47(1): 2014, Netherlands. ISSN: 1359-5997, pp. 199-212.
[15] Kloiber, M., Kunecký, J., Drdácký, M., Tippner, J., Sebera, V.: Experimental and numerical analysis of semi-destructive device for in-situ assessment of wood properties in compression parallel to grain. In: Wood Science and Technology, Vol. 51: 2017. ISSN: 0043-7719, p. 345-356.
[16] Maddox, J., Drdácký, M., Kloiber, M.: In situ assessment of strength of historic wood. In: 9th International Conference on Structural Analysis Historical Constructions, Mexico City, 10/2014, Mexico. ISBN: 04-2014-102011495500-102, 13 pp.
[17] Nowak, T.P., Jasieńko, J., Hamrol-Bielecka, K.: In situ assessment of structural timber using the resistance drilling method – Evaluation of usefulness. In: Construction and Building Materials 102: 2016. ISSN: 0950-0618, 403-415.
[18] Sebera, V., Kloiber, M., Hrivnák, J., Tippner, J., Kunecký, J., Milch, J.: Analysis of Mini-jack technique for *in situ* measurement of strength. In: 3rd International Conference on Timber Bridges Skellefteå, Sweden, 2017.
[19] Vlček, M., Moudrý, I., Novotný, M., Beneš, P., Maceková, V.: Poruchy a rekonstrukce staveb. Nakladatelství ERA, Brno, 2006, 222 s.

Design flaws on Norwegian Timber Bridges

Hauke Burkart
Senior Engineer
Norwegian Public Roads Administration
Oslo, Norway
hauke.burkart@vegvesen.no

Hauke Burkart has worked with timber bridges in the NPRA for the past 8 years, mostly through bridge maintaining and bridge inspection work.

Tormod Dyken
Senior Principle Engineer
Dyken AS
Hyllveien 10C, 3408
Tranby, Norway
tormod.dyken@gmail.com

Tormod Dyken has been active on timber bridges for the past 20 years, mostly within the NPRA but has continued his work after retirement.

Summary

In February 2016 the not yet officially opened Perkolo Bridge in Norway collapsed as a timber lorry passed over it. The collapse was due to a design error. Luckily, no one was seriously injured. The subsequent investigations have, however, uncovered unfavourable choices in the design of timber bridges such as missing focus on structural robustness and non-conservative simplifications. In addition, discussions on how to use Eurocode 5 have shown that the calculated design resistance is very much dependent upon the interpretation of the code, especially for multiple gusset-plate-connections.
Unfortunately, the Perkolo Bridge has not been the only case. Design errors were also discovered on two other bridges, one before and one after the incident of Perkolo Bridge that all were subject to third party control. This is a serious issue for the reputation of timber as an engineering material though the material itself is not to blame. On the good side, strengthening timber bridges afterwards has proven to be relatively easy.

Keywords: Timber, accident, incident, design flaws

1. Introduction

Three uncovered design flaws and one accident within the past two years with Norwegian timber bridges is not a good thing. From being something special, timber bridges have evolved to be a natural consideration in several projects. In comparison to concrete still few timber bridges are built, very few small structures are built out of timber and the number of senior engineers with thorough experience on timber structures is very limited.

After the findings on Perkolo and Sunbyveien bridges and the observation that the errors were related to truss designs, a check for all timber truss bridges with road traffic was called for. A review of these structures was done by a group (see ch. 5) that were to recalculate all bridges. Discussions within the group as with others by the authors are summarised in this paper.

2. Accident and Incidents

The accident on the Perkolo Bridge resulted in insecurity on timber bridges that by the public probably still exists. When the design error on Sunbyveien Bridge was uncovered the insecurity grew and it resulted in three closed timber bridges with following media attention. Before this an incident also had occurred on Kåsa Bridge. All three bridges were subject to third party control where none of the errors was detected. Timber as a structural material is not to blame for any of these incidents.

2.1 Perkolo Bridge

Perkolo Bridge was a truss bridge with one traffic lane and a span length of 47.5 m crossing a future 4 lane highway. The bridge collapsed before official opening of the crossing highway when a lorry with timber passed on the February 17th 2016. The weight of the lorry was said to be about 31 tons. The bridge was designed with Eurocode loads and was opened for lorries with total weight of 60 tons.
The reason for the collapse of Perkolo bridge was faulty design of several connections. Faulty design in the splicing of the lower chord was probably the actuating part. Several of the failed connections experienced various kinds of block shear failure. The course of failure is not known for sure, but the driver reported that the bridge sagged at first before total failure occurred. The warning was insufficient for the driver to act nor did he manage to escape. There were no reports on damage or other signs of overload on the bridge before failure.

Figure 1 Perkolo Bridge after collapse

2.2 Sundbyveien Bridge

Sundbyveien Bridge is a two-lane road bridge with pedestrian lane. The truss bridge opened in 2011, total length is 62 m and largest span is 42 m.
The designers uncovered a design error on Sunbyveien Bridge after the collapse of Perkolo Bridge. Sundbyveien bridge was shortly afterwards closed for traffic and later reopened with one lane before strengthening.

2.3 Kåsa Bridge

Kåsa Bridge is an two-span arch bridge with spans of 27 m opened in 2014 with a dual carriage way and pedestrian lane. At production questions were raised around the fixing of the hangers which were placed in the lower part of the arches close to the surface. It was uncovered that no check on tension perpendicular to fibre was carried out. The bridge was strengthened with screws before mounted at place.

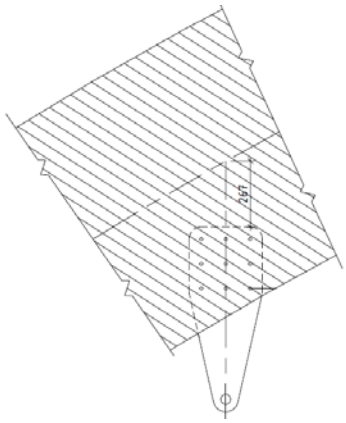

Figure 2 Hangers on Kåsa Bridge

3. Issues discussed during check for truss bridges

Shortly after the failure of Perkolo Bridge, several reports concluded on the reason for failure. The findings on Sundbyveien shortly after collapse of Perkolo resulted in a decision to close all similar bridges with a splicing in the chord, in total three bridges including Sundbyveien Bridge. Luckily, the two others were not in use during winter time anyway, being only used for agricultural purposes.
A group was called for to check all truss bridges owned by the Norwegian Public Roads Administration (NPRA) with road traffic, in total 10 bridges. The report [1] concluded that no other design errors were found. However, unsafe approaches were detected and also dubious interpretations of the design codes for timber. In the following findings from this work and discussions afterwards is presented.

3.1 Multiple shear plane connections

Calculating multiple shear plane connections may not be as straight forward as expected. The geometric design of connections is mostly dependent on other factors than the static part of the connection itself. Multiple shear plane connections may be divided into an outer part, comprising the wood outside the outer gusset plates, and the wood in between the gusset plates. By specifying the dimensions of the chords and webs before calculating the connections, timber parts of different sizes may be connected resulting in a somewhat more complex connection. This may especially be the case when connecting a web to a chord resulting in a much thicker outer part in the chord than required for load transfer.
EC5 requires strain compatibility between the inner and outer parts of the connection. Combining the shear plane capacities by observing the strain compatibility result in a larger total capacity than if only the lowest capacity of each shear plane is combined without taking into account compatibility. Physically, the approach of the code with strain compatibly is more correct, but then the designer also must acknowledge a reduction of the outer thickness t_1 in the case where this is very large. The code [2] works well when t_1 is not greater than $t_2/2$. Thus, having $t_{1,eff} <= t_2/2$ might be a simplified valid limit for the outer thickness. This subject doesn't seem new and Ranta-Maunus and Kevarinmäki [3] have recommended combining the lowest capacity of each shear plane regardless of compatibility. Whatever approach one takes on this, expecting full utilisation of a dowel with very large t_1 in multiple shear plane connections seems not correct.

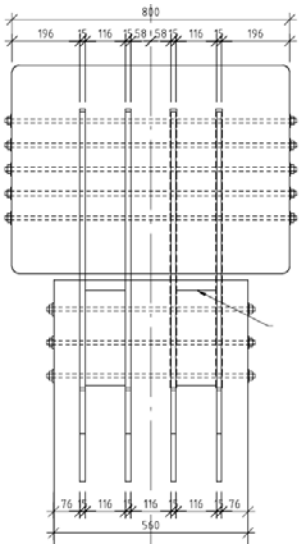

Figure 3 Example of a smaller web connected to a larger chord

3.2 Block shear failure of multiple shear plane connections

One unpleasant surprise on the Perkolo Bridge was the amount of block shear failures in connections. This might also have been the reason why the collapse was that total and no previous overstressing was reported. A beginning of block shear failure is probably very difficult to find, whereas crushed timber behind dowels might be easier. On a note, the NPRA did try particularly to look for signs of block shear failure on one of the truss bridges checked after the Perkolo accident

during inspection by looking for tension failures perpendicular to grain behind tension stressed connections. Distinguishing weather related cracks to stress related cracks seems close to impossible.
When calculating the block shear capacity often the total area of the timber subtracted by the guessed plate connections and dowels is taken. Such an approach does not take into account different stiffness's in different parts of the connections, as for example again in the case where a small web is connected to a larger chord as shown in figure 3. In the outer part plug shear failure may occur. The code [2] gives guidance on how to calculate a single shear plane for block shear failure, but it does not give any guidance on how to deal with multiple shear plane connections. Our recommendation would be to introduce an $t_{1,ef}$ as stated in ch. 3.1 also in the control of block shear tension failure.

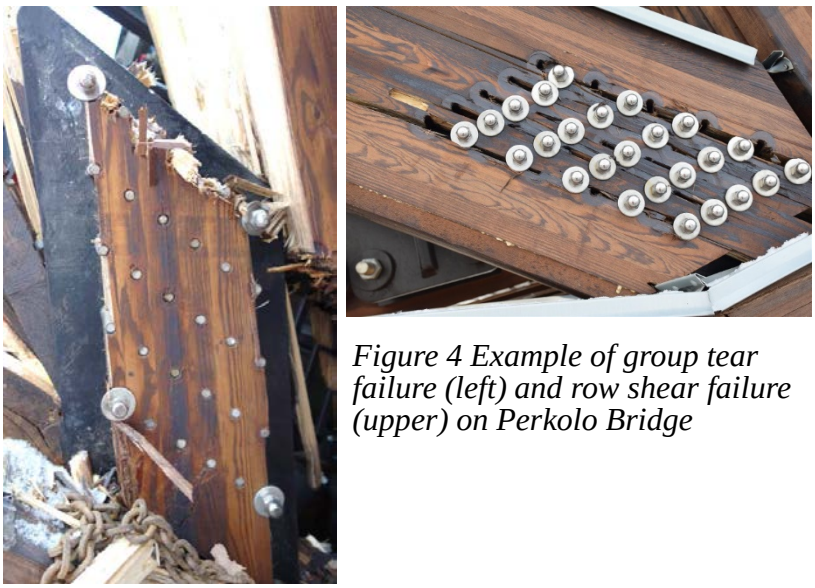

Figure 4 Example of group tear failure (left) and row shear failure (upper) on Perkolo Bridge

3.3 Spacing between dowels in angled connections

On some bridges the connections are at a very small angle. This raises a question on how to interpreted the rules in the code on the edge- and end spacing for dowels. Having a small angle results in a case where the distance from timber edge to dowel is much smaller when taken perpendicular to the cut surface than when measuring in the direction of grain or perpendicular to grain. As the code [2] only gives values on the grain and perpendicular to grain direction, no guidance is given on what the smallest edge distance should be.

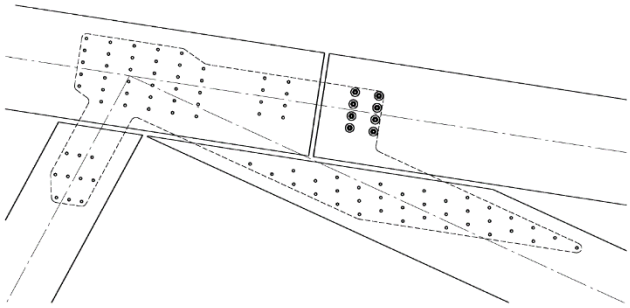

Figure 5 Example of a very angled connection on a timber bridge

Our recommendation is not to cut the timber within the a3-a4 rectangular part. We support an understanding of a reserved area around each connecter as show in figure 6 b).

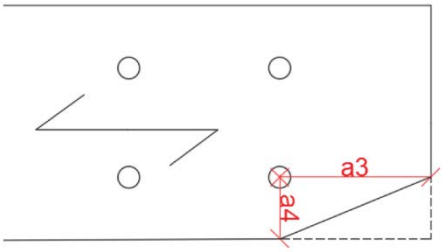

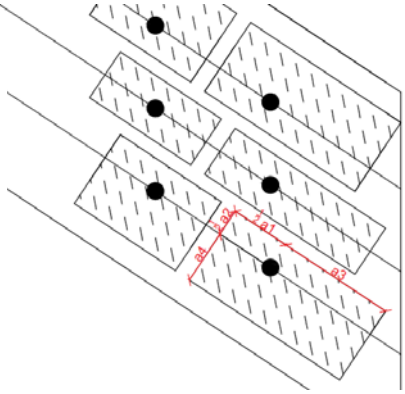

Figure 6

a) left: Cut within the a rectangle a3-a4 of the connection

b) right: Suggestion to an approach of reserved area around each connector

3.4 Very large connections

Timber bridges might be the timber structures with the largest connecters. The code [2] does to our knowledge not give any limitations on the size of a connection. Currently, the only size-dependent factor is that an increase in the distance a_2 between dowels gives an increase in capacity. At some point other factors such as temperature and moisture changes must play a role, such that an increase in or size of the connection must have an upper limit.

3.5 Simplified analysis of trusses

EN-1995 9.2.1 (5) requires a reduction of the utilization of capacity to 70 % when only doing a simplified analysis of a truss. What a simplified analysis is is not stated. Designers probably should at minimum take moments in connections into consideration when not reducing to 70% utilisation.

3.6 Ductility of connections

The code [2] gives guidance on failure resistance, but failure should also be ductile and on this matter no information is given. Preventing block shear failure from happening and tension perpendicular to grain are probably the best way of ensuring a more ductile behaviour. A report by Betkja and Blaβ [4] clearly shows the possibility to ensure ductile behaviour by reinforcing connections against splitting. This should be of interest to all bridge owners, as it probably would allow overloading to be more visible during inspection. Block shear failure could be designed against by introducing a safety factor for it. In reality this would result in connections with fewer dowels in a row probably resulting in trussworks that are more expensive as less timber is utilised, but also using lower quality timber would probably reduce issues regarding block shear failure.

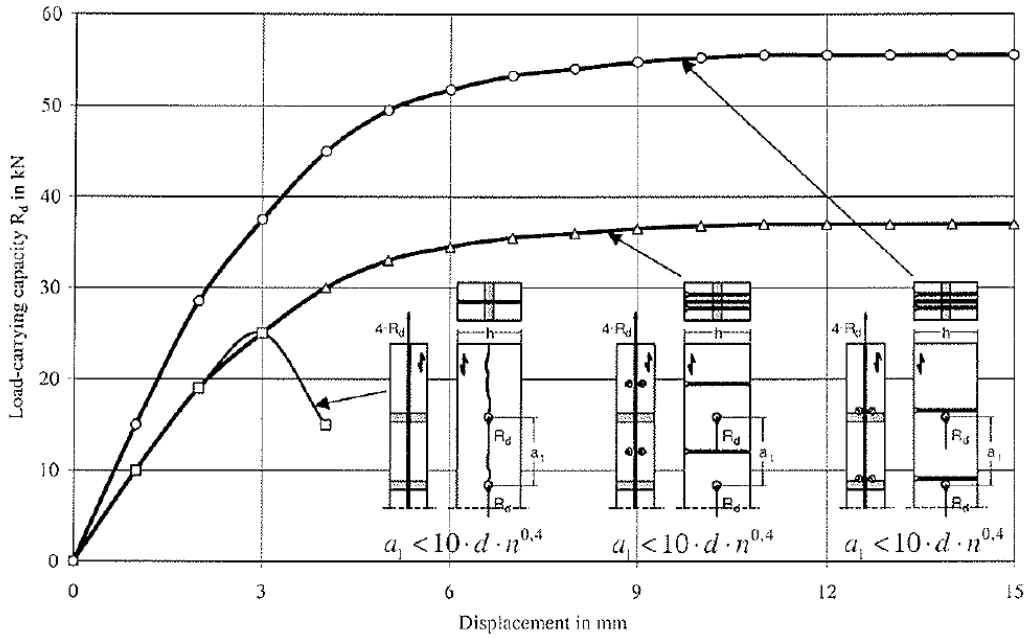

Figure 7 Different failure curves presented by Betkja and Blaβ [4] showing unreinforced and reinforced connections with screws.

3.7 Timber density and connections

EN-14080 *Requirements for glued laminated timber* [5] and also its predecessor [6] allow for very different beam layouts on combined glulam beams with respect to strength class. For bending properties, these different layouts may probably be equal. We do question whether this is fully correct when it comes to connections that often are centred in the middle part of a beam, the weakest part of a combined glulam beam. Using homogenous glulam beams for timber trusses and other structures with connections might be more convenient.
During the check for the timber truss bridges we also encountered some difficulties in recalculating older bridges by newer codes, especially on connections with regard to density properties. There have been several changes during the past 20 years when it comes to strength classes, and the same timber has been classified to different classes. Knowing what properties that can be assumed is difficult as different strength classes by different codes also have been using the same abbreviation. Further, for earlier Norwegian design codes [7] density wasn't part of the equation for dowels. Sorting classes seem to have been more constant and could be useful information to add to as-built drawings for later.

4. Conclusive remarks

Quite simple mistakes on timber truss structures may have disastrous consequences. For timber structures it might be a problem that not enough structures are calculated such that the level of competence by designers and third party controllers might be less than they are for example on concrete structures.

Work on check on all truss bridges owned by the NPRA with road traffic has not uncovered any more design faults, but questions have been raised on how to design timber trusses. This has probably been the first larger structural review of earlier built bridge structures in Norway and might have proven to be quite useful in terms of raising design awareness.

5. Acknowledgements

As stated, the paper is a result of the check on truss bridges aswell as discussions thereafter. A group consisting of the following did the check on timber truss bridges:
NPRA by Jon Henning Prestegarden (group leader)
NTNU by Kjell Arne Marlo and Kolbein Bell
Dr. techn. Olav Olsen AS by Øystein Løset
STRUCTOR by Erling Kristian Langbråthen
in addition to the authors of this article.

More people than mentioned above have contributed in the respective companies and furthermore Norconsult by Per Kristian Ekeberg participated partly.

Further discussions have also been within the NPRA and within the Norwegian comity for Timber Structures.

6. References

[1] Prestegarden, J et.l. «*Kontrollberegning av fagverksbruer i tre*», Norwegian Public Roads Administration report, September 2016.
[2] EN 1995-2:2004 Design of timber structures, part 2: bridges
[3] Ranta-Maunus, A and Kevarinmäki A, «*Reliability of Timber Structures, Theory and Dowel-Type Connection Failures*», CIB-W18/36-7-11, Colorado USA, 2003
[4] Bejtka, I and Blaβ, H J, "Self-Tapping Screws as Reinforcement in Connections with Dowel-Type Fasteners", CIB-W18/38-7-4, Karlsruhe Germany, 2005.
[5] EN-14080:2013 Timber Structures. Glued laminated timber and glued solid timber. Requirements.
[6] EN-1194:1999 Timber Structures. Glued laminated timber. Strength classes and determination of characteristic values.
[7] NS3470:1999 Design of Timber structures, design rules. Part 1 Common rules.

Bjørgum bridge, a roofed timber footbridge in Norway

Asmund Sveen
Project manager
Aas-Jakobsen
Oslo, Norway
asv@aaj.no

M.Sc. from Norwegian Institute of Technology from 1996

Joined Aas-Jakobsen in 1997

Trond Even Eggen
Project engineer
Aas-Jakobsen
tee@aaj.no

PhD. from Nowegian University of Science and Technology, 2000

M.Sc. from Norwegian Institute of Technology, 1993

Joined Aas-Jakobsen in 2010

Yngve O. Aartun
Chief Architect
Plan Arkitekter AS
Trondheim, Norway
yngve@plan.no

M.Arch. from Norwegian Institute of Technology from 1983. Joined the company Plan Arkitekter as a partner in 1996. Specialist in bridge aesthetics and timber bridges

Summary

The Bjørgum bridge is situated 8 km south of Voss in Hordaland county, Norway. It was finished in June 2015. The bridge is part of a new road system for pedestrians intended to provide safer access to nearby schools ad to reduce the need for school buses.

The bridge is a roofed timber bridge where the main load-bearing system consists of two three-hinged glulam arches braced by truss diagonals and a top chord, giving the illusion of a truss bridge with curved chord geometries. These trusses are also the support walls for the roof, and they lean towards each other at an angle of 10 degrees.

The length and width of the bridge walkway is 44.0 m and 2.25m, respectively.

The bridge was ordered by the Norwegian Public Roads Administration, region West and the design is the product of a collaboration between PLAN arkitekter AS and Aas-Jakobsen AS.

Keywords: Timber, truss, arc, roof, footbridge

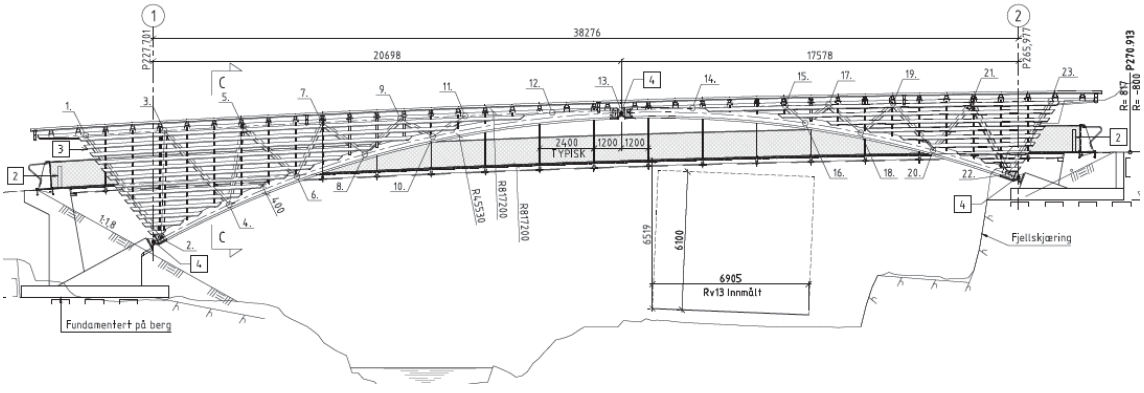

1. Concept

Figure 1 Bjørgum bridge

Bjørgum Bridge is a slender and elegant structure which has been very well received by its users. The positive experience is enhanced by the comprehensive use of timber in the structure.

Before the bridge was built, there were walkways on both sides of county road 13, intersecting the road at a pedestrian crossing with limited visibility. The walkways have now been raised to meet the new bridge, and together they provide a natural choice for pedestrians to reach the other side of the road. The whole road system also caters to people with special needs.

Figure 2 Walkway system around the river Istad Crossing at Bjørgum

The river Istad is a part of the Vosso river system which is a designated national preserve. It is an important part of a landscape rich in variation and contrast, ranging from high mountains, through steep hillsides and deep valleys down to lowlands. Erection of the bridge has only had a negligible impact on the river.

The main load-bearing system of the bridge consists of two three-hinged glulam (glued laminated timber) arches braced by truss diagonals and a top chord, giving the illusion of a truss bridge with curved chord geometries. These trusses are also the support walls for the roof, and they lean towards each other at an angle of 10 degrees. The wooden walkway is suspended by steel hangers from the roof beams which in turn are supported by the trusses. It has stainless steel wiremesh railing on both sides, and these are attached to the hangers.

2. Durability

The bridge is designed for a 100 year life-span and all details are designed with this in mind. Emphasis has been put on diverting water away from the structure, and on ensuring that the wood will dry fast should it get wet. Venetian blinds have been mounted on both sides of the bridge as protection against weather, and the roof has a significant overhang throughout the entire bridge.

All glulam has been subjected to a double preservative treatment. First the individual lamellas have been given an impregnation by copper-salts prior to production of the glulam and then the entire glulam beam is given a light impregnation by creosote oils. The creosote oil treatment is performed after all machining of the glulam beams has been carried out.

The lower part of the frame is prepared for metal cladding (1 mm copper) should it be proved necessary in the future to prevent water from running down the diagonals and into the slotted joints. At this point, the cladding is not installed.

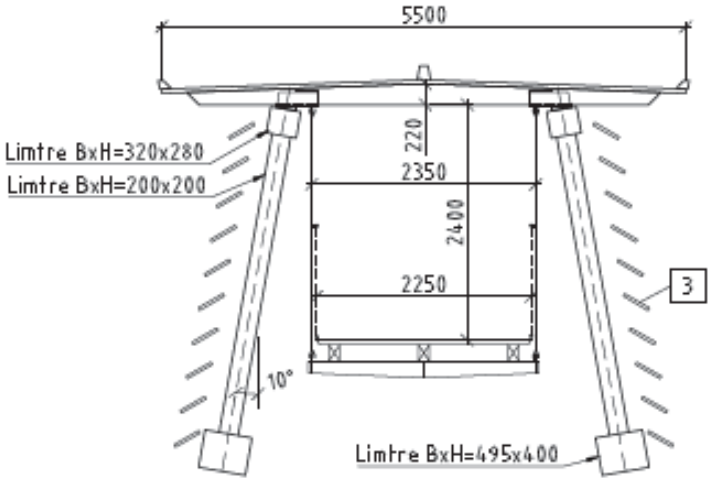
5500
220
2350
2400
2250
Limtre BxH=320x280
Limtre BxH=200x200
3
10°
Limtre BxH=495x400

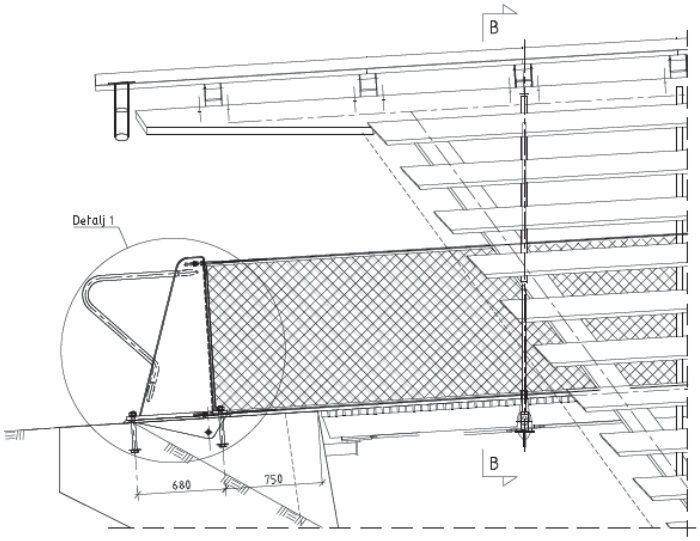
B
Detalj 1
680
750
B

3. Technical description

3.1 BIM-model

Figure 3 BIM-model of Bjørgum bridge

Due to the complexity of its geometry, it was decided to create a 3D model as basis for the design of the bridge. TEKLA has proven a good tool for this in other project, and was chosen as the modelling program.

Emphasis was put on making the model as accurate and complete as possible with respect to geometry, but also with respect to other information such as material properties. All reinforcement in the abutments was also modelled.

The design drawings were "harvested" directly from the 3D model, as were material lists and the bar bending schedule for the abutments. The model was of substantial assistance during the quality assessment of the tender documents, due to the direct link between what was shown in the tender documents and what could be visually inspected in the model. It also proved an invaluable asset in discussions of solutions and details within the design team.

The glulam manufacturer was given the model as part of the design documentation. Due to lack of compatibility between the formats of TEKLA and the format used by the CNC machines used for machining the glulam members, the use of the model for the manufacturer was limited to:

- Support for "understanding" the structure
- Making plans for installation
- As basis for drawings
- Quality assessment of own production drawings

3.2 Analysis

The bridge was designed according to the Eurocode Design Codes. Since the walkway is covered, it was deemed not necessary to design it for service vehicle loads, and barriers are indeed placed at both ends of the walkway to prevent any vehicles from entering. Thus, the bridge was only designed for load from pedestrians in addition to environmental loads from snow and wind.

A 3D model in Focus Konstruksjon was used for static design of the structure, whereas dynamic checks were performed using NovaFrame.

Figure 4 Computation model in Focus Konstruksjon used for analysis and design

3.3 Structural behaviour

Bjørgum bridge is a roofed timber bridge where the main load-bearing system consists of two three-hinged glulam (glued laminated timber) arches braced by truss diagonals and a curved top chord, giving the illusion of a truss bridge with curved chord geometries. These trusses act as support walls for the roof, and they lean towards each other at an angle of 10 degrees.

The roof is built as a rigid plate, transferring horizontal forces on the structure to the steel frames that connect the abutments to the roof at both ends of the bridge. Horizontal bracing under the walkway transfers transversal forces on the walkway to the glulam arches and the abutments.

The walkway is suspended from the roof by steel bars and only transfers transversal forces to the glulam trusses at the two points where the walkway and the glulam arch intersect.

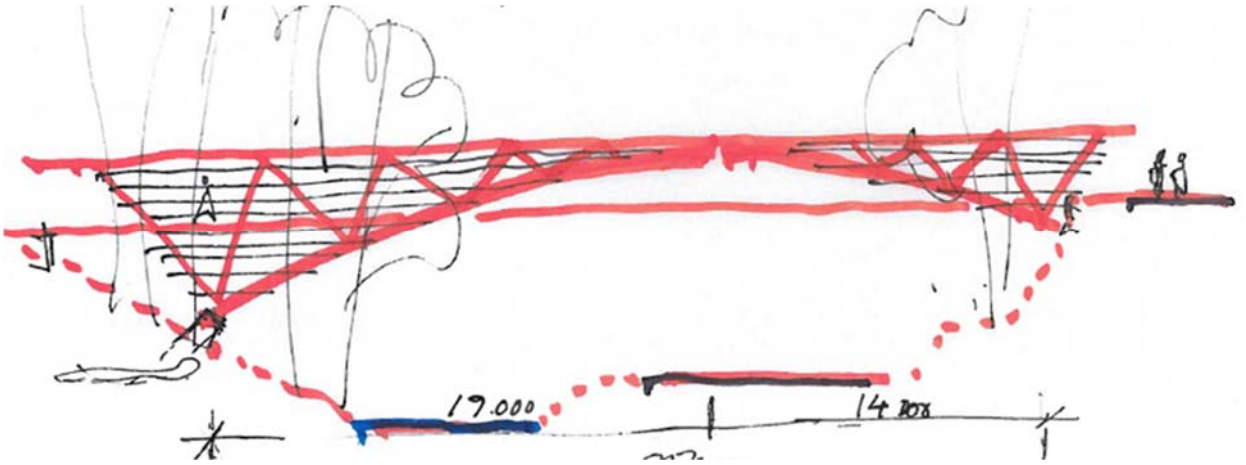

Figure 5 Architectural conceptual sketch

Figure 6 BIM model

Figure 7 Finished bridge

3.4 Details

The walkway:

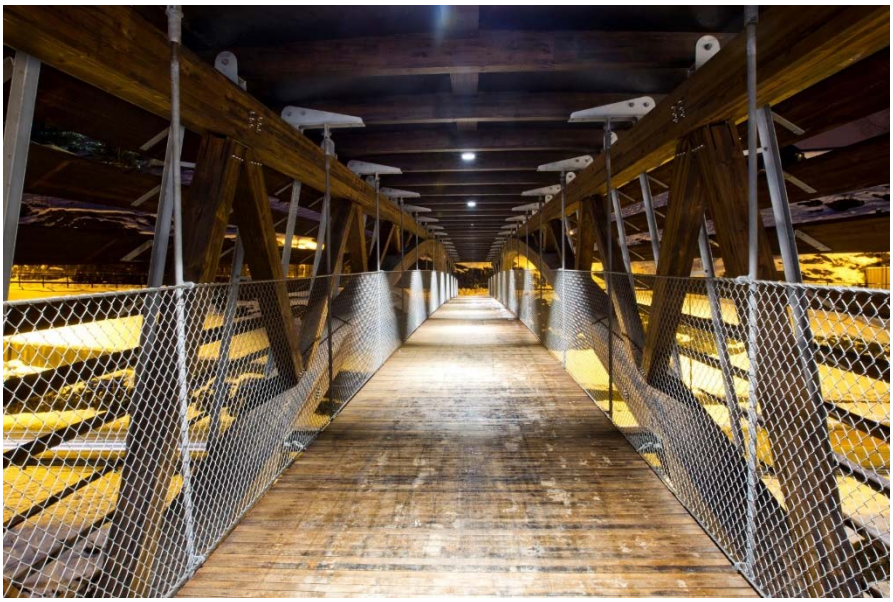

The wooden walkway is suspended by steel hangers from the roof beams. It has stainless steel wiremesh railing on both sides, and these are attached to the hangers.

Details of the roof and the upper bracket for the hanger and the lower fastening for the footpath are shown below (photo and from the BIM-model).

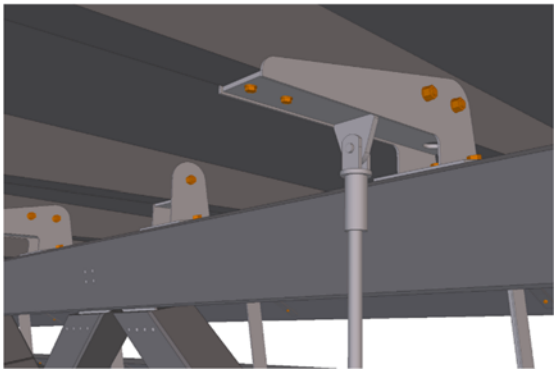

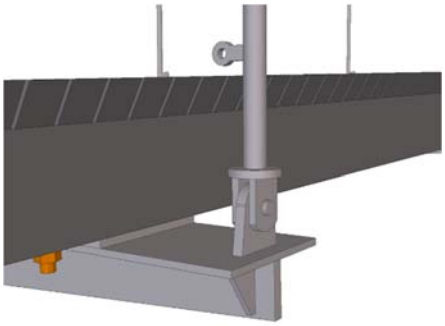

Bracing:

Under the footpath: The horizontal stabilizer system for the footpath, made of steel-crosses and glulam.

Venetian blinds:

Venectian blinds have been mounted on both sides of the bridge as protection against weather, and the roof has a significant overhang throughout the entire bridge. All glulam has been subjected to a double preservative treatment.

4. Fabrication and assembly

The contractor for this bridge has been Moelven Limtre (glulam).

The foundation of the concrete abutments are established directly on bedrock.

The glulam structure was machined and tentatively assembled at the Moelven glulam factory, before all the components were sent for creosote oil treatment and then on to the building site.

The whole bridge is assembled at the construction site.

The 4 parts of the truss come pre-assembled complete with venetian blinds installed. The trusses are hoisted in place one by one by use of a mobile crane.

After the main bearing system has been erected, roof joists and the walkway are assembled before the roof is installed.

Figure 8 Construction of Bjørgum bridge seen from the air. Photo S. Ulvund

Field condition assessment of the first vehicular timber bridge in Korea, Hanareum Bridge

Sang-Joon LEE
Research Scientist (ph.D)
National Institute of Forest Science
Seoul, Republic of Korea
lsjoon@korea.kr

Kwang-Mo KIM
Research Scientist (ph.D)
National Institute of Forest Science
Seoul, Republic of Korea
lovewood@korea.kr

Kug-Bo SHIM
Senior Researcher (ph.D)
National Institute of Forest Science
Seoul, Republic of Korea
kbshim@korea.kr

Summary

Interests in wood and wooden culture including timber structures have been raised up in Korea. As an example of the efforts of National Institute of Forest Science (NIFoS), the first vehicular timber bridge in Korea, Hanareum bridge, was completed in December 2012. DB-24 grade of Korean highway bridge design code with thirty meter long and eight meter wide timber bridge was built. To ensure long-term structural safety of the bridge, field assessments including static and dynamic field loading test and periodic monitoring were conducted for two years. Loading test in 2013 and 2014 proved that the bridge possessed its symmetricity and structural safety. Additionally, the initial finite element model of the bridge was also verified based on these test results. The model can be used for long-term health assessment of the bridge. Up to now, the bridge shows sound status, however long-term monitoring of the bridge can discover potential problems and can be effectively used for setting the next projects of vehicular timber bridges. The monitoring and field assessment of the bridge is planned till 2018, and we believe that this can help not only monitoring the structural safety of Hanareum bridge but also conducting field assessments of possible future cases of timber bridges.

Keywords: Hanareum bridge, Vehicular timber bridge, Field condition assessment, Monitoring

1. Design of the bridge

In 2009, the National Institute of Forest Science in Korea launched a research project for the design of a timber bridge. It started as the development of a bridge deck floor 30m in length. In this design, glue laminated timber (glulam) was used because it can be manufactured in a wide range of shapes, which is appropriate for the construction of a bridge deck floor with a relatively long span. In this research, the pre-stressed glulam deck floor system was designed based on the design guideline by USDA. The required level of pre-stressing and design assumptions such as symmetric behaviour and non-separation at laminated faces were identified and verified.

Following the development of the pre-stressed glulam deck system, research on girder bridges was initiated in 2010. Girder bridges with two lanes and 25, 30 and 35m in length were developed. A sawn lumber deck floor system was adopted for the girder bridge, which was designed with a series of rectangular panels and was supported by 5 main girders. A design and analysis program for the girder bridge was developed and the design procedure was established. The structural behaviours of the bridge design were verified numerically through detailed 3D finite element analyses.

Based on the previous research, comprehensive research for the first vehicular timber bridge in Korea was started in 2011. The research project included the whole process including design, manufacturing, laboratory test, field test, and the construction of the bridge. Among the various bridge types, an arched truss structure was selected for a 30m single-span bridge due to the advantages of structural efficiency and aesthetic value (*Fig. 1*).

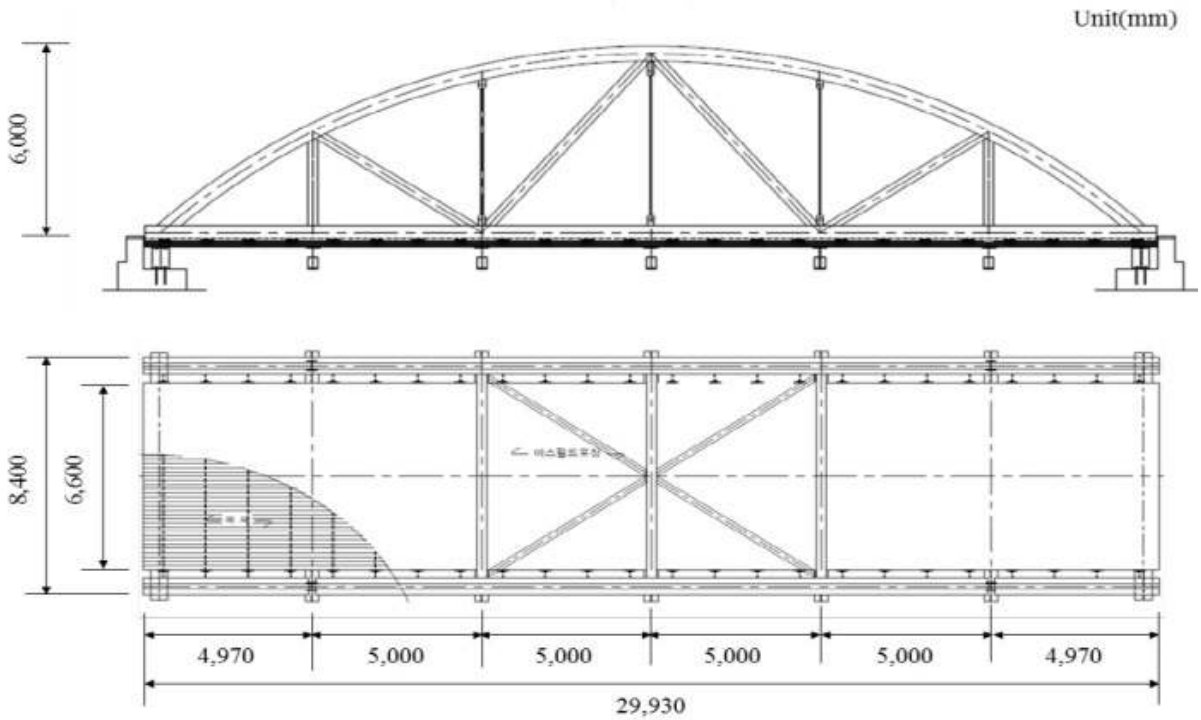

Fig. 1 Longitudinal section and floor plan of bridge designed in 2011 (Named Hanareum bridge)

The main members of the arched truss were made of glulam, and dowel-type joints are used to connect the main members. The vertical members of truss, cross beams, pre-stressing elements, dowel plates and components to assemble were made of steel while the other main members are all made of wood. For the glulam deck system, stressed-laminated system, which was researched in previous studies, was chosen, due to the advantages of prefabrication, installation, and maintenance. A total of 5 cross beams were laid beneath the deck at the intervals of 5m to support the deck floor and to transfer the load from the floor to the truss members. An additional two cross beams were also installed to seat the bridge on the abutments. A number of codes, specifications and guidelines were used to design the truss, joints and other detailed parts of the bridge and the allowable stress

design method was applied. For the material of the main glulam members, pitch pine was chosen because it is one of the most common species of trees in Korea, would be predicted to provide cost-effectiveness for the bridge. Korean Industrial Standard provides the mechanical properties of symmetric laminated pitch pine timber as shown in *Table 1*, classified according to grade of strength. Among them, 10S-30B grade materials were selected for the bridge.

Table 1 Mechanical properties of symmetric laminated pitch pine timber(KS F 3021)

Grade of strength	Allowable Stress(MPa)				Modulus of elasticity(MPa)	
	Flexural		Axial		x-x axis	y-y axis
	x-x axis	y-y axis	Tensile	Compressive		
12S-37B	12.0	8.0	8.0	10.0	11,000	10,000
12S-33B	11.0	7.5	7.0	8.0	10,000	9,000
10S-30B	10.0	7.0	6.5	7.5	9,000	8,000
9S-27B	9.0	6.0	6.0	7.0	8,000	7,000

Using the above research, an arched truss timber bridge for vehicle was completely manufactured and tested in the laboratory before being constructed at the field.

2. Structural performance assessment

Structural performance was assessed with finite element analysis program; MIDAS Civil 2006.This program has strength of infrastructural because it specialized in civil structural analysis. FE model was made of geometry model with timber deck, timber truss member, and steel vertical truss member and load model with DB-24 and self-weight. This paper describes about structural performance of the timber bridge so that the results were classified with timber truss and timber deck.

2.1 Bridge deck performance

Structural performance of bridge deck was analysed with bending moments due to live loads and maximum deflections. As deck was composed of orthotropic plate element model, specific stress data was calculated. Deck moment was computed regarding dead load and live load, respectively (*Table 2*).

Table 2 Results with design and analysis for deck

	Design Values	Analysis Results
Moment due to dead load	18.2 kN·m	13.4 kN·m
Moment due to live load	156 kN·m	111.1 kN·m
Maximum Deflection	12.95 mm	24.75 mm

Deck moment by dead load was 13.4 kN·m (*Fig. 2*). It was lower value than design value at the rate of 36%. In this case, the design value was calculated by Korea Bridge Design Specification (2010). Moment due to live load was 111.1 kN·m. It was also lower value corresponding to 40% of design value. This was why steel cross beam was omitted in the design model. The maximum deck deflection was 24.75mm. It was located at the center of the deck. The deflection shape was below *Fig. 3*.

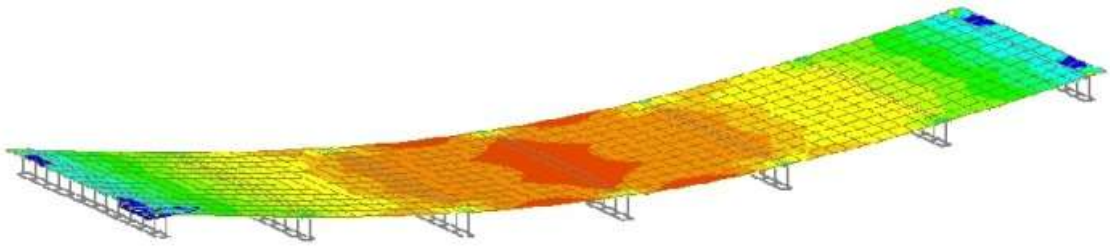

Fig. 2 Deck moment distribution due to dead load

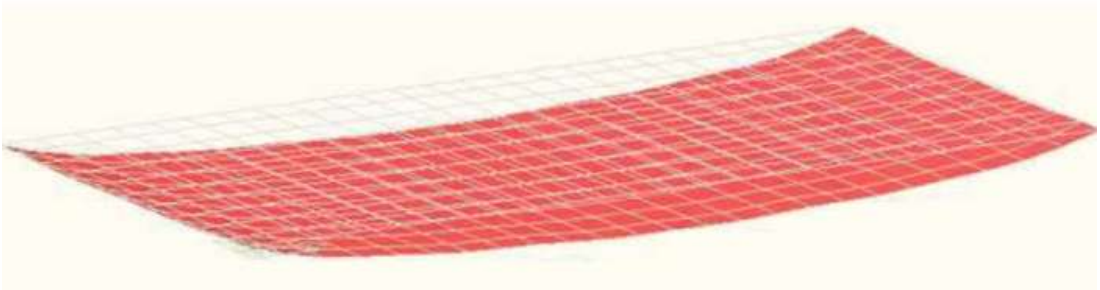

Fig. 3 Deflection shape of bridge deck

2.2 Timber hybrid truss performance

Truss structure performance was estimated by member forces and deflections. The truss structures were made of truss element so that member forces were defined only by axial forces. Finite element analysis was conducted in order to estimate structural behaviour of truss. As a result, member number 3 and 4 had maximum tensile force and number 18 and 20 had maximum compressive force. The number of members is presented in *Fig. 4*.

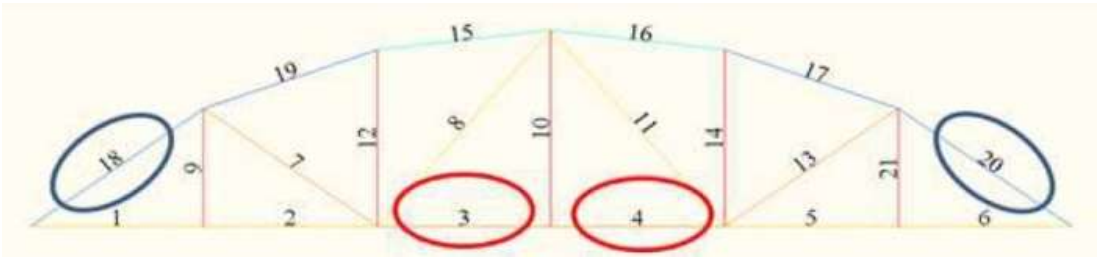

Fig. 4 Numbers of truss member

The force distribution was nearly symmetric because the geometry and load model was symmetric, but material model was orthotropic. The detail values were in *Table 3*. All the forces met the allowable stress standard. Comparing with analysis values, maximum tensile force was 91.05% of design values and maximum compressive force was 92.76% of design value.

Table 3 Truss member forces by finite element analysis

Member Number		Minimum	Maximum
3	Upper Chord	1555.811	640.953
4	Upper Chord	1556.196	940.970
18	Lower Chord	-743.937	-1845.840
20	Lower Chord	-743.888	-1825.920

These results are reasonable value because the design model was truss only design without plate and cross beam. It was 2D truss design model and other structural members were only components with point mass. For this reason, it is natural that 3D finite element model including all parts had more stiffness and analytic value was less than design value. Although the difference existed in the results, difference value was a little small because truss more endured live load which had larger value than dead load.

The maximum deflection occurred at the center of the lower chord, whose value was 30.907mm. The allowable deflection in the Korea Bridge Design Specification was 125mm. Finite element analysis result was only a quarter of design value so that timber truss was enough to play a role as a vehicular bridge and had durable for vehicle to pass through the timber bridge.

2.3 Discussions

Finite element analysis is a useful method to assess structural performance. It could be possible to handle very large scale structures and various conditions such as load condition and environmental condition, even treated behaviour in invisible side. This paper describes vehicular timber bridge assessment and it was the first vehicular timber bridge in Korea so that finite element analysis was a basic research about timber bridges.

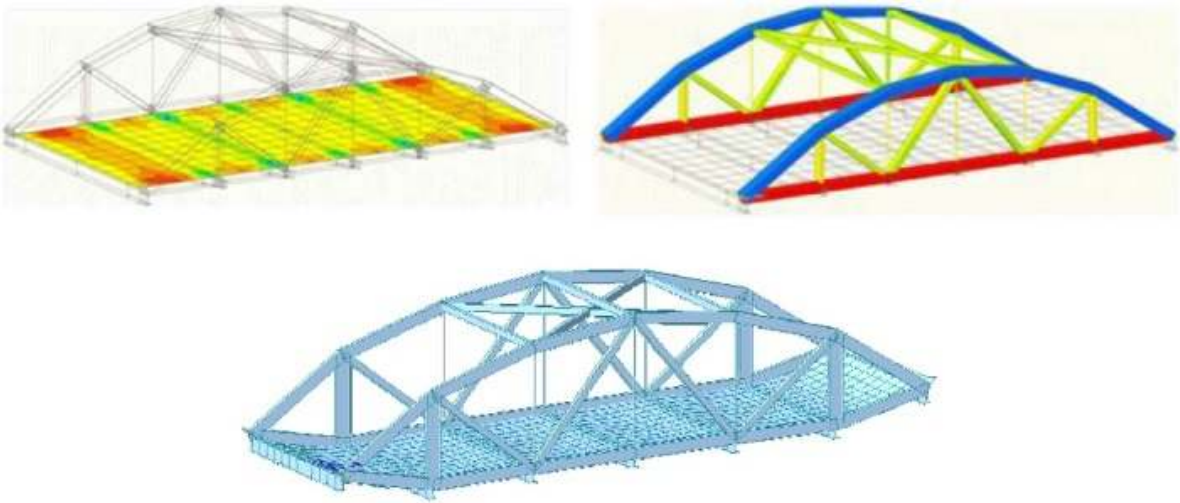

Fig. 5 Results of finite element analysis (deck bending moment, truss axial force distribution and defection shape)

Fig. 5 is a resulting summary of finite element analysis of the timber bridge. The first figure is about bending moment of deck. It was the main result about bridge deck because deck was modeled with orthotropic plate theory. Also, the second figure is about truss axial forces. Upper chords took compressive force, while lower chords did tensile force. The last figure is about deflection of whole truss bridge. These results met the allowable standard and were enough to endure vehicular load.

3. Field load testing

3.1 Construction of the bridge

After the laboratory testing, the bridge was disassembled for transport and reassembled at the construction site. The construction field was located at a forest road of the Micheongol recreational forest, an eastern mountainous region near Yangyang city, Korea. After the installation of a fence and asphalt pavement, the construction of the entire bridge was completed by December 2012, and has been open to the traffic since the official opening ceremony that was held in April 19, 2013.

Fig. 6 3D model of Hanareum bridge

This bridge, given the official name of 'Hanareum bridge', is 30m in length, 8.4m in width and has a maximum load capacity of 110t. As the first vehicular timber bridge in Korea, Hanareum bridge is expected to serve as the groundwork for the construction of many more timber bridges in the future and establishment of Korean design specifications for timber bridges.

In order for that to occur, it is important to assess the present performance of bridge and to apprehend the long-term behaviour like loosen pre-stressing, deterioration etc. Furthermore, it is required to examine whether the bridge performs as it was intended. Therefore, field testing including static and dynamic load testing was performed May 10, 2013.

Fig. 7 Construction of Hanareum bridge

3.2 Configuration of field load testing

The bridge was designed as a two-lane bridge with each lane loaded with a 43.2 ton truck. The loading tests were performed with two gravel loaded 27 ton trucks and corresponding calibration was conducted and the test results were compared to laboratory tests and design values. In order to assess the performance of the bridge and to obtain initial data for investigating its long-term behaviour such as loosen pre-stressing and deterioration, a series of static and dynamic load tests were performed in May, 2013.

The resulting deflections and strains at a series of locations were measured. One of main interests was the integrity of pre-stressed glulam deck. It was assumed that the laminated floor deck would

retain its integrity without the separation of the glulam timbers if the deck was pre-stressed properly. In order to verify this assumption of integrity, a total of 13 LVDT's were installed beneath the deck floor to get a detailed shape of deflections in the lateral direction (*Fig. 8-(a)*). In addition, three more LVDT's were installed across the center cross beam for measuring the mid-span deflection of the bridge (*Fig. 8-(b)*).

(a) Center cross beam (b) Deck floor

Fig. 8 LVDT sensor attachment locations

Strains at important locations were also measured. The locations were identified through finite element analysis, which resulted in a total of 7 locations with the largest strain: 2 of upper chord and 2 of lower chord and 3 of deck floor (*Fig. 9*). Two accelerometers for identifying natural frequencies were installed at the outer sides of bottom deck floor (*Fig. 10*).

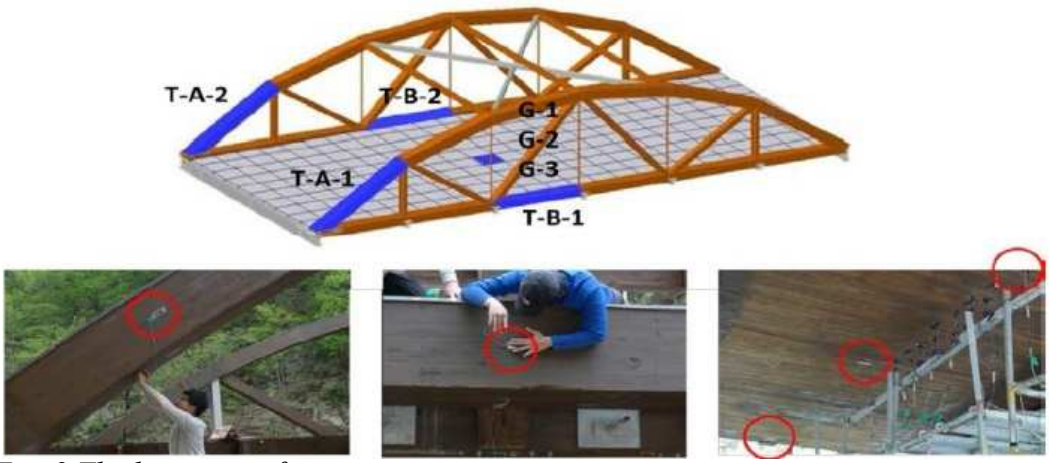

Fig. 9 The locations of strain gauges

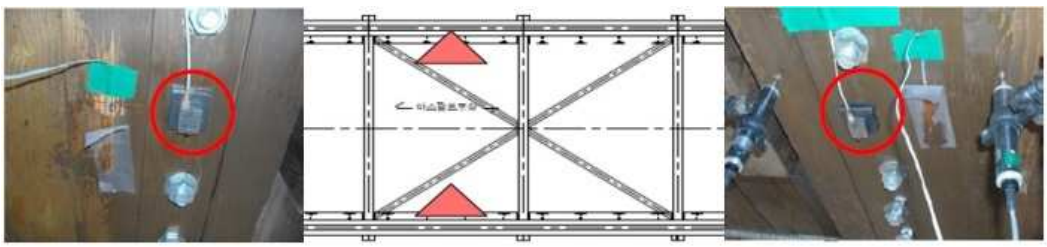

Fig. 10 The locations of accelerometers

In the static loading test, 6 load cases (LC1 - LC6) were set by positioning the truck alone, side by side, and in rows. And in the dynamic loading test, 6 load cases (LC7 - LC12) were set also by letting truck cross the bridge at speeds of 5km/h, 10km/h and 20km/h through each lane (*Fig. 11, 12*).

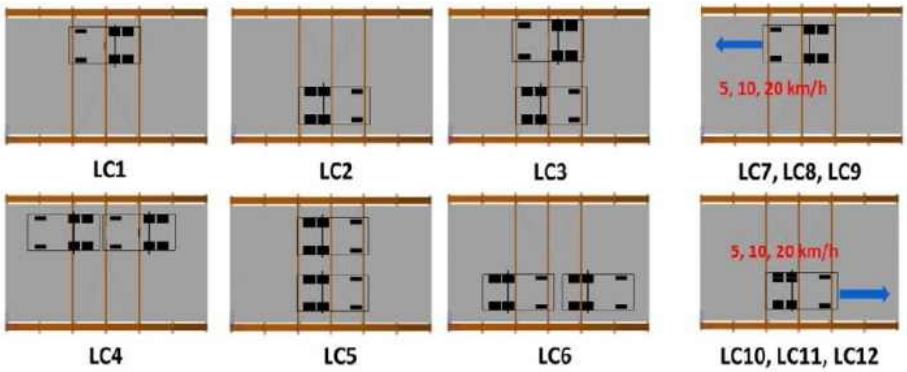

Fig. 11 Load cases for static(LC1-LC6) and dynamic(LC7-LC12) loading test

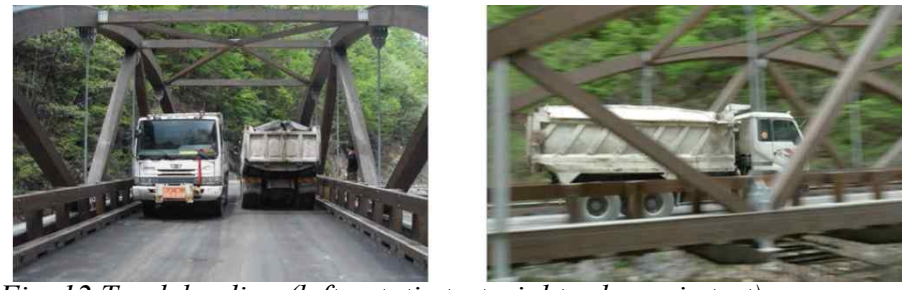

Fig. 12 Truck loading (left : static test, right : dynamic test)

3.3 Results and discussions

The results of the static loading tests are plotted in *Fig. 13*. The displacements of the deck floor and the cross beam at the mid span are compared with their corresponding analysis responses. For a single lane load case, LC2, the results from the laboratory tests were also compared.

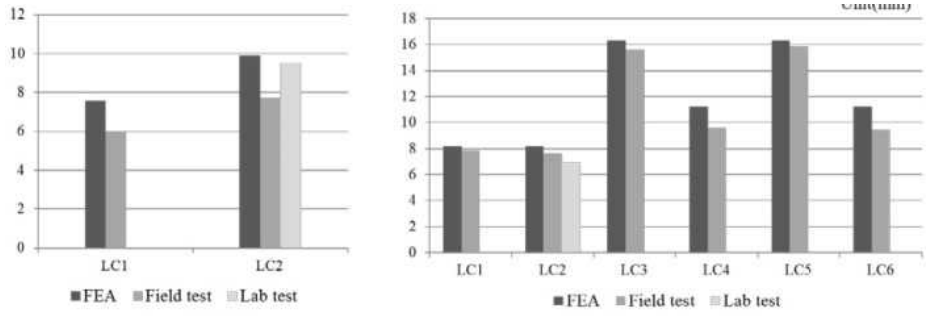

(a) Deck Floor *(b) Center cross beam*

Fig. 13 Maximum vertical displacement for static loading cases

As shown in *Fig. 13*, in general, good consistency was observed between the finite element analysis results and those of the field tests. Larger deflections in the finite element analysis are noted for all the cases, which can be explained by differences in the finite element model and the bridge structure. For example, the connections between timbers were modelled as hinge joints while the bridge has strong connections with dowel plates and bolts which can transfer flexural moment. Furthermore, asphalt pavement and fence, which can strengthen the stiffness of bridge, were not included in the finite element model. This overall stiffness increase is also observed in the comparison of deck floor deflections between laboratory and field test results of LC2.

The purpose of LC3 is to verify the linear behaviour by comparing it with superposition of LC1 and LC2. As shown in table 6, the load-deflection relationship is found to be linear, and the maximum difference between LC3 and LC1+LC2 is 0.3mm.

Table 4 Maximum deflections of cross beam for LC1, LC2 and LC3 (mm)

	LC1	LC2	LC1+LC2	LC3
Left	4.3	7.1	11.4	11.1
Middle	7.8	7.7	15.5	15.4
Right	7.3	4.5	11.8	11.9

The symmetry of right and left lanes is investigated by comparing the deflections of the center cross beam for single lane loading case pairs LC1-LC2 and LC4-LC6, which are single truck and double truck loading cases, respectively. A double lane load case of LC5 was also investigated and the test results are shown in *Fig. 14*, The results indicate that the symmetry of the deflection responses are well maintained, which can be considered to be an indication of the integrity and good quality of the construction of the bridge.

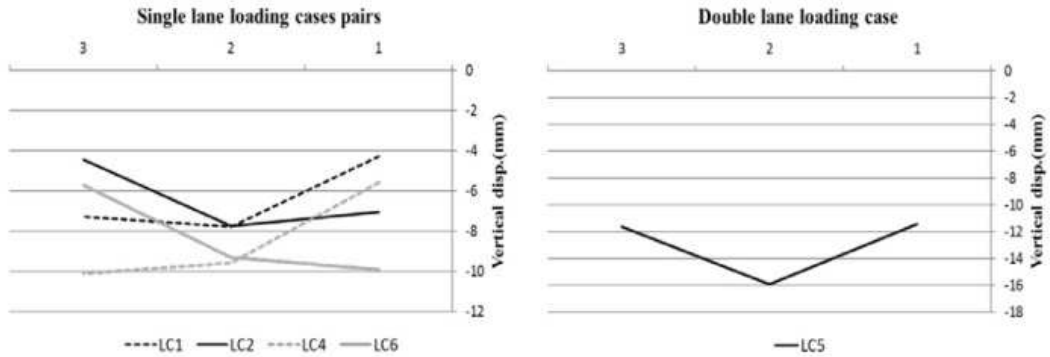

Fig. 14 Deflections of center cross beam for static loading cases

The natural frequencies of the bridge deck were identified from acceleration responses in dynamic loading tests. The first and second mode frequencies were 5.16Hz and 9.06Hz respectively (*Fig. 15*). Those results will be verified through a refined finite element analysis in further research.

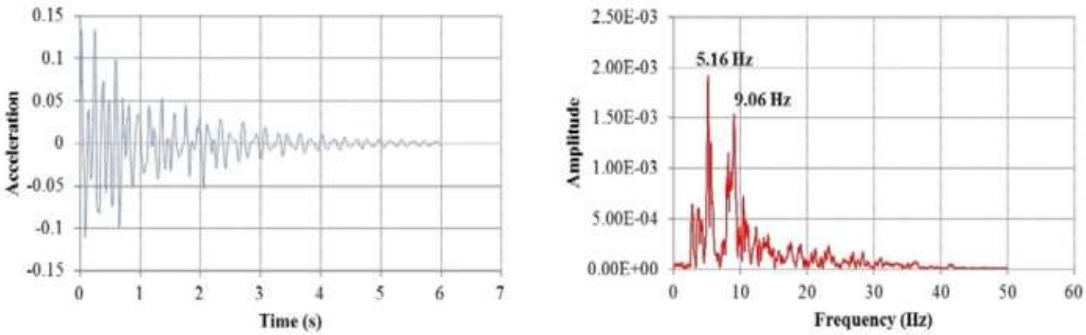

Fig. 15 Acceleration response and its frequency spectrum

In the dynamic loading test, the impact factors were also investigated. The impact factor, defined as the ratio of additional dynamic displacement to corresponding static displacement, depends on the condition of road surface, driving speed, structural characteristics, ratio of live load to dead load, and nature of the response, etc. In this study, for the different speeds of trucks, the maximum vertical displacements of the center cross beam at the crown were measured to calculate the impact factors. The results are depicted in *Fig. 16*. The largest impact factor was evaluated as 0.198 for 20km/h of the 1st lane. These dynamic test results will be analysed through a further analysis using refined 3D finite element model in a future project.

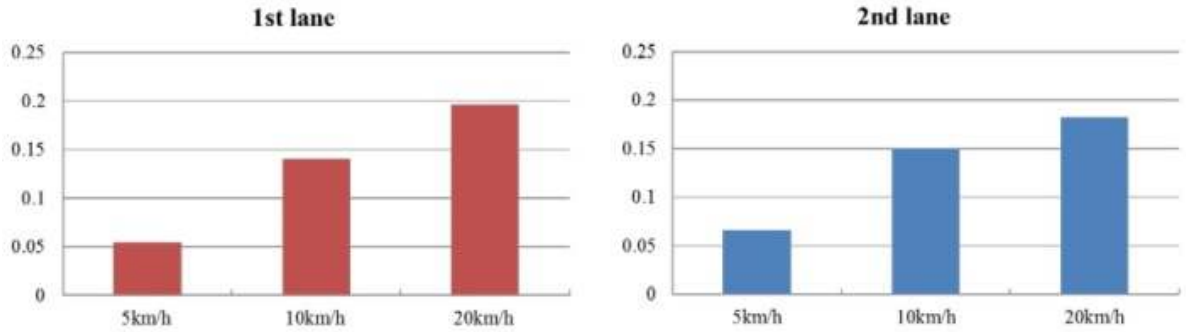

Fig. 16 Impact factors for dynamic load cases

4. Conclusions

Recent research and development activities for the construction of the first vehicular timber bridge in Korea are presented. The results of laboratory and field tests indicate that the manufacturing and fabrication quality of timber members is excellent, and that the bridge can perform as designed.

For the further research, a refined 3D finite element model which reflects the current status of the bridge will be established based on the results of the field tests. To investigate the long term behaviour of the bridge, periodic load testing is planned and the finite element model will be updated based on the corresponding results. The updated model will be used to assess current performance and to establish an appropriate maintenance plan for the bridge.

It would be expected that the successful construction of the Hanareum bridge will lead to the development of more vehicular timber bridges in Korea in the future. The development of new design specifications for timber bridges in Korea is also in the planning stages

References

[1] AASHTO, AASHTO LRFD Bridge Design Specifications, 4th edition, 2008 Interim Revisions, Section 9: Decks and Deck System. Washington, D.C. American Association of State Highway and Transportation Official, 2008.

[2] American Forest & Paper Association, Inc, National Design Specification for wood construction ASD/LRFD, United States, 2005.

[3] Architectural Institute of Korea, Design Manual for timber structure, 2008.

[4] Architectural Institute of Korea, Korea Building Code, 2005.

[5] Korea Concrete Institute, Korea Structural Concrete Design Code Commentary, 2007.

[6] Korea Road and Transportation Association, Korea Bridge Design Specification, 2010.

[7] Lee S. J., Shim K. B., Kim K. M., Kim S., Choi Y.S., Shin H. K., Han Y and Park M. J. : Condition Assessment of The First Vehicular Timber Bridge in Korea. Proc. of the World Conference on Timber Engineering, 2016.

[8] Ritter M. A. : Timber Bridges – Design, Construction, Inspection and Maintenance. 1990.

[9] Shim N. H., Kim D. K.., and Park Y. S. : An Experimental Study for Structural Evaluation of Timber Truss Bridge, Korean Society of Civil Engineers Magazine, Vol.60(9): 52-62. 2012.

[10] Shin Y., Kim K. M., Lee S. J., Park M. J., Yi J. W. and Goh H. M : Structural performance assessment of the first vehicular timber bridge in Korea, Proc. of the World Conference on Timber Engineering, 2014.

[11] Yi J. W., Park W. S., Kim C. Y., Lee S. J., and Koh H. M. : Field Loading Testing of the First Vehicular Timber Bridge in Korea, Proc. of the Intl. conference on Timber Bridges 2013, USA, pp. 337-346. 2013.

Network arch bridge with glulam arches. Lessons learned and further development

Johannes Veie
Senior Principal Engineer
Norwegian Public Roads Administration
Parkgata 81, 2317 HAMAR
Norway
johannes.veie@vegvesen.no

M.sc. in structural engineering from NTH Trondheim 1996. Worked with steel and timber bridge planning since 2000 at the Norwegian Public Roads Administration.

1.1 Summary

In September 2016 the new Steien bridge in Norway opened. The bridge carries two lanes of traffic and two pedestrian lanes and has a single span length of 88 meters. The bridge consist of laminated timber truss arches, network cable system made of steel and a reinforced prestressed concrete slab working as a tie for the arches. The bridge is the first of its kind with glulam arches and has the longest span length in the world for a timber arch bridge.

This paper gives a general description of the bridge and reports the lessons learned from the construction of Steien bridge. The paper also reports the development of a new medium span network arch bridge that is similar to the Steien bridge, but with single arches and integral or semi-integral abutments.

Keywords: Timber bridge, glulam, network arch bridge

2. Introduction

The most recent milestone in the development of timber bridges in Norway was the opening of the Steien bridge, having the world's longest span carried by glulam arches. The bridge is a network arch bridge with trussed glulam arches with a span of 88.2 m and a concrete bridge deck. Since the construction process was as expected and within the planned financial framework, the project has laid the foundation for developing a new type of small and medium-sized network arch bridges in timber that can compete with more traditional solutions.

3. Steien Bridge (Steibrua)

Steien Bridge [1] &[2] is situated in Alvdal municipality. Alvdal is located in Hedmark County, 380 km north of the capital Oslo. The bridge is located in highway 3, which is one of the main roads connecting the east and mid-Norway. Daily traffic is about four thousand vehicles. The bridge crosses the river Glomma and is a new landmark for the village Alvdal.

Figure 1. Steien bridge

The bridge is designed with traffic loads according to EN-1991-2 and with a 100-year design-life.

The network arch bridge has a single span reaching 88 metres. The bridge deck is made of reinforced pre-stressed lightweight concrete that also serves as the tie for the arches. The slab carries the tension load, which is in balance with the arch compression force. The vertical loads acting on the slab are distributed to the arch through 68 tension rods in the system of crossing hangers. One of the main benefits of using this type of bridge in this specific location is addressed to the slenderness of the deck structure. A normal beam bridge would have required the whole road to be elevated to a higher level to overcome a 200 years flooding. The adjusted level would correspond to the height of the girder. The bridge carries two traffic lanes and two 3-meter wide pedestrian walkways.

3.1 Design for the new Steien Bridge

Preliminary studies for the replacement of the existing Steien bridge showed that a network arch bridge where competitive to other relevant alternatives. The tender matching the cost estimates also confirmed this.

The bridge, ref. figure 1 to 2, has a single span width of 88.2 meters and arches that rise 15 meters above the bridge deck. The bridge carries two traffic lanes with a total width of 8 meters and two 3-meter wide pedestrian walkways. The total width of the slab is 19.8 meter.

Arches made of rectangular glulam sections define the bridge. The wind bracings are made of glulam sections in combination with compression steel bars. All glulam elements are treated with both creosote and copper impregnation. The crossing hangers are made of solid steel bars. The arches are inclined 7 degrees inwards.

Figure 2. Steien bridge

The lightweight concrete slab with pre-stressing is made of in situ cast on temporary scaffolding

Zink plates cover the top of the glulam elements.

3.2 Fabrication, transportation and assembly

The bridge was assembled on site. A temporary bridge was placed prior to the demolition of the existing bridges. The abutments and slab were completed before the arch was mounted.

The glulam elements were produced and pre-assembled at the glulam factory. Each arch were divided into four elements supported temporarily by columns rising from the bridge deck, ref. figure 3. Each element was transported to the site complete with steel parts. After the assembly of the hangers connecting the arch and the slab, the framework was lowered and removed.

4. Lessons learned from the construction of Steien Bridge

In general, all operations were performed as planned. There were few surprises. The production of the glulam elements were well within given tolerances. The challenges that were pointed out in the design phase also showed to be those observed under the construction. One of the challenges were addressed to the lowering of the slab. The initial camber of the slab was larger than normal since the tension rods were installed in an un-stressed condition. One lesson learned is that using this method to install and stress the hangers gives a demand for preparing for a large vertical stroke length for adjusting the columns in the scaffolding that carries the framework, and that the lowering must be

done in several rounds to avoid overstressing of the scaffolding.

After the removal of the framework and mobilizing of the hangers, it is preferred to use a jack to check the forces in the hangers. In the case of Steibrua a method based on monitoring the frequency of the tension rods in order to calculate the force was tested. This method is commonly used for instance cable stayed bridges and works well in those cases. In the case of Steien bridge with relatively short tension rods as hangers, the stiffness of the end connections and mass and position of intermediate couplers affects the frequencies in such a way that there is a challenge to get reliable values.

Figure 3. Steien bridge. Installation of truss arches

5. Further development

The consept of Steibrua with truss arches can be used for bridges with larger spans. Next level would typically be spans in the range of 90 to 150 meters. At the present moment it is more focus on the development of new small to medium span network arch bridge types which has similarities with the Steien bridge, but having a more simple design with single arches and integral or semi-integral abutments. These bridges compete with traditional bridges made of steel and concrete.

Examples on such designs are two bridges that in 2017 are under detail planning aiming to start construction in 2017/2018. The first is Hellefossen bridge located in Oppland County spanning 70 meters across the river Etna, and the other is Prestmyrbakken bridge in highway Rv 25 situated in Elverum municipality spanning 35 metres over an access road.

5.1 Hellefossen Bridge.

The reason for choosing a network arch bridge with a slim deck, ref. figure 4, is because the river is covered by environmental protection regulations and it is not allowed to have foundations placed into the river. Another reason, similar to Steien bridge, is to avoid large fillings of the adjacent road due to limited distance from the dimensioning river flood to the top of the road. The bridge will carry two traffic lanes and have semi-integral abutments.

Figure 4. Illustration of Hellefossen bridge

5.2 Prestmyrbakken Bridge.

In this case, in theory, the bridge could be made as a classic arch bridge with a stress laminated timber deck. However, the deck is wide and the distance between the arches is more than 14 meters. This would give relatively tall steel beems to support the stress laminated timber deck. In addition, compared to a concrete deck, a timber deck would have to be elevated more than 1 meter higher above the underlying road to meet the design requirements for accidental loads from vehicles. This would lead to a less favourable road alignment, ref. figure 5.

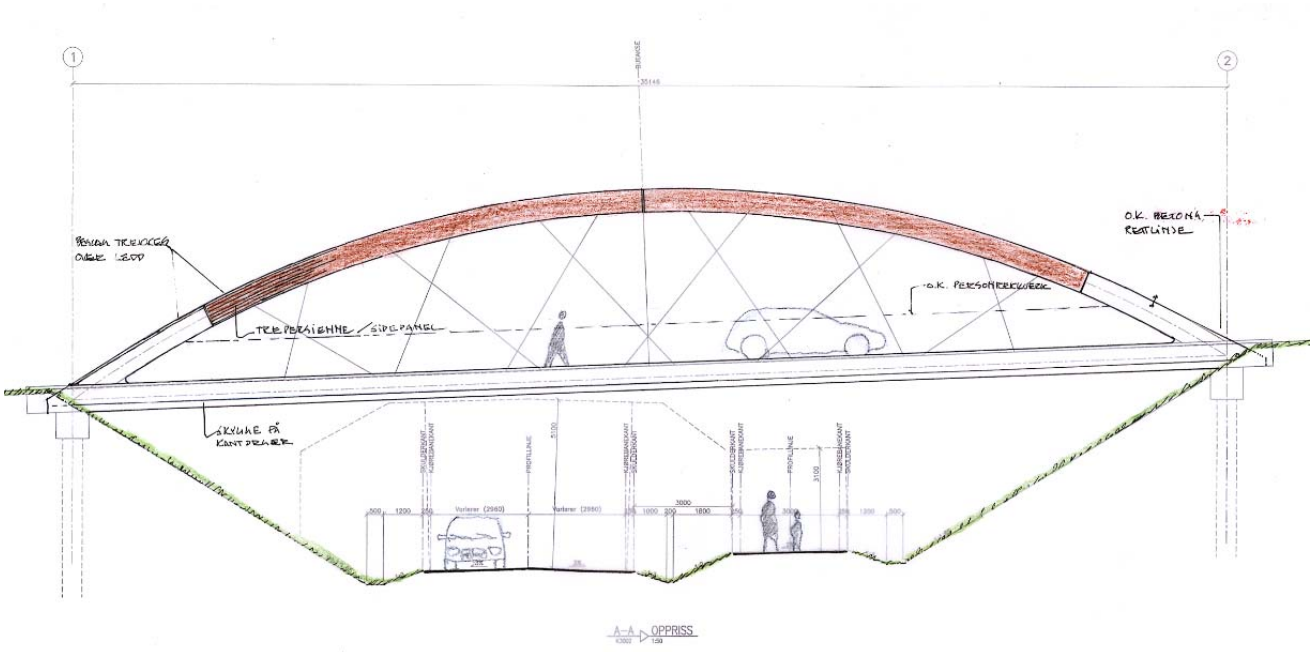

Figure 5. Artistic illustration of Prestmyrbakken bridge

6. Conclusion

The construction of Steien bridge as a timber network arch bridge has been performed without any major surprises and within the planned financial framework. This although the combination of wood, steel and concrete has not been done earlier in a network arch bridge. This project has prepared the way for coming network arch bridges with spans more than 100 meters carried by timber arches. Equally interesting is the possibility of making cost effective small and medium size bridges in the range of 35 to 80 meters that can compete with traditional bridges made of steel and concrete.

7. References

[1] Proceedings of the International Conference Timber Bridges, ICTB2013, Las Vegas, USA September 2013

[2] 21. Internationales Holzbau-Forum IHF 2015, *New dimensions in bridge construction in Norway*. J. Veie, T. A. Stensby, M. A Bjertnæs

Folding System for Timber Truss Bridge

Hideyuki HIRASAWA
Professor
HNCT
Hakodate, Japan
hide@hakodate-ct.ac.jp

Honomi ANSAI
Undergraduate student
Hokkaido Univ.
Sapporo, Japan

Jun TONUMA
President
Tonumaiwasaki Co. Ltd.
Hakodate, Japan

Research and education at Hokkaido Univ. in 1991-2004, Hakodate National College of Technology (HNCT) in 2005-. The Head of Department of Civil Engineering in 2016-. The member of the committe of timber engineering in JSCE in 2009-.

Summary

In Japan, there are so many natural disasters such as typhoon, earthquake, tsunami, rainstorm, landslide and so on in every year and everywhere from north to south. Some people are often isolated in mountain area when roads are divided by these natural disasters. There are a lot of cases in which a bridge is necessary immediately to carry essential commodities or to visit each other. To prepare these accidents, the authors have been developing emergency bridges using wood. A trial model of emergency bridge was designed and manufactured for laboratory experiments. This model, which is Howe truss type, succeeded in making its size compact. In this study, a new unfolding method using mechanical gear box is shown. It is possible to fold and unfold the bridge if only the operation of handling the gear is done in one side of the bridge.

Keywords: timber bridge, emergency bridge, truss bridge, folding, recovery

1. Introduction

Since Japan is located on the Pacific Rim earthquake belt, we are often attacked by big earthquakes and tsunami. In addition to earthquakes, natural disasters such as typhoon, pouring rain, debris flow, etc. descend on our country almost every year. Citizen's life is always influenced by these strong natural rages. Disasters sometimes shut off traffic and lifeline which are ultimately necessary to live for people. Small towns in mountain area are sometimes isolated by the natural disasters. They bring about inconvenient situation to our lives and economical activities even if our towns are not isolated.

For example, the Great East Japan Earthquake of March 11, 2011 and Tsunami made a lot of bridges broken. Therefore, the condition of the trafficability in the area near the seaside got worse and people were forced to take indirect routes. One of the routes after the Tsunami is 50 km longer than the direct route. As another example, the flood in Tochigi, north area of Tokyo, in 2015 was very big and serious. *Fig. 1* shows a broken road bridge which has a short span. A heavy flow of the river runs against the abutments at the left and right sides. The bridge dips and a car and people can not go over it. *Fig. 2* shows a foot bridge which is broken by a big flood. A span in the middle of the bridge was washed away. Grass and trees are entangled in the handrails and piers, which means that the flow was terrible. In this photo, we can see a high riverbank backward. It can be seen that the height of water at the flood is almost the same as the riverbank due to the condition of the entanglement of grass and trees.

Fig. 1 Broken road bridge

Fig. 2 Broken foot bridge

The reason why there are so tremendous disasters in Japan is because the bed slopes of rivers are generally very large as well as a large amount of rain. The distance between the mountain area and the coastal area in Japan is very shorter than that of continental flat land countries. A great deal of water by heavy rain flows in short river from mountain area and gives destructive disasters.

If once a bridge is destroyed by the disaster, a small town in mountain area sometimes is isolated and becomes an out-of-the-way place since the long-term isolation brings serious damage to daily life and economy, rapid recovery is absolutely necessary. In this case, an emergency bridge is required to be constructed quickly. If there is a matter of life-and-death by the disaster, the time of the construction should be as short as possible. The place to assemble the bridge must be restricted right after the disaster in addition to the time. Therefore, this study presents a new emergency bridge without construction time and assembling space.

2. Concept of the Bridge

The bridge presented here is, totally new type, the folding bridge. This bridge can be carried by a middle size track because the size of the bridge is very small under the folded condition. It is folded under transporting, and it is unfolded at the construction site. To develop the bridge, the following conditions are considered and settled[1, 2].

2.1 Conditions of Processing the Member of the Bridge

1) Material is timber for structural use, ready-made and distributed in the local market.

2) Complex processing timber is not necessary and processing time is as short as possible.

3) Necessary strength at the connection is given by bolts and steel plate.

4) Preservatives are not used because of short-term bridge for emergency.

2.2 Conditions of Transportation and Construction.

1) The bridge can be carried by only one track in folding condition.

2) Unfolding time is very short on site.

3) Construction work on site can be done by a small number of workers.

4) Heavy equipment and special tools are not necessary to construct.

5) Only one worker or a small number of workers can operate the bridge to unfold.

3. Folding and Unfolding System

3.1 Rotation Axis on Folding

If we fold some truss panels, two axes of rotation in the truss plate can be considered, one is vertical rotation axis, the other is horizontal rotation axis as shown in *Fig. 3*, where *x*-axis is the direction of bridge span and *y*-axis is the direction of bridge width. The height of a truss is the same before and after unfolding in the type with vertical rotation axis. In the condition of the bridge unfolded completely, the bending stiffness is sufficient. On the other hand, the height of the bridge with horizontal rotation axis becomes lower as it is unfolded. In the condition of unfolded, the stiffness of the bridge becomes small. Therefore, the type with vertical rotation axis is adopted in this study.

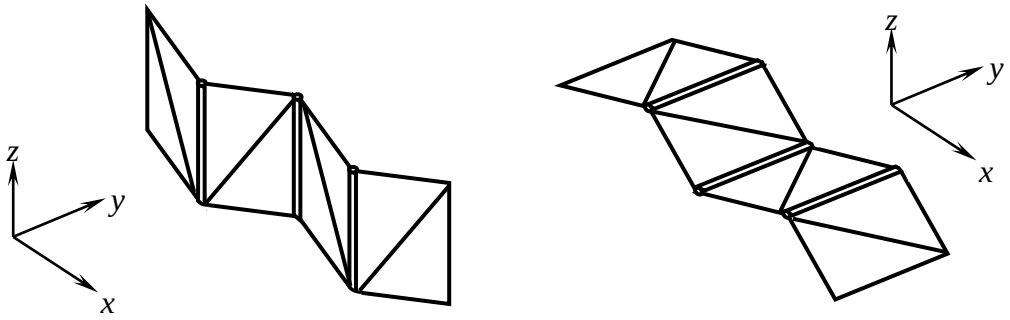

(a) Vertical rotation axis (b) Horizontal rotation axis

Fig. 3 Folding directions

3.2 Scissors Structure and Gear Box

It is necessary to set a device to fold and unfold the bridge as shown in *Fig. 3*. As an easy and simple mechanical device, scissors structure shown in *Fig. 4* is presented in this study. In *Fig. 4* (a), *x*-direction is bridge span direction. If the part *A* at the end of the scissors is moved *y*-direction by a hand power, the scissors are unfolded as shown in *Fig. 4* (b). At first, a trial model of scissors structure is made and checked unfolding movement. *Fig. 5* is the trial model made of 180mm wood bars. As a result of moving this scissors, it is good for moving that the number of bars of scissors is small[3].

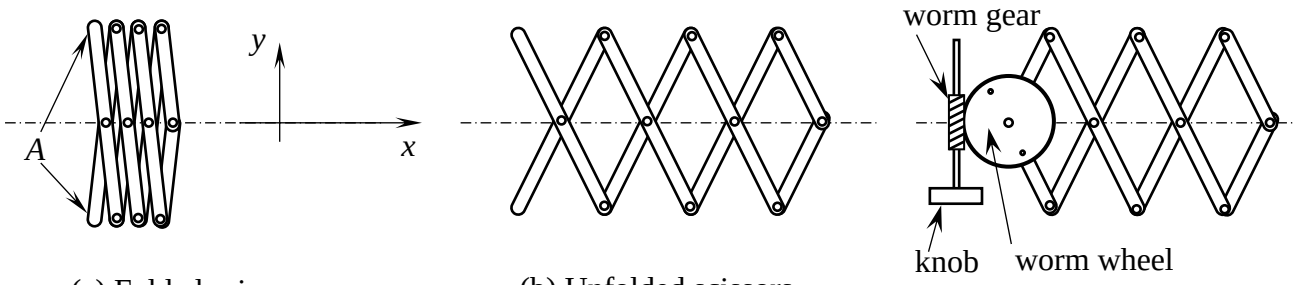

(a) Folded scissors (b) Unfolded scissors (c) Gears attached to scissors

Fig. 4 Scissors structure

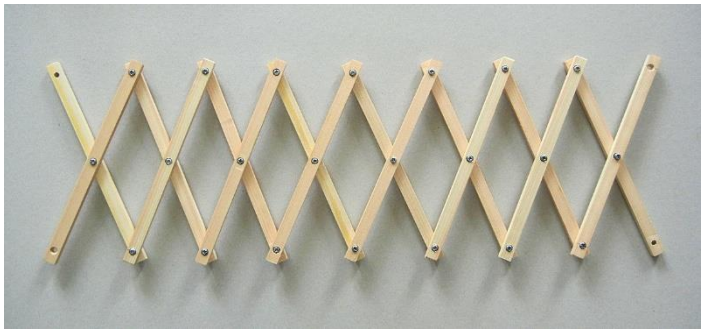

Fig. 5 Trial model of scissors

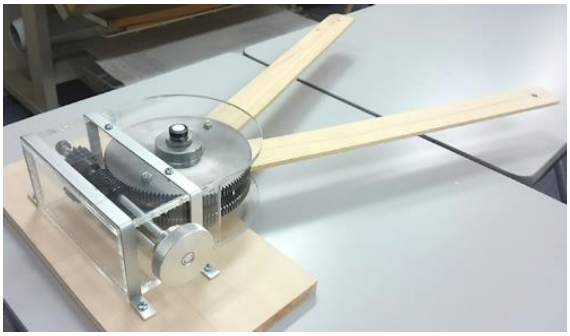

Fig. 6 Gear box and scissors

In order to unfold the scissors by a small hand power, a mechanical device composed of worm gears and worm wheels is developed in this study as shown in *Fig. 4* (c). The worm wheel is attached to the part *A* shown in *Fig. 4* (a) and it can rotate the end bar. To rotate the worm wheel, the operation is only to rotate the worm gear by using the knob. These gears are included in the box made by transparent plastic plates as shown in *Fig. 6*.

3.3 Positioning of Members Considering Folding

To make the bridge compact in size after folding, it is important to consider the position of structural members. It is necessary for a structural member to avoid striking another member each other at folding operation. Here, positioning a cross beam between the both lower chord members in truss bridge is shown.

Fig. 7 shows plane views of parts of truss bridge at the unfolded condition expressed by Step 1, on the way to folded condition by Step 2 and at the completely folded condition by Step 3. A double-circle shows a hinge connection between the lower chord member and the cross beam or between the two lower chord members. The condition as shown in Step 3 should be noted. The cross beam gets out of lower chord members to the outside. Width of this projection is the same as cross beam's width. In this folded condition, the cross beam prevents the folded bridge from becoming compact.

In order to improve this trouble condition, the position of hinge connection points between the cross beam and the lower chord member is changed. Step 1 in *Fig. 8* shows the new connection type which is Type-B. This small change brings a large effect on making the bridge compact after the bridge is folded. As shown in Step 3 in *Fig. 8*, the cross beam is kept in the line of side surface of the lower chord member. Here, the width of the cross beam and the lower chord member are the same. In this study, Type-B is adopted as a connection type between the cross beam and the lower chord member.

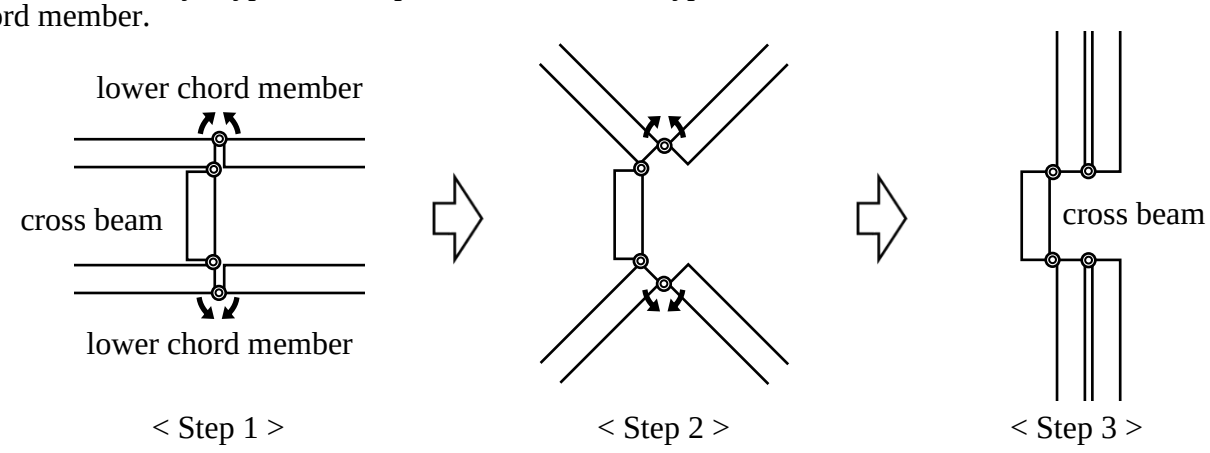

Fig. 7 Folding process of Type-A

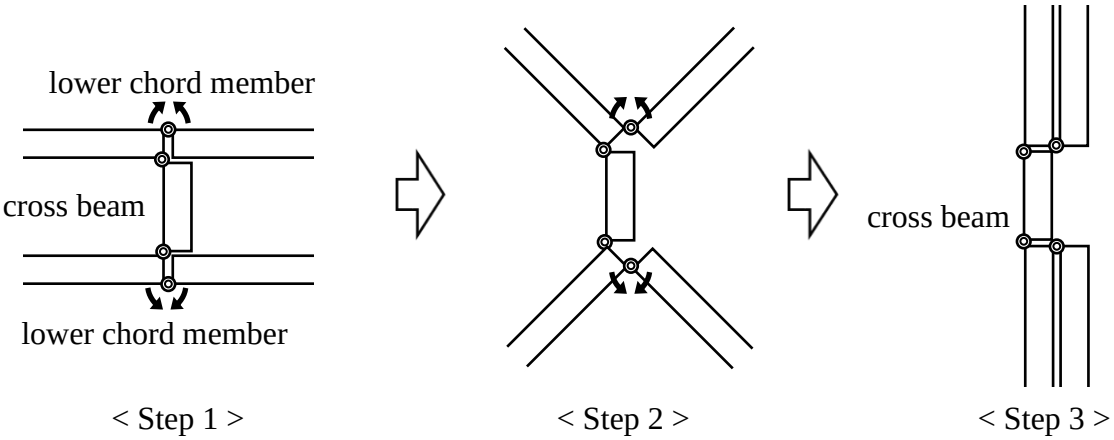

Fig. 8 Folding process of Type-B

4. Bridge Model

4.1 Shape of the Model

The model designed and manufactured is shown in *Fig. 9*. This is a one fifth scale model of a Howe truss foot bridge. Scissors are attached to the bottom of the truss structure. A large triangle frame is settled at the left end to make a fixed support of cantilever. Until the right end lands on the other side, this bridge is cantilever structure. After landing, this bridge becomes a structure with simple supports. It is necessary to have strong connection against the dead load at the left fixed point and against the dead load and live load at the mid-span, for a full scale real bridge.

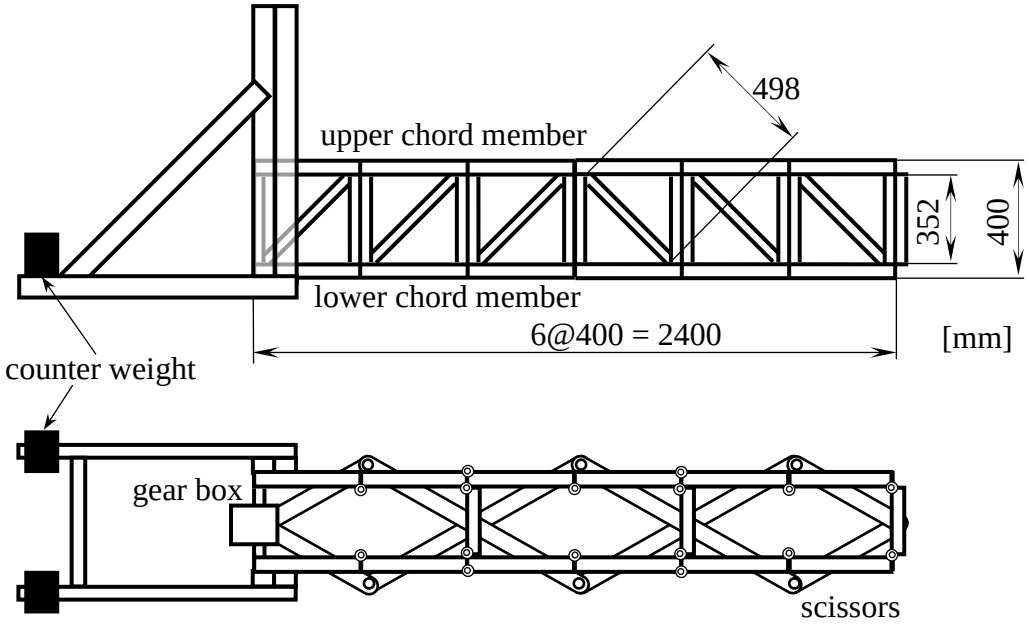

Fig. 9 Bridge model in the unfolded condition

4.2 Structure of Fixed End

A large triangle frame as a role of fixed end in the boundary condition is shown in *Fig. 9*. This triangle consists of a tall column, 1.0m high, a horizontal member and a diagonal member, which are connected by screws. A large size frame is necessary for the truss not to go down during unfolding operation. This column has a structure which can fold like a door with hinges. The end of the truss girder is connected to the column like this door, and can open or close with the move of folding or unfolding for the truss girder. Counter weights are put on the triangle frame to resist the end moment by the dead load. In the real condition, it has to be considered that the counter weight is also carried together with the truss girder by a track. Instead of carrying the weight, the track can play a role of counter weight by treading the horizontal member of the frame.

5. Unfolding Tests

Unfolding tests were performed by applying the rotation to the knob with hand power. At stage 1 in *Fig. 10* (a), folded condition, the bridge is very compact. If the knob is rotated, the bridge structure begin to extend slowly. To extend the bridge to the half length of the bridge span as shown in *Fig. 10* (b) Stage 2, the knob needs to be rotated 8 times. Stage 3 as shown in *Fig. 10* (c) is the condition of the truss girder entirely unfolded. The knob needs to be rotated 21 times to extend the bridge to this condition.

This is a cantilever truss beam and the maximum moment acts on the column of the triangle frame. In this whole structural system, the maximum force acts at the connection point between the upper chord member and the column of triangle frame, where the max axial stress is at the upper chord member, the max shearing stress is at the bolts and column. Any fractures do not occur at this point since the whole truss bridge is not heavy.

(a) Stage 1

(b) Stage 2

(c) Stage 3

Fig. 10 Unfolding tests

After the unfolding action, the free end of the truss girder can touch the abutment in real condition. At this time, the structural system changes from a cantilever girder to a simple girder. The type of this bridge as shown in *Fig. 10* (c) is Howe truss which is suitable for a simple supported timber truss bridge.

If the rotation is applied to the knob, the worm gear rotates and gives the rotation to the worm wheel. The rotation power of worm wheel becomes greater than that of worm gear, although the rotation speed of worm wheel becomes slow. However, on the contrary, if rotation is applied to the worm wheel by the external force such as dead load of the bridge or wind load, the worm wheel cannot give the rotation to the worm gear. The transferring the rotation between the worm gear and worm wheel is irreversible. The worm gear prevent the worm wheel from rotating. This will be good for the construction of the real emergency bridge safely because the unfolding operation does not influenced by external forces.

According to the construction site, the direction of unfolding may be upward or downward. It is possible to unfold in both direction since the rotation power is sufficient.

6. Conclusions

A new type of bridge for recovery from natural disaster is developed. One fifth scale model of the bridge is made from timber and tested to check its unfolding movement. The unfolding movement of this bridge is done smoothly by the movement of worm gears and worm wheels. In the folded condition, it can be carried by a middle size track even if it is designed in full scale size. The next problem of this study is to make the hinges between truss members strong enough for the full scale bridge.

Acknowledgement

The authors would like to acknowledge the financial support of Grants-in-Aid for Scientific Research (C, 15K01267) by Japan Society for the Promotion of Science to this study.

References

[1] Hideyuki H. and Taiga S., "Development of disaster emergency bridge to be constructed instantly", Proceedings of the 14th Symposium on Use of Wood for Civil Engineering, Vol.14, 2015, pp.86-89.(in Japanese)

[2] Hideyuki H., Tomoya Y., Jun T., Tetsuya S. and Hiroshi W., "Timber Truss Bridge for Cascade Use", WCTE2012, 2012.

[3] Hideyuki H. and Kasumi S., "Development of unfolding structure in folding emergency bridge", Proceedings of the 15th Symposium on Use of Wood for Civil Engineering, Vol.15, 2016, pp.46-48.(in Japanese)

Performance evaluation of the cross laminated timber for the bridge decks

Yusuke ARIYAMA
Engineer
RETEC Enginreeing Inc.
6-4-2, Akasaka, Tokyo
Japan
ariyama@retec.co.jp

2008 graduate school of science and engineering at Tokyo Denki University
2008 RETEC Engineering Inc.

Takanobu SASAKI
Professer
Inst. of Wood Tech., Akita Pref. University
Noshiro, Akita, Japan
taka@iwt.akita-pu.ac.jp

Tomoyuki HAYASHI
Professer
Inst. of Wood Tech., Akita Pref. University
Noshiro, Akita, Japan
tomoyuki_hayashi@iwt.akita-pu.ac.jp

Atsushi TOYODA
Chief Engineer
SUNCOH Consultants Co. , Ltd.
1-8-9, Kameido, Koutou-ku,
Tokyo, Japan
a.toyoda@suncoh.co.jp

Humihiko GOTOU
Professer
Faculty of Engineering and Resource Science, Akita University
Akita, Japan
gotou@gipc.akita-u.ac.jp

Katsuhiko TAKAMI
Associate Professor
Faculty of Engineering,
Yamaguchi University
Ube, Yamaguchi, Japan
takami@yamaguchi-u.ac.jp

Shogo ARAKI
Chief Engineer
HATTORI Engineer Inc. Co. , Ltd.
2-2-12, Miroku, Aoi-ku
Shizuoka, Japan
s-araki@hattori-eng.co.jp

Summary

Cross-laminated timber (CLT) is a light-weight construction material, superior in terms of transportability and workability. Applications of CLT slabs include those in civil engineering e.g., soundproofing and bridge decks; however there are no such practical implementations in Japan. This study focuses on the bridge deck application of CLT slabs and examines its potential as an alternative material for concrete bridge decks used in repair work of existing bridges. Repeated load tests and dynamic wheel load tests were conducted to evaluate the fundamental performance of CLT slabs for bridge deck applications of road bridges. The deterioration of wood due to decay is of the highest concern in using CLT slabs for this application. If this deterioration can be prevented, high long-term durability is expected. CLT slabs with improved durability owing to waterproofing treatment were used for a test construction of a forestry road bridge in March 2017.

Keywords: CLT, bridge deck, fatigue test, durability

1. Introduction

There is a total of approximately 700,000 bridges with a minimum length of two meters in Japan. A little over 20% of these are 50 years or older, with approximately 70% estimated to reach this range over the next 20 years. Approximately 70% of the 700,000 bridges are currently managed by municipal governments. The economic burden on municipal governments will be considerable. The development of economically superior construction methods has become a matter of urgency, since an enormous number of bridges will require repairs in the future.

Bridge decks made of cross-laminated timber (CLT), which is a new wooden material, are lighter, stronger, and offer superior workability. This material enables reductions in the cost of steel girder enforcements, and early liberation of traffic lanes owing to improved workability by reducing the load on the main girder. It is expected to form part of the construction method for repair and replacement of bridge decks. It has been reported that CLT slab have been adopted as bridge decks in Scandinavia[1].

Fatigue tests of the form of presumed car loads driving over the bridge repeatedly must be performed prior to the use of CLT slabs as an alternative bridge deck material to concrete. Wheel load tests, with presumed loads of T-14 load (wheel load: 56 kN) and T-25 load (wheel load: 100 kN), were performed to verify the fatigue durability of the material.

The CLT bridge deck was adopted on a trial basis for a newly constructed forestry road bridge, since sufficient performance of the CLT bridge deck was verified for the repeated loads.

2. Test method

2.1 Repeated-load tests

Japanese cedar CLT slabs, comprising 5-layer 7-ply boards of 3,600 mm length, 900 mm width, and 180 mm thickness were used for the repeated load tests (Fig. 1). A resorcinol resin adhesive was used for the laminate adhesion of CLT slab. The repeated load tests were performed using a method involving repeated loading of a concentrated load at the center of a 3-m span between supports. A hydraulic servo fatigue tester (with capacity of 100 kN) was used, as shown in Fig. 2. The loads and displacement of the center were measured. During testing, the load was applied in stages of 17% (20 kN), 25% (30 kN), 33% (40 kN), and 42% (50 kN) of the maximum bending failure load (118.8 kN) derived from a bending failure test using center-concentrated loading on 5-layer 7-ply Japanese cedar CLT slab of the same dimensions, while observing the extent of the damage on the specimen. Furthermore, the targeted load was loaded during the tests using displacement control, since the tester used was not capable of controlling the load. The frequency for the repeated loading was set to 1.0 Hz.

Fig. 1 Laminate composition of CLT slab

Fig. 2 Repeated loading test of CLT slabs

2.2 Dynamic wheel-load tests

The load position was relocated for the case where the design traffic load was applied continuously to perform dynamic wheel load tests to reproduce actual drive-overs by wheel loads. This was for the purpose of verifying the fatigue durability with respect to the traffic loads, which is one of the required performance capabilities of the bridge decks. The design calculation for the actual bridge was performed for the assumed case of replacing steel bridge decks (with a distance between bridge girder centers of approximately 2 m) with CLT bridge decks. Japanese cedar CLT 7-layer 8-ply slabs with a length of 4,000 mm, width of 2,000 mm, and thickness of 240 mm were fabricated for the purpose of these tests. The specimens were secured by bolting CLT bridge decks to the steel H-girders, as shown in Fig. 3 and Fig. 4. The bridge decks were linked by metal joints at the center in the direction of the bridge axis. The wheel load was set to 56 kN (load of one rear wheel for the design load of 140 kN) and 100 kN (load of one rear wheel for the design load of 250

kN), and each of these loads was applied by driving 100,000 round trips to take measurements of the displacements and the strain behaviors of the CLT bridge decks.

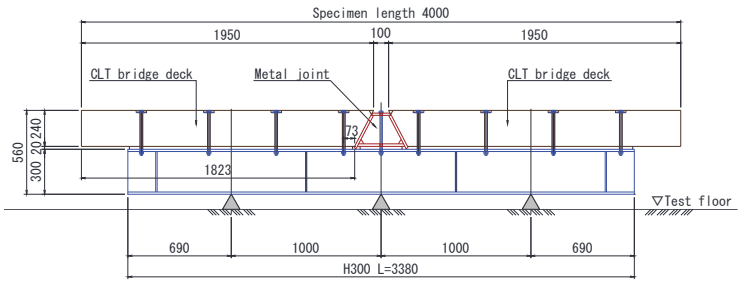

Fig. 3 Specimen for dynamic wheel load test

Fig. 4 State of dynamic wheel load test

3. Test results

3.1 Repeated-load tests

The relationship between the number of repetitions and the loads, as well as center displacements, is shown in Fig. 5. Loads of 17% (20 kN) and 25% (30 kN) of the maximum load, which is the presumed design load level, were applied repeatedly in stages of three million times and four million times, respectively; however, no cracks or adhesion peels were observed in the test specimen. Because the tests were conducted using the displacement control method, it is evident that while the center displacement remained constant, the load declined as the number of repetitions increased. This is surmised to have been due to the bearing stress generated on the specimens at the supporting and loading points, the displacements of which accumulated and led to the same load not being applied even when the input displacement was given; as a consequence, the load gradually decreased.

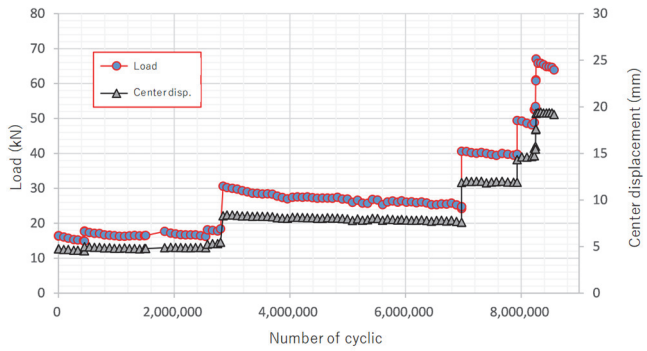

Fig. 5 Results of repeated load tests

However, sufficient fatigue durability of the CLT bridge deck is considered to be indicated since no significant damage was observed on the test specimens that were subjected to repeated loads of several million times. The test continued with elevated load levels of 33% (40 kN) and 42% (50 kN) and a total of 8.5 million repeated loadings was performed; however, no damage to the test specimens was observed.

3.2 Dynamic wheel-load tests

The values of displacements are highest for displacement 1 and displacement 6, as shown in Fig. 6. The relationship between the number of drives with displacement 1 and displacement 6 are shown in Fig. 7. These tests were conducted by varying the wheel load between 56 and 100 kN and the number of drives exceeded 200,000 round trips, but no damage that can trigger fatigue was observed on CLT slabs. The tensile stress of the slab calculated based on the maximum value of the tensile strain in the bridge width direction (approximately 1,000μ) was approximately 3.5 N/mm^2, which correlated well with the design value of 4.2 N/mm^2. These results can be considered to have indicated sufficient fatigue durability of CLT bridge decks, which is similar to the results obtained from the repeated load tests.

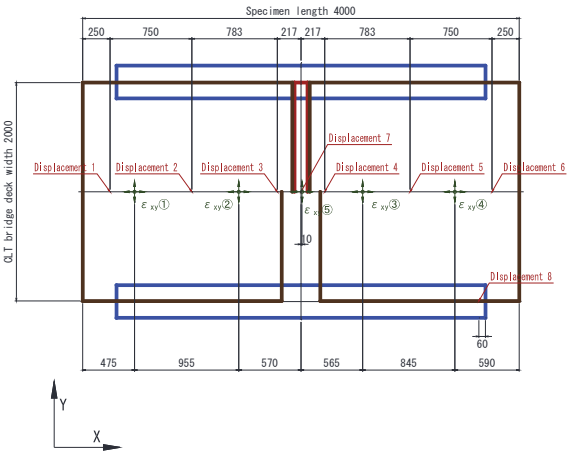

Fig. 6 Positions of measurement devices.

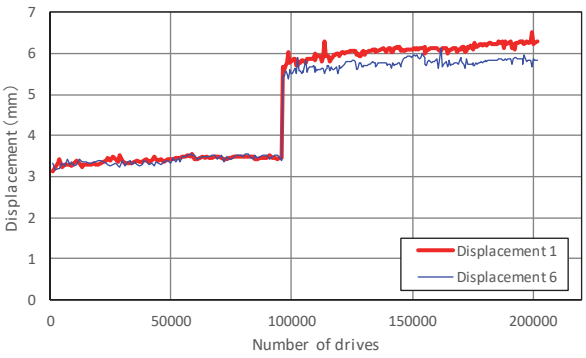

Fig. 7 Example of relationship between number of drives and displacement of CLT slab

4. Test constructions

4.1 Outline of experimental bridge

A general diagram of the experimental bridge is shown in Fig. 8 and Fig. 9. The forestry road bridge was designed to transport cut logs out of the forest, with measurements of 7.0 m in length and 3.86 m in width with a design load of 140 kN. Steel H-beams of 300 x 300 mm cross-section were used for the main and side girders; four Japanese cedar CLT slabs of 3.7 m length, 1.738 m width, and 180 mm thickness were installed adjacent to each other, in the axial direction of the bridge. Incidentally, a 350 x 350 mm steel H-beam was used for the design, with the design load of 200kN, while the thickness of CLT boards was 210 mm. The four CLT slabs all underwent different waterproofing treatments that varied in terms of specifications, with the intention of comparing long-term durability. Polymer cement waterproofing was implemented on the upper surface of the bridge decks, on which the asphalt pavement (thickness of 50 mm) was laid. Three methods of coating, namely (a) wrapping with FRP, (b) covering with polymer cement, and (c) urethane coating, were implemented as waterproofing on the CLT slabs. The state of working of the respective waterproofing treatments conducted in a laboratory at the Institute of Wood Technology of Akita Prefectural University are shown in Fig. 10. Furthermore, a preservation treatment was performed using an oil-based wood preservative coating on the remaining slab of the CLT bridge deck for the purpose of comparison.

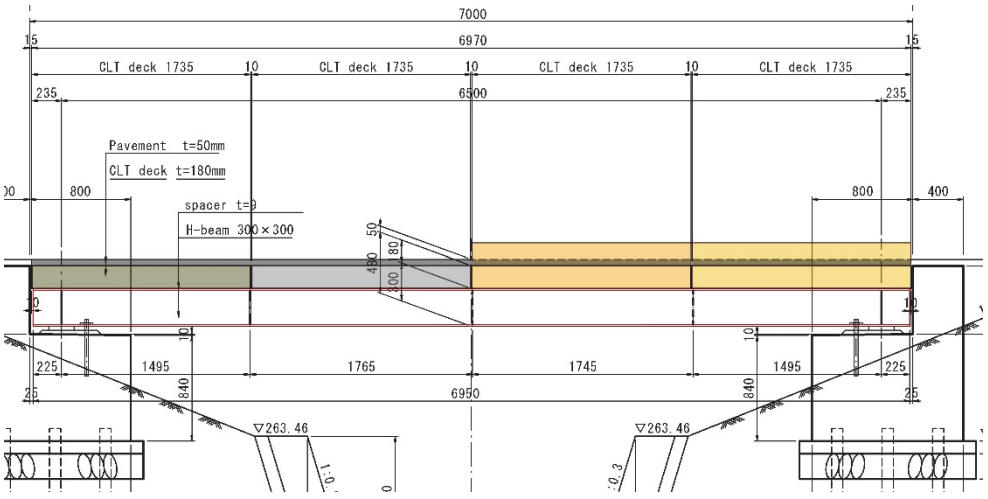

Fig. 8 Side view of experimental bridge

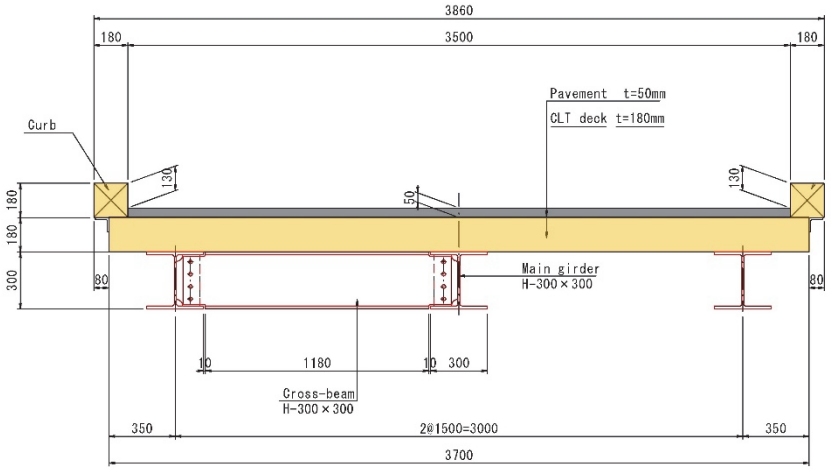

Fig. 9 Front view of experimental bridge

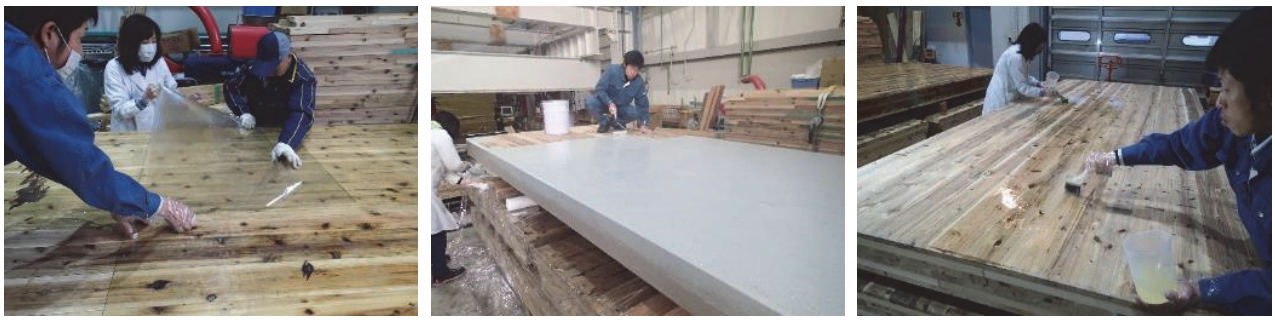

(a) Wrapping with FRP *(b) Covering with polymer cement* *(c) Urethane coating*

Fig. 10 Waterproofing treatments of CLT slabs

4.2 Test constructions

Construction work of the experimental bridge was performed in the Ishikura-stream Prefectural Forest at Tazawa lake in Senboku City of Akita Prefecture. The bridge was constructed using a rough-terrain crane, capable of suspending 50 kN, to install steel H-beams (Fig. 11) and CLT bridge decks (Fig. 12), where each erection was completed in one day. CLT bridge decks were brought to the site after wooden curbs (CLT) of 180 x 180 mm attached to both sides. The weights of bridge decks varied according to the implemented waterproofing treatment, where the heaviest CLT bridge decks that were wrapped with FRP sheets weighed approximately 6 kN. This was lower than the 7 kN for the steel H-beams used as main girders, which confirms the superiority of CLT slabs with regards to transportation and installation work. The CLT bridge decks were secured to the main girders and cross-beams using lug screws (φ16 x 150 mm) on the lower surface of the CLT slabs from the bottom surface of the upper flange of the steel H-beams, as shown in Fig. 13. Holes were drilled in the CLT slabs to enable penetration of the stud bolts (φ16 x 180 mm) (Fig 14.) welded on the upper surface of the flange of the steel H-beam, where driving lug screws from above the abutment was difficult. Then, the bolts were secured with washers and nuts. Furthermore, the bolt holes and the seat-bored sections in the vicinity of the nuts were filled with resin adhesive (Fig. 15). The completed experimental bridge with asphalt pavement is shown in Fig. 16.

Fig. 11 Installation of main girders and cross-beams

Fig. 12 Installation of CLT bridge decks

Fig. 13 Securing CLT bridge decks

Fig. 14 Stud bolts of main girders and cross-beams

Fig. 15 Conditions prior to paving

Fig. 16 Paved experimental bridge

5. Conclusions

CLT bridge decks are confirmed to have sufficient fatigue durability, based on the repeated load tests and the dynamic wheel-load tests. The trial construction of the forestry road bridge using CLT slabs was completed in a total of three days; two days for the bridge installation and one day for the pavement installation. The construction using CLT slabs is confirmed to have superior workability. There is a plan to cut and transport logs out of the forests in the vicinity where the experimental bridge was installed. A load test is planned for the bridge, whereby trucks loaded with logs drive over the bridge. Future work includes the implementation of the investigative research intended for practical implementations, such as the verification of the effectiveness of the waterproofing for the CLT bridge decks.

6. References

[1] Abrahamsen, Rune B., Nyløkken, Trond E., “Bridge deck rehabilitation using cross-laminated timber”, *Proceedings of the International Conference Timber Bridges*, 2010, p371.

Creep behavior of oak pegs under tension in dry and wet conditions

Jiří Kunecký*, Michal Kloiber*, Hana Hasníková*, Jaroslav Hrivnák*, Václav Sebera, Jan Tippner**, Jaromír Milch****
Researcher
***ITAM CAS CR, v.v.i.**
***Prosecká 76, Prague, Czech Rep.**
**** Mendel University in Brno, Faculty of Forestry and Wood Technology, Department of Wood Science**
**** Zemědělská 3, Brno Czech Rep.**
kunecky@itam.cas.cz

The author studied at the Faculty of Transportation Sciences, CTU in Prague where he focused his PhD. thesis on numerical simulation of cellular solids under impact conditions.
Experimental work was focused in biomechanics, later moved to timber structures.

Summary

Carpentry joints equipped with oak pegs are well suited for applications where increased moisture is not a significant factor. However, for the use in outside conditions, e.g. in the repairs of historical timber bridges, the pegs connecting the two halves of the joint may deform and change their original shape. This happens especially during long-term loading and can be augmented significantly by environmental changes. Creep behavior can play a crucial role for some types of carpentry joints, especially when precise contacts of faces in the joint are required. The paper deals with experimental testing of creep behavior of 16 mm oak pegs under dry and wet conditions loaded by the combination of shear and bending between two planks made of spruce in the direction parallel to grain. The results show that the decrease of theoretical stiffness values over time plays a significant role in the force redistribution in the joint especially due to moisture effects (drop 50-70% of the original stiffness).

Keywords: Creep, oak, pegs, dowels, tension.

1. Introduction

1.1 Motivation

In historical timber structures there is a need for sensitive repair methods especially for valuable and old parts of the structure. Such constructions can be made of wood having significant historic value. One of the options for such a repair is the replacement of decayed parts using scarf joints equipped with wooden dowels. This approach looks like a very efficient way both in means of durability and cost. This paper addresses an important issue for design of dowel connections since the distribution of forces in the joint is dependent on the distribution of stiffness of the dowel/surrounding timber system. It is well known that timber suffers highly nonlinear creep behavior, nevertheless, the quantification for the wooden dowels has not been published excessively.

Creep behavior is natural to wood and until 40% of loading does not play significant role in the mechanical response of the whole structure as reported by Holzer et al. in review [1]. In the same publication effects of temperature and moisture content are discussed with moisture being the most significant factor playing main role in creep response. Higher temperature and moisture cycles can lead to big creep deformation and failure. However, the influence is much higher in small specimen sizes than in big structural elements. In exterior exposure creep effects cannot be overlooked.

Duration of load (DOL) can play significant role in both creep deformation and creep failure [2]. Extensive creep deformation is usually important indicator that forces in the element are high enough to produce creep failure. Duration of load is well described by Madison curve [3] relating the ultimate stress to its duration until failure occurs.

Although many papers have been published about wood creep, contributions about mechanical response of wooden dowels to creep have not been found. To check this important issue, especially the change of stiffness of the dowel, the work presented in the article has started.

1.2 Application of creep measurement to lapped scarf joints

Lapped scarf joints have been developed for replacing of the decayed parts of the beams of valuable historical constructions while keeping maximal amount of original timber in the structure [3]. The design of the joints was based on verified analytical model, where stiffness of the coupling elements plays an important role. However, redistribution of forces in the joint according to creep can be significant. The joints (see Fig. 1) are designed for use in all types of loading, however, compression and bending (and their combination) are the most common types of load states. Inclined faces increase load bearing capacity of the joints for moments acting in one direction. Compression is held partly by the inclined face. Pure tension is not optimal type of loading for these joints, nevertheless, in some applications there is the need to transfer high tensile loads (usually between parts oriented parallel to grain). Under these conditions the dowel can be loaded until failure and thus a proper design value is critical. As a solution the designer can take into account relatively low bearing capacity of wooden dowels and apply multiple dowels or use lesser amount of steel dowels with higher load-bearing capacity for tension parallel to grain. Specifically if combination of bending and tension is present, the function of the inclined face can be crucial and should not be avoided by creep-induced gap between the faces. Therefore creep tests of single dowel were performed and are published throughout this conference paper.

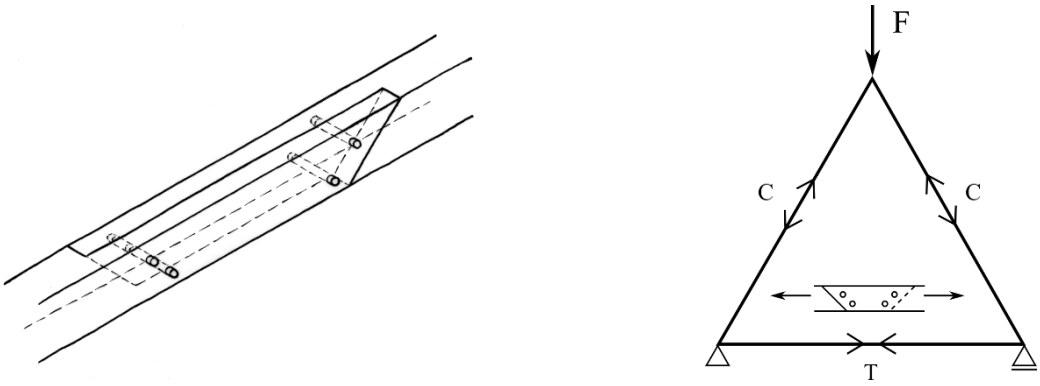

Fig. 1 Lapped scarf joint with inclined faces (left) in a typical structural truss (right) is loaded in tension which is the most demanding type of loading of the joint

The questions and tasks for the work are: 1) What is the size of maximal creep deformation of the dowel? 2) Is it possible to quantify the stiffness drop related to creep? 3) Is there a significant influence of environmental conditions?

2. Materials and methods

2.1 Specimen

Since English Oak (Quercus robur) is a widespread hardwood species with good mechanical properties, it was chosen as a standard for wooden dowels for all the lapped joints tested in the laboratory. A typical softwood is represented in Central Europe by Norway spruce (Picea Abies Karst.) which was used for the joint mass. The connection (see Fig. 2) was manufactured with the pre-drilled hole diameter d=16 mm, dowel itself was processed using turning to match exactly the hole diameter. For completeness, dimensions of the specimen were set: thickness of one half of the joint 1,5d=2,4 cm, together both parts 4,8 cm; length of the necked region 14d=22,4 cm, width 6d=9,6 cm, the place for jaw placement had length 6d=9,6 cm. The specimen was loaded according to Fig. 2 and fastened using bolted connection to the frame.

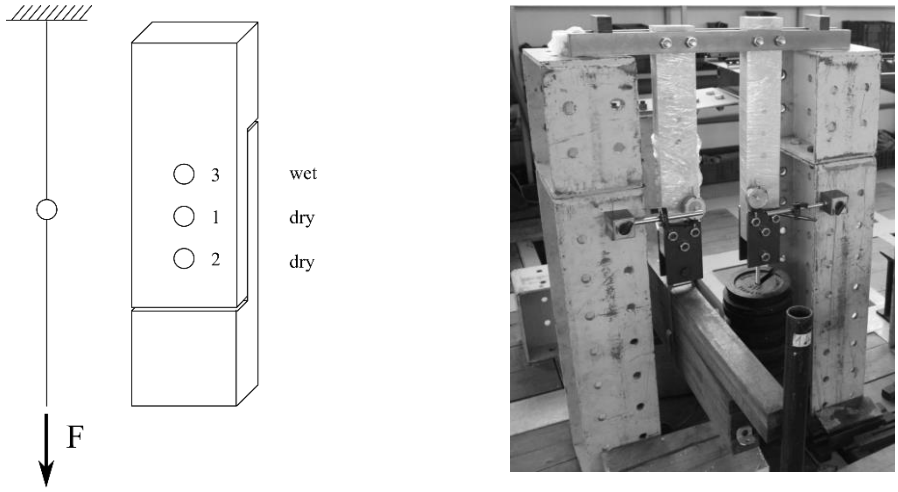

Fig. 2 Scheme of the experiment, typical geometry and numbering the dowels (left), the loaded specimens using weight loading (right)

Table 1 summarizes briefly number of specimens for each type of testing and their moisture content. The hole no. 1 was drilled first in each of the four specimens and the first series of dry specimens with the oak dowel was tested. Next, the second hole was drilled and the creep test was made. Eventually, third series was moisturized and creep measurement was repeated. Thus, there were only four specimen (the same softwood planks) and the results can be independent on the quality of wood. MC was measured using weighting. In the case of wet samples they were immersed in water for one day and, also, small parts of wood were cut out to be proved that the MC until depth 13 mm is 25%. The dowel was completely moisturized. It is worth noting that it is impossible to keep constant conditions inside testing facility since the conditions differ according to outside conditions. However, the wet samples were covered by transparent foil to keep the original moisture content. Average density of the samples was 470 kg/m^3. The dowels were cut of one oak massive.

2.2 Loading

The samples were loaded in tension using weight producing 1.2 kN, as it should be 50% of short-term yield load for this dowel diameter [4]. The recording of the deflection was made every three days using mechanical deflectometers with resolution 10μm. Short-term stiffness of the connection was computed according to the formula presented in [5] as being 2.975 kN/mm.

Tab. 1 Overview of the samples tested in creep

Series No.	Number of samples	Time of loading	Relative moisture content of wood	Average conditions in the facility, season
1	4	55 days	Dry - 12%	60% RH, 25-36 °C, summer
2	4	55 days	Dry - 12%	40% RH, 19 °C, winter
3	3	33 days	Wet - 25%	50% RH, 20 °C, winter/spring

3. Results

The results are summarized in Fig. 3-4. The short term deflection of the curve and first 20 minutes of measurement was cut off since there was a lot of noise and scatter caused primarily by complicated manual loading of the specimens and also a slight difference in the space between the hole and the dowel. The values are adjusted to zero.

The results indicate significant increase in creep deflection which is strongly affected not only by moisture content, but also by environmental condition as can be shown on difference between the

two dry dowel series. The environmental dependency is in agreement with the literature results [1] which states that creep, high temperature and humidity are the most important factors. Although the third series of experiments is scattered and not as large as the other two, it shows clearly with the increase of compliance with the increased moisture content.

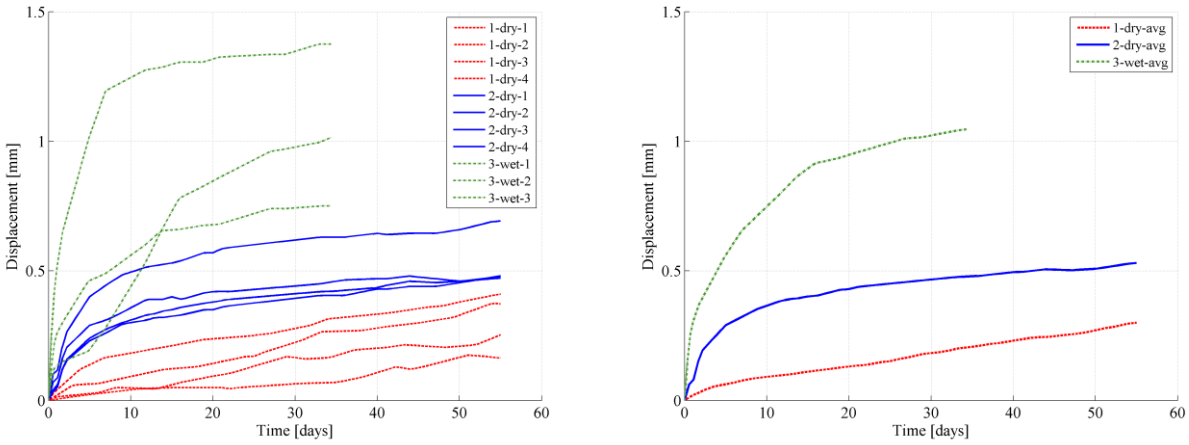

Fig. 3 Creep displacement measured for all samples (left) and averages made for clarity (right)

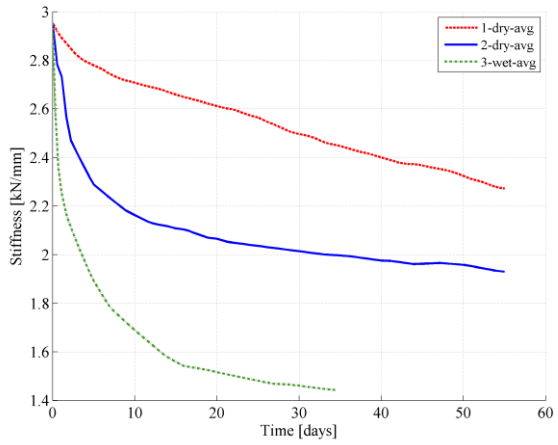

Fig. 4 Stiffness of the doweled connection

In addition, when we focus on the change of the original stiffness, we see a dramatic drop of the values resulting from short-term testing. Although the loading conditions are in the safe area for creep failure (50% of yield, 35% of ultimate load), the stiffness changes significantly and it is worth considering the long-term stiffness to be one half to one third (when higher moisture is present) of the short-term value. The values are already in the secondary creep area and still cannot be taken as the final ones.

4. Discussion and conclusion

Although there is no satisfactory statistics from the data measured, it is clear that even with the moderate changes in temperature, humidity and stiffness there is an obvious change in the mechanical response of the doweled connection. There is an interesting difference between the first and the second series. The first curve is not having a typical creep shape, on the contrary the second having much higher values of creep deflection. The reason can be the different loading state in the holes which was visible also during the measurement: the configuration "2" had slightly more bending as the "1", the longitudinal space between the halves of the joint was wider in the upper part than in the lower part.

The sensitivity of measured data to outside conditions was interesting. Although the temperature was constant in the testing facility, when there was a big temperature drop outside (weather changed), it was immediately visible on the measured values.

As the dowels were slightly deformed after load removal (not visible in the picture, but touchable), it can be concluded that significant amount of the creep as being present in the dowel and not in the

hole.

The preliminary study touching the problems of the creep behavior of the oak dowels should be followed by a bigger experiment group tested at a constant moisture and temperature rate. Also, the bigger diameters of the dowels should be tested.

As a conclusion it is possible to respond questions posed: 1) Maximal creep deformation can be expressed by ratio displacement/radius of the dowel and was about 0,03 in dry and 0,06 in wet conditions and after 55 days still increasing. 2) Stiffness change should be considered as nearly one half or one third of the short-term stiffness. 3) Environmental condition plays important role and should be kept constant and on the unsafety side, i.e. warm and humid.

The lapped joints are designed for the use in dry conditions, in interior or in roof structures, where moisture changes can be neglected. Thus, the problem of high moisture is not so significant. Since the joint is applicable mainly in historic constructions, such amounts of creep does not have significant influence on overall performance of the structure. However, significant redistribution of forces can happen inside doweled joint due to creep deflections.

Acknowledgements

This paper was created with a financial support from grant project DG16P02M026 “Historical Timber Structures: Typology, Diagnostics and Traditional Wood Working”, NAKI program II and project No. LO1219 under the Ministry of Education, Youth and Sports National sustainability programme I.

References

[1] Holzer S.M., Loferski J.R., Dillard D.A.: A review of creep in wood: concepts relevant to develop long-term behaviour predictions for wood structures. Wood and Fiber Science 21(4), 1989, pp. 376-392.

[2] Rosowsky D.V., Bulleit W.M.: Load duration effects in wood members and connections: other statistics and critical loads, Structural safety 24, 2002, p347.-362.

[3] American Forest and Paper Association: National design specification for wood construction, Washington DC, 1997.

[4] Arciszewska-Kedzior, A., Kunecký, J., Hasníková, H., Sebera, V.: Lapped scarf joint with inclined faces and wooden dowels: experimental and numerical analysis. In: Engineering Structures, 94:2015, s. 1-8. ISSN 0141-0296.

[5] German Institute for Standardisation (Deutsches Institut für Normung), DIN 1052-1 (1988-04) Structural use of timber - Design and construction.

[6] Fukuyama, H., Ando N., Inayama M. and Takemura M.: Calculation model and yield process of single shear joint with wood dowel of various slenderness, J. Struct. Constr. Eng., AIJ, Vol. 73 No. 627, 803-810, May, 2008.

Mechanical analysis of scarf joint fastened using cylindrical wooden dowel

Jan Tippner Research assistant Mendel University in Brno, Faculty of Forestry and Wood Technology, Department of Wood Science Zemědělská 3, Brno 619 00 Czech Republic *jan.tippner@mendelu.cz*	**Jaromír Milch** PhD student Mendel University in Brno, Faculty of Forestry and Wood Technology, Department of Wood Science Zemědělská 3, Brno 619 00 Czech Republic *jaromir.milch@mendelu.cz*
Jiří Kunecký Researcher Institute of Theoretical and Applied Mechanics, v.v.i., Prosecká 809, Prague, 190 00 Czech Republic *kunecky@itam.cas.cz*	**Michal Kloiber** Researcher Institute of Theoretical and Applied Mechanics, v.v.i., Centre of Excellence Telč Batelovská 485, Telč, 588 56 Czech Republic *kloiber@itam.cas.cz*
Martin Brabec PhD student Mendel University in Brno, Faculty of Forestry and Wood Technology, Department of Wood Science Zemědělská 3, Brno 619 00 Czech Republic *martin.brabec@mendelu.cz*	**Václav Sebera** Research assistant Mendel University in Brno, Faculty of Forestry and Wood Technology, Department of Wood Science Zemědělská 3, Brno 619 00 Czech Republic *vaclav.sebera@mendelu.cz*

Summary

Traditional all-wooden woodworking joints play an important role in the behaviour of timber structures. These joints are also widely used when historically valuable constructions are being reconstructed and the connections are usually the masterpieces that testify to the high carpentry skills and knowledges of the overall mechanical behaviour. Within historical timber structures traditional carpentry joints were used while wooden dowel fixed mutual position of elements. Main aim of this study was to contribute to knowledge base about prediction and analysis of the mechanical performance of frequently used scarf joints made from spruce wood fastened using oak dowels. The objectives were to determine the joints' slip moduli and load-carrying capacity by means of theoretical and experimental approaches, in next to assess the mechanical behaviour of dowels through experimental investigation, and finally to perform a strain analysis of dowels. For these purposes, the optical technique employing three-dimensional full-field digital image correlation was used. The experiments were done on the full-scale specimens meeting the requirements of European standards (EN 383 and EN 26891), which were made from Norway spruce (*Picea abies* L. Karst.) and English oak (*Quercus robur* L.). The mechanical load consisted in tensile parallel and perpendicular to grain direction within the main components. The results of this study showed good correlation between theoretical approach based on based on Beam on Elastic Foundation theory and European yield model theory and experimental observations.

Keywords: all-wooden joints, scarf joint, dowel, spruce, oak, digital image correlation

1. Introduction

The all-wooden joints are commonly referred as the most critical element in structures, being responsible for the reduction of the overall integrity in 80% of failure cases [1, 2, 3, 4, 5]. Within historical timber structures traditional carpentry joints were used while wooden dowel fixed mutual position of elements. The geometrical parameters of the fastener, mainly diameter and slenderness ratio, influenced the total mechanical joints performance [6, 7]. In the event that the fastener-axis remains more or less unbend (is more "rigid"), the timber load-carrying capacity is exceeded. The related failure mode in this case is "brittle". On the other side, the fastener with a high slenderness ratio is deformed in bending, which reduced a splitting tendency of the joint components. Thus, the load-carrying capacity of the joint is determined by the (moment-) resistance of the fastener itself. However, the bending fastener deformation is limited by the embedment strength of the joint components in the contact zone between fastener and joint components [8, 9]. Therefore, higher load-carrying capacity of the dowel and the appearance of a highly (desired) ductility of the joint are evident [10, 11].

In the past, many studies about this issue have been performed (such as [12, 13] etc.). Johansen [12] proposed the first mathematical model (European yield model – EYM) for joints strength performance. He applied the model for timber-to-timber connection with a steel dowel for ductile failure modes. Larsen [14] continued and developed Johansen's theory further. The validity of this method was confirmed by experimental investigations by Möller [15]. Brungraber [16] was one of the first who performed the experimental tests on individual wooden joints with traditional fasteners - dowels. These joints were tested in the full-scale dimensions for the purpose of detecting local possible failures.

Mechanical behaviour of the wooden dowels is still not precisely known and information about stiffness and bearing capacity is rather scarce [17].

The purpose of this study was to investigate the mechanical properties of single shear dowel-type joints with its detailed performance description where various dowel diameters were tested. The main objectives were: (1) to determine the joints slip moduli (K_{cal} and K_{exp}) and dowel connection load-carrying capacity with determination of the maximal dowel loading in bending and shear deformation modes ($P_{y,EYM,cal}$, $P_{max,exp}$, $P_{y,S,cal}$ and $P_{failure,S,exp}$) with help of theoretical and experimental approaches, (2) to assess the detailed mechanical dowel behaviour through experimental investigation, and (3) to perform a strain analysis of the dowel using digital image correlation (DIC).

2. Materials and Methodology

2.1 Material and experimental analysis

The joints components were made from Norway spruce (*Picea abies* L. Karst.), while its length coincided with the longitudinal direction and a grain angle of 45° on the cross-section was ensured (see Fig. 1). The specimens of joints were assembled by components with similar density (specified in Table 1). English oak (*Quercus robur* L.) was used to make the dowel. Selected wood species represent the most common materials used in reconstructions of historical timber structures in central Europe. The dowels with four nominal diameters (d = {12, 16, 20, 24} mm) were tested. The same dimensions were used to bore the holes in the joint components. The dowels were inserted into predrilled holes, no clearances were allowed.

The mechanical investigations of the full-scale joints (Fig. 1) were carried out according to standards EN 383 and EN 26891. The joints were loaded in tensile parallel and perpendicular to grain in single shear plane. The quasi-static loading rate was 1.5 mm·min^{-1} for all tests. First, the specimen was loaded until 40% of the maximum load ($P_{max,pre}$) and the crosshead position was held for 30 s (this approach results from preliminary test for each series). After this step, each specimen was unloaded to 10% of $P_{max,pre}$ and the crosshead position was held for 30 s again. Finally, specimen was loaded until failure. Fig. 1 and Table 1 present the joints test configurations

including the geometric parameters which were derived from the diameter (*d*) according to Eurocode 5. The joints were placed into a climate chamber and conditioned at 20 °C and 65% relative humidity (RH) until the equilibrium moisture content (EMC) was reached. Moisture content (MC) and density at equilibrium state was then measured gravimetrically according to ASTM D2395 (American Society for Testing and Materials 2014). The mechanical tests were performed using universal testing machine Zwick Z050/TH 3A (Zwick Roell AG, Germany) with 50 kN load cell under crosshead displacement control.

Table 1 The geometrical parameters of the joints derived from dowel diameter (*d*).

Series	***a***	***a*$_{4,c}$**[a]	***l*$_1$**	***l*$_2$**	***a*$_{3,t}$**[a]	***L***	***L*$_1$=*L*$_2$**	***b***	***n***	***w***	***ρ*$_{12}$**	**Material**
	(mm)									(%)	(kg·m^{-3})	
Parallel to grain												
Ø 12	72	36	90	72	84	36	18	19	8	13.0	475 (4.0)[b]	Norway spruce
Ø 16	96	48		96	112	48	24		8	13.3	487 (2.4)	
Ø 20	120	60		120	140	60	30		7	12.9	503 (5.3)	
Ø 24	144	72		144	168	72	36		7	12.4	473 (5.1)	
Perpendicular to grain												
Ø 12	144	72	-	62	83	36	18	-	7	10.3	487 (4.0)	Norway spruce
Ø 16	192	96				48	24				486 (2.8)	
Ø 20	240	120				60	30				443 (4.5)	
Ø 24	288	144				72	36				486 (5.6)	
dowel	**length *L*$_{dowel}$** (mm)					36, 48, 60, 72				12.5	718 (6.1)	English oak
	diameter *d* (mm)					12, 16, 20, 24						
	slenderness ratio (*L*$_{dowel}$/*d*)					3						

[a]Parameters $a_{4,c}$ and $a_{3,t}$ are derived from dowel diameter according to [25] (as 3*d* and 7*d*, respectively), [b]Coefficient of Variation (%) in parenthesis.

The total joints' displacement and complex strain field on the dowels foreheads were examined from captured images during experimental testing using the full-field optical technique based on digital image correlation (DIC). For these purposes, two CCD cameras (AVT Stingray Copper F-504B, cell size of 3.45 µm and resolution of 2452×2056 pixels) equipped with lenses (Pentax C2514-M, focal length of 25 mm) at the stereo-vision configuration (3D) used to capture images (see Fig. 1). The stereo-vision system was centered to the area of interest (AOI), see details in Fig. 1. The images together with applied force were synchronously captured in the acquisition interval of 1.0 s (1 Hz) with help of the hardware trigger device. All captured images were in standard grey scale of 256 levels. The calculation processing of the total displacement and strain distribution at AOI was performed by software Vic-3D v. 2012.

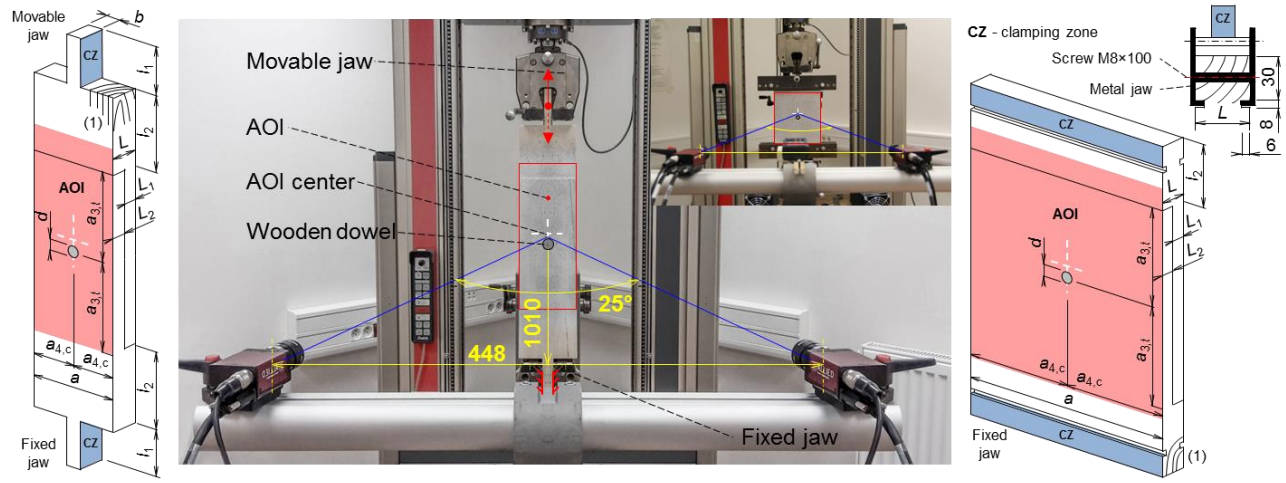

Fig. 1. Experimental test configurations for tensile parallel and perpendicular to grain: joints geometry (left); stereo-vision optical system (3D) for image acquisition of the tests loaded parallel (left) and perpendicular (right) to grain, dimensions in mm; (1) represents the grain direction.

2.2 Theoretical approach – evaluation of dowel-type connection

2.2.1 Slip modulus of the joints

In the following, the theoretical approach derived from Fukuyama et al. [10, 18, 19] based on the Beam on Elastic Foundation (BEF) theory was applied to determine the joints stiffness with taking into account the dowel shear deformation. Material characteristics for Norway spruce and English oak used in the theoretical joints solution are presented in Table 2. These material characteristics were obtained on the basis of load-displacement curves from in-house three-point bending (samples dimension L_b = 300 mm; $R_b = T_b$ = 20 mm) and compression parallel to grain (samples dimension L_c = 30 mm; $R_c = T_c$ = 20 mm) tests. Some of them were adopted from Požgaj et al. [20] and Fukuyama et al. [19], as shown in Table 2.

Firstly, for the theoretical determination of the slip modulus (K_{cal}) the foundation moduli of the joint components (side members k_1 and k_2) are required. These parameters are material properties that need characterization owing to their large variability with the wood species and grain orientation. The components k_1 and k_2 were determined according to the Eq. (1):

$$k_1 = k_2 = \frac{k_e \cdot \alpha_k \cdot k_{cvf}}{k_e + \alpha_k \cdot k_{cvf}} \qquad (\mathrm{N{\cdot}mm^{-3}}) \tag{1}$$

where k_e is the bearing stiffness in timber, in N·mm^{-3}, α_k is the embedment stiffening coefficient owing to kind of dowel material (1.6–3.5), α_k 1.6 was used in this study, and k_{cvf} is the embedding stiffness in dowel, in N·mm^{-3}. Then, k_e is given by Eq. (2):

$$k_e = \frac{MOE_{timber}}{31.6 + 10.9d} \qquad (\mathrm{N{\cdot}mm^{-3}}) \tag{2}$$

where MOE_{timber} is the Young's modulus in compression parallel to grain of the base material (side members of the joint), in N·mm^{-2}, and d is the dowel diameter, in mm.

The slip modulus K_{cal} of single shear dowel-type joints, which takes into account the shear deformation in the dowel, is then given by as less value according to Eq. (3):

$$K_{cal} = min\left\{ \begin{array}{l} \dfrac{k \cdot d^2 \cdot \lambda^2}{2} \cdot \dfrac{1}{4\lambda - 2.4\mu} \\ \dfrac{1}{8}\left(\pi \cdot MOE_{dowel} \cdot k^3 \cdot d^7\right)^{\frac{1}{4}} \cdot \dfrac{1}{\sqrt{1 + \dfrac{MOE_{dowel}}{3G}\left(\dfrac{k \cdot d}{\pi \cdot MOE_{dowel}}\right)^{\frac{1}{2}}}} \end{array} \right. \qquad (\mathrm{N{\cdot}mm^{-1}}) \tag{3}$$

where λ is the slenderness ratio between joint component thickness (L_1 and L_2) and dowel diameter as given by following Eq. (4), μ is the friction coefficient (0.4 was used in this study), $k \rightarrow (k_1 = k_2)$, in N·mm^{-3}, MOE_{dowel} is the elastic bending Young's modulus of the dowel, in N·mm^{-2}, G is the average longitudinal shear elastic modulus of the dowel, in N·mm^{-2},

$$\lambda = \frac{L_{dowel}}{d} \qquad (-) \tag{4}$$

where $L_{dowel} = L_1 + L_2$, is the joint side members (1 and 2) thickness, in mm.

Table 2 The material characteristics used in theoretical solution for single shear dowel-type joints.

	n	MOE_{dowel} [a]	MOE_{timber} [a] ∥	MOE_{timber} [a] ⊥	F_b [a]	G [b]	F_s [c]	$F_{e,exp}$ ∥ or ⊥	F_{cvf} [c]	k_{cvf} [c]	$\alpha_k k_{cvf}$
		(N·mm^{-2})									
Norway spruce	60		12240 (15.8)[d]	327 (16.4)				according to Tables 3 and 4.			
English oak	8	11735 (17.8)			109 (14.0)	1100	24.3		34.4	85.1	65.4

[a]Elastic bending modulus (MOE_{dowel}), normal modulus of compression parallel or perpendicular to grain (MOE_{timber}), and bending strength (F_b) obtained from in-house experiments from n samples, [b]adopted from Požgaj et al. [20], [c]adopted from Fukuyama et al. [19] , [d]Coefficient of Variation (%) in parenthesis.

2.2.2 The dowel load-carrying capacity

The design method for determination of the wooden dowel load-carrying capacity (P_y) derived from Fukuyama et al. [19] and was based on Johansen's yield theory, also known as the European yield model (EYM). This theory predicted the load-carrying capacity of single shear dowel-type joints, per shear plane, loaded laterally to its axis. Fig. 2 illustrates the possible failure modes assumed by EYM for single shear dowel-type joints. The mechanical behaviour of these modes arises from the bending strain deformation (bending capacity – yielding moment) of the dowel and embedment strength of timber.

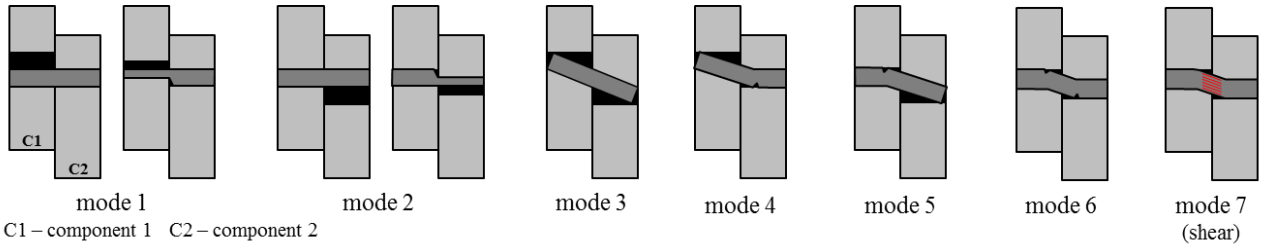

Fig. 2. European yield modes (EYM) for single shear dowel-type joints.

The load-carrying capacity ($P_{y,EYM,cal}$) of the dowel was determined based on the Eq. (5) as the minimal value for individual failure mode according to EYM theory.

$$P_{y,EYM,cal} = \min \begin{cases} d \cdot L_1 \cdot F_{ecp} \quad (\text{mode 1}) \\ d \cdot L_1 \cdot F_{ecp} \cdot \alpha \cdot \beta \quad (\text{mode 2}) \\ d \cdot L_1 \cdot F_{ecp} \cdot \dfrac{\sqrt{\alpha^2 \cdot \beta^3 + (2\alpha^2 + 2\alpha + 2)\beta^2 + \beta} - \beta \cdot (\alpha + 1)}{1 + \beta} \quad (\text{mode 3}) \\ d \cdot L_1 \cdot F_{ecp} \cdot \left[\sqrt{\dfrac{4\beta \cdot M_y}{d \cdot L_1^2 \cdot F_{ecp} \cdot (\beta + 2)} + \dfrac{2\beta \cdot (\beta + 1)}{(\beta + 2)^2}} - \dfrac{\beta}{\beta + 2} \right] \quad (\text{mode 4}) \\ d \cdot L_1 \cdot F_{ecp} \cdot \left[\sqrt{\dfrac{4\beta \cdot M_y}{d \cdot L_1^2 \cdot F_{ecp} \cdot (2\beta + 1)} + \dfrac{2\alpha^2 \cdot \beta^2 \cdot (\beta + 1)}{(2\beta + 1)^2}} - \dfrac{\alpha \cdot \beta}{2\beta + 1} \right] \quad (\text{mode 5}) \\ \sqrt{\dfrac{4d \cdot F_{ecp} \cdot M_y \cdot \beta}{1 + \beta}} \quad (\text{mode 6}) \end{cases} \tag{5}$$

where F_{ecp} is the embedment strength and is defined as the lower value from $F_{e,exp}$ or $\alpha_F F_{cvf}$, in N·mm^{-2}, $F_{e,exp}$ is the embedment strength in joint components and is given by Eq. (6), in N·mm^{-2}, α_F is the amplification coefficient on embedment yield stress (1.9 in this study), F_{cvf} is the embedment yield stress in dowel, in N·mm^{-2}, α is the ratio between side members thickness L_2/L_1, β is the ratio

between embedding wood strength of the joint components 1 and 2, M_y is the plastic capacity moment of the dowel, in N·mm^{-1} and is given by Eq. (7).

$$F_{e,\exp} = \frac{P_{\max,\exp}}{d \cdot L_1} \qquad (\text{N·mm}^{-2}) \tag{6}$$

where: $P_{max,exp}$ is the experimental maximum force specified in Tables 3 and 4, in N.

$$M_y = \left(\frac{\pi \cdot d^3}{32} \right) \cdot F_b \qquad (\text{N·mm}^{-1}) \tag{7}$$

where F_b is the bending strength of dowel, in N·mm^{-2}.

The evaluation of the shear-crack-in-grain capacity ($P_{y,S,cal}$) of the dowel was also taken into account, which is given by equation according to failure mode 7 – shear:

$$P_{y,S,cal} = \frac{F_s \cdot A}{k'} \qquad (\text{mode 7 - shear}) \qquad (\text{N}) \tag{8}$$

where F_s is the shear strength of the dowel, in N·mm^{-2}, A is the dowel cross-sectional area, in mm^2, k' is the revision coefficient of the shear stress (4/3 is given for round cross-section in this study).

2.2.3 Embedment yield deformation

There is an interaction between dowel and joint component surfaces and, therefore, the analyses of the embedment yield deformations (δ_{int} and δ_{ext}) were performed. The δ_{int} and δ_{ext} in the joint components were obtained: (1) through direct measurement after each test using caliper for δ_{int}, and (2) using image analysis for δ_{int} and δ_{ext}, as illustrated Fig. 4. The δ_{int} and δ_{ext} were obtained from image analysis using ImageJ v.1.50h (National Institute of Health, USA). First, the dimensions of the nominal dowel diameter were used for the calibration of the source image (Fig. 3). Then, the Fig. 3 was analyzed using the line measurement tool in ImageJ v.1.50h for determination of the δ_{int} and δ_{ext}, see Table 3. Both measuring techniques were compared and it was found that they differ in range of ± 3–5%.

2.2.4 DIN 1052 – verification

The verification procedure of the predicted numerical force level at the yield point state ($P_{yield,cal,1052}$) was derived based on the Eq. (9) according to DIN 1052 (Deutsches Institut für Normung e.V. 2004). The experimental force level at the yield point $P_{yield,exp}$ was determined using the load-displacement diagrams for each series of the dowels. This point is characterized as transition from the elastic to plastic phase of those diagrams.

$$P_{yield,cal} = 9.5 \cdot d^2 \qquad (\text{N}) \tag{9}$$

3. Result and discussion

3.1 Detailed analysis of the global joints behaviour

The both experimental load-slip curves (Figs. 3A and 3B) show the global joints behaviour. Generally, the dowel-type joints most often indicate an initial consolidation in the first phase of load-slip curves. It is a typical non-linear beginning response of joints at loading, but according to illustrated load-slip curves in Fig. 3 were not observed here. Kunecký et al. [7] presented the similar behaviour in the first phase of the force-deflection curves. This fact may be explained by the fact that the dowels were inserted without clearances into the drilled holes of the joint members with perfect contact between the dowel and joint components. The global joints behaviour with a dowel diameter of 16, 20 and 24 mm loaded parallel to grain showed three phases of the loading process according to load-slip curves, presented in Fig. 3A. The first one is the elastic (linear) till to slip

about of 0.06–0.08*d*. The second one is characterized with a moderate load increase (non-linear) till to slip about of 0.5–0.8*d* (to about of $P_{max,exp}$), and last one is characterized by increasing ductile behaviour with abrupt dowels failure till the ultimate dowel tearing at slip about of 0.6–1.2*d*. The ultimate dowel tearing failure was observed for dowels with nominal diameter of 16, 20 and 24 mm (Fig. 4). Meanwhile, in the joints series with a dowel diameter of 12 mm, different global joints behaviour and dowel failure were observed. These load-slip curves showed also three phases with ductile behaviour, but the third phase was characterized by a continuous development of the joints failure without abrupt dowel tearing. It also confirms Fukuyama et al. [10] who found that the dowels with a small embedment length exhibit a ductile behaviour due to the exceeding of the yield strength in joint components as well as missing dowel tearing. The global joints failure was formed as the combination of the bending with lateral compression stress in the dowel when dowel with a nominal diameter of 12 mm was used (as shows Fig. 4 – left). Therefore, gradual withdrawal of dowel from the joint component holes induced the "opening effect" of the joint components. Based on this, the global joints stiffness was affected due to the small contact area and friction between dowel and hole surfaces of the joint components. It also corresponds to the fact that the angle of dowel rotation was largest for the dowel with a nominal diameter of 12 mm, as shows Fig. 4 at ultimate joints failure.. The last mentioned facts particularly support that the internal embedment yield deformation (δ_{int}) in the joint components was greatest for the dowel with a nominal diameter of 12 mm. The ratio $\delta_{average,int}/d$ was 0.6*d* for a dowel with a nominal diameter of 12 mm, in other cases, these ratios were in range of 0.3–0.4*d*, as summarized in Table 5. In cases of external embedment yield deformation (δ_{ext}), these ratios $\delta_{average,ext}/d$ were not more than 0.1*d* for dowels with nominal diameters of 16, 20 and 24 mm, and are listed in Table 5. In case of dowel with a nominal diameter of 12 mm, the δ_{ext} it was not possible to obtain owing to large rotation and withdrawing of the dowels.

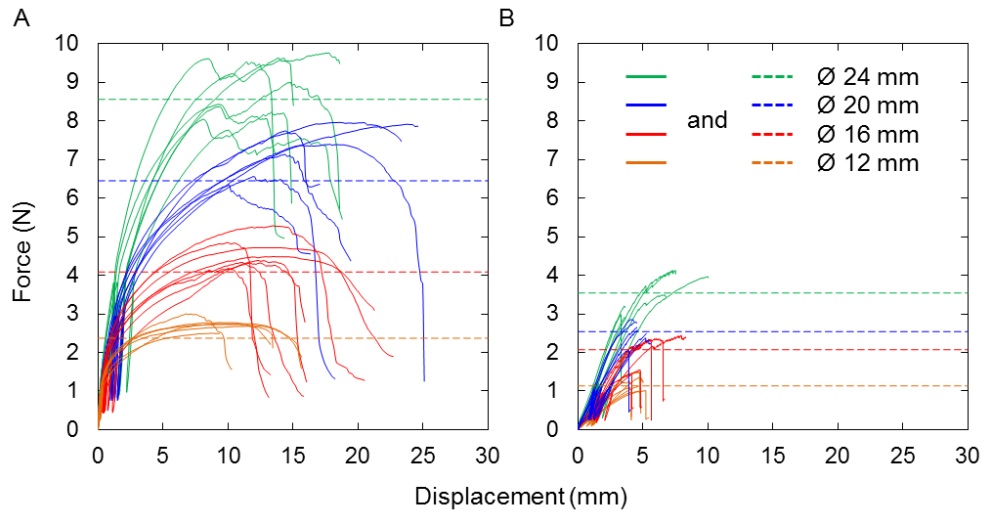

Fig. 3. The experimental results presented by load-displacement curves for dowel diameters 12-24 mm (full coloured lines). The theoretical coloured dashed lines represent prediction for appropriate mode failure which was observed in experiments according to Fig. 2; A - represents tensile parallel to grain; B - represents tensile perpendicular to grain.

On the other hand, the global joints behaviour loaded in tensile perpendicular to grain showed two phases of the loading process according to load-slip curves, presented in Fig. 3B. The first one is the elastic (linear) till to slip about of 3.5 mm for all tested dowel series. The second one is characterized by increasing ductile behaviour with abrupt timber failure (at $P_{max,exp}$) without ultimate dowel tearing or failure.

Table 3 An overview of theoretical and experimental results for single shear dowel-type joints loaded in tensile parallel to grain.

Theoretical results					
	units	d = 12 mm	d = 16 mm	d = 20 mm	d = 24 mm
K_{cal}	(kN·mm^{-1})	2.05	2.98	3.94	4.92
$P_{y,EYM,cal}$ (modes 4 and 5)	(kN)	1.75	2.95	4.74	6.20
$P_{y,EYM,cal}$ (mode 6)	(kN)	2.37	4.09	6.45	8.56
$P_{y,S,cal}$ (shear mode 7)	(kN)	2.06	3.66	5.73	8.25
$P_{yield,cal,1052}$[a]	(kN)	1.03	1.82	2.85	4.10
Experimental results					
		d = 12 mm	d = 16 mm	d = 20 mm	d = 24 mm
K_{exp}	(kN·mm^{-1})	1.74 (8.2)[b]	2.15 (16.7)	2.33 (17.0)	2.93 (19.5)
$P_{yield,exp}$	(kN)	1.20 (3.4)	2.02 (4.5)	3.30 (6.0)	4.40 (2.4)
$P_{max,exp}$	(kN)	2.74 (6.0)	4.63 (7.6)	7.45 (7.2)	8.92 (8.9)
slip at $P_{max,exp}$	(mm)	9.39 (16.5)	12.08 (13.2)	15.25 (30.7)	13.81 (22.4)
$P_{failure,S,exp}$ (shear)	(kN)	-	4.12 (9.8)	6.40 (5.1)	8.70 (6.7)
% from $P_{max,exp}$	(%)	-	90 (4.4)	90 (6.4)	93 (3.5)
slip at $P_{failure,S,exp}$	(mm)	-	6.86 (9.53)	8.78 (6.80)	9.85 (17.06)
$F_{e,exp,\parallel}$	(N·mm^{-2})	12.68 (5.9)	11.63 (5.2)	12.16 (8.8)	10.32 (8.8)

[a]Determined according to [24], [b]Coefficient of Variation (%) in parenthesis.

Table 4 An overview of theoretical and experimental results for single shear dowel-type joints loaded in tensile perpendicular to grain.

Theoretical results					
	units	d = 12 mm	d = 16 mm	d = 20 mm	d = 24 mm
K_{cal}	(kN·mm^{-1})	0.21	0.30	0.38	0.46
$P_{y,EYM,cal}$ (mode 3)	(kN)	0.93	1.71	2.09	2.92
$P_{yield,cal,1052}$[a]	(kN)	1.03	1.82	2.85	4.10
Experimental results					
		d = 12 mm	d = 16 mm	d = 20 mm	d = 24 mm
K_{exp}	(kN·mm^{-1})	0.30 (13.0)[b]	0.45 (22.7)	0.65 (29.1)	0.73 (25.4)
$P_{yield,exp}$	(kN)	0.90 (20.3)	1.52 (19.5)	1.98 (9.4)	2.50 (9.1)
$P_{max,exp}$	(kN)	1.19 (12.1)	2.07 (19.9)	2.54 (10.6)	3.55 (14.9)
slip at $P_{max,exp}$	(mm)	4.52 (10.3)	5.40 (23.6)	4.57 (11.49)	5.99 (42.7)
$F_{e,exp,\perp}$	(N·mm^{-2})	5.51 (16.3)	5.40 (19.8)	4.24 (10.6)	4.10 (14.9)

[a]Determined according to [24], [b]Coefficient of Variation (%) in parenthesis.

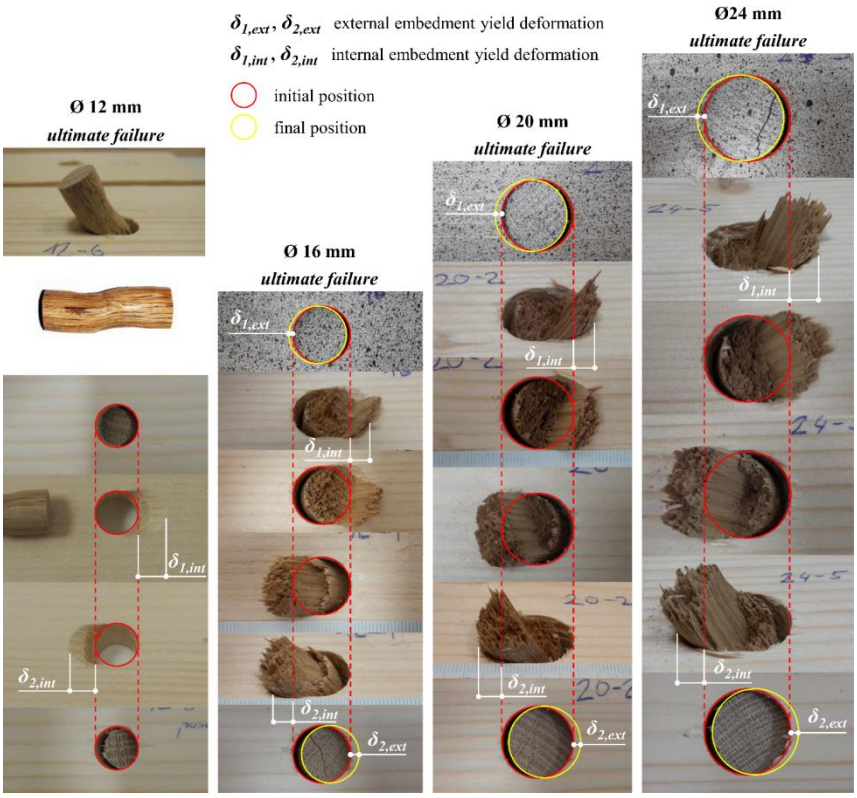

Fig. 4. The dowels deformation description when ultimate joints failure.

Table 5 An external and internal embedment yield deformation in joint components due to the interaction between dowel and components hole surfaces at ultimate joints failure.

	d = 12 mm	d = 16 mm	d = 20 mm	d = 24 mm
$\delta_{1,ext}$ (mm)	-	1.10 (12.6)[a]	1.93 (8.1)	1.92 (18.9)
$\delta_{1,int}$ (mm)	7.28 (12.8)	5.32 (10.4)	7.61 (7.4)	7.30 (23.2)
$\delta_{2,int}$ (mm)	7.42 (10.4)	5.53 (14.4)	8.12 (11.5)	7.73 (19.7)
$\delta_{2,ext}$ (mm)	-	1.07 (11.8)	2.06 (12.3)	2.33 (15.7)
$\delta_{average,int} : d$	0.61	0.34	0.39	0.31
$\delta_{average,ext} : d$	-	0.07	0.10	0.09

[a]Coefficient of Variation (%) in parenthesis.

3.2 The joint slip modulus

The theoretical slip modulus (K_{cal}) of the joints agreed with experimentally determined slip moduli (K_{exp}), which are presented in Tables 3 and 4. Also, the K_{cal} and K_{exp} in this study are in agreement with results made by Fukuyama et al. [10, 19]. Fukuyama et al. [19] reported K_{cal} 1.98 kN·mm^{-1} and K_{exp} 2.71 ± 0.94 kN·mm^{-1} for dowel with a nominal diameter of 18 mm with slenderness ratio 3 made from Oak (*Quercus*) and joint components were made from Japanese cedar (*Cryptomeria japonica* L.f.) loaded in tensile parallel to grain. Further, K_{cal} 1.7 and 4.0 kN·mm^{-1} and K_{exp} 1.2 and 4.8 kN·mm^{-1} for dowels with a nominal diameter 12 and 24 mm and with slenderness ratio 10, respectively, was reported by Fukuyama et al. [10] for joints specimens, which were made of White oak (dowels) and Japanese cedar (joint components). Although those joints were made from different wood species while keeping the physical and mechanical properties, these results are in agreement with the ones presented here. The theoretical approach for determination of the K_{cal} according to Fukuyama et al. [10, 19] has verified a suitable mathematical model for predicting of the total joint stiffness.

3.3 Load-carrying capacity of the dowel

The first dowel failure occurred when the dowel capacity was exceeded and was theoretically characterized as modes 4 and 5 according to EYM (Fig. 2) for tests loaded in tensile parallel to grain. These modes are determined as a minimal value for $P_{y,EYM,cal}$ given by Eq. (5), according to Fig. 2. Based on this, the first theoretical failure should occur inside the joints in the contact zone between the dowel and joint components owing to exceeding the maximal plastic capacity moment (M_y) of the dowel. Nevertheless, in all experiments the failure mode 6 was observed according to EYM (see in Fig. 2). This mode 6 theoretically determined was also evaluated and compared with experimentally predicted load-carrying capacity ($P_{max,exp}$) of the dowels. It was found that the $P_{max,exp}$ was higher about of 14%, 12%, 13% and 4% for the dowel with a nominal diameter of 12, 16, 20 and 24 mm, respectively, than $P_{y,EYM,cal}$ for mode 6, as listed Table 3 for tests in tensile parallel to grain. In tensile perpendicular to grain, the first failure occurred in hole surrounding with subsequent ultimate failure in timber components (Fig. 5A). In experiments the failure mode 3 was observed according to EYM (see in Fig. 2). This mode 3 theoretically determined was evaluated and compared with experimentally predicted load-carrying capacity ($P_{max,exp}$) of the dowels. It was found that the $P_{max,exp}$ was higher about of 22%, 17%, 18% and 18% for the dowel with a nominal diameter of 12, 16, 20 and 24 mm, respectively, than $P_{y,EYM,cal}$ for mode 3, as listed Table 4 for tests in tensile perpendicular to grain. In the both test series, it supports the idea that these differences between theoretically determined and experimentally obtained results of the load-carrying capacity of the dowel are important for design of the joints from their safety perspectives. These facts indicate that this theoretical approach derived from Fukuyama et al. [10, 18, 19] is suitable way for prediction of the load-carrying capacity of the wooden dowel with respect to the design safety level.

Furthermore, as is apparent from Fig. 5B, the yield point ($P_{yield,exp}$) during tensile loading parallel to grain could be properly predicted based on calculation listed in DIN 1052 (Deutsches Institut für Normung e.V. 2004) according to Eq. (9). Nevertheless, for the tests in the tensile perpendicular to grain (Fig. 5C) is not possible to use the same calculation owing to it, that the force level increases linearly with increasing dowel diameter as shows Fig. 5C (magenta dashed line). Therefore, the prediction function should be linear as was estimated in this study (Fig. 5C). However, the presented function cannot be generally applied to any case, because of small amount of experimental measurements. The more measurements should be done.

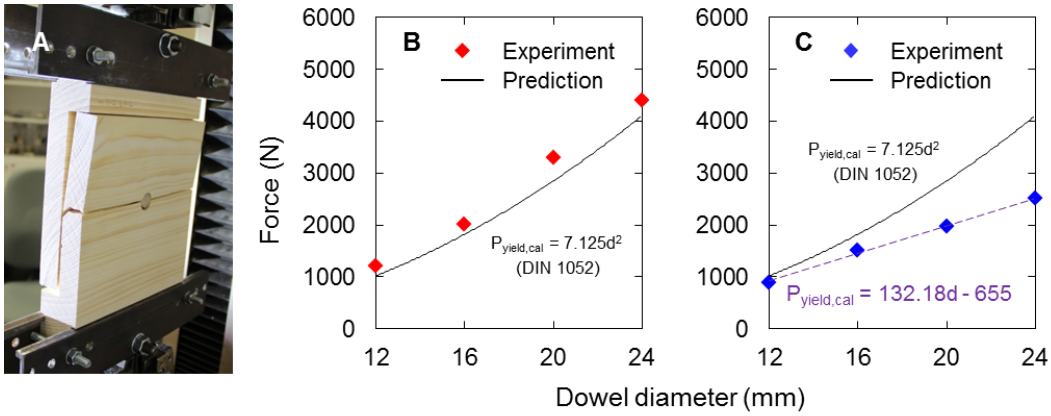

Fig. 5. A - represents the experimental failure at the end of test; B and C – represent the numerical prediction of force at the yield point ($P_{yield,cal,1052}$ and $P_{yield,exp}$) for the tests in tensile parallel and perpendicular to grain, respectively.

3.4 Dowel shear crack capacity

The DIC method was used to determine the force level ($P_{failure,S,exp}$) needed to induce the shear crack in the dowels for tests loaded in tensile parallel to grain. These cracks propagated longitudinally in pith rays on the both foreheads of the dowel with a diameter of 16, 20 and 24 mm, which initiates the failure with a subsequent ultimate tearing of the dowels (see Fig. 4). It was found that the first shear cracks were formed at state about of 92% of the $P_{max,exp}$ determined from the

load-slip curves for the dowels with diameter 16, 20 and 24 mm, as listed in Table 3. Nevertheless, the global joints failure does not occur at this point. The load can increase until the state assumed by $P_{max,exp}$ as confirmed by Fukuyama et al. [10].

The shear crack capacity ($P_{y,S,cal}$) of the dowels was determined theoretically by Eq. (8) for failure shear mode 7. The $P_{y,S,cal}$ showed lower values of 11%, 11% and 5% (for dowels with a nominal diameter of 16, 20 and 24 mm, respectively) when compared to $P_{failure,S,exp}$. The $P_{failure,S,exp}$ corresponds to the force level at the first visible crack in the dowel for each dowel in test series loaded in tensile parallel to grain obtained from DIC processing. These differences between $P_{y,S,cal}$ and $P_{failure,S,exp}$ also indicates that this theoretical approach derived from Fukuyama et al. [10, 18, 19] is convenient way to obtain the shear dowel capacity for the joints design and their safety perspectives. The dowel failure was not occurred in test series loaded in tensile perpendicular to grain. Therefore, the DIC dowel shear analyses were not performed.

4. Conclusion

This study presents the theoretical and experimental approaches for determination of the slip moduli (K_{cal} *and* K_{exp}) of the joints and load-carrying capacity for bending and shear deformation ($P_{y,EYM,cal}$, $P_{max,exp}$, $P_{y,S,cal}$ and $P_{failure,S,exp}$) of the wooden dowels according to design by Fukuyama et al. [10, 18, 19] based on the Beam on Elastic Foundation (BEF) theory with taking account of dowel shear deformation and Johansen's theory for single shear dowel-type joints performance loaded in tensile parallel and perpendicular to grain.

The theoretical and experimental approaches were focused on the solution of the foundation joints properties with detailed description of the mechanical behaviour of the wooden dowels subjected to loads. The theoretical and experimental results show agreement. In terms of solution of the slip moduli of the timber-to-timber joints (K_{cal} and K_{exp}) and load-carrying capacity ($P_{y,EYM,cal}$, $P_{max,exp}$, $P_{y,S,cal}$ and $P_{failure,S,exp}$) of the wooden dowels it has been proved that the mathematical design introduced by Fukuyama et al. [10, 18, 19] is a suitable tool for predicting the all-wooden joints properties with respect to safety level.

Acknowledgement

This paper was created at the Research Center Josef Ressel, Brno-Útěchov, Mendel University in Brno with a financial support from grant project DG16P02M026 “Historical Timber Structures: Typology, Diagnostics and Traditional Wood Working”, NAKI programme II provided by the Ministry of Culture and project No. LO1219 under the Ministry of Education, Youth and Sports National sustainability programme I.

References

[1] Tannert, T, Anthony, R., Kasal, B., Kloiber, M., Piazza, M., Riggio, M., Rinn, F., Widmann, R., Yamaguchi, N.: Recommendation of RILEM TC 215-AST: In-situ assessment of structural timber using semi-destructive techniques. In: Materials and Structures 47(5): 2014, Netherlands. ISSN: 1359-5997, pp. 767–785.

[2] Descamps T, Léoskool L, Van Parys L, Noël J, Aira JR. Sensitivity of old timber hyperstatic frames to the stiffness of step and ridge connections. In: World Conference on Timber Engineering, Quebec City, Canada, 2014.

[3] Branco JM, Descamps T. Analysis and strengthening of carpentry joints. Constr Build Mater 2015; 97: 34–47.

[4] Itany RY, Faherty KF. Structural wood research, state-of-the-art and research needs. American Society of Civil Engineers, New York, 1984.

[5] Shanks JD, Chang WS, Komatsu K. Experimental study on mechanical performance of all-softwood pegged mortice and tenon connections. Biosyst Eng 2008;100: 562–570.

[6] Santos CL, de Jesus AM, Morais JJ, Lousada JL. Quasi-static mechanical behaviour of a double-shear single dowel wood connection. Constr Build Mater 2009; 23:171–182.

[7] Kunecký J, Arciszewska-Kędzior A, Sebera V, Hasníková H. Mechanical performance of dovetail joint related to the global stiffness of timber roof structures. Mater Struct 2015; 49:2315–2327.
[8] Kunecký J, Sebera V, Hasníková H, Arciszewska-Kędzior A, Tippner J, Kloiber M. Experimental assessment of a full-scale lap scarf timber joint accompanied by a finite element analysis and digital image correlation. Constr Build Mater 2015; 76:24–33.
[9] Kessel MH, Augustin R. Load behaviour of connections with oak pegs. Peavy, MD and Schmidt, RJ, trans. Timber Framing, Journal of the Timber Framers Guild 1995;38:6–9.
[10] Kessel MH, Augustin R. Load behaviour of connections with pegs II. Timber Framing, Journal of the Timber Framers Guild 1996;39:8–10.
[11] Fukuyama H, Kairi M, Hirsi Hannu H, Inayama M, Ando N. Shear Characteristics of Wood Dowel Shear Joint and Practical Application Example. In: 10th World Conference on Timber Engineering. Miyazaki, Japan, 2008, pp. 1198-1205.
[12] Oudjene M, Khelifa M. Experimental and Numerical Analyses of Single Double Shear Dowel-Type Timber Joints. In: 11th World Conference on Timber Engineering, Trentino, Italy, 2010, pp. 476–482.
[13] Johansen KW. Theory of timber connections. Inter. Assoc. of Bridge and Structural Engineering, Bern, Switzerland. 1949; 9:249–262.
[14] Bouchair A, Vergne An application of the Tsaï criterion as a plastic flow law for timber bolted joint modelling. Wood Sci Technol 1995; 30:3–19.
[15] Larsen HJ. The yield load of bolted and nailed connections. In: Proceedings IUFRO 5-02, South-Africa, 1973, pp. 646–654.
[16] Möller, T. En ny metod för beräkning av spikförband: New method of estimating the bearing strength of nailed wood connections (in Swedish and English translation). Rep. No. 117. Gothenburg, Sweden: Chalmers Tekniska Högskolas Handlingar, 1950.
[17] Brungraber RL. Traditional timber joinery: a modern analysis. PhD thesis, Department of Civil Engineering, Stanford University, Palo Alto, CA, 1985.
[18] Blass HJ, Ernst W, Werner H. Verbindungen mit Holzstifen. Bauen mit Holz 101, Bruderver Karlsruhe, 1999.
[19] Fukuyama H, Ando N, Inayama M, Takemura M, Inoue M. Proposal of analytical models of wooden dowel shear joint. J Struct Constr Eng AIJ, 2007;72:129–136.
[20] Fukuyama H, Ando N, Inayama M, Takemura M. Calculation model and yield process of single shear joint with wood dowel of various slendernesses. J Struct Constr Eng AIJ, 2008;73:803–810.
[21] Požgaj A, Chovanec D, Kurjatko S, Babiak M. Štruktúra a vlastnosti dreva. Priroda a.s., Bratislava, 1997.
[22] ASTM D2395 (2014). Standard Test Methods for Density and Specific Gravity (Relative Density) of Wood and Wood-Based Materials. American Society for Testing and Materials, Philadelphia, PA, USA.
[23] EN 26891 (1991) Timber structures. Joints made with mechanical fasteners. General Principles for the determination of strength and deformation characteristics. European Committee for Standardization, Brussel.
[24] EN 383 (2007) Timber structures - Test methods - Determination of embedment strength and foundation values for dowel type fasteners. European Committee for Standardization, Brusel.
[25] DIN 1052 (2004) Entwurf, Berechnung und Bemessung von Holzbauwerken - Allgemeine Bemessungsregeln und Bemessungsregeln für den Hochbau. Deutsches Institut für Normung e.V., Berlin.
[26] Eurocode 5 (2004) Design of timber structures, CEN.